Use Authorization

In presenting this thesis in partial fulfillment of the requirements for an advanced degree at Idaho State University, I agree that the Library shall make it freely available for inspection. I further state that permission for extensive copying of my thesis for scholarly purposes may be granted by the Dean of the Graduate School, Dean of my academic division, or by the University Librarian. It is understood that any copying or publication of this thesis for financial gain shall not be allowed without my written permission.

Signature ___________________________

Date ___________________________

Use of Precast Hollow-Core Members in the Construction of Arch Culverts to Improve Aquatic Organism Passage

by

Maria Angelica Tangarife

A thesis

submitted in partial fulfillment

of the requirements for the degree of

Master of Science in the Department of Civil and Environmental Engineering

Idaho State University

Fall 2020

Committee Approval

To the Graduate Faculty:

The members of the committee appointed to examine the thesis of MARIA A. TANGARIFE find it satisfactory and recommend that it be accepted.

Dr. James Mahar
Major Advisor

Dr. Bruce Savage
Committee Member

Dr. Donna Delparte
Graduate Faculty Representative

Dedication

This thesis is dedicated to my amazing parents and sister. I do not think I would have made it this far without your support, love, affection and encouragement.

Acknowledgements

I would like to express the deepest appreciation to my advisor and mentor, Dr. James Mahar, who not only supported and guided me throughout this project, but who provided me with his time and wisdom every step of the way. I would also like to thank Dr. Bruce Savage for initiating this study and allowing me to be part of it. Special thanks to Garrett Thompson and Daniel Garz for providing me with great help during the design and construction of both models. In addition, thank you to Wyatt Radke, Aashish Thapa, Laura-Louise Alicke, Jared Cantrell, Mahesh Acharya, Mahesh Mahat and Tanner Garz for your continued help and support during construction and testing. Special thanks to all of the professors, students and friends who helped contribute to this project and who also made this project successful.

I would also like to thank Idaho State University for sponsoring this project and making this study happen. In addition, special thanks to Strata, Inc. for allowing me to use equipment and materials to perform the various laboratory tests needed for this project. Thank you to Pacific Steel and Recycling for their generous donation of storage boxes.

Finally, I would like to acknowledge with gratitude the love and support of my parents, Patricia Garzon and Edgar Tangarife, and my sister, Adriana Tangarife. Thank you for encouraging me to keep going. I would not have been able to finish without you three by my side.

Table of Contents

List of Figures

List of Tables

Use of Hollow-Core Members in the Construction of Arch Culverts to Improve Aquatic Organism Passage

Thesis Abstract – Idaho State University 2020

Experimental tests on half-scale, hollow-core and cast-in-place concrete arch culvert models were completed along with finite element and STAAD analyses for each. The main objectives were: to evaluate if a hollow-core culvert was able to sustain a 9.03-kip applied load without failure; to assess if hollow-core structure responses were comparable to cast-in-place ones; and to develop computer simulations capable of predicting hollow-core culvert responses of different configurations.

Based on experimental test results, neither concrete culvert is expected to reach its elastic limit in a full-scale application since the soil cover fails in bearing prior to the traffic load reaching the arch. When the load is applied on top of the culverts, both models can sustain the 9.03 kips without undergoing failure. Regarding finite element analyses, simulations developed were unable to be calibrated with experimental data since the program did not appear to include forces acting between the top adjacent segments or the soil bearing failure above the arch.

Key Words: hollow-core, cast-in-place, concrete culvert, experimental test, finite element analyses

Chapter 1: Introduction

1.1. Background

Culverts serve as important underground structures throughout the world as they provide natural drainage, allow for traffic to flow over waterways, prevent erosion and in many cases allow for fish passage. Due to the important role that they play within our communities, providing a proper design, construction and operation throughout the structure's life is of utmost importance.

Currently, the State of Washington is under a federal court order that requires the state to repair or replace culvert structures that are impeding fish and aquatic organism passage. This court ruling was the outcome of legal complaints that 21 northwest Washington tribes submitted to the U.S. District Court in which they stated that the State of Washington had a treaty-based duty to preserve fish runs. The court ruling declared that "the right of taking fish, secured to the tribes in the Stevens Treaties, imposes a duty upon the state to refrain from building or operating culverts under state-maintained roads that hinder fish passage and thereby reduce the number of fish that would otherwise be available for tribal harvest" (Washington State Department of Transportation, 2019). As a result of this ruling, the Washington State Department of Transportation needs to replace approximately 1,012 culverts that are impeding the passage of salmon and steelhead by 2030.

1.2. Purpose and Significance of Study

In an effort to evaluate an efficient and cost-effective solution that could result in rapid culvert construction and that would also provide appropriate Aquatic Organism Passage (AOP), this project evaluated how a precast culvert would perform under a design truck load. The precast culvert used in this study consisted of hollow-core panels with joints bonded by grout. Figure 1 presents a schematic of the model evaluated for this project.

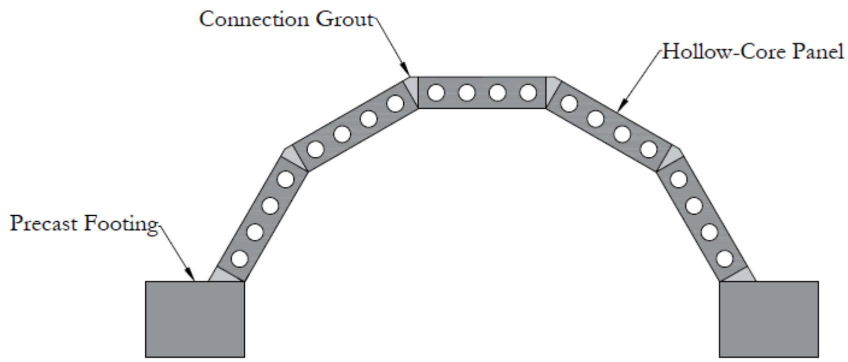

Figure 1 - Hollow-Core Culvert Schematic

An arch-type structure was selected with an open bottom for this project to resemble an "ecological design" in which natural stream conditions are maintained upstream, downstream and within the culvert (Bates et al., 2003). By having an open bottom, the natural streambed is preserved and the impact of the culvert on natural stream conditions and ecological processes is minimized (U.S. General Accounting Office, 2001). This, in turn, is intended to improve aquatic organism passage.

Model dimensions were determined primarily based on tributary width and stress distribution calculations as well as on the geometry that hollow-core panels are typically fabricated in precast plants. To obtain an arch geometry, five panels were used in the hollow-core model (the cast-in-place (CIP) model replicated this design) as this was concluded to be the minimum number of panels needed to obtain a span to height ratio of approximately 2:1. This ratio is typically used for the construction of arch-type structures since they tend to be circular in shape.

The purpose behind utilizing hollow-core panels in the construction of the precast arch culvert was related to the advantages that these members bring in terms of cost and efficiency. The continuous open tubes present in these elements reduce the total weight of the precast slabs making the panels much easier to handle and place. In addition, transportation costs are lowered since more panels can be transported at a time when compared to full sections. Furthermore, in the installation process, the lower weight allows for a shorter set-up time, a smaller number of workers needed and an easier in-situ placement of the precast members, all resulting in overall lower project costs. From a production stand-point, reduction in costs results from the use of uniform cross sections in large production volumes, a decrease in the amount of raw material needed, and an easier handling of the pieces in the production plant.

From an efficiency perspective, opting for precast hollow-core members assures a certifiable quality, a quick and easy installation when compared to CIP elements, high load capacity and durability, and the possibility of utilizing the longitudinal open tubes for other operations (such as post tensioning the slabs). Structurally, hollow-core members have been proven to provide the same efficiency of non-hollow slabs for characteristics such as load capacity, span range and deflection control. The assembly of slabs through keyway grouts can create a basic diaphragm system that is also able to resist lateral loads (PCI Manual for the Design of Hollow Core Slabs and Walls, 2015).

Based on these advantages it seems that, if a precast arch-culvert is able to sustain the design wheel loads imposed on the system, this construction alternative is potentially the most efficient and effective way to construct concrete culverts.

1.3. Project Scope

This project had three main objectives: first, to evaluate if a hollow-core culvert was able to sustain an applied truck load, reduced to a half-size scale model, without failure; second, assess if the response of the precast structure is comparable to that of a monolithic CIP culvert; and third, to develop a FEM simulation, calibrated with experimental data, that would be able to predict the structural responses of different hollow-core culvert configurations.

To achieve the first and second objectives, experimental tests on hollow-core and CIP culvert models were performed. The cast-in-place model served as the basis of comparison of the hollow-core culvert and enabled a performance assessment of the two structures. Both constructed culverts characterized half-scale models and followed the same geometry to obtain comparable designs. Since the inclusion of pre-tensioned or post-tensioned strands within the hollow-core members was not feasible, neither model was reinforced. In order to replicate the conditions around a culvert, both models made use of a soil box. Information obtained from experimental test results was post-processed so that different load and displacement relationships were developed and an assessment of the structural responses of each model were made.

For the third objective, a finite element software (ANSYS Mechanical APDL) was used to develop 2-dimensional and 3-dimensional simulations of the two models. Laboratory tests on the different structural and soil components were performed to obtain the material properties. Results obtained from the finite element (FEM) simulations were compared to those obtained during experimental tests to assess the closeness of the two methods of analysis; and subsequently, the FEM models were refined to yield similar responses to those observed in the laboratory. The ultimate goal of the FEM models was to provide a "calibrated" simulation that could be used in the future for predicting culvert behavior without the need to perform experimental testing.

1.4. Thesis Overview

This research project describes and presents the results of experimental testing performed on a hollow-core and a CIP half-scale model; as well as the numerical computer simulations developed for each. This report is divided into five chapters:

- Chapter 1: Introduction gives a brief overview of the project background as well as an explanation of the purpose and significance of this study, along with a description of the scope and objectives of this research project.
- Chapter 2: Literature Review presents the relevant sources of information used to develop this project. These sources were divided into six main sections which included: aquatic organism passage, culvert structures, cast-in-place concrete in culvert construction, precast concrete in culvert construction, soil-structure interaction, and concrete culvert studies.
- Chapter 3: Cast-in-Place Concrete Culvert Model provides information related to the loading configuration; model design; construction, laboratory and experimental methodologies and results; and FEM simulations developed for the CIP culvert.
- Chapter 4: Precast Hollow-Core Culvert Model presents the same basic information as that in Chapter 3 for the cast-in-place culvert.
- Chapter 5: Conclusions and Recommendations summarizes the experimental and FEM results obtained for each model and provides conclusions drawn from each. In addition, recommendations for future studies are given here.

Chapter 2: Literature Review

2.1. Aquatic Organism Passage (AOP)

2.1.1. Definition of Aquatic Connectivity

Aquatic connectivity can be considered as a continuous biological corridor through which aquatic organisms move, join and interact to fulfill their life cycles. Activities such as acquiring resources, reproducing, rearing and refuging from disturbances and predators are examples of interactions that occur within these water bodies. Movement along this corridor can happen in both the upstream and/or downstream directions, which results in travels through different spatial and temporal frames (U.S. EPA, 2015; Hoffman, Dunham & Hansen, 2012; Evans & Johnston, 1972). Due to the importance of maintaining connectivity throughout water corridors to ensure the necessary life cycle process, it is imperative that structures constructed within the corridors provide adequate aquatic organism passage (AOP).

2.1.2. Effect on AOP

As examined by the U.S. EPA (2015), modifications to naturally existing processes and fluxes within a watershed habitat and between its system components becomes evident and measurable only when human activities and construction are involved. Stream structures (i.e. artificial barriers) are obstacles that do not allow an uninterrupted passage of organisms either up- or downstream. These artificial interventions alter the hydrologic connectivity at different levels (biological, physical and chemical) and dimensions (longitudinal, lateral, vertical and temporal) in water networks; and can ultimately affect organism's population on either side of the barrier.

2.1.3. Examples of Culvert Structures with Good AOP

Natural and artificial passages (i.e. roads and rivers) need a good connectivity in order to be successful. The ultimate goal is to improve the human-built infrastructure in order not to fragment or destabilize the natural ecological levels and dimensions. Culvert structures should maintain habitats, processes and populations, and should never impede the movement of local organisms either up or downstream. In an effort to provide a means of designing crossing structures above a water body, stream simulation design was developed. Stream simulation aims to design a structurally and functionally similar environment to the natural channel, with the objective of creating a passage that presents no further obstacle for organisms, when compared to the one present before human intervention. Open-bottom structures with a continuous streambed type, width, slope and composition along the culvert are good examples of stream simulation designs (Forest Service Stream-Simulation Working Group, 2008). Proper culvert structures should be designed to ensure fish passage 95% of the time within a 1-year period, or 90% of the time within a 6-month period (Evans & Johnston, 1972).

2.1.4. Detrimental Effects of Inadequate AOPs

As per the U.S. EPA (2015), human-related activities and structures distress the connections between streams. Because biological, chemical and physical connections within water networks are directly related, the restrictions to any (or all) of these connections consistently bring about the extinction of one or more aquatic populations throughout the network. These populations refer to "aquatic and semiaquatic organisms that include fish, amphibians, plants, microorganisms and invertebrates" (U.S. EPA, 2015). For instance, a connectivity impediment can cause populations to be fragmented and homogenized, resulting in a reduction of available habitats necessary for their natural life cycles and, hence, an eventual extirpation of the local population.

It is therefore of outmost importance to maintain hydrologic connectivity by creating an appropriate and efficient AOP, as it directly affects the health of all systems present in the stream.

Directly related discoveries of stream modification impacts were found by Hoffman, Dunham and Hansen (2012). Their analysis of the level of potential impacts on different taxa groups and, within these, diverse type of migration behaviors from each group, showed that migratory fish are the most susceptible to the negative effects related to a marginal or total impediment of movement within the stream. Other taxa groups analyzed included amphibians, aquatic insects, crayfish and mussels, whilst other migration behaviors included permanent residents, explorers and dispersers. Regardless of the type of population or their movement habits, it was found they all suffer higher or lower levels of survival when the AOP at water crossings are limited or totally restricted as a result of poor culvert design. Because a poor connectivity can result in a fragmented or reduced habitat and isolated or extinct populations, the work in this study highlights the importance of preserving the processes and connections of water systems.

Migratory barriers, which include human-induced or construction activities and structures, can have both positive and negative impacts on the local species of an aquatic habitat. However, the detrimental effects tend to be higher than the beneficial ones, as stated by Gubernick and others (2008).

These barriers tend to modify and weaken the ability of naturally existing populations to procreate and/or survive by blocking the organisms' movement, delaying their migration and causing them physiological distress (Forest Service Stream-Simulation Working Group, 2008). These effects might be enhanced due to changes in hydraulic and velocity forces that create a substrate displacement that, in turn, have a negative impact on local aquatic organisms, reducing its numbers (Khan & Colbo, 2008).

As culverts create barriers that limit the movement of organisms, if improperly designed they can block their access to essential habitats, possibly having an effect on their genetic diversity and survival. Unfortunately, the main objective of many culvert designs is to provide a maximum hydraulic capacity and not to ensure adequate aquatic organisms' passage (Gregory, McEnroe, Klingeman, & Wyrick, 2004).

2.1.5. Requirements for Properly Designed AOPs

As early as 1956, McKinley and Webb (1956), and Shoemaker (1956) proposed considerations that could create an adequate culvert design, by reducing water flow and augmenting the depth that could increase passage. Considered factors for an effective AOP should take into account the preservation of the entire range of connectivity levels and dimensions, as well as all organisms and their entire cycle of life (Hoffman, Dunham, & Hansen, 2012). Because human-built stream crossings entail a varied range of conditions that can affect AOP, there is a challenge on selecting an adequate design and control method. As such, different culvert construction methods could be compared in one specific site, so as to assess which mechanism or type of construction is more adequate and promotes efficient AOP.

As noted by Gubernick and others (2008), culverts with narrower sections than the natural channel results in higher water velocities inside the culverts, as well as upstream backwater conditions when high flows arrive. On one hand, higher stream velocities might prevent organisms from swimming back upstream. On the other, backwatering during high flows can lead to sediment and debris deposition at the pipe inlet, which in turn become an additional barrier for organism movement. A number of items should be taken into consideration when designing a culvert, these include: eliminating elevation drops at inlets or outlets, removing clogs, maintaining the stream velocity and turbulence within the culvert, considering the existence of bank-edge habitats (for weak-swimming and crawling species), ensuring a sufficient water depth, maintaining water depth and providing a continuous channel substrate. Furthermore, Gubernick (2008) recommends guidelines for culvert designs, including considerations of the stream and road changes over time, suggestions on a minor obstacle introduction to the stream, and advise of avoiding fragmentation of aquatic habitats.

Evans and Johnston (1972) consider that an artificial structure with an adequate passage for upstream moving organisms should include en-route and upstream resting areas, small sized individual jumps, in-range water depths and velocities. The authors also state that the design details should be based on the organism with the lowest swimming ability. Moreover, the selection of the crossing site is of particular importance. For the location selection, the following aspects should be considered: maintaining the water gradient and velocity for at least 100 feet below, above and at the crossing point; the gradient throughout should be as close to zero as possible; and should follow the alignment of the natural channel for at least 100 feet above and below the culvert inlet and outlet. Evans and Johnston opine that "Culverts in fish streams should be designed to pass a 50-year flood at static head and a 100-year flood with ponding head."

Evans and Johnston (1972) conclude that "many fish biologists believe that the arch should be the only acceptable type of culvert to use where any significant fish passage is required. Preferably, the arch culvert has the same bottom width as the natural channel". In addition, due to the high cost of replacing all environmentally inadequate culverts, it is of great importance to examine lower cost alternatives for the creation and construction of culverts that ensure proper organism passage, but that are equally financially attractive to managers (Gregory, McEnroe, Klingeman, & Wyrick, 2004). Thus, the use of hollow-core culverts proposed in this research merit such consideration.

2.1.6. AOP Considerations for Current Project

In an effort to provide proper AOP, this project followed the design considerations to develop culvert structures that would aim to diminish the impact that such barriers have on aquatic organisms. Since arch structures with open-bottoms were considered to be the ideal types of structures for use in water corridors, both the CIP and hollow-core models followed this configuration. Even though the structures were not placed in a natural environment for testing, the design intent was to provide the same width of a natural channel and a continuous open stream bottom with the same width and slope throughout the span.

2.2. Culvert Structures

2.2.1. Definition

Culverts are structures that enable water to flow under roads or trails. For the most part, culverts are embedded structures with an important hydraulic design component, aimed at increasing the water carrying capacity at the crossing point. Culvert design is of outmost importance, and it should not only consider the hydraulic design factor but also comply with the adequate load carrying capacity requirements. Loads affecting culverts are of two types, permanent and transient, each one with several sub-categories need to be considered in the design process.

Depending on the construction material, culverts are classified as either rigid or flexible. Concrete and stone masonry culverts represent the former category, while steel, aluminum and composite materials make up the latter. Rigid culverts have limited deflection allowance, such that their capacities rely primarily on the material itself to resist the culvert loads. On the other hand, flexible culverts depend on the backfill composition and compaction to prevent buckling failure. Both models in this study are rigid culverts.

2.2.2. Culvert Shapes

Culverts come in various sizes and shapes. The selection of a particular design is driven by factors such as depth of cover, headwater elevation, AOP, and structural/ hydraulic requirements and not necessarily by the construction material itself. Figure 2 presents some common culvert shapes.

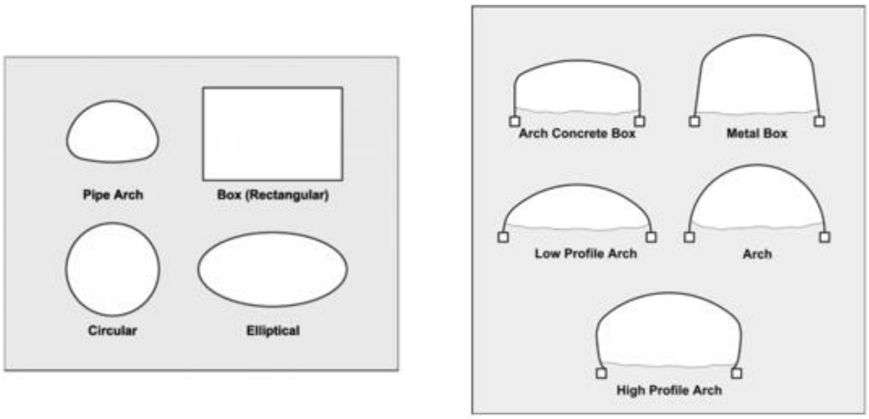

Figure 2 - Closed-bottom culvert shapes (left) and open-bottom culvert shapes (right) (U.S. Department of Transportation, 2012)

- Circular Culverts

  Circular culverts are considered hydraulically and structurally efficient under most conditions, making it the most common shape used in culvert design. However, this shape can result in a limited stream width when low flows occur and it may be more likely to clog, when compared to other culvert shapes. For flexible culverts, special attention needs to be given during backfill placement to properly compact the soil under the haunch and to prevent excessive inward movement of the pipe above the springline.

- Pipe and Elliptical Culverts

  Pipe arch and elliptical culverts are preferred over circular geometries when the distance between the invert and the pavement surface is limited or when low flow levels require a wider section. Pipe arch and elliptical pipes are also likely to clog and have a lower structural efficiency than circular shapes.

- Arch Culverts

These shapes allow for a better passage of the water and can also provide a natural and erosion-resistant stream bottom. For this shape, special attention must be given to footing support.

- Box-Section Culverts

Culverts with a rectangular cross-section are also extensively used as they can easily be adapted to a varied range of site conditions, even though they do not have the same structural efficiency of other shapes.

- Multiple-Barrel Culverts

These shapes are ideal when good hydraulic capacity is needed for low embankments, as well as when waterways are wide. However, they might be likely to clog in areas between the barrels where debris and sediment accumulate.

2.2.3. Culvert Materials

- Precast Concrete

Precast concrete is used for circular, elliptical (long axis is horizontal or vertical), rectangular and arch culverts.

- Cast-in-place Concrete

Cast-in-place concrete is used for rectangular and arch-shaped culverts, although the former is more widely used in practice. Cast-in-place construction is ideal when the culvert needs very specific site requirements, but because of the typically long construction times, pre-cast concrete or corrugated metal culverts are preferred.

- Metal

  Aluminum and steel are typically used in construction of flexible culverts. The most common types of metal culverts are corrugated metal pipes produced in factories or structural plates assembled in the field. The shape selection of flexible culverts depends on span length, clearance distances (horizontal and vertical), peak stream flow and type of terrain.

- Masonry

  Even though stone and brick were widely used in the past, the present practice is to only use stone if the terrain has very acidic runoff. In some cases, stone is selected based on aesthetic requirements, rather than structural considerations.

- Timber

  Timber is used for the construction of box culverts built from individual members. Inspection for construction of a timber structure should be the same than that for a timber bridge.

- Other Materials

  Materials such as iron, stainless steel, terracotta or plastic are very rarely used in culvert construction, as they are considered to be relatively new (in the case of plastic), labor-intensive (if terracotta is considered) or needed only in very specific conditions (iron and stainless steel).

2.3. Cast-in-Place Concrete Culverts

2.3.1. Design Guidelines

2.3.1.1. Design Loads

2.3.1.1.1. <u>Self-Weight (DC):</u>

For self-weight calculations, the unit weight of the concrete should be taken as 150 lb/ft^3. If a uniform load is applied across the top slab, the self-weight can be calculated as:

$$\boldsymbol{W_{DC} = \gamma_{conc}\left(\frac{t}{12}\right)} \text{ (U. S. Department of Transportation, 2012)} \qquad \textbf{(1)}$$

Where:

$t =$ top slab thickness, in.

$\gamma_{conc} =$ unit weight of concrete, pcf

In cases where the is no fill on the top slab, the self-weight calculations should include a ½-inch wearing surface. The thickness of the wearing surface should be considered in the design, but not in the section properties of the top slab.

All relative weights for the top slab, walls and any other structure weights are included in the bottom slab calculations, as these result in an upward reaction from the soil with a corresponding uniform pressure. The weight of the bottom slab is not considered, as it is assumed to be directly supported by the underlying soil.

2.3.1.1.2. <u>Vertical Earth Pressure (EV):</u>

For the vertical earth pressure calculations, the unit weight of soil should be considered as 120 lb/ft^3 if data are not available for the backfill soil. Vertical earth loads include the soil and pavement loads above and in areas adjacent to the culverts. These are calculated based on a soil-structure interaction factor (F_e), which adjusts the vertical earth load applied to the culvert.

$$\boldsymbol{F_e = 1 + 0.20 \cdot \frac{H}{B_c}} \textit{ (U.S. Department of Transportation, 2012)} \tag{2}$$

Where:

H = depth of backfill, ft

B_c = total width of top culvert, ft

2.3.1.1.3. <u>Horizontal Earth Pressure (EH):</u>

This load considers active, at-rest and passive pressures as well as the soil-structure interaction factor. The horizontal pressure acting on the side of the culvert is calculated using the equivalent fluid method. The maximum and minimum values for the fluid unit weights are 0.060 and 0.030 kips per cubic feet, respectively. The horizonal earth pressure is used to calculate shear and moment forces acting on the sidewalls, as well as the axial forces acting on the top and bottom slabs (State of Illinois Bureau of Bridges and Structures Office of Program Development, 2017).

Per the *AASHTO LRFD Bridge Design Specifications* (2017), the horizonal soil pressure at any point that lies beneath the fill surface is calculated using the following formula:

$$\boldsymbol{p = k_h y_s z} \tag{3}$$

Where:

p = lateral earth pressure, psf

k_h = lateral earth pressure coefficient

y_s = unit weight of backfill, pcf

z = distance from the surface to the reference point, ft

The coefficient k_h depends on two factors: the stress history of the soil and the displacement of the culvert. The stress history refers to the level of consolidation of the soil (either normally consolidated (NC) or over consolidated (OC)); whereas the displacement refers to level of flexibility or stiffness of the structure, as well as of the type of soil loading (passive or active).

2.3.1.1.4. Horizontal Earth Load Surcharge (ES):

In cases where a culvert is buried, the fill above the deck level is considered an earth surcharge, which should be considered as a constant horizontal earth pressure addition to the basic existing earth pressure. This constant earth pressure surcharge is given by:

$$\Delta_p = k_s q_s \textit{ (AASHTO, 2017)} \tag{4}$$

Where:

Δ_p = constant horizontal earth pressure, psf

k_s = coefficient of earth pressure due to surcharge

q_s = uniform surcharge acting on upper surface of an active earth wedge, psf

2.3.1.1.5. Horizontal Water Pressure (WA):

Culverts should be designed assuming that a static water pressure acts on the inside of the walls, for the full design height. The following gives the WA relationships used at the top and bottom elevations:

$$WA_{top} = 0.00 \tag{5}$$

$$WA_{bottom} = y_w \cdot Rise \cdot w \textit{ (AASHTO, 2017)} \quad \textbf{(6)}$$

Where:

WA = horizontal water pressure, pounds per linear foot

γ_w = unit weight of water, pcf

$Rise$ = height of water column, ft

w = width of water column, ft

In addition, the design should also take into consideration groundwater pressures acting on the outside of the walls for the full design height. Similar relationships as those given in equations 5 and 6 are used to determine the corresponding groundwater pressures.

2.3.1.1.6. Transient Live Loads (LL):

Per the *AASHTO LRFD Bridge Design Specifications* (2017), box culverts should be designed based on calculations made for a HL-93 truck and/or tandem vehicular live loads. The approximate strip method is used in design with the 1-foot wide design strip oriented parallel with the span. For box culverts with spans of 15 feet or greater, lane loads are also applied to the top slabs of box culverts.

2.3.1.1.7. Transient Live Load Surcharge (LS):

According to AASHTO's design guide (2017), a live load surcharge should be applied whenever a vehicular load is expected to act on the surface of the backfill within a distance equal to 1/2 the wall height behind the back face of the wall. The increase in horizontal pressure due to LS is given by:

$$\Delta_p = k_a \gamma_s h_{eq} \quad \textbf{(7)}$$

Where:

Δ_p = constant horizontal earth pressure due to live surcharge, psf

k_a = coefficient of lateral earth pressure

γ_s = total unit weight of soil, pcf

h_{eq} = equivalent height of soil from vehicular load location, ft

2.3.1.1.8. Transient Dynamic Load Allowance (IM):

The dynamic load allowance (IM) for culverts and other buried structures is proportional to the depth of fill over the culvert. *AASHTO LRFD Bridge Design Specifications* (2017) requires that IM be considered for fill heights of up to 8 ft. The equation to calculate the dynamic load allowance for the strength and service limit states is:

$$\boldsymbol{IM = 33 \cdot (1.0 - 0.125 \cdot D_E) \geq 0\%} \tag{8}$$

Where:

IM = dynamic load allowance

D_E = minimum depth of earth cover above the structure, ft

2.4. Precast Concrete in Culvert Construction

2.4.1. Hollow-Core Members

A hollow-core slab is a precast element of prestressed concrete that has longitudinal open tubes of different forms and sizes, whose geometry depends on the use and the loads to which the element is subjected to. The continuous voids reduce the total weight of the precast slabs, making them an economical and efficient alternative for floor and roof systems, as well as wall panels, spandrel elements and bridge slabs (PCI Manual for the Design of Hollow Core Slabs and Walls, 2015).

From a cost perspective, hollow-core members are an ideal solution in terms of production, transportation, and installation for culverts. First, a reduction in production costs results from the use of uniform cross sections in large production volumes, a decrease in the amount of raw material (i.e. concrete and prestressing steel) and easier handling of the pieces in the production plant. With a lower weight, transport costs are also reduced. The lower weight allows for a shorter set-up time, a smaller number of workers and a more efficient erection process, all of which results in lower overall project costs (PCI Manual for the Design of Hollow Core Slabs and Walls, 2015).

From an efficiency stand point, opting for precast hollow-core members assures a certifiable quality and fire resistance, a high load capacity and durability, and the possibility of utilizing the longitudinal void spaces for other systems (ventilation or wire concealment). Based on past experience, hollow-core members provide the same structural efficiency as non-hollow slabs for characteristics such as load capacity, span range and deflection control. Assembly of slabs using keyway grouts can create a basic diaphragm system that is also able to resist lateral loads (PCI Manual for the Design of Hollow Core Slabs and Walls, 2015).

Precast hollow-core members used in floor systems can be combined with top surfaces, which can be either prepared with feathered latex cement joints between slabs, by installing a ½- to 2-inch thick non-structural topping or by casting a structural concrete topping.

In practice, hollow-core members are cast on beds that range from 300 to 600 feet in length. Once the elements are cured, the slabs are sawcut to the desire length for each specific project. When evaluating different products in the design of a project, it is important to consider repetitive form and size slabs, since this will result in a higher efficiency, both in terms of production and installation (PCI Manual for the Design of Hollow Core Slabs and Walls, 2015). Finally, the sawcut process allows the slabs to be cut to the appropriate lengths which minimizes the transport volume of the slabs to the project site.

2.4.2. Methods of Manufacturing

Currently, there are seven major manufacturing systems for the production of machine-cast hollow core slabs. The systems depend on the manufacturer's patent allowing other producers to build hollow-cores as a franchise or with a license from the original manufacturer. Table 1 shows the seven available manufacturing systems, the types of machines used for each one, the concrete type and slump, and their core form.

Table 1 - Hollow-Core Slab Systems (PCI Manual for the Design of Hollow Core Slabs and Walls, 2015)

Manufacturer	Machine Type	Concrete Type/Slump	Core Form
Dynaspan	Slip form	Dry/low	Tubes
Echo	Slip form	Dry/low	Tubes
Elematic	Extruder	Dry/low	Auger/tube
Flexicore	Fixed form	Wet/normal	Pneumatic tubes
Spancrete	Slip form	Dry/low	Tubes
SpanDeck	Slip form	Wet/normal	Filler aggregate
Ultra-Span	Extruder	Dry/low	Augers

Based on the above table, there are two basic manufacturing techniques: the dry-cast and the wet-cast methods.

2.4.2.1. Dry-Cast Method

In this method, low-slump concrete is used, limiting the water content to just above that needed to hydrate the cement. Water-cement ratios are around 0.30. For this technique, special attention needs to be given to the mixing process, as the low water content must be dispersed throughout the mix. The low-slump concrete is then passed through a casting machine that has cores around which the concrete consolidates through compaction and vibration. The cores can be formed using either augers or tubes.

In this process, admixtures that reduce water content can be used to lower the water requirements of the mix without compromising concrete compaction by the machine. However, air-entraining admixtures are not ideal since low water-cement ratios combined with compaction placing methods do not allow for proper air dispersion and maintenance.

In the case of zero-slump concrete, dry-cast extruded hollow-core slabs, the *Commentary to the ACI Code I* (2011) gives cautions on the existing development length equations. In this commentary, an explanation is given on why shear and bond strength depend on the degree of compaction of the concrete as well as on the concrete mix design, which also depend on the specific machine employed in slab production (PCI Manual for the Design of Hollow Core Slabs and Walls, 2015).

2.4.2.2. Wet-Cast Method

This technique employs a typical slump concrete, with water-cement ratios ranging between 0.40 and 0.45. The production of concrete depends on the mix proportions and the addition of admixtures and must always be stiff enough to hold its shape consistent with the forming technique used. In the west-cast method, the forming technique varies depending on the size of the slabs and the cores. For the former, it is possible to use either stationary, fixed or machine-attached forms. For the latter, the form is given by "either lightweight aggregate fed through tubes attached to the casting machine, pneumatic tubes anchored in a fixed form, or long tubes attached to the casting machine that slip form the cores" (PCI Manual for the Design of Hollow Core Slabs and Walls, 2015).

2.4.3. Design Guidelines

The design of hollow-core slabs should be made in accordance with the *Building Code Requirements for Structural Concrete (ACI 318-11)* and its *Commentary (ACI 318R-11)*, published by the American Concrete Institute (ACI) (2011). Consistent with other prestressed concrete members, hollow-core slabs must be designed to resist the different stresses that occur from production to erection. These stresses include: force transfer stress, handling stress, service load stress, deflections, shear and bending. The *PCI Design Handbook: Precast and Prestress Concrete* (2017) and the *PCI Standard Design Practice* (2003) present a number of charts and tables which provide useful information in the design of prestressed members, and also provide design practice guidelines for the precast and prestressed concrete industry. In addition, manufacturers usually present load tables that are useful when considering uniform load cases, since they have already considered the forces and stresses a given element can withstand for production purposes. These references aim to aid the designer in obtaining relevant data for slab design. For projects in which the loads are not uniform, the following design factors should be considered:

2.4.3.1. Flexural Design

According to Chapter 18 of *ACI 318-11* (2011), prestressed flexural members are classified as either Class U, Class T or Class C, depending on the variable f_t, corresponding to the extreme fiber stress in tension in the pre-compressed tensile zone, and f_c', corresponding to the specified compressive strength of concrete. For Class U and Class T flexural members, the uncracked section can be used to calculate the stresses at service loads. For Class C flexural members, these same stresses should be computed using the cracked transformed section. The following are the f_t and f_c' relationships for the different classes of flexural members:

- Class U

$$\boldsymbol{f_t \leq 7.5\sqrt{f'_c}} \quad \textbf{(9)}$$

- Class T:

$$\boldsymbol{7.5\sqrt{f'_c} < f_t \leq 12\sqrt{f'_c}} \quad \textbf{(10)}$$

- Class C:

$$\boldsymbol{f_t > 12\sqrt{f'_c}} \quad \textbf{(11)}$$

Sections 9 and 18 of *ACI 318-11* (2011) provide further information on permissible stresses at transfer and service loads, loss of prestress, required strength and minimum reinforcement.

2.4.3.2. Shear Design

In dry-cast systems, if the applied shear is greater than the shear strength, the use of stirrups is not recommended since their placement in these systems is very difficult. Stirrups could be considered a viable method to improve shear capacity in wet-cast systems, since it is easier to place them than in a dry-cast member. Shear strength can also be increased by reducing the number of cores in a slab, which can be achieved by removing a full-length core from the slab, or by breaking into the cores locally and filling them while the slab concrete is still fresh. According to ACI (2011), it is possible to assume that the "prestressing force increases linearly from zero at the member end to full effective prestress in a length equal to 50 strand diameters.

If de-bonded strands are used, transfer of prestress for the de-bonded strands must also be considered" (PCI Manual for the Design of Hollow Core Slabs and Walls, 2015).

Chapter 11 of *ACI 318-11* (2011) presents additional guidelines for shear design.

2.4.3.3. Camber and Deflection

Camber is defined as the upward deflection of a prestressed concrete member. Because camber depends on prestressing forces and eccentricity, both of which are defined by the design loads and the span length, camber will change depending on the design, and should not be considered a design parameter. Deflections, although also defined by prestressing forces, can be independent of the prestress level if the tensile stresses are smaller than the cracking stress.

Both, cambers and deflections are susceptible to changes in time, as a result of creep in the concrete, and loss of prestress in the members. Instantaneous cambers and deflections, as well as their changes over time need to be considered when designing the hollow-core members. The instantaneous values are easy to calculate when the properties of the materials are known. However, time-dependent changes are not easily and accurately calculated, as such the values are only estimates. Based on experience, producers typically have a more accurate knowledge of long-term deflections, but final calculations and approximates should be carried out in order to correlate manufacturer experience with design needs.

Chapter 9 of *ACI 318-11* presents in-depth information and calculations regarding camber and deflection parameters and design considerations.

2.4.3.4. Strand Developments

In the precast industry, particularly related to prestressed hollow-core members, each slab is given a number of prestressing strands which provide structural reinforcement to the entire member. Strands can vary in size and length and can be arranged in various strand patterns. Prestressing strands play a huge role in determining the load carrying capacity of a hollow-core member. In fact, the moment capacity of a member is a function of the maximum strength of the prestressing strands. It is therefore important to consider strand development, which analyses the strengths and stresses along the prestressing strands within a hollow-core member (PCI Manual for the Design of Hollow Core Slabs and Walls, 2015).

Per Section 12.9 of *ACI 318-11*, the development lengths of the prestressed strands are calculated using the following formula:

$$\boldsymbol{l_d = \left(\frac{f_{se}}{3000}\right) d_b + \left(\frac{f_{ps}-f_{se}}{1000}\right) d_b = (f_{ps} - 2/3 f_{se}) d_b} \qquad \textbf{(12)}$$

where,

l_d = development length, in.

f_{se} = effective stress in prestressing steel, psi

f_{ps} = stress in prestressing steel at nominal flexural strength, psi

d_b = nominal diameter of bar, wire, or prestressing strand, in.

Equation 12 covers two bond mechanisms in the calculation. The first, l_t or strand transfer length, is the bond length needed to transfer f_{se} (the effective stress after all prestress losses) to the concrete. This term is represented in the first part of the equation as:

$$\boldsymbol{l_t = \left(\frac{f_{se}}{3000}\right) d_b} \qquad \textbf{(13)}$$

The second bond mechanism that must be considered is the flexural bond length (l_f), which corresponds to the bond length once the steel stress exceeds the effective stress f_{se}. The flexural bond length considers the full stress in the strand that corresponds to f_{ps} (stress in prestressed reinforcement at the nominal strength of the component), from which the additional bond length is calculated using:

$$\boldsymbol{l_f = \left(\frac{f_{ps} - f_{se}}{1000}\right) d_b} \qquad \textbf{(14)}$$

This analysis is depicted in Figure 3:

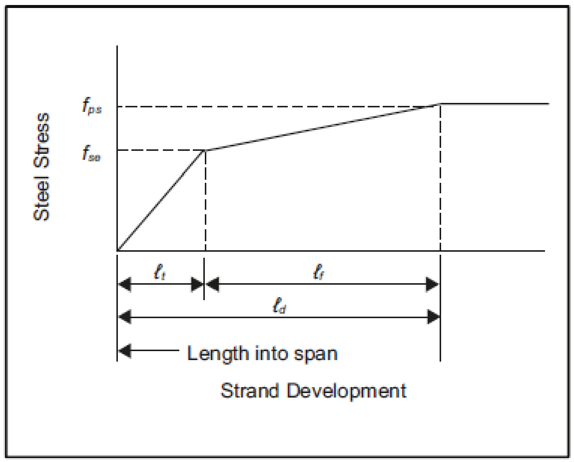

Figure 3 - Steel Stress vs. Strand Development (PCI Manual for the Design of Hollow Core Slabs and Walls, 2015)

Although *ACI 318-11* references the development length analysis only at maximum moment sections where the element needs to have full strength under the considered loads, there are cases in which a steep rate of moment increases within l_t which can produce critical sections at locations other than at the maximum moments. This might result in flexural cracking within l_t, if the required strand strength is higher than f_{se} in a section where the strand cannot accept additional stress without causing bond failure. Thus, within l_t, the maximum flexural strength that can be sustained is directly related to the cracking moment.

This is not the case for l_f, where the strand stress can exceed f_{se}, but never to full f_{ps}. This means that there exists additional flexural capacity beyond the cracking moment but the stress level cannot reach full nominal strength. When flexural cracking occurs in the l_f interval, the maximum value of f_{ps} is calculated as follows:

$$\boldsymbol{f_{px} = f_{se} + \frac{(x - l_t)}{l_f}\left(f_{ps} - f_{se}\right) = \frac{x}{d_b} + \frac{2}{3} f_{se}} \qquad \textbf{(15)}$$

Where x is the distance from the end of the element to the section of interest.

Nominal capacity should be calculated based on the above maximum strand stress.

2.4.3.5. Diaphragm Action

Lateral loads act on hollow-core slabs as lateral earth pressures. The function of the diaphragm is to receive loads from places where they originate and transmit them to resisting elements. Lateral earth pressures are determined by the type of the soil, which also determines the lateral movement needed to obtain a minimum active earth pressure or a maximum passive earth pressure (Withiam, 2003).

The horizonal earth pressures are used to calculate shear and moment forces acting on the sidewalls, as well as the axial forces acting on the top and bottom slabs (State of Illinois Bureau of Bridges and Structures Office of Program Development, 2017). Per the *AASHTO LRFD Bridge Design Specifications* (2017), the horizonal soil pressure on any point below the fill surface is determined using the following equation:

$$\boldsymbol{p = k_h y_s z} \qquad \textbf{(16)}$$

where:

p = lateral earth pressure;

k_h = lateral earth pressure coefficient;

y_s = unit weight of backfill soil;

z = distance from the surface to the reference point.

The coefficient k_h depends on two factors: the stress history of the soil and the displacement of the culvert. The stress history refers to the level of consolidation of the soil (either normally consolidated (NC) or over consolidated (OC)); whereas the displacement refers to level of flexibility or stiffness of the structure, as well as to the nature of soil load (passive or active) (Withiam, 2003).

Horizontal earth pressures on the sidewalls should be calculated considering an initial or at rest value ($\boldsymbol{k_o}$) of 0.5 and an estimated unit weight of $\boldsymbol{y_s}$ depending on the type of backfill soil placed against the wall. Per Article 3.11. of the *AASHTO LRFD Bridge Design Specifications* (2017), the minimum horizontal earth pressures should be equal to 50% of the maximum pressure (State of Illinois Bureau of Bridges and Structures Office of Program Development, 2017).

2.5. Soil-Structure Interaction

2.5.1. Fundamental Concepts and Background

Soil-structure interaction (SSI), according to Katona and others (1976), can be understood as the way in which a buried culvert deforms when earth-load distributions are applied. This means that there is a continuous interaction between the response of the soil to the motion of the structure, and the influence of that motion on the structural response. Models that analyze specific SSIs help in calculating the loads that act on buried structures, and also aid in determining the level of distress and deformation in the structure (Katona, 2018).

In order to use an adequate methodology for calculation and design of buried culverts, a number of researchers have developed a variety of approaches, solutions and methods. The first SSI models were developed by Marston and Spangler in the 1920s, followed by Burns and Richard, and, subsequently, by the more recent Finite Element Method (FEM) approach (Katona 2018). Computer programs such as Culvert Analysis Design (CANDE), introduced in the 1970s, have enabled a more detailed analysis of any type and geometry of culvert and, as a result, have often been used in buried culvert design (McGrath, 2018; Katona, 2018).

When analyzing culvert behavior and performance, it is important to consider adequate soil support of the structure. Because it is difficult to know beforehand the earth pressure and shear traction acting on a buried culvert, an SSI analysis can be used to determine the load distribution on a given structure. With the implementation of SSI analysis, it is possible to determine whether the loads acting on the structure will result in negative or positive arching. In the first case, which occurs in rigid structures, the culvert stiffness is greater than the soil stiffness and, consequently, the pipe attracts the soil load. Conversely, in the second case, the culvert stiffness is less than the soil stiffness, as is the case of flexible pipes (Katona, 2018)

Appropriate installation of buried culverts has always been difficult due to factors including a lack of contractor knowledge and time and cost-related issues of a project including the additional expense for installation inspection (McGrath, 2018). It is therefore important to have efficient and realistic methods for calculating and designing these structures, inviting contractors to understand and make use of them, thus ensuring proper culvert performance.

2.5.2. Analytical Methodologies

2.5.2.1. Marston-Spangler Approach

The Marston-Spangler approach is a traditional conceptual method created in the 1920s, which is an empirical approach based on one-dimensional sliding soil columns (see Figure 4).

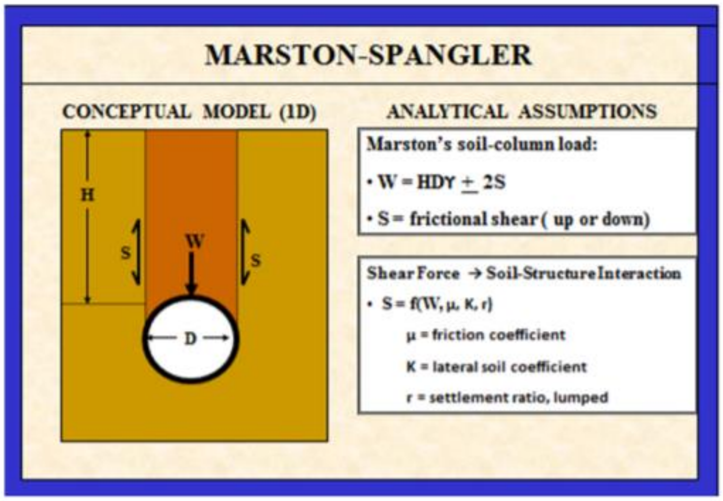

Figure 4 - Marston-Spangler Model (Katona, 2018)

The method is a combination of "Marston's estimation of effective vertical load acting on the structure and Spangler's assumption for the load distribution around the culvert" (Katona, Smith, Odello, & Allgood, 1976).

In this method, the net vertical load, W, acting at the crown of the conduit is the weight of the soil column with the addition or subtraction of the shear traction, S, that acts on both sides of the column. The magnitude and direction of the shear traction are determined by a settlement ratio parameter, which in turn depends on the relative stiffness of the culvert compared to that of the soil. In flexible structures, S will act upwards, whereas in rigid pipes the traction acts in a downward direction. The final calculated soil weight, W, is equivalent to the net vertical load acting on the conduct crown.

Once the load W is calculated, the Marston-Spangler approach becomes dependent on the rigidness or flexibility of the culvert. Depending on the type of culvert, the analysis is extended to include other conditions needed to finalize the specifics of the culvert design. For rigid buried structures, the Marston-Spangler 'equivalent' D-load (load capacity of the structure) is calculated, from which the wall section is then designed to satisfy the corresponding load at the top of the conduit. For flexible conduits, the load distribution around the structure and the corresponding deflection or flattening are estimated. The culvert is designed to counteract the bending stresses by having sufficient stiffness in the same plane to limit the total deflection to 5% or less than the diameter of the pipe (Katona, 2018).

2.5.2.2. Burns and Richard Solution

The Burns and Richard approach is a closed-form analytical elastic solution (Katona et al 1976). As an analytical method, it is based on classic elasticity and shell theory and thus generates more exact solutions (when compared with numerical methods that use approximation techniques). Moreover, the Burns and Richard's method is a "closed-form solution for a thin shell encased in an infinite elastic medium with overburden loading" (Katona, Smith, Odello, & Allgood, 1976).

For this model, basic assumptions in four main elements are key. First, the soil is analyzed using "continuum theory with an infinite soil expanse in plane strain and characterized by two elastic parameters" (Young's modulus and Poisson ratio) (Katona, 2018). Second, the structure is analyzed through a cylindrical shell theory, including plain strain formulation with hoop stiffness (EA) and bending stiffness (EI). Third, the structure-soil interface is assumed to be frictionless and perfectly bonded solution alternatives are obtained. Finally, the soil gravity loading is estimated by "applying the free field soil pressure (γH) as a uniform surface pressure" (Katona, 2018). Regardless of some simplifying assumptions, it is considered a quite accurate prediction of soil-structure interaction (Katona, Smith, Odello, & Allgood, 1976).

2.5.2.3. Finite Element Method (FEM)

The Finite Element Method (FEM) is a numerical method, which has become the preferred method in present culvert analysis. Because the analysis includes a wide array of variables such as the type of embankment, incremental soil loading, variable bedding configurations and complex structure shapes, it is the main method for design of both rigid and flexible culverts. In addition, this method is appropriate when considering incremental construction and non-linear behavior. However, the time required for mesh preparation and code debugging along with the need for trained analysts are downsides for use of the FEM technique in culvert design (Katona, Smith, Odello, & Allgood, 1976; Katona, 2018).

FEM includes two- and three- dimensional analysis. Two-dimensional analysis that can be either linear or non-linear include small or large deformation theory. When additional forces, other than stresses and deformations on transverse sections are considered, a linear three-dimensional approach can be implemented (Allgood & Takahashi, 1978).

2.6. Concrete Culvert Studies

The following sections provide overviews on experimental and numerical culvert studies.

2.6.1. Numerically Modeling of the Structural Behavior of Precast Three-Sided Arch Bridges for Analysis and Design (Jensen, 2012)

This work involved laboratory testing and design validation of a three-sided, bottomless precast concrete structure manufactured by Foley Products Company. Both field and laboratory tests were carried out on the structure.

- Field testing: the field tests were conducted in Midland, NC on an active project in which a 42-foot clear span arch structure was constructed. The service load level tests were done by backfilling around the structure and driving a known-weight truck over the culvert while stopping at different points.
- Laboratory testing: the laboratory tests were performed on a 20-foot and 36-foot clear span structures. The lab tests were performed at the Auburn University Structural Research Laboratory, with pre-installed gauges for data collection. Both structures were loaded to failure using hydraulic load actuators. Upon testing completion, the computer program SAP2000 was used to develop two structural models which were then correlated with the structural analyses and the results obtained in the laboratory. Nonlinear behavior was accounted for in the analytical phase, and moment hinges were incorporated in the structural model to match the deflection magnitudes calculated in the analysis with the deflection measurements made in the laboratory tests.

After developing and correlating the SAP2000 structural models, the design methodology for the Foley Arch was evaluated. The designers used a RISA 3-D program to develop a structural computer model to predict the point of maximum moment. The RISA 3-D and the SAP2000 models were compared to assess the extent of correspondence between the two programs. The results indicated that the structure strength was adequate and that the design methodology was reasonable and safe (Jensen, 2012).

2.6.2. Finite-Element Modeling of Reinforced Concrete Arch Under Live Load (McGrath and Mastroianni, 2002)

This study used two, 28-foot span, reinforced concrete arch culverts to conduct full-scale field tests. The tests included subjecting the structures to service live loads, meeting AASHTO design criteria for strength and serviceability with depths of cover ranging from 1 to 3 feet. At a 1-foot fill level, the culverts were loaded with a simulated single-axle live load greater than 980kN (220,000 lb). Computer models were developed based on the cover depth. The field data included arch deflection, interface pressure, concrete strain and strain in the reinforcing steel. Two and three-dimensional finite element analyses were conducted in which non-linear material models for the backfill soil and the reinforced concrete were included.

Results from the finite element analysis were then compared to the field data. The comparison indicated that the two-dimensional models were limited in their ability to predict longitudinal spreading of the live load forces, as well as to predict maximum moments larger than those experienced by the actual structure. The three-dimensional deflection predictions were dependent on the properties used to characterize the concrete material model; however, the design parameters (moment, thrust, and shear) did not show the same level of sensitivity. Results suggest that, for a typical structural design, material parameters may be approximated without seriously degrading the accuracy of predicted design parameters (McGrath & Mastroianni, 2002).

2.6.3. Predicting the Ultimate Load Carrying Capacity of Long-Span Precast Concrete Arch Culverts (Zoghi and Hastings, 2000)

This study was conducted on the second phase of a full-scale, live load test research project conducted on a 36-foot precast reinforced concrete arch culvert. The project had two main objectives: investigate the failure mode of the test culvert using a modified CANDE finite-element computer program; and analyze the soil-structure interaction characteristics of long-span precast concrete culverts. The results of the first phase were used as a baseline.

In the finite-element model, beam-column elements were used to simulate the actual structure, whereas rectangular or triangular elements were used to model the backfill and cover soil, as well as foundation footings and bedding. The first simulation considered the foundation with no backfill and, subsequently, soil lifts were added until backfill was completed around and over the culvert. Vehicular traffic loads were replicated by applying loads on the surface of the top layer of soil.

This study revealed that the ultimate load capacity of the arch culvert was approximately 340 kips. It was also determined that high quality soil compaction was paramount in the overall structural integrity and soil-structure interaction (Zoghi & Hastings, 2000).

2.6.4. Structural Behavior of Three-Sided Arch Span Bridge (McGrath, Selig and Beach, 1996)

This study aimed to evaluate the methodology used in the structural design of three-sided culverts with arched top slabs. In order to perform the assessment, a three-sided arch structure was constructed and tests were conducted during initial installation and after 6 months, 1 year, 18 months and 2 years of construction. The test structure consisted of a 3.4-meter (11-foot) high and

11-meter (36-foot) span bridge, composed of ten 1.6-meter (5.2-foot) wide precast concrete segments. Field tests were conducted by imposing an HS-25 +30% live load on soil covers ranging between 0.3 and 0.9 meters (1 and 3 feet). In three of the ten segments, soil stress cells and anchor pins were mounted on the legs of the bridge. A tape extensometer was used to measure changes in the shape of the structure. Survey data was collected on the instrumented segments during each test. In addition, visual observations were made for crack development.

Results from this study indicated that the bridge underwent smaller movement when subjected to the HS-25 +30% live load than when subjected to the 0.9-meter soil cover earth pressure. Data collected throughout the 2-year time period showed that soil stress and span width had increased, but the overall structural performance was within acceptable limits. In addition, correlation between the experimental and analytical results indicated that, even though the actual live load effects were much smaller than anticipated in the design phase, the use of finite-element analysis to design these types of structures was beneficial (McGrath, Selig, & Beach, 1996).

2.6.5. Load Test Report and Evaluation of a Precast Concrete Arch Culvert (Beach, 1988)

Extensive field tests and theoretical analyses were performed on a three-sided box-arch shaped precast concrete culvert as part of this study. A field load test was conducted to compare the actual performance and predicted structural behavior of the culvert. In addition, the finite element computer program CANDE, was used to perform an in-depth analysis of the effects of existing field conditions on the performance of the structure.

Results of the study showed a good correlation between the predicted behavior using finite element analysis and actual performance of the culvert. The capacity of the culvert in extreme overload conditions exceeded expectations (Beach, 1988).

2.6.6. Observed Behavior of a Concrete Arch Culvert (Oswald and Furlong, 1993)

During a 5-year period, measurements of soil pressures and strains were made in arch of a concrete culvert. The outcomes of study were synthesized in this publication which supported six different conclusions. First, the methods used to design the arch segments were successful in supporting the soil and environmental forces. Second, the use of steel reinforcement in the floor slab, as a tension member, was beneficial under a deep fill (±20 feet.). Third, design of similar structures can be based on AASHTO recommended practices for strength design of concrete if the soil unit weight is 130 pcf instead of 120 pcf. Fourth, analytic procedures must include consideration of creep deformation, to obtain the corresponding displacement responses. Fifth, the soil-structure interaction-related redundancies produce favorable redistributions of resistance to soil loads on the arch. Lastly, there was a good correlation between stress and displacement values obtained using an analytical model of the structural system and the in-situ measurements (considering that the analytical model should include very specific data regarding soil properties and concrete creep response time effects) (Oswald & Furlong, 1993).

2.6.7. Live Load Distribution on Concrete Box Culverts (Abdel-Karim, Tadros and Benak, 1990)

In this study, separate considerations were made on the distributions of wheel loads applied through pavement, embankment soil and culvert top slabs. To perform this evaluation, full-scale tests were performed on a functioning cast-in-place concrete box culvert. Load dispersions found in field tests were compared with AASHTO provisions and theoretically predicted values using a Boussinesq elastic solution. Results from this study showed similar load distributions in both the transverse and longitudinal directions between the field tests and predicted values. The authors also concluded that the AASHTO 1.75 distribution factor is appropriate when considering fill heights less than 2 feet and greater than 8 feet. In addition, rigid pavements and culvert top slab distributions are discussed with emphasis on empirical solutions for appropriate incorporation in structural design (Abdel-Karim, Tadros, & Benak, 1990).

2.6.8. Structural Response of Full-Scale Concrete Box Culvert (Abdel-Karim, Tadros and Benak, 1993)

An extensive field investigation was conducted on the behavior of a double-cell cast-in-place concrete box culvert. The investigation included measurements of soil pressure as well as arch deflection. Moment was calculated by analyzing strains in the outer and inner strands of the concrete walls using vibrating-wire gages that were installed in the laboratory before placing them in the structure. Continuous measurements were made during the construction and backfilling phases. The live load measurements were taken at 2-feet fill increments, beginning with the exposed top slab. Results of the full-scale tests on the box culvert, together with a detailed discussion of the measurements on the structural response to soil and truck loading are given in the Abdel-Karim, Benak, & Tadros (1993) study.

Chapter 3: Cast-in-Place (CIP) Culvert Model

3.1. Introduction

The purpose of the CIP model was to assess how a monolithic concrete culvert would perform under an applied 9-kip load, reduced for a half-scale model. Results from this testing provided a basis of comparison with the hollow-core culvert and enabled a performance assessment of the two. The CIP model included two phases of analysis: experimental testing and finite element modeling. The latter was utilized to first, predict the behavior of the CIP model under the previously mentioned load, and later, refine the model based on the experimental data obtained.

The CIP model constructed characterized a half-scale prototype and followed the same geometry used for the assembled precast hollow-core panels to provide a comparable design. The following sections present information pertinent to the load determinations, CIP model design, methodologies, laboratory and experimental results, and finite element model (FEM) analyses.

3.2. Vehicular Loading

Guidelines presented in the *AASHTO LRFD Bridge Design Specifications* (American Association of State Highway and Transportation Officials, 2017) were followed to determine the truck load and load area that the half-size model needed to be subjected to, in order to replicate the loading conditions that culvert structures are designed to sustain. Based on Section 3.6.1.3.3. of the aforementioned manual, HL-93 design vehicular live loading for the top culvert slabs should only consider axle loads of the design truck or design tandem with an associated dynamic load allowance. After review of the characteristics of both the design truck and design tandem, axle loading of the design truck were concluded to better represent the conditions that this study was aiming to evaluate. Figure 5 below presents the characteristics of the design truck.

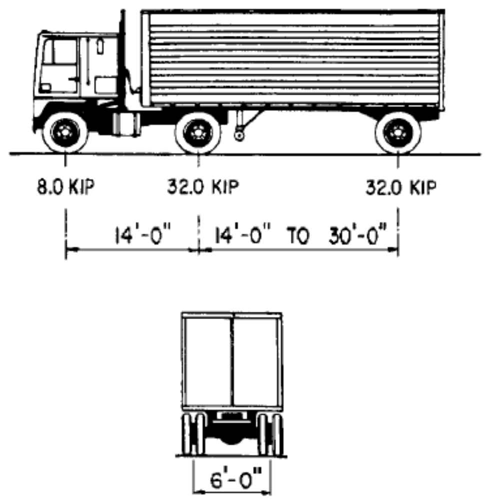

Figure 5 - Design truck characteristics (American Association of State Highway and Transportation Officials, 2017)

Based on the design truck presented above and assuming a maximum culvert span of 20 feet, established on the definition presented by the Federal Highway Administration in Publication No. FHWA-HIF-07-033 *Design for Fish Passage at Roadway-Stream Crossings: Synthesis Report* in which it is specified that "a culvert differs from a bridge in that it usually consists of structural material around its entire perimeter and has a total span (width) of less than 6.1 m (20 ft)" (Federal Highway Administration, 2007); then the most critical loading scenario consisted of a 32-kip axle load placed at the center of the span. Notice that, with a maximum culvert span of 20 feet, no two axles would lie on the culvert at the same time.

Since the tire spacing of the AASHTO design truck is 6 feet and a two-dimensional model was evaluated as part of this project to simplify the analysis (ignores the two-way action of the culvert which ultimately makes for a more conservative approach), then each 16-kip wheel load is held by a tributary width of approximately 6 feet in a full-scale structure. Using a factor of λ = ½ to represent a half-scale model, the resulting suggested tributary width will result in approximately 3 feet. In addition, the imposed wheel load would be further reduced by ¼, based on the total model area, and would result in a value of 4 kips.

To calculate the total imposed load that the model needed to be tested under, a dynamic load allowance (IM), in percent, was determined:

$$\boldsymbol{IM = 33(1.0 - 0.125D_E) \geq 0\%} \tag{17}$$

where,

D_E = minimum depth of earth cover above the structure, ft

In addition, a dynamic load allowance factor that was applied to the static load condition was also calculated:

$$\boldsymbol{Dynamic\ Load\ Allowance\ Factor = 1 + \frac{IM}{100}} \tag{18}$$

Based on the above equations and using a one-foot soil cover, an IM of 28.88% and a dynamic load allowance factor of 1.29 were obtained.

To determine the static load, a Strength I Limit State load combination was used since the structures modeled were underground structures, and Strength I is the basic load combination for normal vehicular use of a bridge structure without wind (American Association of State Highway and Transportation Officials, 2017). Based on Table 3.4.1-1 of the *AASHTO LRFD Bridge Design Specifications*, the static Strength I Limit State load factor for truck live load (LL) is 1.75. See Appendix A – AASHTO Design Truck Loading for vehicular loading references. With this, the total imposed load needed for the model was calculated by the following equation:

$$\boldsymbol{Total\ Imposed\ Load = 1.75LL\ (dynamic\ load\ allowance\ factor)} \tag{19}$$

And resulted in:

$$Total\ Imposed\ Load = 1.75(4\ kips)(1.29)$$

$$Total\ Imposed\ Load = 9.03\ kips$$

The AASHTO manual also specifies a tire contact area or loading patch dimension of 20 inches wide and 10 inches long for a full-scale structure. Reducing this loading patch to half, for the laboratory model, resulted in an assumed loaded area of 10 inches wide by 5 inches long. Based on a one-foot soil cover over the half-scale culvert structure and a 60º stress distribution of the soil mass, the resulting loaded area on top of the culvert was calculated to be approximately 22 inches wide by 17 inches long (1.83 feet by 1.42 feet).

3.3. CIP Culvert Model Design

The CIP model dimensions were determined primarily based on the tributary width and stress distribution calculations presented above, and the geometry that hollow-core panels are typically fabricated to at precast yards. Based on the stress distribution and tributary area calculations, the dimensions of the top culvert segment had to be greater than 17 inches long and between 22 and 36 inches wide. In an effort to avoid having a structure in which stress concentrations would emerge at the interfaces between the top segment and adjacent east and west sections, and to provide enough space for the distribution of stresses to develop within the soil mass, a final culvert configuration consisting of segments with approximate dimensions of 27 inches long by 31 inches wide by 6 inches deep was created in model scale.

To obtain an arch-type geometry, the hollow-core panels were connected at a 30º angle between the top segment and the adjacent sections, and at a 60º angle between the adjacent sections and the bottom segments. In addition, two footings, with dimensions of 18.6-inch × 14.2-inch × 31-inch, each, were placed at each end.

To replicate the conditions around a culvert, a soil box was also erected. The box walls were made of a combination of prime whitewood and oriented strand boards (OSB); and were located approximately 33 inches away from the outside-edges of the culvert footings (x-direction) and at the front and back faces of the culvert structure (z-direction). The space in between the culvert and the walls was filled with medium sand from the bottom footing elevation to a height of 50 inches, or the top of the concrete structure, and with coarse sand from a height of 50 inches to a height of 62 inches on either side of the top concrete segment. From the top segment to a height of 62 inches, the volume was filled with either pea gravel for the first test, ¾-inch road base for the second test, or a concrete trapezoid prism backfilled with coarse sand for the third test. Figure 6 below presents the side view of the CIP culvert with dimensions and material types. Note that the location of the concrete trapezoid prism is provided by means of red lines above the top segment, for reference, and was only used to conduct the third CIP test.

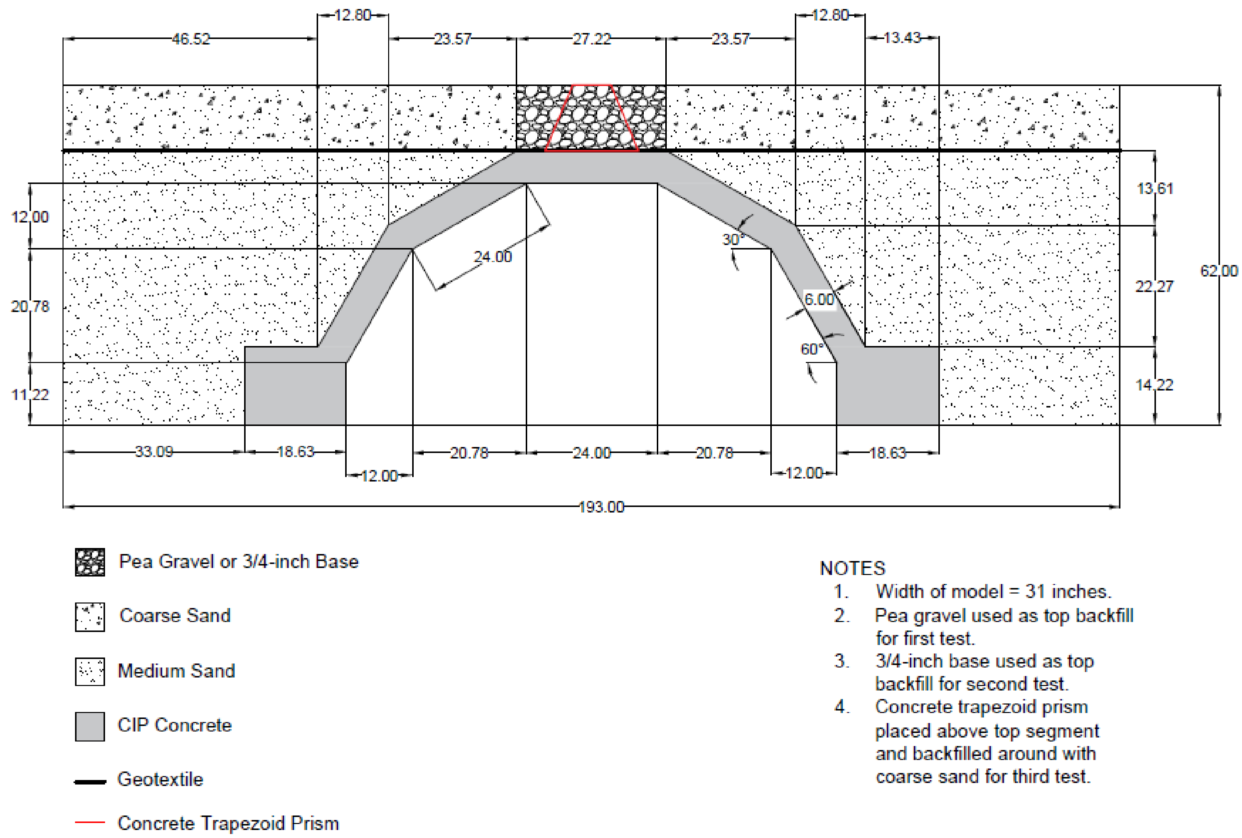

Figure 6 - CIP Culvert Model Geometry

3.4. Methodology

Procedures followed for the construction and assembly of the CIP model, as well as for laboratory and in-situ testing of the structural and soil materials, and for the experimental testing are presented in the following sections.

3.4.1. CIP Model Assembly

The first step in the construction of the CIP model included the design and construction of the base frame and the formwork for the cast-in-place culvert erection. Panel and truss design for this task was done by graduate student Garrett Thompson who was the lead in the construction of this unit. The base frame for the model consisted of three, 7/8-inch APA rated sturd-I-floors, which were designed to sustain a maximum pressure of 613.4 lb/ft^2. The sturd-I-floors were placed over a bed of steel tubes which were welded together to provide stability for the model during transportation.

In addition, formwork for the CIP culvert included four planar trusses each comprised of a floor beam, a polygon arch top chord, two intermediate beams and four intermediate posts located under the structure. Intermediate beams and posts were placed at approximately 10 ¼- inches on center. To connect all trusses, four crossbeams were used. All truss elements consisted of 2-inch by 4-inch Douglas Fir Larch No.2 lumber. In addition, to form the footings and provide segment covers, panels consisting of a combination of OSB and 2-inch by 4-inch lumber were placed on top of the trusses. Figure 7 below presents the assembled CIP formwork. Refer to Appendix B – Formwork Design Calculations and Drawings for formwork design calculations and additional CIP drawings.

Figure 7 - Assembled CIP Formwork

The second step in the process included placement of concrete within the forms. Concrete having a target 28-day compressive strength of 4,000 psi was used for the CIP portion of this project.

Refer to Section 3.4.2 for additional mix design information and concrete placement procedures. A total of 3.5 cubic yards of concrete were used to create the CIP structure. Figure 8 shows concrete placement activities of the footings.

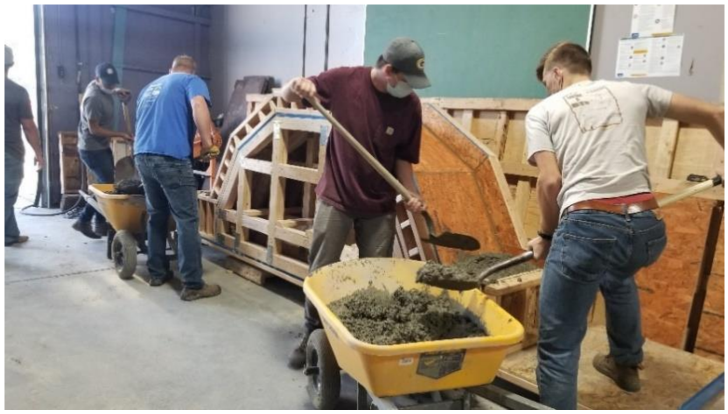

Figure 8 - Footing Placement

Following concrete placement, the culvert was left covered for 28 days to complete the curing cycle. During this time, retaining walls for the soil box were designed and constructed by graduate student Daniel Garz. A total of four retaining walls were constructed. Two walls were assembled for the front and back sides of the model, and two for the side areas. In an effort to allow access to the interior portion of the culvert and facilitate subsequent backfilling activities, the front wall was assembled in two separate segments with the bottom part having an opening in the middle. All retaining walls had longitudinal and crossbeam elements made of a combination of 2-inch by 4-inch lumber, 2-inch by 8-inch lumber, and OSB panels. Appendix C – Retaining Wall Design Calculations provides the wall design calculations along with the respective wall drawings.

The next step in the process entailed setting up the loading equipment for model testing. Due to the height of the CIP model and the dimensions of the actuator loading machine, the loading frame had to be elevated approximately 12 inches off the ground by means of I-beams. In addition, the actuator beam had to be raised to the highest possible position within the reaction frame. Refer to Section 3.4.6.1 of this report for additional test set up information.

Once the testing area was set up, the culvert was moved into place. Moving of the culvert was done by means of a forklift and a pallet jack which were located on either end of the structure. At the time of relocation, it was observed that the base steel frame was detached from the lower wood formwork. To provide a safe and successful travel way and avoid flexure of the structure, a secondary wood frame was built around the model. Figure 9 presents the added frame as well as the equipment used for transportation of the culvert to the testing area (left) and the final CIP culvert location (right).

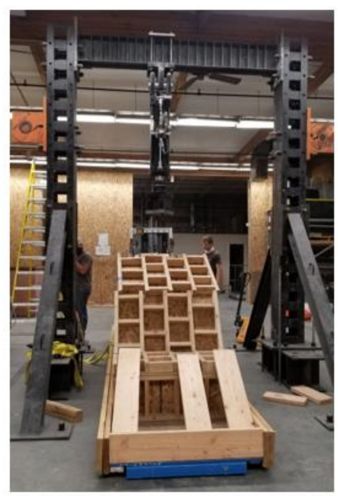

Figure 9 - Relocation Activities and Final Positioning of CIP Culvert

After relocation of the culvert into the structural lab was accomplished, the added frame and the top formwork were stripped off the CIP model. Removal of the formwork revealed a void in the top left concrete panel at the interface between the vertical and horizontal forms (see left image of Figure 10). Due to the size of the void, repair by means of a concrete patcher was accomplished and the section was allowed to cure for 24 hours prior to removal of the lower formwork.

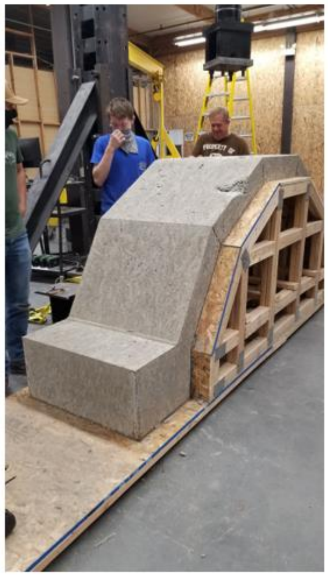 

Figure 10 - Void on the top left panel of the front face (left) and repaired spot (right)

Once the concrete patch was cured, the lower forms were removed, the CIP culvert was painted for crack monitoring purposes, and assembly of the retaining walls was performed. In order to prevent the migration of soil particles from the top of the structure (backfill areas) to the spaces between the culvert and the retaining walls, DAPtex plus foam was sprayed along the front and back faces of the concrete. Immediately after spraying, the walls were assembled and secured by means of ratchet straps. Figure 11 presents the assembled walls.

Figure 11 - CIP Initial Wall Assembly

After wall placement, gaps were observed between the bottom OSB and the walls. To prevent soil migration into the floor through the gaps and provide a seal between adjacent OSB panels, Great Stuff Gaps and Cracks insulating foam was sprayed along the edges. In addition, and in order to provide a secondary means of containment of the backfill soil at the interface between the walls and the concrete, 1-inch wide by 0.5-inches thick wood members were positioned and secured along the edges.

Backfilling began once all gaps were sealed. The medium sand was the first material placed followed by the coarse sand and the pea gravel. Moisture conditioning, placing and compaction activities of all soil units complied with the methodologies presented in Section 3.4.4.6 of this report. The medium sand was placed to a height of 50 inches above the bottom culvert elevation; and the coarse sand and pea gravel from a height of 50 inches to a height of 62 inches. Density determinations of the medium sand and pea gravel were achieved by calculating volumes and soil masses at the top locations as well as by performing sand cone tests. Refer to Sections 3.4.5.2.2 and 3.4.5.2.3 of this report for additional density information.

The final step in the CIP model assembly entailed instrumenting the model. In general, the key areas of interest for data acquisition included the bottom face of the top segment, the loading plate, the loading cell, and the reaction beam. Equipment used to obtain displacement, strain, and load information during experimental testing at these and select additional locations included a combination of string pots, linear potentiometers, and load cells. Refer to Section 3.4.6.1.2 for supplementary instrumentation information. All instrumentation mounted on the CIP model was linked to the LoggerNet 4.5 DAQ, developed by Campbell Scientific, Inc., which was used to record and display real-time data during testing.

Once all model components were designed, constructed, erected, and assembled; the structure was ready for testing. At first, only one test was anticipated to be conducted on the CIP model. However, due to the load transferring difficulties experienced during the initial test between the pea gravel and the concrete structure in which the pea gravel underwent punching and bearing failures, additional tests had to be conducted. Differences between subsequent rounds of tests were related to the materials placed on top of the upper concrete segment which were ultimately, the mechanisms by which load was being transferred to the concrete structure. In general, the second round of testing replaced the pea gravel with ¾-inch road base, to diminish the void spaces between soil particles and attempt to provide a stiffer material; and the third and final round of testing replaced the ¾-inch road base with a concrete trapezoid prism to, once again, increase the stiffness of the load transferring material. Refer to Sections 3.4.6 and 3.5.4 for additional testing information.

3.4.2. Mix Design and Concrete Placement

3.4.2.1. Cast-in-Place Concrete

The mix design used for construction of the CIP model was a common concrete mix designs used in the industry for construction of underground concrete culverts. Pocatello Ready Mix, Inc., a local ready-mix concrete provider, was consulted regarding the ideal mix design for fabrication of the CIP model. Based on their experience with similar structures, a mix design with a target 28-day concrete compressive strength of 4,000 psi was suggested. Appendix D – Concrete and Grout Mix Designs presents the mix design utilized for the CIP model construction and Table 2 presents the CIP mix quantities used, along with material specifications. The concrete mix design and concrete (Class 40A) utilized for this project was produced and provided by Pocatello Ready Mix, Inc.

Table 2 - Mix Material Quantities and Specifications

Material	Weight (lb)	Volume (ft^3)	Specification
Cement	479	2.44	Type I, II
Fly Ash	85	0.58	Type F
Sand	1,425	8.72	Specific Gravity 2.62
Coarse Aggregate	1,755	10.65	Specific Gravity 2.64
Water	254	4.07	
Air	2.0	0.54	
Water Reducing Admixtures	3 fl. oz/cwt	16.9 fl. oz/Y3	

Erection of the culvert structure necessitated approximately 3.5 cubic yards of concrete to be completed. The sequence of concrete placement included:

1. Filling the two side footings with concrete;
2. Vibrating the concrete in the footings using an electric concrete vibrator;
3. Finishing the surface by means of a trowel;
4. Placing the footing covers;
5. Placing the bottom segment covers on either side of the structure;
6. Filling the two bottom segments with concrete;
7. Vibrating the concrete in the two bottom segments;
8. Repeating steps 4 to 6 for the remaining side segments;
9. Filling the top segment with concrete;
10. Vibrating the concrete inside the top segment;
11. Finishing the surface by means of a trowel; and
12. Placing the top member cover

Figure 12 presents concrete placement activities of the arch segments.

Figure 12 - Vibration of bottom right segment (left) and finishing of top segment (right)

3.4.2.2. Concrete for Trapezoid Prism

Due to the top soil bearing failures and the resulting decrease in load transferring capabilities, an alternative that utilized a stiffer material to transfer load onto the underlying structure was used. This alternative consisted of erecting a concrete trapezoid with dimensions that resembled a 60° stress distribution, based on a 5-inch by 10-inch loaded plate.

To create the concrete prism, Rapid Set Concrete Mix was utilized. This product was selected based on its fast setting and early strength capabilities. Refer to Appendix D – Concrete and Grout Mix Designs for mix composition and product specifications. Approximately 240 pounds of mix material, yielding about 2 ft^3, were utilized. The following presents the concrete mixing and placing procedures carried out to erect the trapezoid prism.

1. Positioned the cement mixer in place;
2. Placed the first 60 lb concrete mix into the cement mixer;
3. Added approximately 4 quarts of water to the mix;
4. Blended the material until a flowable and smooth texture was achieved;
5. Transferred the blend to 5-gallon buckets;
6. Placed the concrete into the trapezoid prism form;
7. Vibrated the concrete inside the form by means of a tamping rod;
8. Repeated steps 2 to 7 until the prism was filled;
9. Finished the surface by means of a trowel; and
10. Placed a wet burlap on the upper face and covered with plastic.

Once the prism was erected, the structure was allowed to cure for one and a half days, before removing the forms. Figure 13 presents the cured concrete trapezoid prism.

Figure 13 - Concrete trapezoid prism

3.4.3. Concrete Sample Casting

In order to test and obtain the compressive strength, modulus of elasticity and Poisson's ratio of the CIP concrete at different time periods, test specimens were casted at the time of concrete placement and were later cured under controlled laboratory conditions. Casting and curing of the test specimens were performed in accordance with *ASTM C192/C192M-19, Standard Practice for Making and Curing Concrete Test Specimens in the Laboratory* (ASTM International, 2019) requirements. The following presents a summary of the steps completed for concrete cylinder casting and subsequent test specimen curing:

1. Placed the mold on a rigid surface free from vibration and other disturbances;
2. Placed the first layer of concrete in the mold using a scoop (filled to approximately 1/3 of the height);
3. Stroke the concrete 25 times using a 3/8-inch diameter tamping rod;
4. Tapped the outside of the mold lightly 10 to 15 times with a mallet or open hand;

5. Repeated steps 2 to 4 for the remaining two layers;
6. Stroke off the surface of the concrete with the tamping rod to obtain a level finish;
7. Covered the top of the mold with a lid;
8. Left casted cylinder in an undisturbed area for the next 24 hours;
9. After 24 hours removed cylinder from the mold, marked and placed the sample in a water bath cure.

For this project, CIP test specimens consisted of either 4-inch diameter, 8-inch tall concrete cylinders casted using Gilson steel molds; or 6-inch diameter, 12-inch tall concrete cylinders casted using Gilson plastic molds. A total of nine 4- by 8-inch cylinders and three 6- by 12-inch cylinders were made during the CIP concrete placement. Figure 14 displays test specimen casting activities and Figure 15 presents the water tank used for curing of samples.

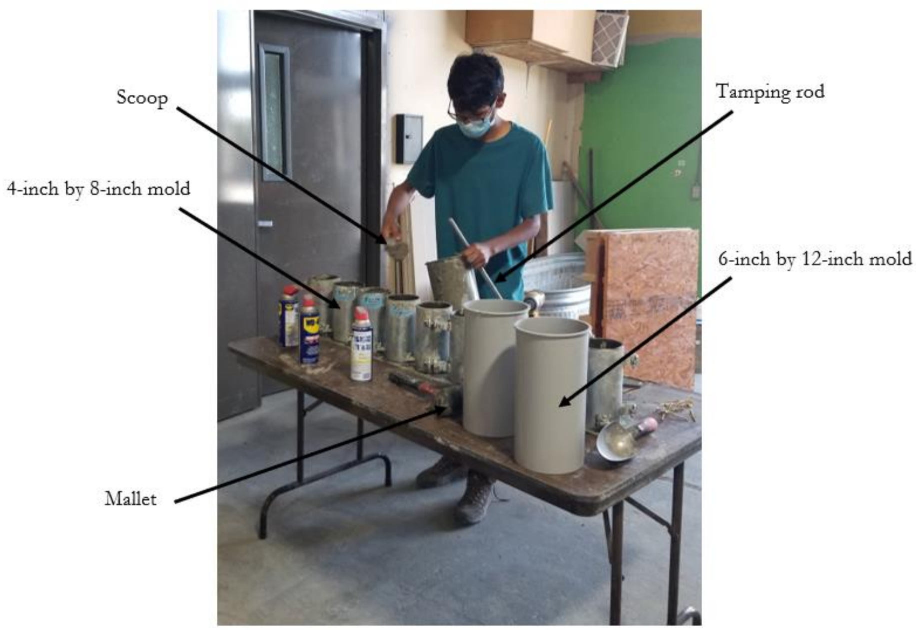

Figure 14 - Cylinder Casting

Figure 15 - Water Tank for Moist Curing of Samples

Concrete cylinders were also casted during placement of the concrete trapezoid prism, to obtain the compressive strength of the material before model testing. Casting and curing of these cylinders followed the same procedures as those presented above for the CIP concrete. Two 4-inch by 8-inch cylinders were produced during prism placement.

3.4.4. Soil Backfill and Geotextile

In an effort to replicate the conditions of an underground culvert structure, the CIP model was backfilled with medium sand to a height of 50 inches, with coarse sand from the top of culvert to a height of 62 inches on either side of the top segment, and with pea gravel/ ¾-inch road base/concrete trapezoid prism with coarse sand from the top segment to 62 inches directly above. To prevent migration of fines between the medium sand, coarse sand, and pea gravel/¾-inch road base layers, a separation geotextile was placed at the interface between the soil units. Refer to Figure 6 in Section 3.3 for soil and geotextile location information.

3.4.4.1. Medium Sand

Medium sand was selected as the main backfill material for this project due to its workability characteristics and its resemblance to backfill material used in the industry around underground structures. The workability characteristics of medium sand refer to the ease of moisture conditioning and compacting of the soil to (or close to) optimum requirements to obtain ideal density conditions.

In order to obtain a relatively clean medium sand and avoid moisture conditioning challenges that can arise when using finer material, a fines content of less than 15% was selected as the threshold for this project. Material that met this specification was Pocatello Ready Mix's medium sand, which was used to backfill around both the CIP and precast hollow-core culverts. To ensure that the fines content of the medium sand used was kept below the 15% threshold, a sieve analysis test was performed on the material. Refer to Sections 3.4.5.1.3, 3.5.2.3 and Appendix E – Laboratory Test Results for gradation procedures, results, and additional soil analysis data.

Sand used for this project was stored in 4-ft by 4-ft by 4-ft cardboard boxes kept at the facility. Figure 16 displays the stored material.

Figure 16 - Stored Sand Material

3.4.4.2. Coarse Sand

Coarse sand was used to backfill the upper one foot of the CIP model, on either side of the top segment, in order to provide additional strength to the primary soil section. Coarse sand was also placed around the concrete trapezoid prism, for the third round of testing, to provide confinement. Coarse sand used for this project was supplied by Pocatello Ready Mix, Inc. and was also stored in 4-ft by 4-ft by 4-ft cardboard boxes. As with the medium sand, a sieve analysis was performed to obtain the particle size distribution. Refer to Section 3.5.2.3and Appendix E – Laboratory Test Results for gradation results and additional coarse sand soil analysis data.

3.4.4.3. Pea Gravel

Pea gravel was used to backfill the area on top of the upper CIP segment (24-inches by 12-inches by 31-inches), in order to provide additional strength to the primary soil section being compressed during the first round of testing. Pea gravel for this project was obtained from Home Depot and was supplied by Greensmix in 60-pound bags. As with the medium and coarse sands, a gradation test was performed to obtain the particle size distribution. Refer to Section 3.5.2.3and Appendix E – Laboratory Test Results for pea gravel gradation results and additional soil analysis data.

3.4.4.4. ¾ -inch Road Base

In an effort to provide a stiffer material that was capable of transferring the applied 9-kip load to the underlying structure for the second round of testing, ¾ -inch road base was placed on top of the upper CIP segment. The ¾-inch road based was obtained from the Idaho Rock and Sand yard located in Pocatello and was also tested to obtain the particle size distribution prior to experimental testing. Refer to Section 3.5.2.3and Appendix E – Laboratory Test Results for ¾-inch road base gradation results and additional soil analysis data.

3.4.4.5. Geotextile

In order to prevent the migration of fines between the medium sand, coarse sand and pea gravel/ ¾-inch road base backfill material, a separation geotextile was placed at the interface between the soil units or a height of 50 inches above the ground surface. The Matrix Grid Weed Control Fabric produced by Vigoro was the separation geotextile utilized for this project. The matrix grid consisted of two nonwoven layers with a matrix mesh in-between. Figure 17 displays the Vigoro geotextile used.

Figure 17 – Vigoro geofabric

3.4.4.6. Backfilling Process

Backfilling activities around and on top of the CIP culvert began once the culvert was positioned in the testing area, the soil box walls were assembled around the structure, and the soil material was moisture conditioned. Moisture conditioning consisted of increasing the soil's moisture content with the intent of achieving a required density once the material was compacted. In the construction industry, compacting the soil material to the highest possible state (or close to the highest state) aids in minimizing settlement of the soil when loads are applied to the soil mass. An indication of the highest density and the corresponding moisture content that a soil can achieve is obtained through compaction laboratory testing.

For this project, guidelines presented in *ASTM D698-12, Standard Test Methods for Laboratory Compaction Characteristics of Soil Using Standard Effort (12 400 ft-lbf/ft^3 (600 kN-m/m^3))* (ASTM International, 2012) were followed to obtain the relationship between molding water content and dry unit weight of the medium and coarse sands. Compaction testing only applies to soils that have 30% or less by mass of particles retained on the 3/8 -inch sieve. Since the pea gravel had more than 30% retained in the 3/8 -inch sieve, the material was too coarse to be tested. Refer to Section 3.4.5.1.4 of this report for additional compaction testing information.

The density of the compacted soil is one of the factors that determines how the soil mass will behave under an applied load and the amount of settlement it will undergo. As such, working the soil material close to the optimum moisture contents is beneficial. For this project, moisture conditioning activities entailed two main steps:

1. Determination of stored sand moisture content: In order to estimate the amount of water needed to be added to the stored medium sand, coarse sand, and ¾-inch road base and achieve close to optimum requirements, moisture content determinations were carried out prior to the start of backfilling operations. One moisture content test was performed per storage box (east and west sides). Refer to Sections 3.4.5.2.1 and 3.5.3.1. for moisture content test procedures and results.
2. Addition of water: Hoses were utilized to add water to the sand and ¾-inch road base material located inside the storage boxes. Since both the medium and coarse sands did not evince an important rise in unit weight with moisture, having an exact amount of added water was not considered to significantly impact the model. Instead, moisturizing the soil with a hose until the material was observed to be at a state similar

to the optimum requirements allowed for a more rapid backfilling process and yielded similar density results.

Once moisture conditioning was completed, backfilling activities began. Backfilling of the medium sand material was done in lifts of approximately 6 inches. The backfilling process entailed placing a layer of material, compacting said layer by means of a 8-inch by 8-inch hand tampers, scarifying the top and placing the next lift. This process was maintained until the compacted material reached a height of 50 inches above ground surface. To maintain equilibrium within the culvert member, backfilling was performed on both sides of the CIP culvert simultaneously. Figure 18 presents compaction activities of the medium sand (left) and the completed top layer of medium sand material (right).

Figure 18 - Backfilling operations of the medium sand

To determine the density and, therefore, the compactness of the top segment of medium sand, the material was placed in 5-gallon buckets and weighed prior to insertion into the model from a height of 36.5 inches to a height of 50 inches on both sides. The weights, in conjunction with the volume calculations of the selected areas, allowed for the determination of the "as compacted" unit weight of the medium sand. In addition, a sand cone test was performed on either side of the top segment to verify the density results. Refer to Sections 3.4.5.2.2, 3.4.5.2.3, 3.5.3.2. and 3.5.3.3. for density procedures and results.

Once the compacted medium sand reached a height of 50 inches, the Vigoro geofabric was placed along the entire model length. Immediately after placement of the geofabric, backfilling operations of the coarse sand at either side of the top segment commenced. To avoid mixing the coarse sand with the pea gravel/ ¾-inch road base material, OSB boards were positioned vertically at the interface between the top and adjacent east and west concrete segments extending to the top of the retaining walls. The coarse sand was then placed and was also compacted using square hand tampers. As with the medium sand, moisture conditioning was performed prior to backfilling and compaction of the material in the soil box. For the first and second tests, density determinations were not performed on the coarse sand since the backfill areas were not expected to experience any of the compression loading imposed on the model (areas were out of the 60° distribution zone). For the third test, however, a sand cone test was performed on the coarse sand since additional coarse sand was added on the sides of the trapezoid, and the material was in close proximity to the loaded zone.

Upon completion of the coarse sand backfill process, pea gravel filling and compaction was performed for the first test. The pea gravel extended from the top segment elevation to 62 inches above grade. This soil unit was placed in 6-inch loose lifts which were also compacted by means of hand tampers. For the second test, the pea gravel was replaced with ¾-inch road base. Compaction of the medium sand, coarse sand, pea gravel, and ¾-inch road base was performed until a firm unyielding condition was observed in every lift placed. Determination of the "as compacted" unit weight of the pea gravel and ¾-inch road base followed a similar methodology as that of the medium sand in terms of weight and volume calculations.

Figure 19 displays backfilling activities of the coarse sand (left) and pea gravel (right).

Figure 19 - Backfilling operations of the coarse sand (left) and pea gravel (right)

In addition, Figure 20 presents a view of the completed backfilled model prior to the start of the first experimental test.

Figure 20 - Backfilled CIP model

3.4.5. Concrete and Soil Testing

In the civil engineering profession, particularly in the geotechnical, structural and transportation fields, it is common practice to perform field and laboratory tests on the different materials used in construction to obtain material properties. This is primarily done to verify that the parameters utilized in design and analysis, correlate to those present in the field. For this project, the main driving factor for field and laboratory testing was the need to obtain accurate material properties of the components used in the FEM modeling/analysis of the CIP and precast hollow-core culverts.

The following sections present the laboratory and field testing performed for the CIP portion of the project.

3.4.5.1. Laboratory Testing

3.4.5.1.1. <u>Concrete Compression Test and Unit Weight Determination</u>

Determination of the compressive strength and unit weight of cylindrical concrete specimens followed the guidelines presented in *ASTM C39/C39M-20, Standard Test Method for Compressive Strength of Cylindrical Concrete Specimens* (ASTM International, 2020). Cylinders were used to determine the compressive strength of CIP cylinders after 28-days of curing and at the time of culvert testing. Compression testing was done by means of a Gilson Compression Testing Machine presented in Figure 21.

Figure 21 - Gilson Compression Testing Machine

A summary of the concrete compression testing procedure is presented below:

1. Removed specimen from water bath;

2. Measured and recorded the diameter of the specimen at right angles (mid height) for cross-sectional area calculations;
3. Measured and recorded the height of the cylinder at three different locations, spaced evenly, for volume calculations;
4. Weighed the cylinder and recorded its mass for density (unit weight) calculations;
5. Placed the plain bearing block on the platen of the testing machine directly under the spherically seated bearing block, and placed concrete test specimen on the lower bearing block;
6. Aligned the axis of the specimen with the center of thrust of the spherically seated block;
7. Zeroed the testing machine prior to testing of the specimen;
8. Applied the load continuously at an approximate rate of 440 lb/s ± 88 lb/s until the load indicator showed that the load was decreasing steadily and the specimen displayed a well-defined fracture pattern (Figure 22);

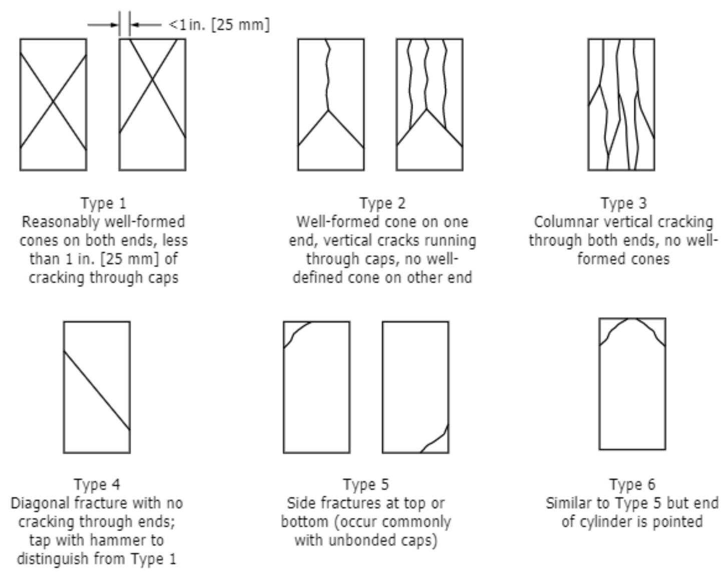

Figure 22 - Typical Fracture Patterns (ASTM International, 2020)

9. Recorded the maximum load carried by the specimen during the test; and
10. Retracted the loading disc, removed the broken specimen, and noted the type of fracture pattern.

3.4.5.1.2. Modulus of Elasticity and Poisson's Ratio Test

Two of the direct inputs needed for the FEM simulation of the CIP culvert were the modulus of elasticity and Poisson's ratio of concrete. In order to obtain these values, procedures set forth in *ASTM C469/C469M-14, Standard Test Method for Static Modulus of Elasticity and Poisson's Ratio of Concrete in Compression* (ASTM International , 2014) were followed. This test was performed in conjunction with the compression test. As such, only one cylinder was used for the modulus of elasticity/Poisson's ratio test and the maximum load at failure obtained from the compression test was utilized to obtain the 40% load value needed for testing. In general, the modulus of elasticity/ Poisson's ratio test entailed:

1. Removing a concrete specimen from the water bath;
2. Measuring and recording the diameter of the specimen at right angles (mid height) for cross-sectional area calculations;
3. Measuring and recording the height of the cylinder at three different locations, spaced evenly, for volume calculations;
4. Weighing the cylinder and recording its mass for density calculations;
5. Measuring the distance from the dial gage to the pivot rod of the compressometer-extensometer as well as the distance from the contact screw to the pivot rod;

6. Straightening the compressometer/extensometer so that all yolks aligned, checking that the pivot rod had proper placement between the top and bottom yolk, and tightening bracing screws
7. Placing the specimen inside the compressometer-extensometer (centered) and tightening all anchor screws to contact the cylinder to prevent movement within the compressometer/extensometer;
8. Placing the specimen, with the strain-measuring equipment attached, on the lower platen of the testing machine and aligning the axis of the specimen with the center of thrust of the spherically seated upper bearing block;
9. Unscrewing all bracing screws from the top and bottom rings and one of the transverse bracing screws from the center ring to allow movement when testing;
10. Zeroing out the longitudinal and transverse dial gauges;
11. Loading the specimen to 40% of the maximum compression load (obtained from compression test) at a rate of approximately 440 lb/s ± 88 lb/s;
12. Recorded, without interruption of loading, the applied load, transverse and longitudinal strains at the point when:
    a. The longitudinal strain reached 0.0002625 inches
    b. The load reached 10,000 lbs
    c. The load reached 20,000 lbs
    d. The load reached 30,000 lbs
13. Upon reaching the maximum load, reducing the load to zero at the same rate at which it was applied;
14. Repeating the test 3 additional times;
15. Removing specimen with measuring devices from the testing machine;

16. Screwing in all bracing screws and unscrewing all anchor screws; and
17. Removing the test specimen from the compressometer/extensometer and discarding it; and
18. Determining the stress, longitudinal strain and transverse strain for each loading cycle and calculating the modulus of elasticity and Poisson's ratio.

The testing apparatus used to perform the modulus of elasticity/Poisson's ratio test is presented in Figure 23.

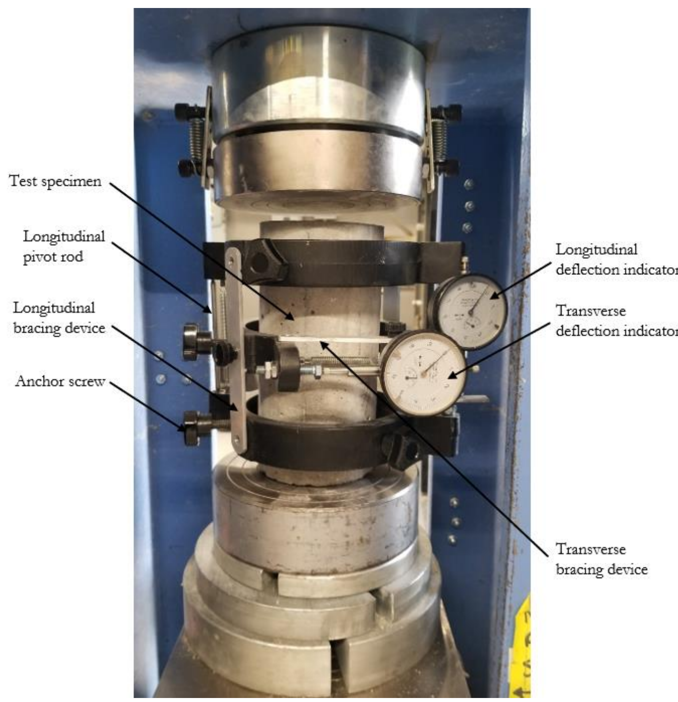

Figure 23 - Modulus of Elasticity/Poisson's Ratio Testing Apparatus

The Rapid Set Concrete Mix, used for the construction of the trapezoid prism which was placed on top of the concrete culvert to conduct experimental tests number 3, 4, and 5, also necessitated a modulus of elasticity determination for use in the FEM analysis. Due to time constraints and the inability to obtain the testing apparatus used to conduct the modulus of elasticity/Poisson's ratio test of the CIP cylinders, a variation of the modulus of elasticity test was performed. Even though this test method did not follow all recommendations set forth in ASTM C469, it did yield the necessary information needed to calculate the stresses and longitudinal strains and, thus, obtain the modulus of elasticity of the concrete. The following presents a summary of the steps performed to obtain the elastic modulus of the Rapid Set Concrete Mix:

1. Removed a concrete specimen from the water bath;
2. Measured and recorded the diameter of the specimen at right angles (mid height) for cross-sectional area calculations;
3. Measured and recorded the height of the cylinder at three different locations, spaced evenly, for volume calculations;
4. Weighed the cylinder and recorded its mass for density calculations;
5. Instrumented the loading frame with a linear potentiometer to record deflection in the longitudinal direction:
6. Placed a 2165SFQX-225K load cell on the loading frame to record vertical loading:
7. Placed the test specimen on top of the load cell for testing;
8. Connected the load cell and linear potentiometer to a LoggerNet 4.5 DAQ to record load and displacements at 0.2 second intervals;
9. Zeroed out all instrumentation;
10. Loaded the test specimen to 40% of the maximum compression load at a rate of approximately 440 lb/s ± 88 lb/s using a manual loading machine;
11. Recorded, without interruption of loading, the applied load and longitudinal displacements every 0.2 seconds;
12. Upon reaching the maximum load, reduced the load to zero at the same rate at which it was applied;

13. Removed the specimen from the testing machine;
14. Determined the stress and longitudinal strain every 5,000 lbs up to a maximum load of 20,000 lbs and calculated the resulting modulus of elasticity.

The loading machine, load cell, linear potentiometer, and test specimen used to perform the modulus of elasticity test of the Rapid Set Concrete Mix are presented in Figure 24.

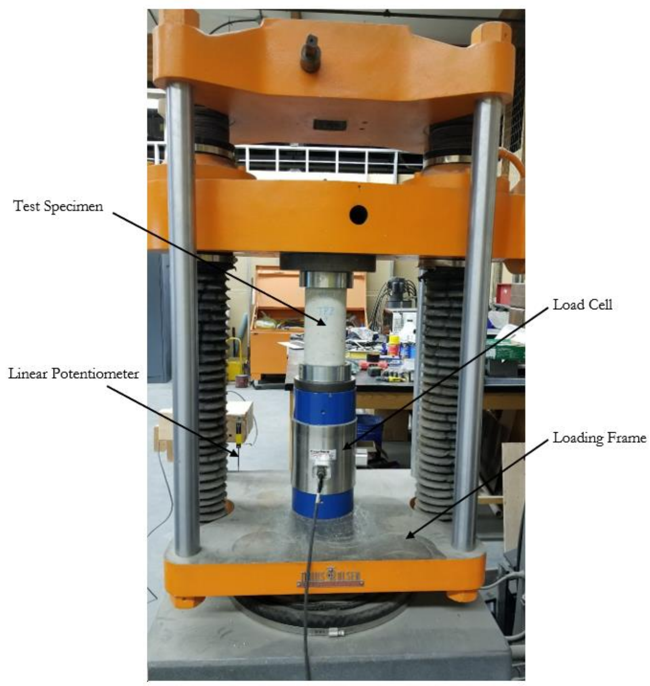

Figure 24 - Testing equipment modulus of elasticity test (variation)

3.4.5.1.3. <u>Sieve Analysis Tests</u>

Determination of the particle size distribution of the medium sand, coarse sand, pea gravel and ¾-inch road base followed the guidelines presented in *ASTM C136/C136M-19, Standard Test Method for Sieve Analysis of Fine and Coarse Aggregates* (ASTM International, 2019). A summary of the sieve analysis procedure is presented below:

1. Used a quartering process to obtain a sample size of approximately 3,000 g;
2. Dried the sample to a constant mass, recorded the dry mass and determined the moisture content of the sample as received;
3. Washed the test fraction over the No. 200 sieve;
4. Re-dried the sample to a constant mass and recorded the new dried mass;
5. Selected the sieves that had suitable openings for the test sample;

Table 3 - Sieve Sizes for Gradation Analysis

Sieve No.	Size (in)	Size (mm)
3/4"	0.750	19.000
1/2"	0.500	12.500
3/8"	0.375	9.500
No. 4	0.187	4.750
No. 8	0.0937	2.360
No. 10	0.0787	2.000
No. 16	0.0469	1.180
No. 30	0.0234	0.600
No. 40	0.0165	0.425
No. 50	0.0117	0.300
No. 100	0.0059	0.150
No. 200	0.0029	0.075

6. Placed the sieve arrangement on a mechanical sieve shaker, dropped the soil material on the top screen and secured the sieve arrangement;
7. Shook the material for a total of 8 minutes using the mechanical sieve shaker;
8. Used a scale to determine the mass of material retained on each sieve;

9. Calculated the percent passing in all size screens based on the total mass of initial dry sample (step 4); and
10. Discarded the material used.

Figure 25 presents the equipment used to perform the gradation tests. For all tests, two different sets of shakers were used. One for the particles bigger than the No. 4 sieve (left sieve arrangement) and one for the particles smaller than the No. 4 sieve (right sieve arrangement).

Figure 25 - Gradation Equipment

3.4.5.1.4. <u>Proctor Compaction Tests</u>

To determine the relationship between molding water content and dry unit weight of soil having less than 30% by mass retained on the 3/8-inch sieve, a proctor compaction test was performed. For this project, the medium sand, coarse sand and ¾-inch road base were tested using a Method B standard proctor. Guidelines presented in *ASTM D698-12, Standard Test Methods for Laboratory Compaction Characteristics of Soil Using Standard Effort (12 400 ft-lbf/ft^3(600 kN-m/m^3))* (ASTM International, 2012) were followed when performing each test.

The procedure for the proctor compaction test included:

1. Determining the water content of the test fraction;
2. From the test fraction, using a quartering process to obtain five sub specimens weighing approximately 2,300 grams;
3. Increasing the moisture content of the first sub specimen by 2% starting from in-situ conditions and mixing the test fraction thoroughly;
4. Progressively increasing the water content of each additional sub specimen by 2% with respect to the previous tested specimen, and mixing each test fraction thoroughly;
5. Determining and recording the mass of the mold and base plate;
6. Assembling and securing the mold and collar to the base plate, and resting the mold on a uniform rigid foundation;
7. Placing the first lift of loose soil from the first compaction point into the mold and spreading into a layer of uniform thickness;
8. Lightly tamping the soil until fluffiness of the first lift was removed using a manual rammer;
9. Compacting the first lift with 25 blows, using a manual rammer weighing approximately 5.50 lb and falling freely through a distance of 12 inches from the surface of the specimen, in such a manner as to provide complete uniform coverage of the specimen surface (Figure 26);

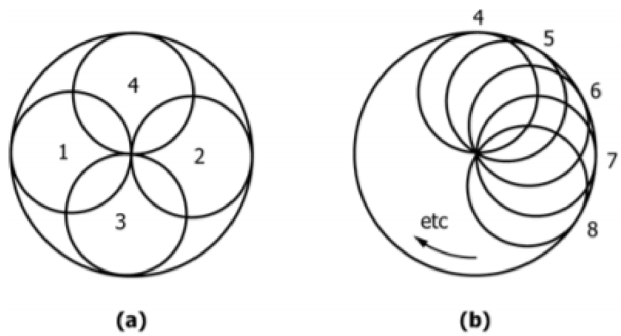

Figure 26 - Rammer Pattern of Compaction (ASTM International, 2012)

10. Repeating steps 8 through 10 for the second and third layers;
11. Removing the collar and trimming the excess soil extending above the top of the mold by means of a straightedge.
12. Removing excess soil from the outside of the mold and base plate;
13. Determining and recording the mass of the specimen, mold and base plate;
14. Removing the material from the mold and obtaining a 150 g sub specimen for molding water content determination;
15. Determining the molding water content of the first compaction point;
16. Discarding all material used for the first compaction point;
17. Repeating steps 7 through 16 for the rest of the sub specimens prepared in step 5; and
18. Calculating the moist and dry densities of each proctor point and plotting a compaction curve of the dry density vs. molding water content.

Equipment used for the proctor compaction test is shown in Figure 27.

Figure 27 - Equipment for Proctor Compaction Test

3.4.5.2. In-Situ Testing

3.4.5.2.1. <u>Moisture Content Test</u>

Moisture content tests were carried out prior to moisture conditioning of the backfill material to determine the "as stored" water content of the soil and after moisturizing the soil. To conduct said tests, *ASTM D2216-19, Standard Test Method for Laboratory Determination of Water (Moisture) Content of Soil and Rock by Mass* (ASTM International, 2019) was used as a reference. Due to the amount of moisture content tests needed to be carried out and the need for prompt results, a microwave was used to dry the samples. In general, moisture determination tests included:

1. Selecting a representative test specimen of approximately 100 g;
2. Weighing the testing container and recording its mass;
3. Placing the moist test specimen in the container and determining the mass of the container and the moist specimen;

4. Placing the container with the test specimen in the microwave and drying for a period of one (1) minute;
5. Removing and weighing the container with soil sample;
6. Repeating steps 4 and 5 until a change in mass of 0.1% or less between drying cycles was achieved;
7. Calculating the water content of the material.

3.4.5.2.2. Density of Compacted Medium Sand and Pea Gravel

In an effort to determine the density of the compacted medium sand (top segment) and pea gravel, the following measurements were taken at the time of backfilling operations:

1. Measured and recorded the dimensions of the area where the material was going to be located (backfilled);
2. Placed the moisturized material in 5-gallon buckets;
3. Weighed and recorded the mass of each bucket used;
4. Placed and compacted the material in 6-inch lifts;
5. Verified that the compacted material was in a firm and unyielding state;
6. Calculated the volume and total mass of material used; and
7. Determined the compacted density of the material.

3.4.5.2.3. Sand-Cone Test

To determine the density and moisture content of the compacted medium sand (after all rounds of testing were accomplished) and coarse sand (after trapezoid prism was positioned in place and backfilled) and, consequently, obtain an indication of the compaction state; sand cone tests were performed on the top layers. The sand cone tests were completed in accordance with *ASTM D1556/1556M-15e1, Standard Test Method for Density and Unit Weight of Soil in Place by Sand-Cone Method* (ASTM International, 2015). The test included:

1. Filling the cone container with conditioned sand for which the bulk density had already been determined;
2. Preparing the surface of the location where the test was performed so that it was a level plane;
3. Seating the base plate on the plane surface, making sure there was contact with the ground surface around the edge of the flanged center hole;
4. Digging the test hole through the center hole in the base plate, being careful to avoid disturbing or deforming the soil that was bounding the hole;
5. Placing all excavated soil in a moisture tight container for subsequent moisture determination;
6. Inverting the sand-cone funnel into the flanged hole, opening the valve to allow the sand to fill the hole, and closing the valve once flow of sand material stopped;
7. Determining the mass of the apparatus with the remaining sand;
8. Determining the mass of the mass of the moist material that was removed from the test hole;
9. Determining the water content of the removed material;
10. Calculated the volume of the test hole, and the wet and dry densities of the material tested.

Figure 28 displays the testing apparatus.

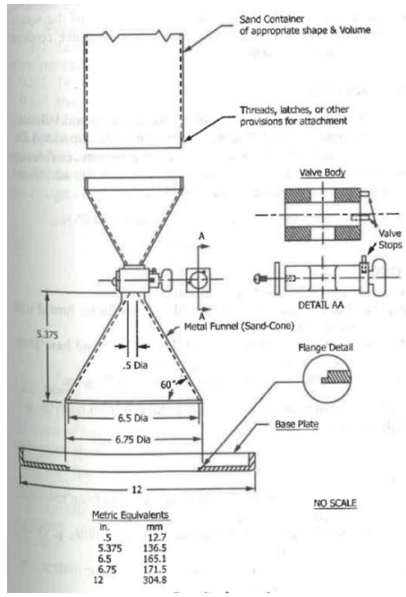

Figure 28 - Sand Cone Apparatus (ASTM International, 2015)

3.4.6. Experimental Testing of CIP Culvert Model

Experimental testing of CIP model was performed to obtain real-life structure responses of a monolithic concrete culvert under applied compressive forces. Information obtained from this test aided in assessing if such a structure would be able to sustain a design compressive load of 9.03 kips (half-scale equivalent of a 16-kip wheel load with applied load combination) without undergoing any failure. The following sections present the test setup, loading procedure and crack monitoring activities performed during experimental testing.

3.4.6.1. Test Setup

3.4.6.1.1. Loading Equipment

Load testing of the CIP culvert was performed by means of a displacement-controlled actuator, connected to a CLC-300K Transducer Techniques load cell and attached to a 5-inch by 10-inch steel plate, which ultimately transferred the imposed load to the model. The displacement-controlled actuator had an approximate compression capacity of 160,000 pounds and pulling capacity of 110,000 pounds. The actuator was mounted onto a reaction frame that consisted of a cross beam and two steel columns, which were elevated by means of I-beams to obtain the appropriate testing height. In addition, a lateral bracing system was positioned on each side. Figure 29 presents a schematic of the testing setup.

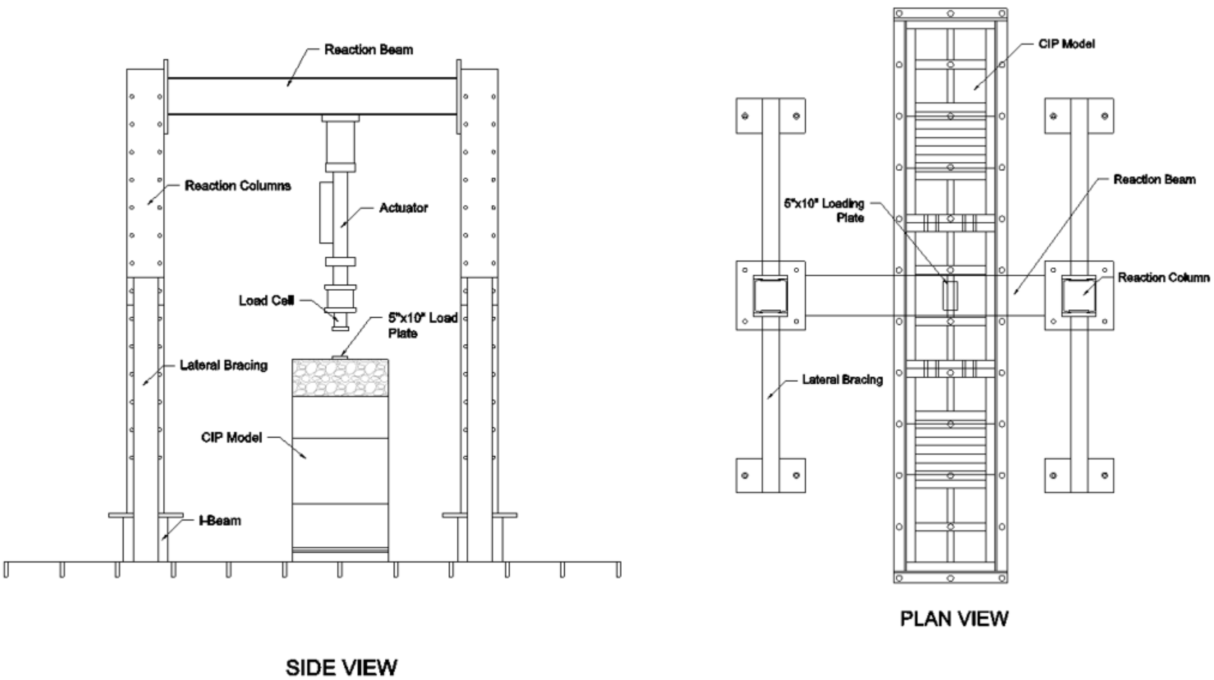

Figure 29 - Testing Setup Schematic

3.4.6.1.2. Instrumentation

In order to measure the load, displacements and strains at specific model locations, load cells, linear potentiometers, and string pots were used. Data obtained from these instruments was utilized to calibrate the FEM model developed for the CIP culvert. Figure 30 and Figure 31 present all instrumentation used for testing.

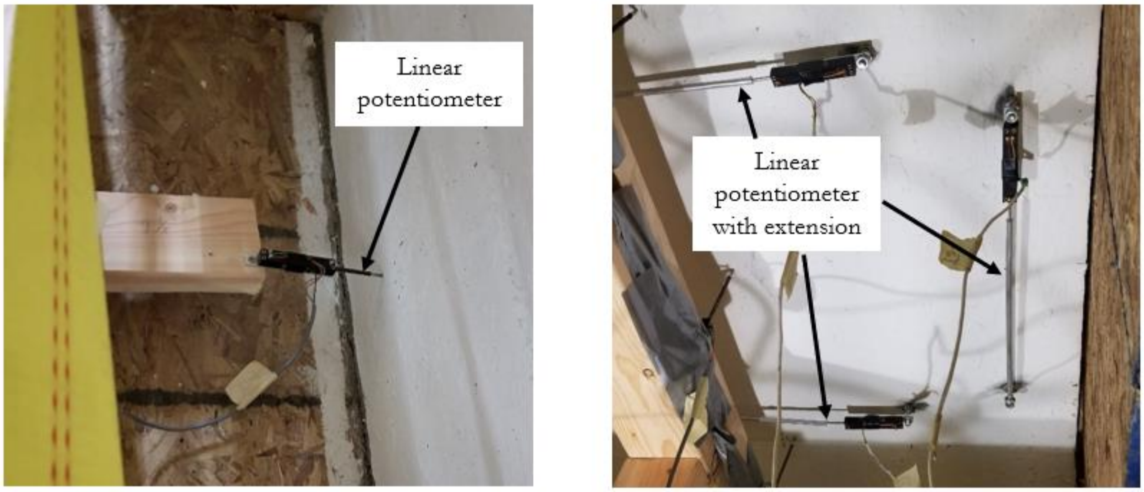

Figure 30 - Linear potentiometers with and without extensions

Figure 31 - String pot (left) and load cell (right)

A total of 18 linear potentiometers and one string pot were utilized to measure the horizontal and vertical displacements of the CIP model for the first, second and third rounds of testing. The fourth test used a total of 12 potentiometers (discarding the 3 placed on the corners of the soil box and relocating LS2 to the second long wall of the model). Furthermore, the fifth test used four instruments (TCY2, LS1, LS2 on the north side, and the BEAM) since the structure was taken to failure.

The linear potentiometers and the string pot used were capable of reading displacements to the nearest thousandths of an inch. Prior to mounting the instrumentation on the model, all potentiometers and string pots were wired to a wiring board which, in turn, was connected to a computer with installed LoggerNet 4.5 DAQ software and calibrated to ensure good functioning of all equipment. Refer to Section 3.4.6.1.3 of this report for additional DAQ information.

For the first four tests, three of the potentiometers were mounted on the center line (long direction) of the bottom face of the upper culvert segment to measure vertical deflection of the concrete. An additional four potentiometers were mounted perpendicular to these, to measure strain in the X- and Z-directions. Two more potentiometers were placed in the inside bottom portion of the culvert to measure outward movement of the bottom concrete segments. Additionally, horizontal displacements of the top half wall were measured by means of two other potentiometers. To obtain the total vertical deflection imposed on the plate, a string pot was placed on the actuator; and to find the true displacement of the plate a final potentiometer was mounted on the reaction beam. Furthermore, for tests 1, 2, and 3, three potentiometers were mounted on the southwest and northeast box corners in the X-, Y-, and Z-directions to measure toppling and potential expansion of the box.

A compression load cell was used to measure the applied force on the 5-inch by 10-inch steel plate which came in contact with the upper soil layer. The CLC-300K load cell had a capacity of approximately 300,000 pounds. Calibration of this load cell was done in the laboratory by comparing load increment readings with a 2165FQX -225K load cell, recently calibrated. Calibration activities evinced that the CLC-300K used a calibration factor of approximately 2.2229 for a 20,000-pound load. Refer to Appendix G – Equipment Calibrations for calibration data.

Figure 32 presents a schematic of all instrumentation used for the CIP model. The names of each instrument used are presented beside each piece of equipment.

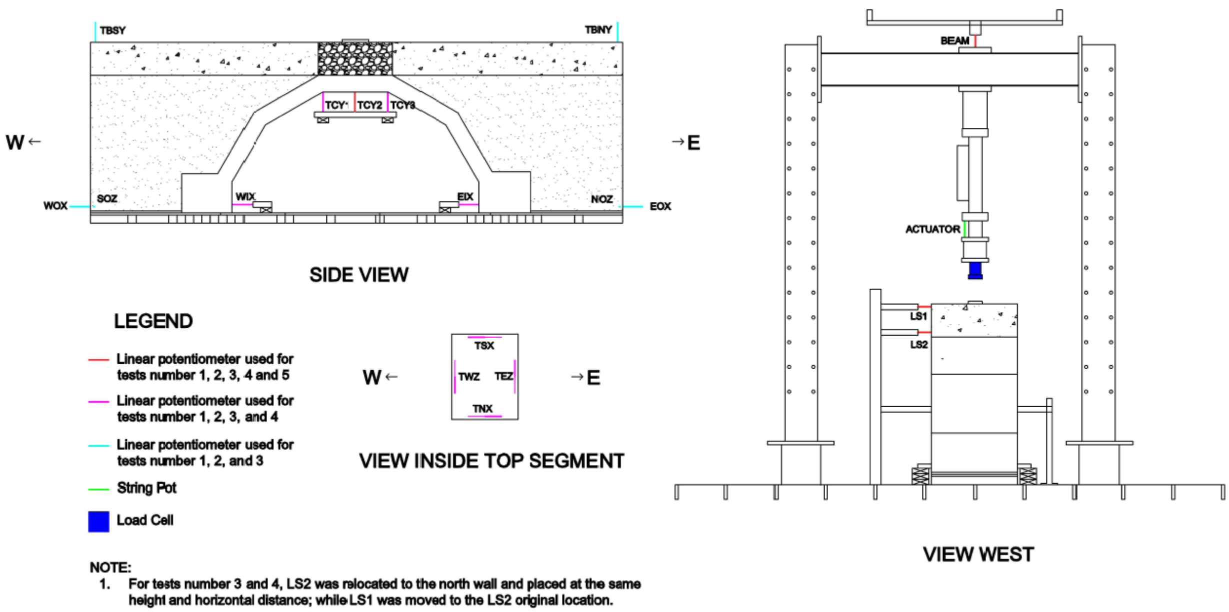

Figure 32 - Instrumentation Schematic

3.4.6.1.3. <u>Data Acquisition System</u>

All instrumentation used for compression testing of the CIP model was linked to a LoggerNet 4.5 DAQ which aided in collecting experimental data. Due to the number of instruments installed, two sensor cards were needed to link the instrumentation to the computer program. The CR6-1 sensor card carried instrumentation for the BEAM (potentiometer), ACTUATOR (string pot) and LOAD CELL, while the CDM-1 sensor card carried the remaining 17 potentiometers installed around the model itself. Table 4 presents the breakdown of instrumentation channels used for the CIP test.

Table 4 - Instrumentation Channel, Designation and Location

Sensor Card	Instrument Type	Instrument Designation	Location
CR6-1	Load Cell	LOAD CELL	Load cell, y-direction
CR6-1	String Pot	ACTUATOR	Actuator, y-direction
CR6-1	Linear Potentiometer	BEAM	Reaction beam, y-direction
CDM-1	Linear Potentiometer	TCY1	Bottom face of top concrete segment, west side, center line, y-direction
CDM-1	Linear Potentiometer	TCY2	Bottom face of top concrete segment, middle, center line, y-direction
CDM-1	Linear Potentiometer	TCY3	Bottom face of top concrete segment, east side, center line, y-direction
CDM-1	Linear Potentiometer	TNX	Bottom face of top concrete segment, north edge, x-direction
CDM-1	Linear Potentiometer	TSX	Bottom face of top concrete segment, south edge, x-direction
CDM-1	Linear Potentiometer	TEZ	Bottom face of top concrete segment, east edge, z-direction
CDM-1	Linear Potentiometer	TWZ	Bottom face of top concrete segment, west edge, z-direction
CDM-1	Linear Potentiometer	EIX	Interior face of footing, east side, x-direction
CDM-1	Linear Potentiometer	WIX	Interior face of footing, west side, x-direction
CDM-1	Linear Potentiometer	NOZ	Exterior face of soil box, northeast corner, z-direction

Sensor Card	Instrument Type	Instrument Designation	Location
CDM-1	Linear Potentiometer	EOX	Exterior face of soil box, northeast corner, x-direction
CDM-1	Linear Potentiometer	TBNY	Exterior face of soil box, northeast corner, y-direction
CDM-1	Linear Potentiometer	SOZ	Exterior face of soil box, southwest corner, z-direction
CDM-1	Linear Potentiometer	WOX	Exterior face of soil box, southwest corner, x-direction
CDM-1	Linear Potentiometer	TBSY	Exterior face of soil box, southwest corner, y-direction
CDM-1	Linear Potentiometer	LS1	Exterior face of south retaining wall, top, y-direction
CDM-1	Linear Potentiometer	LS2	Exterior face of south retaining wall, middle, y-direction

During testing, the LoggerNet 4.5 DAQ used a scan rate of 4 samples per second for each instrument. All data processing was achieved using Microsoft Excel.

3.4.6.2. Loading Procedure

Initially, the loading procedure for experimental testing of the CIP model was planned to be performed by imposing load steps of 500 pounds to the 5-inch by 10-inch plate (positioned at the center of the model), with intermediate observation time, until a total load of 9.03-kips was reached. Since the actuators available for testing were all displacement-based, the loading procedure program had to be changed to displacement increments. Although not ideal, the displacement increments were kept small enough to prevent rapid loading of the model (0.02 inches per step) while also allowing the actuator to respond to small displacement changes. In this way, if more than one displacement increment was needed to be run back-to-back to achieve an approximate 500 to 700-pound increase in load, it could be performed without compromising the observation time needed between the ideal 500 pounds of application per step. On this note, separate displacement steps were written to accommodate the needed observation time between load steps and avoid rushing or waiting for long periods of time during testing.

The displacement loading procedure was maintained throughout all rounds of testing and followed a linear increasing scheme. This meant that the model was not unloaded and reloaded between steps but rather, it was loaded, the load was held during observation time, and then increased again based on the next displacement increment. Originally, one round of testing was anticipated to be accomplished for the CIP model. However, due to difficulties with the load transferring capabilities of the pea gravel at loads higher than approximately 4,000 pounds, additional testing had to be performed.

3.4.6.2.1. Test Number 1 – Pea Gravel Backfill

The first model tested used 12 inches of clean pea gravel as cover material between the upper concrete segment and the loading plate. For this test, the loading plate was accidentally misplaced, and the long side (10-inch edge) was positioned parallel to the culvert span at the center of the model. Subsequent tests corrected this and positioned the loading plate with the long edge in the direction of the culvert width. Figure 33 presents a schematic of Test No. 1.

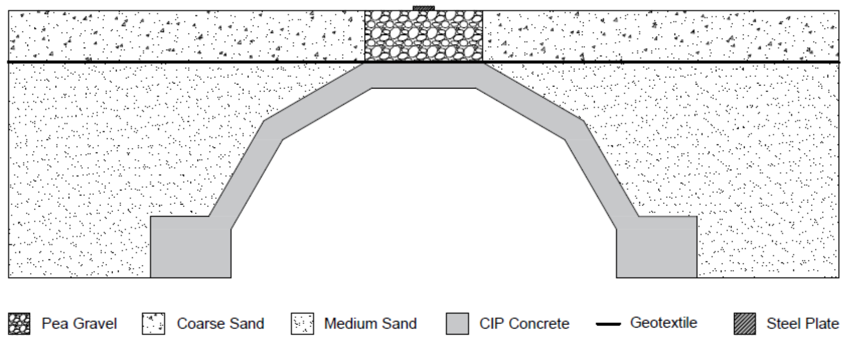

Figure 33 - Schematic Test No. 1 CIP Model

Testing of this model occurred on October 5th, 2020 and took approximately 2 hours and 10 minutes to complete. A total of 84 load steps were driven to carry out this test, with a resulting overall actuator elongation of approximately 1.68 inches (0.02 inches per step).

Loading up to approximately 4,000 pounds necessitated an average of 4 displacement steps to achieve 500-pound increments. After 4,000 pounds, 7 steps were driven to achieve the maximum loading obtained during testing (4,361 pounds) and an additional 45 steps were run, thereafter, to verify that the material could not hold any additional load. Due to difficulties with actuator responses to displacement steps imposed after long waiting periods (observation periods), two loading steps had to be driven at certain times.

3.4.6.2.2. Test Number 2 – ¾-inch Road Base Backfill

Since the pea gravel used for the first test failed in bearing capacity at approximately 4,300 pounds but the structure did not show major signs of damage up to that load, the backfill material of the upper segment was replaced with ¾-inch road base. The purpose of using this type of soil was to fill most of the voids between gravel particles with fines (silt and clay) and potentially obtain a higher strength. Figure 34 presents a schematic of Test No. 2.

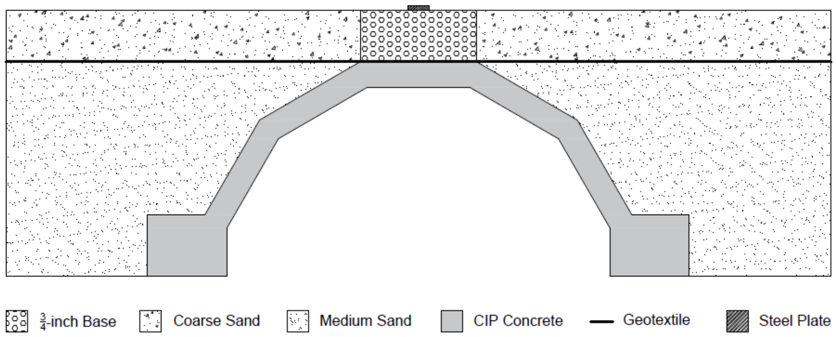

Figure 34 - Schematic Test No. 2 CIP Model

Testing of this model occurred on October 6th, 2020 and took approximately 2 hours and 15 minutes to complete. For this test, the loading plate was positioned with the long edge perpendicular to the culvert span to fulfill AASHTO recommendations. A total of 53 load steps were driven during testing which resulted in an overall actuator elongation of approximately 1.06 inches. Up to approximately 4,000 pounds, an average of 2 displacement steps were needed to achieve the desired 500-pound increments. After 4,000 pounds, the step number increased to between 6 and 10, and after 5,000 pounds a total of 18 steps were driven to achieve the last and maximum load of approximately 5,538 pounds. Since load gain became slower from approximately 3,800 pounds onward, two step increments were driven at a time after step number 18.

3.4.6.2.3. <u>Test Number 3 – Concrete Trapezoid Prism with Coarse Sand Backfill</u>

In an effort to utilize a mechanism capable of transferring the entirety of the test load (9.03 kips) to the culvert structure without failing, but also preserve the 12-inch cover principle, a concrete trapezoid prism was erected. The trapezoid prism's dimensions replicated the 60º stress distribution developed on a soil mass under surface loading. This meant that the top of the prism had similar dimensions to that of the loading plate (5-inches by 10-inches), but the bottom face was widened by 6 inches on each side (17-inches by 22-inches) based on a total height of 12 inches. By using concrete, the stiffness of the system was greatly increased, and the load transferring capabilities were enhanced. This system replicated an extreme loading condition in which the structure would be immediately loaded as would be the case if a truck was travelling directly on top of the culvert. In addition, to provide confinement to the newly added structure, coarse sand was placed and compacted around it. Figure 35 presents a schematic of Test No. 3.

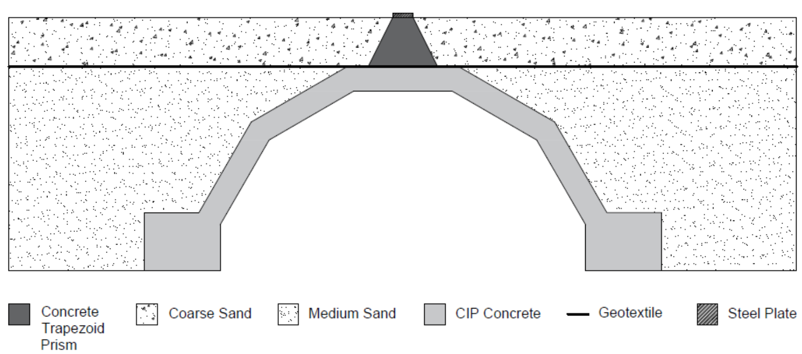

Figure 35 - Schematic Test No. 3 CIP Model

Figure 36 presents the erected trapezoid prism over the culvert structure, backfilled with coarse sand, and instrumented with the loading plate and load cell.

Figure 36 - Backfilled Concrete Trapezoid Prism for Test No. 3

Testing of this model occurred on October 9th, 2020 and took approximately 45 minutes to complete. A total of 16 load steps were driven during testing which resulted in an overall actuator elongation of approximately 0.32 inches. Due to the stiffness of the load transferring mechanism, load increments of 500 pounds were not able to be accomplished. Instead, loading was increased by an average of 1,500 pounds per 0.02-inch step from the beginning of testing until a load of approximately 18,200 pounds was reached. Between 18,200 pounds and the end of testing, or a load of 19,300 pounds, the loads between displacement steps varied between 200 and 800 pounds.

3.4.6.2.4. <u>Test Number 4 – Concrete Trapezoid Prism with No Soil Backfill</u>

To evaluate the capacity of the concrete culvert without the aid of the backfill soil, which ultimately puts the structure in a compression state and increases to some extent it's capacity, all backfill material was removed from the top and sides. Only the medium sand placed from the base to the top of footing elevation was left in place. As with Test No. 3, the concrete trapezoid prism was used as the load dissipating mechanism which ultimately loaded the structure immediately after the application of loads. Figure 37 presents a schematic of Test No. 4 and Figure 38 presents the model setup.

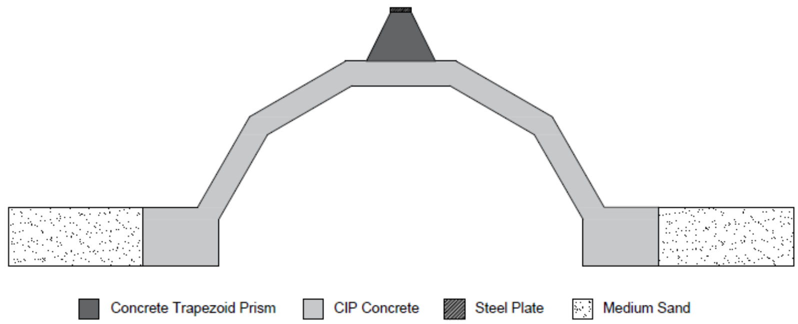

Figure 37 - Schematic Test No. 4 CIP Model

Figure 38 - Model Setup for Test No. 4 CIP Model

Testing of this model occurred on October 13th, 2020 and took approximately 30 minutes to complete. A total of 10 load steps were driven during testing which resulted in an overall actuator elongation of approximately 0.2 inches. As with Test No. 3, load increments of 500 pounds were not attained, but rather loading was increased by approximately 1,500 to 2,500 pounds per displacement step. Test No. 4 was carried out until a load of approximately 21,000 pounds was achieved (similar to Test No. 3) to avoid collapse of the structure and potential damage of the instrumentation placed in the inner face of the structure.

3.4.6.2.5. Test Number 5 – Concrete Trapezoid Prism No Soil Backfill to Failure

To assess the ultimate capacity of the concrete culvert without backfill soil, one final test was performed. As with Test No. 4, only the medium sand at the footing level was left in place and the concrete trapezoid prism was used as the load dissipating mechanism. To avoid damage to instrumentation, only the center middle gauge (TCY2) was left in place and all other equipment was removed from underneath the culvert. In addition, the side wall gauges (LS1 and LS2) were also left in place. Figure 39 presents a schematic of Test No. 5.

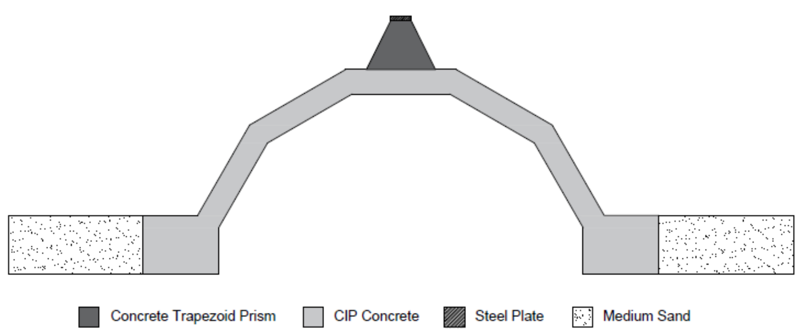

Figure 39 - Schematic Test No. 5 CIP Model

Testing of this model occurred on October 13th, 2020 and took approximately 30 minutes to complete. A total of 19 load steps were driven during testing which resulted in an overall actuator elongation of approximately 0.38 inches. During testing, loading was increased by approximately 1,500 to 2,500 pounds per displacement step. Test No. 5 was carried out until failure occurred at a load of approximately 31,200 pounds.

3.4.6.3. Crack Monitoring

During all rounds of testing, crack monitoring activities were performed. Crack monitoring of the lower portion of the structure consisted of observing the interior face of the culvert after a 500 pound or displacement step increment was applied (whichever yielded a higher load increment), and looking for crack formation, extension and/or widening. To avoid missing potential cracks not evident from the observation point during testing, cameras were also positioned in the interior face of the structure. Cameras used were pointed in the direction of the top and the two adjoining segments. After testing, video records were reviewed and crack formation/extension/widening times were noted down and then correlated with the respective load increment steps.

For the upper portion of the structure, crack monitoring was performed at different stages post testing. For tests number 1, 2, and 3, crack observation was performed once all soil was removed from the sides of the structure on October 12, 2020. For tests number 4 and 5, crack monitoring was performed once each test was finalized and the structure was unloaded.

For the front and back faces of the culvert, crack monitoring was only possible after all rounds of testing were performed and the retaining walls were unmounted. Although not ideal, cracks observed during this stage were able to be correlated to specific rounds of testing.

3.5. Results

3.5.1. Introduction

This section presents the laboratory and in-place test results of all testing performed on the structural and soil components of the CIP model, as well as the experimental test results of the compression testing carried out on the CIP model as a whole. Material properties obtained from laboratory and in-place testing were used as input parameters in the finite element analysis model for the CIP culvert. In addition, experimental compression test results were used to calibrate the FEM model in order to have a fair basis of comparison when assessing the performance of the hollow core culvert.

3.5.2. Laboratory Test Results

3.5.2.1. Concrete Compression Test Results and Unit Weight Determinations

Compression testing of CIP concrete cylinders was performed at 32-days and on the days of testing of the CIP model to evaluate the structure's strength at each stage. In addition, compression testing of the concrete used in the construction of the trapezoid prism was also accomplished on the day that Test No. 3 was conducted. Compression testing of the latter cylinders was only used to assess if the maximum load intended to be applied on the trapezoid was going to be resisted by said structure without inducing failure.

The compressive strengths of the concrete cylinders were calculated by dividing the maximum compressive load of each by the average cross-sectional area. Equation 20 below presents said relationship.

$$f'_c = \frac{P}{A_{avg}} \tag{20}$$

where,

$f'_c =$ compressive strength of concrete, psi

$P =$ maximum compressive load resisted by concrete specimen, lb

$A_{avg} =$ Average cross-sectional area of concrete cylinder, in^2

In addition, the specimens' unit weight was calculated by diving the weight of each cylinder by its volume.

$$\gamma = \frac{W}{V} \tag{21}$$

where,

$\gamma =$ unit weight of concrete specimen, pcf

$W =$ mass of specimen, lb

$V =$ volume of specimen computed from the average dimensions, ft^3

Table 5 the results of the CIP compression tests and the unit weight determinations. Refer to Appendix E – Laboratory Test Results for additional test data.

Table 5 - Compressive Strength and Unit Weight of CIP Concrete Cylinders

Specimen No.	Cross-Sectional Area (in^2)	Volume (in^3)	Weight (lb)	Max. Load (lb)	Compressive Strength (psi)	Unit Weight (pcf)	Age
HC 5 (07/24/20)	12.425	100.480	8.424	76,730	6,175	144.87	32-day
HC 7 (07/24/20)	12.466	100.601	8.456	83,305	6,683	145.25	73-day

Specimen No.	Cross-Sectional Area (in²)	Volume (in³)	Weight (lb)	Max. Load (lb)	Compressive Strength (psi)	Unit Weight (pcf)	Age
HC 9 (07/24/20)	12.466	99.757	8.448	86,230	6,917	146.34	74-day
HC 1 (07/24/20)	12.444	99.607	8.391	86,735	6,970	145.56	77-day

Based on the above test results, the test specimens showed an increase of strength with increasing time. A gain of approximately 800 psi was evinced between the 32-day and 77-day tests. On average, the compressive strength of the concrete during testing was of 6,857 psi. Additionally, all test results demonstrated that the target compressive strength of the mix (4,000 psi) was achieved and surpassed by approximately 54 to 74%.

Table 6 presents the results of the concrete trapezoid's compression tests and the unit weight determinations.

Table 6 - Compressive Strength and Unit Weight of Trapezoid Concrete Cylinders

Specimen No.	Cross-Sectional Area (in²)	Volume (in³)	Weight (lb)	Max. Load (lb)	Compressive Strength (psi)	Unit Weight (pcf)	Age
TPZ 1 (10/07/20)	12.450	100.035	7.920	53,025	4,259	136.81	2-day
TPZ 2 (10/07/20)	12.371	99.224	7.960	48,030	3,883	138.62	2-day

On average, concrete used in the construction of the trapezoid prism evinced a compressive strength of 4,071 psi after 2 days of placement. Experimental testing of the CIP model anticipated an applied load of 9.03 kips. Based on the above test results, the concrete trapezoid was capable of withholding the experimental test load without failing.

3.5.2.2. Modulus of Elasticity and Poisson's Ratio Test Results

In order to determine the modulus of elasticity and Poisson's ratio of the CIP concrete, an ASTM C469 test was performed. As presented in Section 3.4.5.1.2 of this report, dimensions of the test specimen and equipment were taken prior to the start of testing in order to calculate the longitudinal and transverse deformations. Refer to Appendix E – Laboratory Test Results for cylinder and compressometer/extensometer dimensions.

A total of four loading cycles were conducted on specimen HC 2 (07/24/20) to obtain the load, longitudinal and transverse deflections. Calculations of the vertical deformation of the specimen were based on the following equation:

$$\boldsymbol{d = \frac{g e_r}{e_r + e_g}} \qquad \textbf{(22)}$$

where,

$d =$ total longitudinal deformation of specimen throughout effective gauge length, in.

$g =$ longitudinal gauge reading, in.

$e_r =$ perpendicular distance from the pivot rod to the vertical plane passing through the two support points of the rotating yoke, in.

$e_g =$ perpendicular distance from the gauge to the vertical plane passing through the two support points of the rotating yoke, in.

Horizontal deformations were calculated using a similar relationship:

$$\boldsymbol{d' = \frac{g' e'_h}{e'_h + e'_g}} \qquad \textbf{(23)}$$

where,

$d' =$ total transverse deformation of specimen diameter, in.

$g' =$ transverse gauge reading, in.

$e'_h =$ perpendicular distance from the hinge to the vertical plane passing through the support points of the middle yoke, in.

$e'_g =$ perpendicular distance from the gauge to the vertical plane passing through the support points of the middle yoke, in.

Determination of the modulus of elasticity and Poisson's ratio of the CIP test specimen also required the determination of the stresses and strains at the different load increments. Stress calculations used the same relationship as that presented in Equation 20. In addition, strain calculations used the following formula:

$$\boldsymbol{\varepsilon} = \frac{\Delta \boldsymbol{L}}{\boldsymbol{L}} \tag{24}$$

where,

$\varepsilon =$ longitudinal or transverse strain, in/in

$\Delta L =$ change in length which corresponds to d for the longitudinal calculations or d' for the transverse calculations, in

$L =$ total length which corresponds to the specimen's height for the longitudinal calculations or the specimen's diameter for the transverse calculations, in

Once all stresses and strains were determined, the following relationships were utilized to calculate the modulus of elasticity and Poisson's ratio of the specimen:

$$E = \frac{S_2 - S_1}{\varepsilon_{l2} - \varepsilon_{l1}} \quad (25)$$

where,

E = modulus of elasticity, psi

S_2 = stress corresponding to 40% of the ultimate load, psi

S_1 = stress corresponding to a longitudinal strain, ε_{l1}, of 0.00026 in/in, psi

ε_{l2} = longitudinal strain produced by stress S_2, in/in

$$\mu = \frac{\varepsilon_{t2} - \varepsilon_{t1}}{\varepsilon_{l2} - \varepsilon_{l1}} \quad (26)$$

where,

μ = Poisson's ratio

ε_{t2} = transverse strain at midheight of the specimen produced by stress S_2, in/in

ε_{t1} = transverse strain at midheight of the specimen produced by stress S_1, in/in

Test results and the calculated parameters are presented in Table 7 and Table 8.

Table 7 - Modulus of Elasticity and Poisson's Ratio Test Results for CIP Concrete

Test No.	Load	Vertical Deflection (in)	Horizontal Deflection (in)	Long. Specimen Deformation (in)	Trans. Specimen Deformation (in)
1	1,350	0.00026	0.00000	0.000129	0.000000
	10,000	0.00260	0.00000	0.001280	0.000000
	20,000	0.00500	0.00015	0.002462	0.000065
	30,700	0.00745	0.00055	0.003669	0.000238
2	1580	0.00026	0.00000	0.000129	0.000000
	10,000	0.00255	0.00000	0.001256	0.000000

Test No.	Load	Vertical Deflection (in)	Horizontal Deflection (in)	Long. Specimen Deformation (in)	Trans. Specimen Deformation (in)
	20,000	0.00470	0.00015	0.002314	0.000065
	30,600	0.00733	0.00050	0.003609	0.000216
3	1440	0.00026	0.00000	0.000129	0.000000
	10,000	0.00260	0.00000	0.001280	0.000000
	20,000	0.00490	0.00010	0.002413	0.000043
	30,700	0.00747	0.00048	0.003678	0.000208
4	1360	0.00026	0.00000	0.000129	0.000000
	10,000	0.00255	0.00000	0.001256	0.000000
	20,000	0.00490	0.00012	0.002413	0.000052
	31,000	0.00750	0.00050	0.003693	0.000216

Table 8 – CIP Concrete Modulus of Elasticity and Poisson's Ratio Determinations

Test No.	Stress (psi)		Long. Strain (in/in)		Trans. Strain (in/in)		Modulus of Elasticity, E (psi)	Poisson's Ratio, μ
1	S_1 =	108	ε_1 =	1.61E-05	ε_{t1} =	0.00E+00	5.35E+06	0.14
	S_3 =	802	ε_3 =	1.59E-04	ε_{t3} =	0.00E+00		
	S_4 =	1,604	ε_4 =	3.06E-04	ε_{t4} =	1.63E-05		
	S_2 =	2,461	ε_2 =	4.56E-04	ε_{t2} =	5.97E-05		
2	S_1 =	127	ε_1 =	1.61E-05	ε_{t1} =	0.00E+00	5.38E+06	0.13
	S_3 =	802	ε_3 =	1.56E-04	ε_{t3} =	0.00E+00		
	S_4 =	1,604	ε_4 =	2.88E-04	ε_{t4} =	1.63E-05		
	S_2 =	2,453	ε_2 =	4.49E-04	ε_{t2} =	5.43E-05		
3	S_1 =	115	ε_1 =	1.61E-05	ε_{t1} =	0.00E+00	5.32E+06	0.12
	S_3 =	802	ε_3 =	1.59E-04	ε_{t3} =	0.00E+00		
	S_4 =	1,604	ε_4 =	3.00E-04	ε_{t4} =	1.09E-05		
	S_2 =	2,461	ε_2 =	4.57E-04	ε_{t2} =	5.21E-05		
4	S_1 =	109	ε_1 =	1.61E-05	ε_{t1} =	0.00E+00	5.37E+06	0.12
	S_3 =	802	ε_3 =	1.56E-04	ε_{t3} =	0.00E+00		
	S_4 =	1,604	ε_4 =	3.00E-04	ε_{t4} =	1.30E-05		
	S_2 =	2,486	ε_2 =	4.59E-04	ε_{t2} =	5.43E-05		

Figure 40 presents the relationship between the stress and longitudinal strain for the four load increments performed on the HC 2 (07/24/20) specimen.

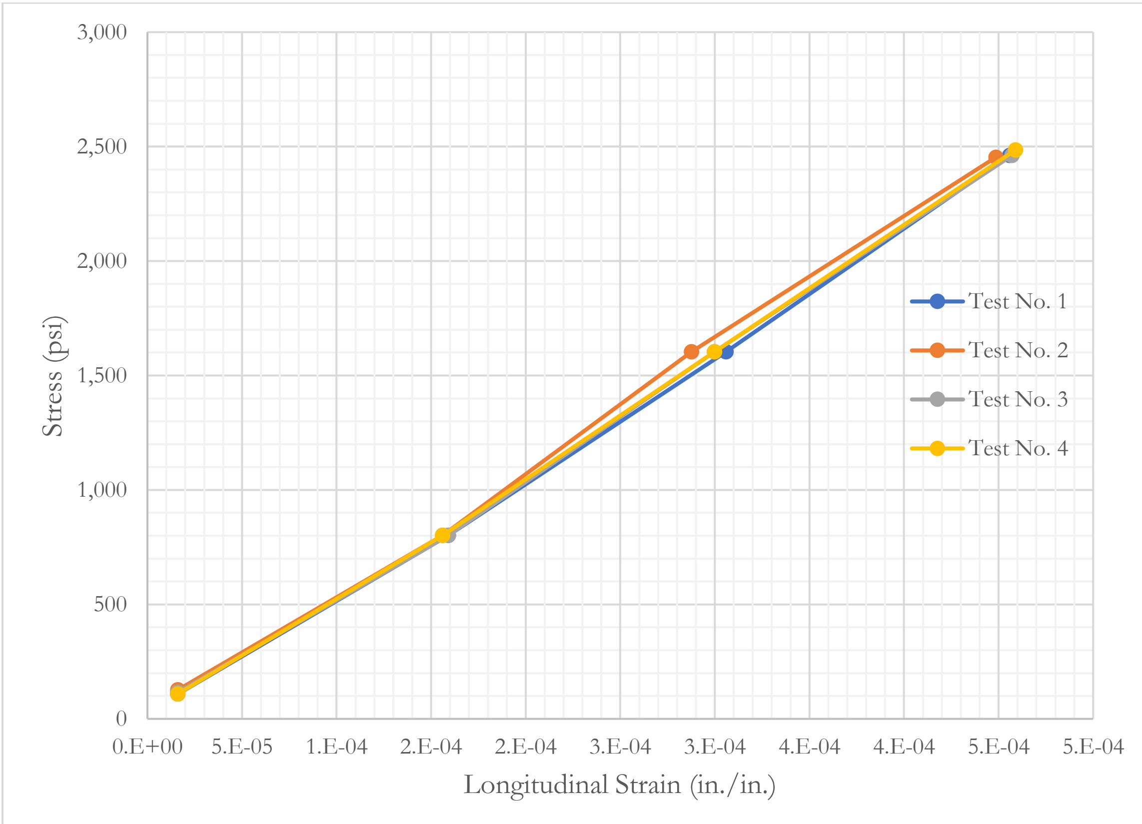

Figure 40 - Stress vs. Strain Relationship of CIP Concrete Test Specimen

Based on the above graph, testing was only performed in the linear elastic portion of the material. Since the proportional limit was not reached in any of the tests, the test specimen was able to return to its original state upon load removal and no permanent deformation was experienced between each consecutive test. Test results for each load cycle appear to follow similar paths and have comparable longitudinal strains for the different load increments. Since test results evinced low variability, the modulus of elasticity and Poisson's ratio of the test specimen was taken as the average of the four load cycles. Namely, $E = 5.35 \times 10^6$ psi and $\mu = 0.13$. These test results appear to lie within published

E and μ ranges for concrete which generally include 2×10^6 to 6×10^6 psi values for the modulus of elasticity and 0.1 to 0.2 values for the Poisson's ratio.

For the Ready Set Concrete Mix (concrete used for the trapezoid prism), a modulus of elasticity test was also performed. Test specimen TPZ 2 (10/07/20) was the cylinder used for testing. For this test, some variations in the original testing equipment and procedure were performed due to time constraints and the inability to obtain the testing apparatus needed to perform both the modulus of elasticity and Poisson's ratio tests simultaneously. Refer to Section 3.4.5.1.2 for additional details. Even though not ideal, the variation test conducted yielded the necessary information needed to obtain the elastic modulus of the Ready Set Concrete Mix.

Calculations of the stress and longitudinal strain of the test specimen used the same relationships as those provided in equations 20 and 24. Namely, the stress was obtained by dividing the applied load by the cross-sectional area, and the longitudinal strain was calculated by dividing the change in height by the specimen's initial height. Refer to Appendix D – Concrete and Grout Mix Designs for the Ready Set Concrete Mix test results and calculated parameters. Figure 41 provides the stress-strain relationship of the test specimen up to an approximate applied load of 20,000 pounds.

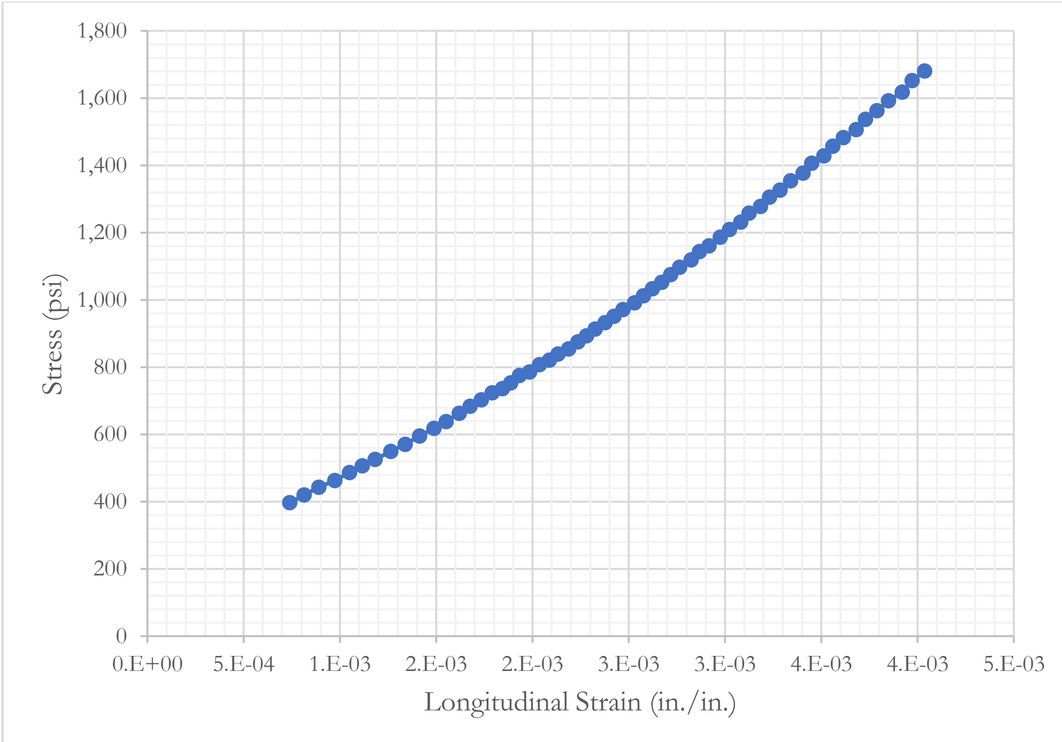

Figure 41 - Stress vs. Strain Relationship of Rapid Set Concrete Test Specimen

As with the CIP specimens, testing of the Rapid Set Concrete Mix was only performed in the linear elastic portion of the material. Based on the above graph, the modulus of elasticity (slope of the line) of the Rapid Set Concrete Mix was approximately 4.49×10^5 psi. Based on published literature, this number appears to be one order of magnitude lower than typical concrete ranges (2×10^6 to 6×10^6 psi) and it is likely that the instrumentation used for testing may not have accurately recorded the changes in height experienced by the test specimen. As such, this test result will not be taken into consideration for the material properties of the concrete trapezoid prism in the FEM models.

3.5.2.3. Sieve Analysis Test Results

For this project, gradation determinations were performed on the different backfill materials used for the CIP model to assess the particle size distribution of each and predict how the material would perform under loading. Sieve analyses also allowed for the classification of the soil which was later used to obtain additional material properties from correlation charts.

To determine the particle size distribution of the different soil units, test specimens were allowed to pass through an arrangement of sieves which progressively decreased in mesh size. Based on the amounts of material retained on each sieve size, gravel, sand and silt/clay quantities were determined. Per *ASTM D2487-17e1, Standard Practice for Classification of Soils for Engineering Purposes (Unified Soil Classification System)* (ASTM International, 2017), gravel material includes particles of rock that pass the 3-in sieve and are retained on the No. 4 sieve; sand material includes particles of rock that pass the No. 4 sieve and are retained on the No. 200 sieve; and silt/clay is material that passes the No. 200 sieve. Gravel and sand are further subdivided into categories based on the coarseness or fineness of the soil. Coarse gravel is defined as material passing the 3-in sieve but retained on the ¾-in sieve and fine gravel includes all material passing the ¾-in sieve but retained on the No. 4 sieve. For the sand unit, coarse sand includes particles passing the No. 4 sieve and retained on the No. 10 sieve; medium sand includes material passing the No. 10 sieve and retained on the No. 40 sieve; and fine sand includes soil passing the No. 40 sieve and retained on the No. 200 sieve. The following tables present the particle size distribution of the four soil units tested.

- <u>Medium sand</u>: this soil unit was placed around the right and left sides of the CIP culvert up to a height of 50 inches or the top culvert elevation. The medium sand test specimen evinced the following particle size distribution. Refer to Appendix E – Laboratory Test Results for the cumulative particle size distribution curve.

Table 9 - Sieve Analysis of Medium Sand

Sieve Size	Metric Equivalent	Percent Passing
1/2 - inch	12.500 mm	100
3/8 - inch	9.500 mm	99
No. 4	4.750 mm	99
No. 8	2.360 mm	93
No. 10	2.000 mm	87
No. 16	1.180 mm	64
No. 30	0.600 mm	40
No. 40	0.425 mm	32
No. 50	0.300 mm	24
No. 100	0.150 mm	15
No. 200	0.075 mm	11.1

Based on the above data, the medium sand consisted of approximately 1.4% gravel particles, 87.5% sand particles, and 11.1% silt particles. In order to evaluate the evenness of this distribution, the coefficients of uniformity (C_u) and curvature (C_c) were computed. The following equations present the C_u and C_c formulas used.

$$\boldsymbol{C_u = \frac{D_{60}}{D_{10}}} \tag{27}$$

where,

$D_{60} =$ particle size diameter corresponding to 60% of material passing on the cumulative particle size distribution curve, in

$D_{10} =$ particle size diameter corresponding to 10% of material passing on the cumulative particle size distribution curve, in

$$C_c = \frac{(D_{30})^2}{D_{10} \times D_{60}} \quad (28)$$

where,

D_{30} = particle size diameter corresponding to 30% of material passing on the cumulative particle size distribution curve, in.

For the medium sand, a C_u equal to 20.6 and a C_c equal to 2.65 were obtained. Based on the Unified Soil Classification System (USCS), sand having a C_u higher than or equal to 4 and a C_c between 1 and 3 results in a well graded sand. Based on the particle size distribution results and the coefficients of curvature and uniformity, the medium sand was classified as Well Graded Sand with Silt (GP-GM).

- Coarse sand: this soil unit was placed from a height of 50 inches to a height of 62 inches, or the top model elevation, on either side of the top concrete segment. The gradation results for the coarse sand test specimen are presented below. Refer to Appendix E – Laboratory Test Results for the cumulative particle size distribution curve.

Table 10 - Sieve Analysis of Coarse Sand

Sieve Size	Metric Equivalent	Percent Passing
1/2 - inch	12.500 mm	100
3/8 - inch	9.500 mm	100
No. 4	4.750 mm	87
No. 8	2.360 mm	36
No. 10	2.000 mm	28
No. 16	1.180 mm	19
No. 30	0.600 mm	15

Sieve Size	Metric Equivalent	Percent Passing
No. 40	0.425 mm	15
No. 50	0.300 mm	14
No. 100	0.150 mm	14
No. 200	0.075 mm	13.8

Based on the above gradation results, the coarse sand consisted of approximately 13.1% gravel particles, 73.1% sand particles, and 13.8% silt particles. Based on the USCS, this material was classified as Silty Sand (SM).

- Pea gravel: this soil unit was placed from a height of 50 inches to a height of 62 inches, or the top model elevation, on the upper part of the top concrete segment for the first test. Table 11 below provides the sieve analysis results of the pea gravel test specimen. Refer to Appendix E – Laboratory Test Results for the cumulative particle size distribution curve.

Table 11 - Sieve Analysis of Pea Gravel

Sieve Size	Metric Equivalent	Percent Passing
1 - inch	25.000 mm	100
3/4 - inch	19.000 mm	100
1/2 - inch	12.500 mm	100
3/8 - inch	9.500 mm	58
No. 4	4.750 mm	3
No. 8	2.360 mm	3
No. 10	2.000 mm	3
No. 16	1.180 mm	3
No. 30	0.600 mm	3
No. 40	0.425 mm	3
No. 50	0.300 mm	3
No. 100	0.150 mm	3

Sieve Size	Metric Equivalent	Percent Passing
No. 200	0.075 mm	2.7

Based on the above gradation results, the pea gravel consisted of approximately 97.3% gravel particles, 0% sand particles, and 2.7% silt particles. As with the medium sand, the evenness of the particle size distribution was evaluated by means of the coefficients of uniformity and curvature. For the pea gravel a C_u equal to 1.81 and a C_c equal to 0.97 were obtained. Based on the USCS, gravel having a C_u lower than 4 and/or a C_c lower than 1 or higher than 3 results in a poorly graded gravel. Based on the particle size distribution results and the coefficients of curvature and uniformity, the pea gravel was classified as Poorly Graded Gravel (GP) per the USCS.

- ¾-inch Road Base: this soil unit was placed from a height of 50 inches to a height of 62 inches, or the top model elevation, on the upper part of the top concrete segment for the second test. Table 12 below provides the sieve analysis results of the ¾-inch road base test specimen. Refer to Appendix E – Laboratory Test Results for the cumulative particle size distribution curve.

Table 12 - Sieve Analysis of ¾-inch Road Base

Sieve Size	Metric Equivalent	Percent Passing
1 - inch	25.000 mm	100
3/4 - inch	19.000 mm	100
1/2 - inch	12.500 mm	94
3/8 - inch	9.500 mm	88
No. 4	4.750 mm	65
No. 8	2.360 mm	51
No. 10	2.000 mm	49

Sieve Size	Metric Equivalent	Percent Passing
No. 16	1.180 mm	43
No. 30	0.600 mm	39
No. 40	0.425 mm	38
No. 50	0.300 mm	37
No. 100	0.150 mm	35
No. 200	0.075 mm	34.3

Based on the above gradation results, the ¾-inch road base consisted of approximately 34.8% gravel particles, 30.9% sand particles, and 34.3% silt particles. These soil percentages resulted in a USCS classification of Silty Gravel with Sand (GM).

3.5.2.4. Proctor Compaction Test Results

Standard proctor compaction tests were performed on test specimens of the medium sand, coarse sand, and ¾-inch road base to establish the maximum unit weights that the soil materials could achieve using controlled compactive efforts. Proctor test results were used in conjunction with in-place density results (see Sections 3.4.5.1.4 and 3.5.2.4during backfill activities to determine the degree of soil density of these three units. Compaction testing was only done for the medium and coarse sands and ¾-inch road base materials since this test method can only be performed on material that has 30% or less by mass of particles retained on the 3/8 -inch sieve. Since the pea gravel had more than 30% retained in the 3/8 -inch sieve, the material was too coarse to be tested.

The Figure 42, Figure 43, and Figure 44 present the moisture-density relationship curves of the medium sand, coarse sand and ¾-inch road base, respectively.

Based on Figure 42, the maximum dry density that the medium sand can achieve is 112 pcf with a corresponding optimum moisture content of 9.9%. The moisture-density relationship curve presented above also evinces that the dry unit weight of the medium sand does not appear to be highly influenced by changes in moisture content. This can be observed by the flatness of the curve and the minimal change in dry density (approximately 2.5 pcf) between the moisture contents presented.

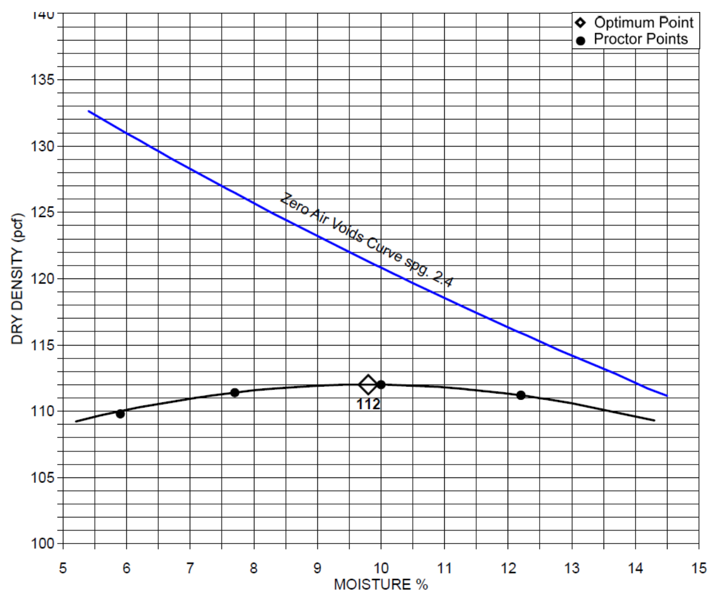

Figure 42 - Moisture-Density Relationship of Medium Sand

Based on Figure 43, the maximum dry density that the coarse sand can achieve is 106 pcf with a corresponding optimum moisture content of 7.7%. As with the medium sand, moisture changes of the coarse sand do not appear to significantly impact the dry unit weight of the material.

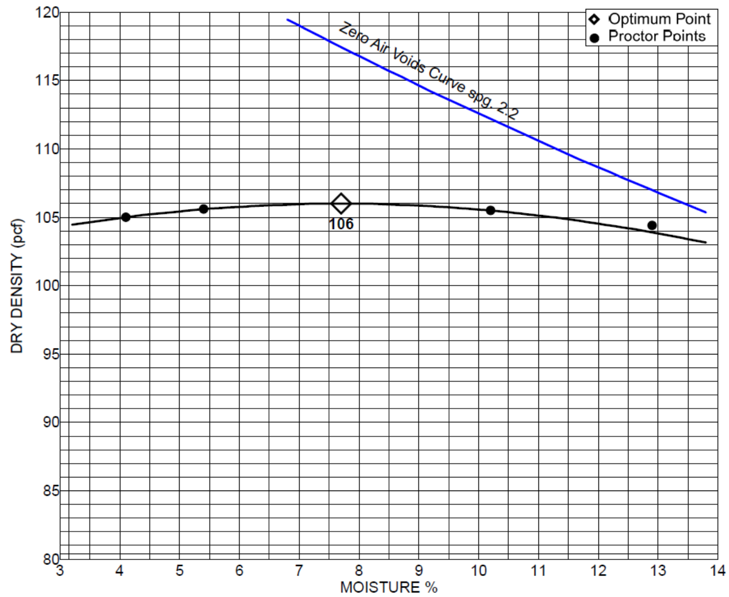

Figure 43 - Moisture-Density Relationship of Coarse Sand

Based on Figure 44, the maximum dry density that the ¾-inch road base can achieve is 136.8 pcf with a corresponding optimum moisture content of 7.9%. Different than the previous soil units tested, the dry density of the ¾-inch road base appears to be fairly controlled by the moisture content and the compaction efforts. For instance, soil having a 4% moisture and being compacted with standard compaction methods can achieved a maximum dry unit weight of approximately 125 pcf. Differently, soil having a moisture of about 7.8% with the same compaction efforts can achieve a maximum dry density of approximately 138 pcf. This results in a dry density increase of about 13 pcf which, compared to the sand unit, is an important amount.

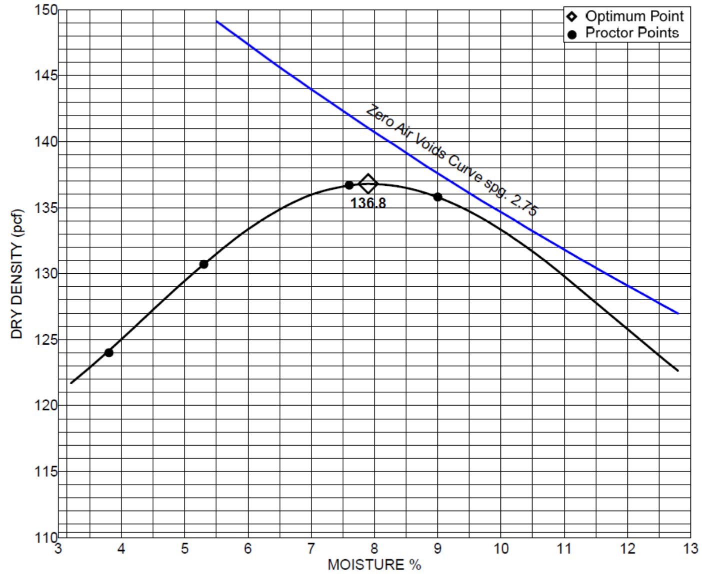

Figure 44 - Moisture-Density Relationship of 3/4-inch Road Base

3.5.3. In-Situ Test Results

3.5.3.1. Moisture Content Test Results

To determine the water content of the backfill soil material prior to and immediately after moisture conditioning activities were achieved, moisture content tests were performed. Equation 29 below provides the moisture content formula utilized to determine the water percentage in each case. In addition, Table 13, Table 14 and Table 15 provide the calculated water contents of the medium sand, coarse sand, and ¾-inch road base backfill material.

$$w\% = \frac{W_w}{W_s} \times 100\% \quad (29)$$

Table 13 - Moisture Content of Medium Sand

Test No.	Location	State	Moisture (%)	Date
1	Top 1/3 of Storage Box 2, right of model	Stored	4.78	09/28/2020
2	Top 1/3 of Storage Box 1, left of model	Stored	4.75	09/28/2020
3	4 inches from top of form (bottom half wall), right of model	Moisturized Storage Box #2	6.97	09/28/2020
4	4 inches from top of form (bottom half wall), left of model	Moisturized Storage Box #1	6.45	09/28/2020
5	At top segment elevation (50 inches), right of model	Moisturized Storage Box #3	5.40	09/29/2020
6	10 inches below top segment elevation, left of model	Moisturized Storage Box #4	4.20	09/29/2020

The stored medium sand in boxes 1 and 2 had an approximate moisture content of 4.75% prior to moisture conditioning activities. With the addition of water, moisture contents for the material in these boxes raised by about 2.2% and 1.75% on the east and west sides, respectively. Soil from storage boxes 1 and 2 allowed for backfilling up to 30 inches in height. For the remaining height, or the additional 20 inches, material from storage boxes 3 and 4 was utilized. Moisture contents for these boxes were not performed prior to moisture conditioning activities. Instead, water contents were run on the moisturized material. The results show that the upper layers had a decrease in moisture content with respect to the bottom layers of approximately 1.6% on the east side and 2.3% on the west side. Possible reasons for these differences could have been related to the lower moisture contents of the stored material in storage boxes 3 and 4, and a decrease in added water to said storage boxes when moisture conditioning was taking place.

Table 14 - Moisture Content of Coarse Sand

Test No.	Location	State	Moisture (%)	Date
1	Top model elevation (62 inches), right of model	Moisturized Storage Box #5	6.53	09/29/2020
2	Top model elevation (62 inches), left of model	Moisturized Storage Box #6	11.65	09/29/2020
3[1]	Top elevation (62 inches), left of trapezoid prism	Moisturized Storage Box #6	5.14	10/08/2020

1. Moisture content test performed in preparation for experimental Test No. 3. Coarse sand placement around trapezoid prism conducted after experimental Tests No. 1 and 2 were finalized and pea gravel/ ¾-inch road base material was removed from model.

Based on the above results, the coarse sand on the right side of the model (moisture tests number 1 and 2) appears to have had less water than the left side during moisture conditioning activities. Even though the difference between these two numbers is approximately 5.2%, the proctor compaction curve, presented in Figure 43, shows a difference in dry unit weight of approximately 1 pcf based on standard compaction efforts. Therefore, it is anticipated that the dry unit weight at both locations is comparable.

The third water content test was performed after the concrete trapezoid was placed on top of the upper concrete segment, and the remaining area was backfilled with coarse sand. This was done in preparation for experimental Test No. 3 and was achieved at a later time than that of moisture content tests number 1 and 2. Based on the third water content test results and the proctor compaction curve for this material, under standard compaction effort the coarse sand around the trapezoid prism would have an approximate dry density of 105.5 pcf.

Table 15 - Moisture Content of ¾-inch Road Base

Test No.	Location	State	Moisture (%)	Date
1	Top model elevation (56 inches), above upper concrete segment	Moisturized Bucket	5.92	10/05/2020
2	Top model elevation (62 inches), above upper concrete segment	Moisturized Bucket	6.11	10/05/2020

The moisturized ¾-inch road base, used as the upper backfill material of the top concrete segment for experimental Test No. 2, had similar values for the first and second lifts (moisture tests number 1 and 2). Based on the proctor compaction curve for this soil unit, the moisture content values laid on the left portion of the graph and represented a dry density, under standard compaction efforts, of approximately 133.5 pcf.

3.5.3.2. Density of Compacted Medium Sand and Pea Gravel Results

Density determinations of the top section of the compacted medium sand (right and left locations), pea gravel and ¾-inch road base were achieved by means of volume calculations and mass data obtained during backfilling activities. Once all rounds of testing were finalized, additional density determinations of the medium sand were achieved by means of sand cone tests. Refer to Section 3.5.3.3. for sand cone test results. The following table presents the backfill area dimensions as well as the total mass of material used and its corresponding wet density.

Table 16 - Density of Compacted Medium Sand and Pea Gravel

Material	Location	Total Volume (ft^3)	Total Mass (lb)	Wet Density (pcf)	Dry Density (pcf)
Medium Sand	East – from 36.5' to 50" high	17.16	1,956.6	114.0	108.2[1]
Medium Sand	West - from 36.5' to 50" high	17.03	1,840.9	108.1	103.7[2]
Pea Gravel	Middle – from 50" to 62" high	5.63	557.6	99.1	-
¾-inch Road Base	Middle – from 50" to 62" high	5.63	800.6	142.2	134.0[3]

1. Dry density calculated based on a moisture content of 5.4% obtained as part of moisture density determinations (see Section 3.5.3.1.)
2. Dry density calculated based on a moisture content of 4.2% obtained as part of moisture density determinations.
3. Dry density calculated based on a moisture content of 6.11% obtained as part of moisture density determinations.

Based on the dry density values presented in Table 16 and the proctor compaction curve for the medium sand (Figure 42), the east and west locations appear to have been compacted to approximately 96.6% and 92.6% of the maximum dry density, respectively. These density values translate to an approximate percent relative density of 62 (medium dense) for the east medium sand and 56 (medium dense) for the west medium sand based on the *Representative Values of Relative Density* correlation chart developed by McCarthy and presented as Table 4-3 on the *Essentials of Soil Mechanics and Foundations, Basic Geotechnics* book (McCarthy, Representative Values of Relative Density, 2007).

The percent relative density and condition of the compacted gravel, based on the *Representative Values of Relative Density* correlation chart, resulted in a value of 49% and a descriptive condition of medium dense. The moist density was used for calculating the percent relative of the pea gravel since the pea gravel is a free draining material and the moisture content is not anticipated to have been significantly high.

The ¾-inch road base appears to have been compacted to approximately 98% of the maximum dry density, based on the proctor curve, and have a percent relative density of 85 (very dense) according to the correlation chart. All values obtained from this correlation chart were calculated based on linear interpolation. Refer to Appendix H – Correlation Charts for the *Representative Values of Relative Density* correlation chart used.

3.5.3.3. Sand Cone Test Results

Determinations of the in-place wet and dry densities of the medium sand (post testing) and coarse sand (around concrete trapezoid prism) were obtained by means of sand cone tests. The calculation portion of the sand cone test first required the determination of the test hole volume, water content of the extracted soil and bulk-density of the calibration sand. The following provide the equations used for each:

- Bulk density of sand:

$$\boldsymbol{\rho_1 = \frac{M_5}{V_1}} \tag{30}$$

where,

ρ_1 = bulk density of sand, lb/ft^3

M_5 = mass of sand to fill calibration container, lb

V_1 = volume of calibration container, ft^3

- Volume of test hole:

$$\boldsymbol{V = \frac{M_1 - M_2}{\rho_1}} \tag{31}$$

where,

$V =$ volume of test hole, ft^3

$M_1 =$ mass of sand used to fill test hole, funnel and base plate, lb

$M_2 =$ mass of sand used to fill funnel and base plate, lb

ρ_1 = bulk density of sand, lb/ft^3

Once all three parameters were obtained, the wet and dry densities were calculate using the following formulas:

- Wet density

$$\boldsymbol{\rho_m = \frac{M_3}{V}} \tag{32}$$

where,

ρ_m = wet density of tested material, lb/ft^3

$V =$ volume of test hole, ft^3

$M_3 =$ moist mass of soil from test hole, lb

- Dry density

$$\boldsymbol{\rho_d = \frac{M_4}{V}} \tag{33}$$

where,

ρ_d = dry density of tested material, lb/ft^3

$V =$ volume of test hole, ft^3

$M_4 =$ dry mass of soil from test hole, lb

Based on the sand-cone tests results, the right top lift of the medium sand evinced a wet density (ρ_w) of 112.4 lb/ft^3, a moisture content (w) of 4.0%, and a resulting dry density

(ρ_d) of 108.1 lb/ft^3. Similarly, the western top lift of medium sand had a ρ_w equal to 110.9 lb/ft^3, a w equal to 3.7% and a ρ_d equal to 107.0 lb/ft^3. Comparing these values with the maximum dry density obtained from the proctor compaction curve results in approximate compactive efforts of 96.5% and 95.5% of the maximum dry density, respectively, for the east and west areas. These same results translate to an approximate percent relative density of 62 (medium dense) for the east medium sand and 61 (medium dense) for the west medium sand based on the *Representative Values of Relative Density* correlation chart developed by McCarthy and presented as Table 4-3 on the *Essentials of Soil Mechanics and Foundations, Basic Geotechnics* book (McCarthy, Representative Values of Relative Density, 2007). Refer to Appendix E – Laboratory Test Results for the recorded and calculated sand cone values for the two tests conducted on the medium sand.

Test results of the coarse sand determined that the top lift of material (on the left side of the concrete trapezoid) had a wet density of 109.0 lb/ft^3, a moisture content of 5.1% and a dry density of 104.8 lb/ft^3. Based on the previously mentioned correlation chart, the percent relative density of the coarse sand resulted in a value of 57% and a descriptive condition of medium dense. Appendix E – Laboratory Test Results provides the test results for this material.

3.5.4. Experimental Test Results of CIP Model

To obtain structure responses of the CIP structure under compression loading, experimental testing was performed. As explained in Section 3.4.6.2, originally only one test was planned to be completed for this model; however, due to bearing failures experienced by the pea gravel during Test No. 1, additional rounds of testing were executed. A total of five tests were performed on the CIP model. During testing, the instrumentation mounted on the models recorded vertical displacements and strains of the inner face of the upper segment, horizontal displacements of the inner faces of the foundations, outward deflection of the box (z-direction), displacements in the x-, y-, and z-directions of the southwest and northeast corners of the soil box for toppling/expansion effects, and vertical deflections of the beam and actuator. The following sections present the results obtained from each round of testing.

3.5.4.1. Test Number 1 – Pea Gravel Backfill

Refer to Figure 33 for the model schematic of this test. Testing of this model was performed until the pea gravel backfill material could not sustain any additional load with increases in actuator displacements and complete bearing failure was experienced. To reach this state, a total of 84 displacement steps were driven by the actuator which resulted in an approximate vertical movement of the loading plate of -1.5729 inches. This distance was calculated by taking the difference between the total actuator's displacement (-1.578284 in) and the total reaction beam deflection (-0.005372). The negative sign indicates downward movement. Note that for this test, the loading plate was positioned with the 10-inch edge located parallel to the culvert span. This positioning was corrected for subsequent tests.

Figure 45 presents the load vs. time and displacement vs. time relationships observed during the first round of testing of the CIP model.

Based on the load vs. time graph, during the majority of testing the loaded pea gravel experienced creep after each displacement step was applied. This behavior was shown by the plotted peak loads followed by a continuous reduction in sustained load prior to the application of the next displacement step. Possible reasons for this trend may have been related to the rearrangement of gravel particles as loading was applied. From approximately

11:51 a.m. the material was unable to sustain additional loading with increases in actuator displacement (method of loading). This was the result of a bearing failure that occurred within the pea gravel soil mass after reaching a maximum load of approximately 4,300 pounds. At this stage, creep occurring within the backfill material was particularly evident since the soil was unable to sustain additional loading and load peaks were rapidly reduced after its initial application.

During testing, the deflection of the inner face of the upper concrete segment was monitored by means of three linear potentiometers. The first was located at the center of the segment (TCY2) and the other two located at the interfaces between the east and west adjacent panels along the centerline (TCY3 and TCY1).

Based on the figure below, deflections of all linear potentiometers were observed to follow a linear pattern up to 11:51 a.m. From that time to the end of testing, or 1:04 p.m., the pea gravel started undergoing a bearing failure and additional loading was not being sustained with increases in actuator distance. Due to this, increases in displacement of the inner concrete panel were observed to remain approximately constant up to the end of testing. Additionally, gauges appeared to rebound during this time between displacement steps. This is seen by the decrease in deflection with time between specific periods (when no additional load was imposed) and the re-engagement of displacement after a new load increment was applied. The rebound is likely the result of the material staying within its linear elastic range and recovering as the load between displacement steps was eased off.

As shown in Figure 45, out of the three gauges, the east potentiometer (TCY3) underwent the greatest deflection during testing. Based on the linear portion of the graph, the west, center, and east instruments experienced maximum deflections of approximately -0.0060 inches, -0.0091 inches, and -0.01091 inches, respectively. A possible reason for the higher east deflection may have been related to the hairline crack that formed along the entire length of the inner interface between the upper and east segments at 11:47 a.m. when a load of approximately 4,000 pounds was applied.

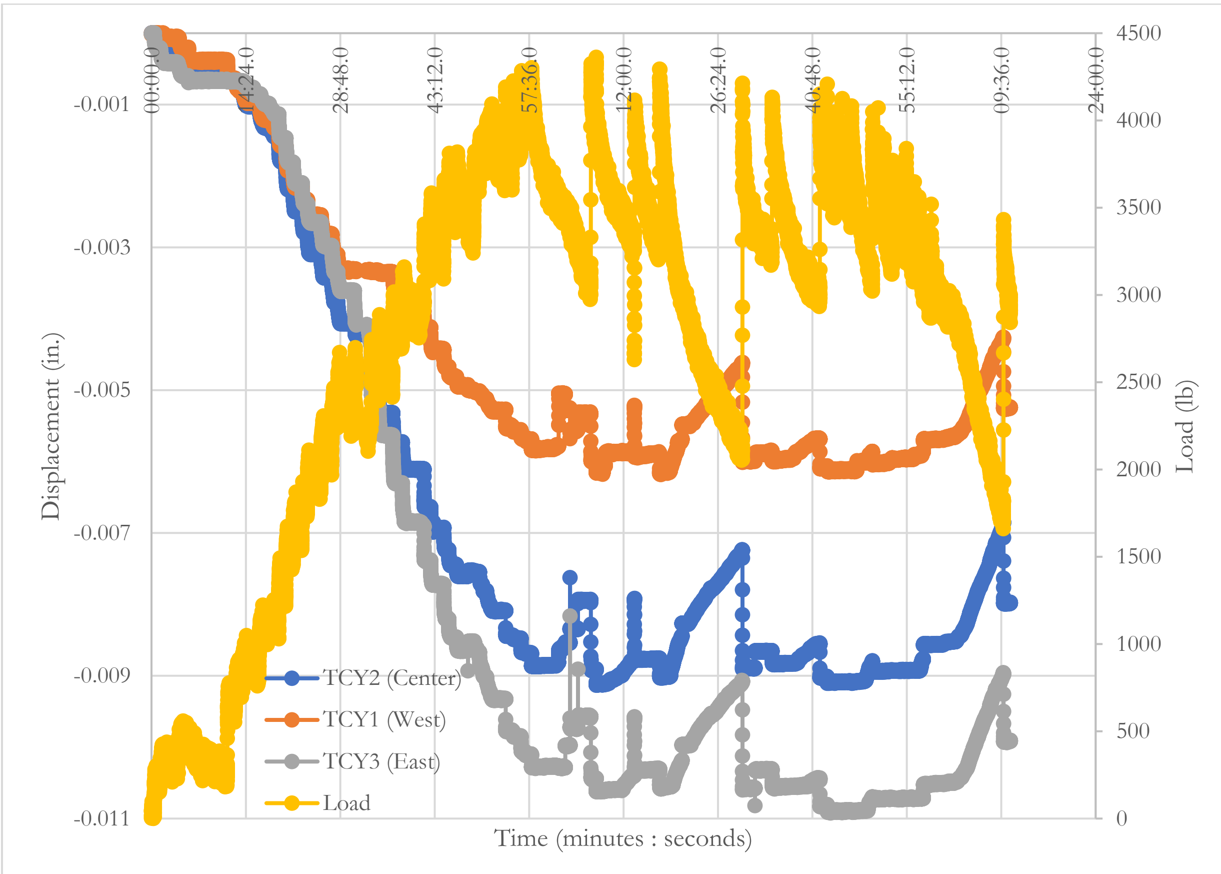

Figure 45 - Load and Displacement vs. Time and Displacement vs. Time Test No. 1

Figure 46 presents the load vs. displacement relationship obtained at the centroid of the upper concrete segment (TCY2). Since the scan rate for the duration of testing corresponded to four readings per second per instrument, the number of data points recorded was approximately 38,700 for each instrument. To reduce the data to a manageable size and ignore the data points that were recorded between load steps, which generally showed constant displacements, only the data points that corresponded to a change in displacement based on an increase in loading were taken into consideration. In addition, information obtained after the bearing failure had occurred (11:51 a.m.) was disregarded since no significant change in displacement was observed during this period of time.

Based on Figure 46, the concrete structure appears to have remained within the linear elastic range during testing since increases in loading were followed by corresponding proportional increases in displacements. Additionally, the maximum loading achieved during testing corresponded to approximately 4,260 pounds. Furthermore, the hairline crack observed during testing does not appear to have affected the strength capacity of the structure. Appendix I – Experimental Test Results presents the raw experimental data obtained for all instruments.

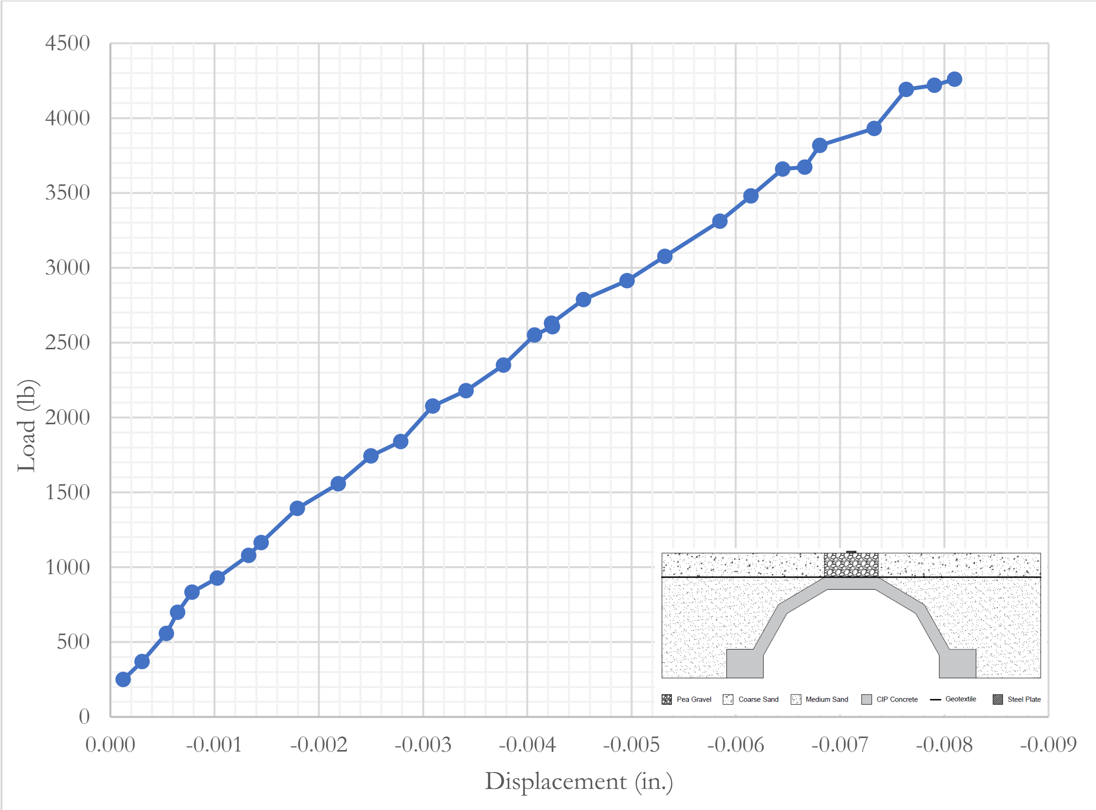

Figure 46 - Load vs. Vertical Displacement Relationship of Upper Concrete Segment at Centroid – Test No. 1

3.5.4.2. Test Number 2 – ¾-inch Road Base Backfill

Refer to Figure 34 for the model schematic of this test. Testing of this model was performed until the ¾-inch road base backfill material could not hold any additional load with increases in actuator displacements and complete bearing failure was experienced, as was the case in Test No. 1. During testing of the ¾-inch road base model a total of 53 displacement steps were driven by the actuator which resulted in an approximate vertical movement of the loading plate of -0.9576 inches. For this test, the loading plate was repositioned with the 10-inch edge located perpendicular to the culvert's span.

As was the case for Test No. 1, this test also evinced significant creep effects after each displacement step was applied. This behavior was likely the result of the punching failure that was occurring within the soil mass as loading was applied and the consequential side displacement of soil particles. From approximately 11:41 a.m. the material was unable to sustain any additional loading with increases in actuator displacement. Once again, this was the result of a bearing failure that occurred within the backfill soil after reaching a maximum load of approximately 5,540 pounds. Based on the maximum load achieved, the ¾-inch road base provided a higher stiffness to the system than the pea gravel material, which failed at 4,260 pounds.

Deflections of all linear potentiometers were observed to follow a linear pattern during testing. From approximately 11:12 a.m., the west gauge showed rebounding after the application of displacement steps. For this test, the center potentiometer recorded the highest deflection with a value of approximately -0.01 inches. The east and west potentiometers recorded maximum displacements of approximately -0.00942 inches and -0.00849, respectively. During testing no additional cracking, other than the hairline crack developed during Test No. 1, was observed.

Figure 47 presents the load vs. time and displacement vs. time relationships of the three upper linear potentiometers observed during the second round of testing of the CIP model.

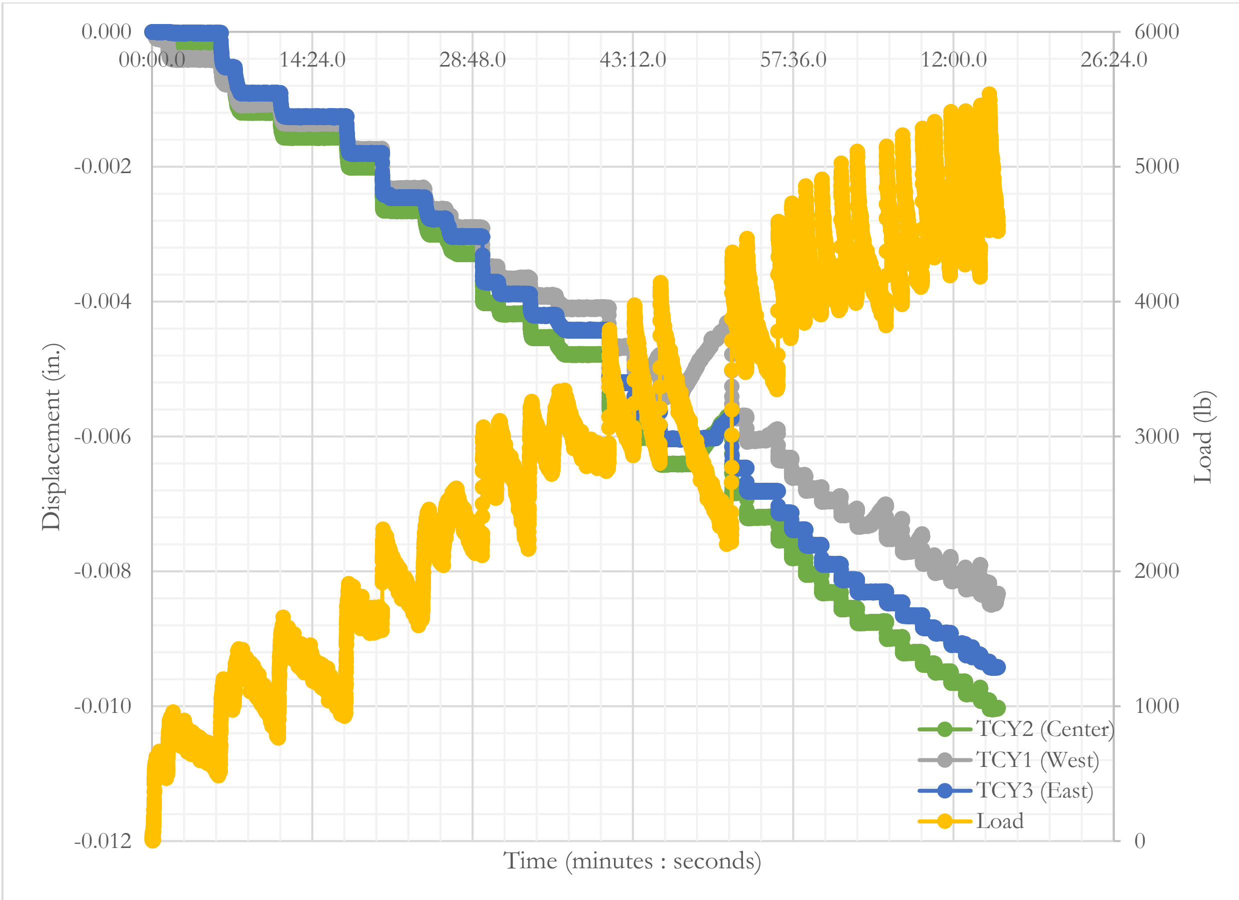

Figure 47 - Load and Displacement vs. Time Test No. 2

Figure 48 presents the load vs. displacement relationship obtained at the centroid of the upper concrete segment (TCY2). As was done for Test No. 1, data reduction activities were performed obtain a manageable data size and ignore irrelevant records.

The load vs. displacement graph presented below evinces a mostly linear relationship throughout the test duration. This suggests that the concrete structure remained within the linear elastic range and no permanent deformation was imposed on the structure. Based on the test results, the inner face of the upper concrete segment began undergoing detectable deflections after a load of approximately 680 pounds was imposed into the model. Maximum loading experienced by the system was approximately 5,500 pounds which resulted in a displacement of the upper concrete panel of approximately -0.01 inches.

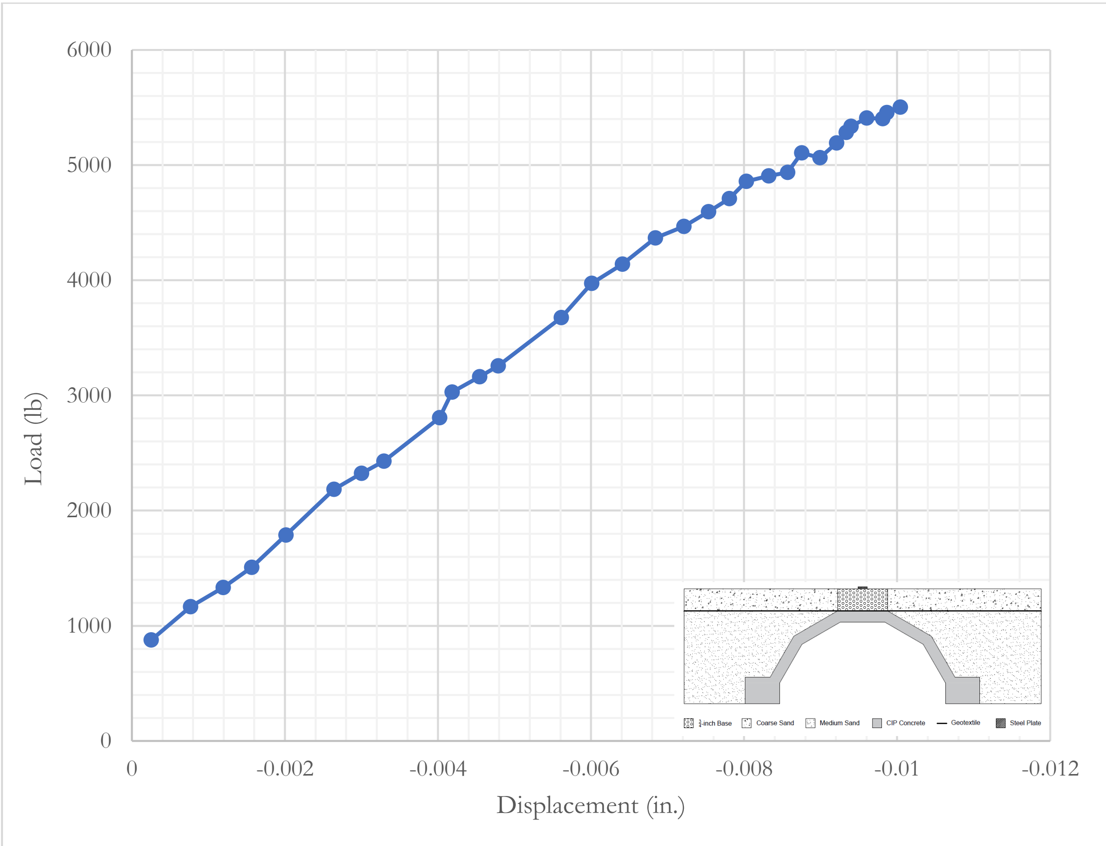

Figure 48 - Load vs. Vertical Displacement Relationship of Upper Concrete Segment at Centroid – Test No. 2

3.5.4.3. Test Number 3 – Concrete Trapezoid Prism and Coarse Sand Backfill

To overcome the bearing failures that were experienced during Tests No. 1 and 2, a concrete trapezoid was erected on top of the upper concrete segment with dimensions that corresponded to a 60° stress distribution of a soil mass. This system replicated an extreme loading condition in which the structure was immediately loaded as would be the case if a truck was travelling directly on top of the culvert. Refer to Figure 35 for the model schematic of this test. Testing of this model was performed until a load of approximately

19,300 pounds was achieved. This represented approximately double the load that the model was intended to sustain.

For this test, a total of 16 displacement steps were driven by the actuator which resulted in an approximate vertical movement of the loading plate of -0.14675 inches. Creep effects were not as evident during this round of testing as compared to Tests. No. 1 and 2. This may be the result of an increase in stiffness of the load distribution material used for testing (concrete vs. soil). On this same note, displacement steps yielded much higher load increments than the previous tests conducted. For this test a maximum load of approximately 19,300 pounds was carried by the arch.

As was the case with the previous two tests, deflections of all linear potentiometers for Test No. 3 were observed to follow a linear pattern. Rebounding effects were not observed at any point during testing in any of the gauges. For this test, the east potentiometer recorded the highest deflection with a value of approximately -0.0396 inches. The center and west potentiometers recorded maximum displacements of approximately -0.0374 inches and -0.0309 inches, respectively. No additional cracking, other than the hairline crack which developed during Test No. 1, was observed.

The following figure presents the load and displacement vs. time relationships observed during the third round of testing of the CIP model.

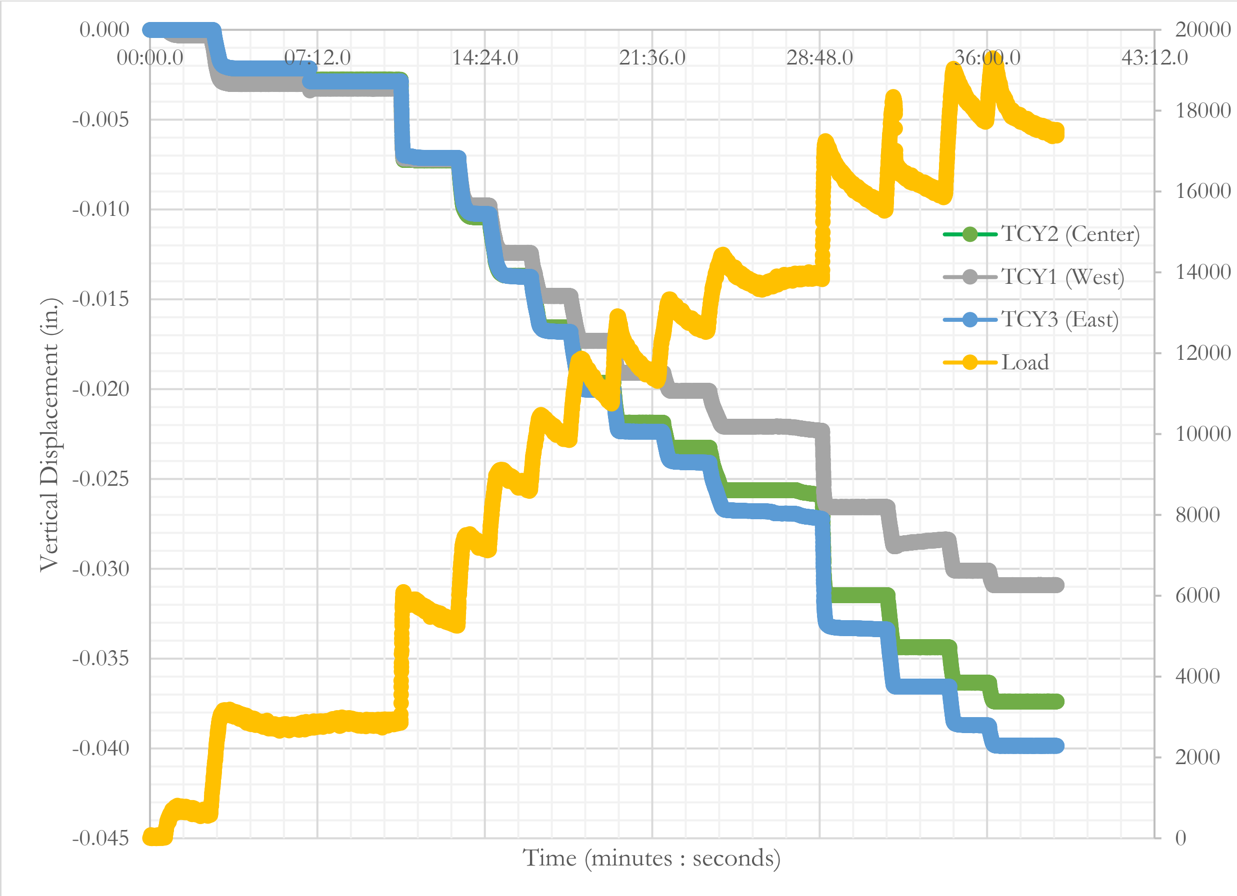

Figure 49 - Load and Displacement vs. Time Test No. 3

Figure 50 presents the load vs. displacement relationship obtained at the centroid of the upper concrete segment (TCY2) throughout Test No. 3. Based on this graph, the concrete structure appears to have remained, once again, within the linear elastic range throughout testing. Maximum displacement experienced by the centroid of the upper panel was approximately -0.03738 inches which corresponded to a load of approximately 19,300 pounds.

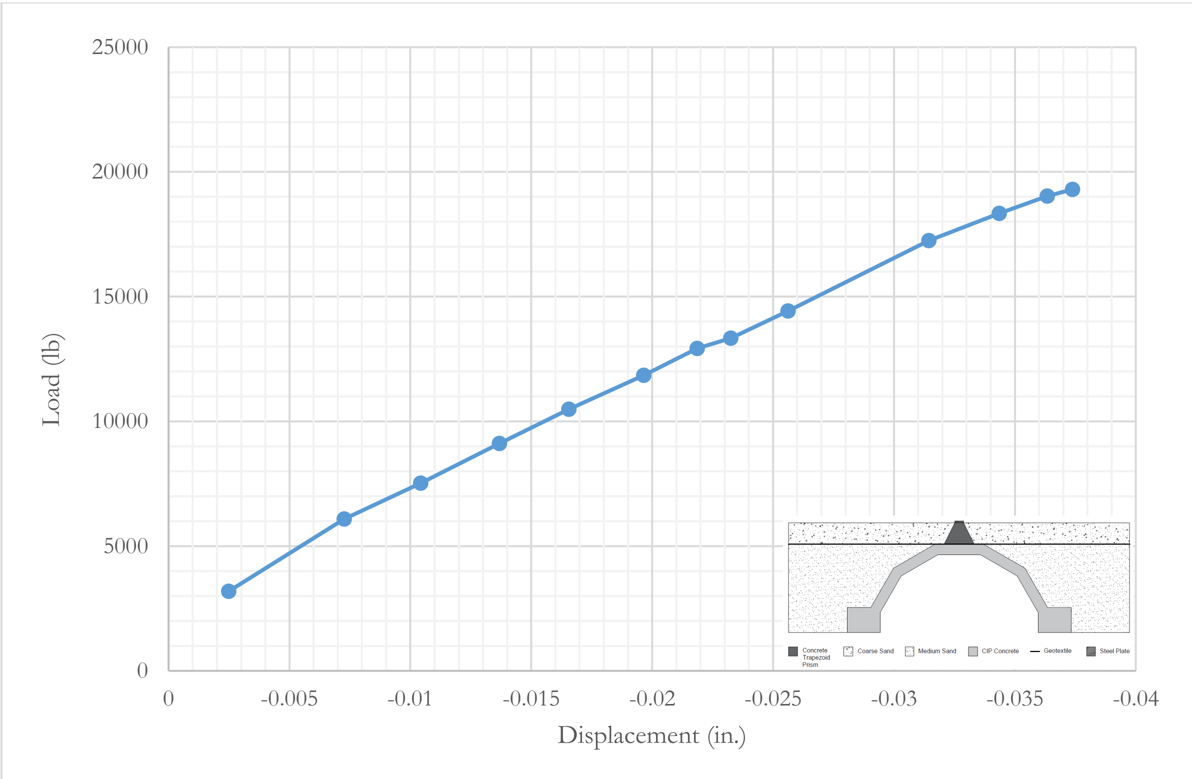

Figure 50 - Load vs. Vertical Displacement Relationship of Upper Concrete Segment at Centroid – Test No. 3

Horizontal movement of the structure was monitored by a set of two linear potentiometers that were positioned in the inner face of the east and west foundations. The following graph shows the displacements obtained for each.

Based on Figure 51, the east and west footings appear to have undergone horizontal deflections of approximately 0.0110 and 0.0126 inches, respectively, during testing. The positive deflections obtained reflect outward movement of the structure, meaning sliding was detected. Comparing the horizontal deflections obtained at the inner face of the footings against the vertical deflection obtained at the centroid of the upper segment results in an approximate outward movement of the east and west faces of 29% and 34% of the vertical displacement, respectively.

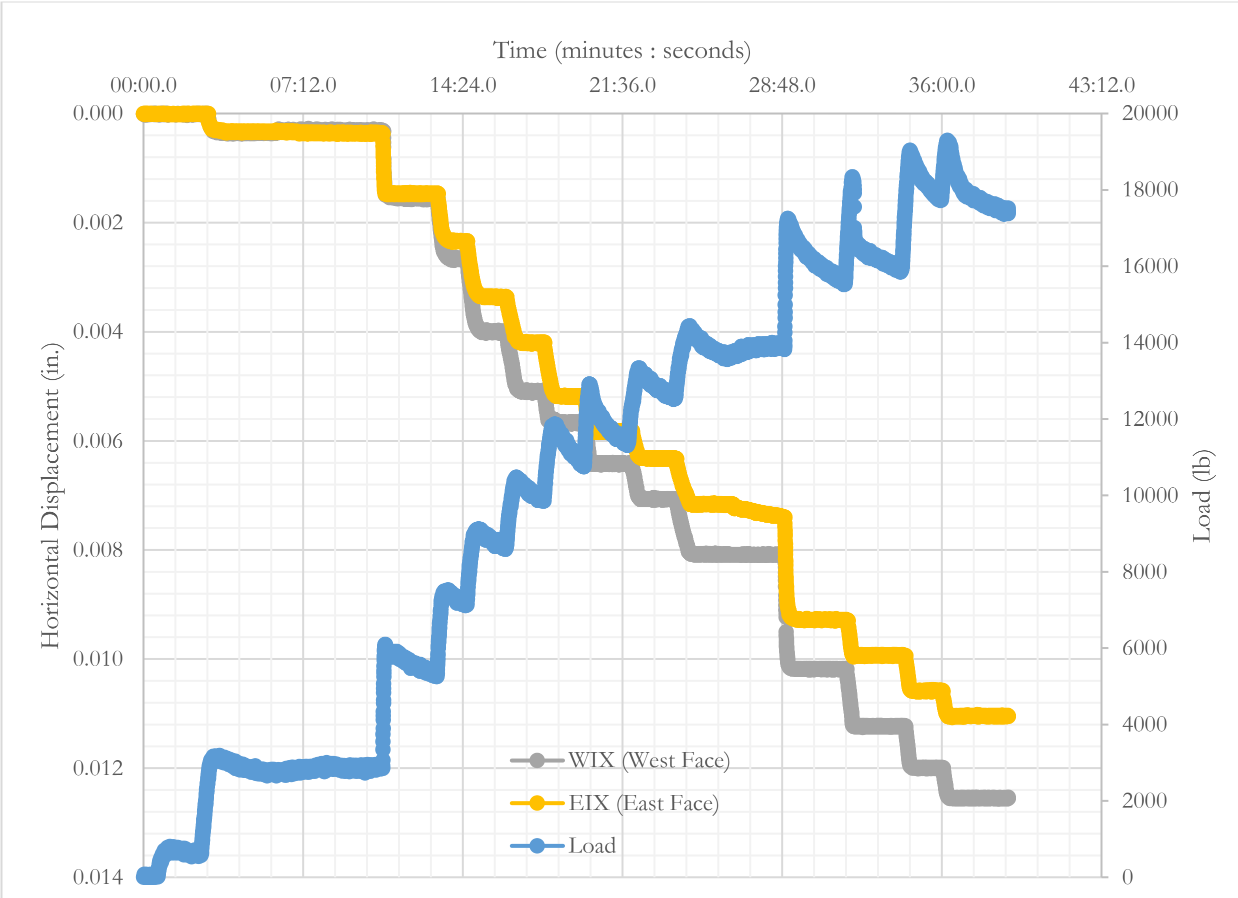

Figure 51 - Load and Horizontal Displacement and vs. Time of Inner Face of Footings – Test No. 3

Strains in the x- and z-directions were also monitored by means of four linear potentiometers positioned along the north, south, east and west edges of the upper concrete segment. Namely, instruments TNX, TSX, TEZ and TWZ were used. Prior to the start of testing, the length of each potentiometer with its corresponding extension were measured. Strains were then obtained by dividing the initial length by the maximum and minimum changes in length recorded by the instrument. In general, instruments TNX, TEZ and TWZ did not evince any major changes in length throughout testing. In fact, data recorded for all three instruments appeared to generally fluctuate between 0.00002 inches and -0.00002 inches, passing through the zero position frequently. TSX, however, did show a higher movement, with a couple of positive peaks at around 12:43 p.m. and 12:56 p.m., when loads of 5,925 lb and 14,442 lb were being imposed on the system, respectively. In addition, some negative peaks were observed towards the end of testing at around 01:04 p.m. and 1:09 p.m., when loads of 17,217 lb and 19,299 lb were being applied.

Table 17 below presents the strain results based on maximum and minimum displacement values obtained during testing for each instrument.

Table 17 - Strains of Upper Concrete Segment

Instrument	Initial Length (in.)	Change in Length (in.)		Strain (in./in.)	
		Max.	Min.	Max.	Min.
TNX	14.500	0.0000314	-0.0000247	0.00000217	-0.00000170
TSX	14.625	0.0001023	-0.0000561	0.00000699	-0.00000384
TEZ	14.750	0.0000372	-0.0000308	0.00000252	-0.00000209
TWZ	14.625	0.0000234	-0.0000265	0.00000160	-0.00000181

The changes in length obtained during experimental testing appear to have been minimal. Based on the accuracy of the instruments used (0.0001 inches), the values obtained may have been highly influenced by the sensitivity of each potentiometer. All in all, significant strains in the x- and z-directions do not appear to have developed during testing in the inner face of the upper concrete segment.

Movement of the soil box walls was also monitored by means of two sets of three linear potentiometers located at the northeast and southwest corners of the model. See Figure 32 for instrument locations.

Figure 52 presents the displacement recorded in the x-direction. Based on this figure, the soil box underwent movement towards the west during testing. This is evinced by the negative displacements recorded by WOX (linear potentiometer shortening) and the positive displacements of EOX (linear potentiometer extending). Movement of the west wall started occurring at approximately 12:46:48 p.m. when an approximate vertical load of 8,600 pounds was being imposed on the system. Conversely, movement of the east wall started occurring at a later time (01:03:12 p.m.), when the actuator was compressing the model with an approximate load of 15,700 pounds. Total displacements of the east and west walls in the x-direction were of 0.00240 inches and -0.00467 inches, respectively. All in all, the model appears to have experienced minor sliding towards the west, with the west wall experiencing almost double the movement than that of the east wall.

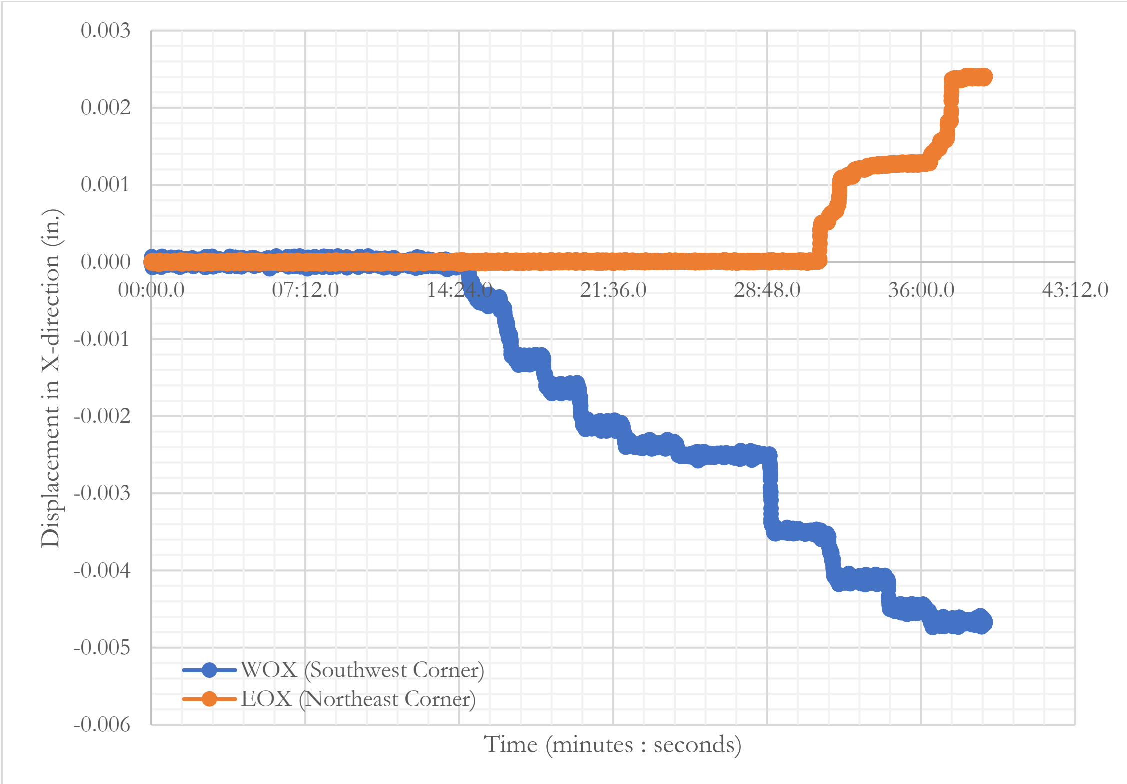

Figure 52 - Displacement of Soil Box in X-Direction – Test No. 3

Figure 53 presents the displacement recorded in the y-direction. Downward movement of the east and west walls were recorded by linear potentiometers TBNY and TBSY. The south portion of the west wall appears to have moved approximately 0.00235 inches downward and the north portion of the east wall approximately 0.00114 inches downward. Detectable displacements at these locations started occurring after an approximate 4,800 pounds compressive load was imposed on the model. Toppling effects do not seem to have occurred during testing.

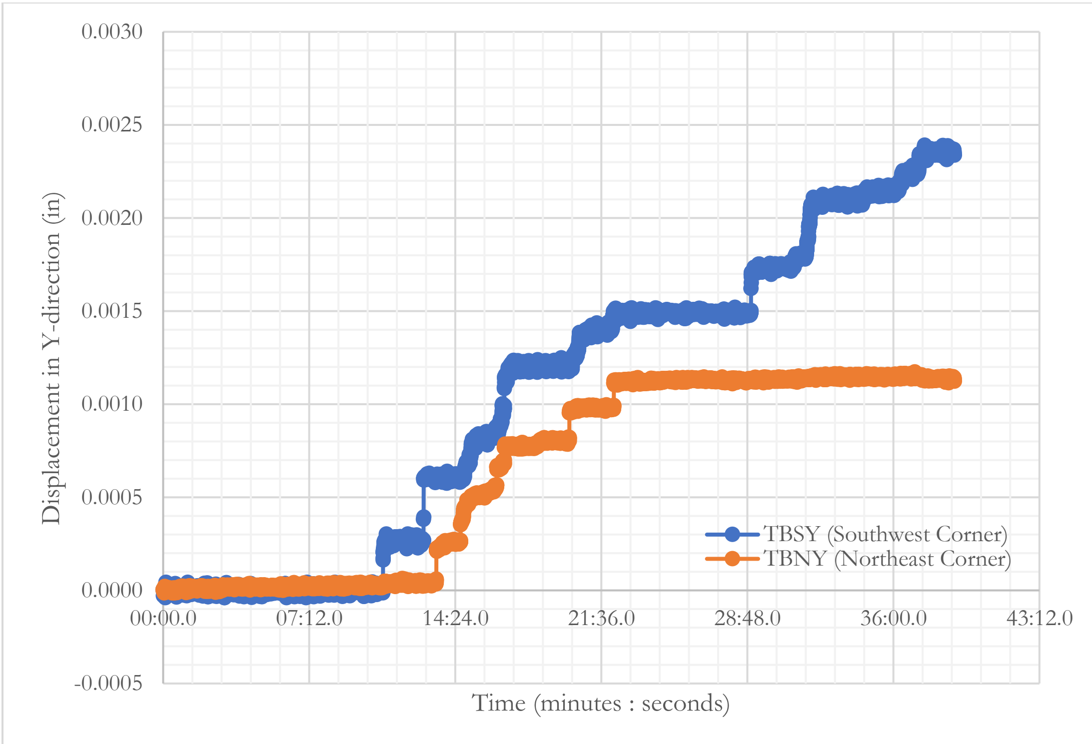

Figure 53 - Displacement of Soil Box in Y-Direction – Test No. 3

Figure 54 presents the displacement recorded in the z-direction. Outward movement of the north and south walls was detected by linear potentiometers NOZ and SOZ. Based on Figure 54, the eastern portion of the north wall underwent an approximate displacement of -0.00328 inches during testing. Similarly, the western portion of the south wall underwent an approximate displacement of -0.00432 inches. The negative signs of both potentiometers, indicate that instruments were contracting and the wall was moving outward.

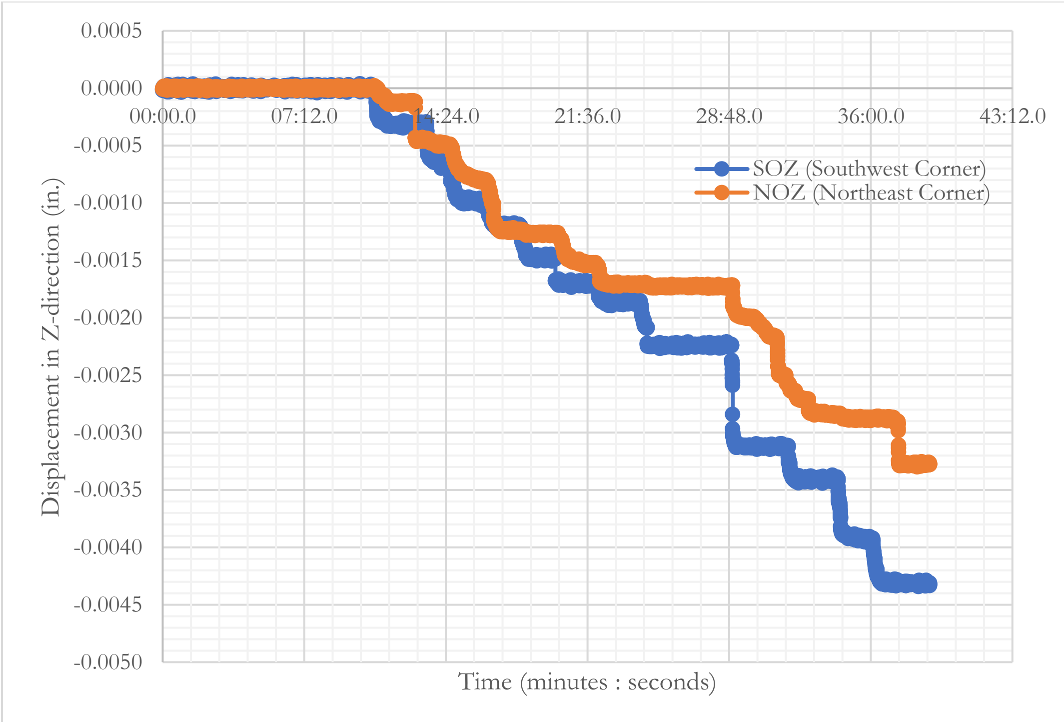

Figure 54 - Displacement of Soil Box in Z-Direction – Test No. 3

3.5.4.4. Test Number 4 – Concrete Trapezoid Prism with no Backfill

To evaluate the strength of the concrete structure without the aid of the backfill material, which ultimately influenced the structure by putting into compression and aiding in obtaining a higher strength, a fourth test was conducted. Refer to Figure 37 for the model schematic of this test. For this test, only the soil placed next to the footings was left in place and the rest of the backfill material was removed from the model. Testing of this model was performed until a load similar to that obtained during Test No. 3 was reached. A total of 10 displacement steps were driven by the actuator which resulted in an approximate vertical movement of the loading plate of -0.1387 inches.

During this round of testing, creep effects were evident after a load of approximately 20,200 pounds was reached. At this point, peaks were observed followed by a decrease in loading immediately after, and a regain in load to a value somewhere between the maximum and minimum peaks. The maximum compressive load obtained during testing corresponded to a value of approximately 21,030 pounds.

In addition, deflections of all linear potentiometers were observed to follow a linear pattern up to approximately 14:39, at which point significantly higher deflections were recorded by all instruments. During this portion of testing, the model was experiencing spikes in loading followed by immediate drops in load and then regain to an “average load”. Similar to Test No. 3, the east potentiometer recorded the highest deflection with a value of approximately -0.08902 inches. The center and west potentiometers recorded maximum displacements of approximately -0.08262 inches and -0.06552 inches, respectively. No additional cracking, other than the hairline crack developed during Test No. 1, was observed during testing. However, the east hairline crack was observed to widen during testing to approximately 1/16-inch.

The following figure presents the load & displacement vs. time relationships observed during the fourth round of testing of the CIP model.

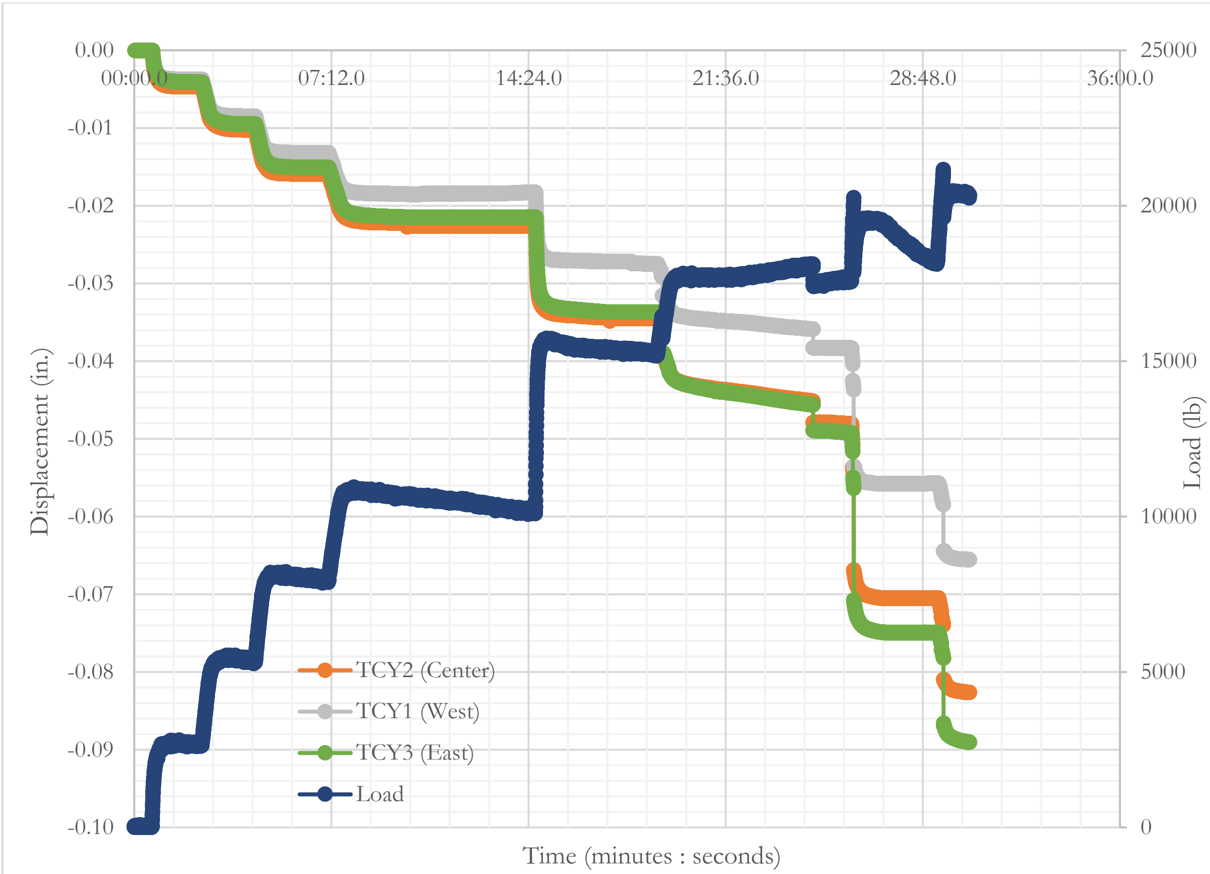

Figure 55 - Load & Displacement vs. Time Test No. 4

Figure 56 presents the load vs. displacement relationship obtained at the centroid of the upper concrete segment (TCY2) throughout Test No. 4. This graph evinces a mostly linear relationship up to a load of approximately 15,700 pounds (yield strength). From a load of 15,700 pounds onward, the structure appears to be within the strain hardening state, and permanent deformation of the structure is anticipated to have developed. During this round of testing, the structure did not reach the ultimate strength and additional cracking, other than the hairline developed as part of Test No. 1, was not observed. Based on the test results, the maximum load experienced by the system was of approximately 21,170 pounds which resulted in a displacement of the upper concrete panel of -0.08261 inches.

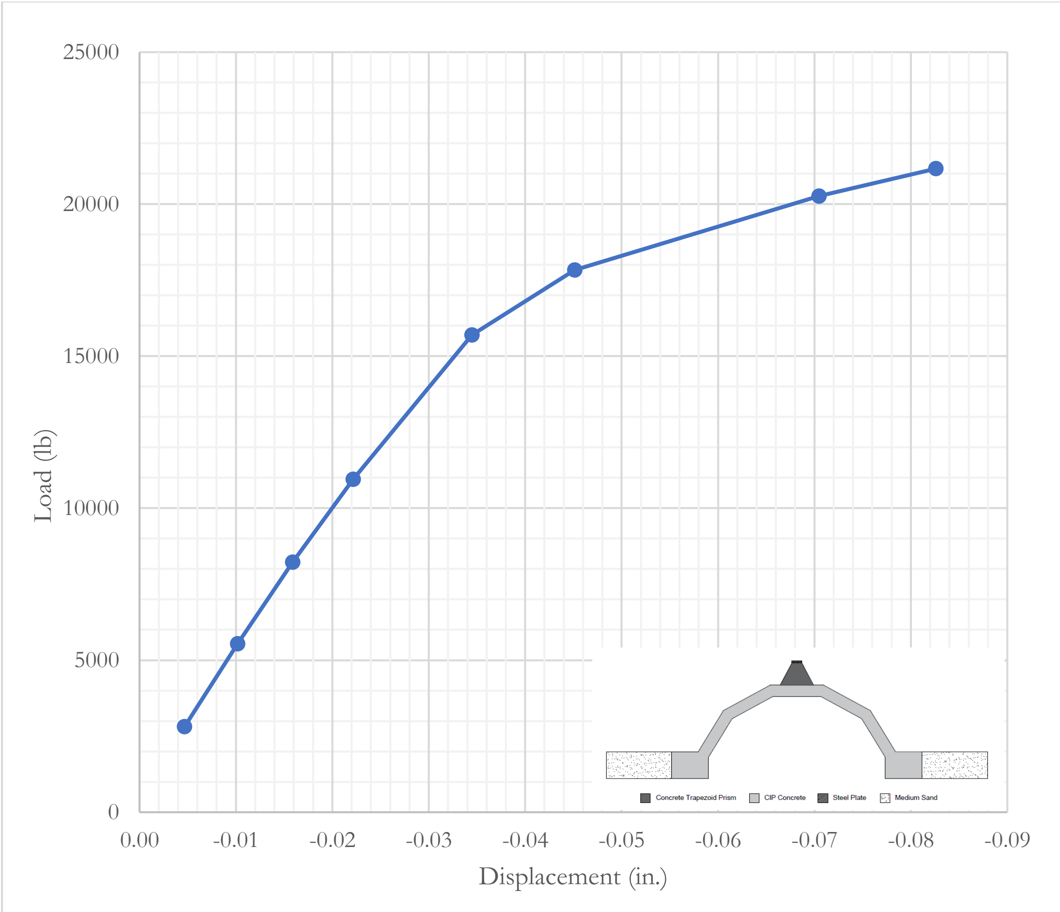

Figure 56 - Load vs. Vertical Displacement Relationship of Upper Concrete Segment at Centroid – Test No. 4

3.5.4.5. Test Number 5 – Concrete Trapezoid Prism with no Backfill to Failure

Test No. 5 consisted of testing the model, once more, without the backfill soil and taking the structure to failure. This test resembled Test No. 4 with the only differences being that the maximum load achieved was higher and only three linear potentiometers were left in place. Refer to Figure 39 for the model schematic of this test. One instrument was used to record vertical deflection at the centroid of the upper concrete panel, and the other two measured lateral deflection of the soil box at the north and south walls. A total of 18 displacement steps were driven by the actuator which resulted in an approximate vertical movement of the loading plate of -0.255 inches.

During this round of testing, creep effects were evident after a load of approximately 19,260 pounds was achieved. As was the case with Test No. 3 and 4, after this load, peaks were observed followed by a decrease in loading immediately after, and a regain in load to a value somewhere between the maximum and minimum peaks. The maximum compressive load reached during testing, which ultimately resulted in failure of the structure, was of approximately 31,270 pounds. Failure of the model is evinced in the above graph by the peak load and the significant decrease in load immediately after.

Additionally, Deflections of the upper concrete segment appeared to follow a somewhat linear pattern up to approximately 15:25. From that point onward, the recorded deflections had a higher increase per displacement step. At approximately 15:36:30 a significant increase in displacement was observed which reflected the failure that occurred within the structure. Total deflection of the center gauge was of approximately -0.254 inches.

Figure 57 presents the load & displacement vs. time relationships observed during the fifth round of testing of the CIP model.

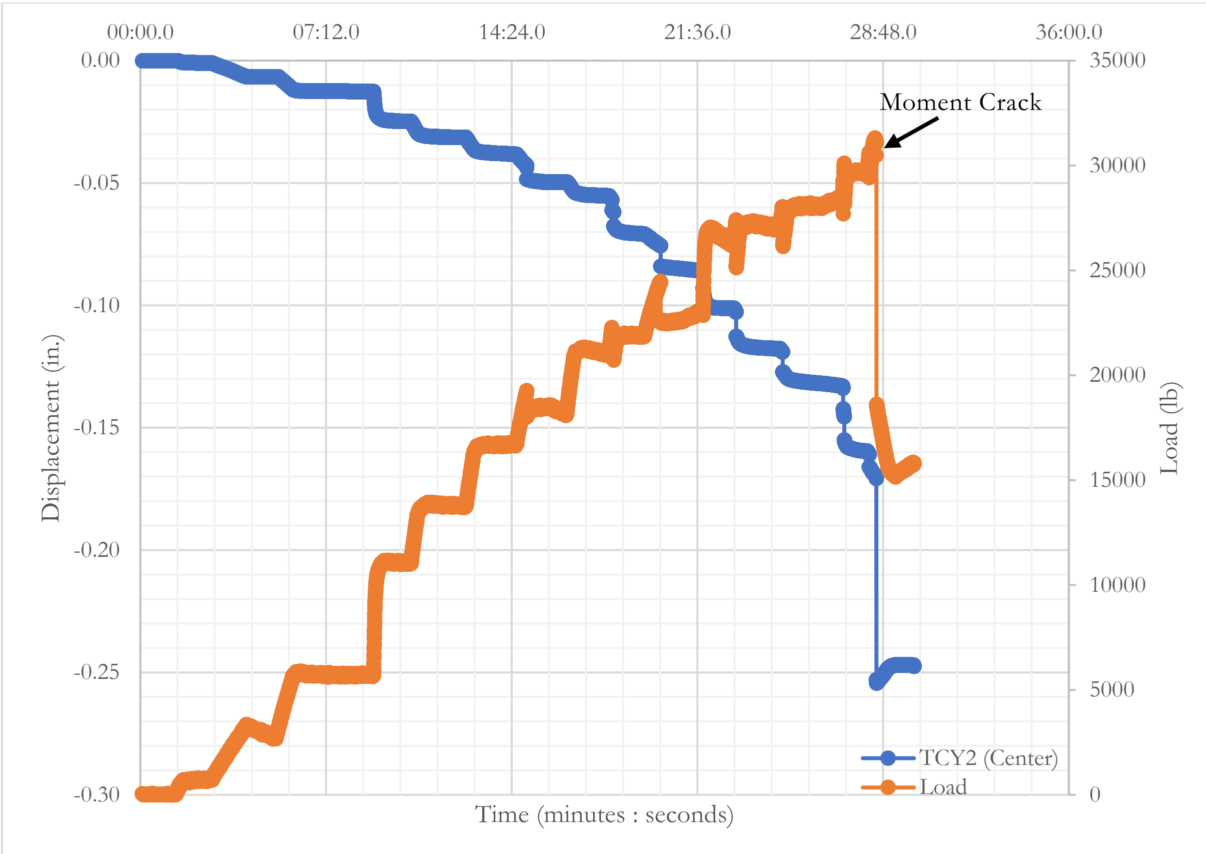

Figure 57 - Load vs. Time Test No. 5

Figure 58 presents the load vs. displacement relationship obtained at the centroid of the upper concrete segment (TCY2) throughout Test No. 5. Similar to Test No. 4, the load vs. displacement graph evinces a mostly linear relationship up to a load of approximately 16,670 pounds. From 16,670 pounds to 30,115 pounds, the structure appears to be within the strain hardening state and the ultimate point is anticipated to correspond to the latter load. From that point onward, the model presents a necking behavior until reaching its final fracturing point at a load of approximately 15,140 pounds.

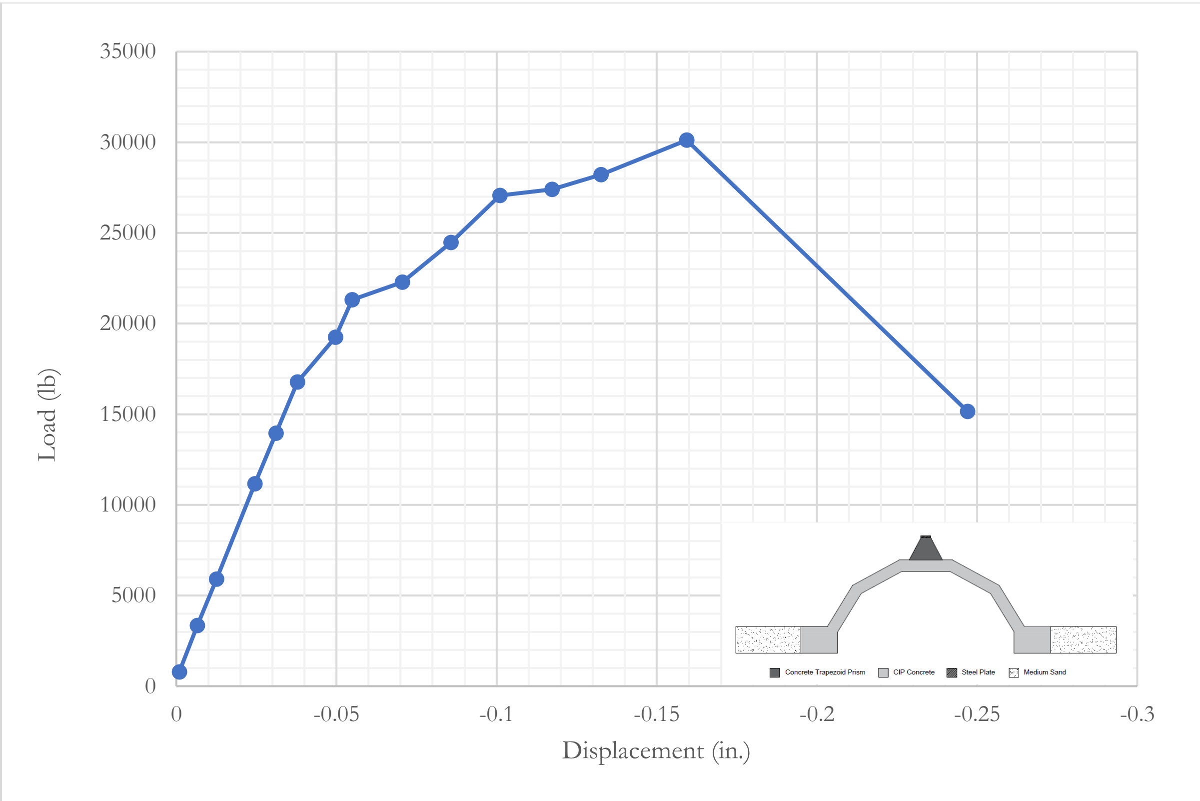

Figure 58 - Load vs. Vertical Displacement Relationship of Upper Concrete Segment at Centroid – Test No. 5

During this round of testing, the hairline crack that developed during Test No. 1 was observed to widen to approximately 1/16-inch during the majority of testing, but prior to fracturing of the structure. In addition, after the last displacement increment, a moment crack developed along the centerline of the upper concrete segment. The crack was observed to extend through the panel’s thickness, meaning the east and west portions of the structure were divided through that crack. Additionally, the hairline crack on the east interface closed once the moment fracture developed; but it extended through the segment’s thickness. Figure 59 through Figure 62 show the cracks observed at the conclusion of Test No. 5.

Figure 59 - Moment crack along centerline and hairline crack along top/east interface. Inner face view (north direction to the left of the photograph).

Figure 60 - Top view of crack at interface between top/east segments. View west.

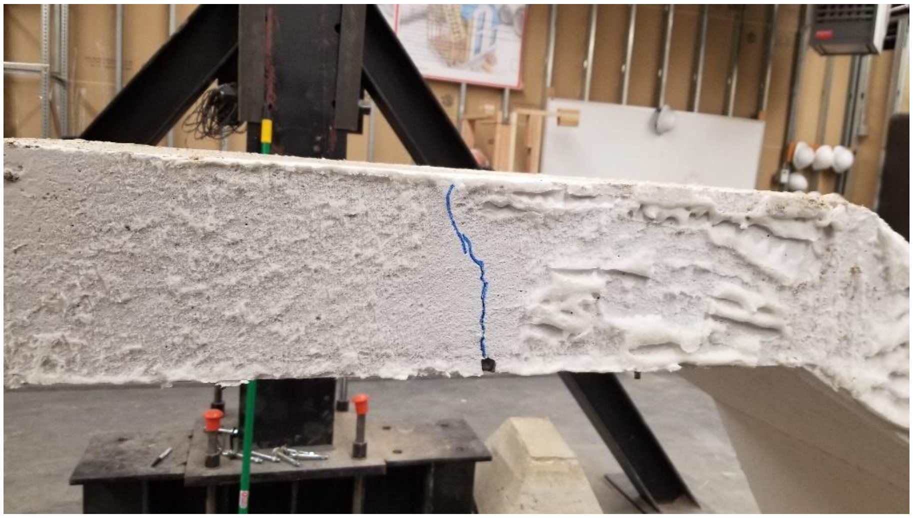

Figure 61 - Moment crack. View South.

Figure 62 - Moment crack. View North.

In addition, movement of the north and south retaining walls was monitored by means of LS1 and LS2 linear potentiometers. For this test, LS2 was relocated to the north (upper center) wall. Data recorded by LS1 and LS2 showed an overall similar behavior and total deflection (0.02 inches of total movement) of the south and north walls. LS1, located on the south wall, presented negative displacements meaning the linear potentiometer was contracting and movement was happening towards the south side. LS2, located on the north wall, displayed positive displacements which resulted in an extension of the instrument and a southward movement. Possible reasons for these results are likely related to the observed southward tilt of the CIP culvert observed prior to the start of experimental testing. This tilt was the result of the non-perpendicularity of some forms when concrete for the culvert was being placed.

Figure 63 presents the movement recorded for LS1 (south wall) and LS2 (north wall).

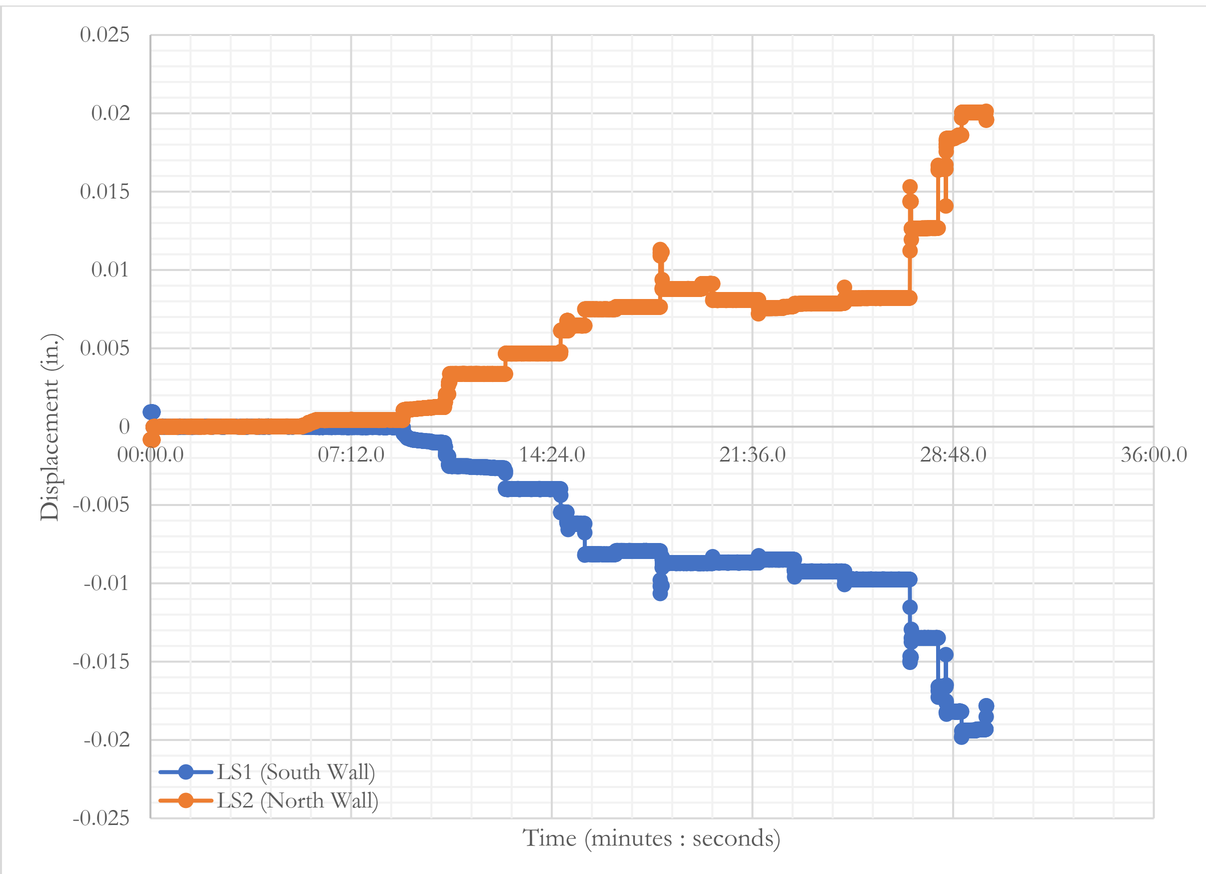

Figure 63 - Displacement in Z-Direction of North and South Walls - Test No. 5

3.5.4.6. Effect of Soil-Structure Interaction

To assess the soil-structure interaction component of the study, the actuator load increment was plotted against the measured deflection in the center of the CIP culvert for all five tests (see Figure 64). In Test No. 3, the steel plate representing the AASHTO traffic load was placed on the concrete trapezoid bearing on the crown of the culvert. The trapezoid was surrounded by compacted soil which did not loosen and cause a reduction in stiffness adjacent to the loaded area. In Tests No. 1 and 2, the load from the steel plate was transferred to the top of the culvert through one foot of compacted soil. The soil failed in bearing above and adjacent to the culvert at loads well below the structural capacity of the arch. In fact, the culvert did not take additional load once the soil failed in bearing below the steel plate. The effect of the bearing failure was to reduce the stiffness of the soil against the haunch area of the culvert which in turn allowed greater deflection of the arch. In Tests No. 4 and 5, the structure itself was tested by removing the soil above the anchor blocks and by applying the load through the concrete trapezoid.

The sequence of tests from Test No. 3 to Tests No. 4/5 represents a reduction in the effect of the soil in restraining the vertical/lateral deformation of the culvert arch. The vertical deflection was greatest where the structure was loaded without soil support and was least where the soil provided a passive resistance against the sides and top of the culvert. In Tests No. 1 and 2, the deflection was intermediate where the soil was present in the haunch area but underwent a bearing failure and thus a loss of confinement in the haunch area of the culvert.

Even though there was some variability in the load-displacement data, the CIP concrete arch exhibited linear elastic behavior during all five tests.

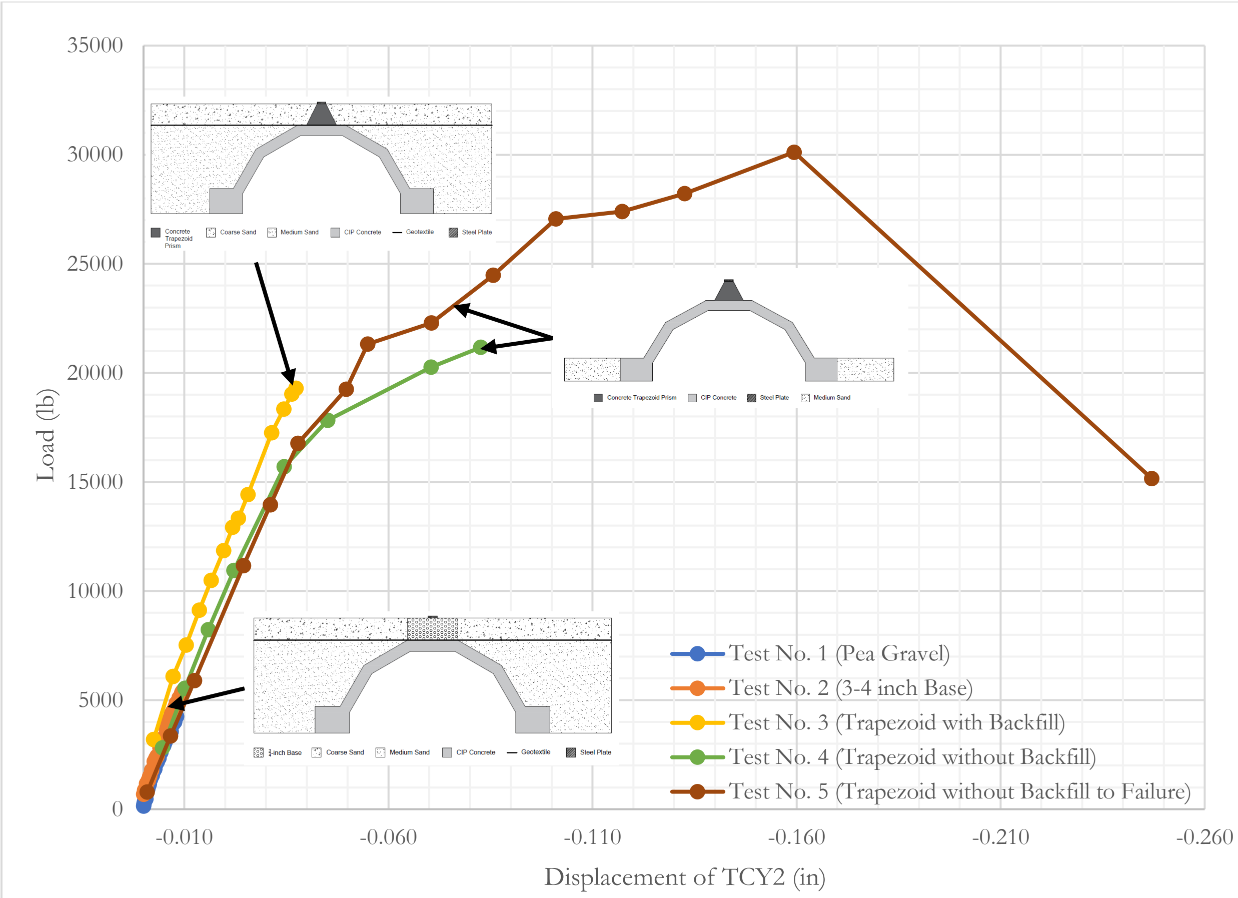

Figure 64 - Compilation of Load vs Displacement Data of TCY2 for all Rounds of Testing

Table 18 was developed to summarize the effect of soil confinement on the deflection (stiffness) of the culvert at common load increments. At a load of 4,000 pounds, Test No. 1 (pea gravel) and Test No. 2 (¾-in. road base) with soil bearing failures showed equal or slightly lower deflections than those measured in the structure itself (Test No. 4 with no backfill soil). However, the crown deflection recorded in Test No. 3 at the same load increment was approximately one-half that experienced in the structure by itself (Test No. 4). In the remaining load increments above 4,000 pounds, lower deflections were recorded when the structure was confined by the surrounding soil. The test results indicated that the effect of the soil-structure interaction increases with increasing load (see Figure 64).

Table 18 - Centroidal Displacement Comparison all Rounds of Testing

	Displacement (in)					Deflection Differences
Load (lb)	Test No. 1	Test No. 2	Test No. 3	Test No. 4	Test No. 5	Test No. 3 vs. Test No. 4/5
4,000	-0.0074	-0.0061	-0.0043	-0.0073	-0.0082	-0.003 to -0.0039
9,000	-	-	-0.0138	-0.0176	-0.0195	-0.0038 to -0.0057
15,000	-	-	-0.027	-0.032	-0.033	-0.005 to -0.006

3.6. Finite Element Method (FEM) Analysis

The second phase of this project entailed modeling the CIP culvert, under the same loading conditions as those described in Section 3.3, using finite element software. The computer program used for the development of the numerical model was ANSYS, Mechanical APDL. ANSYS was the program of choice due to its elastic, inelastic, 2-D and 3-D modeling capabilities and the familiarity that the researcher of this project had with the software. In an effort to develop the most reliable model, 2-D and 3-D simulations were created. Results obtained from these simulations were compared to those obtained during experimental testing to assess the closeness of the two methods of analysis; and subsequently, the FEM model was refined to yield similar responses as those observed in the laboratory. The ultimate goal of the FEM model was to provide a "calibrated" simulation that could be used to obtain structure responses of different underground system configuration.

The following sections present the methods and results of each simulation developed for the CIP culvert.

3.6.1. Model Configuration Methodology

3.6.1.1. Geometric Properties

The numerical CIP model was created to represent the same scale as that of the experimental model. As such, the CIP FEM model had an approximate overall length of 193 inches and a height of 62 inches. The depth component for the 3D simulation was cut in half (15.5 inches) since the stresses and deflections right below the loaded area were of interest. This meant that the model was sliced in the middle (along the long dimension).

For the 2D analysis, Solid, Quad 4 Node 182 (also known as PLANE182) elements were used. In general, PLANE182 elements are defined by four nodes with two degrees of freedom per node which allow for translation in the x- and y- directions. Plasticity, hyperelasticity, stress stiffening, large deflection and large strain capabilities can be assigned to these members (Ansys, Inc., 2018). For the 2-D CIP analysis, a plane stress behavior was selected since the stresses of interest lied mostly on the x- and y-plane and the model was not assumed to be infinitely long.

For the 3D model, solid Brick 8 Node 185 (also known as SOLID185) elements were specified. SOLID185 nodes are defined by eight nodes, each having three degrees of freedom or translation in the x-, y- and z-directions. As with the PLANE182, these elements have plasticity, hyperelasticity, stress stiffening, large deflection and large strain capabilities, in addition to creep.

To create the 2D and 3D configurations, KeyPoints were developed. The KeyPoints reflected vertex locations of different portions of the model which were then connected to create the solid areas. Figure 65 displays the KeyPoints used for both configurations (2D and 3D simulations) for each round of testing. It is important to note that the only difference between Test No. 1 and the subsequent rounds of testing was the position of the loading plate. As it was mentioned in Section 3.4.6.2.1, for Test No.1 the loading plate was misplaced and the long side (10-inch edge) was positioned parallel to the culvert span at the center of the model. To have a fair basis of comparison, the FEM simulation for Test No. 1 reflected this same plate positioning. As such, the Key Points that variated were those specified for the steel plate. Refer to Appendix J – FEM Simulations for KeyPoint numbers and additional geometric information.

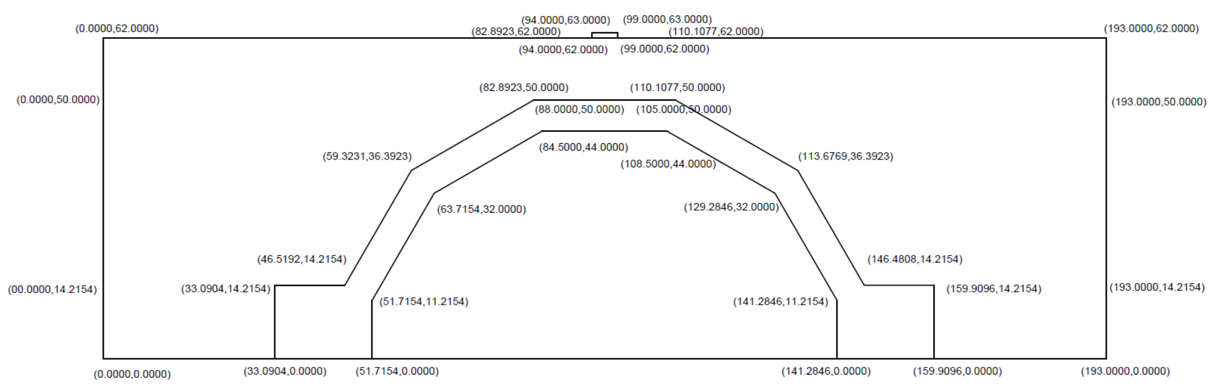

Figure 65 - KeyPoints used for 2D and 3D CIP FEM Models for all Rounds of Testing

To create volumes for the 3D simulation, the previously assembled areas were extruded to half the width of the model. In other words, only the middle half of the structure (in the long direction) was analyzed so that the stresses and displacements right below the loading plate were easily identified.

3.6.1.2. Material Properties

Since the physical CIP concrete structure remained within the linear-elastic range after the application of the 9.03-kip load was imposed, and the culvert did not show significant cracking during this portion of experimental testing, the FEM 2D and 3D simulations only included linear-elastic analyses. As a result, linear, elastic, and isotropic conditions were assigned to the concrete, soil and steel elements. Table 19 below provides the material specifications assigned to each unit.

Table 19 - CIP FEM Material Properties

ID	Material	Modulus of Elasticity (psi)	Poisson's Ratio
1	CIP Concrete	5.35×10^6	0.13
2	Medium Sand	5.2×10^3	0.3
3	Coarse Sand	2.08×10^3	0.35
4	Pea Gravel	13.9×10^3	0.3
5	Steel Plate	29×10^6	0.3
6	¾-inch Road Base	20.8×10^3	0.35
7	Concrete Trapezoid	3.36×10^6	0.2

Values used for the CIP concrete were based on the Modulus of Elasticity and Poisson's Ratio laboratory test results presented in Section 3.5.2.2. For the Rapid Set Concrete Mix trapezoid prism, the modulus of elasticity value was based on the equation presented in ACI 318 (Section 19.2.2.1(a)) which relates the unit weight of concrete with its corresponding compressive strength. This value was preferred over the laboratory test result obtained due to its resemblance with published E modulus ranges for concrete (the laboratory test result was one order of magnitude lower than what the published ranges present). The Poisson's ratio selected for this material was also based on published literature since a Poisson's ratio test was not conducted for the Rapid Set Concrete Mix specimen. See Appendix H – Correlation Charts for published elastic modulus and Poisson's ratio values of concrete.

In addition, material properties of the soil elements were obtained by correlating the lowest unit weight of the compacted sands, pea gravel, and ¾-inch road base to the apparent density and soil condition description (either loose, medium, dense or very dense) of each material, and selecting the corresponding elastic modulus and Poisson's ratio values.

The lowest dry unit weight obtained for the medium sand (well graded sand with silt) resulted in an approximate value of 103.7 pcf which corresponded to a 56% apparent density and a medium dense condition description (McCarthy, Representative Values of Relative Density, 2007). Based on the *Range of Values: Modulus of Elasticity and Poisson's Ratio* table presented in the *Essentials of Soil Mechanics and Foundations, Basic Geotechnics* book by David F. McCarthy, the modulus of elasticity of a medium dense sand generally ranges between 3,500 and 6,950 psi and the Poisson's ratio between 0.25 and 0.4. For the FEM model, a modulus of elasticity and Poisson's ratio of 5,200 psi and 0.3 were used.

For the coarse sand (silty sand), dry unit weight approximations were computed based on the sand cone test performed. Refer to Section 3.5.3.3. for sand cone test results. The dry unit weight of the coarse sand was calculated to be approximately 104.8 pcf which corresponded to a 57% apparent density and a medium dense condition. Based on the previously cited table developed by David F. McCarthy, the modulus of elasticity of a medium dense silty sand generally ranges between 1,042 and 3,125 psi and the Poisson's ratio between 0.2 and 0.4. For the FEM model, a modulus of elasticity and Poisson's ratio of 2,080 psi and 0.35 were used.

The pea gravel (poorly graded gravel) had an approximate moist unit weight of 99.1 pcf which resulted in a 49% apparent density and a medium dense condition. Based on the cited chart above, these values corresponded to a modulus of elasticity of approximately 13,900 psi and a Poisson's ratio of 0.3.

The dry unit weight obtained for the ¾-inch road base (silty gravel with sand) resulted in an approximate value of 134.0 pcf which corresponded to a 85% apparent density and a very dense condition description (McCarthy, Representative Values of Relative Density, 2007). Based on the correlation charts, the modulus of elasticity of a dense sand and gravel ranges between 13,900 and 27,800 psi and the Poisson's ratio between 0.3 and 0.45. For the CIP model, values of 20,800 psi and 0.35 were used for the modulus of elasticity and Poisson's ratio of the ¾-inch road base.

For the steel plate, the material properties used corresponded to those of typical stainless-steel members.

3.6.1.3. Loading Configuration

Loading configurations within the FEM models were setup to mimic the conditions of the physical model. The supports used for the 2D and 3D models included rollers at the right and left face lines of the soil edges to prevent movement from happening in the x-direction. This confinement was provided by the short walls in the physical model. In addition, to simulate the floor connection, all bottom edge lines were fixed. Furthermore, for the 3D model, rollers were placed on the front and back face lines of the culvert and soil edges to confine movement in the z-direction. This retention was provided by the long walls in the physical model.

To model the compressive surface load applied during experimental testing, a line load of 1,806 lb/in acting over a 5-inch length was used for the 2D simulation. Similarly, a pressure of 180.6 ln/in^2 acting over a 5-inch by 10-inch area was used for the 3D model. These values corresponded to a point load of 9.03 kips. Figure 66 provides a graphical representation of the 3D model with the corresponding supports and surface load.

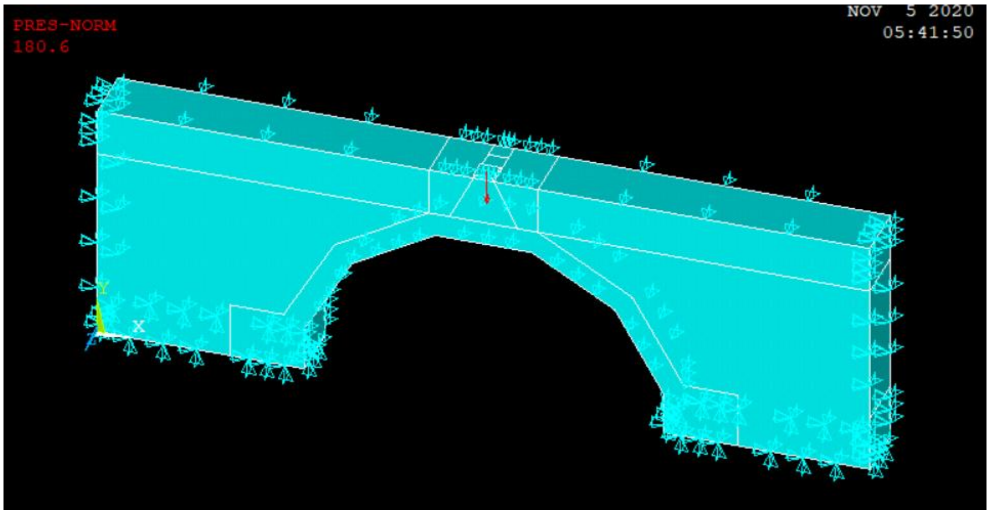

Figure 66 - Loading Configuration Test No. 3 - 3D Model

3.6.1.4. Meshing

Different size meshes were used within the 2D and 3D simulations to provide varying levels of detail within the model. For both models, meshing was done manually, and the element sizes entered attempted to make use of most elements allowed by the software (maximum 256,000 elements). Division numbers were based on the sensitivity of the element within the model. For instance, the loaded soil layer or trapezoid prism had a finer mesh than that used for the bottom sand backfill since more detail was needed for elements located directly below the loaded area.

Table 20 below presents the element sizes used for each material within the 2D and 3D simulations for all rounds of testing.

Table 20 - Mesh divisions used for the 2D and 3D models

Component	Test No. 1		Test No. 2		Test No. 3		Test No. 4	
	2D	3D	2D	3D	2D	3D	2D	3D
CIP Culvert Structure	0.2	1.5	0.2	1.5	0.2	1.5	0.1	1
Medium Sand Backfill (East and West)	1	3	1	3	1	3.0	0.5	2
Coarse Sand Backfill (East and West)	1	3	1	3	1	3.0	0.5	-
Pea Gravel Backfill	0.2	1	-	-	-	-	-	-
Steel Plate	0.5	2	0.5	2	0.5	2.0	0.5	1
3/4-inch Road Base Backfill	-	-	0.2	1	-	-	-	-
Concrete Trapezoid	-	-	-	-	0.2	2.0	0.1	1

Mesh divisions for the 3D models required a coarser mesh for all materials since it in included a depth component.

Figure 67 presents the meshed 2D CIP model for Test No. 3.

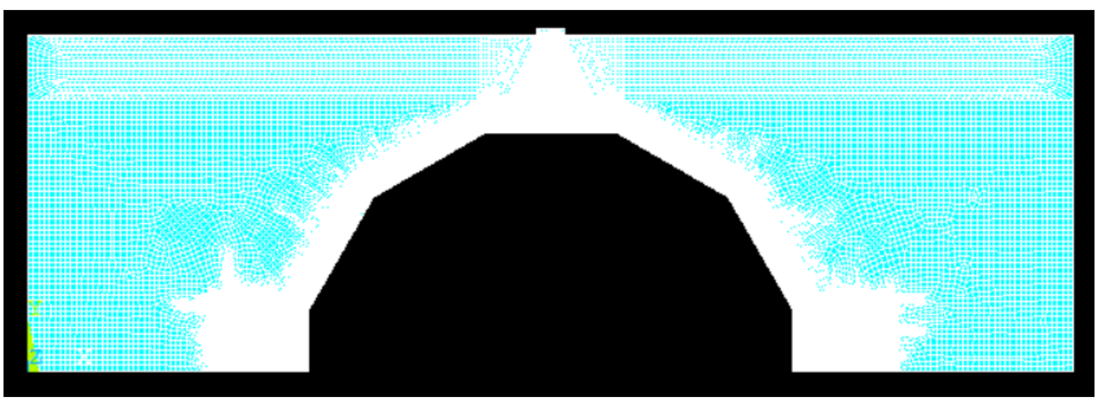

Figure 67 - Meshed 2D CIP Model - Test No. 3

3.6.2. Model Analysis Results

One of the main focuses of this study was to develop a calibrated FEM simulation that could be used to predict structure responses of different culvert configurations under similar loading conditions. To achieve this, a model was developed and refined to first produce similar structure responses as those observed during experimental testing of the CIP model; and then predict the response that a precast hollow core culvert structure would have under similar loading conditions.

The main basis of comparison and refinement between the FEM simulation and the physical model were the displacements and strains obtained at specific locations. In general, longitudinal deflections (y-direction) of interest were obtained at the loading plate, at the interior face of the top segment and at the northeast and southwest corners of the soil box. In addition, transverse deflections and strains (x-direction) were evaluated at the interior faces of the footings and at the interior north and south edges of the top segment. All locations listed matched the areas where potentiometers were mounted on the physical model.

3.6.2.1. Initial Model Predictions

After obtaining the main material properties of the components used for the construction of the CIP model, an initial FEM simulation was developed and analyzed to predict deflections for all rounds of testing. The following table presents the predicted displacements at select model locations for all tests. Note that location designations used match the naming conventions of instrumentation mounted on the physical CIP model.

Table 21 - Displacement Predictions – Tests No. 1 and 2

Location	Location	Displacement (in)			
		Test No. 1		Test No. 2	
		2D	3D	2D	3D
TCY1	Bottom face of top concrete segment, west side, center line, y-direction	-0.11541	-0.0018472	-0.057949	-0.0018410
TCY2	Bottom face of top concrete segment, middle, center line, y-direction	-0.16366	-0.0025828	-0.082483	-0.0025662
TCY3	Bottom face of top concrete segment, east side, center line, y-direction	-0.11540	-0.0018437	-0.057948	-0.0018378
EIX	Interior face of footing, east side, x-direction	0.00053961	0.000039759	0.00027065	0.000039668
WIX	Interior face of footing, west side, x-direction	-0.00053962	-0.000036185	-0.00027065	-0.000036095

Table 22 - Displacement Predictions – Tests No. 3 and 4

Location	Location	Displacement (in)			
		Test No. 3		Test No. 4	
		2D	3D	2D	3D
TCY1	Bottom face of top concrete segment, west side, center line, y-direction	-0.052314	-0.0015632	-0.052738	-0.0018458
TCY2	Bottom face of top concrete segment, middle, center line, y-direction	-0.065989	-0.0019736	-0.067101	-0.0021976
TCY3	Bottom face of top concrete segment, east side, center line, y-direction	-0.052312	-0.0015623	-0.052483	-0.0018481
EIX	Interior face of footing, east side, x-direction	0.00026026	0.000030599	0.00021219	0.000048610
WIX	Interior face of footing, west side, x-direction	-0.00026026	-0.000030998	-0.00022489	-0.000048374

Based on the above predictions, it was anticipated that the upper concrete segment was going to undergo deflections between -0.0018 and -0.16 inches for Test No 1; between -0.0018 and -0.08 inches for Test No. 2; between -0.0016 and -0.066 inches for Test No. 3; and between -0.0018 and -0.067 inches for Test No. 4. This meant that the tests that used soil material on the top and sides of the structures were going to cause higher deflections to the structure than those that used the trapezoid prism with and without soil on the sides. In addition, minimal outward movement of the footings was expected.

The following figures show the nodal plot of the vertical displacements that were predicted for Test No. 1. Similar deformed plots were obtained for the other three rounds of testing. The only difference between each was the amount of displacement predicted by the simulation at each location.

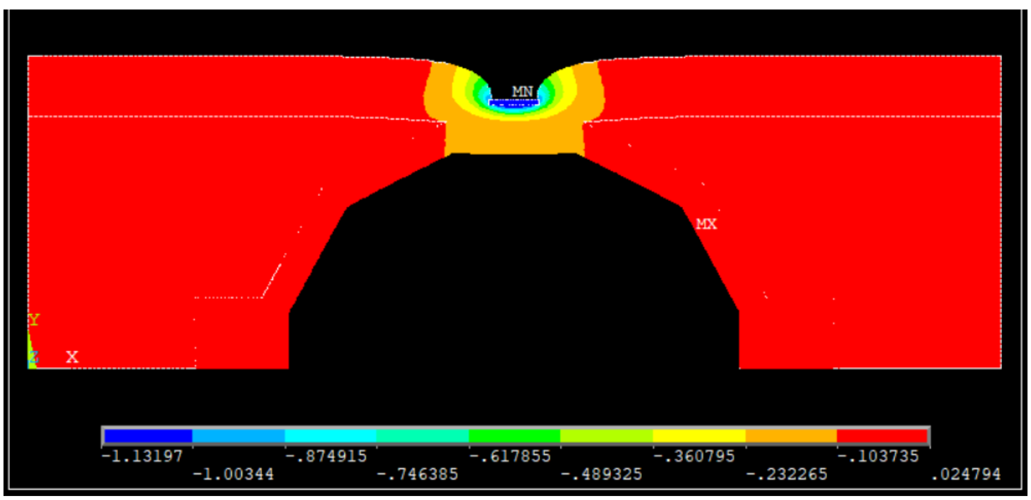

Figure 68 – 2D Nodal Solution of Predicted Displacements for Test No. 1 - CIP Model

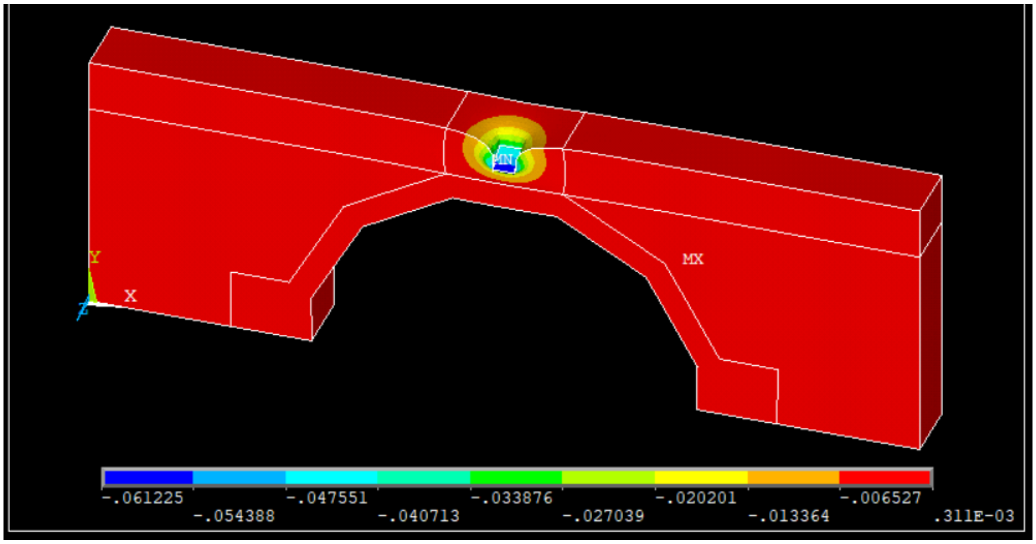

Figure 69 - 3D Nodal Solution of Predicted Displacements for Test No. 1 - CIP Model

Based on the above graphs, the highest deflections were anticipated to occur at and above the upper concrete segment. The rest of the model was not expected to undergo significant displacements.

3.6.2.2. Model Calibration

In order to obtain comparable deflections to those recorded during experimental testing, the ANSYS models for Tests No. 3 and 4 were further refined. Calibration activities mostly entailed refinement of the material properties of the different model elements. The modulus of elasticity and Poisson's ratio of the soil materials were the first parameters changed before the models were rerun. Subsequently, the material properties of the concrete trapezoid prism were refined and, finally, those pertaining to the cast-in-place concrete culvert. Since displacements at the centroid of the inner face of the top segment (TCY2) were of primary interest, calibration activities focused on this location. The following tables presents all runs performed for the 2D and 3D models.

For the first rerun, the modulus of elasticity of the medium sand was decrease to a value of 3,470 psi, which was the lower end of the range presented in the *Range of Values: Modulus of Elasticity and Poisson's Ratio* table developed by David F. McCarthy for a medium dense sand. In addition, the modulus of elasticity of the coarse sand was changed to a value of 1,390 psi, which was the mid-range value given for a silty sand material since this unit had significant fines. The Poisson's ratio values of both materials were left unchanged.

For the second rerun, the modulus of elasticity of the concrete trapezoid prism was lowered to a value of 2×10^6 psi, which was the lower end of the range based on published modulus of elasticity values for concrete. Once again, the Poisson's ratio was left unchanged. For the third rerun, the modulus of elasticity of the CIP concrete was changed to a value of 4.84×10^6 psi. This value was obtained by using ACI's modulus of elasticity equation for concrete which relates the unit weight of the specimen with its unconfined compressive strength. The values used for the unit weight and compressive strength of concrete were based on laboratory test results. See Section 3.5.2.1. For the final round of testing, the modulus of elasticity of the concrete was once again lowered. This time, a value of 2×10^6 psi was used. This was done in order to assess to what extend this material property influenced the displacements obtained.

For Test No. 3, the closest load obtained from the load vs. displacement graph (Figure 50) to the desired half-scale resulting truck load (9.03 kips), was of approximately 9,119 lb. To have a fair basis of comparison between the experimental and numerical data, the ANSYS model for Test No. 3 reflected the same loading conditions. Namely, a point load of 9,119 lb was used which corresponded to a line load of 1823.8 lb/in for the 2D model and a pressure of 182.38 lb/in^2 for the 3D model. The following table provides the displacements obtained at the centroid of the upper concrete segment for Test No. 3. In addition, Figure 70 and Figure 71 present the 2D and 3D nodal plots of the vertical displacements at the centroid for the first rerun. It is important to note that subsequent reruns showed the same overall deformed shape, but deflections obtained varied.

Table 23 - ANSYS Reruns for Test No. 3 - CIP Model

Rerun No.	Material Properties			Test No. 3		
	Type	Modulus of Elasticity, psi	Poisson's Ratio	2D TCY2	3D TCY2	Experimental Testing TCY2
1	CIP Concrete	5.35×10^6	0.13	-0.06698	-0.002001	-0.01369131
	Med. Sand	3.47×10^3	0.3			
	Coarse Sand	1.39×10^3	0.35			
	Steel Plate	29×10^6	0.3			
	Concrete Trapezoid	3.36×10^6	0.2			
2	CIP Concrete	5.35×10^6	0.13	-0.07120	-0.002132	-0.01369131
	Med. Sand	3.47×10^3	0.3			
	Coarse Sand	1.39×10^3	0.35			
	Steel Plate	29×10^6	0.3			
	Concrete Trapezoid	2.00×10^6	0.2			
3	CIP Concrete	4.84×10^6	0.13	-0.07767	-0.002326	-0.01369131
	Med. Sand	3.47×10^3	0.3			
	Coarse Sand	1.39×10^3	0.35			
	Steel Plate	29×10^6	0.3			
	Concrete Trapezoid	2.00×10^6	0.2			
4	CIP Concrete	2.00×10^6	0.13	-0.16784	-0.005004	-0.01369131
	Med. Sand	3.47×10^3	0.3			
	Coarse Sand	1.39×10^3	0.35			
	Steel Plate	29×10^6	0.3			
	Concrete Trapezoid	2.00×10^6	0.2			

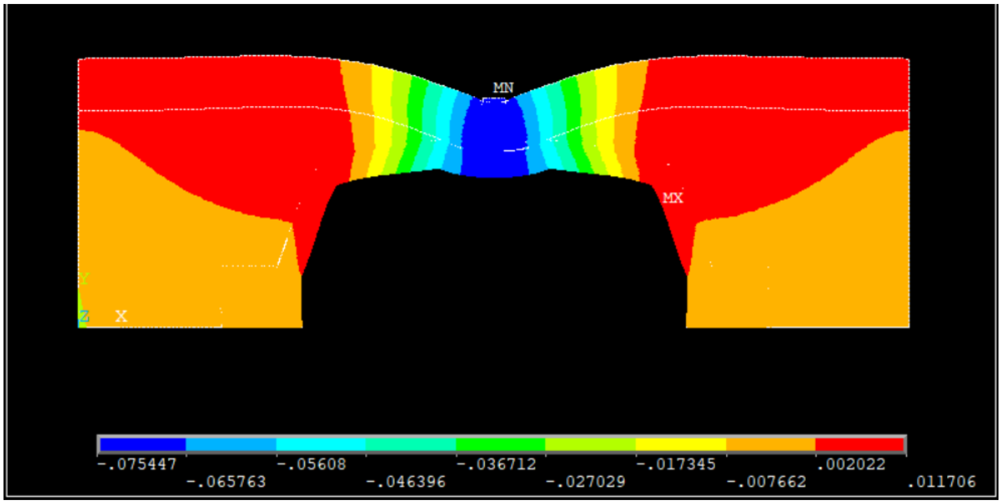

Figure 70 - 2D Rerun No. 1 Nodal Solution for Test No. 3 - CIP Model

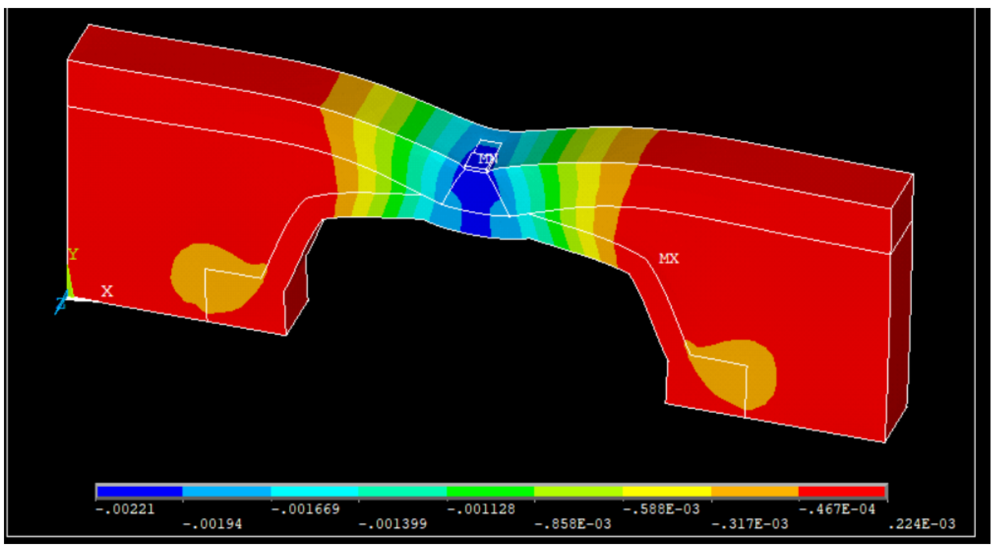

Figure 71 - 3D Rerun No. 1 Nodal Solution for Test No. 3 - CIP Model

For Test No. 4, the closest load obtained from the load vs. displacement graph (Figure 56) to the desired half-scale resulting truck load (9.03 kips), was of approximately 10,947 lb. To have a fair basis of comparison between the experimental and numerical data, the ANSYS model for Test No. 4 reflected the same loading conditions, meaning a load of 10,947 pounds was imposed on the system. Namely, a point load of 10,947 lb was used which corresponded to a line load of 2189.4 lb/in for the 2D model and a pressure of

218.94 lb/in^2 for the 3D model. The following table provides the displacements obtained at the centroid of the upper concrete segment for Test No. 4. In addition, present the 2D and 3D nodal plots of the vertical displacements at the centroid for the second rerun. It is important to note that subsequent reruns showed the same overall deformed shape, but deflections obtained varied.

Table 24 - ANSYS Reruns for Test No. 4 - CIP Model

Rerun No.	Material Properties			Test No. 4		
	Type	Modulus of Elasticity, psi	Poisson's Ratio	2D[1] TCY2	3D[1] TCY2	Experimental Testing[1] TCY2
1	CIP Concrete	5.35×10^6	0.13	-0.08136	-0.002879	-0.022154
	Med. Sand	3.47×10^3	0.3			
	Coarse Sand	1.39×10^3	0.35			
	Pea Gravel	10.4×10^3	0.3			
	Steel Plate	29×10^6	0.3			
	3/4-inch Road Base	3.12×10^3	0.3			
	Concrete Trapezoid	3.36×10^6	0.2			
2	CIP Concrete	5.35×10^6	0.13	-0.08650	-0.003062	-0.022154
	Med. Sand	3.47×10^3	0.3			
	Coarse Sand	1.39×10^3	0.35			
	Pea Gravel	10.4×10^3	0.3			
	Steel Plate	29×10^6	0.3			
	3/4-inch Road Base	3.12×10^3	0.3			
	Concrete Trapezoid	2.00×10^6	0.2			
3	CIP Concrete	4.84×10^6	0.13	-0.09445	-0.003345	-0.022154
	Med. Sand	3.47×10^3	0.3			
	Coarse Sand	1.39×10^3	0.35			
	Pea Gravel	10.4×10^3	0.3			
	Steel Plate	29×10^6	0.3			
	3/4-inch Road Base	3.12×10^3	0.3			
	Concrete Trapezoid	2.00×10^6	0.2			

Rerun No.	Material Properties			Test No. 4		
	Type	Modulus of Elasticity, psi	Poisson's Ratio	2D[1] TCY2	3D[1] TCY2	Experimental Testing[1] TCY2
4	CIP Concrete	2.00×10^6	0.13	-0.20733	-0.005829	-0.022154
	Med. Sand	3.47×10^3	0.3			
	Coarse Sand	1.39×10^3	0.35			
	Pea Gravel	10.4×10^3	0.3			
	Steel Plate	29×10^6	0.3			
	3/4-inch Road Base	3.12×10^3	0.3			
	Concrete Trapezoid	2.00×10^6	0.2			

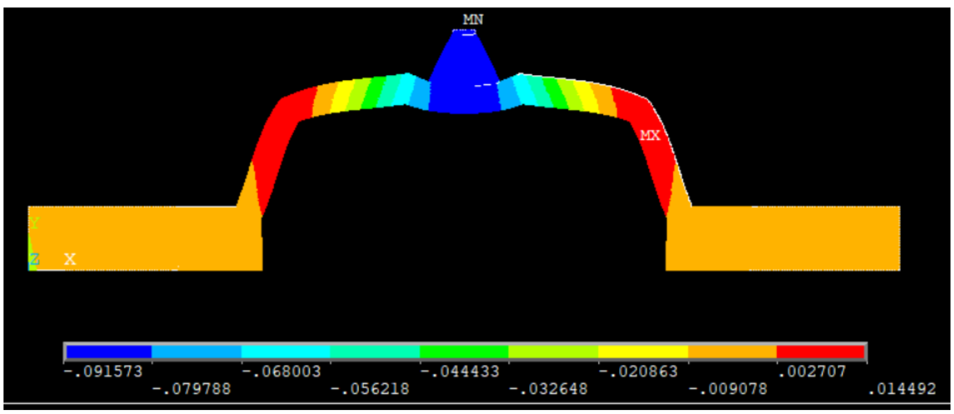

Figure 72 - 2D Rerun No. 2 Nodal Solution for Test No. 4 - CIP Model

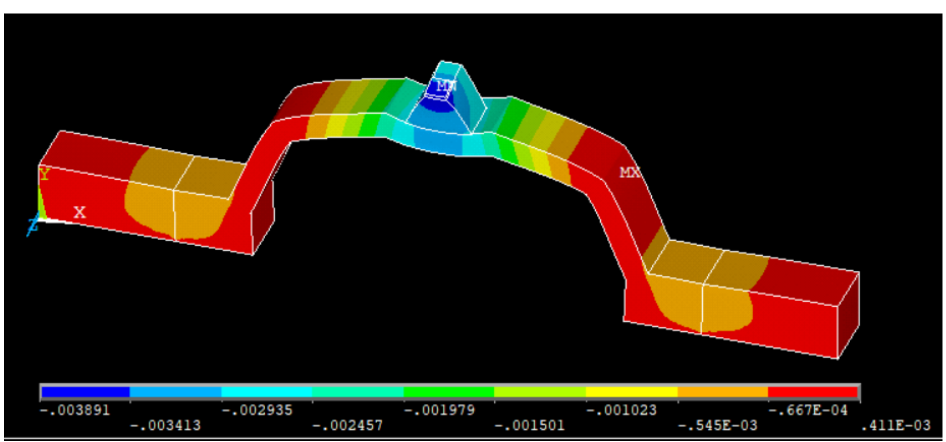

Figure 73 - 3D Rerun No. 2 Nodal Solution for Test No. 4 - CIP Model

Based on the above results, it is evident that the 2D simulations were over-predicting the deflections of the center gauge for all reruns and tests; and the 3D models were underpredicting the displacements of the center gauge for all reruns and tests. The overprediction of the 2D model was expected, as these simulations were more simplified by not taking into consideration the depth component of the geometry. However, the 3D models were expected to show closer results to the ones obtained experimentally.

In general, the 2D models overpredicted the displacements of the center gauge by approximately between 389% and 467% for Test No. 3, and between 267% and 326% for Test No. 4 for the first 3 reruns. The fourth rerun for the 2D models had an exponentially higher overprediction. However, the modulus of elasticity of the concrete used for this rerun was highly questionable. In addition, the 3D models underpredicted the displacements of the center gauge by approximately between 83% and 87% for both tests. Once again, rerun number 4 had a smaller underprediction (between 63% and 68%), but the values used for the CIP concrete was not realistic.

In an effort to check the ANSYS displacements obtained, structural analysis of the top concrete segment (beam analysis) was conducted. STAAD Pro was the program used to perform this analysis. Results obtained from the simulation was then compared to those obtained for the predictions of Test No. 4 to evaluate if the ANSYS models were providing erroneous data.

Since it was not known if the connections between the upper concrete segment and the east and west adjacent segments were fixed or pinned; two configurations, one using fixed reactions and another using pinned reactions, were developed for the beam model. For all analyses, the self-weight of the beam, as well as the weight imposed by the trapezoid prism and the steel plate were included in addition to the applied line load of 531.2 lb/in (6,370 lb/ft), corresponding to a point load of approximately 9.03 kips applied 12 inches above the segment and having a 60º load distribution. To closely replicate the conditions specified in the ANSYS program, the material properties assigned to the concrete beam were based on laboratory test results.

- Top beam analysis - fixed connection

  The following figure presents the load diagram analyzed for the fixed beam reaction simulation, along with the displacement plot. Refer to Appendix K – STAAD Analyses for additional analysis data including, reactions and shear and moment diagrams.

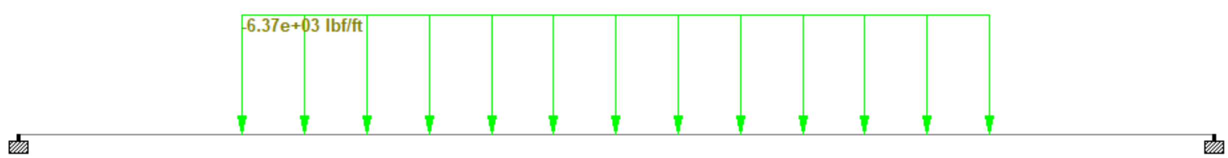

Figure 74 - STAAD Load Diagram 27-inch Beam - Fixed Connection

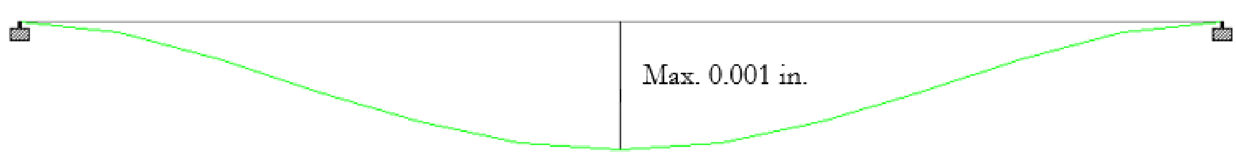

Figure 75 - STAAD Displacement Diagram 27-inch Beam - Fixed Connection

- Top beam analysis – pinned connection

  The following figure presents the displacement plot output of the pinned beam reaction simulation. Refer to Appendix K – STAAD Analyses for additional analysis data including, reactions and shear and moment diagrams.

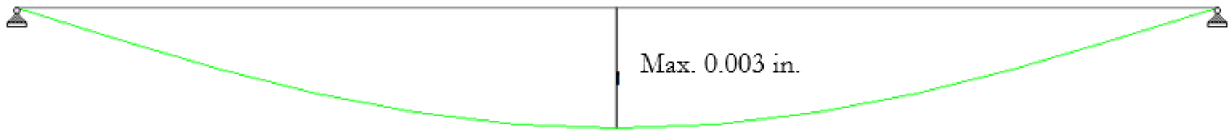

Figure 76 - STAAD Displacement Diagram 27-inch Beam - Pinned Connection

Based on the above figures, the STAAD program predicted center beam deflections of -0.001 inches and -0.003 inches for the fixed and pinned connections, respectively. These results go hand in hand with the displacement predictions that the ANSYS program provided for Test No. 4; namely, -0.0022. This means that, from a structural stand-point, the ANSYS program appears to be outputting realistic results when the top beam is analyzed as a beam. However, the geometry of the culvert may be playing a role when it comes to the interaction between the upper segment and the adjacent east and west sections.

To assess if the ANSYS program may take into consideration the impacts of this geometry, the top three members were analyzed. Results for a fixed simulation are provided below.

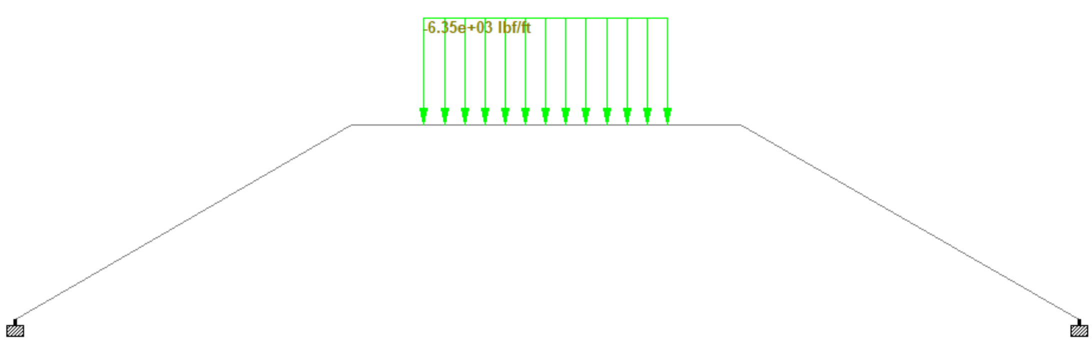

Figure 77 - STAAD Load Diagram Three 27-inch Segments - Fixed Connection

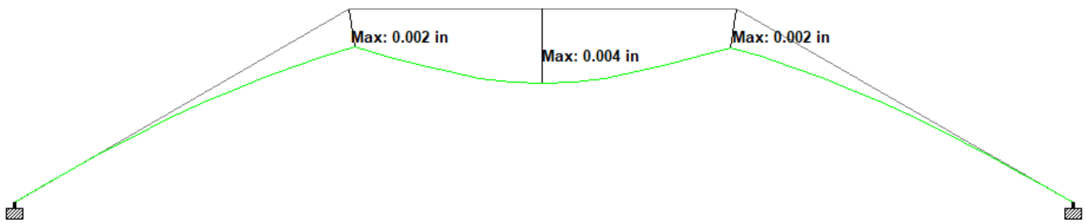

Figure 78 - STAAD Displacement Diagram Three 27-inch Segments - Fixed Connection

Based on Figure 78, a center beam deflection of -0.004 inches was predicted. This result is approximately one order of magnitude lower than the deflection obtained experimentally. Once again, the difference in displacements appears to be the result of the inability of the computer program to take into considerations internal forces that are likely to be acting within the system.

Since the model is not a perfect arch and the adjacent segments have a shallow angle with respect to the horizontal plane (30°), the model may be acting more like a longer beam with the adjacent segments attached to it. In other words, instead of having a 27-inch-long upper section, the model itself may acting more as a 81-inch long beam.

To evaluate this conclusion, a third set of structural analysis was performed. This time, a beam length of three times the segment length was used. Results for the fixed simulation is provided below.

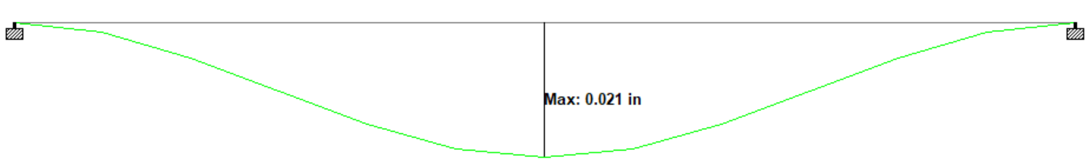

Figure 79 - STAAD Displacement Diagram 81-inch Beam - Fixed Connection

The displacement obtained for the fixed connection of the longer beam appears to resemble more closely the results obtained experimentally for Test No. 4 of the CIP model. Namely, the STAAD analysis predicts a deflection of -0.021 inches at the center of the member and the experimental results show a displacement of -0.0022 inches at this same location. This supports, to some extent, the thesis statement presented previously which attempted to explain the difference obtained between the experimental results and the numerical outputs.

Chapter 4: Precast Hollow-Core Culvert Model

4.1. Introduction

The purpose of the precast model was to assess how a hollow-core concrete culvert would perform under an applied 9-kip load, reduced for a half-scale model. Results from this testing were compared to those obtained from the CIP model and performance assessment of the two was conducted. As with the CIP model, the hollow-core model included two phases of analysis: experimental testing and finite element modeling. The latter was utilized to first, predict the behavior of the hollow-core model under the previously mentioned load, and later, refine the model based on the experimental data obtained.

The assembled hollow-core model followed the same geometry used for the construction of the CIP model to provide a comparable design. The following sections present information pertinent to the hollow-core model design, methodologies, laboratory and experimental results, and FEM analyses.

4.2. Hollow Core Culvert Model Design

The arch geometry utilized for the assemblage of the hollow-core model as well as the construction of the CIP culvert was mainly dictated by the geometry that hollow-core panels are typically fabricated to in precast plants and the shape that an assembly of five of those panels would make to forma an arch culvert. To provide an arch-like geometry, these segments were connected at 30º angle between the top segment and the adjacent east and west sections, and at a 60º angle between the east and west adjacent sections and the bottom segments. In addition, two footings, with dimensions of 18.6-inch × 14.2-inch × 31-inch, each, were placed at each end to provide support for the structure. Footings were spaced approximately 89.5 inches apart.

To replicate the conditions around a typical culvert, as was done with the CIP model, a soil box was erected around the precast structure. The box walls used for this model were the same ones used in the construction of the CIP model. Refer to Section 3.4.1 for additional information on wall dimensions, materials and location. For the first and second tests, the spaces in between the culvert and the walls were filled with medium sand from the bottom footing elevation to a height of 50 inches, or the top of the concrete structure, and with coarse sand from a height of 50 inches to a height of 62 inches on either side of the top concrete segment. From the top segment to a height of 62 inches, the volume was filled with ¾-inch road base for the first test, or a concrete trapezoid prism backfilled with coarse sand for the second test. Figure 80 below presents the side view of the hollow-core culvert with dimensions and material types. Note that the location of the concrete trapezoid prism is provided by means of red lines above the top segment, for reference, and was only used to conduct the second and third hollow-core tests.

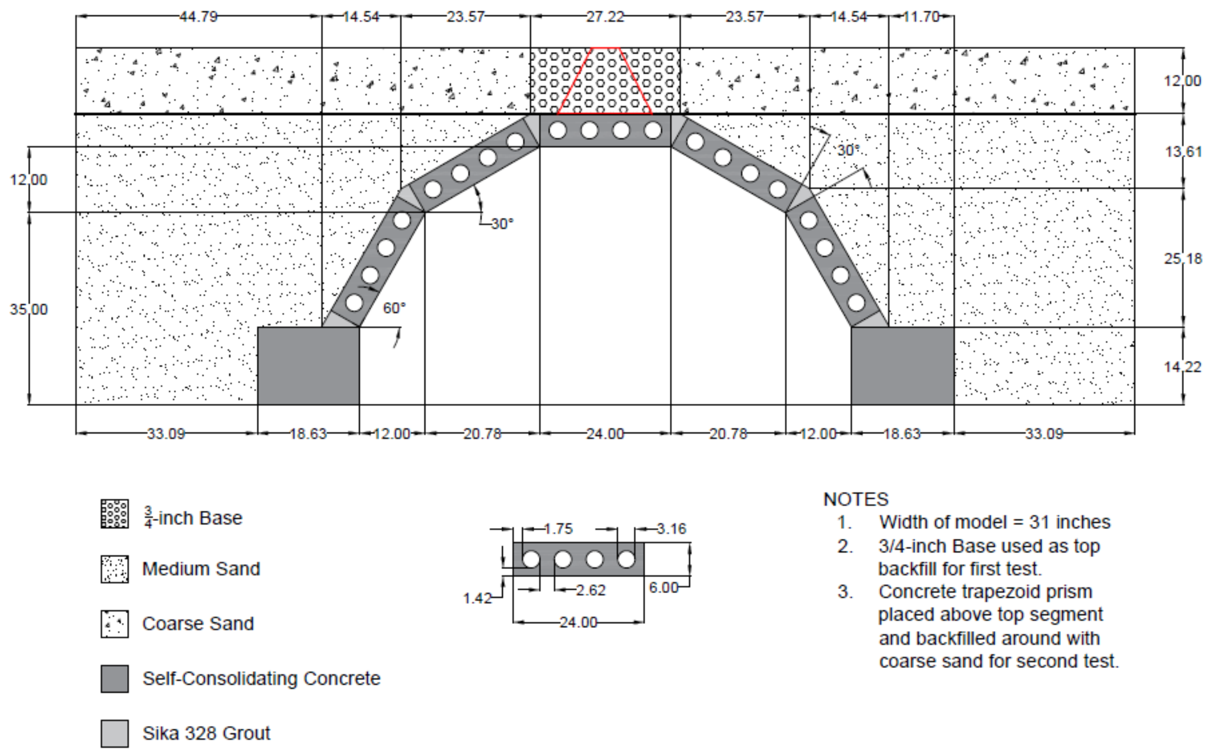

Figure 80 - Hollow-Core Culvert Model Geometry

4.3. Methodology

Procedures followed for the construction and assembly of the hollow-core model, as well as for laboratory and in-situ testing of the structural and soil materials, and for the experimental testing are presented in the following sections.

4.3.1. Hollow Core Culvert Model Assembly

The first step in the construction of the hollow-core model included the construction of the formwork for the panel and footing erection. Formwork for each panel and footing consisted of a combination of OSB and 4-inch Douglas Fir Larch No.2 lumber. In addition, four 3-inch diameter mailing tubes with end caps were positioned at approximately 5.5 inches on-center with a 1.5-inch vertical cover and 1.75-inch horizontal cover in each panel. In an effort to prevent the tubes from squashing during concrete placement, the hollow space was filled with sand. Figure 81 below presents the formwork for one of the hollow core panels. In addition, Appendix B – Formwork Design Calculations and Drawings provides the formwork drawings.

Figure 81 - Hollow-Core Panel Formwork

Once forms were assembled, placement of concrete within the forms was achieved. Self-consolidating concrete having a target 28-day compressive strength of 7,000 psi was used for the construction of the hollow-core panels. Refer to Section 4.3.2.1 for additional mix design information and concrete placement procedures. A total of approximately 26 cubic feet of concrete were used to create the hollow core panels and footings. For this project, 7 hollow-core panels, five for use and two additional ones for backup. Hollow-core panels and footings were left covered for 28 days to complete the curing cycle. Figure 82 presents self-consolidating concrete placement activities of the footings.

Figure 82 - Concrete placement activities of footing for hollow-core model

Since this model was moved into the structural lab following completion of experimental testing of the CIP culvert, the reaction frame used for model testing was left in place and no further loading equipment setup was needed. Refer to Section 3.4.6.1 of this report for additional test set up information and for test configuration drawings.

To assemble the hollow-core panels to form the precast culvert structure, the base frame and the four planar trusses used for the erection of the CIP culvert were reutilized. Refer to Section 3.4.1 for dimension and material information of the base frame and truss forms. Assembly of the hollow core footings/panels was achieved within the loading area and entailed:

1. Cleaning the base frame after removal of the CIP model;
2. Marking the location of the east and west footings used for the precast culvert;
3. Moving the footings in place;
4. Placing the lumber trusses an OSB boars between the footings and securing them by means of cross beams;
5. Removing the sand from the hollow-cores and placing the east and west lower panels against the footings;

6. Securing the lower panels by means of ratchet straps; and
7. Repeating steps 5 and 6 for the remaining panels.

In order to bond the panels to the footings and to each other, Sika grout 328 was utilized. Grouting placement was achieved immediately after positioning of the hollow-core panels. Refer to Section 4.3.2.4 for additional grout information and placement procedures. To allow for strength development of the grout, the model was left curing for approximately 2 days.

Once the grout was cured, the lower forms were removed, the precast culvert was painted for crack monitoring purposes, and assembly of the retaining walls was performed. Once again, the retaining walls used for the CIP model were reutilized for the hollow-core model. In order to prevent the migration of soil particles from the top of the structure (backfill areas) to the spaces between the culvert and the retaining walls, DAPtex plus foam was sprayed along the front and back faces of the concrete. Immediately after spraying, the walls were assembled and secured by means of ratchet straps.

After wall placement, Great Stuff Gaps and Cracks insulating foam was sprayed along the edges of the bottom OSBs on the east and west sides to prevent soil migration into the floor during backfilling activities. In addition, and as was done for the previous model to provide a secondary means of containment of the backfill soil at the interface between the walls and the concrete, 1-inch wide by 0.5-inches thick wood members were positioned and secured along the edges of the structure.

Once all gaps were sealed, backfilling activities began. This model followed a similar backfilling process as that performed for the CIP model. Meaning, the medium sand was placed to a height of 50 inches above the bottom culvert elevation; and the coarse sand from a height of 50 inches to a height of 62 inches on either side of the top hollow-core panel. The only difference was related to the material placed between the upper concrete segment and the top elevation of the culvert (62 inches) which consisted of ¾-inch road base material instead of pea gravel. Density determinations of the medium sand and ¾-inch road base were achieved by calculating volumes and soil masses at the top locations. Refer to Section 3.4.5.2.2 of this report for the density procedures.

The final step in the hollow-core model assembly entailed instrumenting the model. Instrumentation of this model followed the same schematic as that used for the CIP culvert. In other words, the key areas of interest for data acquisition included the bottom face of the top segment, the loading plate, the loading cell, and the reaction beam. Equipment used to obtain displacement, strain, and load information during experimental testing at these and select additional locations also included a combination of string pots, linear potentiometers, and load cells. Refer to Section 3.4.6.1.2 for supplementary instrumentation information. All instrumentation mounted on the CIP model was linked to a LoggerNet 4.5 DAQ which was used to record and display real-time data during testing.

Once all model components were designed, constructed, erected, and assembled; the structure was ready for testing. Three tests were anticipated to be conducted on the hollow-core model, based on the CIP structure response experience. The first round of testing included using the ¾-inch road base material, located on top of the upper hollow-core panel, as the main mechanism to transfer the load to the structure. Since a bearing failure was anticipated to occur prior to achieving the 9.03 kips of loading or failure of the structure, the second round of testing included using the trapezoid prism to load the model. The third and final round included testing the model without the use of backfill soil around the culvert. Refer to Sections 4.3.5.2.1, 4.3.5.2.2, and 4.3.5.2.3 for additional testing information.

4.3.2. Mix Designs and Concrete/Grout Placements

4.3.2.1. Precast Mix Design

The mix design used for construction of the hollow-core panels resembled common self-consolidating concrete (SCC) mix designs used in precast plants for the fabrication of these structural members. Various precast companies, including Oldcastle Infrastructure, Forterra Structural Precast and Teton Prestress Concrete, were consulted to develop the most appropriate mix design. Based on their experience with similar structures, a mix design with a target 28-day concrete compressive strength of approximately 7,000 psi was suggested. The control mix developed for the precast hollow-core model followed the guidelines presented in the *American Concrete Institute (ACI) Standard Practice for Selecting Proportions for Normal, Heavyweight, and Mass Concrete (ACI 211.1-91)* Absolute Volume Method of Concrete Mix Design.

Table 25 presents the CIP mix quantities used, along with material specifications. The concrete mix used for this project was produced in-house.

Table 25 - Control Mix Material Quantities and Specifications of Precast Members

Material	Quantity per 1 CY	Quantity per 1 ft^3	Specification	Supplier
Cement	729 lb	27 lb	Type I/II	Home Depot
Fly Ash	183.2 lb	6.78 lb	Type F	Pocatello Ready Mix
Coarse Sand	1,701 lb	63 lb	3/8" minus	Idaho Rock and Sand
Fine Pea Gravel	810 lb	30 lb	½" minus	Idaho Rock and Sand

Material	Quantity per 1 CY	Quantity per 1 ft^3	Specification	Supplier
Water	364.5 lb	13.5 lb	-	-
High-Range Water Reducing (HRWR) Agent	10.4 fl. oz/cwt	10.4 fl. oz/cwt	MasterGlenium 1466	Master Builder Solutions

Production of the seven hollow-core panels and two footings necessitated approximately 26 cubic feet of SCC concrete. The sequence of concrete placement included:

1. Weighing the mix material (cement, fly ash, sand, gravel, water and HRWR) separately using buckets to produce the necessary batch (Figure 83 left);
2. Using an electric concrete mixer to blend in all materials necessary to produce the SCC mix (Figure 83 right);
3. Filling the panel and footing forms;
4. Vibrating the concrete in the footings and panels using an electric concrete vibrator;
5. Finishing the surface by means of a trowel; and
6. Placing wet burlap and plastic on the free face of each form;

Figure 83 - Weighing of material for SSC mix (left) and blending all components together (right)

4.3.2.2. Concrete for Trapezoid Prism

The same trapezoid prism erected to perform Tests No. 3, 4 and 5 for the CIP model was reutilized for Tests No. 2 and 3 of the hollow-core model. Refer to Section 3.4.2.2 for trapezoid prism construction procedures.

4.3.2.3. Grout for Hollow-Core Connections

To provide an arch-like geometry, the hollow core segments were connected at 30º angle between the top segment and the adjacent east and west sections, and at a 60º angle between the east and west adjacent sections and the bottom segments. To fill the spaces left between adjacent panels, Sika grout 328 was used. This product was selected based on its high performance, non-shrink and extended working time capabilities. Refer to Appendix D – Concrete and Grout Mix Designs for mix composition and product specifications. Approximately 225 pounds of mix material, yielding about 1.04 ft^3, were used. The following presents the concrete mixing and placing procedures carried out to fill the connections between adjacent members.

1. Placed a third of the first 50 lb grout mix into a bucket;
2. Added approximately 2.4 quarts of water to the mix;
3. Blended the material until a flowable and smooth texture was achieved;
4. Placed the grout into the space between the east footing and the adjacent hollow-core panel;
5. Vibrated the concrete inside the form by means of a tamping rod;
6. Used a mallet to hit the sides of the forms;
7. Repeated steps 1 to 6 until the all connections were filled;
8. Placed a wet burlap on the upper face and covered the model with plastic.

Once the connections were filled, the structure was allowed to cure for two days, before removing the forms. Figure 84 presents the cured hollow-core model.

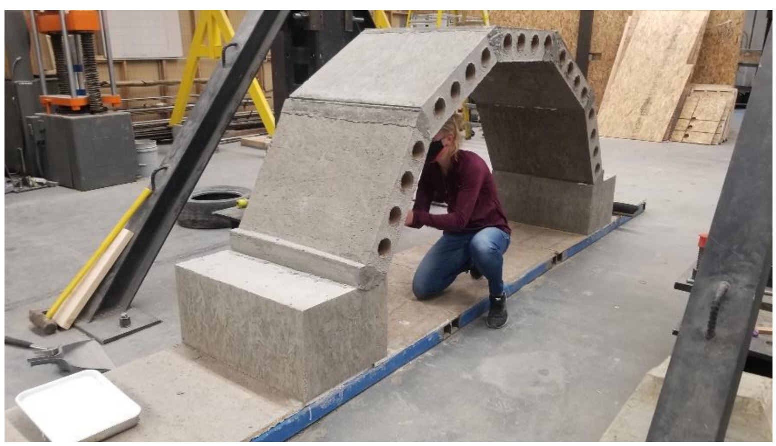

Figure 84 - Cured hollow-core model

4.3.2.4. Concrete/Grout Sample Casting

4.3.2.4.1. <u>Cylinder Casting</u>

Cylinder casting for this model followed the procedures presented in Section 3.4.3 of this report. For this project, SCC test specimens consisted of either 4-inch diameter, 8-inch tall concrete cylinders casted using Gilson steel molds; or 6-inch diameter, 12-inch tall concrete cylinders casted using Gilson plastic molds. A total of 15 4- by 8-inch cylinders and four 6- by 12-inch cylinders were made during the SCC concrete placement. As was done with the CIP cylinders, the SCC concrete cylinders were cured, after 24 hours of placement, in a water bath.

4.3.2.4.2. Cube Casting

In order to test and obtain the compressive strength of the Sika 328 grout at different time periods, cube test specimens were casted at the time of grout placement and were later cured under controlled laboratory conditions. Casting and curing of the test specimens were performed in accordance with *ASTM C109/C109M-20b, Standard Test Method for Compressive Strength of Hydraulic Cement Mortars (Using 2-in. or [50 mm] Cube Specimens)* (ASTM International, 2020) requirements. The following presents a summary of the steps completed for cube casting and subsequent test specimen curing:

1. Placed the molds on a rigid surface free from vibration and other disturbances;
2. Applied a thin coating of WD40 to the interior faces of the mold and base plates;
3. Placed the first layer of grout in the mold using a scoop (filled to approximately 1/2 of the height);
4. Tamped the grout in each cube compartment 32 times using a rectangular tamper;

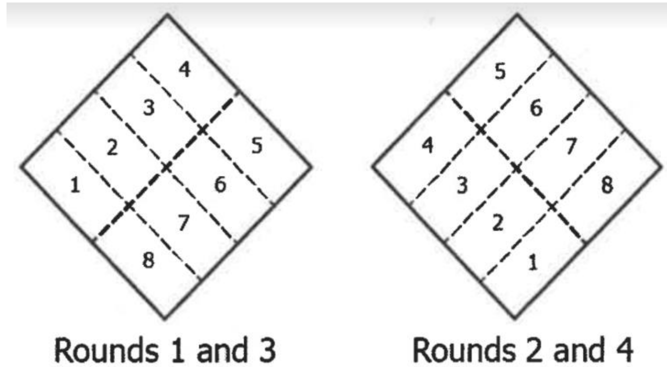

Figure 85 - Order of Tamping in Molding of Test Specimens (ASTM International, 2020)

5. Placed the second layer of grout in the mold using a scoop (filled to top);
6. Repeated step 4 for the second layer;
7. Stroke off the surface of the grout with a trowel to obtain a level finish;
8. Placed the top cover on the mold and secured the assembly by means of screws;
9. Left casted cubes in an undisturbed area for the next 24 hours;
10. After 24 hours removed cubes from the mold, marked and placed the samples in a water bath cure.

For this project, a total of six grout cubes were casted.

4.3.3. Soil Backfill and Geotextile

As was done with the CIP model, the hollow-core model was backfilled with medium sand to a height of 50 inches, with coarse sand from the top of culvert to a height of 62 inches on either side of the top segment, and with ¾-inch road base/concrete trapezoid prism with coarse sand from the top segment to 62 inches directly above. To prevent migration of fines between the medium sand, coarse sand, and ¾-inch road base layers, a separation geotextile was placed at the interface between the soil units. The medium sand, coarse sand and ¾-inch road base material used to backfill the CIP model was the reutilized for the hollow-core model. See Sections 3.4.4.1, 3.4.4.2, and 3.4.4.4 for additional soil information. In addition, the same type of geotextile material was used for the hollow-core model. Refer to Section 3.4.4.5 of this report for further geotextile information. In addition, Section 3.4.4.6 provides additional backfilling details. It is important to note that, for the hollow-core model, pea gravel was not used as backfill material on top of the upper panel. Instead, ¾-inch road base/trapezoid prism with coarse sand was placed at that location to conduct Tests. No. 1 and 2, respectively.

Figure 86 presents backfilling activities and geotextile placement achieved for the hollow-core model.

Figure 86 - Backfilling activities of medium sand (left) and geotextile placement (right)

4.3.4. Material Testing

To verify the parameters used in the hollow-core FEM analysis, material testing was also performed on the members/components utilized in the hollow-core model. The following sections present the laboratory and field testing performed for this portion of the project.

4.3.4.1. Laboratory Testing

4.3.4.1.1. Concrete Compression Test and Unit Weight Determination

Determination of the compressive strength and unit weight of cylindrical SCC specimens followed the guidelines presented in *ASTM C39/C39M-20, Standard Test Method for Compressive Strength of Cylindrical Concrete Specimens* (ASTM International, 2020). Refer to Section 3.4.5.1.1 for compression testing procedures.

4.3.4.1.2. Grout Compression Test and Unit Weight Determination

Determination of the compressive strength and unit weight of grout cube specimens followed the guidelines presented in *ASTM C109/C109M-20b, Standard Test Method for Compressive Strength of Hydraulic Cement Mortars (Using 2-in. or [50 mm] Cube Specimens)* (ASTM International, 2020). 2-inch by 2-inch by 2-inch cubes were used to determine the compressive strength of the grout used in the connections between hollow-core panels and the footings at the time of culvert testing (approximately 10, 11 and 15 days after placement). Compression testing was done by means of a Gilson Compression Testing Machine and used a steel member to raise the cubes to the appropriate heights. Figure 87 below presents the equipment used to perform grout compression testing.

Figure 87 – Equipment used for compression testing of grout cubes

A summary of the grout compression testing procedure is presented below:

11. Removed specimen from water bath;
12. Removed sand grains and any other incrustations from the faces of the test specimen;
13. Measured and recorded the length, width and height of the cube, for volume calculations;
14. Weighed the cube and recorded its mass for density (unit weight) calculations;
15. Placed the cube on the steel pedestal with the casting face facing the front;
16. Aligned the axis of the specimen with the center of thrust of the spherically seated block;
17. Zeroed the testing machine prior to testing of the specimen;

18. Applied the load continuously at an approximate rate of 400 lb/s until the load indicator showed that the load was decreasing steadily and the specimen displayed a well-defined fracture pattern;
19. Recorded the maximum load carried by the specimen during the test; and
20. Retracted the loading surface and removed the broken specimen.

4.3.4.1.3. Modulus of Elasticity and Poisson's Ratio Test

A modulus of elasticity and Poisson's Ratio test was performed on one of the SCC cylindrical specimens casted. To perform this test, guidelines set forth in *ASTM C469/C469M-14, Standard Test Method for Static Modulus of Elasticity and Poisson's Ratio of Concrete in Compression* (ASTM International , 2014) were followed. See Section 3.4.5.1.1 for modulus of elasticity/Poisson's ratio procedures.

4.3.4.1.4. Sieve Analysis Tests

The medium sand, coarse sand and ¾-inch road base soils used to backfill around the CIP culvert were reused to backfill around the hollow-core structure. As such, the sieve analysis tests presented in Section 3.4.5.1.3 as well as the results presented in Section 3.5.2.3 are applicable to this model. Sieve analysis determinations followed the guidelines presented in *ASTM C136/C136M-19, Standard Test Method for Sieve Analysis of Fine and Coarse Aggregates* (ASTM International, 2019).

4.3.4.1.5. Proctor Compaction Tests

As was the case with the sieve analysis determinations, the proctor compaction tests performed as part of the CIP tests were used to determine the relationship between dry density and moisture content for the hollow-core model since the same soil materials were used to backfill around both culvert structures. Refer to Section 3.4.5.1.4 for additional standard proctor procedures.

4.3.4.2. In-Situ Testing

4.3.4.2.1. Moisture Content Test

Moisture content tests were carried out after moisture conditioning of the backfill material had been performed to determine the water content of the which the soil was being compacted. Moisture content tests followed the guidelines presented in *ASTM D2216-19, Standard Test Method for Laboratory Determination of Water (Moisture) Content of Soil and Rock by Mass* (ASTM International, 2019). Procedures presented in Section 3.4.5.2.1 of this report were the same steps followed for this portion of the project.

4.3.4.2.2. Density of Compacted Medium Sand and Pea Gravel

As was done for the CIP model, to determine the density of the compacted medium sand (top segment) and ¾-inch road base, measurements of specific backfill locations were taken and the weight of the material placed at these locations were recorded. Refer to Section 3.4.5.2.2 of this report for density determination procedures.

4.3.5. Experimental Testing of CIP Culvert Model

Experimental testing of hollow-core model was performed to obtain real-life structure responses of an assembled precast concrete culvert under applied compressive forces. Information obtained from this test aided in assessing if such a structure would be able to sustain a design compressive load of 9.03 kips (half-scale equivalent of a 16-kip wheel load with applied load combination) without undergoing any failure. In addition, the model behavior obtained from this model was compared to that obtained during experimental testing of the CIP model to evaluate the similarities and differences between the two systems. The following sections present the test setup, loading procedure and crack monitoring activities performed during experimental testing.

4.3.5.1. Test Setup

4.3.5.1.1. Loading Equipment

This model used the same loading setup and equipment that was used for experimental testing of the CIP model. In fact, the reaction frame and base frame were not removed from the testing area between tests. See Section 3.4.6.1.1 for loading equipment information.

4.3.5.1.2. Instrumentation

To obtain load, displacement and strain data at equivalent locations as those of the CIP model, the same set of instruments were utilized during experimental testing of the hollow-core model. Data obtained from these instruments was also used to calibrate the FEM model developed for the hollow-core culvert. Refer to Section 3.4.6.1.2 for additional instrument information. Note that, for the hollow-core model, the 18 linear potentiometers were used to record displacements for the first and second rounds of testing. For Test No. 3, eight of the inner linear potentiometers were removed, leaving only the center potentiometer in place, since the structure was going to be taken to failure and potential collapse of the panels could have occurred. In addition, the two sets of three linear potentiometers positioned at the northeast and southwest corners were removed since no major movement was anticipated to occur at these locations as the soil was removed from within the model for this round of testing. In addition, and as was done for the last round of testing of the CIP model, LS1 was repositioned and mounted on the north (center) wall to monitor outward or inward movement of the soil box.

4.3.5.1.3. Data Acquisition System

All instrumentation used for compression testing of the hollow-core model was linked to the LoggerNet 4.5 DAQ which aided in collecting experimental data. The two sensor cards used for testing of the CIP model, namely CR6-1 and CDM-1, were also used for this model. In fact, the channels to which each instrument was wired to matched the channels used for testing of the previous model. A scan rate of of 4 samples per second was also employed for this model. Refer to Section 3.4.6.1.3 of this report for additional DAQ information.

4.3.5.2. Loading Procedure

Since the actuator used for testing was displacement-based, the loading procedure program was based on displacement increments instead of load increments. As was done with the previous model, 0.02 inches of displacement were advanced per step. Displacement increments were run back to back, when needed, to achieve an approximate 500 to 700-pound increase in load, before observations were made. This displacement loading procedure was maintained throughout all rounds of testing and followed a linear increasing scheme for the majority of tests. This meant that the model was not unloaded and reloaded between steps but rather, it was loaded, the load was held during observation time, and then increased again based on the next displacement increment. This was done for Tests No. 1 and 3. However, for Test No. 2, the model was loaded in displacement increments up to a load of approximately 6,500 lb and then completely unloaded. The model was then reloaded continually (by running 4 displacement steps at once) to achieve a similar load, and then continued the regular displacement loading procedure explained above. The purpose behind the loading, unloading, and reloading activities was to assess how the load and displacements recorded at TCY2 were being affected by the displacement steps during testing. loading conclusions on how displacement steps. The following subsections provide a summary of the procedures conducted for each test.

4.3.5.2.1. Test Number 1 – ¾-inch Road Base Backfill

The first model tested used 12 inches of ¾-inch road base as cover material between the upper concrete segment and the loading plate. Figure 88 presents a schematic of Test No. 1.

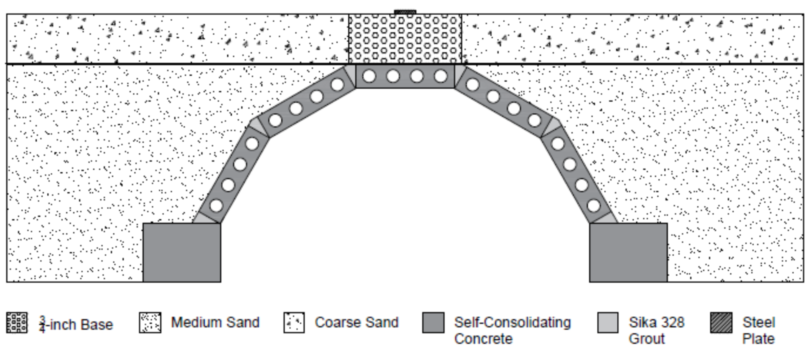

Figure 88 - Schematic Test No. 1 Hollow-Core Model

Testing of this model occurred on November 4th, 2020 and took approximately 18 minutes to complete. A total of 30 displacement steps were driven to carry out this test, with a resulting overall actuator elongation of approximately 0.58 inches (0.02 inches per step).

For this test, various displacement steps were needed to achieve the desired 500-pound increments. From the start to a load of approximately 1,670, about 3 displacement increments were driven to achieve the chosen load increment. After a load of approximately 1,200 pounds, the model required 12 displacement steps to get to the next 500 pounds. This soil was capable withstanding a maximum load of 2,050 pounds before experiencing a punching failure.

4.3.5.2.2. Test Number 2 – Concrete Trapezoid Prism with Coarse Sand Backfill

In an effort to utilize a mechanism capable of transferring the entirety of the test load (9.03 kips) to the culvert structure without failing, while preserving the 12-inch cover principle, the concrete trapezoid prism constructed for testing of the CIP model was reused. By using concrete, the stiffness of the system was greatly increased, and the load transferring capabilities were enhanced. This system replicated an extreme loading condition in which the structure was immediately loaded as would be the case if a truck was travelling directly on top of the culvert. In addition, to provide confinement to the newly added structure, coarse sand was placed and compacted around it. Figure 89 presents a schematic of Test No. 2.

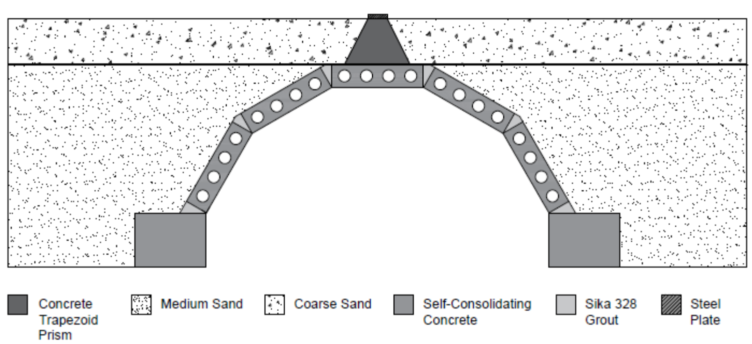

Figure 89 - Schematic Test No. 2 Hollow-Core Model

Testing of this model occurred on November 5th, 2020 and was done in two parts. Test No. 2A entailed loading the model up to approximately 6,500 pounds in four displacement steps and then unloading the specimen. Test 2B consisted of loading the first four displacement increments at once, and then continuing with a one displacement step increment up to a load of approximately 14,500 pounds. For Test No. 2A a total of four displacement steps were driven which took approximately 10 minutes to complete. For Test No. 2B a total of 14 load steps were driven during testing which resulted in an overall actuator elongation of approximately 0.28 inches. Due to the stiffness of the load transferring mechanism, load increments of about 1,000 pounds were achieved per displacement step for Test No. 2B up to a load of 12,000 pounds. Between 12,000 pounds and the end of testing, or a load of 13,600 pounds, the loads between displacement steps varied between 300 and 800 pounds.

4.3.5.2.3. Test Number 3 – Concrete Trapezoid Prism with No Soil Backfill

To evaluate the capacity of the hollow-core culvert without the aid of the backfill soil, which ultimately puts the structure in a compression state and increases to some extent it's capacity, all backfill material was removed from the top and sides. Only the medium sand, placed from the base to the top of footing elevation, was left in place. As with Test No. 2, the concrete trapezoid prism was used as the load dissipating mechanism which ultimately represented an extreme loading condition which transferred the load to the structure instantly. Figure 90 presents a schematic of Test No. 3.

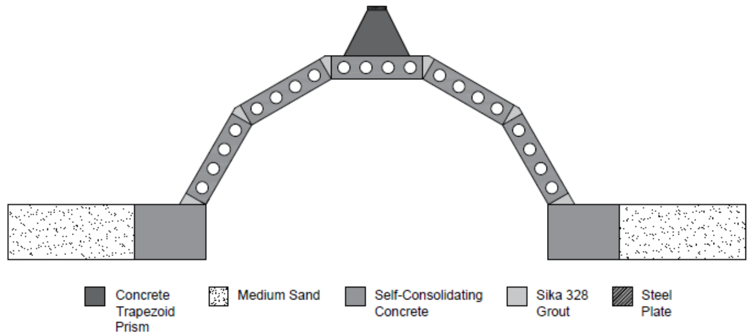

Figure 90 - Schematic Test No. 3 Hollow-Core Model

Testing of this model occurred on November 9th, 2020 and took approximately 37 minutes to complete. A total of 40 load steps were driven during testing which resulted in an overall actuator elongation of approximately 0.8 inches. Test No. 3 was carried out until shear failure of the structure was achieved.

4.3.5.3. Crack Monitoring

The same crack monitoring procedures as those described in Section 3.4.6.3 of this report were carried out during experimental testing of the hollow-core model. For the upper portion of the structure, crack monitoring of tests number 1 and 2 was performed once all soil was removed from the sides of the structure on November 6th, 2020. For test number 3, crack monitoring was performed once the test was finalized and the structure was unloaded. For the front and back faces of the culvert, crack monitoring was only possible after all rounds of testing were performed and the retaining walls were unmounted. Although not ideal, cracks observed during this stage were able to be correlated to specific rounds of testing.

4.4. Results

4.4.1. Introduction

This section presents the laboratory and in-place test results of all testing performed on the structural and soil components of the hollow-core model, as well as the experimental test results of the compression testing carried out on the hollow-core model as a whole. Material properties obtained from laboratory and in-place testing were used as input parameters in the finite element analysis model for the hollow-core culvert. In addition, experimental compression test results were used to calibrate the FEM model.

4.4.2. Laboratory Test Results

4.4.2.1. Concrete Compression Test Results and Unit Weight Determinations

Compression testing of SCC concrete cylinders was performed at 32-days and on the days of testing of the hollow-core model to evaluate the structure's strength at each stage. As was done with the CIP cylinders, compressive strengths of the SCC cylinders were calculated by dividing the maximum compressive load of each by the average cross-sectional area. Refer to Section 3.5.2.1 of this report for the equations used.

Table 26 presents the results of the SCC compression tests and the unit weight determinations. Refer to Appendix E – Laboratory Test Results for additional test data.

Table 26 - Compressive Strength and Unit Weight of SCC Cylinders

Specimen No.	Cross-Sectional Area (in^2)	Volume (in^3)	Weight (lb)	Max. Load (lb)	Compressive Strength (psi)	Unit Weight (pcf)	Age
HCPC-4A	12.606	100.568	8.0695	87,855	6,979	138.65	32-day
HCPC-3A	12.372	98.467	8.3110	100,390[1]	8,114	145.85	89-day
HCPC-1A	12.260	98.725	8.3525	100,290[1]	8,180	146.34	90-day
HCPC-3B	12.519	100.154	8.2305	105,840	8,454	142.00	94-day

1. Testing of HCPC-3, HCPC-1 was stopped when a load of approximately 100,000 pounds was achieved for safety reasons. These cylinders did not experience failure during testing.

Based on the above test results, and as is expected with concrete, the test specimens showed an increase in strength with time. A gain of approximately 1,201 psi was evinced between the 32-day and 90-day tests. On average, the compressive strength of the concrete during testing was of 8,250 psi. Additionally, all test results demonstrated that the target compressive strength of the mix (7,000 psi) was achieved and surpassed by approximately 16-20% between the 89- and 94-day tests.

4.4.2.2. Grout Compression Test Results and Unit Weight Determinations

Compression testing of grout cubes was performed at on the days of testing of the hollow-core model to evaluate the connection's strength at each stage. As was done with the CIP and hollow-core cylinders, compressive strengths of the grout cubes were calculated by dividing the maximum compressive load of each by the average cross-sectional area.

Table 27 presents the results of the SCC compression tests and the unit weight determinations. Refer to Appendix E – Laboratory Test Results for additional test data.

Table 27 - Compressive Strength and Unit Weight of Grout Cubes

Specimen No.	Cross-Sectional Area (in^2)	Volume (in^3)	Weight (lb)	Max. Load (lb)	Compressive Strength (psi)	Unit Weight (pcf)	Age
GRT-1	4.250	8.500	0.680	26,560	6,249	138.24	9-day
GRT-4	4.256	8.248	0.668	32,725	7,689	139.95	9-day
GRT-2	4.118	8.496	0.682	29,765	7,228	138.71	10-day
GRT-5	4.250	8.237	0.664	29,560	6,955	139.20	10-day
GRT-3	4.080	8.132	0.666	38,850	9,512	141.52	14-day
GRT-6	4.058	8.092	0.656	38,645	9,523	139.99	14-day

On average, the compressive strength of the cubes during testing was of 7,859 psi. This value, compared to the compressive strength of the SSC concrete during testing was approximately 391 psi or 5% lower. However, for Tests No. 1 and 2, the difference between the SCC and grout compressive strengths was approximately 1,118 or 14%.

4.4.2.3. Modulus of Elasticity and Poisson's Ratio Test Results

In order to determine the modulus of elasticity and Poisson's ratio of the CIP concrete, an ASTM C469 test was performed. A total of three loading cycles were conducted on specimen HCPC-4B to obtain the load, longitudinal and transverse deflections. Calculations of the vertical and horizontal deformations as well as the modulus of elasticity and Poisson's ratio used the equations presented in Section 3.5.2.2 of this report.

Test results and the calculated parameters are presented in Table 28 and

Table 29.

Table 28 - Modulus of Elasticity and Poisson's Ratio Test Results of SSC Specimen

Test No.	Load (lb)	Vertical Deflection (in)	Horizontal Deflection (in)	Long. Specimen Deformation (in)	Trans. Specimen Deformation (in)
1	2,700	0.00026	0.00000	0.000129	0.000000
	10,000	0.00170	0.00035	0.000837	0.000151
	20,000	0.00415	0.00075	0.002044	0.000324
	30,000	0.00690	0.00110	0.003398	0.000476
	35,000	0.00800	0.00135	0.003939	0.000584
2	2,300	0.00026	0.00000	0.000129	0.000000
	10,000	0.00210	0.00020	0.001034	0.000086
	20,000	0.00450	0.00045	0.002216	0.000195
	30,000	0.00670	0.00800	0.003299	0.000346
	35,000	0.00775	0.00110	0.003816	0.000476
3	2,300	0.00026	0.00000	0.000129	0.000000
	10,000	0.00210	0.00015	0.001034	0.000065
	20,000	0.00440	0.00060	0.002167	0.000259
	30,000	0.00690	0.00110	0.003398	0.000476
	35,000	0.00810	0.00140	0.003989	0.000605

Table 29 – SCC Modulus of Elasticity and Poisson's Ratio Determinations

Test No.	Stress (psi)	Long. Strain (in/in)	Trans. Strain (in/in)	Modulus of Elasticity, E (psi)	Poisson's Ratio, μ
1	S_1 = 216	ε_1 = 1.62E-05	ε_{t1} = 0.00E+00	5.41E+06	0.31
	S_3 = 799	ε_3 = 1.05E-04	ε_{t3} = 3.79E-05		
	S_4 = 1,598	ε_4 = 2.56E-04	ε_{t4} = 8.12E-05		
	S_5 = 2,397	ε_5 = 4.26E-04	ε_{t4} = 1.19E-04		
	S_2 = 2,796	ε_2 = 4.93E-04	ε_{t2} = 1.46E-04		
2	S_1 = 184	ε_1 = 1.62E-05	ε_{t1} = 0.00E+00	5.66E+06	0.26
	S_3 = 799	ε_3 = 1.30E-04	ε_{t3} = 2.17E-05		
	S_4 = 1,598	ε_4 = 2.78E-04	ε_{t4} = 4.87E-05		
	S_5 = 2,397	ε_5 = 4.13E-04	ε_{t4} = 8.67E-05		
	S_2 = 2,796	ε_2 = 4.78E-04	ε_{t2} = 1.19E-04		
3	S_1 = 184	ε_1 = 1.62E-05	ε_{t1} = 0.00E+00	5.40E+06	0.31
	S_3 = 799	ε_3 = 1.30E-04	ε_{t3} = 1.63E-05		
	S_4 = 1,598	ε_4 = 2.71E-04	ε_{t4} = 6.50E-05		
	S_5 = 2,397	ε_5 = 4.26E-04	ε_{t4} = 1.19E-04		

Test No.	Stress (psi)		Long. Strain (in/in)		Trans. Strain (in/in)		Modulus of Elasticity, E (psi)	Poisson's Ratio, μ
	S_2 =	2,796	ε_2 =	5.00E-04	ε_{t2} =	1.52E-04		

Figure 91 presents the relationship between the stress and longitudinal strain for the three load increments performed on the HCPC-4 specimen.

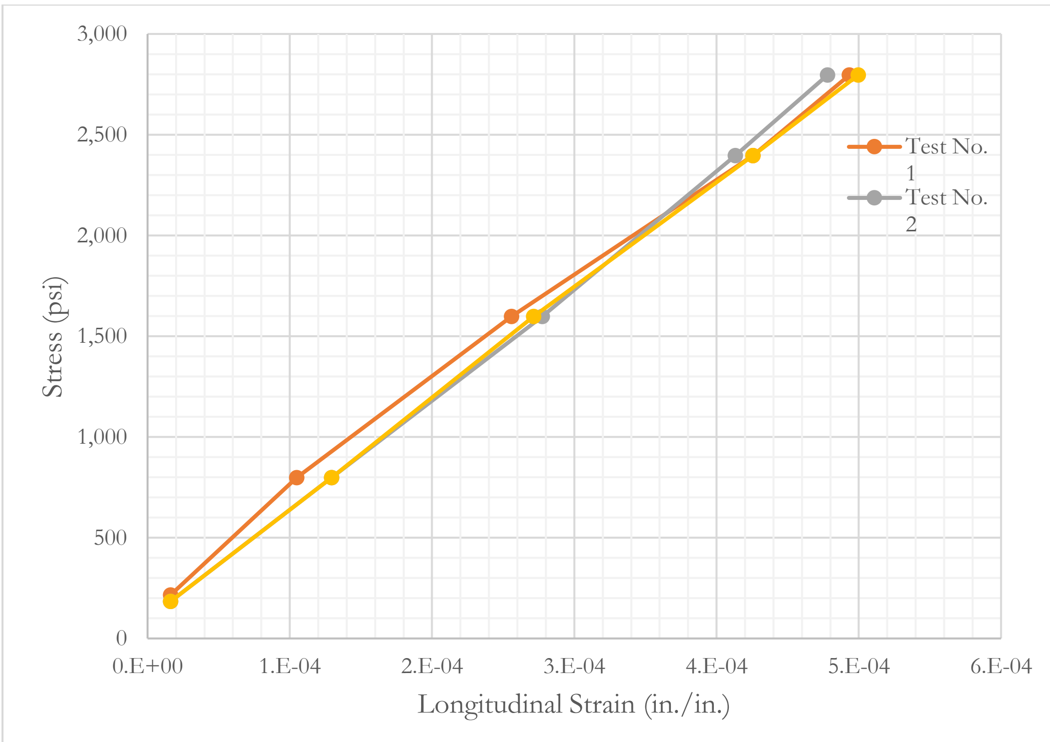

Figure 91 - Stress vs. Strain Relationship of CIP Concrete Test Specimen

Based on the above graph, testing was only performed in the linear elastic portion of the material. Since the proportional limit was not reached in any of the tests, the test specimen was able to return to its original state upon load removal and no permanent deformation was experienced between each consecutive test. Test results for each load cycle appear to follow similar paths and have comparable longitudinal strains for the different load increments. Since test results evinced low variability, the modulus of elasticity and

Poisson's ratio of the test specimen was taken as the average of the three load cycles. Namely, $E = 5.49 \times 10^6$ psi and $\mu = 0.29$. The modulus of elasticity test result appears to lie within published E ranges for concrete which generally include 2×10^6 to 6×10^6 psi values. However, the Poisson's ratio value appears to be slightly higher than the μ published values which generally range between 0.1 to 0.2.

4.4.2.4. Sieve Analysis Test Results

Since the backfill soil used for this model was the same soil used for the CIP model, the sieve analyses tests performed for these materials and presented in Section 3.5.2.3 are applicable to this portion of the project.

4.4.2.5. Proctor Compaction Test Results

As was the case with the sieve analysis results, the proctor compaction test results presented in Section 3.5.2.4 are applicable to this portion of the project.

4.4.3. In-Situ Test Results

4.4.3.1. Moisture Content Test Results

To determine the water content of the backfill soil immediately after moisture conditioning activities were achieved, moisture content tests were performed. Equation 29, presented in Section 3.5.3.1. of this report, was the moisture content formula utilized to determine the water percentage Table 30, Table 31, and Table 32 provide the calculated water contents of the medium sand, coarse sand, and ¾-inch road base backfill material.

Table 30 - Moisture Content of Medium Sand

Test No.	Location	State	Moisture (%)	Date
1	1 ft above bottom of footing elevation, right side	Moisturized	6.44	10/29/2020
2	1 ft above bottom of footing elevation, left side	Moisturized	4.52	10/29/2020
5	At top segment elevation (53 inches), right side	Moisturized	4.50	11/02/2020
6	At top segment elevation (53 inches), left side	Moisturized	3.53	11/02/2020

The results show that the upper layers had a decrease in moisture content with respect to the bottom layers of approximately 1.9% on the right side and 1.0% on the left side. Possible reasons for these differences could have been related to the lower moisture contents of the stored material within storage boxes and a decrease in added water to said storage boxes when moisture conditioning was taking place.

Table 31 - Moisture Content of Coarse Sand

Test No.	Location	State	Moisture (%)	Date
1	Top model elevation (65 inches), right side	Moisturized	2.83	11/02/2020
2	Top model elevation (65 inches), left side	Moisturized	2.53	11/02/2020

Based on the above results, the two moisture contents obtained for the right and left portion of the model appear to be comparable. However, the numbers appear to lie within the lower range based on the proctor compaction curve, presented in Figure 43.

Table 32 - Moisture Content of ¾-inch Road Base

Test No.	Location	State	Moisture (%)	Date
1	Top model elevation (65 inches), above upper concrete segment	Moisturized	3.99	11/02/2020

Based on the proctor compaction curve for this soil unit, the moisture content values laid on the left portion of the graph and represented a dry density, under standard compaction efforts, of approximately 125 pcf.

4.4.3.2. Density of Compacted Medium Sand and ¾-inch Road Base Results

Density determinations of the top section of the compacted medium sand (east and west locations) and ¾-inch road base were achieved by means of volume calculations and mass data obtained during backfilling activities. The following table presents the backfill area dimensions as well as the total mass of material used and its corresponding wet density.

Table 33 - Density of Compacted Medium Sand and ¾-inch Road Base

Material	Location	Total Volume (ft^3)	Total Mass (lb)	Wet Density (pcf)	Dry Density (pcf)
Medium Sand	Right – from 38.4" to 53" high	17.93	2,016.8	112.5	107.7[1]
Medium Sand	Left - from 36.4" to 53" high	20.63	2,212.6	107.3	103.6[2]

Material	Location	Total Volume (ft^3)	Total Mass (lb)	Wet Density (pcf)	Dry Density (pcf)
¾-inch Road Base	Middle – from 53” to 65” high	5.49	725.1	132.1	127.0[3]

4. Dry density calculated based on a moisture content of 4.5% obtained as part of moisture density determinations.
5. Dry density calculated based on a moisture content of 3.53% obtained as part of moisture density determinations.
6. Dry density calculated based on a moisture content of 3.99% obtained as part of moisture density determinations.

Based on the dry density values presented in Table 33 and the proctor compaction curve for the medium sand (Figure 42), the right and left locations appear to have been compacted to approximately 96.2% and 92.5% of the maximum dry density, respectively. These density values translate to an approximate percent relative density of 62 (medium dense) for the right medium sand and 55 (medium dense) for the left medium sand based on the *Representative Values of Relative Density* correlation chart developed by McCarthy and presented as Table 4-3 on the *Essentials of Soil Mechanics and Foundations, Basic Geotechnics* book (McCarthy, Representative Values of Relative Density, 2007).

The ¾-inch road base appears to have been compacted to approximately 92.8% of the maximum dry density, based on the proctor curve, and have a percent relative density of 82 (dense) according to the correlation chart. All values obtained from this correlation chart were calculated based on linear interpolation. Refer to Appendix H – Correlation Charts for the *Representative Values of Relative Density* correlation chart used.

4.4.4. Experimental Test Results

To obtain structure responses of the hollow-core structure under compression loading, experimental testing was performed. A total of three tests were performed on the hollow-core model. During testing, the instrumentation mounted on the models recorded vertical displacements and strains of the inner face of the upper segment, horizontal displacements of the inner faces of the foundations, outward deflection of the box (z-direction), displacements in the x-, y-, and z-directions of the southwest and northeast corners of the soil box for toppling/expansion effects, and vertical deflections of the beam and actuator. The following sections present the results obtained from each round of testing.

4.4.4.1. Test Number 1 – ¾-inch Road Base Backfill

Refer to Figure 88 for the model schematic of this test. Testing of this model was performed until the ¾-inch road base backfill material could not hold any additional load with increases in actuator displacements and complete bearing failure was experienced, as was the case with Tests No. 1 and 2 of the CIP model. During testing of the ¾-inch road base model a total of 30 displacement steps were driven by the actuator which resulted in an approximate vertical movement of the loading plate of -0.5596 inches.

This test evinced significant creep effects after each displacement step was applied. This behavior was likely the result of the punching/bearing failure that was occurring within the soil mass as loading was applied and the consequential side displacement of soil particles. From approximately 13:08 the material was unable to sustain any additional loading with increases in actuator displacement. This was the result of the punching failure that occurred within the backfill soil after reaching a maximum load of approximately 2,070 pounds.

Additionally, deflections of all linear potentiometers were observed to follow a linear pattern during testing. For this test, the center potentiometer recorded the highest deflection with a value of approximately -0.00319 inches. The east and west potentiometers recorded maximum displacements of approximately -0.002 inches and -0.00249 inches, respectively. No cracks were observed.

Figure 92 presents the load & displacement vs. time relationships observed during the second round of testing of the CIP model.

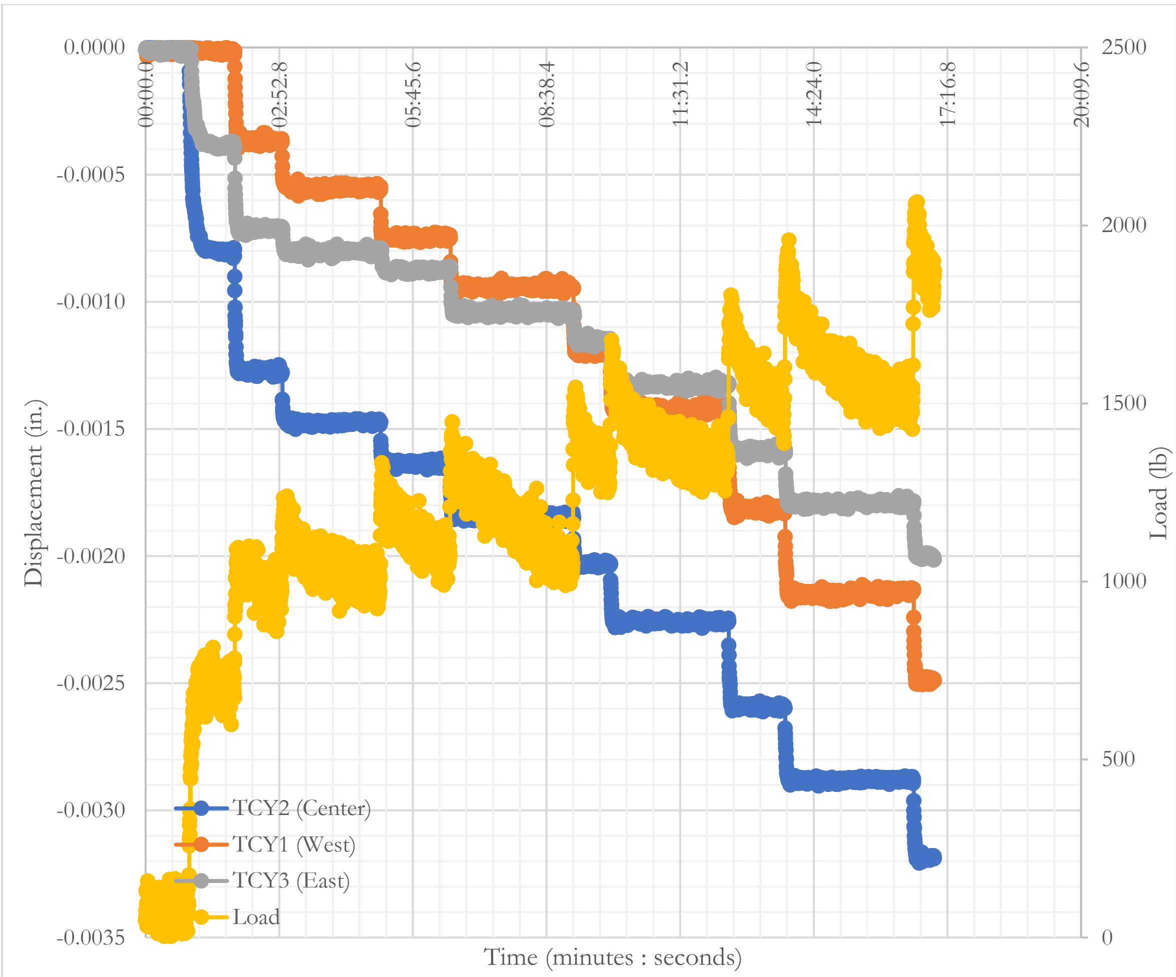

Figure 92 - Load & Displacement vs. Time Hollow Core Model - Test No. 1

Figure 93 presents the load vs. displacement relationship obtained at the centroid of the upper concrete segment (TCY2). This graph evinces a mostly linear relationship throughout the test duration. This suggests that the hollow-core structure remained within the linear elastic range and no permanent deformation was imposed on the structure.

Based on the test results, the maximum loading experienced by the system was approximately 2,070 pounds which resulted in a displacement of the upper concrete panel of approximately -0.00321 inches.

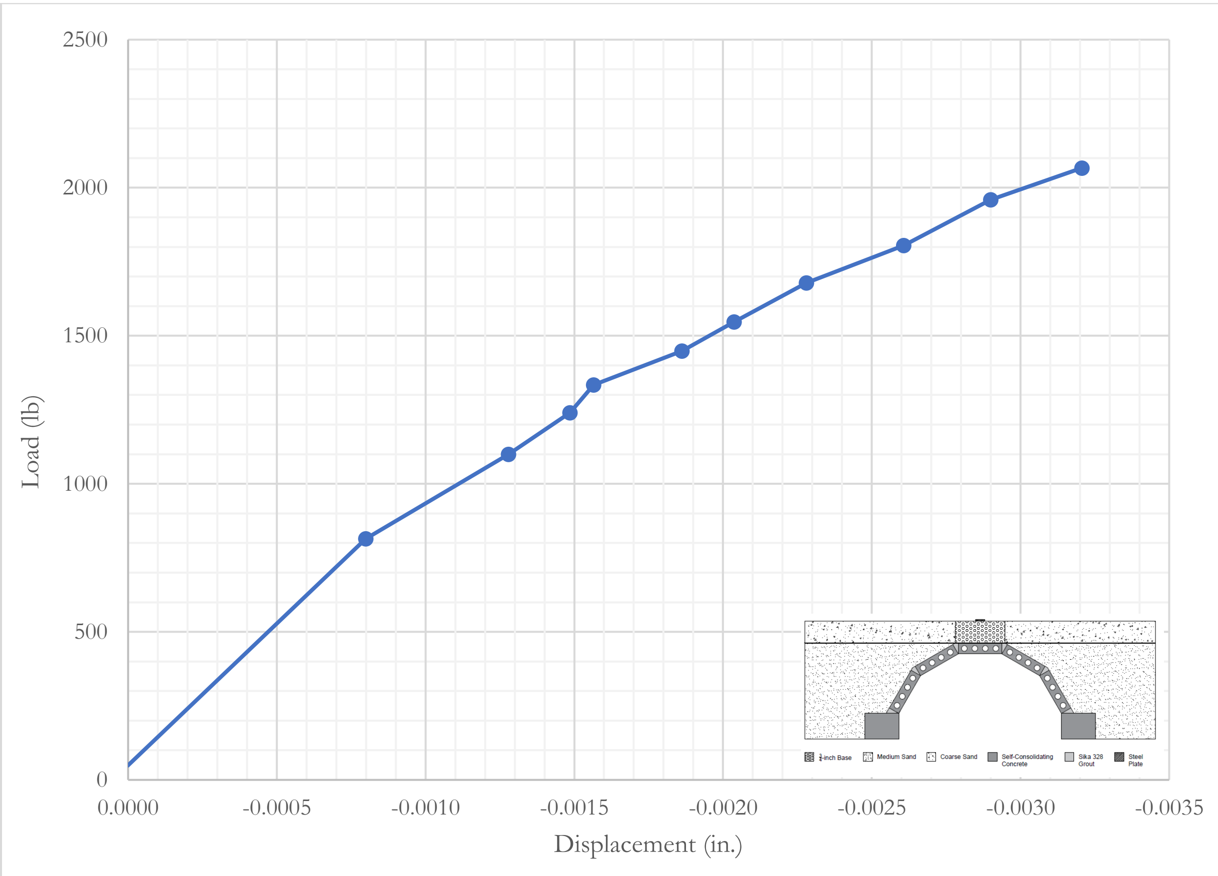

Figure 93 - Load vs. Vertical Displacement Relationship of Upper Hollow-Core Segment at Centroid – Test No. 1

4.4.4.2. Test Number 2 – Concrete Trapezoid Prism and Coarse Sand Backfill

To overcome the punching failure that was experienced during Test No. 1, a concrete trapezoid was erected on top of the upper concrete segment with dimensions that corresponded to a 60º stress distribution of a soil mass. This system replicated an extreme loading condition in which the structure was immediately loaded as would be the case if a truck was travelling directly on top of the culvert. Refer to Figure 89 for the model schematic of this test.

Testing of this model was performed in two parts: part A included loading the model up to a load of approximately 6,500 pounds in four displacement steps and then unloading the specimen; and part B entailed loading the first four displacement increments at once, and then continuing with a one displacement step increment up to a load of approximately 14,500 pounds was achieved. This represented approximately 1.6 times the load that the model was intended to sustain.

For this test, a total of four displacement steps were driven for part A and 14 displacements steps for part B. This resulted in an approximate vertical movement of the loading plate of -0.23955 inches. Test No. 2a was used to assess the lag observed between maximum load and maximum displacement achieved by the model; and correlate that lag with the load and displacement achieved at the beginning of testing of Test No. 2b. Figure 94 present the load & displacement vs. time relationships observed during Tests No. 2a for the hollow-core model.

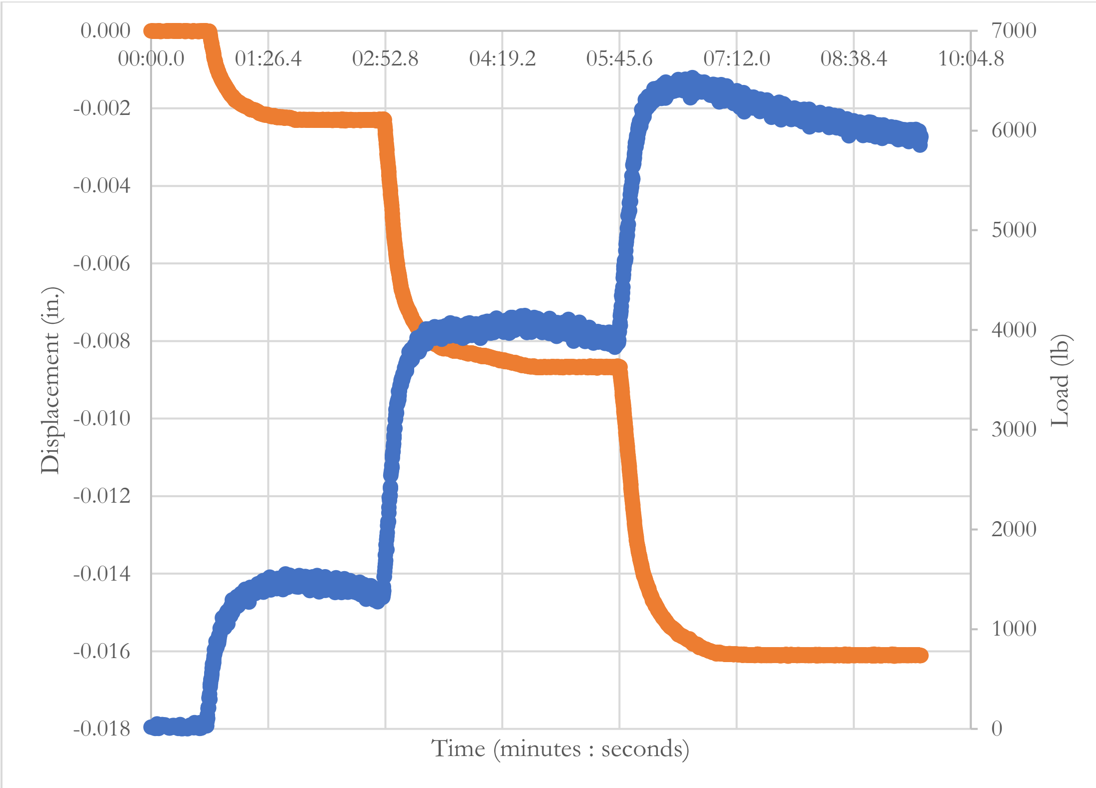

Figure 94 - Load vs. Time Hollow-Core Model Test No. 2A

Figure 95 present the load & displacement vs. time relationships observed during Tests No. 2b for the hollow-core model.

During Test No. 2B creep effects were not as evident during this round of testing as compared to Tests. No. 1. This may be the result of an increase in stiffness of the load distribution material used for testing (concrete vs. soil). On this same note, displacement steps yielded much higher load increments than the previous tests conducted. For this test a maximum load of approximately 14,500 pounds was imposed into the system.

In addition, deflections of all linear potentiometers for Test No. 2B were observed to follow a linear pattern up to approximately 11:06 a.m. Thereafter, the system was observed to have higher increases in displacement with time. Up to approximately 10:50 a.m., TCY1 and TCY2 followed a similar pattern; however, after this time, TCY1 appeared to experience much higher increases in displacement with time. This was likely the result of the crack that was observed to form after the 6th displacement step was driven. For this test, the west potentiometer recorded the highest deflection with a value of approximately -0.224 inches. The center and west potentiometers recorded maximum displacements of approximately -0.160 inches and -0.0927 inches, respectively.

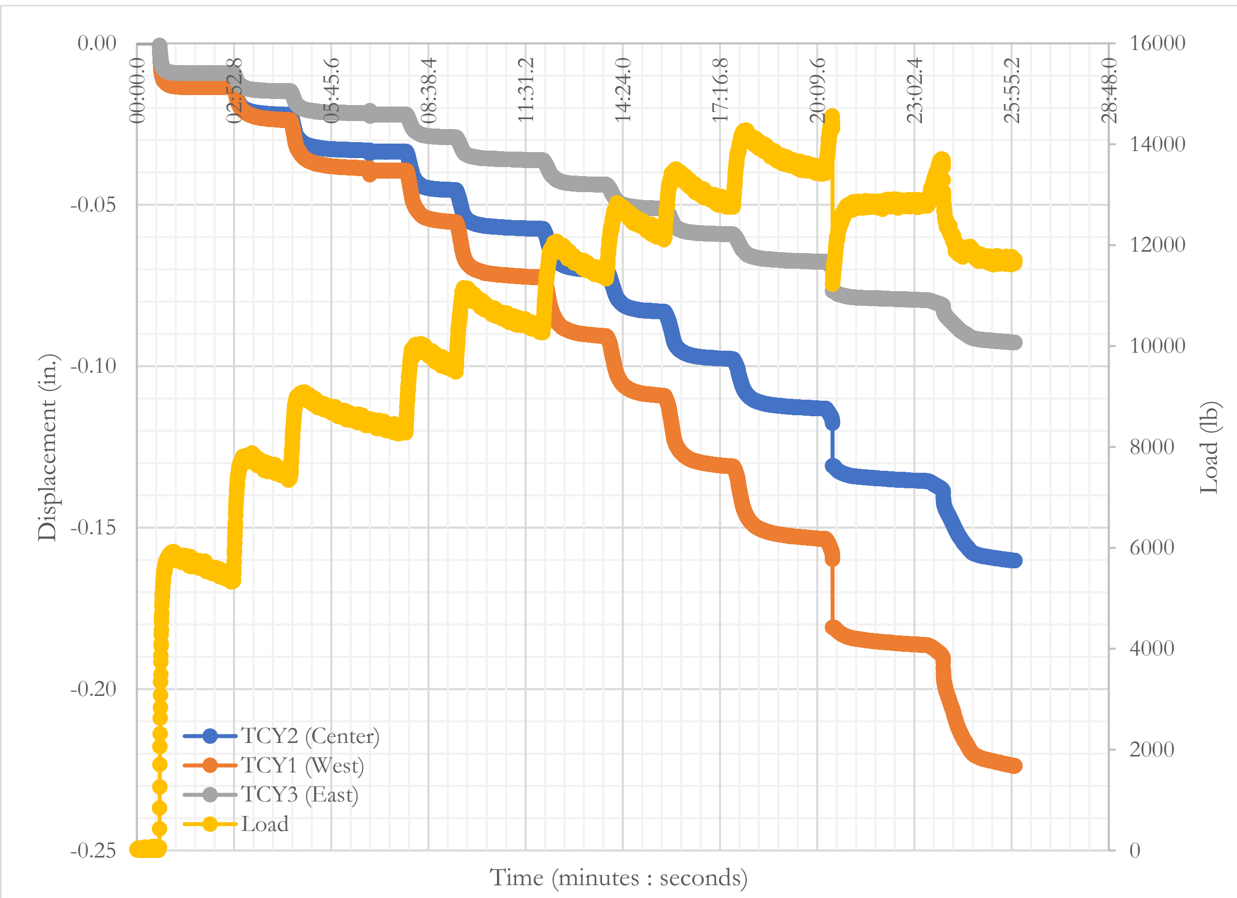

Figure 95 - Load & Displacement vs. Time Hollow-Core Model Test No. 2B

Figure 96 presents the load vs. displacement relationship obtained at the centroid of the upper concrete segment (TCY2) throughout Test No. 2B. This graph evinces a mostly linear relationship up to a load of approximately 8,000 pounds (yield strength). From a load of 8,000 pounds onward, the structure appears to be within the strain hardening state, and permanent deformation of the structure is anticipated to have developed. The ultimate strength of the structure appears to have been reached at a load of 14,560 pounds corresponding to a deflection of -0.1353 inches. Based on the test results, the maximum displacement experienced by the system was of approximately -0.1602 inches which was the result of a 13,700-pound applied load.

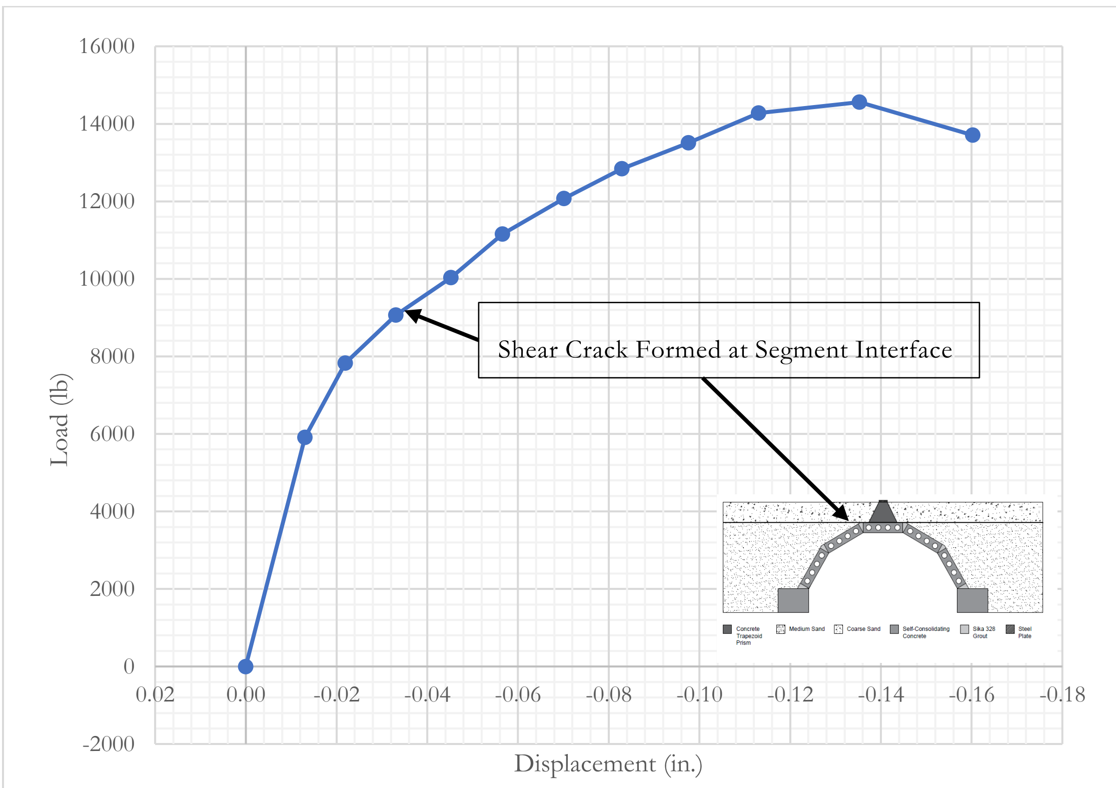

Figure 96 - Load vs. Vertical Displacement Relationship of Upper Hollow-Core Segment at Centroid – Test No. 2B

Cracking was observed to develop at a load of 9,600 pounds along the connection between the upper hollow-core panel and the west segment, more specifically between the grout and upper panel. This crack was observed to open 1/16- inch during testing. Upon removal of soil from the top and sides of the structure, the crack was observed to have extended through the thickness of the member, making it a shear crack. See Figure 97 and Figure 98 for crack location and extents.

Figure 97 - Shear crack along top/west interface. Inner face view (east direction to the bottom of the photograph).

Figure 98 - Shear crack along top/west interface. Top face view (east direction to the top of the photograph).

Horizontal movement of the structure was monitored by a set of two linear potentiometers that were positioned in the inner face of the east and west foundations. Figure 99 shows the displacements obtained for each. Based on this graph, the east and west footings appear to have undergone horizontal deflections of approximately 0.0141 and 0.0271 inches, respectively, during testing. The positive deflections obtained reflect outward movement of the structure, meaning sliding was detected. The west face appears to have experienced almost double the deflection of the east face. This may be due to the shear crack that was observed to have developed along the top and upper west segments.

Comparing the horizontal deflections obtained at the inner face of the footings against the vertical deflection obtained at the centroid of the upper segment results in an approximate outward movement of the east and west faces of 8.8% and 17% of the vertical displacement, respectively.

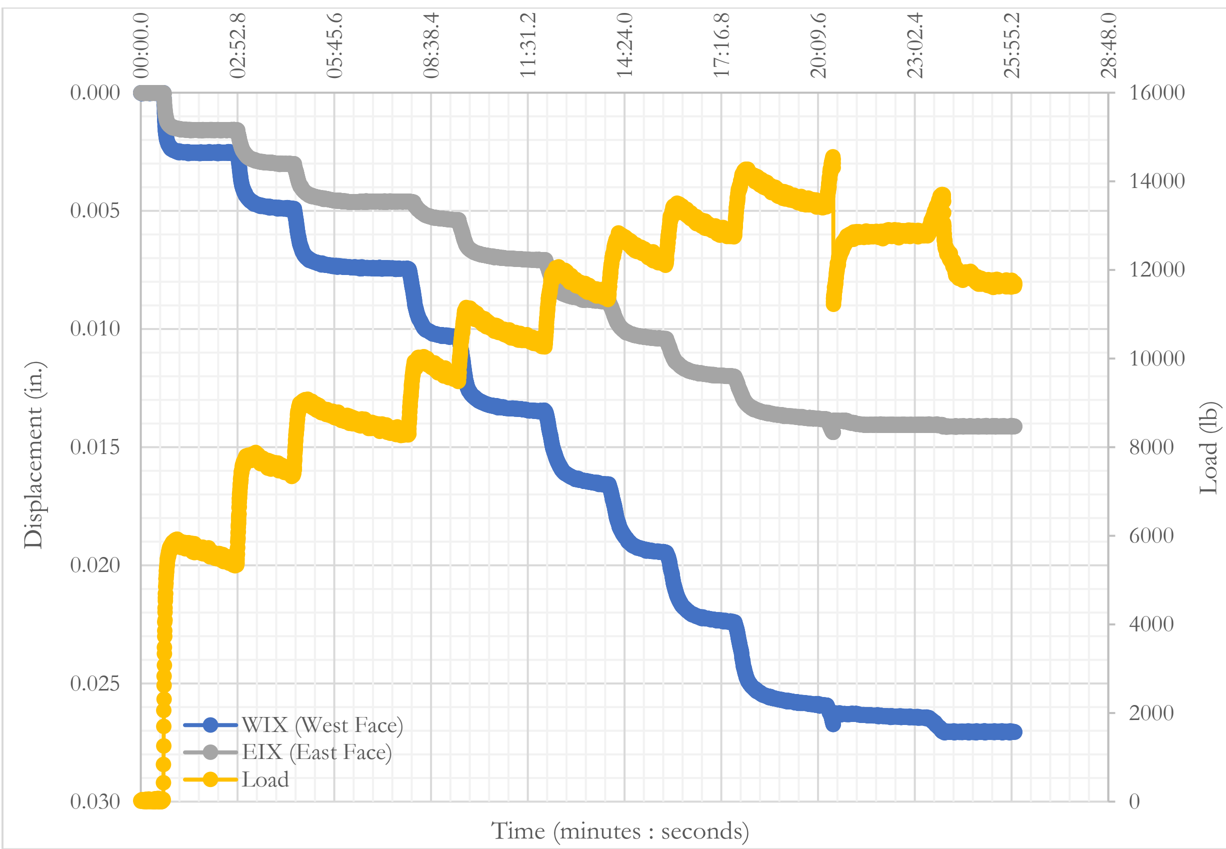

Figure 99 – Load & Horizontal Displacement vs. Time of Inner Face of Footings – Test No. 3

Strains in the x- and z-directions were also monitored by means of four linear potentiometers positioned along the north, south, east and west edges of the upper concrete segment. Namely, instruments TNX, TSX, TEZ and TWZ were used. Prior to the start of testing, the length of each potentiometer with it's corresponding extension were measured. Strains were then obtained by dividing the initial length by the maximum and minimum changes in length recorded by the instrument. In general, instruments TNX, TEZ and TWZ did not evince any major changes in length throughout testing. In fact, data recorded for all three instruments appeared to lie between 0.001 inches and -0.001 inches. TSX, however, did show a higher movement, with peaks in the positive and negative directions (extension and retraction).

Table 34 below presents the strain results based on maximum (extension) and minimum (retraction) displacement values obtained during testing for each instrument.

Table 34 - Strains of Upper Hollow-Core Panel

Instrument	Initial Length (in.)	Change in Length (in.)		Strain (in./in.)	
		Max.	Min.	Max.	Min.
TNX	15.4375	0.000808	NA	0.0000523	NA
TSX	14.6875	0.0088	-0.0254	0.0005991	-0.0017294
TEZ	15.4375	0.0000525	-0.0000525	0.0000034	-0.0000034
TWZ	15.1250	NA	-0.00105	NA	-0.0000069

The changes in length obtained during experimental testing appear to have been minimal. Based on the accuracy of the instruments used (0.001 inches), the values obtained may have been highly influenced by the sensitivity of each potentiometer. The only significant strains that appear to have developed during testing are those for the TSX instrument. However, the fluctuations observed between the positive and negative values, make the recorded displacements uncertain.

Movement of the soil box walls was also monitored by means of two sets of three linear potentiometers located at the northeast and southwest corners of the model (see Figure

32 for instrument locations). Figure 100 presents the displacements recorded in the x-direction. Based on this diagram, the east and west footings appear to have undergone horizontal deflections of approximately 0.0141 and 0.0271 inches, respectively, during testing. The positive deflections obtained reflect outward movement of the structure, meaning sliding was detected. The west face appears to have experienced almost double the deflection of the east face. This may be due to the shear crack that was observed to have developed along the top and upper west segments.

Comparing the horizontal deflections obtained at the inner face of the footings against the vertical deflection obtained at the centroid of the upper segment results in an approximate outward movement of the east and west faces of 8.8% and 17% of the vertical displacement, respectively.

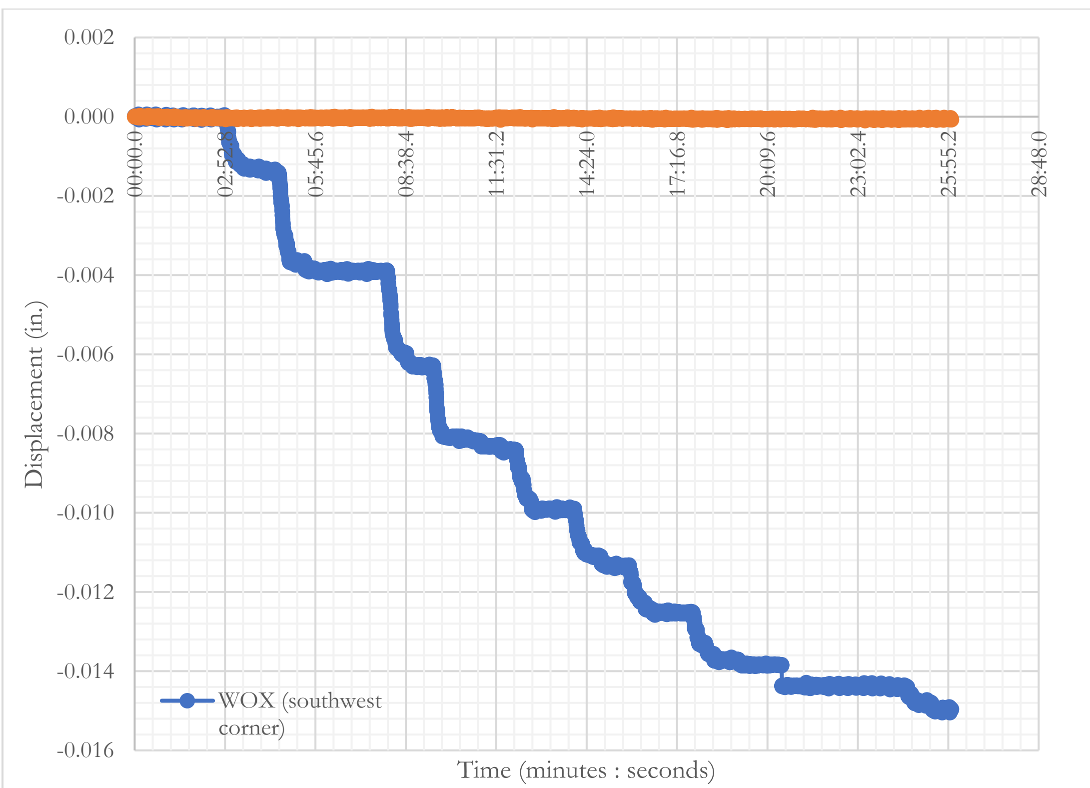

Figure 100 - Displacement of Soil Box in X-Direction – Hollow-Core Model

Figure 101 presents the displacements recorded in the y-direction. Downward movement of the east and west walls were recorded by linear potentiometers TBNY and TBSY. The south portion of the west wall appears to have moved approximately 0.004 inches downward and the north portion of the east wall approximately 0.0003 inches downward. Detectable displacements at these locations started occurring after the first set of displacement steps were imposed on the model, for the southeast corner, and after an approximate 8,700 pounds compressive load was imposed on the model. Toppling effects do not seem to have occurred during testing.

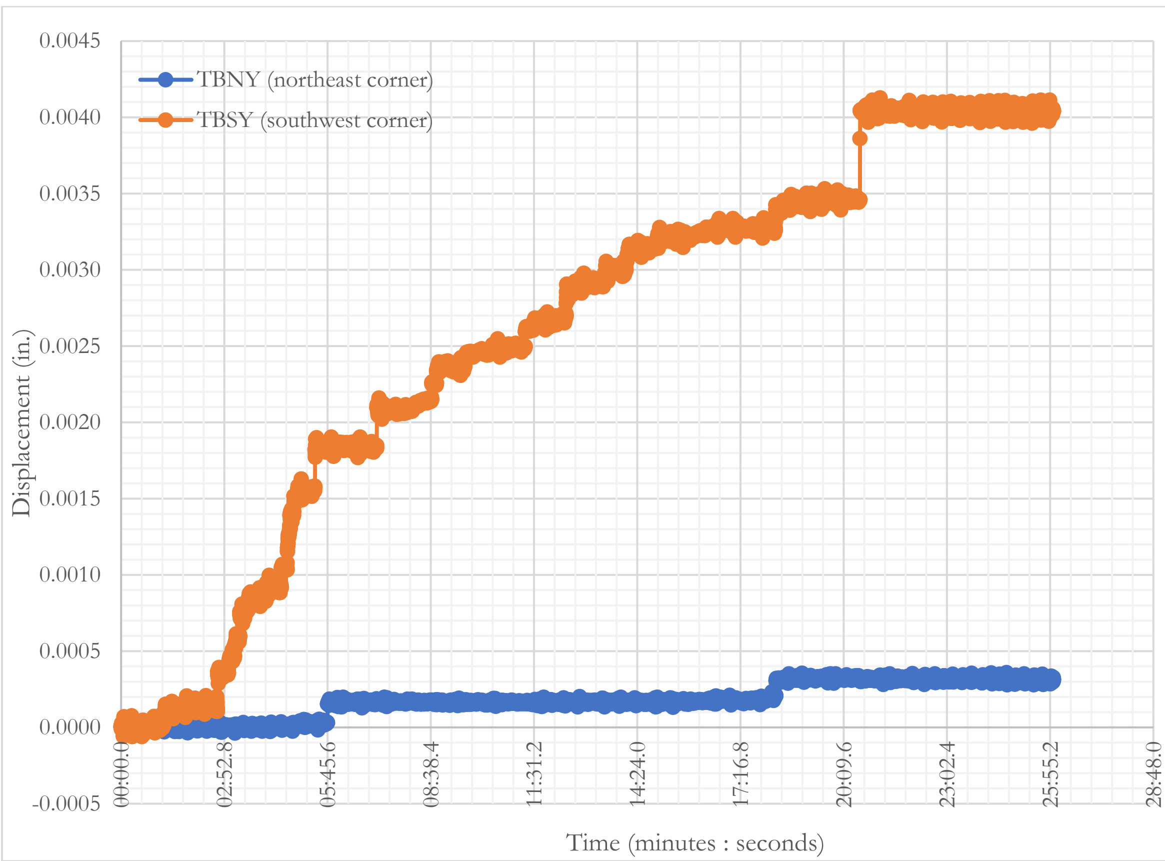

Figure 101 - Displacement of Soil Box in Y-Direction – Hollow-Core Model

Figure 102 presents the displacements recorded in the z-direction. Movement of the north wall was not detected during testing of this model. Differently, the south wall underwent an approximate displacement of -0.015 inches. The negative sign of this potentiometer indicates that the instrument was contracting and the wall was moving outward.

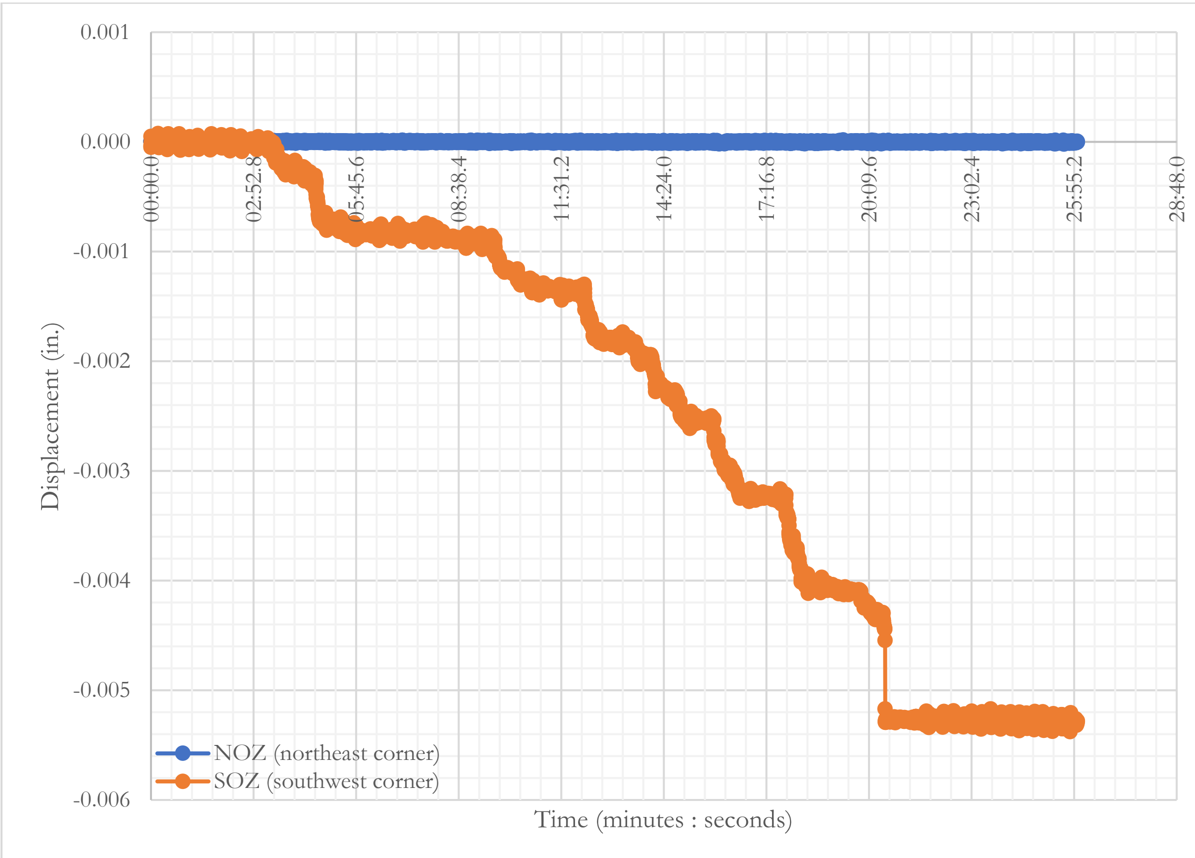

Figure 102 - Displacement of Soil Box in Z-Direction – Hollow-Core Model

4.4.4.3. Test Number 3 – Concrete Trapezoid Prism with no Backfill

To evaluate the strength of the hollow-core structure without the aid of the backfill material, which ultimately influenced the structure by putting it into compression and aiding in obtaining a higher capacity, a third test was conducted. For this test, only the soil placed next to the footings was left in place and the rest of the backfill material was removed from the model. Refer to Figure 90 for the model schematic of this test. Testing of this model was performed until the structure was not able to sustain additional load with increasing actuator displacement. Since the model was anticipated to be taken to ultimate failure (collapse), only three linear potentiometers were left in place. One instrument was used to record vertical deflection at the centroid of the upper hollow-core panel, and the other two measured lateral deflection of the soil box at the north and south walls. For this test, a total of 40 displacement steps were driven by the actuator which resulted in an approximate vertical movement of the loading plate of -0.8032 inches.

During this round of testing, residual displacement along the shear crack was evident after a load of approximately 3,500 pounds was reached. At this point, peaks were observed followed by a rapid decrease in load. The behavior was the result of the residual shear strength along the crack at the west interface (Test No. 2b). The arch remained on compression throughout the full load application. The maximum load obtained during this round of testing corresponded to a value of approximately 5,660 pounds.

Additionally, deflections experienced by the upper hollow-core segment appear to correspond to the residual strength of the system. This is due to the fact that, during the second round of testing, the yield point of the system was reached (load of 14,560 lb) and permanent deformation of the structure occurred. For Test No. 3 total deflection of the center gauge was of approximately -0.711 inches.

The following figure presents the load & displacement vs. time relationships observed during the third round of testing of the hollow-core model.

Figure 103 - Load & Displacement vs. Time Hollow-Core Model Test No. 3

Figure 104 presents the load vs. displacement relationship obtained at the centroid of the upper concrete segment (TCY2) throughout Test No. 3. The load vs. displacement graph evinces a mostly linear relationship up to a load of approximately 3,530 pounds. From that load onward, the structure appears to be within the residual strength state. Based on the test results, the maximum load experienced by the system was of approximately 5,660 pounds which resulted in a displacement of the upper concrete panel of -0.5234 inches.

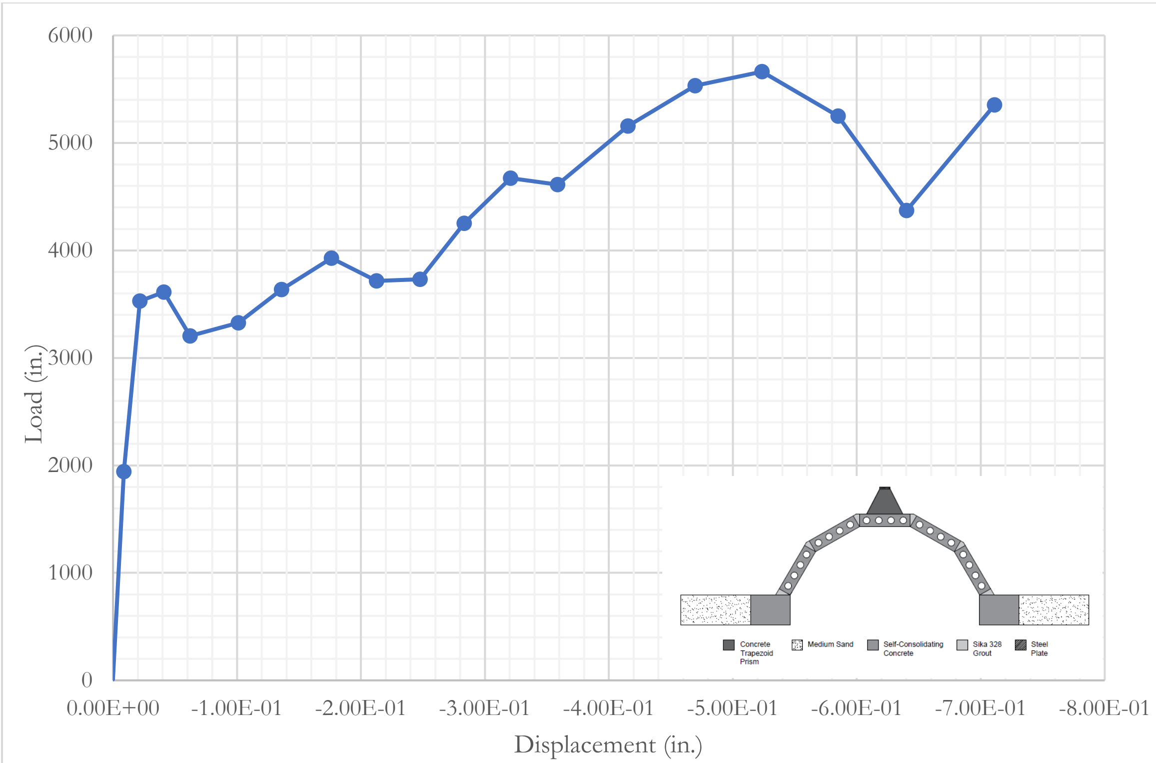

Figure 104 - Load vs. Vertical Displacement Relationship of Upper Hollow-Core Segment at Centroid – Test No. 3

During testing, the shear crack that had developed at interface between the west grout connection and the upper hollow-core segment during Test No. 2b, was observed to shift vertically. In other words, shear failure was observed to have developed at this location. At the end of testing, the west panel had moved vertically approximately 1.375 inches with respect to the top hollow-core segment. Figure 105 and Figure 106 show the shear failure. It is important to note that the culvert remained in compression as a result of the arch action.

Figure 105 - Shear failure observed at interface between top hollow-core panel and west connecting grout. Side and top view.

Figure 106 - Shear failure observed at interface between top hollow-core panel and west connecting grout. Bottom view.

In addition, a moment crack developed between the upper and lower east panels at approximately at a load of approximately 5,270 lb. The crack extended along the full length and thickness of the segment. At the end of testing, this crack had an opening of approximately 0.1875 inches. Figure 107 and Figure 108 below show the moment crack observed in the structure.

Figure 107 - Moment crack observed at interface between top east and bottom east hollow-core panels at the connection grout. Top view.

Figure 108 - Moment crack observed at interface between top east and bottom east hollow-core panels at the connection grout. Side view.

Movement of the north and south retaining walls was monitored by means of LS1 and LS2 linear potentiometers. For this test, LS1 was relocated to the north (upper center) wall. Data recorded by LS1 and LS2 showed that wall movement was occurring towards the south. This is evinced by the positive displacements of LS1 (located on the north wall), meaning the instrument was undergoing elongation; and the negative displacements of LS2 (located on the south wall) which corresponded to a contraction experienced by the potentiometer. Possible reasons for these results are likely related to the observed southward tilt of the hollow-core culvert observed during assembly and prior to the start of the test. Figure 109 presents the movement recorded for LS1 and LS2.

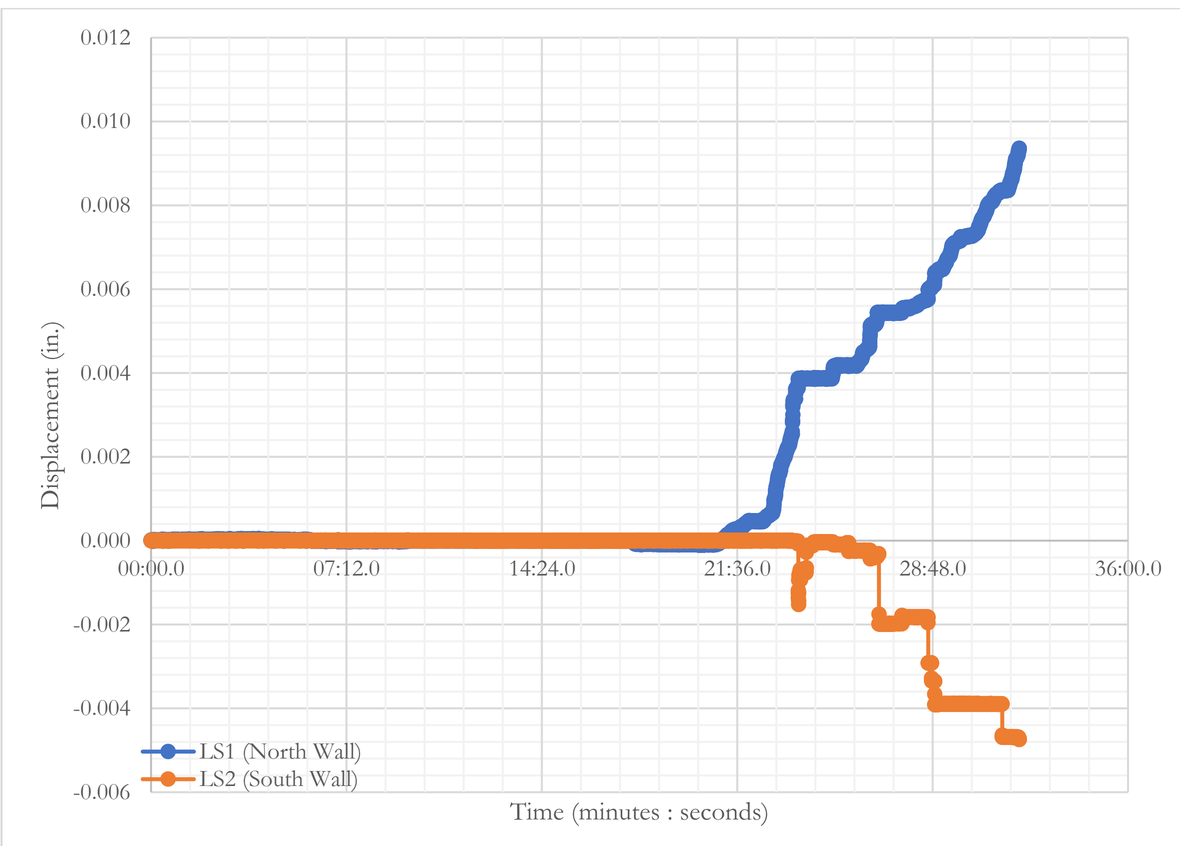

Figure 109 - Displacement in Z-Direction of North and South Walls of Hollow-Core Model - Test No. 3

4.4.4.4. Comparison Hollow-Core Test Results

In an effort to assess the similarities and differences in the hollow-core test results, specifically related to the centroid on the inner face of the upper concrete segment, the load vs. displacement graphs developed for all tests were compiled in one plot. Figure 110 below presents said relationships.

Based on this figure, the linear elastic region of Tests No. 1 and 2B appear to follow a similar path. Test No. 1 and 2B showed slightly more stiffness than Test No. 3 due to the compression state of the backfill soil around the structure (soil absent during Test No. 3). Additionally, considering Test No. 3 was likely run on the "residual strength" of the system since the ultimate strength of the model was reached at the end of Test No. 2, the stiffness of the structure was compromised. This can be seen by the shallower slope at the beginning of test and the rapid increase in deflection, from approximately 3,530 pounds to the end of testing, with minor increases in loading.

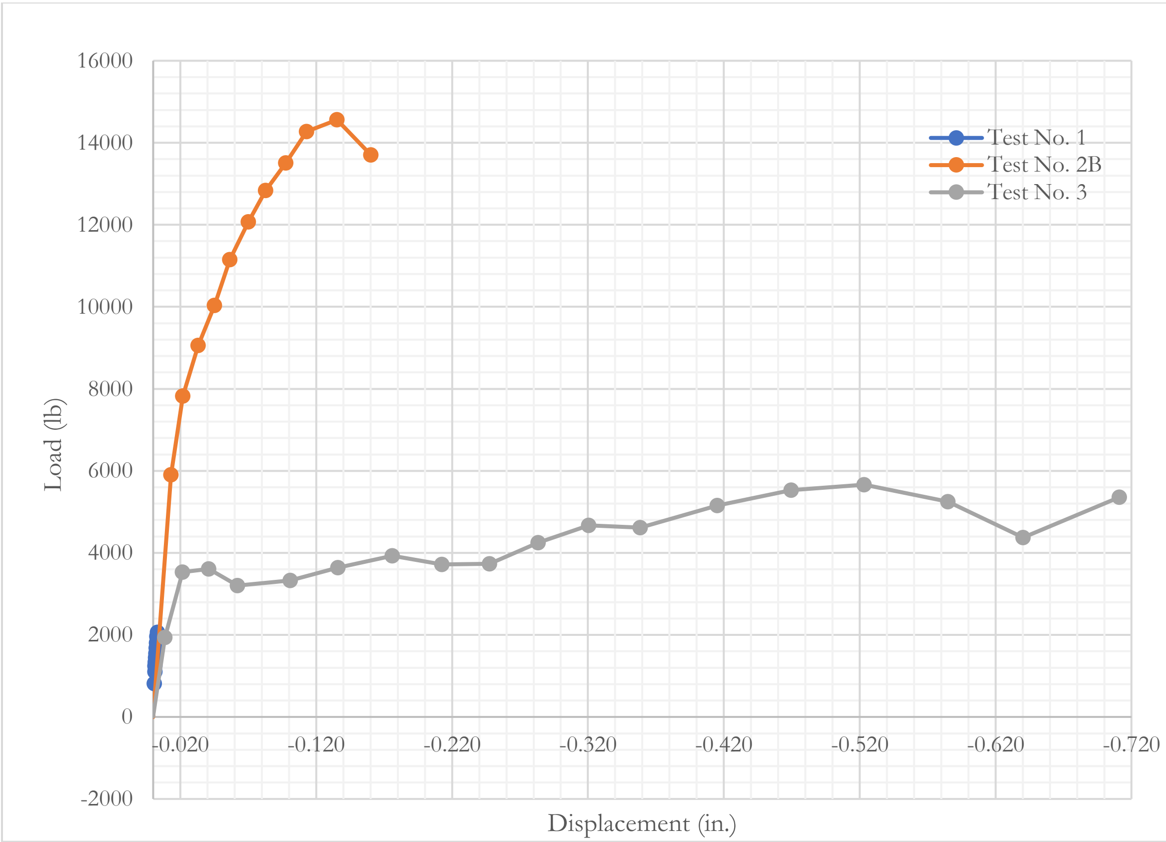

Figure 110 - Compilation of Load vs Displacement Data of TCY2 for all Rounds of Testing of Hollow-Core Model

In an effort to compare the test results obtained from the CIP and hollow-core models and assess the similarities between select rounds of testing (soil cover and concrete trapezoid with backfill); Figure 111 and Figure 112 were developed.

In Figure 111, results obtained for Tests No. 1 and 2 of the CIP model were compared to those obtained for Test No. 1 of the hollow-core model since these were the tests that used backfill soil as the cover material. In general, all three tests showed similar linear elastic relationships with highly comparable slopes. Interestingly, Tests No. 1 of both models had almost identical load vs. displacement relationships even though the backfill material used differed (pea gravel for the CIP and ¾-inch road base for the hollow-core).

Test No. 2 of the CIP displayed a higher initial stiffness and a greater ultimate bearing capacity compared with the other tests, most likely because of the greater compactive state of the soil. The soil backfill above the hollow-core arch underwent a bearing failure at an axial load of roughly 2,100 pounds, which was much lower than in the CIP tests.

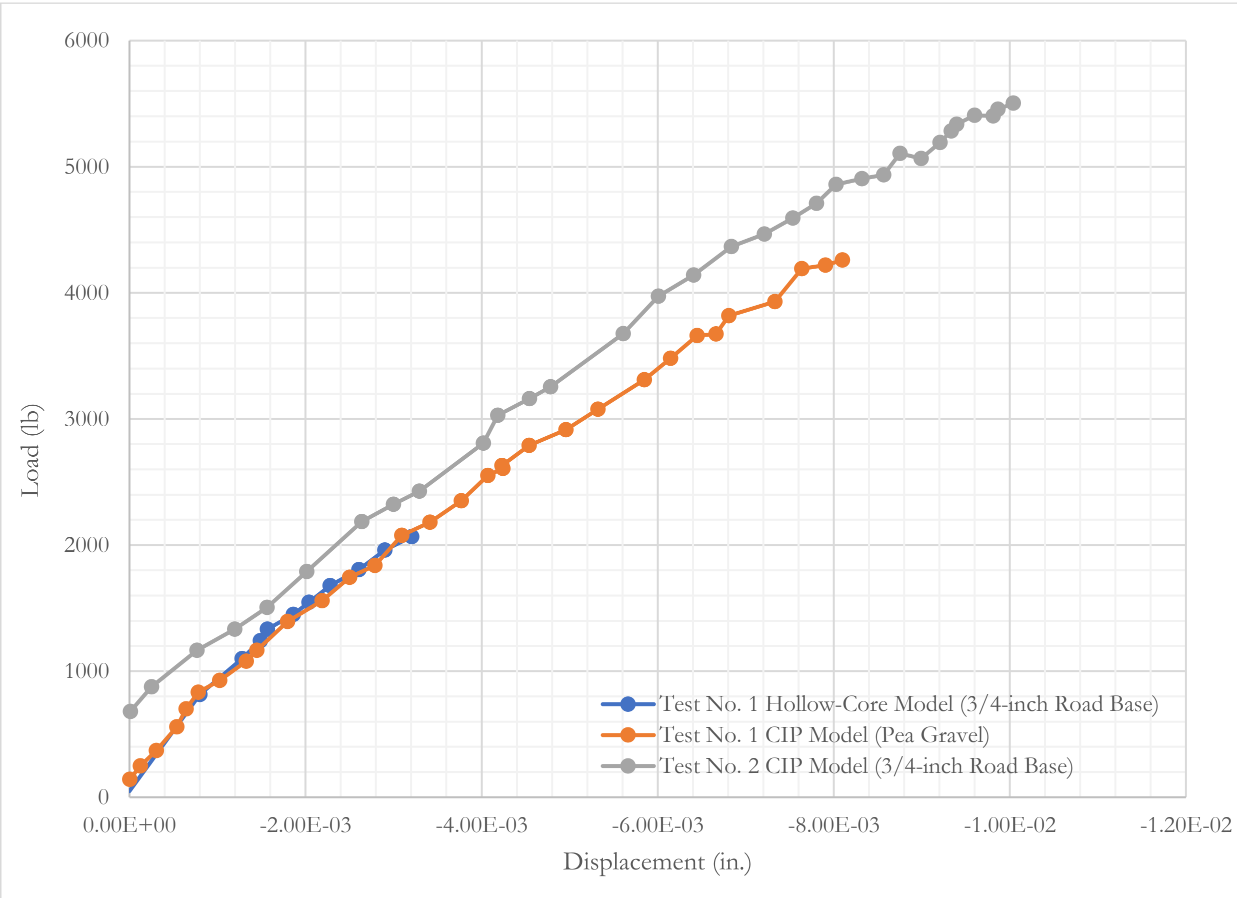

Figure 111 - Comparison of Load vs Displacement Data of TCY2 for Test No. 1 of Hollow-Core Model and Tests No. 1 and 2 of CIP Model

For Figure 112, results obtained for Test No. 3 of the CIP model were compared to those obtained for Test No. 2B of the hollow-core model since these were the tests that used the trapezoid prism with backfill soil on top of the upper concrete segment. In general, Test No. 3 of the CIP model evinced higher stiffness and strength than that of the hollow-core arch, based on the steeper linear elastic slope, lower centerline deflection and the higher ultimate load. These differences in behavior are likely related to the use of a monolithic structure (CIP model) compared with the assembled model (hollow-core model) which had grouted joints to connect different segments. This means that, the monolithic structure was acting as one continuous arch whereas the hollow-core arch acted more like a segmental structure. Moreover, the hollow-core arch failed along a grouted joint before reaching capacity of the segment section.

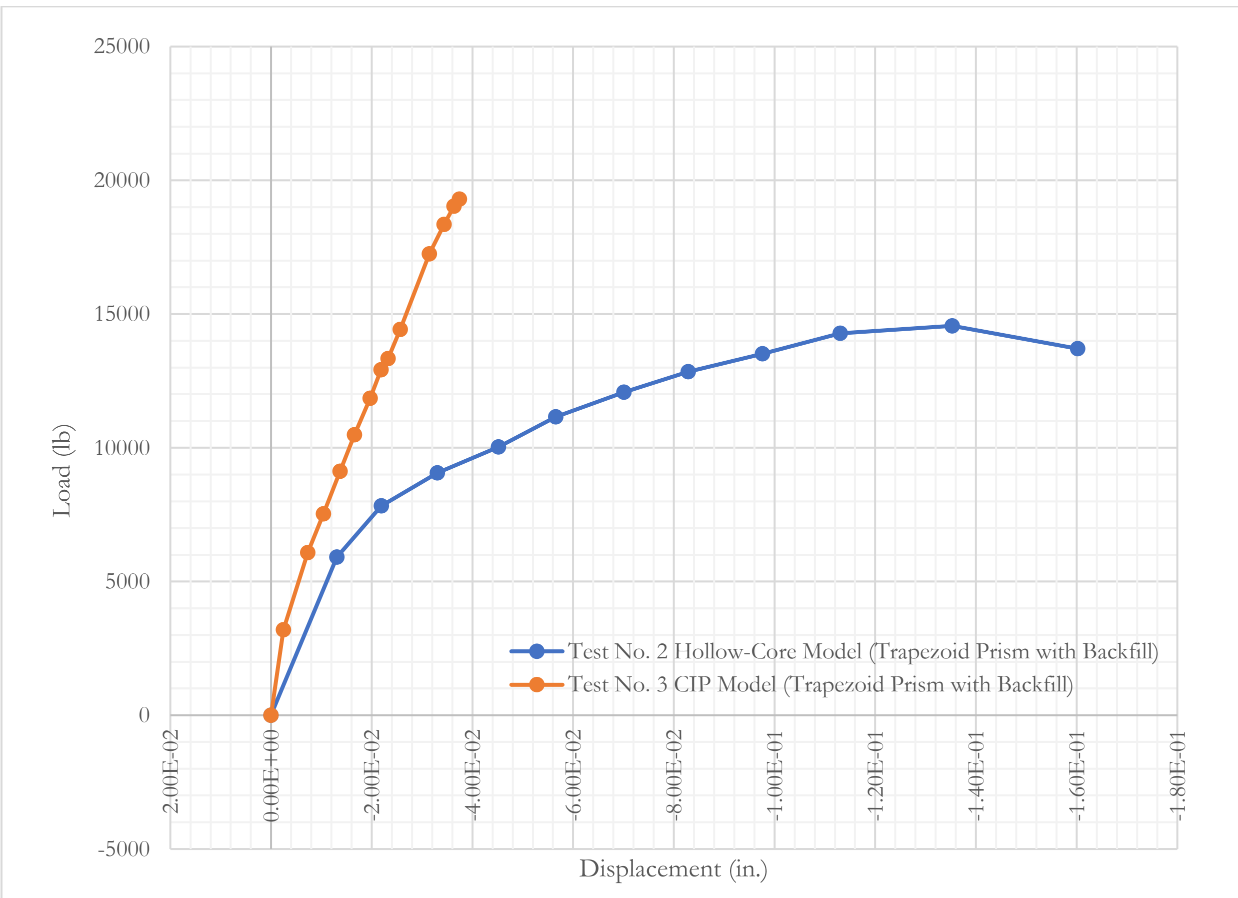

Figure 112 - Comparison of Load vs Displacement Data of TCY2 for Test No. 2B of Hollow-Core Model and Test No. 3 of CIP Model

4.5. FEM Analysis

The fourth phase of this project entailed modeling the hollow-core culvert, under the same loading conditions as those described in Section 3.3, using finite element software. As was done with the CIP model, ANSYS Mechanical APDL was utilized to develop 2-D and 3-D simulations for the three tests performed on the hollow-core structure. Results obtained from these simulations were compared to those obtained during experimental testing to assess the closeness of the two methods of analysis; and subsequently, the FEM model was refined to yield similar responses as those observed in the laboratory. The ultimate goal of the FEM model was to provide a "calibrated" simulation that could be used to obtain structure responses of different underground system configurations.

The following sections present the methods and results of each simulation developed for the hollow-core culvert.

4.5.1. Model Configuration Methodology

4.5.1.1. Geometric Properties

The numerical hollow-core model was created to represent the same scale as that of the experimental model. As such, the hollow-core FEM model had an approximate overall length of 193 inches and a height of 65 inches. The depth component for the 3D simulation was cut in half (15.5 inches) since the stresses and deflections right below the loaded area were of interest.

The same elements as those used for the 2D and 3D CIP simulations were used for the hollow-core models. Refer to Section 3.6.1 for additional element information.

To create the 2D and 3D configurations, KeyPoints were developed. The KeyPoints reflected vertex locations of different portions of the model which were then connected to create the solid areas. Figure 113 displays the KeyPoints used for both configurations (2D and 3D simulations) for each round of testing. Refer to Appendix J – FEM Simulations for KeyPoint numbers and additional geometric information.

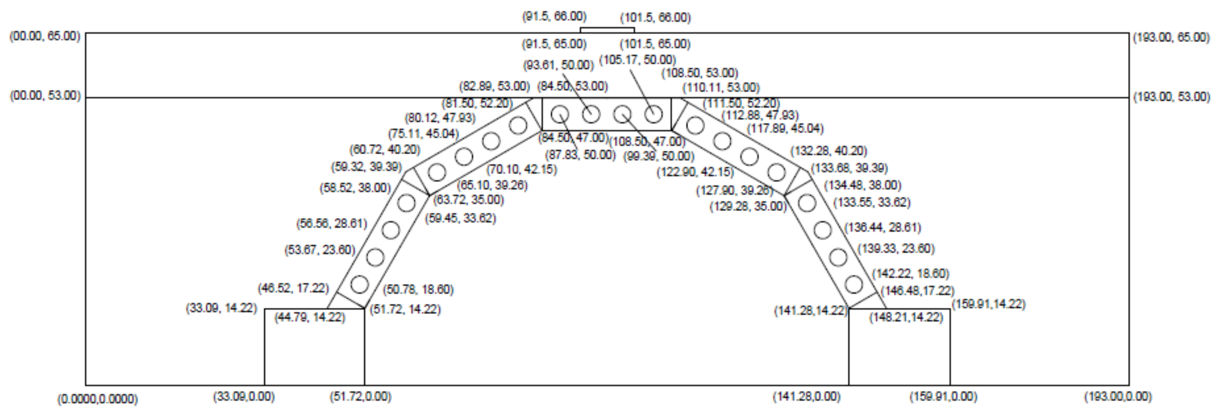

Figure 113 - KeyPoints used for 2D and 3D Hollow-Core FEM Models for all Rounds of Testing

To create volumes for the 3D simulation, the previously assembled areas were extruded to half the width of the model. In other words, only the middle half of the structure (in the long direction) was analyzed so that the stresses and displacements right below the loading plate were easily identified.

4.5.1.2. Material Properties

Since the physical hollow-core concrete structure remained within the linear-elastic range up to the application of the 9.03-kip load was imposed, and the culvert did not evince significant cracking during this portion of experimental testing, the FEM 2D and 3D simulations only included linear-elastic analyses. As a result, linear, elastic, and isotropic conditions were assigned to the concrete, soil and steel elements. Table 35 Table 19 below provides the material specifications assigned to each unit.

Table 35 – Hollow-Core FEM Material Properties

ID	Material	Modulus of Elasticity (psi)	Poisson's Ratio
1	SCC	5.49×10^6	0.29
2	Medium Sand	5.2×10^3	0.3
3	Coarse Sand	2.08×10^3	0.35
4	¾-inch Road Base	20.8×10^3	0.3
5	Steel Plate	29×10^6	0.3
6	Concrete Trapezoid	3.36×10^6	0.2
7	Sika 328 Grout	4.24×10^6	0.25

Values used for the SCC were based on the Modulus of Elasticity and Poisson's Ratio laboratory test results presented in Section 4.4.2.3. For the Sika 328 grout, the modulus of elasticity value was based on the equation presented in ACI 318 (Section 19.2.2.1(a)) which relates the unit weight of concrete with its corresponding compressive strength. The Poisson's ratio selected for this material was based on published literature (Allan & Philippacopoulos, 1999). For the Rapid Set Concrete Mix, the modulus of elasticity value was also based on the ACI 318 (Section 19.2.2.1(a)) equation. This value was preferred over the laboratory test result obtained due to its resemblance with published E modulus ranges for concrete (the laboratory test result was one order of magnitude lower than what the published ranges present). The Poisson's ratio selected for this material was also based on published literature. See Appendix H – Correlation Charts for published elastic modulus and Poisson's ratio values of concrete.

In addition, material properties of the soil elements were obtained by correlating the lowest unit weight of the compacted sands and ¾-inch road base to the apparent density and soil condition description (either loose, medium, dense or very dense) of each material, and selecting the corresponding elastic modulus and Poisson's ratio values.

The lowest dry unit weight obtained for the medium sand (well graded sand with silt) resulted in an approximate value of 103.6 pcf which corresponded to a 55% apparent density and a medium dense condition description (McCarthy, Representative Values of Relative Density, 2007). Based on the *Range of Values: Modulus of Elasticity and Poisson's Ratio* table presented in the *Essentials of Soil Mechanics and Foundations, Basic Geotechnics* book by David F. McCarthy, the modulus of elasticity of a medium dense sand generally ranges between 3,500 and 6,950 psi and the Poisson's ratio between 0.25 and 0.4. For the FEM model, a modulus of elasticity and Poisson's ratio of 5,200 psi and 0.3 were used.

For the coarse sand (silty sand), the dry unit weight was obtained by correlating the moisture contents with the proctor compaction curve for this material. Based on a moisture content of 2.5%, an approximate dry unit weight of 103 pcf was obtained, which corresponded to a 55% apparent density and a medium dense condition. Based on the previously cited table developed by David F. McCarthy, the modulus of elasticity of a medium dense silty sand generally ranges between 1,042 and 3,125 psi and the Poisson's ratio between 0.2 and 0.4. For the FEM model, a modulus of elasticity and Poisson's ratio of 2,080 psi and 0.35 were used.

The dry unit weight obtained for the ¾-inch road base (silty gravel with sand) resulted in an approximate value of 127.0 pcf which corresponded to a 82% apparent density and a dense condition description (McCarthy, Representative Values of Relative Density, 2007).

Based on the correlation charts, the modulus of elasticity of a dense sand and gravel ranges between 13,900 and 27,800 psi and the Poisson's ratio between 0.3 and 0.45. For the hollow-core model, values of 20,800 psi and 0.35 were used for the modulus of elasticity and Poisson's ratio of the ¾-inch road base.

For the steel plate, the material properties used corresponded to those of typical stainless-steel members.

4.5.1.3. Loading Configuration

Loading configurations within the FEM models were setup to mimic the conditions of the physical model. The supports used for the 2D and 3D models included rollers at the right and left face lines of the soil edges to prevent movement from happening in the x-direction. This confinement was provided by the short walls in the physical model. In addition, to simulate the floor connection, all bottom edge lines were fixed. Furthermore, for the 3D model, rollers were placed on the front and back face lines of the culvert and soil edges to confine movement in the z-direction. This retention was provided by the long walls in the physical model.

To model the compressive surface load applied during experimental testing, a line load of 1,806 lb/in acting over a 5-inch length was used for the 2D simulation. Similarly, a pressure of 180.6 ln/in^2 acting over a 5-inch by 10-inch area was used for the 3D model. These values corresponded to a point load of 9.03 kips. Figure 114 provides a graphical representation of the 3D model with the corresponding supports and surface load for Test No. 2.

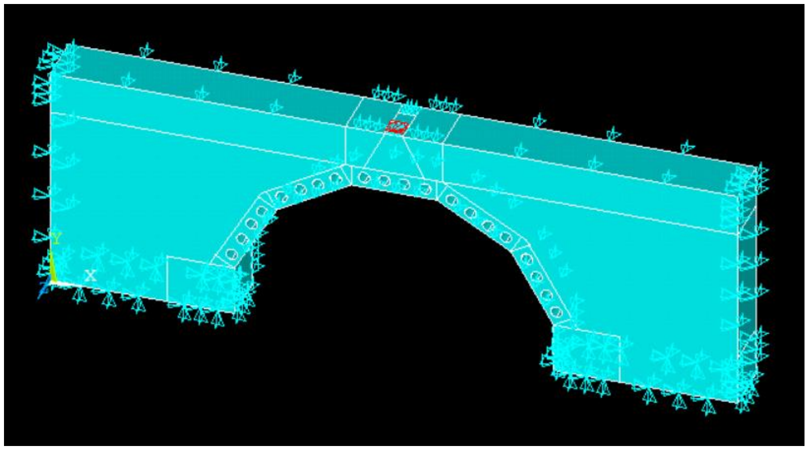

Figure 114 - 3D Model with Supports for Test No. 2

4.5.1.4. Meshing

Different size meshes were used within the 2D and 3D simulations to provide varying levels of detail within the model. For both models, meshing was done manually, and the element sizes entered attempted to make use of most elements allowed by the software (maximum 256,000 elements). Division numbers were based on the sensitivity of the element within the model. For instance, the loaded soil layer or trapezoid prism had a finer mesh than that used for the bottom sand backfill since more detail was needed for elements located directly below the loaded area.

Table 36 below presents the element sizes used for each material within the 2D and 3D simulations for all rounds of testing.

Table 36 - Mesh divisions used for the 2D and 3D models

Component	Test No. 1		Test No. 2b		Test No. 3	
	2D	3D	2D	3D	2D	3D
Hollow-Core Culvert	0.2	2-3	0.2	2-3	0.1	2
Medium Sand Backfill (East and West)	1	3	1	3	0.5	1

Component	Test No. 1		Test No. 2b		Test No. 3	
	2D	3D	2D	3D	2D	3D
Coarse Sand Backfill (East and West)	1	3	1	3	-	-
3/4-inch Road Base Backfill	0.2	2	-	-	-	-
Steel Plate	0.5	2	0.5	2	0.2	2
Concrete Trapezoid	-	-	0.2	2	0.2	2
Sika 328 Grout	0.1	1	0.1	1	0.1	1

Mesh divisions for the 3D models required a coarser mesh for all materials since it in included a depth component.

4.5.2. Model Analysis Results

One of the main focuses of this study was to develop a calibrated FEM simulation that could be used to predict structure responses of different culvert configurations under similar loading conditions. To achieve this, a model was developed and refined to produce similar structure responses as those observed during experimental testing of the hollow-core model.

The main basis of comparison and refinement between the FEM simulation and the physical model were the displacements obtained at specific locations. In general, longitudinal deflections (y-direction) of interest were obtained at the loading plate, at the interior face of the top segment and at the northeast and southwest corners of the soil box. In addition, transverse deflections and strains (x-direction) were evaluated at the interior faces of the footings and at the interior north and south edges of the top segment. All locations listed matched the areas where potentiometers were mounted on the physical model.

4.5.2.1. Initial Model Predictions

After obtaining the main material properties of the components used for the construction of the hollow-core model, an initial FEM simulation was developed and analyzed to predict deflections for all rounds of testing. The following table presents the predicted displacements at select model locations for all tests. Note that location designations used match the naming conventions of instrumentation mounted on the physical hollow-core model.

Table 37 - Displacement Predictions – Tests No. 1 and 2 Hollow-Core Model

Location	Location	Displacement (in)			
		Test No. 1		Test No. 2b	
		2D	3D	2D	3D
TCY1	Bottom face of top concrete segment, west side, center line, y-direction	-0.083523	-0.0022605	-0.075442	-0.0018261
TCY2	Bottom face of top concrete segment, middle, center line, y-direction	-0.11639	-0.0030904	-0.091086	-0.0022049
TCY3	Bottom face of top concrete segment, east side, center line, y-direction	-0.081694	-0.0022294	-0.072747	-0.0018050
EIX	Interior face of footing, east side, x-direction	0.00039585	0.000024457	0.00026182	0.000024835

Location	Location	Displacement (in)			
		Test No. 1		Test No. 2b	
		2D	3D	2D	3D
WIX	Interior face of footing, west side, x-direction	-0.00042517	-0.00002629	-0.00026933	-0.000024887

Table 38 - Displacement Predictions – Test No. 3 Hollow-Core Model

Designation	Location	Displacement (in)	
		Test No. 3	
		2D	3D
TCY1	Bottom face of top concrete segment, west side, center line, y-direction	-0.077518	-0.0019946
TCY2	Bottom face of top concrete segment, middle, center line, y-direction	-0.093076	-0.0024659
TCY3	Bottom face of top concrete segment, east side, center line, y-direction	-0.074354	-0.0019666
EIX	Interior face of footing, east side, x-direction	0.00024218	0.000038594
WIX	Interior face of footing, west side, x-direction	-0.00023715	-0.00003668

Based on the above predictions, it was anticipated that the upper hollow-core panel was going to undergo deflections between -0.0022 and -0.11 inches for Test No 1; between -0.0018 and -0.09 inches for Test No. 2b; and between -0.002 and -0.093 inches for Test No. 3. This meant that the test that used soil material on the top and sides of the structure was going to cause higher deflections to the structure than those that used the trapezoid prism with and without soil on the sides. In addition, minimal outward movement of the footings was expected.

The following figures show the nodal plot of the vertical displacements that were predicted for Test No. 2b. Similar deformed plots were obtained for the other three rounds of testing. The only difference between each was the amount of displacement predicted by the simulation at each location.

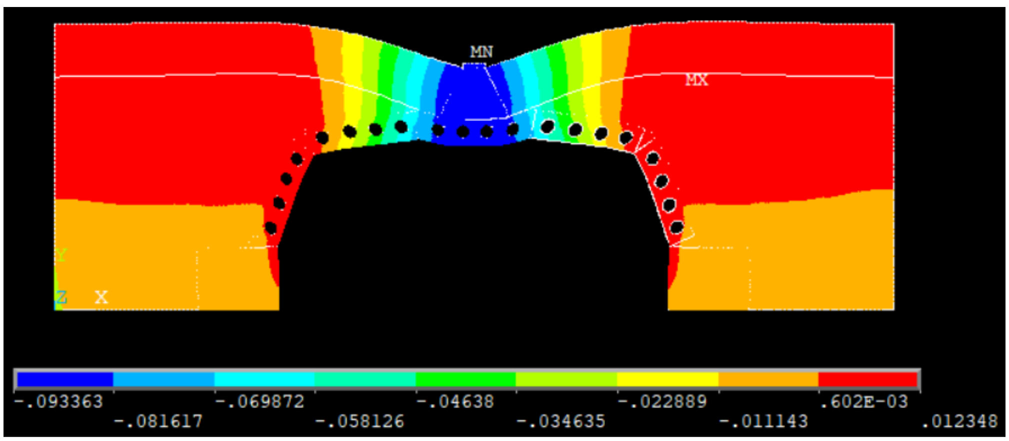

Figure 115 - 2D Nodal Solution of Predicted Displacements for Test No. 2b – Hollow-Core Model

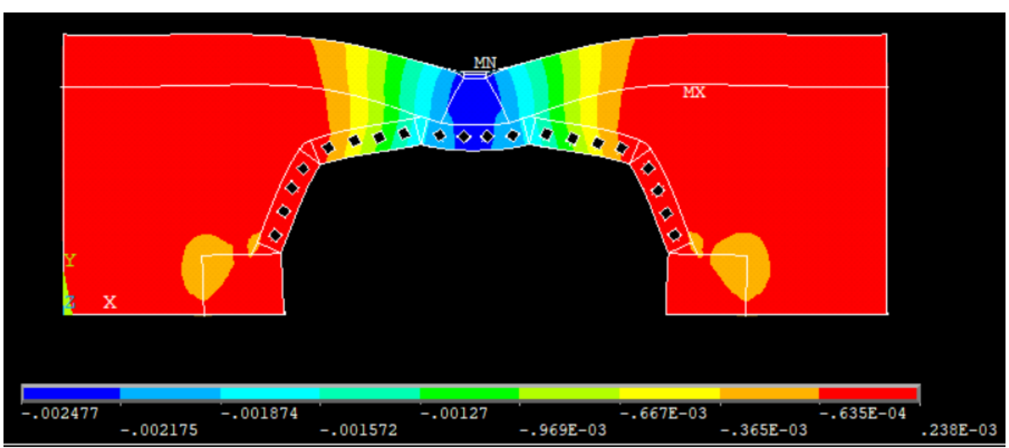

Figure 116 - 3D Nodal Solution of Predicted Displacements for Test No. 2b – Hollow-Core Model

Based on the above graphs, the highest deflections were anticipated to occur at and above the upper concrete segment. The rest of the model was not expected to undergo significant displacements.

4.5.2.2. Model Calibration

In order to obtain comparable deflections to those recorded during experimental testing, the ANSYS model for Test No. 2b was further refined. Calibration activities mostly entailed refinement of the material properties of the different model elements. The modulus of elasticity and Poisson's ratio of the medium and coarse sands were the first parameters changed before the models were rerun. Subsequently, the material properties of the concrete trapezoid prism were refined and, finally, those pertaining to the SCC of the hollow-core panels. The following table presents all of the runs performed for the 2D and 3D models. Models for Test No. 1 and 3 were not refined since the ¾-inch road base experienced a punching failure at a considerably low load (2,070 pounds) during Test No. 1; and Test No. 3 was conducted in the inelastic range.

As was the case for the first rerun of the CIP model, the modulus of elasticity of the medium sand was decrease to a value of 3,470 psi, which was the lower end of the range presented in the *Range of Values: Modulus of Elasticity and Poisson's Ratio* table developed by David F. McCarthy for a medium dense sand. In addition, the modulus of elasticity of the coarse sand was changed to a value of 1,390 psi, which was the mid-range value given for a silty sand material since this unit had significant fines. The Poisson's ratio values of both materials were left unchanged.

For the second rerun, the modulus of elasticity of the concrete trapezoid prism was lowered to a value of 2×10^6 psi, which was the lower end of the range based on published modulus of elasticity values for concrete. Once again, the Poisson's ratio was left unchanged. For the third rerun, the modulus of elasticity of the SCC concrete was changed to a value of 5.28×10^6 psi. This value was obtained by using ACI's modulus of elasticity equation for concrete which relates the unit weight of the specimen with its unconfined compressive strength. The values used for the unit weight and compressive strength of concrete were based on laboratory test results. See Section 4.4.2.1. In addition, the modulus of elasticity of the grout was changed to a value of 2×10^6 psi based on published reports (Allan & Philippacopoulos, 1999). For the final round of testing, the modulus of elasticity of the concrete was once again lowered. This time, a value of 2×10^6 psi was used. This was done in order to assess to what extend this material property influenced the displacements obtained.

For Test No. 2b, the closest load obtained from the load vs. displacement graph (Figure 96) to the desired half-scale resulting truck load (9.03 kips), was of approximately 9,062 lb. To have a fair basis of comparison between the experimental and numerical data, the ANSYS model for Test No. 2b reflected the same loading conditions. Namely, a point load of 9,062 lb was used which corresponded to a line load of 1812.4 lb/in for the 2D model and a pressure of 181.24 lb/in^2 for the 3D model. The following table provides the displacements obtained at the centroid of the upper concrete segment for Test No. 2b. In addition, Figure 117 and Figure 118 present the 2D and 3D nodal plots of the vertical displacements at the centroid for the first rerun. It is important to note that subsequent reruns showed the same overall deformed shape, but deflections obtained varied.

Table 39 - ANSYS Reruns for Test No. 2b – Hollow Core Model

Rerun No.	Material Properties: Type	Modulus of Elasticity, psi	Poisson's Ratio	Test No. 2b: 2D TCY2	3D TCY2	Experimental Testing TCY2
1	CIP Concrete	5.49×10^6	0.29	-0.091969	-0.0022561	-0.0330475
	Med. Sand	3.47×10^3	0.3			
	Coarse Sand	1.39×10^3	0.35			
	Steel Plate	29×10^6	0.3			
	Sika 328 Grout	4.24×10^6	0.25			
	Concrete Trapezoid	3.36×10^6	0.2			
2	CIP Concrete	5.49×10^6	0.29	-0.097144	-0.0025239	-0.0330475
	Med. Sand	3.47×10^3	0.3			
	Coarse Sand	1.39×10^3	0.35			
	Steel Plate	29×10^6	0.3			
	Sika 328 Grout	4.24×10^6	0.25			
	Concrete Trapezoid	2.0×10^6	0.2			
3	CIP Concrete	5.28×10^6	0.29	-0.10663	-0.0026209	-0.0330475
	Med. Sand	3.47×10^3	0.3			
	Coarse Sand	1.39×10^3	0.35			
	Steel Plate	29×10^6	0.3			
	Sika 328 Grout	2.0×10^6	0.25			
	Concrete Trapezoid	2.0×10^6	0.2			
4	CIP Concrete	2.0×10^6	0.29	-0.23305	-0.0056973	-0.0330475
	Med. Sand	3.47×10^3	0.3			
	Coarse Sand	1.39×10^3	0.35			
	Steel Plate	29×10^6	0.3			
	Sika 328 Grout	2.0×10^6	0.25			
	Concrete Trapezoid	2.0×10^6	0.2			

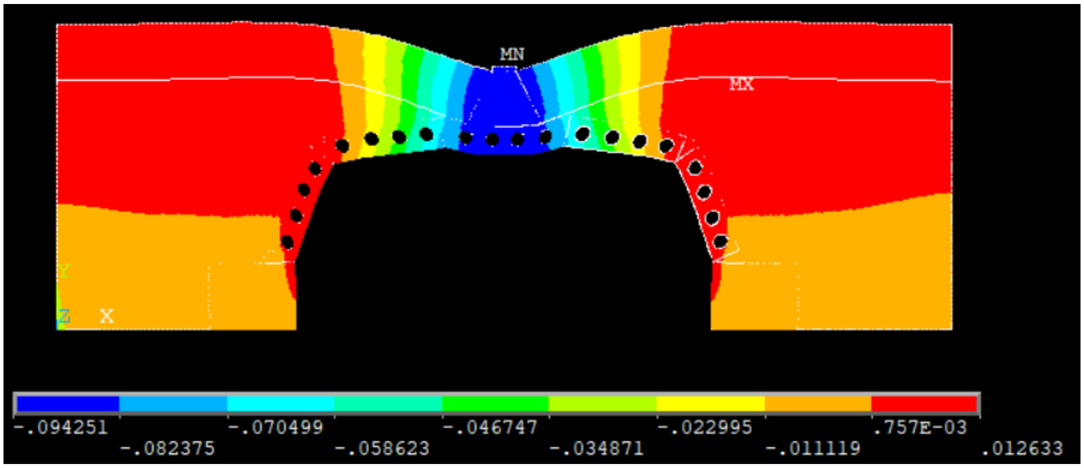

Figure 117 - 2D Rerun No. 1 Nodal Solution for Test No. 2b – Hollow-Core Model

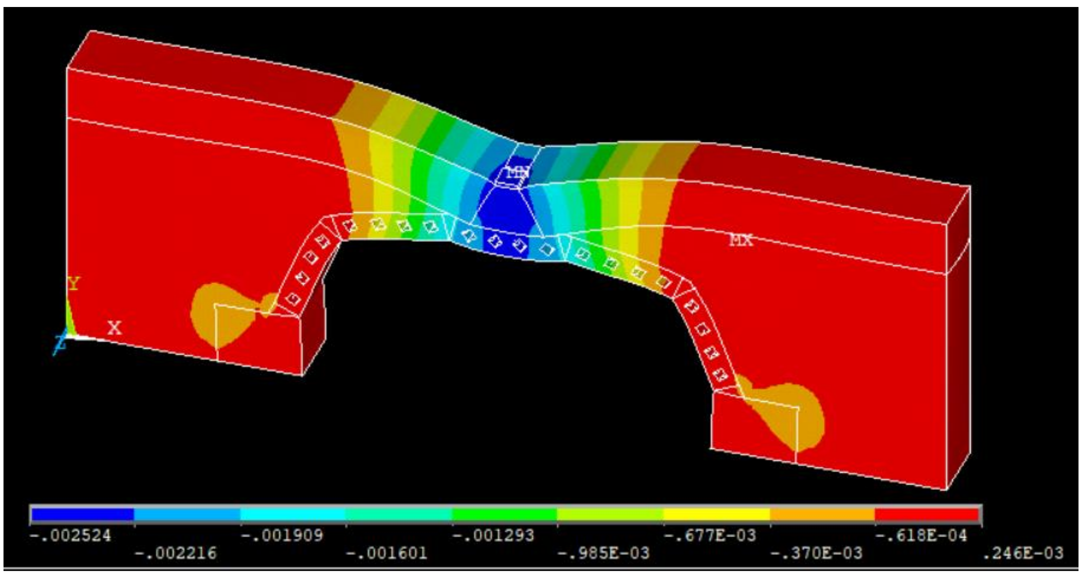

Figure 118 - 3D Rerun No. 1 Nodal Solution for Test No. 2b – Hollow-Core Model

Based on the above results, it is evident that the 2D simulations were over-predicting the deflections of the center gauge for all reruns and tests; and the 3D models were underpredicting the displacements of the center gauge for all reruns and tests. The overpredictions of the 2D models were expected, as these simulations were more simplified by not taking into consideration the depth component of the geometry.

However, the 3D models were expected to show closer results to the ones obtained experimentally.

As was the case with the CIP models, the 2D simulations for the hollow-core model overpredicted the displacements of the center gauge by approximately between 178% and 222%; and the 3D simulations underpredicted the displacements by approximately between 92% and 93%. The fourth rerun for the 2D and 3D models had exponentially higher overpredictions and underpredictions, respectively. However, the modulus of elasticity of the concrete used for this rerun was highly questionable.

A similar conclusion to that made for the CIP ANSYS models was made for the hollow-core ANSYS models. The geometry of the culvert appears to be playing a role when it comes to the interaction between the upper segment and the adjacent east and west sections. Since the model is not a perfect arch and the east and west adjacent segments have a shallow angle with respect to the horizontal plane, the model may be acting more like a longer beam with the east and west segments attached to it. In other words, instead of having a 27-inch-long upper section, the model itself may acting as a 81-inch long beam. This behavior does not appear to be detected by the FEM simulation which may be the reason why lower deflections are being predicted.

Chapter 5: Conclusions and Recommendations

This project had three main objectives: first, to evaluate if a hollow-core culvert was able to sustain a truck load, reduced to a half-size scale model, of 9.03 kips; second, to assess if the response of said structure was comparable to that of a monolithic cast-in-place structure; and third, to develop a numerical simulation, calibrated based on experimental data, that would be able to predict the structural responses of different CIP/hollow-core culvert configurations. The following sections present the conclusions drawn for each model based on the experimental and numerical studies. Recommendation for future studies are given at the end of the section.

5.1. CIP Culvert Test Results

The CIP model consisted of a monolithic structure with two footing and five segments formed at different angles to provide and arch-like geometry. Concrete segments had approximate dimensions of 27 inches long by 31 inches wide by 6 inches deep. In addition, the two outside footings used had dimensions of 18.6 inches wide by 14.2 inches high by 31 inches deep each. Footings were spaced approximately 89.6 inches apart. To replicate the conditions around an actual culvert, a soil box was also erected. The box walls were located approximately 33 inches away from the outside-edges of the culvert footings (x-direction) and along the front and back faces of the culvert structure (z-direction). The space in between the culvert and the box walls was filled with compacted soil up to a height of 62 inches above the invert, depending on the test conditions.

A total of five (5) experimental tests were conducted on the CIP model. Tests No. 1 and 2 had 12 inches of soil cover above the culvert arch. A steel plate representing the AASHTO traffic load applied the load from a ram through the soil onto the underlying structure. Because of bearing failures in the soil cover, Tests No. 3, 4 and 5 required the use of a concrete trapezoidal prism to stress the culvert to levels above the strength of the soil.

5.1.1. Test No. 1

For this test, pea-gravel was used as the soil cover material. Testing of this model was performed until the pea gravel could not sustain any additional load with increases in actuator displacement. The maximum load of approximately 4,300 pounds resulted in a bearing failure of the soil above the arch culvert. During testing a hairline crack developed at the interface between the upper and east segments. One explanation for formation of this crack is related to the development of stress concentrations in the arch along the corner of the top and lower segments in response to the 60º stress distribution of the soil mass. In this test, the long dimension of the loading plate was placed parallel with culvert span, which increased the distributed load area to locations close to the east and west interfaces of the crown slab. Other than the hairline crack at the inner interface, the structure did not show any evidence of damage or fatigue. Moreover, in this as well as subsequent tests, the structure performed in the linear elastic range.

One of the main conclusions from this test, as well as Test No. 2, is that in practice the soil above the arch will fail first in bearing and/or punching from the applied truck loads and the structural capacity of the culvert will not be reached.

5.1.2. Test No. 2

In an effort to overcome the bearing failure in the pea gravel, a stiffer soil (¾-inch road base) was used as backfill above the arch. The culvert was loaded until the soil failed in bearing and additional load could not be placed on the structure. A maximum load of approximately 5,538 pounds was attained prior to the soil undergoing a complete bearing failure. During the test, no additional cracks were observed in the arch and the crack observed in Test No. 1 did not widen.

Once again, this test proved that the soil above the culvert is much weaker than the arch concrete and would undergo failure prior to reaching the elastic limit of the structure.

5.1.3. Test No. 3

In order to achieve the required 9.03-kip load, a concrete trapezoidal prism was placed on the culvert. The prism shape and dimensions replicated the 60º stress distribution developed in a soil mass under the surface load. Use of the trapezoidal prism is an extreme loading condition in which the structure was immediately stressed similar to a truck travelling directly on top of the culvert. To provide soil-structure interaction adjacent to the loaded area, coarse sand was placed and compacted around the prism. A load of approximately 19,300 pounds was carried by the arch confined by the soil, which is more than two times greater the 9.02-kip target load. Based on the experimental results, the structure did not exceed its linear elastic range and no permanent deformation was recorded. The maximum vertical deflection in the crown was of -0.03738 inches.

5.1.4. Test No. 4

A fourth and then a fifth test was conducted to evaluate the structural capacity of the concrete culvert. In both trials, the medium sand backfill was removed down to the tops of the anchor blocks. The load on the culvert was applied by the concrete trapezoid block. The culvert in Test No. 4 was loaded to approximately 21,170 pounds before the test was terminated to avoid collapse of the structure and potential damage to the underlying instrumentation. The maximum deflection of the arch was of -0.08261 inches which was at least twice the deflection when the culvert was confined by soil. The structure appeared to surpass its linear elastic range but remain within the strain hardening state. Additional cracking, other than the hairline crack formed at the start of Test No. 1, was not observed.

In general, the culvert in Test No. 4 experienced higher deflection per load increment than in Test No. 3. The differences in deflection are the direct effect of the soil-structure interaction. In Test No. 3, the soil backfill compacted around and above the culvert not only placed the structure in compression but also provided confinement in the haunch area. Thus, the added compression and soil stiffness decreased the vertical deflection compared to that experienced by the structure alone.

5.1.5. Test No. 5

To determine the ultimate capacity of the concrete culvert, one final test was performed to failure. The test set-up was the same as in Test No 4. The load vs. displacement data from Test No. 5 showed a nearly linear relationship up to a load of approximately 16,670 pounds. Above 16,670 pounds, the structure underwent strain hardening up to an ultimate load of 30,115 pounds at which point a moment crack developed along the centerline of the middle panel. Even though the culvert was unreinforced, the arch had residual capacity and continued to carry load up to a final fracturing point at a load of approximately 15,140 pounds. The maximum displacement at the centroid of the upper segment (inner face) was -0.254 inches.

The centerline moment crack extended through the full thickness of the crown panel. A discontinuous hairline crack also developed in the outer fiber of the culvert along the interface between the arch and the sloping east side panel. The moment failure observed in the center panel was expected since the lower face of the segment was put into tension and the structure lacked reinforcement. The vertical deflection of each load increment in the structure alone were greater than those when the culvert was surrounded by soil backfill as in Test No. 3.

5.1.6. General Conclusions

In practice, the cast-in-place culvert design is not expected to undergo inelastic deformation and certainly will not fail under the design traffic load because the pavement will fail in bearing well before the ultimate structural capacity of the arch is reached. Further, the results of Tests No. 1, 2 and 4 show that when the soil fails in bearing above the culvert, the soil-structure interaction has a limited effect on reducing the deflection of the arch. A bearing failure in the one-foot interval of soil cover above the culvert lowers the stiffness of the medium in the haunch area and thus significantly reduces the effectiveness of the soil confinement in limiting the vertical deflection.

Even when the load was applied directly to the arch by a concrete trapezoid, as in Tests No. 4 and 5, the CIP structure itself was able to carry the target 9.03-kips without undergoing adverse deflection or failure. In a comparable test (No. 3), the presence of the compacted soil backfill above the culvert and around the trapezoid significantly reduced the vertical deflection and thus the moments in the arch.

As expected for a flat crown, monolithic structure, ultimate failure was in moment.

5.2. CIP Model FEM Simulation

A total of eight FEM simulations were carried out on the CIP model. One 2D simulation and one 3D simulation were developed per test. In general, the 2D models overpredicted the deflections obtained during experimental testing, whereas the 3D models underpredicted the same test displacements. However, experimental data lie within the range of values obtained in the 2D and 3D analyses. The 2D models were observed to be less accurate due to the lack of the z-dimension; whereas 3D models took into account out-of-plane behavior. During model calibration it was evident that the 3D FEM simulations did not take into consideration the forces acting between the top and the adjacent segments, which ultimately resulted in lower predictions of vertical displacement. One plausible explanation is the complex geometry of the test culvert, which did not form a circular, uniform arch. Based on STAAD structural analysis estimates of vertical deflection compared with the test results, the top three segments of the culvert appear to act more like a long beam than an arch; which may explain the higher deflections obtained in the experimental tests compared with the 3D analysis. Overall, a calibrated FEM simulation of the test results was not obtained in this study.

5.3. Hollow-Core Model Experimental Testing

The hollow-core model consisted of a series of five individual pre-cast concrete panels connected by grout and supported on two end footings (one on each leg). For comparison purposes, the geometry of the culvert was essentially the same as that of the CIP model. The individual hollow-core panels had dimensions of approximately 24 inches long by 31 inches wide by 6 inches thick and contained four, 3-inch diameter tubes oriented perpendicular to the long dimension of the panel. The hollow-core culvert was erected in an elongated soil box. The footings were located approximately 33 inches laterally from the ends of the box and the front and back faces of the culvert were flush with the long sides of the box. The space in between the outside surface of the culvert and the box walls was filled with sand or gravel or left open depending on the test conditions.

A total of three (3) tests were performed on the hollow-core culvert. In Test No. 1, 12 inches of ¾-inch road base was compacted above the culvert arch and the steel loading plate representing the truck wheels was placed on the surface of the soil. In Tests No. 2 and 3 the concrete trapezoidal prism was used to apply the ram load.

5.1.7. Test No. 1

Test No 1 had results similar to Tests No. 1 and 2 on the cast-in-place arch. The soil below the steel plate failed in bearing and loads greater than 2,070 pounds could not be applied to the culvert arch. No cracking or failure of the structure was observed during the test. Simply stated, the hollow-core culvert is much stronger that the soil and thus the soil underlying the pavement will fail well before the culvert experiences the full 9.03 kips of load.

5.1.8. Test No. 2b

In the next test, the same concrete trapezoidal block was placed in the center of the culvert arch in order to reach the 9.03-kip target load. This system represents an extreme loading condition in which the structure would be immediately loaded as if a truck was travelling directly on top of the culvert. To provide confinement similar to the behavior of an actual culvert, coarse sand was placed and compacted around the trapezoid and above the culvert. The arch exhibited linear behavior up to a load of approximately 8,000 pounds (yield strength). Above 8,000 pounds, the structure appeared to undergo strain hardening, reaching ultimate strength at a load of approximately 14,560 pounds and a corresponding deflection of -0.1353 inches.

At a load of approximately 9,600 pounds, a shear crack developed along the interface between the crown panel and the adjacent west side panel. This crack opened 1/16- inch during the test. After the soil was removed from the top and sides of the structure, the crack extended through the thickness of the joint along the vertical interface between the crown panel and the grout. No cracks were observed in the panels themselves. The maximum vertical, centerline deflection was -0.1602 inches.

This test results demonstrated that if the soil cover has sufficient strength to transmit the load to the arch, the hollow-core culvert is capable of carrying the target 9.03-kip load without developing cracks. In comparing the two culverts, the hollow-core structure underwent greater deflection per load increment and failed at a much lower load (approximately half) that the CIP culvert. The difference in behavior is explained by differences in the modes of failure: the hollow-core arch failed in bond/shear along the grouted interface, whereas failure of the CIP arch was in the structural section of the panel. Moreover, the bond along the upper hollow-core joints was not sufficient to mobilize the structural strength of the crown panel. Still, the ultimate load carrying capacity of the hollow-culvert was 5.2 kips greater that the 9.3-kip target load.

5.1.9. Test No. 3

To evaluate the post-crack behavior of the hollow-core culvert alone, the ram load was removed and the soil backfill was excavated from around the arch above the anchor blocks. As in Test No. 2, the concrete trapezoid prism was used to reload the arch. The crack that developed along the interface between the grout and the joint in Test No. 2b continued to offset vertically with increasing load. At the end of the test, the west panel had moved vertically approximately 1.375 inches with respect to the crown segment. The failure was in pure shear. In addition, a moment crack developed along the grouted joint between the upper and lower east side panels at a load of approximately 5.2 kips. The moment crack extended along the entire full length and across the full thickness of the joint. At the end of testing, the crack opened approximately 0.1875 inches at the top and was hairline at the bottom of the joint. Clearly the weakness in the culvert was along the grouted joint connections and not in the hollow-core panels themselves. The hollow-core arch was able to carry a residual load up to 5.6 kips with a displacement of 0.7 in. without collapse.

5.1.10. General Conclusions

The hollow-core culvert was much stronger than the soil above the arch which failed in bearing under a 2.0-kip load. Further, the arch carried the 9.03-kip target load without cracking even under severe loading conditions where the concrete trapezoid was placed on the culvert crown. The hollow-core culvert had an ultimate load carrying capacity of approximately 14,560 pounds at a corresponding deflection of -0.1353 inches. In addition, the hollow-core culvert had significant post-crack capacity (up to 5.7 kips) because the arch remained in compression even with a total downward movement of 1.38 in. The bond strength between the joints must be increased in order to mobilize the full structural capacity of the hollow-core panels.

In the absence of soil backfill, the deflections measured at the centroid of the upper hollow-core panel were more than twice those recorded under similar loads at the same location for the CIP model (-0.0330 inches vs. -0.0137 inches). This means that the hollow-core arch was not as stiff as the monolithic CIP structure.

5.4. Hollow-Core Model FEM Simulation

A total of six FEM simulations were developed for the hollow-core model. One 2D simulation and one 3D simulation were developed per test. As was the case with the CIP model, the hollow-core 2D model was overpredicting the deflections measured in the experimental tests, whereas the 3D model underpredicted said displacements. However, experimental deflection data was within the ranges obtained between the two analyses. With open tubes and joints between the panels, the hollow-core FEM geometry was much more complicated than the CIP simulation, where similar analytical results were obtained. Even though the joints were grouted to form a continuous arch, the ultimate behavior was affected by the joint properties which is not accounted for in the FEM elastic analysis.

5.5. Recommendations for Future Studies

It is clear that the hollow-core culverts show promise in the transportation industry for breaching streams. However, additional tests must be performed before the technology is accepted by designers and manufacturers. As a minimum, the structural capacity of the individual panels in bending as well as the impact of applying the load at other locations above the culvert (such as at the joints) need to be assessed. Another possibility is to utilize an equivalent half-size tandem load, in which both sets of wheels act on the structure at the same time. Further, studies must also include strengthening of the joint connections such as by improving the bond and/or reinforcing the interfaces in order to mobilize the structural capacity of the panel. One possibility would be to used resin grouted dowel connections similar to those used in the pre-cast concrete segments in the tunneling industry. Finally, similar tests should be carried out on box structures in which hollow-core panels are used in the walls and the top of the culvert.

In future analytical studies, alternative software such as CANDE or SAP2000 may yield more realistic results. In addition, performing analyses outside of the linear-elastic range or using simulations with joint elements may also provide better results than the ANSYS program used in this study.

References

Abdel-Karim, A. M., Benak, J. V., & Tadros, M. K. (1993). Structural Response of Full-Scale Concrete Box Culvert. *Journal of Structural Engineering, 119*(11).

Abdel-Karim, A. M., Tadros, M. K., & Benak, J. V. (1990). Live Load Distribution on Concrete Box Culverts. *Transportation Research Record, 1288*, 136-151.

Allan, M. L., & Philippacopoulos, A. J. (1999). *Properties and Performance of Cement-Based Grouts for Geothermal Heat Pump Applications.* Washington D.C.: United States Department of Energy.

Allgood, J. R., & Takahashi, S. K. (1978). Balanced Design and Finite-Element Analysis Culverts. *Highway Research Record*(413), 45-46.

American Association of State Highway and Transportation Officials. (2017). *AASHTO LRFD Bridge Design Specifications.* Washington D.C.: American Association of State Highway and Transportation Officials.

American Concrete Institute. (2002). *Standard Practice for Selecting Proportions for Normal, Heavyweight, and Mass Concrete (ACI 211.1-91).* Detroit: American Concrete Institute.

American Concrete Institute. (2011). *Building Code Requirements for Structural Concrete (ACI 318-11) and Commentary.* Farmington Hills: American Concrete Institute.

Ansys, Inc. (2018, 02). PLANE182. Retrieved 09 23, 2020, from https://www.mm.bme.hu/~gyebro/files/ans_help_v182/ans_elem/Hlp_E_PLANE182.html

ASTM International . (2014). *ASTM C469/469M-14, Standard Test Method for Static Modulus of Elasticity and Poisson's Ratio of Concrete in Compression.* West Conshohocken: ASTM International.

ASTM International. (2012). *ASTM D698-12, Standard Test Methods for Laboratory Compaction Characteristics of Soil Using Standard Effort (12 400 ft-lbf/ft3 (600 kN-m/m3)).* West Conshohocken: ASTM International.

ASTM International. (2015). *ASTM D1556/1556M-15e1, Standard Test Method for Density and Unit Weight of Soil in Place by Sand-Cone Method.* West Conshohocken: ASTM International.

ASTM International. (2017). *ASTM D2487-17e1, Standard Practice for Classification of Soils for Engineering Purposes (Unified Soil Classification System)* . West Conshohocken: ASTM International.

ASTM International. (2019). *ASTM C136/C136M-19, Standard Test Method for Sieve Analysis of Fine and Coarse Aggregates.* West Conshohocken: ASTM International.

ASTM International. (2019). *ASTM C192/C192M-19, Standard Practice for Making and Curing Concrete Test Specimens in the Laboratory.* West Conshohocken: ASTM International.

ASTM International. (2019). *ASTM D2216-19, Standard Test Methods for Laboratory Determination of Water (Moisture) Content of Soil and Rock by Mass.* West Conshohocken: ASTM International.

ASTM International. (2020). *ASTM C109/C109M-20, Standard Test Method for Compressive Strength of Hydraulic Cement Mortars (Using 2-in. or [50 mm] Cube Specimens).* West Conshohocken: ASTM International.

ASTM International. (2020). *ASTM C39/C39M-20, Standard Test Method for Compressive Strength of Cylindrical Concrete Specimens.* West Conshohocken: ASTM International.

Bates, K., Barnard, B., Heiner, B., Klavas, J. P., & Powers, P. D. (2003). *Design of Road Culverts for Fish Passage.* Olympia: Washington Department of Fish and Wildlife.

Beach, T. J. (1988). Load Test Report and Evaluation of a Precast Concrete Arch Culvert. *Transportation Research Record*(1191), 12-21.

Evans, W. A., & Johnston, B. (1972). *Fish Migration and Fish Passage: A Practical Guide to Solving Fish Passage Problems.* Washington, D.C.: Forest Service USDA.

Federal Highway Administration. (2007). *Design for Fish Passage at Roadway-Stream Crossings: Synthesis Report.* McLean, Virginia, United States: Federal Highway Administration.

Forest Service Stream-Simulation Working Group. (2008). *Stream Simulation: An Ecological Approach to Providing Passage for Aquatic Organisms at Road-Stream Crossings.* San Dimas: USDA.

Gregory, S., McEnroe, J., Klingeman, P., & Wyrick, J. (2004). *Fish Passage Through Retrofitted Culverts.*

Gubernick, R. A., Cenderelli, D. A., Bates, K. K., Johansen, D. K., & Jackson, S. D. (2008). *Stream Simulation: An Ecological Approach to Providing Passage for Aquatic Organisms at Road-Stream Crossings.* United States Department of Agriculture, Forest Service. San Dimas: United States Department of Agriculture. Retrieved 04 20, 2020, from https://www.fs.usda.gov/Internet/FSE_DOCUMENTS/fsm91_054564.pdf

Hoffman, R. L., Dunham, J. B., & Hansen, B. P. (2012). *Aquatic Organism Passage at Road-Stream Crossings— Synthesis and Guidelines for Effectiveness Monitoring.*

Idaho Transportation Department. (2018). *2018 Standard Specifications for Highway Construction.* Boise, Idaho, United States of America: Idaho Transportation Department.

Jensen, T. J. (2012). *Numerically Modeling Structural Behavior of Precast Three-Sided Arch Bridges for Analysis and Design.*

Katona, M. G. (2018). History of Soil–Structure Interaction Models for Buried Culverts. *Transportation Research Circular, E-C230*, 13-20.

Katona, M. G., Smith, J. M., Odello, R. S., & Allgood, J. R. (1976). *CANDE - A Moden Approach For The Structural Design and Analysis of Buried Culverts.* Washington, D.C.: Federal Highway Administration.

Khan, B., & Colbo, M. H. (2008). The Impact of Physical Disturbance on Stream Communities: Lessons From Road Culverts. *Hydrobiologia 600*, 229-235.

McCarthy, D. F. (2007). Range of Values: Modulus of Elasticity and Poisson's Ratio. In D. F. McCarthy, *Essentials of Soil Mechanics and Foundations, Basic Geotechnics* (p. 496). Upper Saddle River: Pearson Prentice Hall.

McCarthy, D. F. (2007). Representative Values of Relative Density. In D. F. McCarthy, *Essentials of Soil Mechanics and Foundations, Basic Geotechnics* (7th ed., p. 88). Upper Saddle River: Pearson Prentice Hall.

McGrath, T. J. (2018). Development of Design and Analysis Methods for Buried Culverts. *Transportation Research Circular, E-C230*, 1-12.

McGrath, T. J., & Mastroianni, E. P. (2002). Finite-Element Modeling of Reinforced Concrete Arch Under Live Load. *Transportation Research Record*(1814), 203-210.

McGrath, T. J., Selig, E. T., & Beach, T. J. (1996). Structural Behavior of Three-Sided Arch Span Bridge. *Transportation Research Record*(1541), 112-119.

McKinley, W. R., & Webb, R. D. (1956). A Proposed Correction of Migratory Fish Problems at Box Culverts. *Fish Res. Papers 1*, 33-45.

O'Shaughnessy, E., Landi, M., Januchowski-Hartley, S. R., & Diebel, M. (2016). Conservation Leverage: Ecological Design Culverts also Return Fiscal Benefits. *Fisheries, 41*, 750-757.

Oswald, C. S., & Furlong, R. W. (1993). *Observed Behavior Of A Concrete Arch Culvert.* Austin.

PCI Committee on Building Code. (2003). PCI Standard Design Practice. *PCI Journal*, 15-30.

PCI Manual for the Design of Hollow Core Slabs and Walls (3rd ed.). (2015). PCI Hollow Core Slab Producers Committee.

Precast/Prestressed Concrete Institute. (2017). *PCI Design Handbook.* Chicago: Precast/Prestressed Concrete Institute.

Shoemaker, R. H. (1956). Hydraulics of Box Culverts with Fish-Ladder Baffles. *Highway Research Board Proceedings 35*, 196-209.

State of Illinois Bureau of Bridges and Structures Office of Program Development. (2017). *Culvert Manual.* Springfield: Illinois Department of Transportation.

U.S. Department of Transportation. (2012). *Hydraulic Design of Highway Culverts, Third Edition.* U.S. Department of Transportation Federal Highway Administration.

U.S. EPA. (2015). *Connectivity of Streams and Wetlands To Downstream Waters: A Review and Synthesis of the Scientific Evidence (Final Report).* Washington, DC: U.S. EPA.

U.S. General Accounting Office. (2001). *Restoring Fish Passage through Culverts on Forest Service and BLM Lands in Oregon and Washington Could Take Decades.* Washington D.C. : House of Representatives .

Washington State Department of Transportation. (2019). *Federal Court Injunction for Fish Passage*. Retrieved 11 13, 2020, from Washington State Department of Transportation: https://wsdot.wa.gov/Projects/FishPassage/CourtInjunction.htm

Withiam, J. L. (2003). Implementation of the AASHTO LRFD Bridge Design Specifications for Substructure Design. In *Limit State Design in Geotechnical Engineering Practice*. World Scientific.

Zoghi, M., & Hastings, J. (2000). *Predicting the ultimate load carrying capacity of long-span precast concrete arch culverts*. Dayton: University of Dayton.

Appendix A – AASHTO Design Truck Loading

Table 3.4.1-1—Load Combinations and Load Factors

Load Combination Limit State	*DC DD DW EH EV ES EL PS CR SH*	*LL IM CE BR PL LS*	*WA*	*WS*	*WL*	*FR*	*TU*	*TG*	*SE*	Use One of These at a Time *EQ*	*BL*	*IC*	*CT*	*CV*
Strength I (unless noted)	γ_P	1.75	1.00	—	—	1.00	0.50/1.20	γ_{TG}	γ_{SE}	—	—	—	—	—
Strength II	γ_P	1.35	1.00	—	—	1.00	0.50/1.20	γ_{TG}	γ_{SE}	—	—	—	—	—
Strength III	γ_P	—	1.00	1.00	—	1.00	0.50/1.20	γ_{TG}	γ_{SE}	—	—	—	—	—
Strength IV	γ_P	—	1.00	—	—	1.00	0.50/1.20	—	—	—	—	—	—	—
Strength V	γ_P	1.35	1.00	1.00	1.00	1.00	0.50/1.20	γ_{TG}	γ_{SE}	—	—	—	—	—
Extreme Event I	1.00	γ_{EQ}	1.00	—	—	1.00	—	—	—	1.00	—	—	—	—
Extreme Event II	1.00	0.50	1.00	—	—	1.00	—	—	—	—	1.00	1.00	1.00	1.00
Service I	1.00	1.00	1.00	1.00	1.00	1.00	1.00/1.20	γ_{TG}	γ_{SE}	—	—	—	—	—
Service II	1.00	1.30	1.00	—	—	1.00	1.00/1.20	—	—	—	—	—	—	—
Service III	1.00	γ_{LL}	1.00	—	—	1.00	1.00/1.20	γ_{TG}	γ_{SE}	—	—	—	—	—
Service IV	1.00	—	1.00	1.00	—	1.00	1.00/1.20	—	1.00	—	—	—	—	—
Fatigue I—*LL, IM & CE* only	—	1.75	—	—	—	—	—	—	—	—	—	—	—	—
Fatigue II—*LL, IM & CE* only	—	0.80	—	—	—	—	—	—	—	—	—	—	—	—

3.6.2—Dynamic Load Allowance: *IM*

3.6.2.1—General

Unless otherwise permitted in Articles 3.6.2.2 and 3.6.2.3, the static effects of the design truck or tandem, other than centrifugal and braking forces, shall be increased by the percentage specified in Table 3.6.2.1-1 for dynamic load allowance.

The factor to be applied to the static load shall be taken as: $(1 + IM/100)$.

The dynamic load allowance shall not be applied to pedestrian loads or to the design lane load.

Table 3.6.2.1-1—Dynamic Load Allowance, *IM*

Component	IM
Deck Joints—All Limit States	75%
All Other Components:	
• Fatigue and Fracture Limit State	15%
• All Other Limit States	33%

C3.6.2.1

Page (1976) contains the basis for some of these provisions.

The dynamic load allowance (*IM*) in Table 3.6.2.1-1 is an increment to be applied to the static wheel load to account for wheel load impact from moving vehicles.

Dynamic effects due to moving vehicles may be attributed to two sources:

- hammering effect is the dynamic response of the wheel assembly to riding surface discontinuities, such as deck joints, cracks, potholes, and delaminations, and
- dynamic response of the bridge as a whole to passing vehicles, which may be due to long undulations in the roadway pavement, such as those caused by settlement of fill, or to resonant excitation as a result of similar frequencies of vibration between bridge and vehicle.

3.6.2.2—Buried Components

The dynamic load allowance for culverts and other buried structures covered by Section 12, in percent, shall be taken as:

$$IM = 33(1.0 - 0.125D_E) \geq 0\% \qquad (3.6.2.2\text{-}1)$$

where:

D_E = the minimum depth of earth cover above the structure (ft)

3.6.1.2.2—Design Truck

The weights and spacings of axles and wheels for the design truck shall be as specified in Figure 3.6.1.2.2-1. A dynamic load allowance shall be considered as specified in Article 3.6.2.

Except as specified in Articles 3.6.1.3.1 and 3.6.1.4.1, the spacing between the two 32.0-kip axles shall be varied between 14.0 ft and 30.0 ft to produce extreme force effects.

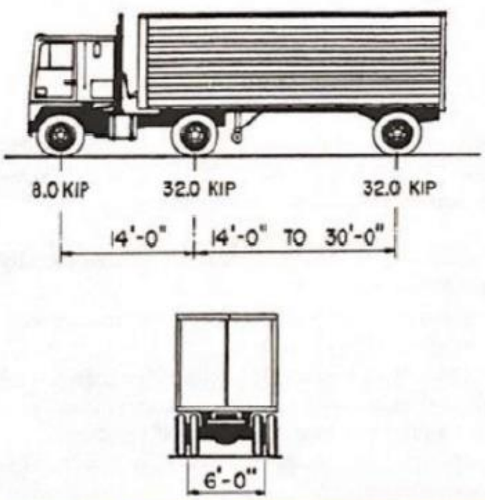

Figure 3.6.1.2.2-1—Characteristics of the Design Truck

3.6.1.2.5—Tire Contact Area

The tire contact area of a wheel consisting of one or two tires shall be assumed to be a single rectangle, whose width is 20.0 in. and whose length is 10.0 in.

The tire pressure shall be assumed to be uniformly distributed over the contact area. The tire pressure shall be assumed to be distributed as follows:

- On continuous surfaces, uniformly over the specified contact area, and
- On interrupted surfaces, uniformly over the actual contact area within the footprint with the pressure increased in the ratio of the specified to actual contact areas.

For the design of orthotropic decks and wearing surfaces on orthotropic decks, the front wheels shall be assumed to be a single rectangle whose width and length are both 10.0 in. as specified in Article 3.6.1.4.1.

C3.6.1.2.5

The area load applies only to the design truck and tandem. For other design vehicles, the tire contact area should be determined by the engineer.

As a guideline for other truck loads, the tire area in in.[2] may be calculated from the following dimensions:

Tire width = $P/0.8$

Tire length = $6.4\gamma(1 + IM/100)$

where:

γ = load factor
IM = dynamic load allowance percent
P = design wheel load (kip)

Appendix B – Formwork Design Calculations and Drawings

B1 – CIP Culvert Formwork

Garrett Thompson | Formwork Calcs. | Panel Design | 1/6

$\gamma_c = 145\ \text{lb/ft}^3$

$\gamma_s = 125\ \text{lb/ft}^3$

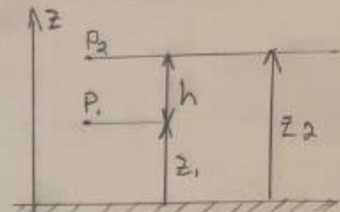

$P_2 - P_1 = -\gamma(z_2 - z_1) = -\gamma h$

PANEL DESIGN

Maximum pressure at base of formwork.

$h = 50.78\text{in} = 4.23\text{ft}$

Controlling pressure used for design.

$P = -145\ \text{lb/ft}^3(4.23\text{ft}) = -613.35\ \text{lb/ft}^2$

From APA Panel Design Specification Manual: Table 1d Uniform loads on Plywood Structural 1 Sturd-I-Floor Span rating 32" o.c.

F.S.

$\boxed{P_u = 1.4\ (613\ \text{lb/ft}^2) = 859\ \text{lb/ft}^2}$

$\phi_b = 0.85 \quad \phi_v = 0.75 \quad \lambda = 1.0 \quad C_D = 1.0$

	12" Center to Center Spacing	
L/360	3,111 > 859	OK
L/240	4,666 > 859	OK
L/180	6,221 > 859	OK
Bending	875 > 859	OK
Shear	1,040 > 859	OK

Note: Conservati[ve] beams are space 7.6875" not 12" o.c.

Therefore use 7/8" APA Rated Sturd-I-Floor

BEAM DESIGN $P_u = 859 \text{ lb/ft}^2$

Beam Length = 24"

Tributary width for center beam = 10.25"

$P_u = 859 \text{ lb/ft}^2 (0.85 \text{ ft}) = 733.7 \text{ lb/ft}$

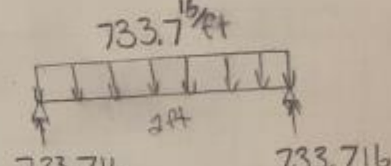

NDS Supplement, Table 4A pg. 32

Assumption: Douglas Fir Larch No. 2

$F_b = 900$ psi $F_v = 180$ psi

$F_t = 575$ psi

$SG = 0.5$

Adjustment Factors $C_r = 1.15$ $C_F = 1.5$

$C_M = 1.0$ $C_t = 1.0$

$F_b^* = 900(1.15)(1.5)(1.0)(1.0) = 1{,}552.5$ psi

From NDS eqn 3.3-6 $F_b' = F_b^* C_L$

$$C_L = \frac{1 + (F_{bE}/F_b^*)}{1.9} - \sqrt{\left[\frac{1 + (F_{bE}/F_b^*)}{1.9}\right]^2 - \frac{F_{bE}/F_b^*}{0.95}}$$

$F_{bE} = \dfrac{1.2 E'_{min}}{R_B^2}$ $E'_{min} = E_m(1)(1) = 580{,}000$ psi

Garrett Thompson | Formwork Calcs | Beam Design Cont. | 3/6

$R_B = \sqrt{\frac{l_e d}{b^2}}$ $\quad l_e = 1.37 l_u + 3d = 1.37(24") + 3(3.5")$

$l_e = 43.38 in$

$R_B = \sqrt{\frac{43.38(3.5)}{1.5^2}} = 8.2$

$F_{bE} = \frac{1.2(580,000)}{8.2^2} = 10,350.98 psi$

$F_{BE}/F_b^* = \frac{10,350.98 psi}{1552.5} = 6.667$

$\frac{1 + (F_{BE}/F_b^*)}{1.9} = 4.035$

$C_L = 4.035 - \sqrt{4.035^2 - \frac{6.667}{0.95}}$

$C_L = 0.9914$

$F_b' = F_b^* C_L = 1,552.5 psi (0.9914) = 1,539.15 psi$

$F_b' = 1540 psi$ $\quad * \boxed{F_b' = 3080 psi \text{ with 2 beams side by side}}$

Shear

$F_v' = F_v C_m C_t = 180 psi (1)(1) = 180 psi$

$F_v' = 180 psi$ $\quad * \boxed{F_v' = 360 psi \text{ with 2 beams side by side}}$

Modulus of Elasticity

$* \boxed{E' = E C_m C_t C_i = E(1)(1)(1) = 1,600,000 psi}$

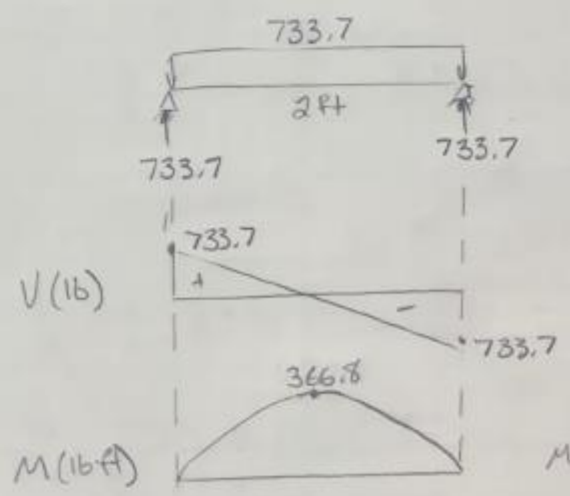

$M_{max} = 366.8\,(12)\frac{in}{ft}$
$= 4402$ lbin

Bending

$$f_b = \frac{M_{max}}{S_x} \quad \frac{4402 \text{ lbin}}{3.06} = 1438 \text{ psi}$$

$f_b = 1438$ psi $< F'_b = 3080$ psi OK ✓

Shear

$$f_v = 1.5\,\frac{V_{max}}{A} = \frac{1.5\,(733.7)}{10.5}$$

$f_v = 104.8$ psi $< F'_v = 360$ psi OK ✓

Deflection

$$\Delta = \frac{P L^3}{48 E I_x} = \frac{(1467 \text{ lb})(24 \text{ in})^3}{48(1{,}600{,}000 \text{ psi})(5.359 \text{ in}^4)}$$

$\Delta = 0.0000246$ in OK ✓

Therefore use two 2x4" Douglas Fir Larch No. 2 @ 10.25" on center. 3 trusses total

COLUMN DESIGN

↓ 733 lb $\quad P_u = 733\text{ lb}$

$38.03'' = l_e$

↑ 733 lb

Assumption: Entire column unbraced. This is conservative becase the beam is braced in two locations along the length

$f_c = 733\text{ lb}/5.25\text{ in}^2 = 139.6\text{ psi}$

$F_c^* = F_c C_M C_t$ $\quad F_c = 1{,}350\text{ psi}$ ← NDS Suppl. Table 4A

$F_c' = F_c^* C_P$

$$C_P = \frac{1 + (F_{cE}/F_c^*)}{2c} - \sqrt{\left(\frac{1 + (F_{cE}/F_c^*)}{2c}\right)^2 - \frac{F_{cE}/F_c^*}{c}}$$

$$F_{cE} = \frac{0.822 E_{min}'}{(l_e/d)^2} \qquad c = 0.8$$

$$= \frac{0.822(580{,}000)}{(38.03''/3.5'')^2} = 3883.47\text{ psi}$$

$F_{cE} = 3{,}883.5\text{ psi}$

$$\frac{1 + (F_{cE}/F_c^*)}{2c} = \frac{1 + (3883.5/1350)}{2(0.8)} = 2.4$$

$$C_P = 2.4 - \sqrt{2.4 - \frac{3883.5/1350}{0.8}}$$

$C_P = 0.9288$

$F'_c = F^*_c C_p = 1350\,\text{psi}\,(0.9288)$

$F'_c = 1254\,\text{psi} < \underline{f'_c = 139.6\,\text{psi}}$ OK ✓

Therefore use 2"x4" for each horizontal and vertical column.

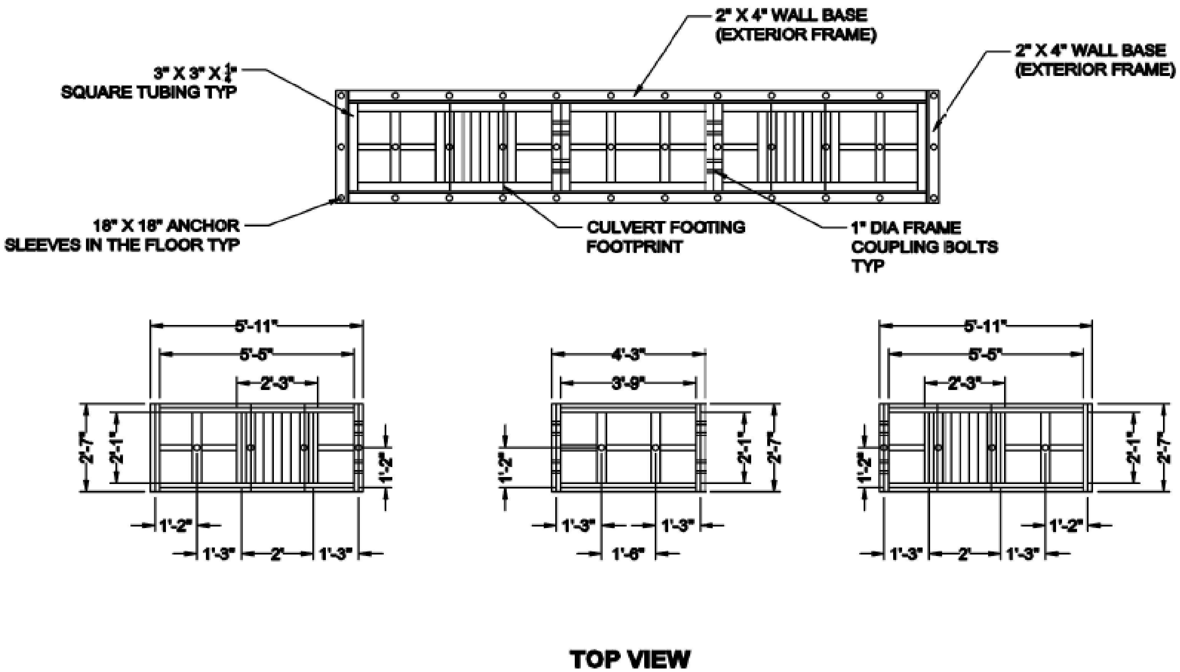

PRODUCED BY AN AUTODESK STUDENT VERSION

Issue	Date	Description
1	07/28/2020	Base Frame Layout

IDAHO STATE UNIVERSITY

College of Science and Engineering

Department of Civil and Environmental Engineering

Project Supervisor: Dr. James Maher

Project Title

Use of Precast Hollow-Core Members in the Construction of Arch Culverts under Roadways

Drawing Name

Base Frame Layout

Engineered by : G. Thompson Date : 07/2020
Drawn by : G. Thompson Date : 07/2020

Drawing Scale 1:2

Sheet No:

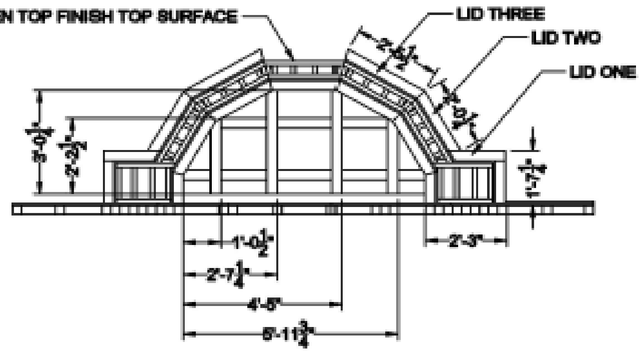

PROFILE VIEW

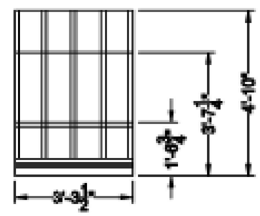

SIDE VIEW

Issue	Date	Description
1	07/28/2020	CIP Formwork

IDAHO STATE UNIVERSITY

College of Science and Engineering

Department of Civil and Environmental Engineering

Project Supervisor: Dr. James Mahar

Project Title

Use of Precast Hollow-Core Members in the Construction of Arch Culverts under Roadways

Drawing Name

CIP Formwork

Engineered by : G. Thompson Date : 07/2020
Drawn by : G. Thompson Date : 07/2020

Drawing Scale 1:2

Sheet No:

B2 – Hollow-Core Panel Formwork

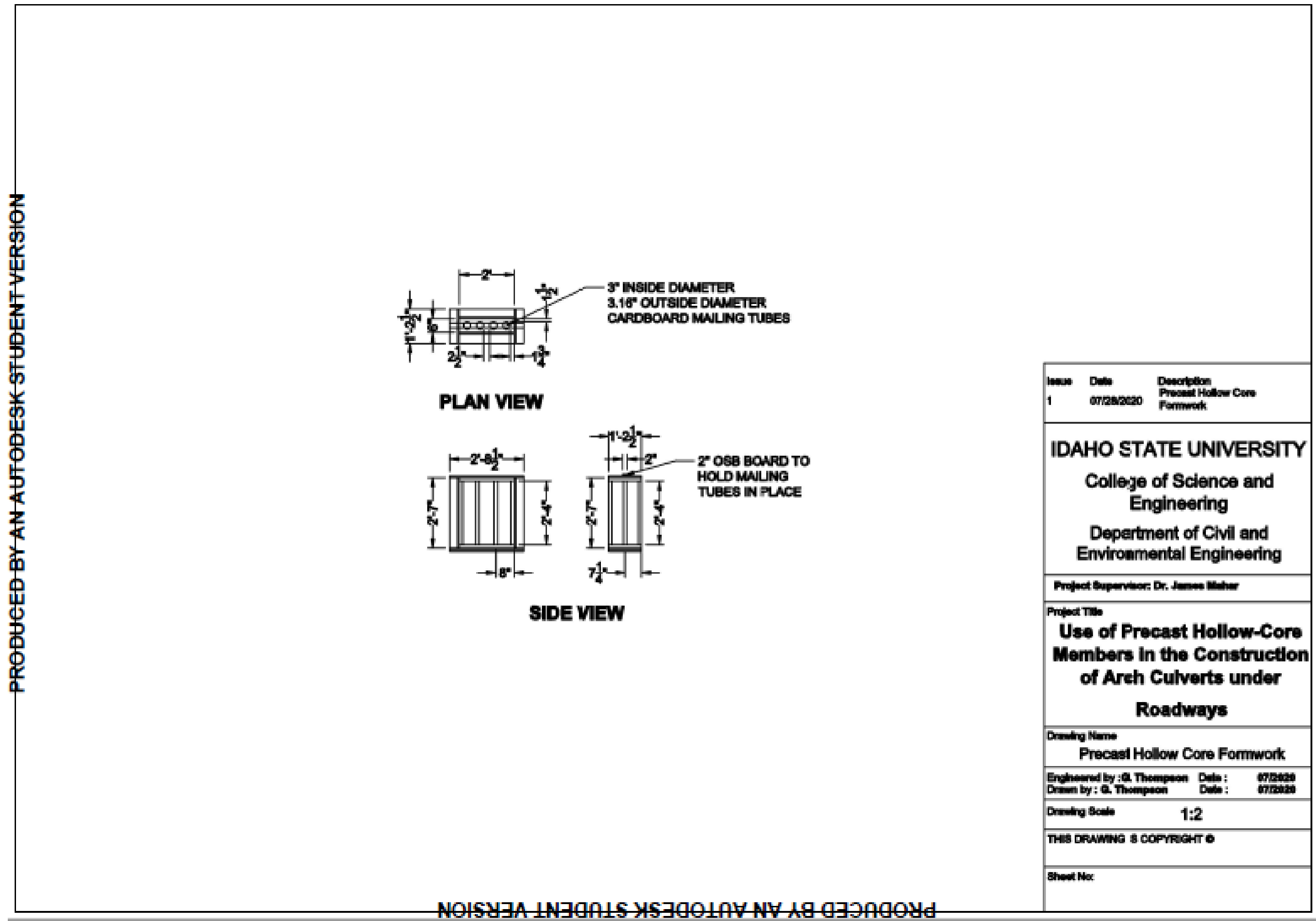

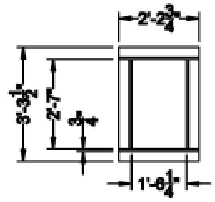

PLAN VIEW

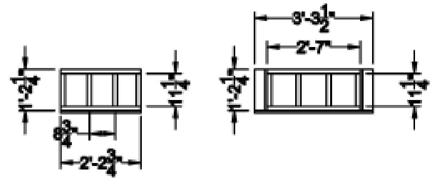

SIDE VIEW

Issue	Date	Description
1	07/28/2020	Precast Footing Formwork

IDAHO STATE UNIVERSITY

College of Science and Engineering

Department of Civil and Environmental Engineering

Project Supervisor: Dr. James Maher

Project Title

Use of Precast Hollow-Core Members in the Construction of Arch Culverts under Roadways

Drawing Name

Precast Footing Formwork

Engineered by : G. Thompson Date : 07/2020
Drawn by : G. Thompson Date : 07/2020

Drawing Scale 1:2

Sheet No:

PRODUCED BY AN AUTODESK STUDENT VERSION

Appendix C – Retaining Wall Design Calculations

C1 – Lateral Earth Pressures

D. Garz Hollow Core Culvert 2020.06.29.Horizontal.Loading

Soil Loading

Active Pressure

$$P_A = \frac{1}{2} \times K_A \times \gamma \times H^2$$

$$K_A = \frac{1}{3}$$

$$\gamma = 125\ \frac{lbf}{ft^3}$$

$$H = 65.78\ in\ \times \frac{1\ ft}{12\ in} = 5.48\ ft$$

$$P_A = 626 \frac{lbf}{ft}$$

Horizontal Soil Pressure

$$\overline{\sigma_H} = K_0 \times \overline{\sigma_V}$$

$$K_0 = .5$$ McCarthy Equation for Dense Sand

$$\overline{\sigma_V} = \gamma \times H$$

$$\overline{\sigma_V} = 685\ \frac{lbf}{ft^2}$$

$$\overline{\sigma_H} = 342\ \frac{lbf}{ft^2}$$

$$P_{\overline{\sigma_H}} = \frac{1}{2} \times \overline{\sigma_H} \times H$$

$$P_{\overline{\sigma_H}} = 937\ \frac{lbf}{ft}$$

Compare Active and Horizontal Pressure

$$P_A = 626 \frac{lbf}{ft} < 937 \frac{lbf}{ft} = P_{\sigma_H}$$

Therefore, use Horizontal Soil Pressure

$$P_{Design} = F.S. \times P_{Nominal}$$

$$F.S. = 1.5$$

$$P_{Nominal} = 342 \frac{lbf}{ft^2}$$

$$P_{Design} = 514\ \frac{lbf}{ft^2}$$

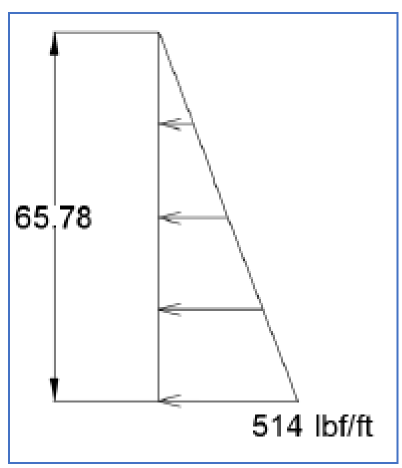

Figure 1: Horizontal Soil Loading

Stud Loading

$W_{Design} = P_{Design} \times Tributary\ Width$

$Tributary\ Width = 1ft$

$W_{Design} = 514\frac{lbf}{ft}$ at depth of 65.78 in for Stud A

$W_{Design} = 195\frac{lbf}{ft}$ at depth of 25.00 in for Stud B

$W_{Design} = 93.4\ \frac{lbf}{ft}$ at depth of 12.00 in for Stud C

Lateral Pressure Due to Vertical Loading

Boussinesq Equation for Vertical Stress

$\Delta\sigma_v = \frac{3Q}{2\pi}\frac{z^3}{(z^2+x^2)^{\frac{5}{2}}}$ (McCarthy EQ 9-6a)

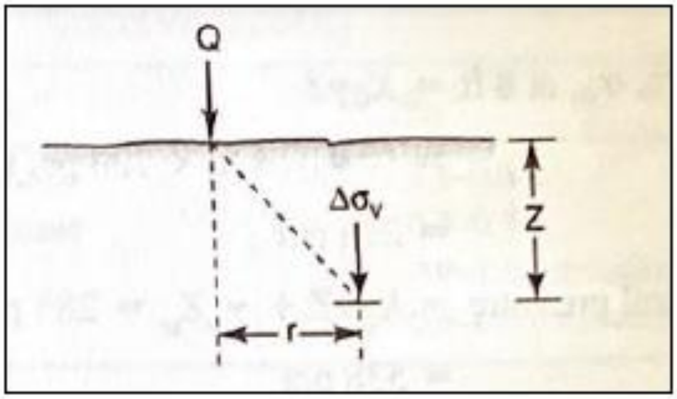

Figure 2: McCarthy Figure 9-5 Boussinesq Term Definitions

$Q = 18.2\ k$

$Z = 12\ in$

$r = 12.5\ in$

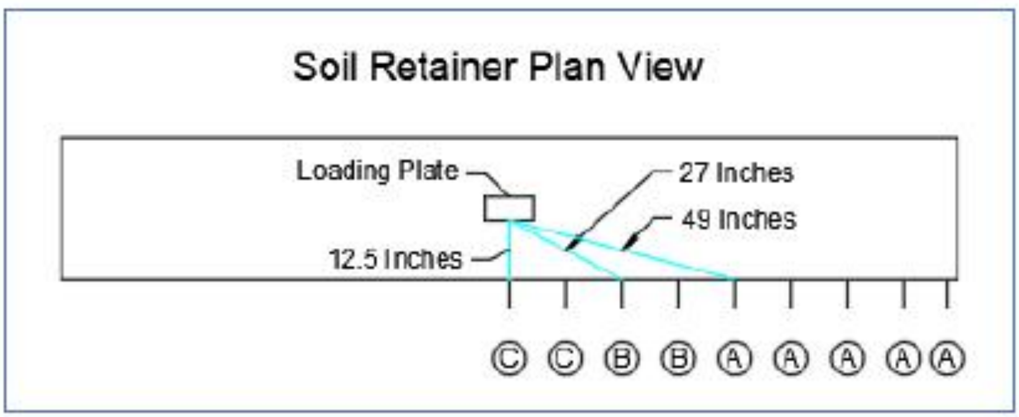

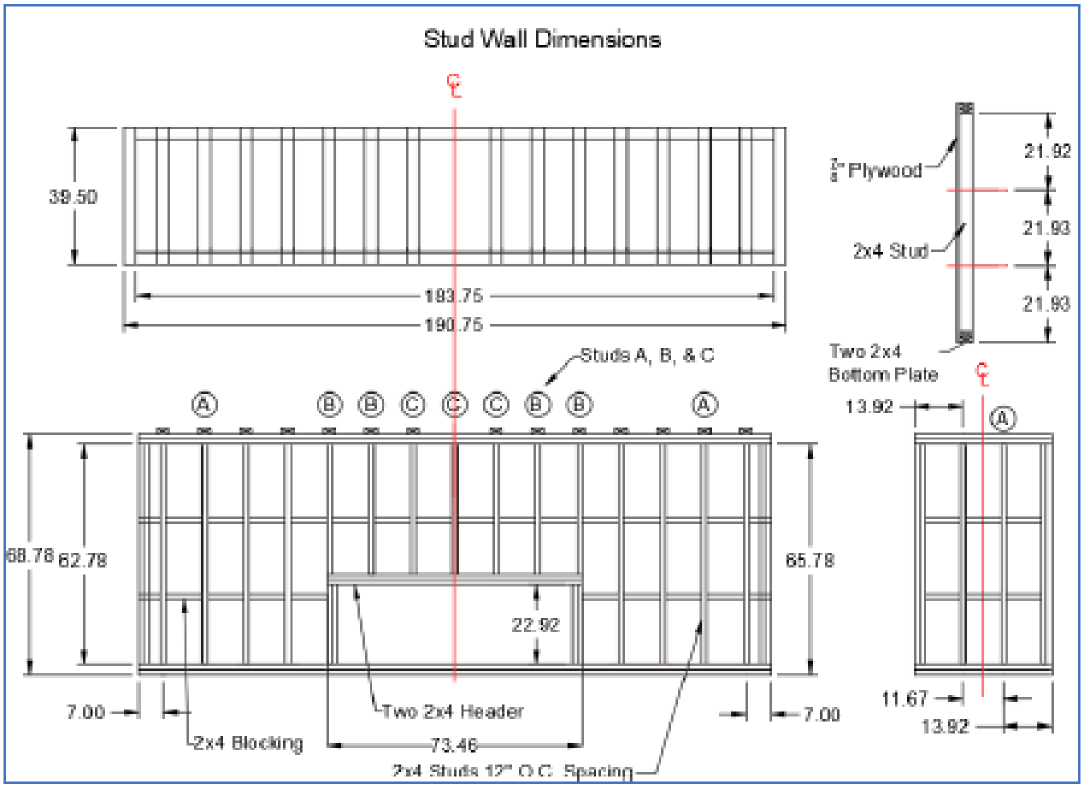

Figure 3: Stud Plans

$$\Delta\sigma_v = \frac{3(18.2\ k)}{2\pi}\frac{(12\ in)^3}{[(12\ in)^2 + (12.5\ in)^2]^{\frac{5}{2}}}$$

$$\Delta\sigma_v = 0.0096\ \frac{k}{in^2}$$

$$\Delta\sigma_v = \frac{3Q}{2\pi}\frac{z^3}{(z^2+x^2)^{\frac{5}{2}}}$$ (McCarthy EQ 9-6a)

$$Q = 18.2\ k$$

$$Z = 1\ ft$$

$$r = 1.04\ ft$$

$$\Delta\sigma_v = \frac{3(18.2\ k)}{2\pi}\frac{(1\ ft)^3}{[(1\ ft)^2 + (1.04\ ft)^2]^{\frac{5}{2}}}$$

$$\Delta\sigma_v = 1.384\ \frac{k}{ft^2} = 0.0096\ \frac{k}{in^2}$$

Calculating Horizontal Pressure

$\Delta\sigma_h = \Delta\sigma_v \times k_0$

$$k_0 = 0.5$$

$$\Delta\sigma_h = 1.384\,\frac{k}{ft^2} \times 0.5$$

$$\Delta\sigma_h = 0.692\,\frac{k}{ft^2}$$

$$\Delta\sigma_h = 692\,\frac{lbf}{ft^2}$$

Boussinesq Equation is applied at a constant distance of 12.5 inches away from the loading at various depths (Z) from 1 to 12 inches. The vertical pressure values are then converted using a K_o factor of 0.5. The values are plotted in a graph and an approximate triangular distribution is assumed for the horizontal loading.

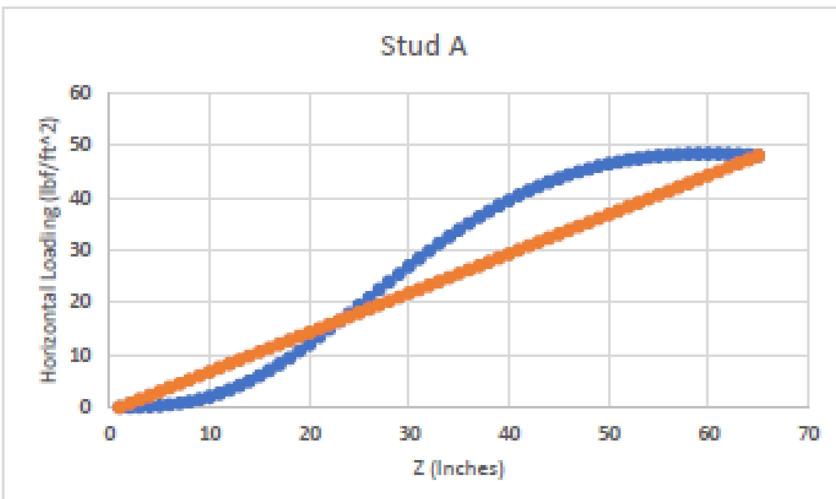

Figure 4: Horizontal Pressure at Stud A

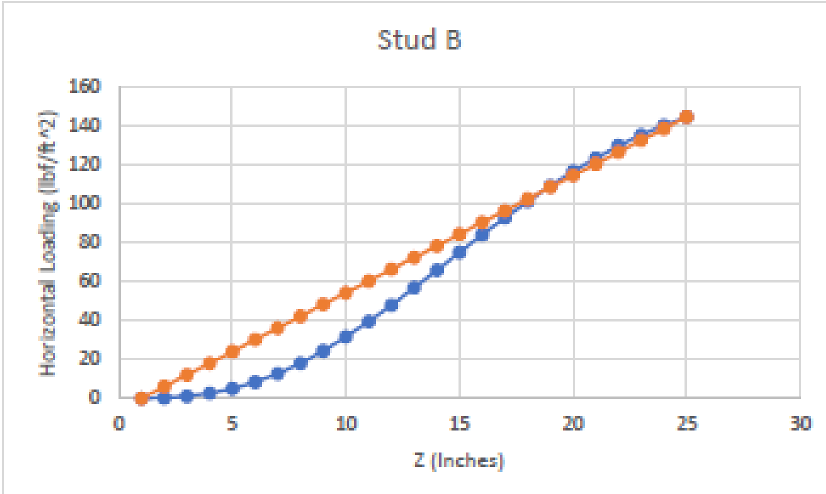

Figure 5: Horizontal Pressure at Stud B

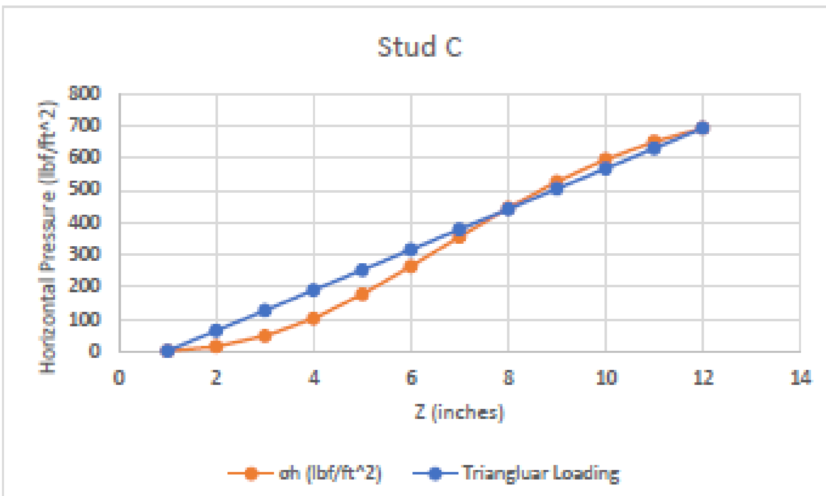

Figure 6: Horizontal Pressure at Stud C

Use a factor of safety of 1.5 for design loading.

$W_{Design} = 80\,\frac{lbf}{ft}$ at depth of 65.78 in for Stud A

$W_{Design} = 216\,\frac{lbf}{ft}$ at depth of 25.00 in for Stud B

$W_{Design} = 138\,\frac{lbf}{ft}$ at depth of 12 in for Stud C

Combined Loading

$W_{Design} = 594 \frac{lbf}{ft}$ at depth of 65.78 in for Stud A

$W_{Design} = 411 \frac{lbf}{ft}$ at depth of 25.00 in for Stud B

$W_{Design} = 1131 \frac{lbf}{ft}$ at depth of 12 in for Stud C

Appendix

Appendix 1: Stud A Horizontal Pressure Values

Stud A			
Q	18.2	k	
r	49	in	
k0	0.5		
x	y	y	
Z (in)	σ_v (lbf/ft^2)	σ_h (lbf/ft^2)	Triangluar Loading
1	0.004	0.002	0.002
2	0.035	0.018	0.753
3	0.118	0.059	1.505
4	0.279	0.139	2.256
5	0.540	0.270	3.007
6	0.922	0.461	3.758
7	1.445	0.722	4.509
8	2.124	1.062	5.261
9	2.972	1.486	6.012
10	4.000	2.000	6.763
11	5.214	2.607	7.514
12	6.618	3.309	8.265
13	8.211	4.105	9.017
14	9.990	4.995	9.768
15	11.951	5.976	10.519
16	14.085	7.042	11.270
17	16.381	8.191	12.021
18	18.827	9.413	12.773
19	21.408	10.704	13.524
20	24.109	12.055	14.275
21	26.914	13.457	15.026
22	29.804	14.902	15.777
23	32.763	16.382	16.529
24	35.774	17.887	17.280
25	38.817	19.409	18.031
26	41.877	20.939	18.782
27	44.937	22.469	19.533
28	47.982	23.991	20.285
29	50.996	25.498	21.036
30	53.967	26.983	21.787
31	56.881	28.440	22.538
32	59.727	29.864	23.289
33	62.496	31.248	24.041
34	65.178	32.589	24.792
35	67.766	33.883	25.543
36	70.252	35.126	26.294
37	72.632	36.316	27.045
38	74.901	37.450	27.797
39	77.055	38.527	28.548
40	79.092	39.546	29.299
41	81.011	40.506	30.050
42	82.811	41.405	30.801
43	84.491	42.245	31.553
44	86.052	43.026	32.304
45	87.495	43.748	33.055
46	88.823	44.411	33.806
47	90.036	45.018	34.558
48	91.138	45.569	35.309
49	92.131	46.066	36.060
50	93.019	46.510	36.811
51	93.805	46.903	37.562
52	94.492	47.246	38.314
53	95.084	47.542	39.065
54	95.585	47.793	39.816
55	95.998	47.999	40.567
56	96.328	48.164	41.318
57	96.578	48.289	42.070
58	96.752	48.376	42.821
59	96.854	48.427	43.572
60	96.888	48.444	44.323
61	96.857	48.429	45.074
62	96.765	48.383	45.826
63	96.616	48.308	46.577
64	96.412	48.206	47.328
65	96.158	48.079	48.079

Appendix 2: Stud B Horizontal Pressure Values

Stud B			
Q	18.2	k	
r	27	in	
k0	0.5		
x	y	y	
Z (in)	σ_v (lbf/ft^2)	σ_h (lbf/ft^2)	Triangluar Loading
1	0.087	0.043	0.043
2	0.688	0.344	6.080
3	2.283	1.142	12.116
4	5.286	2.643	18.153
5	10.020	5.010	24.189
6	16.698	8.349	30.225
7	25.423	12.711	36.262
8	36.179	18.090	42.298
9	48.853	24.426	48.335
10	63.240	31.620	54.371
11	79.069	39.534	60.407
12	96.025	48.012	66.444
13	113.767	56.883	72.480
14	131.949	65.974	78.516
15	150.237	75.119	84.553
16	168.323	84.162	90.589
17	185.931	92.966	96.626
18	202.825	101.413	102.662
19	218.811	109.406	108.698
20	233.739	116.869	114.735
21	247.496	123.748	120.771
22	260.011	130.005	126.808
23	271.242	135.621	132.844
24	281.179	140.589	138.880
25	289.834	144.917	144.917

Appendix 3: Stud C Horizontal Pressure Values

Stud A			
Q	18.2	k	
r	12.5	in	
k0	0.5		
x	y	y	
Z (in)	σ_v (lbf/ft^2)	σ_h (lbf/ft^2)	Triangluar Loading
1	4.036	2.018	2.018
2	30.794	15.397	64.755
3	96.247	48.123	127.492
4	205.663	102.832	190.229
5	353.664	176.832	252.966
6	527.428	263.714	315.703
7	711.150	355.575	378.440
8	889.929	444.965	441.177
9	1052.173	526.087	503.914
10	1190.462	595.231	566.651
11	1301.291	650.646	629.388
12	1384.240	692.120	692.125

Appendix 4: Design Loading

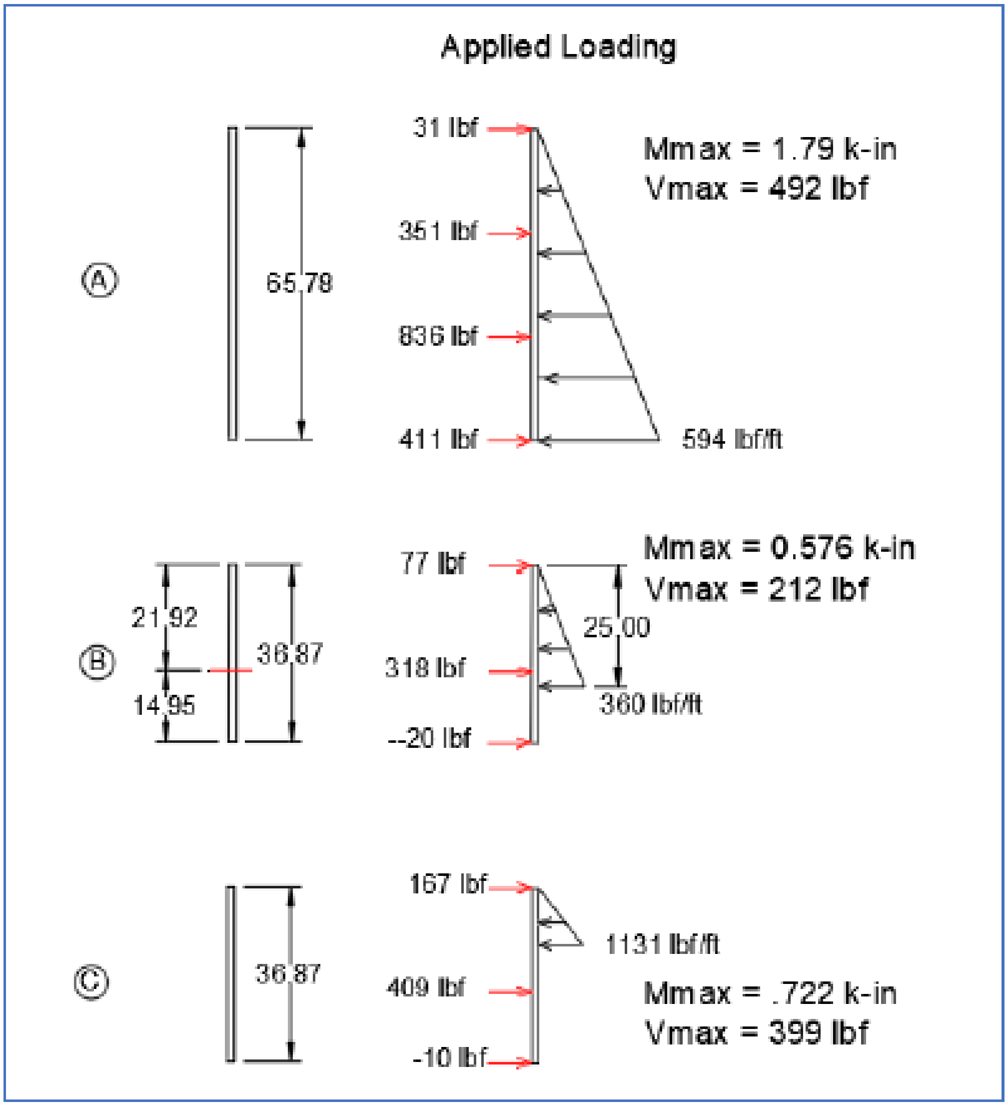

C2 – Cross-Beam Design Calculations

D. Garz | Hollow Core Culvert | 2020.07.02 Cross Beam Design

Stud A Beam Calculation

Stud "A" has the largest bending moment applied and therefore controls the stud wall design. Figure 1 shows Studs A, B, and C along with their maximum shear and moments.

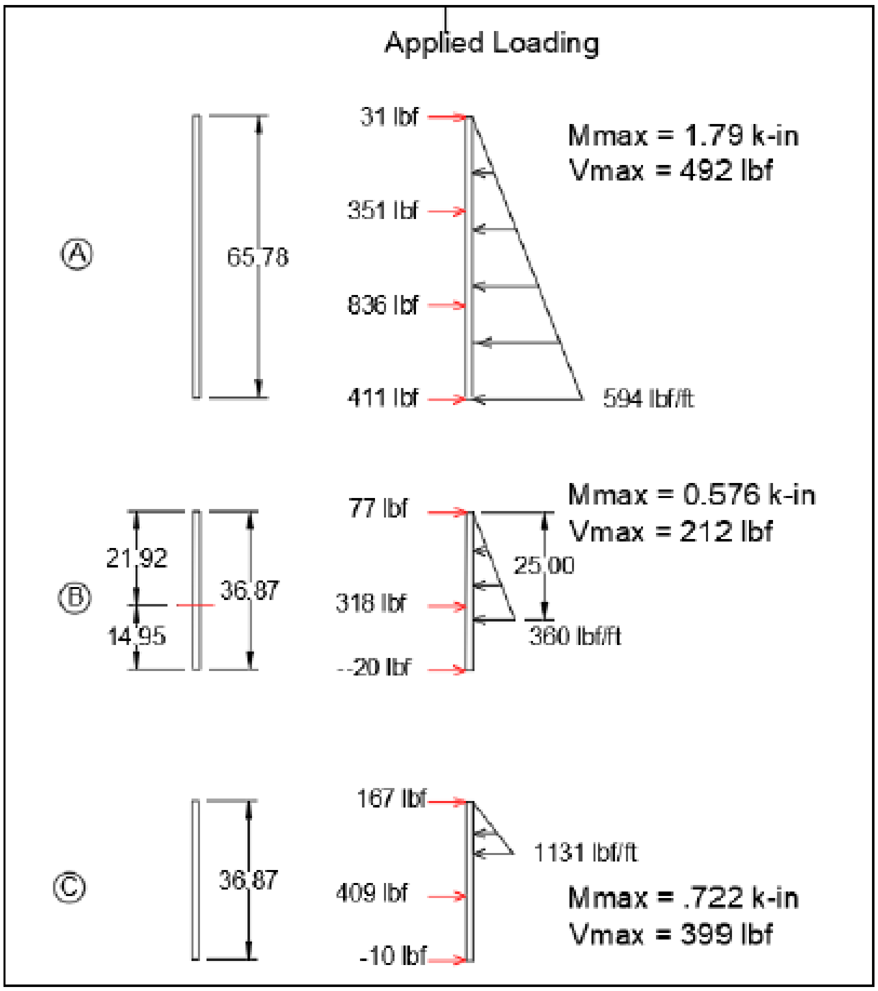

Figure 1: Stud FBD, Shears, and Moments

$f_b^* = F_b(C_D C_M C_t C_F \text{ or } C_V C_r)$ *Note no* C_L

$f_b^* = 900\ psi$ NDS Reference Manual Table 4A for No. 2 Douglas Fir-Larch
$C_D = 1.25$ NDS Table 2.3.2 Duration Factor for Construction

$C_M = 1$ Table 4A of NDS Reference Manual, Moisture Content > 19%
$C_t = 1$ Normal Temperatures
$C_F = 1$ Table 4A of NDS Reference Manual for 2x8
$C_r = 1.15$ Table 4A of NDS Reference Manual

$$f_b^* = 900\,psi(1.25 \times 1 \times 1 \times 1 \times 1.15) = 1294\,psi$$

$$F_{BE} = \frac{1.2\ E'_{min}}{R_B^2}$$

$E'_{min} = 580{,}000\ psi$ NDS Reference Manual Table 4A for Douglas-Fir Larch

$$R_B = \sqrt{\frac{l_e \times d}{b^2}} = Slenderness\ Ratio$$

$l_e = effective\ unbraced\ length\ of\ beam\ from\ NDS\ Table\ 3.3.3$

$$\frac{l_u}{d} = 21.93\ in \div 3.5\ in = 6.09 < 7$$

Therefore, $l_e = 2.06 \times l_u = 45.17\ inches$

$$R_B = \sqrt{\frac{45.17\ inches \times 3.5 inches}{1.5^2\ \ inches^2}} = 8.38$$

$$F_{BE} = \frac{1.2\ E'_{min}}{R_B^2} = 1.2 \times \frac{580{,}000\ psi}{40.36^2} = 9905\ psi$$

$$F_{BE} / F_b^* = \frac{9905\ psi}{1294\ psi} = 7.65$$

$$C_L = \frac{1 + (F_{BE}/F_b^*)}{1.9} - [(\frac{1 + (F_{BE}/F_b^*)}{1.9})^2 - \frac{(F_{BE}/F_b^*)}{0.95}]^{0.5} = \frac{1 + 7.65}{1.9} - \sqrt{(\frac{1 + 7.65}{1.9})^2 - \frac{7.65}{.95}}$$

$C_L = 0.9926$

$F'_b = F_b^* C_L = 1294\ psi \times 0.9926 = 1284\ psi$

$M_{max_{Design}} = 1.79\ kip\ in$

$M_{max_{Allowable}} = F'_B \times S = 1284\ psi \times 3.06\ in^3 = 3929\ lbf\ in = 3.929\ kip\ in$

Cross Beam One

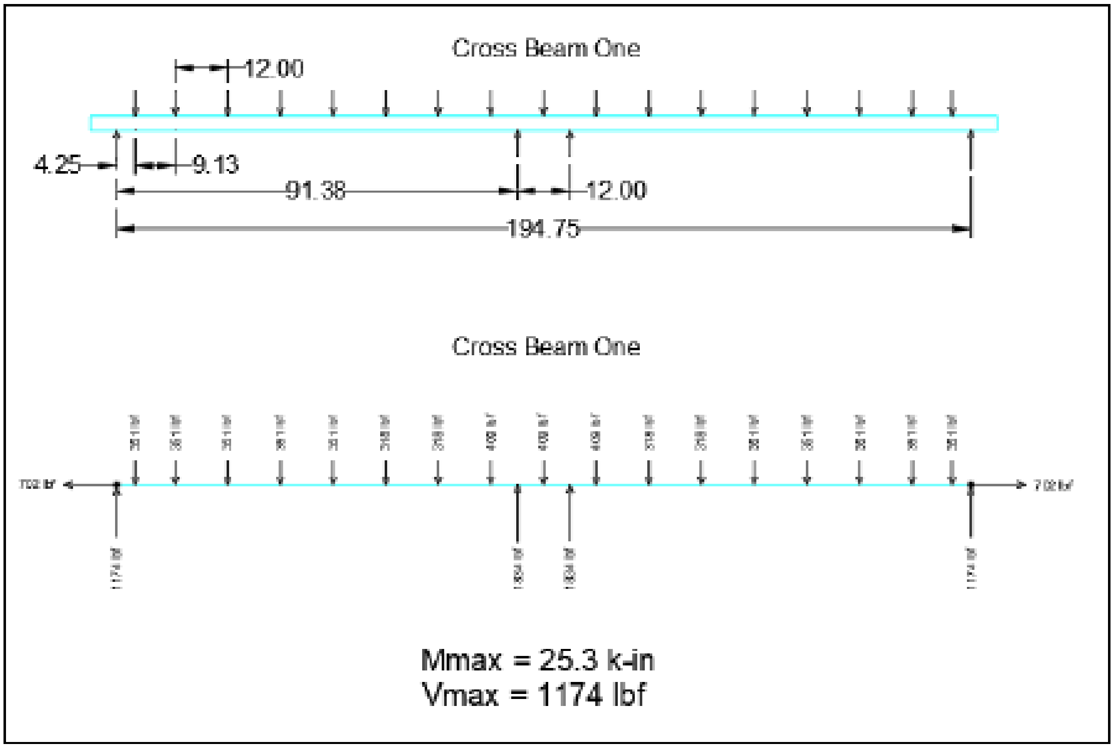

Figure 2: Cross Beam 1 FBD, Shears, and Moments

Beam Made of Two 2x8 Studs

$D = 7.25\ in$

$B = 3\ in$

$S = 26.28\ in^3$

$f_b^* = F_b(C_D C_M C_t C_F\ or\ C_V C_r)\ Note\ no\ C_L$

$f_b^* = 900\ psi$ NDS Reference Manual Table 4A for No. 2 Douglas Fir-Larch
$C_D = 1.25$ NDS Table 2.3.2 Duration Factor for Construction
$C_M = 1$ Table 4A of NDS Reference Manual, Moisture Content > 19%
$C_t = 1$ Normal Temperatures
$C_F = 1$ Table 4A of NDS Reference Manual for 2x8
$C_r = 1$ Table 4A of NDS Reference Manual

$$f_b^* = 900\,psi(1.25 \times 1 \times 1 \times 1 \times 1) = 1125\,psi$$

$F_{BE} = \dfrac{1.2\,E'_{min}}{R_B^2}$

$E'_{min} = 580{,}000\,psi$ NDS Reference Manual Table 4A for Douglas-Fir Larch

$R_B = \sqrt{\dfrac{l_e \times d}{b^2}} = Slenderness\ Ratio$

$l_e = effective\ unbraced\ length\ of\ beam\ from\ NDS\ Table$ 3.3.3

$\frac{l_u}{d} = 24\,in \div 7.15\,in = 3.31 < 7$

Therefore, $l_e = 2.06 \times l_u = 49.44\,inches$

$R_B = \sqrt{\dfrac{49.44\,inches \times 7.25\,inches}{3^2\ inches^2}} = 6.31$

$F_{BE} = \dfrac{1.2\,E'_{min}}{R_B^2} = 1.2 \times \dfrac{580{,}000\,psi}{6.31^2} = 17475\,psi$

$F_{BE}/F_b^* = \dfrac{17475\,psi}{1294\,psi} = 7.65$

$C_L = \dfrac{1 + (F_{BE}/F_b^*)}{1.9} - [(\dfrac{1 + (F_{BE}/F_b^*)}{1.9})^2 - \dfrac{(F_{BE}/F_b^*)}{0.95}]^{0.5}$

$C_L = 0.9967$

$F_b' = F_b^* C_L = 1125\,psi \times 0.9967 = 1121\,psi$

$M_{max_{Design}} = 25.3\,kip\,in$

$M_{max_{Allowable}} = F_B' \times S = 1121\,psi \times 26.28\,in^3 = 29{,}464\,lbf\,in = 29.464\,kip\,in$

Cross Beam Two

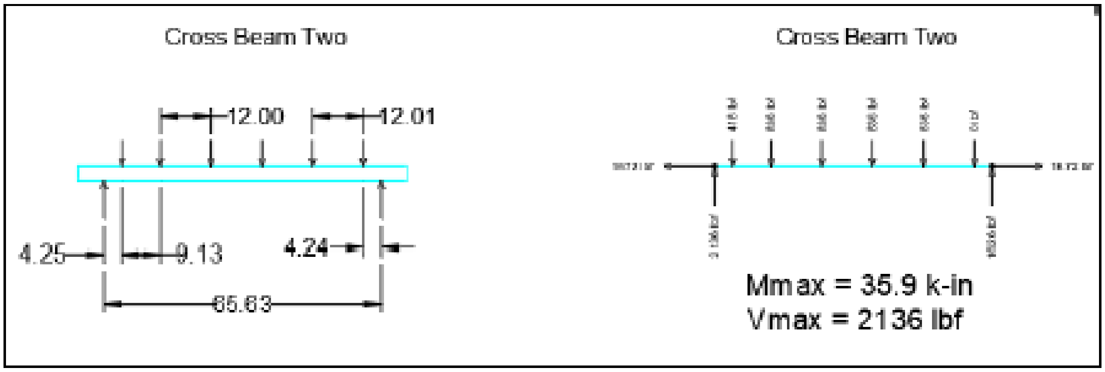

Figure 3: Cross Beam 2 FBD, Shear, and Moment

Beam Made of Three 2x8 Studs

$D = 7.25\ in$

$B = 3\ in$

$S = 39.42\ in^3$

$$f_b^* = F_b(C_D C_M C_t C_F \ or\ C_V C_r)\ Note\ no\ C_L$$

$f_b^* = 900\ psi$ NDS Reference Manual Table 4A for No. 2 Douglas Fir-Larch
$C_D = 1.25$ NDS Table 2.3.2 Duration Factor for Construction
$C_M = 1$ Table 4A of NDS Reference Manual, Moisture Content $> 19\%$
$C_t = 1$ Normal Temperatures
$C_F = 1$ Table 4A of NDS Reference Manual for 2x8
$C_r = 1$ Table 4A of NDS Reference Manual

$$f_b^* = 900\ psi(1.25 \times 1 \times 1 \times 1 \times 1) = 1125\ psi$$

$$F_{BE} = \frac{1.2\ E'_{min}}{R_B^2}$$

$E'_{min} = 580{,}000\ psi$ NDS Reference Manual Table 4A for Douglas-Fir Larch

$$R_B = \sqrt{\frac{l_e \times d}{b^2}} = Slenderness\ Ratio$$

$l_e = effective\ unbraced\ length\ of\ beam\ from\ NDS\ Table$ 3.3.3

$$\frac{l_u}{d} = 24\ in \div 7.15\ in = 3.31 < 7$$

Therefore, $l_e = 2.06 \times l_u = 49.44\ inches$

$$R_B = \sqrt{\frac{49.44\ inches \times 7.25\ inches}{4.5^2\ \ inches^2}} = 4.21$$

$$F_{BE} = \frac{1.2\ E'_{min}}{R_B^2} = 1.2 \times \frac{580{,}000\ psi}{3.21^2} = 39320\ psi$$

$$F_{BE}\big/F_b^* = \frac{39320\ psi}{1294\ psi} = 34.95$$

$$C_L = \frac{1 + (F_{BE}/F_b^*)}{1.9} - [(\frac{1 + (F_{BE}/F_b^*)}{1.9})^2 - \frac{(F_{BE}/F_b^*)}{0.95}]^{0.5}$$

$$C_L = 0.9985$$

$$F_b' = F_b^* C_L = 1125\ psi \times 0.9985 = 1123\ psi$$

$$M_{max_{Design}} = 35.9\ kip\ in$$

$$M_{max_{Allowable}} = F_B' \times S = 1123\ psi \times 39.32\ in^3 = 44{,}282\ lbf\ in = 44.282\ kip\ in$$

Cross Beam Three and Four

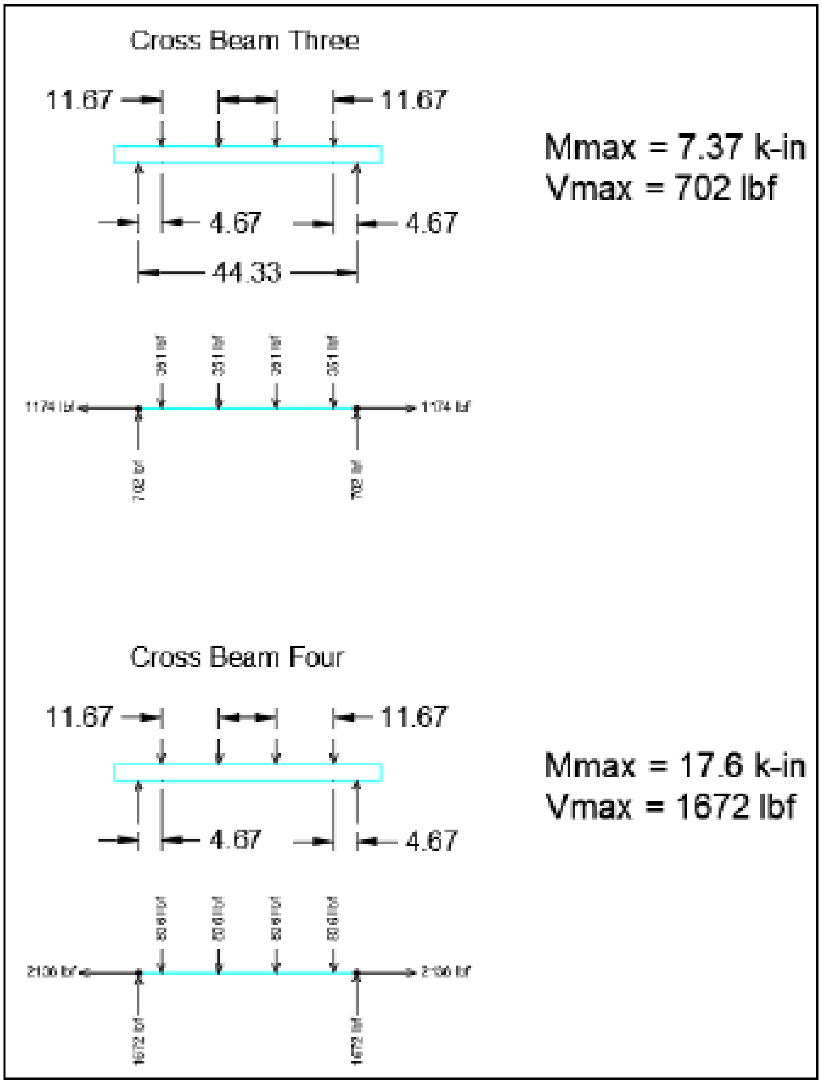

Figure 4: Cross Beams 3 and 4 FBD, Shears, and Moments

Beam Made of Two 2x8 Studs

The maximum moment of cross beams three and four (7.37 and 17.6 kip in) are smaller than cross member one. Two 2x8 members are assumed to be sufficient.

Header

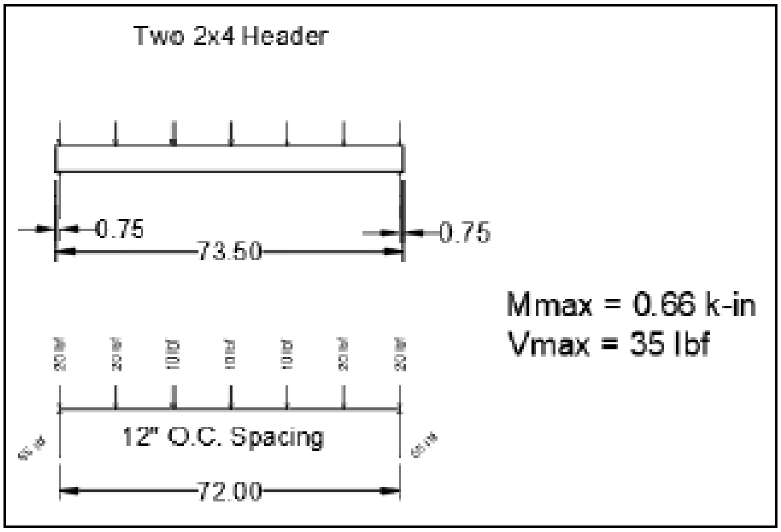

Figure 5: Header FBD, Shear, and Moment

Beam Made of Two 2x4 Studs

$D = 3.5\ in$

$B = 3\ in$

$S = 6.125\ in^3$

$f_b^* = F_b(C_D C_M C_t C_F\ or\ C_V C_r)\ Note\ no\ C_L$

f_b^* = 900 psi NDS Reference Manual Table 4A for No. 2 Douglas Fir-Larch
C_D = 1.25 NDS Table 2.3.2 Duration Factor for Construction
C_M = 1 Table 4A of NDS Reference Manual, Moisture Content > 19%
C_t = 1 Normal Temperatures
C_F = 1 Table 4A of NDS Reference Manual for 2x8
C_r = 1 Table 4A of NDS Reference Manual

$$f_b^* = 900\ psi(1.25 \times 1 \times 1 \times 1 \times 1) = 1125\ psi$$

$$F_{BE} = \frac{1.2\ E'_{min}}{R_B^2}$$

E'_{min} = 580,000 psi NDS Reference Manual Table 4A for Douglas-Fir Larch

$$R_B = \sqrt{\frac{l_e \times d}{b^2}} = Slenderness\ Ratio$$

$l_e = effective\ unbraced\ length\ of\ beam\ from\ NDS\ Table$ 3.3.3

$$\frac{l_u}{d} = 72\ in \div 3.5\ in = 20.57 < 7$$

Therefore, $l_e = 1.84 \times l_u = 132.48\ inches$

$$R_B = \sqrt{\frac{132.48\ inches \times 3.5\ inches}{3^2\ \ inches^2}} = 7.18$$

$$F_{BE} = \frac{1.2\ E'_{min}}{R_B^2} = 1.2 \times \frac{580{,}000\ psi}{7.18} = 13509\ psi$$

$$F_{BE}/F_b^* = \frac{13509\ psi}{1125\ \ psi} = 12.08$$

$$C_L = \frac{1 + (F_{BE}/F_b^*)}{1.9} - [(\frac{1 + (F_{BE}/F_b^*)}{1.9})^2 - \frac{(F_{BE}/F_b^*)}{0.95}]^{0.5}$$

$C_L = 0.9955$

$F_b' = F_b^* C_L = 1125\ psi \times 0.9955 = 1120\ psi$

$M_{max_{Design}} = 0.66\ kip\ in$

$M_{max_{Allowable}} = F_B' \times s = 1120\ psi \times 6.07\ in^3 = 6{,}859\ lbf\ in = 6.859\ kip\ in$

C3 – Cross-Beam Connection Design Calculations

D. Garz

Hollow Core Culvert

2020.07.16 Cross Beam Connection Design

Loading

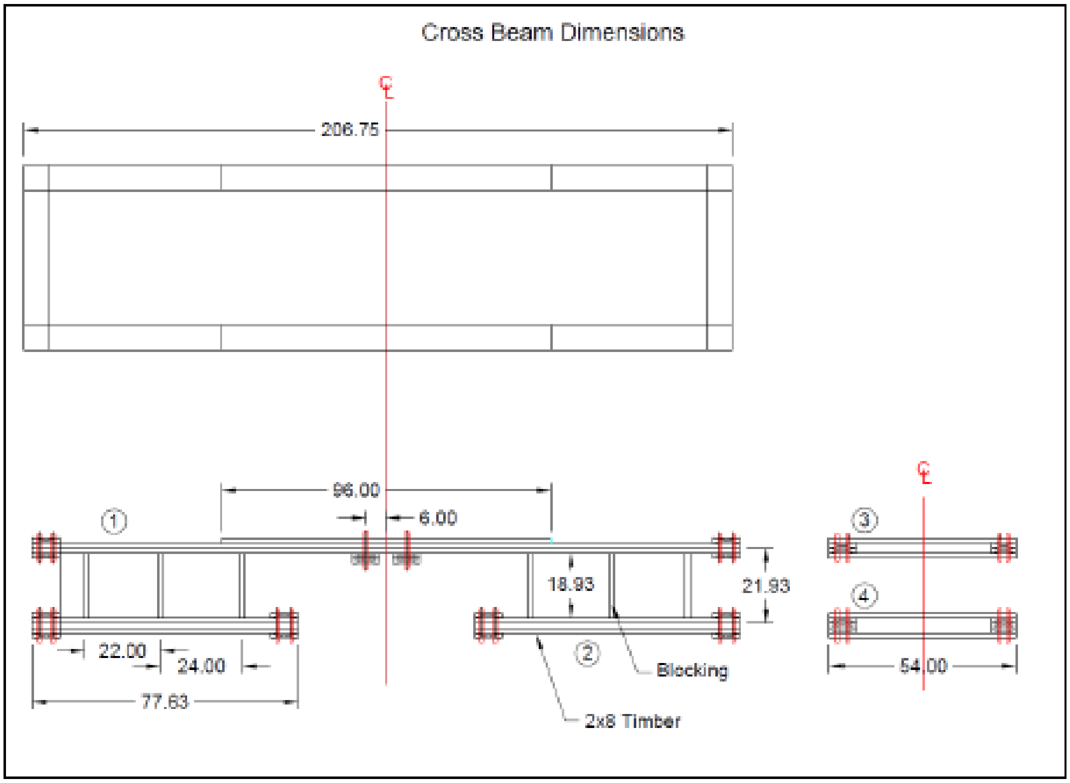

Figure 1: Cross Beams

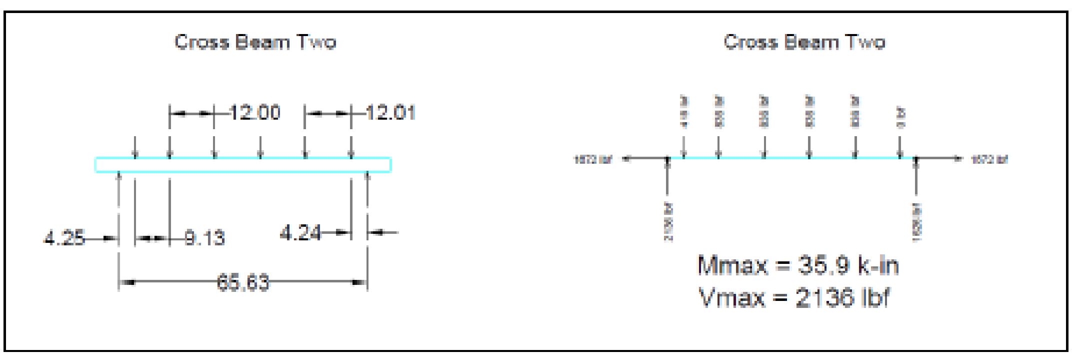

Figure 2: Cross Beam Two Loading and FBD

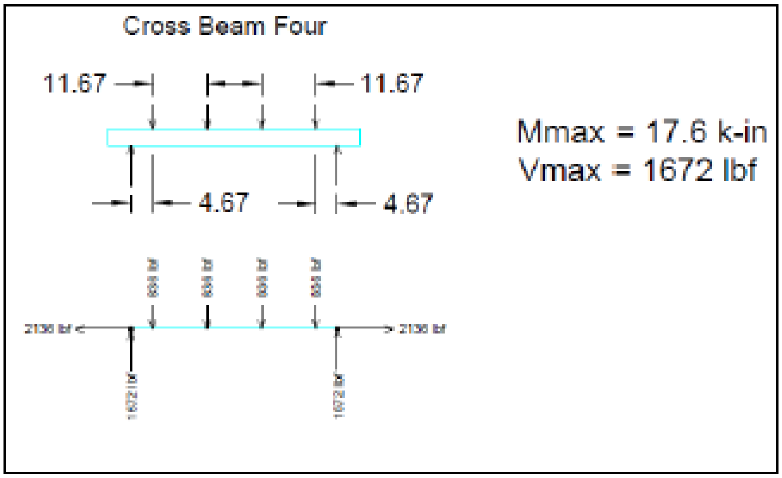

Figure 3: Cross Beam Four Loading and FBD

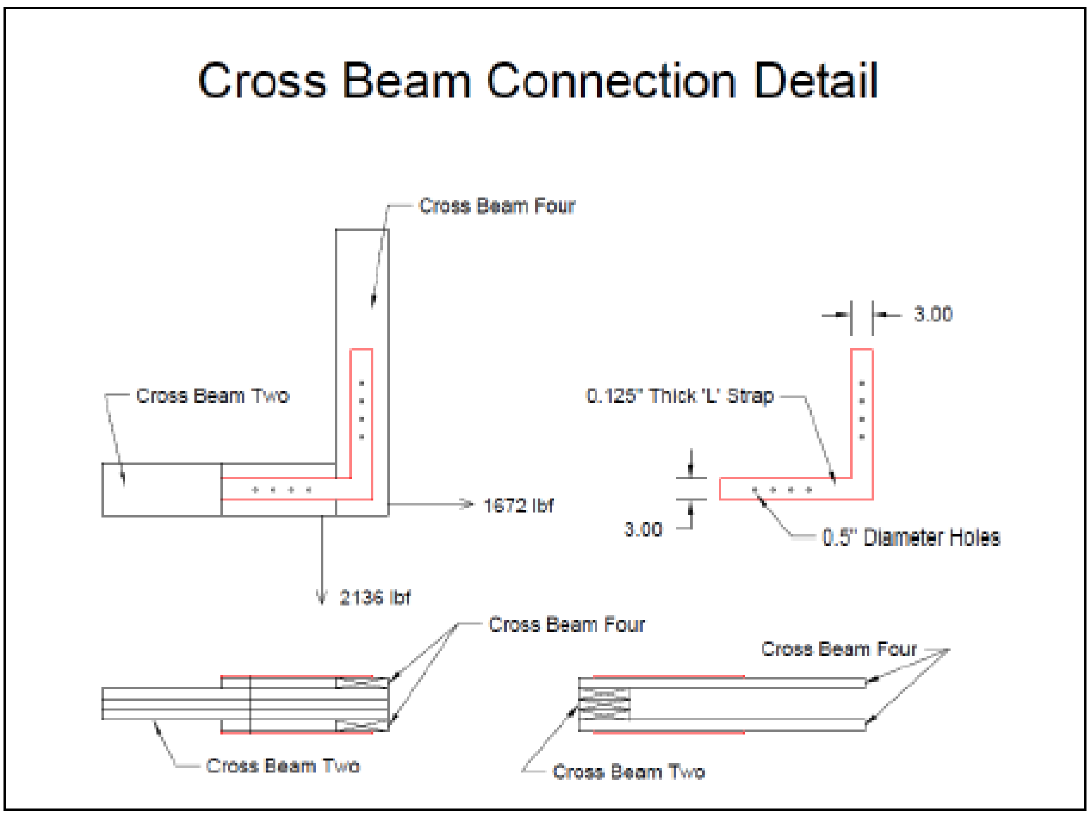

Figure 4: Cross Beam Connection Detail

Cross Beam Connection

Bolt Capacity

(Following Example 13.4 pg 737 of Design of Wood Structures)

$Z' = Z \times C_D \times C_M \times C_t \times C_g \times C_\Delta \times C_{eg} \times C_{di} \times C_{tn}$

$Douglas\ Fir\ Larch\ Specific\ Gravity, G = 0.5\ (NDS\ T11.3.3a)$

$Z = Smallest\ value\ from\ Figure\ 3$

$$F_{em} = F_{e\theta} = \frac{F_{e||} \times F_{e\perp}}{F_{e||}(\sin\theta)^2 + F_{e\perp}(\cos\theta)^2}$$

$F_{e||} = 11{,}200G$

$F_{e\perp} = 6{,}100G^{1.45}D^{-0.5}$

$G = 0.49\ (Douglas\ Fir - Larch\ Northern\ NDS\ T11.3.3A)$

$\boldsymbol{D = 1.0\ inch}$

$F_{e||} = 5488\ psi$

$F_{e\perp} = 2168\ psi$

$\theta = 52°$

$F_{em} = 2813\ psi$

$F_{es} = 1.5\ F_u$

$F_u = 58{,}000\ psi\ for\ A36\ Steel$

$F_{es} = 87{,}000\ psi$

$$R_e = \frac{F_{em}}{F_{es}}$$

$R_e = 0.03233$

$l_m = 4.5\ in$

$l_s = 0.25\ in$

$$R_t = \frac{l_m}{l_s} = 18\ in$$

$$K_\theta = 1 + \frac{\theta}{360}$$

$K_\theta = 1.144$

$F_{yb} = 45{,}000\ psi(Assumed\ for\ A307\ Bolt)$

Table 1: Rd Calculation Table

Failure Mode	R_d	R_d
I_m	$R_d = 4K_\theta$	4.58
I_s	$R_d = 4K_\theta$	4.58
II	$R_d = 3.6K_\theta$	4.12
III_m	$R_d = 3.2K_\theta$	3.66
III_s	$R_d = 3.2K_\theta$	3.66
IV	$R_d = 3.2K_\theta$	3.66

$$k_1 = \frac{\sqrt{R_e + 2R_e^2(1 + R_t + R_t^2) + R_t^2R_e^3} - R_e(1 + R_t)}{(1 + R_e)} = 16.9$$

$$k_2 = -1 + \sqrt{2(1 + R_e) + \frac{2F_{yb}(1 + 2R_e)D^2}{3F_{em}l_m^2}} = 0.620$$

$$k_3 = -1 + \sqrt{\frac{2(1 + R_e)}{R_e} + \frac{2F_{yb}(2 + R_e)D^2}{3F_{em}l_s^2}} = 19.3$$

Table 2: Bolt Capacity Calculation Table

Failure Mode	*Double Shear Z*	Z
I_m	$Z = \frac{Dl_mF_{em}}{R_d}$	2766 lbf
I_s	$Z = \frac{2Dl_sF_{es}}{R_d}$	9502 lbf
II	$Z = \frac{k_1Dl_sF_{es}}{R_d}$	89,012 lbf
III_m	$Z = \frac{k_2Dl_mF_{em}}{(1 + 2R_e)R_d}$	**2014 lbf**
III_s	$Z = \frac{2k_3Dl_sF_{em}}{(2 + R_e)R_d}$	3641 lbf
IV	$Z = \frac{2D^2}{R_d}\sqrt{\frac{2F_{em}F_{yb}}{3(1 + R_e)}}$	4938 lbf

$Z = 2014\ lbf$

$C_D = 1.25\ (NDS\ 2.3.2)$

$C_M = C_t = 1.0$

Group Action Factors, C_g

$C_g = 1.0$ $(Each\ Cross\ Beam\ Has\ One\ Bolt)$

$Geometry\ Factor, C_{\Delta}$

$C_{\Delta} = 1.0$

End Grain Factor, C_{eg}

$C_{eg} = 1.0$ $(NDS\ Section\ 11.5.2)$

Diaphragm Factor, C_{di}

$C_{di} = 1.0$ $(NDS\ Section\ 11.5.3)$

Toe-Nail Factor, C_{tn}

$C_{tn} = 1.0$ $(NDS\ Section\ 11.5.4)$

$Z' = 2014 \times 1.25$

$Z' = 2518\ lbf$

$P = n \times Z'$

$P = 2712\ lbf$

$n = 1.077$

$\therefore \boldsymbol{Use\ Two\ 1\ in\ Diameter\ Bolts}$

$\boldsymbol{Edge\ Distance\ from\ Loaded\ Edge = 4\ in}$

$\boldsymbol{Edge\ Distance\ from\ Unloaded\ Edge = 1.5\ in}$

$\boldsymbol{End\ Distance = 7\ in}$

Net Section Tension

$$Z'_{NT} = F'_t A_n$$

Equation 1: Net Section Tension (NDS Eq. E.2-1)

$F'_t = adjusted\ tension\ design\ value\ parallel\ to\ grain, psi\ (CH\ 7)$

$F'_t = F_t(C_D)(C_M)(C_t)(C_F)(C_i)$

$F_t = 400\ \frac{lbf}{in^2}$ $(Douglas\ Fir\ Larch\ North\ NDS\ Supplement\ T4A)$

$C_D = 1.25$

$C_M = 1.0$

$C_t = 1.0$

$C_F = 1.2$

$C_i = 1.0$

$F_t' = 600\,\frac{lbf}{in^2}$

$A_n = net\ cross - sectional\ area\ of\ tension\ member, in^2\ (CH\ 7)$

$A_n = A_g - \sum A_h$

$A_g = 7.25\ in\ \times 4.5\ in = 32.6\ in^2$

$\sum A_h = 1.125\ in\ \times 4.5\ in = 5.06\ in^2$

$A_n = 27.6\ in^2$

$Z'_{NT} = 16.5\ kips$

Stud to Plate Connection

Use Simpson Strong-Tie joist hangers model numbers LUS24 and LUS24-2. Both hangers are rated for 870 pounds of loading. Simpson Strong-Tie recommends two fasteners model number SD9212 for the joist (stud) and four fasteners model number SD9112 for the face (stud plates). See appendix for screenshot of rating table.

Top Plate to Tension Member Connection

Use two screws at each connection

Middle Plate Connection

$Z' = Z \times C_D \times C_M \times C_t \times C_g \times C_\Delta \times C_{eg} \times C_{di} \times C_{tn}$

$Douglas\ Fir\ Larch\ Specific\ Gravity, G = 0.5\ (NDS\ T11.3.3a)$

$Z = Smallest\ value\ from\ Figure\ 3$

$G = 0.5\ (Douglas\ Fir - Larch\ NDS\ T11.3.3A)$

$\boldsymbol{D = 0.164\ inch}$

$F_{em} = 16{,}600G^{1.84}$

$F_{em} = 4637\ psi$

$F_{es} = F_{em}$

$F_{es} = 4637\ psi$

$R_e = \frac{F_{em}}{F_{es}}$

$R_e = 1$

$l_m = 1.5\ in$

$l_s = 1.4\ in$

$R_t = \frac{l_m}{l_s} = 1.07\ in$

$K_\theta = 1 + \frac{\theta}{360}$

$\theta = 90°$

$K_\theta = 1.25$

$F_{yb} = 45{,}000\ psi (Assumed\ for\ A307\ Bolt)$

$R_d = K_D\ (D < 0.25\ in)$

$K_D = 2.2\ (D \leq 0.17\ in)$

$$k_1 = \frac{\sqrt{R_e + 2R_e^2(1 + R_t + R_t^2) + R_t^2R_e^3} - R_e(1 + R_t)}{(1 + R_e)} = 16.9$$

$$k_2 = -1 + \sqrt{2(1 + R_e) + \frac{2F_{yb}(1 + 2R_e)D^2}{3F_{em}l_m^2}} = 0.620$$

$$k_3 = -1 + \sqrt{\frac{2(1 + R_e)}{R_e} + \frac{2F_{yb}(2 + R_e)D^2}{3F_{em}l_s^2}} = 19.3$$

Table 3: Nail Connection Capacity

Failure Mode	*Single Shear Z*	Z
I_m	$Z = \frac{Dl_mF_{em}}{R_d}$	$518\ lbf$
I_s	$Z = \frac{Dl_sF_{es}}{R_d}$	$484\ lbf$
II	$Z = \frac{k_1Dl_sF_{es}}{R_d}$	$248\ lbf$
III_m	$Z = \frac{k_2Dl_mF_{em}}{(1 + 2R_e)R_d}$	$183\ lbf$
III_s	$Z = \frac{k_3Dl_sF_{em}}{(2 + R_e)R_d}$	$172\ lbf$
IV	$Z = \frac{D^2}{R_d}\sqrt{\frac{2F_{em}F_{yb}}{3(1 + R_e)}}$	$\mathbf{102\ lbf}$

$Z = 102\ lbf$

$C_D = 1.25\ (NDS\ 2.3.2)$

$C_M = C_t = 1.0$

Group Action Factors, C_g

$C_g = 1.0\ (Appendix\ C, NDS\ 10.3.6)$

$Geometry\ Factor, C_\Delta$

$C_\Delta = 1.0$

End Grain Factor, C_{eg}

$C_{eg} = 1.0\ (NDS\ Section\ 11.5.2)$

Diaphragm Factor, C_{di}

$C_{di} = 1.0\ (NDS\ Section\ 11.5.3)$

Toe-Nail Factor, C_{tn}

$C_{tn} = 1.0\ (NDS\ Section\ 11.5.4)$

$Z' = 102 \times 1.25$

$Z' = 127.5\ lbf$

$P = n \times Z'$

$P = 836\ lbf$ Per 12 in of Length

$n = 6.56$

$\therefore \boldsymbol{Use\ Eight\ \#8\ 3\ in\ Length\ Wood\ Screws\ Per\ 12\ in\ of\ Length}$

$\boldsymbol{Edge\ Distance\ from\ Loaded\ Edge = 0.656\ in}$

$\boldsymbol{Edge\ Distance\ from\ Unloaded\ Edge = 0.246\ in}$

$\boldsymbol{End\ Distance = 1.15\ in}$

Appendix

Appendix A: NDS Table 11.3.1A

Table 11.3.1A Yield Limit Equations

Yield Mode	Single Shear		Double Shear	
I_m	$Z = \dfrac{D\,\ell_m\,F_{em}}{R_d}$	(11.3-1)	$Z = \dfrac{D\,\ell_m\,F_{em}}{R_d}$	(11.3-7)
I_s	$Z = \dfrac{D\,\ell_s\,F_{es}}{R_d}$	(11.3-2)	$Z = \dfrac{2D\,\ell_s\,F_{es}}{R_d}$	(11.3-8)
II	$Z = \dfrac{k_1\,D\,\ell_s\,F_{es}}{R_d}$	(11.3-3)		
III_m	$Z = \dfrac{k_2\,D\,\ell_m\,F_{em}}{(1+2R_e)\,R_d}$	(11.3-4)		
III_s	$Z = \dfrac{k_3\,D\,\ell_s\,F_{em}}{(2+R_e)\,R_d}$	(11.3-5)	$Z = \dfrac{2k_3\,D\,\ell_s\,F_{em}}{(2+R_e)\,R_d}$	(11.3-9)
IV	$Z = \dfrac{D^2}{R_d}\sqrt{\dfrac{2\,F_{em}\,F_{yb}}{3\,(1+R_e)}}$	(11.3-6)	$Z = \dfrac{2D^2}{R_d}\sqrt{\dfrac{2\,F_{em}\,F_{yb}}{3\,(1+R_e)}}$	(11.3-10)

Notes:

$$k_1 = \frac{\sqrt{R_e + 2R_e^2(1+R_t+R_t^2) + R_t^2R_e^3} - R_e(1+R_t)}{(1+R_e)}$$

$$k_2 = -1 + \sqrt{2(1+R_e) + \frac{2F_{yb}(1+2R_e)D^2}{3F_{em}\ell_m^2}}$$

$$k_3 = -1 + \sqrt{\frac{2(1+R_e)}{R_e} + \frac{2F_{yb}(2+R_e)D^2}{3F_{em}\ell_s^2}}$$

D = diameter, in. (see 11.3.7)
F_{yb} = dowel bending yield strength, psi
R_d = reduction term (see Table 11.3.1B)
R_e = F_{em}/F_{es}
R_t = ℓ_m/ℓ_s
ℓ_m = main member dowel bearing length, in.
ℓ_s = side member dowel bearing length, in.
F_{em} = main member dowel bearing strength, psi (see Table 11.3.3)
F_{es} = side member dowel bearing strength, psi (see Table 11.3.3)

DOWEL-TYPE FASTENERS

Appendix B: Specific Gravities

Table 11.3.3A Assigned Specific Gravities

Species Combination	Specific[1] Gravity, G	Species Combi
Alaska Cedar	0.47	Douglas Fir-Larch
Alaska Hemlock	0.46	E=1,900,000 ps
Alaska Spruce	0.41	E=2,000,000 ps
Alaska Yellow Cedar	0.46	E=2,100,000 ps
Aspen	0.39	E=2,200,000 ps
Balsam Fir	0.36	E=2,300,000 ps
Beech-Birch-Hickory	0.71	E=2,400,000 ps
Coast Sitka Spruce	0.39	Douglas Fir-Larch (N
Cottonwood	0.41	E=1,900,000 ps
Douglas Fir-Larch	0.50	E=2,000,000 ps
Douglas Fir-Larch (North)	0.49	E=2,300,000 ps
Douglas Fir-South	0.46	Douglas Fir-Larch (S

Appendix C: Group Action Factors

10.3.6 Group Action Factors, C_g

10.3.6.1 Reference lateral design values for split ring connectors, shear plate connectors, or dowel-type fasteners with $D \leq 1"$ in a row shall be multiplied by the following group action factor, C_g:

$$C_g = \left[\frac{m(1-m^{2n})}{n\left[(1+R_{EA}m^n)(1+m)-1+m^{2n}\right]}\right]\left[\frac{1+R_{EA}}{1-m}\right] \quad (10.3\text{-}1)$$

where:

C_g = 1.0 for dowel type fasteners with $D < 1/4"$

n = number of fasteners in a row

R_{EA} = the lesser of $\frac{E_sA_s}{E_mA_m}$ or $\frac{E_mA_m}{E_sA_s}$

E_m = modulus of elasticity of main member, psi

E_s = modulus of elasticity of side members, psi

A_m = gross cross-sectional area of main member, in.^{2}

A_s = sum of gross cross-sectional areas of side members, in.^{2}

$m = u - \sqrt{u^2 - 1}$

$u = 1 + \gamma \frac{s}{2}\left[\frac{1}{E_mA_m} + \frac{1}{E_sA_s}\right]$

s = center to center spacing between adjacent fasteners in a row, in.

γ = load/slip modulus for a connection, lbs/in.

= 500,000 lbs/in. for 4" split ring or shear plate connectors

= 400,000 lbs/in. for 2-1/2" split ring or 2-5/8" shear plate connectors

= $(180{,}000)(D^{1.5})$ for dowel-type fasteners in wood-to-wood connections

= $(270{,}000)(D^{1.5})$ for dowel-type fasteners in wood-to-metal connections

D = diameter of dowel-type fastener, in.

Group action factors for various connection geometries are provided in Tables 10.3.6A, 10.3.6B, 10.3.6C, and 10.3.6D.

10.3.6.2 For determining group action factors, a row of fasteners is defined as any of the following:

(a) Two or more split rings or shear plate connector units, as defined in 12.1.1, aligned with the direction of load.

(b) Two or more dowel-type fasteners of the same diameter loaded in single or multiple shear and aligned with the direction of load.

Where fasteners in adjacent rows are staggered and the distance between adjacent rows is less than 1/4 the distance between the closest fasteners in adjacent rows measured parallel to the rows, the adjacent rows shall be considered as one row for purposes of determining group action factors. For groups of fasteners having an even number of rows, this principle shall apply to each pair of rows. For groups of fasteners having an odd number of rows, the most conservative interpretation shall apply (see Figure 10B).

10.3.6.3 Gross section areas shall be used, with no reductions for net section, when calculating A_m and A_s for determining group action factors. When a member is loaded perpendicular to grain its equivalent cross-sectional area shall be the product of the thickness of the member and the overall width of the fastener group (see Figure 10B). Where only one row of fasteners is used, the width of the fastener group shall be the minimum parallel to grain spacing of the fasteners.

Appendix F: End Grain Factor

11.5.2 End Grain Factor, C_{eg}

11.5.2.1 Where lag screws are loaded in withdrawal from end grain, the reference withdrawal design values, W, shall be multiplied by the end grain factor, $C_{eg} = 0.75$.

11.5.2.2 Where dowel-type fasteners are inserted in the end grain of the main member, with the fastener axis parallel to the wood fibers, reference lateral design values, Z, shall be multiplied by the end grain factor, $C_{eg} = 0.67$.

Appendix G: Diaphragm and Toe-Nail Factors

11.5.3 Diaphragm Factor, C_{di}

Where nails or spikes are used in diaphragm construction, reference lateral design values, Z, are permitted to be multiplied by the diaphragm factor, $C_{di} = 1.1$.

11.5.4 Toe-Nail Factor, C_{tn}

11.5.4.1 Reference withdrawal design values, W, for toe-nailed connections shall be multiplied by the toe-nail factor, $C_{tn} = 0.67$. The wet service factor, C_M, shall not apply.

11.5.4.2 Reference lateral design values, Z, for toe-nailed connections shall be multiplied by the toe-nail factor, $C_{tn} = 0.83$.

Appendix D: End Distance Requirements

Table 11.5.1A End Distance Requirements

Direction of Loading	End Distances: Minimum end distance for $C_\Delta = 0.5$	End Distances: Minimum end distance for $C_\Delta = 1.0$
Perpendicular to Grain	2D	4D
Parallel to Grain, Compression: (fastener bearing away from member end)	2D	4D
Parallel to Grain, Tension: (fastener bearing toward member end)		
for softwoods	3.5D	7D
for hardwoods	2.5D	5D

(b) For loading at an angle to the fastener, where dowel-type fasteners are used, the minimum shear area for $C_\Delta = 1.0$ shall be equivalent to the shear area for a parallel member connection with minimum end distance for $C_\Delta = 1.0$ (see Table 11.5.1A and Figure 11E). The minimum shear area for $C_\Delta = 0.5$ shall be equivalent to ½ the minimum shear area for $C_\Delta = 1.0$. Where the actual shear area is greater than or equal to the minimum shear area for $C_\Delta = 0.5$, but less than the minimum shear area for $C_\Delta = 1.0$, the geometry factor, C_Δ, shall be determined as follows:

$$C_\Delta = \frac{\text{actual shear area}}{\text{minimum shear area for } C_\Delta = 1.0}$$

Appendix E: Edge Distance Requirements

Table 11.5.1C Edge Distance Requirements[1,2]

Direction of Loading	Minimum Edge Distance
Parallel to Grain:	
where $\ell/D \leq 6$	1.5D
where $\ell/D > 6$	1.5D or ½ the spacing between rows, whichever is greater
Perpendicular to Grain:[2]	
loaded edge	4D
unloaded edge	1.5D

1. The ℓ/D ratio used to determine the minimum edge distance shall be the lesser of:
   (a) length of fastener in wood main member/D = ℓ_m/D
   (b) total length of fastener in wood side member(s)/D = ℓ_s/D
2. Heavy or medium concentrated loads shall not be suspended below the neutral axis of a single sawn lumber or structural glued laminated timber beam except where mechanical or equivalent reinforcement is provided to resist tension stresses perpendicular to grain (see 3.8.2 and 10.1.3).

Appendix H: Joist Hanger Ratings

Load Values with Strong-Drive® SD Connector Screws

Allowable Loads for LUS Model Hangers with SD Screws

Model No.	Fasteners		DF/SP Allowable Loads (lbs)				SPF/HF Allowable Loads (lbs)			
	Joist	Face	Uplift (160)	Floor (100)	Snow (115)	Roof (125)	Uplift (160)	Floor (100)	Snow (115)	Roof (125)
LUS24	(2) SD9212	(4) SD9112	495	870	1000	1085	425	605	695	755
LUS26	(4) SD9212	(4) SD9112	1180	1055	1210	1315	1015	760	875	950
LUS28	(4) SD9212	(6) SD9112	1335	1395	1570	1570	1130	985	1135	1230
LUS210	(4) SD9212	(8) SD9112	1240	1735	1995	2170	1065	1210	1390	1510
LUS24-2	(2) SD9212	(4) SD9112	495	870	1000	1085	425	590	680	740
LUS26-2	(4) SD9212	(4) SD9112	1180	1055	1210	1315	1015	735	845	920
LUS28-2	(4) SD9212	(6) SD9112	1335	1395	1570	1570	1100	960	1105	1200
LUS210-2	(6) SD9212	(8) SD9112	1240	1920	2210	2400	1065	1325	1525	1660
LUS214-2	(6) SD9212	(10) SD9112	1995	2265	2605	2830	1645	1550	1785	1940
LUS26-3	(4) SD9212	(4) SD9112	1180	1055	1210	1315	1015	735	845	920
LUS28-3	(4) SD9212	(6) SD9112	1335	1395	1570	1570	1100	960	1105	1200
LUS210-3	(6) SD9212	(8) SD9112	1240	1735	1995	2170	1065	1185	1360	1480
LUS36	(4) SD9212	(4) SD9112	1180	1055	1210	1315	1015	735	845	920
LUS310	(4) SD9212	(6) SD9112	1240	1395	1570	1570	1065	960	1105	1200
LUS44	(2) SD9212	(4) SD9112	495	870	1000	1085	425	590	680	740
LUS46	(4) SD9212	(4) SD9112	1180	1055	1210	1315	1015	735	845	920
LUS48	(4) SD9212	(6) SD9112	1335	1395	1570	1570	1100	960	1105	1200
LUS410	(6) SD9212	(8) SD9112	1240	1920	2210	2400	1065	1325	1525	1660
LUS414	(6) SD9212	(10) SD9112	1995	2265	2605	2830	1645	1550	1785	1940

Appendix D – Concrete and Grout Mix Designs

D1 – CIP Mix Design

POCATELLO HORROCKS AM. FALLS READY MIX

9659 N. Philbin Rd, Pocatello, Idaho 83201 • Phone: (208) 233-4134 • Fax: (208) 233-4135
577 Frontage Rd., Blackfoot, Idaho 83221 • Phone: (208) 785-6426 • Fax: (208) 785-6949
100 Whitman, American Falls, ID 83211 • Phone: (208) 226-2541

Orig.Date: 5-Oct-06
Cement Type: 2

Application: MIX # 07NA
4000 PSI

Bag Mix	6.0	%FA	15	Mix Vol:	27 ft3
Air	2.0	RepRatio	1	W/C:	0.45
S/Agg(%)	45.0				

		SP GR:	ABSORP
Sand Source:	PW 84	2.62	0.00
Agg 1 Source:	PW 84	2.64	0.00
Agg 2 Source:	PW 84	2.62	0.00

	Weight(lbs)		Vol (ft3)
Cement	479		2.44
Fly Ash	85		0.58
Silica F.	0.0		0.00
Water	254	30.5 Gal	4.07
Air	2.0		0.54
Sand	1425		8.72
C.Agg 1	1755		10.65
C.Agg 2	0		0.00
Total Wt	3998.0		27.00 Cubic Feet

Unit Wt 148.1 PCF Total Silica Fume: 0.0 %

Tot.Mortar 60.5 % Tot. Paste: 28.3 %

Admixtures (liquid)

	oz/cwt	oz/Y3
Silica F	0	0.0
WRA	3	16.9
Retard	0	0.0
Accel	0	0.0
Super	0	0.0
Cl2 Inh't	0	Gallons/Y3

Admixtures (solid)

Silica F	0	lbs/Y3
Fibers	0	lbs/Y3
Ice	0	lbs/Y3

Slump:
Super P:

C. Michael Horrocks
Submitted By

8-Feb-19
Date

Pocatello Ready Mix Inc.

Corporate Office

9659 N. Philbin Rd. Pocatello, Idaho 83201

Phone (208) 233-7041 - Fax (208) 233-4135

Phone (208) 785-6428 - Blackfoot

Phone (208) 226-2541 - American Falls

DELIVERY TICKET

CONDITIONS OF SALE:
Concrete is a perishable product and becomes the property of the customer upon batching. We assume no responsibility for damage when required to deliver off of public road. Customers are required to provide suitable road to point of delivery. Towing and standby costs are the responsibility of the customer. All deliveries are considered C.O.D. unless other arrangements are approved prior to delivery. A service [illegible] per month added to any unpaid amount [illegible] on which the same becomes due, the customer agrees to pay all costs including reasonable attorney's fees necessary to collect the same. Pocatello Ready Mix Inc. standards and terms shall apply to all quotations and sales.

TICKET	DATE	TIME
001-171083	07/16/20	08:50 AM

SOLD TO: ISU3500 ENGINEERING & SCIENCE ISU

JOB ID: 000013 1030 S 2ND AVE
POCATELLO

<UNKNOWN>

CARRIER: 70 : H, COLEMAN LOAD NBR. 1 TOTAL YDS. 3.5 SLUMP 5.00

PRODUCT	DESCRIPTION	T	QUANTITY	U/M	PRICE	AMOUNT
40AF1	40 AF-1	01	3.50	CY		
MID RANGE	MID RANGE PLASTICIZER	01	3.50	CY		
DC	DELIVERY - NON TAX	01	3.50	CY		
ML	MIN LOAD DELIVERY CHARGE	01	1.00	EA		

CORNER PUTNAM & S 2ND

LEAVE PLANT	ARRIVE JOB	START DISCHARGE	END DISCHARGE	LEAVE JOB	RETURN PLANT	SLUMP (IN)	% AIR	TEMP(F)	CYL. TAKEN	REV
:	:	:	:	:	:					

WATER ADDED - Seller assumes no responsibility in results to concrete caused by adding water at jobsite. If water is added, amount must be shown and customer's signature at bottom of ticket acknowledges this amount of water added.
WARNING – Ready mixed concrete, freshly mixed, may be harmful to the skin. Avoid direct contact where possible and wash exposed skin areas promptly with water. If any cementitious materials get into eyes or mucous membranes, wash immediately with water and seek prompt medical attention.

RECEIVED BY
(FULL NAMES, NO INITIALS) X ______________________

GAL. WATER ADDED

MISC:

SUB-TOTAL	473.25
TAX	0.00
TICKET TOTAL	473.25
PREV. BAL	
GRAND TOTAL	

Pocatello Ready Mix Inc.

Corporate Office

9659 N. Philbin Rd. Pocatello, Idaho 83201

Phone:(208) 233-7041 - Fax:(208) 233-4136

Phone:(208) 785-6426 - Blackfoot

Phone:(208) 226-2541 - American Falls

DELIVERY TICKET

CONDITIONS OF SALE:
Concrete is a perishable product and becomes the property of the customer upon batching. We assume no responsibility for damage when required to deliver off of public road. Customers are required to provide suitable road to point of delivery. Towing and standby costs are the responsibility of the customer. All deliveries are considered C.O.D. unless other arrangements are approved prior to delivery. A service charge of 1% per month added to any unpaid amount beginning on the date on which the same becomes due, the customer agrees to pay all costs including reasonable attorney's fees necessary to collect the same. Pocatello Ready Mix Inc. standards and terms shall apply to all quotations and sales.

TICKET	DATE	TIME
001-171379	07/24/20	07:46 AM

SOLD TO: ISU3500 ENGINEERING & SCIENCE ISU

JOB ID: 000013 1030 S 2ND AVE
POCATELLO

MISC OUTSIDE FLAT

CARRIER: 100 : D, TONY   LOAD NBR: 1   TOTAL YDS: 1.5   SLUMP: 5.00

PRODUCT	DESCRIPTION	T	QUANTITY	U/M	PRICE	AMOUNT
40AF1	40 AF-1	01	1.50	CY		
MID RANGE	MID RANGE PLASTICIZER	01	1.50	CY		
DC	DELIVERY - NON TAX	01	1.50	CY		
ML	MIN LOAD DELIVERY CHARGE	01	1.00	EA		

CORNER PUTNAM & S 2ND

LEAVE PLANT	ARRIVE JOB	START DISCHARGE	END DISCHARGE	LEAVE JOB	RETURN PLANT	SLUMP (IN)	% AIR	TEMP(F)	CYL. TAKEN	REV.
:	:	:	:	:	:					

WATER ADDED - Seller assumes no responsibility in results to concrete caused by adding water at jobsite. If water is added, amount must be shown and customer's signature at bottom of ticket acknowledges this amount of water added.
WARNING – Ready mixed concrete, freshly mixed, may be harmful to the skin. Avoid direct contact where possible and wash exposed skin areas promptly with water. If any cementitious materials get into eyes or mucous membranes, wash immediately with water and seek prompt medical attention.

RECEIVED BY
(FULL NAMES, NO INITIALS) X ____________________

_____ GAL. WATER ADDED

MISC:

SUB-TOTAL	244.25
TAX	00.00
TICKET TOTAL	244.25
PREV. BAL	
GRAND TOTAL	

D2 – Self-Consolidating Concrete Mix Design

Self-Consolidating Mix Design

Mix Quantities by Unit Volume		
Volume	1.00	yd^3
Cement	729	lb
Fly Ash	183.2	lb
Coarse Sand	1701	lb
Fine Pea Gravel	810	lb
Water	364.5	lb
Master Glenimum 1466	10.4	fl.oz/cwt

Mix Quantities by Unit Volume		
Volume	1.00	ft^3
Cement	27	lb
Fly Ash	6.785185185	lb
Coarse Sand	63	lb
Fine Pea Gravel	30	lb
Water	13.5	lb
Master Glenimum 1466	10.4	fl.oz/cwt

Mix Quantities for Total Precast Volume		
Volume	20.00	ft^3
Cement	540	lb
Fly Ash	135.7037037	lb
Coarse Sand	1260	lb
Fine Pea Gravel	600	lb
Water	270	lb
Master Glenimum 1466	28.08	fl.oz

Mix Quantities for Single Batch		
Volume	6.67	ft^3
Cement	180.09	lb
Fly Ash	45.25718519	lb
Coarse Sand	420.21	lb
Fine Pea Gravel	200.1	lb
Water	90.045	lb
Master Glenimum 1466	9.36468	fl.oz

D3 – Sika Grout 328

BUILDING TRUST

PRODUCT DATA SHEET

SikaGrout®-328

HIGH PERFORMANCE, PRECISION, GROUT WITH EXTENDED WORKING TIME

PRODUCT DESCRIPTION

SikaGrout®-328 is a non-shrink, non-metallic, cementitious precision grout powered by ViscoCrete technology. This grout provides extended working time and exceptional physical performance at fluid consistency. A structural, precision grout, SikaGrout®-328 can be placed from fluid to dry pack.

USES

- Where exceptional one day and ultimate compressive strengths are required.
- Applications requiring a pumpable grout.
- Non-shrink grouting of machinery and equipment, base plates sole plates, precast panels, beams, columns and curtain walls.
- Applications where a non-shrink grout is needed for maximum effective bearing area to transfer optimum load.
- For underwater application in conjunction with Sikament® 100 SC. Consult Technical Service for dosage information. Independent test data is available however on site testing is recommended to confirm performance under actual field conditions.
- For grouting rebar, bolts, dowels and pins, etc.

CHARACTERISTICS / ADVANTAGES

- Multiple fluidity with one material
- Reaches 10,000 psi in dry pack consistency
- Outstanding performance in fluid state
- Extended working time
- Excellent fluidity - sufficient time for placement
- Contains premium quality quartz aggregate
- Hardens free of segregation
- Non-metallic, will not stain or rust
- Shows positive expansion

APPROVALS / STANDARDS

- Meets ASTM-C 1107 (Grade B & C)
- SikaGrout®-328 is USDA certifiable

PRODUCT INFORMATION

Packaging	50 lb (22.7 kg) bag
Appearance / Color	Gray powder
Shelf Life	9 months from date of production if stored properly in original, unopened and undamaged sealed packaging
Storage Conditions	Store dry at 40–95 °F (4–35 °C) Protect from moisture. If damp, discard material

TECHNICAL INFORMATION

Compressive Strength

(ASTM C-109) 73 °F (23 °C) 50 % R.H.	Dry Pack	Plastic	Flowable	Fluid
1 day	5,000 psi (34.4 MPa)	4,500 psi (31 MPa)	4,000 psi (27.6 MPa)	3,500 psi (24.1 MPa)
3 day	8,000 psi (55.2 MPa)	6,500 psi (44.8 MPa)	6,000 psi (41.4 MPa)	5,500 psi (37.9 MPa)
14 day	9,200 psi (63.4 MPa)	7,000 psi (48.3 MPa)	6,700 psi (46.2 MPa)	6,500 psi (44.8 MPa)
28 day	10,000 psi (69 MPa)	8,200 psi (56.5 MPa)	8,000 psi (55.2 MPa)	7,500 psi (51.7 MPa)

Flexural Strength

	Fluid
3 day	1,100 psi (7.6 MPa)
7 day	1,200 psi (8.6 MPa)
28 day	1,300 psi (9 MPa)

(ASTM C-293) 73 °F (23 °C) 50 % R.H.

Splitting Tensile Strength

	Fluid
3 day	350 psi (2.4 MPa)
7 day	400 psi (2.8 MPa)
28 day	650 psi (4.5 MPa)

(ASTM C-496) 73 °F (23 °C) 50 % R.H.

Shear Strength

	Fluid
3 day	950 psi (6.6 MPa)
7 day	1,750 psi (12.1 MPa)
28 day	2,000 psi (13.8 MPa)

*Mortar scrubbed into substrate at 73 °F (23 °C) and 50 % R.H.

(ASTM C-882 modified*)

Freeze-Thaw Stability 300 Cycles 99 % (ASTM C-666)

APPLICATION INFORMATION

Mixing Ratio

Dry Pack	Plastic	Flowable	Fluid
5.5–6.0 pts (2.6–2.8 L)	6.5–7.0 pts (3.1–3.3 L)	7.0–7.5 pts (3.3–3.5 L)	8.0–8.5 pts (3.8–4 L)

Coverage 0.44 ft^3 (0.01 m^3) per bag at hfluid consistency
(Coverage figures do not include allowance for surface profile and porosity or material waste)

Layer Thickness

Min.	Max.
1/2" (12.7 mm)	6" (152.4 mm)

For application thicknesses of 6" or greater, consult Sika®'s Technical Service Department.

Flowability

Dry Pack	Plastic[1]	Flowable[1]	Fluid[2]
10–25 %	100–125 %	124–145 %	20–60 sec

[1]ASTM C-1437
[2]ASTM C-939

Product Temperature 65–75 °F (18–24 °C)

Ambient Air Temperature > 45 °F (7 °C)

Substrate Temperature > 45 °F (7 °C)

Set Time

	Dry Pack	Plastic	Flowable	Fluid
Initial	<15 min	>2 hr	>3 hr	>4 hr
Final	<2 hr	<6 hr	<7 hr	<8 hr

SURFACE PREPARATION

- Surface must be clean and sound. Remove all deteriorated concrete, dirt, oil, grease, and other bond-inhibiting materials from the area to be repaired.
- Anchor bolts to be grouted must be de-greased with suitable solvent.
- Concrete must be sound and roughened to promote mechanical adhesion.
- To ensure optimum repair results, the effectiveness of decontamination and preparation should be assessed by a pull-off test.
- Substrate should be Saturated Surface Dry (SSD) with clean water prior to application. No standing water should remain during application.

FORMING

- For pourable grout, construct forms to retain grout without leakage.
- Forms should be lined or coated with bond-breaker for easy removal.
- Forms should be sufficiently high to accommodate head of grout.
- Where grout-tight form is difficult to achieve, use SikaGrout®-328 in dry pack consistency.

MIXING

- Pour the water in the recommended proportion into a suitable mixing container.
- DO NOT OVER WATER!
- Ambient and material temperature should be as close as possible to 70 °F. If higher, use cold water; if colder, use warm water.
- While mixing slowly, add the powder to the water.
- Mix thoroughly for at least 5 minutes with low speed (400-600 rpm) using a Sika mixing paddle or a jiffy paddle to avoid entraining too much air and until homogenous with no lumps.

EXTENSION WITH AGGREGATES

- For deeper applications (plastic and flowable consistancy only), 25 lbs. of 3/8" (9.5 mm) coarse aggregate can be added.
- The aggregate must be non-reactive (reference ASTM C-1260, C-227 and C-289), clean, well graded, saturated surface dry, have low absorption and high density, and comply with ASTM C-33 size number 8 per Table 2.
- Variances in aggregate may result in different strengths.
- Add pea gravel after the water and SikaGrout®-328.

APPLICATION

- Within 60 minutes after mixing, place grout into forms in normal manner to avoid air entrapment.
- Vibrate, pump, or ram grout as necessary to achieve flow or compaction.
- SikaGrout®-328 must be confined leaving minimum exposed surface.
- After grout has achieved final set, remove forms, trim or shape exposed grout shoulders to designed profile.
- SikaGrout®-328 is an excellent grout for pumping, even at high flow. For pump recommendations, contact Technical Service.

CURING TREATMENT

- Wet cure for a minimum of 3 days or apply a curing compound which complies with ASTM C-309 on exposed surfaces.

LIMITATIONS

- Do not use as a patching or overlay mortar or in unconfined areas.
- As with all cement based materials, avoid contact with aluminum to prevent adverse chemical reaction and possible product failure. Insulate potential areas of contact by coating aluminum bars, rails, posts etc.with an appropriate epoxy such as Sikadur 32 Hi-Mod.

BASIS OF PRODUCT DATA

Results may differ based upon statistical variations depending upon mixing methods and equipment, temperature, application methods, test methods, actual site conditions and curing conditions.

OTHER RESTRICTIONS

See Legal Disclaimer.

ENVIRONMENTAL, HEALTH AND SAFETY

For further information and advice regarding transportation, handling, storage and disposal of chemical products, user should refer to the actual Safety Data Sheets containing physical, environmental, toxicological and other safety related data. User must read the current actual Safety Data Sheets before using any products. In case of an emergency, call CHEMTREC at 1-800-424-9300, International 703-527-3887.

DIRECTIVE 2004/42/CE - LIMITATION OF EMISSIONS OF VOC

0 g/l (EPA method 24)

LEGAL DISCLAIMER

- **KEEP CONTAINER TIGHTLY CLOSED**
- **KEEP OUT OF REACH OF CHILDREN**
- **NOT FOR INTERNAL CONSUMPTION**
- **FOR INDUSTRIAL USE ONLY**
- **FOR PROFESSIONAL USE ONLY**

Prior to each use of any product of Sika Corporation, its subsidiaries or affiliates ("SIKA"), the user must always read and follow the warnings and instructions on the product's most current product label, Product Data Sheet and Safety Data Sheet which are available at usa.sika.com or by calling SIKA's Technical Service Department at 1-800-933-7452. Nothing contained in any SIKA literature or materials relieves the user of the obligation to read and follow the warnings and instructions for each SIKA product as set forth in the current product label, Product Data Sheet and Safety Data Sheet prior to use of the SIKA product.

SIKA warrants this product for one year from date of installation to be free from manufacturing defects and to meet the technical properties on the current Product Data Sheet if used as directed within the product's shelf life. User determines suitability of product for intended use and assumes all risks. User's and/or buyer's sole remedy shall be limited to the purchase price or replacement of this product exclusive of any labor costs. **NO OTHER WARRANTIES EXPRESS OR IMPLIED SHALL APPLY INCLUDING ANY WARRANTY OF MERCHANTABILITY OR FITNESS FOR A PARTICULAR PURPOSE. SIKA SHALL NOT BE LIABLE UNDER ANY LEGAL THEORY FOR SPECIAL OR CONSEQUENTIAL DAMAGES. SIKA SHALL NOT BE RESPONSIBLE FOR THE USE OF THIS PRODUCT IN A MANNER TO INFRINGE ON ANY PATENT OR ANY OTHER INTELLECTUAL PROPERTY RIGHTS HELD BY OTHERS.**

Sale of SIKA products are subject to the Terms and Conditions of Sale which are available at https://usa.sika.com/en/group/SikaCorp/termsandconditions.html or by calling 1-800-933-7452.

Sika Corporation
201 Polito Avenue
Lyndhurst, NJ 07071
Phone: +1-800-933-7452
Fax: +1-201-933-6225
usa.sika.com

Sika Mexicana S.A. de C.V.
Carretera Libre Celaya Km. 8.5
Fracc. Industrial Balvanera
Corregidora, Queretaro
C.P. 76920
Phone: 52 442 2385800
Fax: 52 442 2250537

D4 – Rapid Set Concrete Mix

CTS CEMENT | Rapid Set Construction Cement

CTS Cement Cement Manufacturing Corporation
11065 Knott Avenue, Suite A
Cypress, CA 90630
Phone: (800) 929-3030 • Fax: (714) 379-8270
info@ctscement.com
www.ctscement.com

Rapid Set® Concrete Mix — DATASHEET
Very Fast-Setting Concrete

PRODUCT DESCRIPTION:
When mixed with water CONCRETE MIX produces a workable, high quality concrete material that is ideal where fast strength gain, high durability and low shrinkage are desired. Apply CONCRETE MIX in thicknesses from 2-in to 24-in. Durable in wet environments. *SETS IN 15 MINUTES & IS READY FOR TRAFFIC IN 1-HOUR.* One 60-lb. bag of Rapid Set® CONCRETE MIX will yield approximately 0.5 cubic feet.

USES:
CONCRETE MIX is a multipurpose, Fast-Setting product that can be used for repair and construction of pavements, formed work, footings, setting posts, industrial floors, machine bases, and concrete repair.

COMPOSITION:
Rapid Set® CONCRETE MIX is a high performance blend of Rapid Set® hydraulic cement and quality aggregates. CONCRETE MIX is non-metallic and no chlorides are added. Rapid Set® CONCRETE MIX is similar in appearance to portland cement concrete and may be applied using similar methods.

COLOR: [Light Grey]
The final color of CONCRETE MIX may vary due to application techniques and environmental conditions.

LIMITATIONS:
Not intended for applications thinner than 2-in, for thin sections use Rapid Set® Cement ALL or Rapid Set® Mortar Mix. For applications where bonding is important, at least one test section should be prepared to evaluate the suitability of the materials and procedures.

TECHNICAL DATA:

- **Set Time**
  ASTM C-191(Mod.) at 70ºF
  Initial Set 15-minutes
  Final Set 35-minutes

- **Compressive Strength**
  ASTM C-109 Mod.
  Age: Compressive Strength:
  1-hour* 2800-psi
  3-hour 3600 -psi
  7-day 5000 -psi
  28-day 6000-psi

- **Flexural Strength**
  ASTM C-78 Mod.

2-hour* 420-psi
1-day 650-psi
28-day 750-psi

* After Final Set.

Using CONCRETE MIX

SURFACE PREPARATION:
Where bonding is important, the adjacent surfaces shall be clean, sound and free from any materials that may inhibit bond such as oil, asphalt, curing compounds, acids, dirt and loose debris. Roughen surfaces and remove all unsound concrete. Immediately prior to placement the repair surface shall be thoroughly saturated with no standing water.

MIXING:
The use of a power driven mechanical mixer, such as a mortar mixer or a drill mounted mixer, is recommended. Organize work so that all personnel and equipment are in place before mixing. Use clean Potable water. Rapid Set® CONCRETE MIX may be mixed using 3 to 5 quarts of water per 60 lb. bag. Use less water to achieve higher strengths. Do NOT exceed 5 quarts of water per bag. For increased fluidity and workability use Rapid Set® FLOW CONTROL® plasticizing admixture from the Concrete Pharmacy®. Place the desired quantity of mix water into the mixing container. While the mixer is running add Rapid Set® CONCRETE MIX. Mix for the minimum amount of time required to achieve a lump-free, uniform consistency (usually 1 to 3 minutes). Do NOT re-temper.

PLACEMENT:
Rapid Set® CONCRETE MIX may be placed using traditional methods. Organize work so that all personnel and equipment are ready before placement. Place, consolidate and screed quickly to allow for maximum finishing time. Do NOT wait for bleed water, apply final finish as soon as possible. Rapid Set® CONCRETE MIX may be troweled, floated or broom finished. On flat work Do NOT install in layers, install full depth sections and progress horizontally. Do NOT install on frozen surfaces. Use a method of consolidation that eliminates air voids. To extend working time use Rapid Set® SET CONTROL® set retarding admixture.

CURING:
Water cure all Rapid Set® CONCRETE MIX installations. Begin curing as soon as the surface has lost its moist sheen. Keep exposed surfaces wet for a minimum of 1 hour. When experiencing extended setting times, due to cold temperature or the use of retarder, longer cure times may be required. The objective of water curing shall be to maintain a continuously wet surface until the product has achieved sufficient strength.

TEMPERATURE:
Warm environmental and materials temperatures will reduce the working time of CONCRETE MIX. To compensate for warm temperatures, keep material cool and use chilled mix water. Temperatures below 70ºF (21ºC) will decrease the rate of strength gain and CONCRETE MIX should not be applied if surface or ambient temperature is below 45ºF (7.2ºC).

LIMITED WARRANTY:
CTS Cement Manufacturing Corporation warrants its material to be of good quality, and, at its sole option, within one year from date of sale, will replace defective materials or refund the purchase price thereof and such replacement or refund shall be the limit of CTS's responsibility. Except for the foregoing, all warranties, express or implied including merchantability and fitness for a particular purpose are excluded. CTS shall not be liable for any consequential, incidental, or special damages arising directly or indirectly from the use of the material.

CAUTION:
CONCRETE MIX contains cement-itious materials and may cause irritation to lungs, eyes and skin. Avoid contact. Use only in adequate ventilation. Do NOT breath dust. Wet mixture may cause burns. Wear suitable gloves, eye protection and protective clothing. In case of skin contact, wash thoroughly with soap and water. In case of eye contact, flush immediately and repeatedly with large quantities of water and get prompt medical attention. In case of difficulty breathing, remove person to fresh air. If difficulty breathing persists, seek medical attention.

Appendix E – Laboratory Test Results

E1 – Unconfined Compressive Strength

Compressive Strength of CIP Concrete Report

Sample Description:	CIP Concrete
Sampled By:	M. Mahat
Date Sampled:	7/24/2020
Date Received:	8/25/2020, 10/05/2020, 10/06/2020 and 10/09/2020

Specimen No.	Diameter (in)		Height (in)		Cross-Sectional	Volume	Weight	Unit Weight	Max. Load	Compressive	Age	Fracture
	Reading	Average	Reading	Average	Area (in^2)	(in^3)	(lbs)	(pcf)	(lbs)	Strength (psi)		Type
HC 5 (07/24/20)	3.980 3.975 -	3.978	8.100 8.075 8.085	8.087	12.425	100.480	8.424	144.87	76,730	6,175	32-day	Type 4
HC 7 (07/24/20)	3.983 3.985 -	3.984	8.1 8.05 8.06	8.07	12.466	100.601	8.456	145.25	83,305	6,683	73-day	Type 2
HC 9 (07/24/20)	3.976 3.992 -	3.984	8 8.003 8.004	8.002	12.466	99.757	8.448	146.34	86,230	6,917	74-day	Type 4
HC 1 (07/24/20)	3.983 3.978 -	3.981	8.009 8.004 8.000	8.004	12.444	99.607	8.391	145.56	86,735	6,970	77-day	Type 4

Compressive Strength of SCC Concrete Report

Sample Description:	Self-Consolidating Concrete
Sampled By:	M. Mahat
Date Sampled:	8/7/2020
Date Received:	09/08/2020, 11/04/2020, 11/05/2020, 11/09/2020

Specimen No.	Diameter (in)		Height (in)		Cross-Sectional Area (in^2)	Volume (in^3)	Weight (lbs)	Unit Weight (pcf)	Max. Load (lbs)	Compressive Strength (psi)	Age	Fracture Type
	Reading	Average	Reading	Average								
HCPC-4A	4.003 4.014 4.002	4.006	7.975 7.978 7.980	7.978	12.606	100.568	8.0695	138.65	87,855	6,969	32-day	3
HCPC-3A	4.000 3.938 -	3.969	8.000 7.938 7.938	7.959	12.372	98.467	8.3110	145.85	100,390	8,114	89-day	None
HCPC-1A	3.951 3.951 -	3.951	8.063 8.063 8.031	8.052	12.260	98.725	8.3525	146.20	100,290	8,180	90-day	None
HCPC-3B	4.000 3.985 -	3.993	8.000 7.938 8.063	8.000	12.519	100.154	8.2305	142.00	105,840	8,454	94-day	5

Compressive Strength of Sika 328 Grout Report

Sample Description:	Sika 328 Grout
Sampled By:	M. Tangarife
Date Sampled:	10/26/2020
Date Received:	11/04/2020, 11/05/2020, 11/09/2020

Specimen No.	Width (in)	Length (in)	Height (in)	Cross-Sectional Area (in^2)	Volume (in^3)	Weight (lbs)	Unit Weight (pcf)	Max. Load (lbs)	Compressive Strength (psi)	Age
GRT-1	2.125	2.000	2.000	4.250	8.500	0.680	138.24	26,560	6,249	9-day
GRT-4	2.063	2.063	1.938	4.256	8.248	0.668	139.95	32,725	7,689	9-day
GRT-2	2.125	1.938	2.063	4.118	8.496	0.682	138.71	29,765	7,228	10-day
GRT-5	2.125	2.000	1.938	4.250	8.237	0.664	139.20	29,560	6,955	10-day
GRT-3	2.011	2.031	1.991	4.084	8.132	0.666	141.52	38,850	9,512	14-day
GRT-6	2.030	1.999	1.994	4.058	8.092	0.656	139.99	38,645	9,523	14-day

Compressive Strength of Rapid Set Concrete Report

Sample Description:	Rapid Set Concrete Mix
Sampled By:	M. Tangarife
Date Sampled:	10/7/2020
Date Received:	10/9/2020

Specimen No.	Diameter (in)		Height (in)		Cross-Sectional Area (in^2)	Volume (in^3)	Weight (lbs)	Unit Weight (pcf)	Max. Load (lbs)	Compressive Strength (psi)	Age	Fracture Type
	Reading	Average	Reading	Average								
	3.984		8.003									
TPZ 1 (10/07/20)	3.979	3.982	8.100	8.035	12.450	100.035	7.920	136.81	53,025	4,259	2-day	Type 4
	-		8.001									
	4.000		8.000									
TPZ 2 (10/07/20)	3.938	3.969	8.000	8.021	12.371	99.224	7.960	138.62	48,030	3,883	2-day	Type 4
	-		8.063									

E2 – Modulus of Elasticity and Poisson's Ratio

Modulus of Elasticity and Poisson's Ratio of CIP Concrete Report

Sample Description:	CIP Concrete
Sampled By:	M. Mahat
Date Sampled:	7/24/2020
Date Received:	8/25/2020

Specimen No.	Diameter (in)		Height (in)		Cross-Sectional Area (in^2)	Volume (in^3)	Weight (lbs)	40% of Max Load (lbs)	40% of 32 day Compressive Strength (psi)	Gauge Length (in)	Distance from vertical gauge to center of cylinder (in)	Distance from vertical pivot to center of cylinder (in)	Distance from horz. gauge to center of cylinder (in)	Distance from horz. pivot to center of cylinder (in)
	Reading	Average	Reading	Average										
HC 2 (07/24/20)	3.980 3.990 -	3.985	8.035 8.065 8.040	8.047	12.472	100.360	8.418	30,692	2,461	5.25	4.1875	4.0625	3.9375	3.0000

Test No.	Load (lb)	Vertical Deflection (in)	Horizontal Deflection (in)	Long. Specimen Deformation (in)	Transv. Specimen Deformation (in)	Stress (psi)	Long. Strain (in/in)	Trans. Strain (in/in)	Modulus of Elasticity, E (psi)	Poisson's Ratio, μ
1	1,350	0.00026	0.00000	0.000129	0.000000	$S_1 =$ 108	$\varepsilon_1 =$ 1.6064E-05	$\varepsilon_{t1} =$ 0.0000E+00	5.35E+06	0.14
	10,000	0.00260	0.00000	0.001280	0.000000	$S_3 =$ 802	$\varepsilon_3 =$ 1.5911E-04	$\varepsilon_{t3} =$ 0.0000E+00		
	20,000	0.00500	0.00015	0.002462	0.000065	$S_4 =$ 1,604	$\varepsilon_4 =$ 3.0598E-04	$\varepsilon_{t4} =$ 1.6277E-05		
	30,700	0.00745	0.00055	0.003669	0.000238	$S_2 =$ 2,461	$\varepsilon_2 =$ 4.5591E-04	$\varepsilon_{t2} =$ 5.9683E-05		
2	1580	0.00026	0.00000	0.000129	0.000000	$S_1 =$ 127	$\varepsilon_1 =$ 1.6064E-05	$\varepsilon_{t1} =$ 0.0000E+00	5.38E+06	0.13
	10,000	0.00255	0.00000	0.001256	0.000000	$S_3 =$ 802	$\varepsilon_3 =$ 1.5605E-04	$\varepsilon_{t3} =$ 0.0000E+00		
	20,000	0.00470	0.00015	0.002314	0.000065	$S_4 =$ 1,604	$\varepsilon_4 =$ 2.8762E-04	$\varepsilon_{t4} =$ 1.6277E-05		
	30,600	0.00733	0.00050	0.003609	0.000216	$S_2 =$ 2,453	$\varepsilon_2 =$ 4.4857E-04	$\varepsilon_{t2} =$ 5.4258E-05		
3	1440	0.00026	0.00000	0.000129	0.000000	$S_1 =$ 115	$\varepsilon_1 =$ 1.6064E-05	$\varepsilon_{t1} =$ 0.0000E+00	5.32E+06	0.12
	10,000	0.00260	0.00000	0.001280	0.000000	$S_3 =$ 802	$\varepsilon_3 =$ 1.5911E-04	$\varepsilon_{t3} =$ 0.0000E+00		
	20,000	0.00490	0.00010	0.002413	0.000043	$S_4 =$ 1,604	$\varepsilon_4 =$ 2.9986E-04	$\varepsilon_{t4} =$ 1.0852E-05		
	30,700	0.00747	0.00048	0.003678	0.000208	$S_2 =$ 2,461	$\varepsilon_2 =$ 4.5713E-04	$\varepsilon_{t2} =$ 5.2087E-05		
4	1360	0.00026	0.00000	0.000129	0.000000	$S_1 =$ 109	$\varepsilon_1 =$ 1.6064E-05	$\varepsilon_{t1} =$ 0.0000E+00	5.37E+06	0.12
	10,000	0.00255	0.00000	0.001256	0.000000	$S_3 =$ 802	$\varepsilon_3 =$ 1.5605E-04	$\varepsilon_{t3} =$ 0.0000E+00		
	20,000	0.00490	0.00012	0.002413	0.000052	$S_4 =$ 1,604	$\varepsilon_4 =$ 2.9986E-04	$\varepsilon_{t4} =$ 1.3022E-05		
	31,000	0.00750	0.00050	0.003693	0.000216	$S_2 =$ 2,486	$\varepsilon_2 =$ 4.5897E-04	$\varepsilon_{t2} =$ 5.4258E-05		
								Average	**5.35E+06**	**0.13**

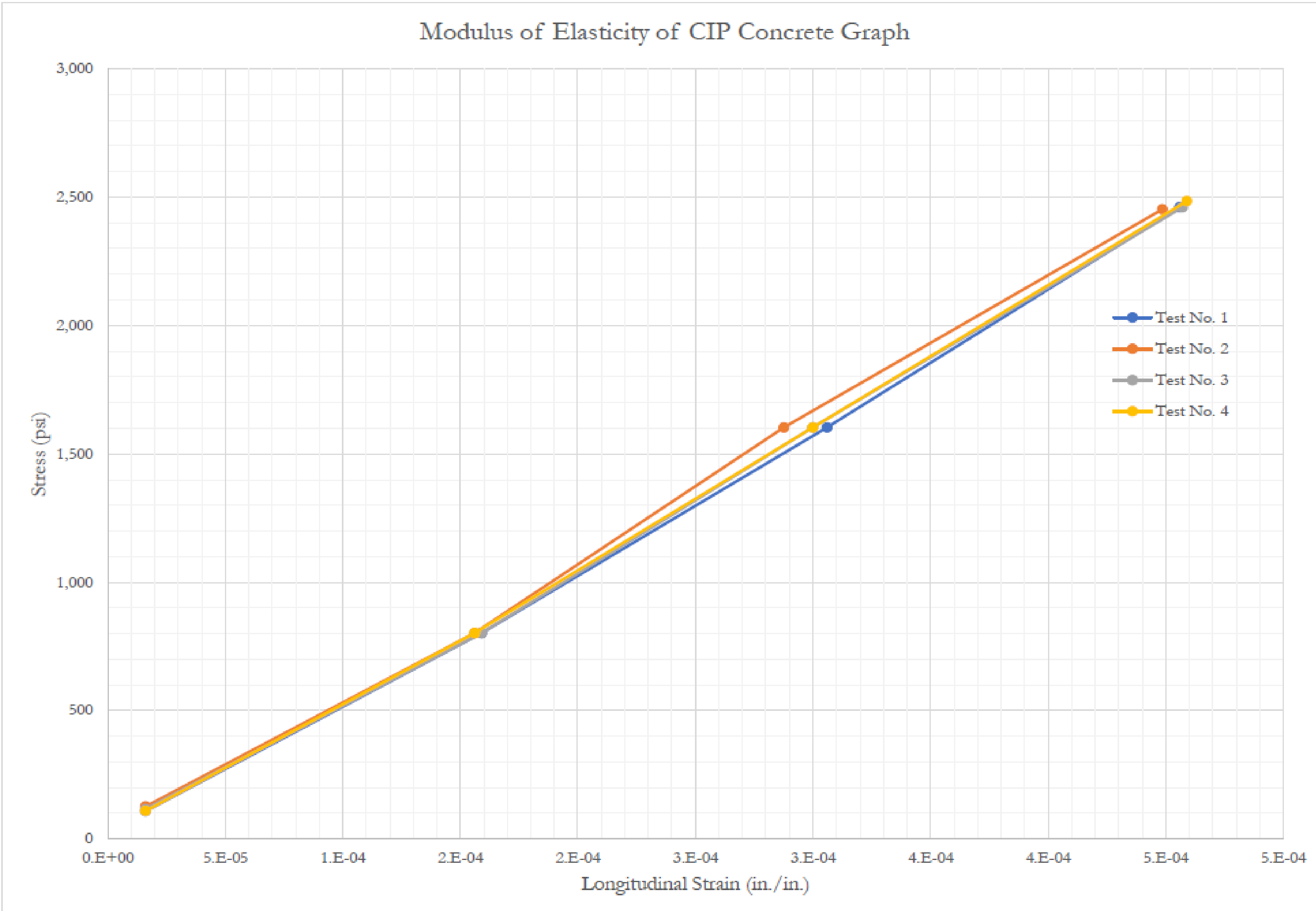
Modulus of Elasticity of CIP Concrete Graph
3,000
2,500
2,000
1,500
1,000
500
0
Stress (psi)
0.E+00
5.E-05
1.E-04
2.E-04
2.E-04
3.E-04
3.E-04
4.E-04
4.E-04
5.E-04
5.E-04
Longitudinal Strain (in./in.)
Test No. 1
Test No. 2
Test No. 3
Test No. 4

Modulus of Elasticity and Poisson's Ratio of SCC Report

Sample Description:	Self-Consolidating Concrete
Sampled By:	M. Mahat
Date Sampled:	8/7/2020
Date Received:	9/8/2020

Specimen No.	Diameter (in) Reading	Diameter (in) Average	Height (in) Reading	Height (in) Average	Cross-Sectional Area (in^2)	Volume (in^3)	Weight (lbs)	40% of Max Load (lbs)	40% of 90 day Compressive Strength (psi)	Gauge Length (in)	Distance from vertical gauge to center of cylinder (in)	Distance from vertical pivot to center of cylinder (in)	Distance from horz. gauge to center of cylinder (in)	Distance from horz. pivot to center of cylinder (in)
HCPC-4B	3.976 4.008 -	3.992	7.985 7.985 7.980	7.983	12.516	99.921	8.109	35,142	2,808	5.25	4.1875	4.0625	3.9375	3.0000

Test No.	Load (lb)	Vertical Deflection (in)	Horizontal Deflection (in)	Long. Specimen Deformation (in)	Transv. Specimen Deformation (in)	Stress (psi)	Long. Strain (in/in)	Trans. Strain (in/in)	Modulus of Elasticity, E (psi)	Poisson's Ratio, μ
1	2,700	0.00026	0.00000	0.000129	0.000000	S_1 = 216	ε_1 = 1.6191E-05	ε_{t1} = 0.0000E+00	5.41E+06	0.31
	10,000	0.00170	0.00035	0.000837	0.000151	S_3 = 799	ε_3 = 1.0486E-04	ε_{t3} = 3.7914E-05		
	20,000	0.00415	0.00075	0.002044	0.000324	S_4 = 1,598	ε_4 = 2.5598E-04	ε_{t4} = 8.1244E-05		
	30,000	0.00690	0.00110	0.003398	0.000476	S_5 = 2,397	ε_5 = 4.2560E-04	ε_{t5} = 1.1916E-04		
	35,000	0.00800	0.00135	0.003939	0.000584	S_2 = 2,796	ε_2 = 4.9345E-04	ε_{t2} = 1.4624E-04		
2	2,300	0.00026	0.00000	0.000129	0.000000	S_1 = 184	ε_1 = 1.6191E-05	ε_{t1} = 0.0000E+00	5.66E+06	0.26
	10,000	0.00210	0.00020	0.001034	0.000086	S_3 = 799	ε_3 = 1.2953E-04	ε_{t3} = 2.1665E-05		
	20,000	0.00450	0.00045	0.002216	0.000195	S_4 = 1,598	ε_4 = 2.7757E-04	ε_{t4} = 4.8746E-05		
	30,000	0.00670	0.00080	0.003299	0.000346	S_5 = 2,397	ε_5 = 4.1327E-04	ε_{t5} = 8.6660E-05		
	35,000	0.00775	0.00110	0.003816	0.000476	S_2 = 2,796	ε_2 = 4.7803E-04	ε_{t2} = 1.1916E-04		
3	2,300	0.00026	0.00000	0.000129	0.000000	S_1 = 184	ε_1 = 1.6191E-05	ε_{t1} = 0.0000E+00	5.40E+06	0.31
	10,000	0.00210	0.00015	0.001034	0.000065	S_3 = 799	ε_3 = 1.2953E-04	ε_{t3} = 1.6249E-05		
	20,000	0.00440	0.00060	0.002167	0.000259	S_4 = 1,598	ε_4 = 2.7140E-04	ε_{t4} = 6.4995E-05		
	30,000	0.00690	0.00110	0.003398	0.000476	S_5 = 2,397	ε_5 = 4.2560E-04	ε_{t5} = 1.1916E-04		
	35,000	0.00810	0.00140	0.003989	0.000605	S_2 = 2,796	ε_2 = 4.9962E-04	ε_{t2} = 1.5165E-04		
								Average	**5.49E+06**	**0.29**

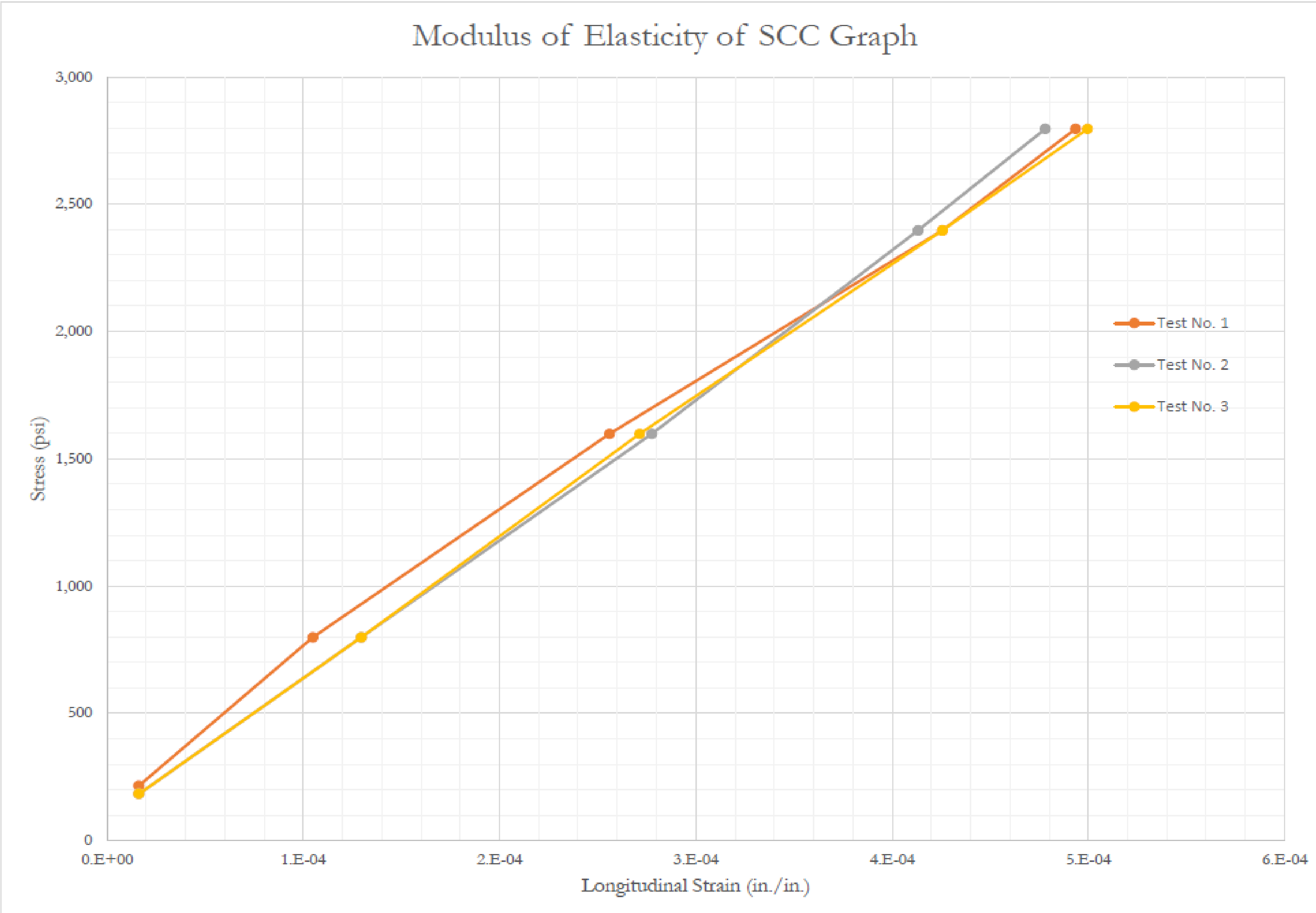
Modulus of Elasticity of SCC Graph
Stress (psi)
3,000
2,500
2,000
1,500
1,000
500
0
0.E+00
1.E-04
2.E-04
3.E-04
4.E-04
5.E-04
6.E-04
Longitudinal Strain (in./in.)
Test No. 1
Test No. 2
Test No. 3

Modulus of Elasticity Report

Sample Description:	Rapid Set Concrete Mix
Sampled By:	M. Tangarife
Date Sampled:	10/7/2020
Date Received:	10/9/2020

Specimen No.	Diameter (in)		Height (in)		Cross-Sectional Area (in^2)	Volume (in^3)	Weight (lbs)	40% of Max Load (lbs)	40% of 2 day Compressive Strength (psi)
	Reading	Average	Reading	Average					
TPZ 2 (07/24/20)	4.000 3.938 -	3.969	8.000 8.000 8.063	8.021	12.372	99.239	7.96	21,210	1,714

Time	Load (lb)	Long. Displ. (in)	Stress (psi)	Long. Strain (in/in)
36:21.4	4,910	0.005932961	397	7.3968E-04
36:21.6	5,195	0.006526761	420	8.1371E-04
36:21.8	5,478	0.007147261	443	8.9107E-04
10/9/2020 14:36	5,724	0.007804761	463	9.7304E-04
36:22.2	6,016	0.008419161	486	1.0496E-03
36:22.4	6,265	0.008950361	506	1.1159E-03
36:22.6	6,500	0.009485161	525	1.1825E-03
36:22.8	6,794	0.010141561	549	1.2644E-03
10/9/2020 14:36	7,060	0.010735361	571	1.3384E-03
36:23.2	7,359	0.011333361	595	1.4130E-03
36:23.4	7,649	0.011939061	618	1.4885E-03
36:23.6	7,894	0.012442061	638	1.5512E-03
36:23.8	8,202	0.012995661	663	1.6202E-03
10/9/2020 14:36	8,456	0.013443361	683	1.6760E-03
36:24.2	8,690	0.013914561	702	1.7348E-03
36:24.4	8,950	0.014368861	723	1.7914E-03

Time	Load (lb)	Long. Displ. (in)	Stress (psi)	Long. Strain (in/in)
36:24.6	9,105	0.014785561	736	1.8434E-03
36:24.8	9,318	0.015134361	753	1.8868E-03
10/9/2020 14:36	9,594	0.015499661	775	1.9324E-03
36:25.2	9,717	0.015927561	785	1.9857E-03
36:25.4	9,985	0.016332761	807	2.0362E-03
36:25.6	10,160	0.016750861	821	2.0884E-03
36:25.8	10,378	0.017110661	839	2.1332E-03
10/9/2020 14:36	10,571	0.017552061	854	2.1883E-03
36:26.2	10,828	0.017937561	875	2.2363E-03
36:26.4	11,049	0.018298161	893	2.2813E-03
36:26.6	11,300	0.018650861	913	2.3253E-03
36:26.8	11,530	0.019071061	932	2.3776E-03
10/9/2020 14:36	11,771	0.019436061	951	2.4231E-03
36:27.2	12,011	0.019813961	971	2.4703E-03
36:27.4	12,258	0.020294361	991	2.5302E-03
36:27.6	12,523	0.020668961	1,012	2.5769E-03
36:27.8	12,776	0.021040761	1,033	2.6232E-03
10/9/2020 14:36	13,016	0.021421461	1,052	2.6707E-03
36:28.2	13,304	0.021796561	1,075	2.7174E-03
36:28.4	13,576	0.022166861	1,097	2.7636E-03
36:28.6	13,837	0.022651961	1,118	2.8241E-03
36:28.8	14,153	0.023004061	1,144	2.8680E-03
10/9/2020 14:36	14,363	0.023400961	1,161	2.9175E-03
36:29.2	14,677	0.023858761	1,186	2.9745E-03
36:29.4	14,956	0.024251661	1,209	3.0235E-03
36:29.6	15,236	0.024711061	1,231	3.0808E-03
36:29.8	15,560	0.025062661	1,258	3.1246E-03
10/9/2020 14:36	15,804	0.025545561	1,277	3.1848E-03
36:30.2	16,146	0.025916461	1,305	3.2311E-03
36:30.4	16,407	0.026360461	1,326	3.2864E-03
36:30.6	16,749	0.026796761	1,354	3.3408E-03
36:30.8	17,030	0.027315261	1,376	3.4055E-03
10/9/2020 14:36	17,400	0.027674161	1,406	3.4502E-03
36:31.2	17,669	0.028183861	1,428	3.5138E-03

Time	Load (lb)	Long. Displ. (in)	Stress (psi)	Long. Strain (in/in)
36:31.4	18,024	0.028559861	1,457	3.5606E-03
36:31.6	18,343	0.028994461	1,483	3.6148E-03
36:31.8	18,642	0.029528861	1,507	3.6814E-03
10/9/2020 14:36	19,011	0.029911661	1,537	3.7292E-03
36:32.2	19,338	0.030390061	1,563	3.7888E-03
36:32.4	19,695	0.030866361	1,592	3.8482E-03
36:32.6	20,019	0.031448861	1,618	3.9208E-03
36:32.8	20,445	0.031857161	1,652	3.9717E-03
10/9/2020 14:36	20,792	0.032378961	1,681	4.0368E-03

Modulus of Elasticity, E (psi) = **4.4858E+05**

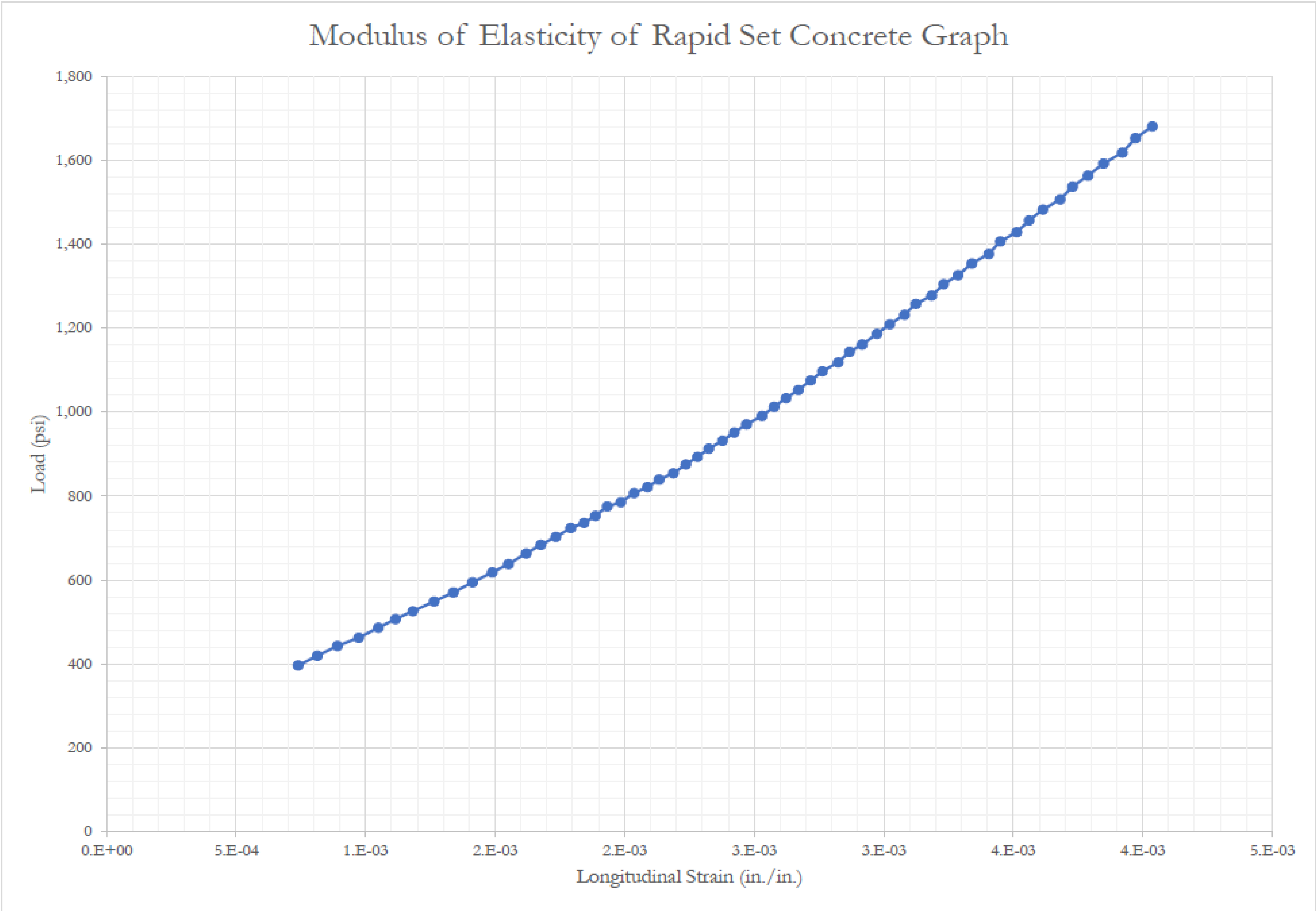

Modulus of Elasticity of Rapid Set Concrete Graph
Load (psi)
1,800
1,600
1,400
1,200
1,000
800
600
400
200
0
0.E+00
5.E-04
1.E-03
2.E-03
2.E-03
3.E-03
3.E-03
4.E-03
4.E-03
5.E-03
Longitudinal Strain (in./in.)

E3 – Proctor Compaction

Standard Proctor Raw Data - Medium Sand

Sample Source:	Pocatello Ready Mix
Sample Location:	Medium Sand Stockpile
Sample Description:	Well graded sand with silt (SW-SM)
Sampled By:	M. Tangarife
Date Sampled:	9/11/2020
Date Received:	9/12/2020

DENSITY					
Target Moisture	In-situ	2%	4%	6%	5%
Weigth of Mold (g)	4292.2	4292.2	4292.2	4292.2	4292.2
Weight of Mold and Moist Soil (g)	6058.3	6097.7	6145.0	6170.5	6155.3
Weight of Moist Soil (g)	1766.1	1805.5	1852.8	1878.3	1863.1
Weigth of Moist Soil (lb)	3.894	3.981	4.086	4.142	4.108
Mold Diameter (in)	4	4	4	4	4
Mold Height (in)	4.5625	4.5625	4.5625	4.5625	4.5625
Mold Area (in^2)	12.566	12.566	12.566	12.566	12.566
Mold Volume (in^3)	57.334	57.334	57.334	57.334	57.334
Mold Volume (ft^3)	0.033	0.033	0.033	0.033	0.033
Wet Density (pcf)	117.0	119.6	122.7	124.4	123.4

MOISTURE					
Pan ID	115	Smoke	Home	514	508
Tare Weight (g)	271	300.9	188	274.5	303.6
Weigth of Moist Soil and Tare (g)	788.4	826.0	665.2	769.3	830.0
Weigth of Dry Soil and Tare (g)	759.7	788.6	621.9	715.4	778.9
Moisture Lost (g)	28.7	37.4	43.3	53.9	51.1
Weight of Dry Soil (g)	488.7	487.7	433.9	440.9	475.3
Moisture Content (%)	5.873	7.669	9.979	12.225	10.751
Dry Density (pcf)	110.5	111.0	111.6	110.8	111.4

MOISTURE-DENSITY RELATIONSHIP CURVE
ASTM D698
Method B

Sample Location: Fine Sand - Pocatello Ready Mix
Sample Classification: Well-Graded Sand with Silt (GP-GM)
Date Sampled: 09/11/2020
Date Tested: 09/12/2020
Rammer Type: Manual

GRADING ANALYSIS

SCREEN SIZE	% PASSING	AS TESTED
6 inch		
3 inch		
2 inch		
3/4 inch	100	100
3/8 inch	99	
#4 screen	99	

Maximum Dry Density, pcf :
Optimum Moisture Content, %:

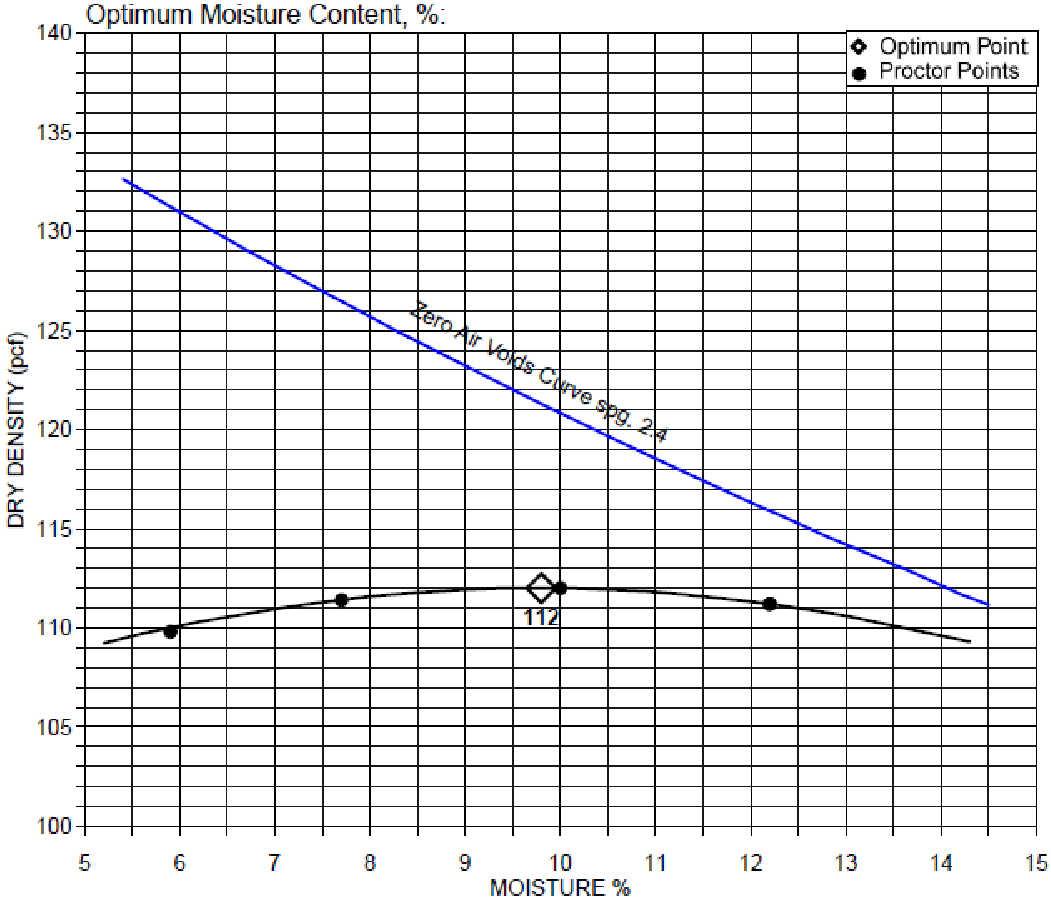

Standard Proctor Raw Data - Coarse Sand

Sample Source:	Pocatello Ready Mix
Sample Location:	Coarse Sand Stockpile
Sample Description:	Silty Sand (SM)
Sampled By:	M. Tangarife
Date Sampled:	9/11/2020
Date Received:	9/12/2020

DENSITY					
Target Moisture	In-situ	2%	4%	6%	8%
Weigth of Mold (g)	4292.5	4292.5	4292.5	4292.5	4292.5
Weight of Mold and Moist Soil (g)	5937.0	5970.2	6008.2	6048.2	6068.1
Weight of Moist Soil (g)	1644.5	1677.7	1715.7	1755.7	1775.6
Weigth of Moist Soil (lb)	3.626	3.700	3.783	3.872	3.915
Mold Diameter (in)	4	4	4	4	4
Mold Height (in)	4.5625	4.5625	4.5625	4.5625	4.5625
Mold Area (in^2)	12.566	12.566	12.566	12.566	12.566
Mold Volume (in^3)	57.334	57.334	57.334	57.334	57.334
Mold Volume (ft^3)	0.033	0.033	0.033	0.033	0.033
Wet Density (pcf)	108.9	111.1	113.6	116.3	117.6

MOISTURE					
Pan ID	Smoke	Wendy	Home	115	508
Tare Weight (g)	300.9	187.5	188.1	270.8	303.6
Weigth of Moist Soil and Tare (g)	833.0	756.8	705.2	843.7	900.3
Weigth of Dry Soil and Tare (g)	812.1	727.8	667.7	790.5	831.9
Moisture Lost (g)	20.9	29.0	37.5	53.2	68.4
Weight of Dry Soil (g)	511.2	540.3	479.6	519.7	528.3
Moisture Content (%)	4.088	5.367	7.819	10.237	12.947
Dry Density (pcf)	104.6	105.4	105.4	105.5	104.1

MOISTURE-DENSITY RELATIONSHIP CURVE
ASTM D698
Method B

Sample Location: Coarse Sand - Pocatello Ready Mix
Sample Classification: Silty Sand (SM)
Date Sampled: 09/11/2020
Date Tested: 09/14/2020
Rammer Type: Manual

GRADING ANALYSIS

SCREEN SIZE	% PASSING	AS TESTED
6 inch		
3 inch		
2 inch	100	
3/4 inch	100	
3/8 inch	100	100
#4 screen	87	

Maximum Dry Density, pcf : 106.0
Optimum Moisture Content, %: 7.7

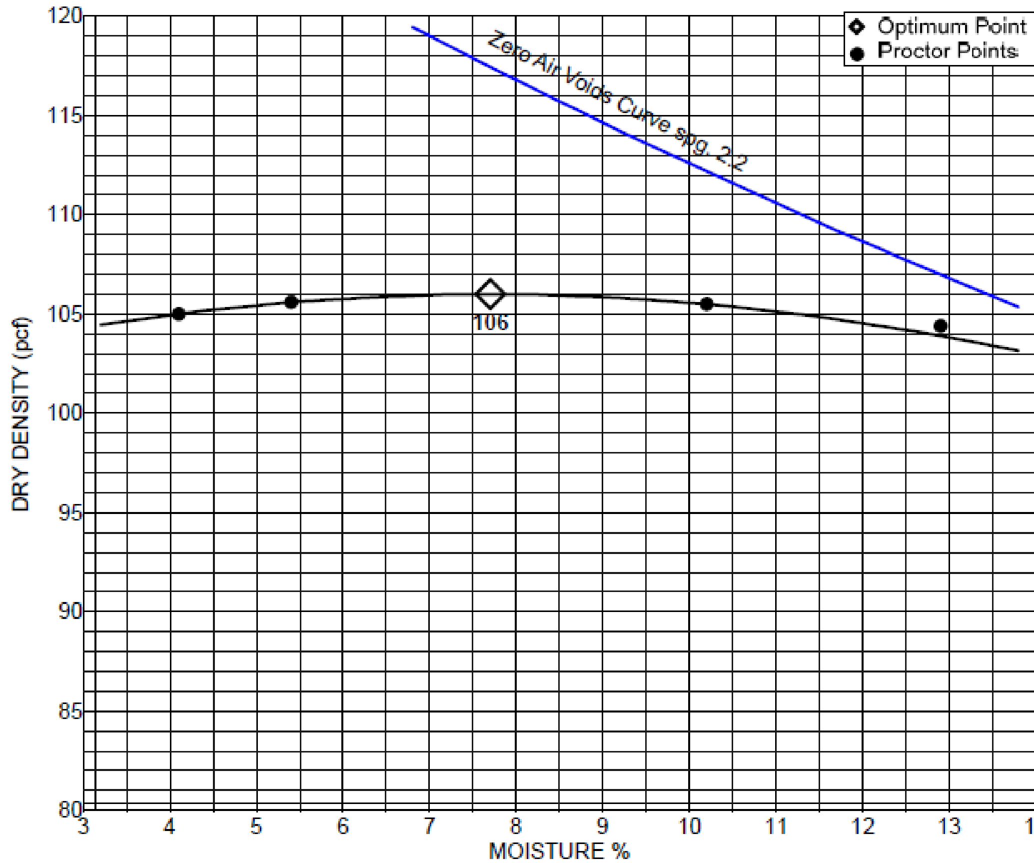

Standard Proctor Raw Data - 3/4-inch Base

Sample Source:	Idaho Rock and Sand
Sample Location:	3/4-inch Base Stockpile
Sample Description:	Silty Gravel with Sand (GM)
Sampled By:	M. Tangarife
Date Sampled:	10/5/2020
Date Received:	10/19/2020

DENSITY				
Target Moisture	In-situ	2%	4%	6%
Weigth of Mold (g)	4291.7	4291.7	4291.7	4291.7
Weight of Mold and Moist Soil (g)	6215.3	6370.8	6513.6	6528.3
Weight of Moist Soil (g)	1923.6	2079.1	2221.9	2236.6
Weigth of Moist Soil (lb)	4.242	4.585	4.900	4.932
Mold Diameter (in)	4	4	4	4
Mold Height (in)	4.5625	4.5625	4.5625	4.5625
Mold Area (in^2)	12.566	12.566	12.566	12.566
Mold Volume (in^3)	57.334	57.334	57.334	57.334
Mold Volume (ft^3)	0.033	0.033	0.033	0.033
Wet Density (pcf)	127.4	137.7	147.1	148.1

MOISTURE				
Pan ID	514	115	Smoke	508
Tare Weight (g)	274.4	270.8	300.9	303.6
Weigth of Moist Soil and Tare (g)	721.0	798.9	896.4	942.2
Weigth of Dry Soil and Tare (g)	704.6	772.2	854.4	889.6
Moisture Lost (g)	16.4	26.7	42.0	52.6
Weight of Dry Soil (g)	430.2	501.4	553.5	586
Moisture Content (%)	3.812	5.325	7.588	8.976
Dry Density (pcf)	122.7	130.7	136.8	135.9

MOISTURE-DENSITY RELATIONSHIP CURVE
ASTM D698
Method C

Sample Location: 3/4-inch Base - Idaho Rock and Sand
Sample Classification: Silty Gravel with Sand (GM)
Date Sampled: 10/5/2020
Date Tested: 10/19/2020
Rammer Type: Manual

GRADING ANALYSIS

SCREEN SIZE	% PASSING	AS TESTED
6 inch		
3 inch		
2 inch	100	
3/4 inch	93	100
3/8 inch	75	
#4 screen	66	

Maximum Dry Density, pcf : 136.8
Optimum Moisture Content, %: 7.9

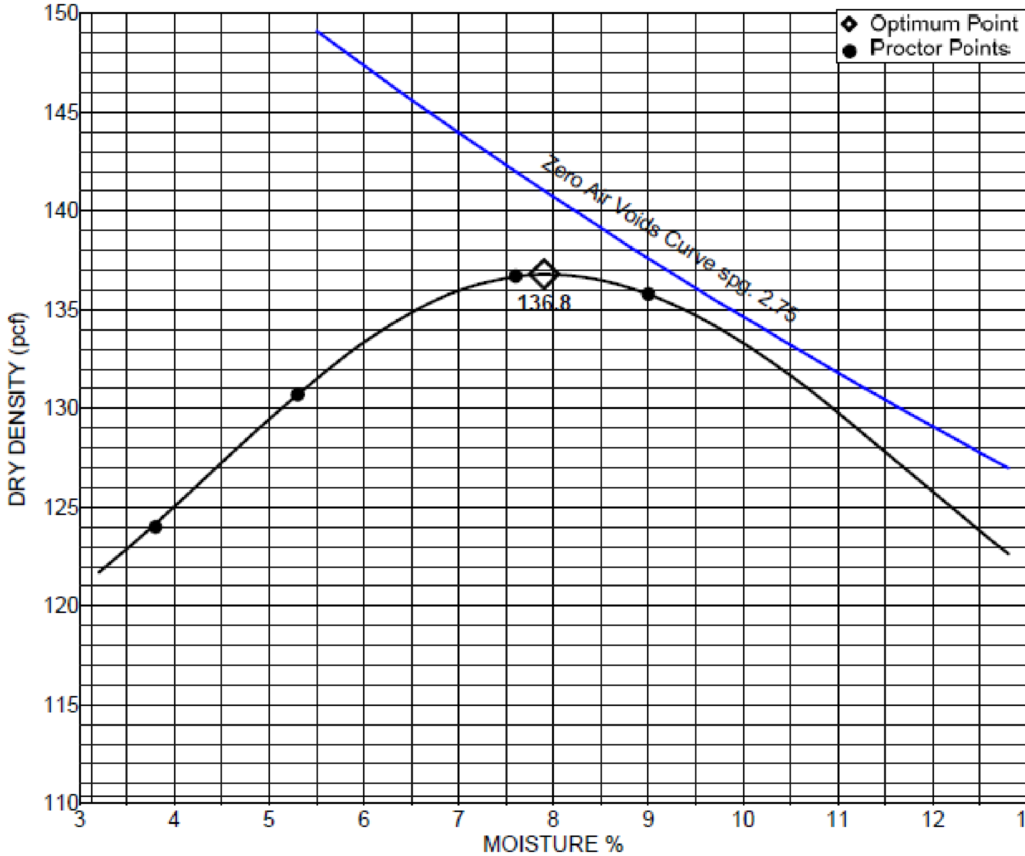

E4 – Sieve Analysis

Sieve Analysis Laboratory Report
Medium Sand

Sample Source:	Pocatello Ready Mix
Sample Location:	Medium Sand Stockpile
Sample Description:	Well graded sand with silt (SW-SM)
Sampled By:	M. Tangarife
Date Sampled:	9/11/2020
Date Received:	9/12/2020

Sieve Size	Metric	Percent Passing
1/2"	12.5 mm	100
3/8"	9.5 mm	99
No. 4	4.75 mm	99
No. 8	2.36 mm	93
No. 10	2.00 mm	87
No. 16	1.18 mm	64
No. 30	0.6 mm	40
No. 40	0.425 mm	32
No. 50	0.3 mm	24
No. 100	0.15 mm	15
No. 200	0.075 mm	11.1

GRADATION ANALYSIS
ASTM C136

Sample Location: Fine Sand - Pocatello Ready Mix
Sample Classification: Well-Graded Sand with Silt (GP-GM)
Date Sampled: 09/11/2020
Date Tested: 09/12/2020

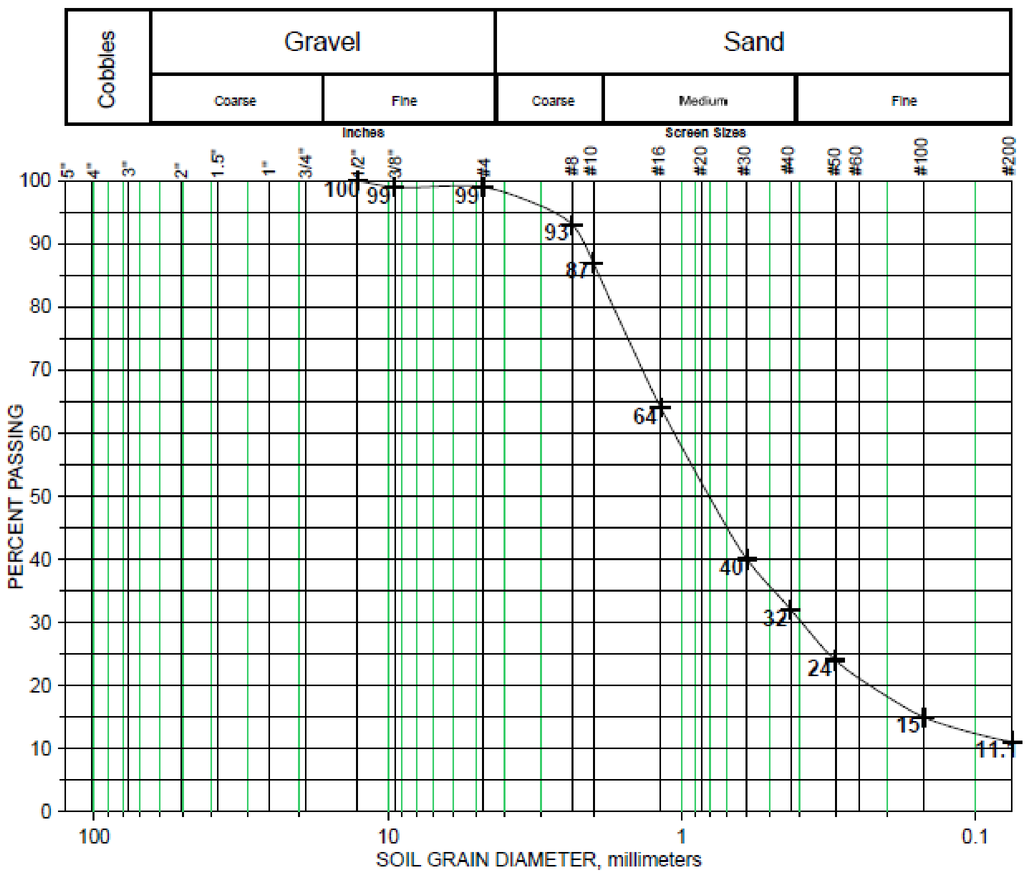

Sieve Analysis Laboratory Report
Coarse Sand

Sample Source:	Pocatello Ready Mix
Sample Location:	Coarse Sand Stockpile
Sample Description:	Silty Sand (SM)
Sampled By:	M. Tangarife
Date Sampled:	9/11/2020
Date Received:	9/12/2020

Sieve Size	Metric	Percent Passing
1/2"	12.5 mm	100
3/8"	9.5 mm	100
No. 4	4.75 mm	87
No. 8	2.36 mm	36
No. 10	2.00 mm	28
No. 16	1.18 mm	19
No. 30	0.6 mm	15
No. 40	0.425 mm	15
No. 50	0.3 mm	14
No. 100	0.15 mm	14
No. 200	0.075 mm	13.8

GRADATION ANALYSIS
ASTM C136

Sample Location: Coarse Sand - Pocatello Ready Mix
Sample Classification: Silty Sand (SM)
Date Sampled: 09/11/2020
Date Tested: 09/14/2020

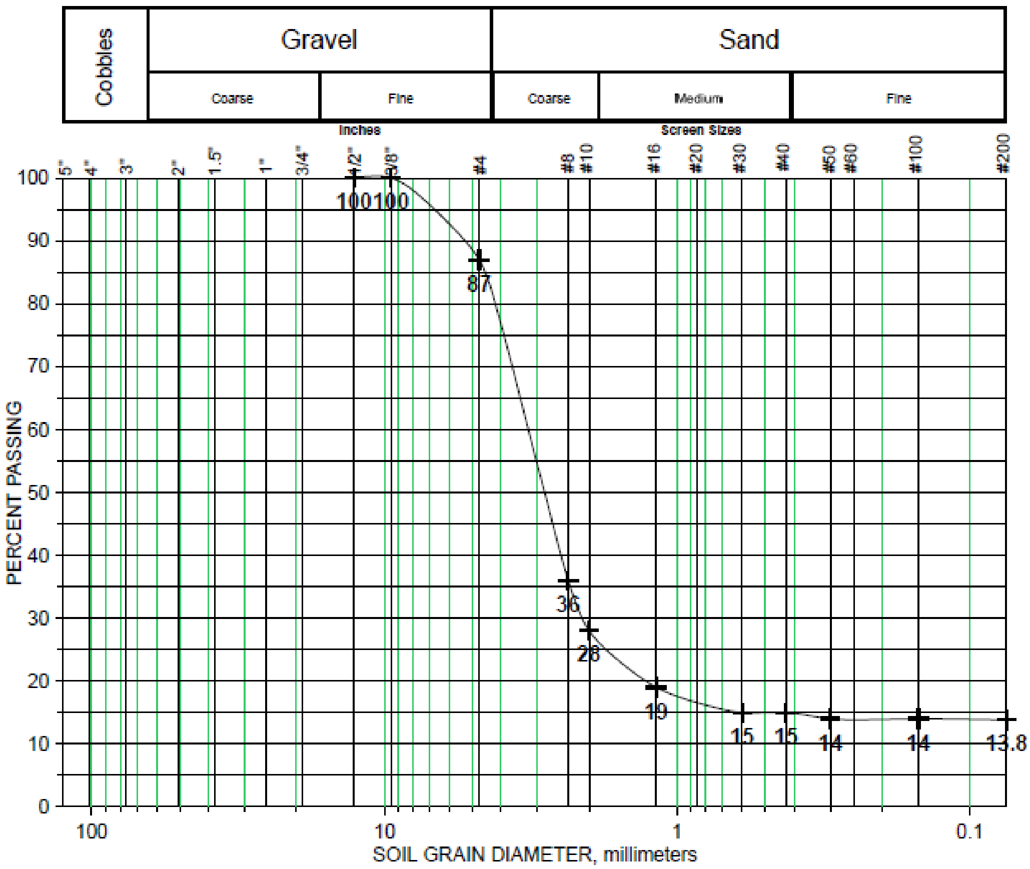

Sieve Analysis Laboratory Report
Pea Gravel

Sample Source:	Greensmix
Sample Location:	The Home Depot
Sample Description:	Poorly graded gravel (GP)
Sampled By:	M. Tangarife
Date Sampled:	9/21/2020
Date Received:	9/22/2020

Sieve Size	Metric	Percent Passing
1/2"	12.5 mm	100
3/8"	9.5 mm	58
No. 4	4.75 mm	3
No. 8	2.36 mm	3
No. 10	2.00 mm	3
No. 16	1.18 mm	3
No. 30	0.6 mm	3
No. 40	0.425 mm	3
No. 50	0.3 mm	3
No. 100	0.15 mm	3
No. 200	0.075 mm	2.7

GRADATION ANALYSIS
ASTM C136

Sample Location: Pea Gravel - The Home Depot
Sample Classification: Poorly Graded Gravel (GP)
Date Sampled: 9/21/2020
Date Tested: 9/22/2020

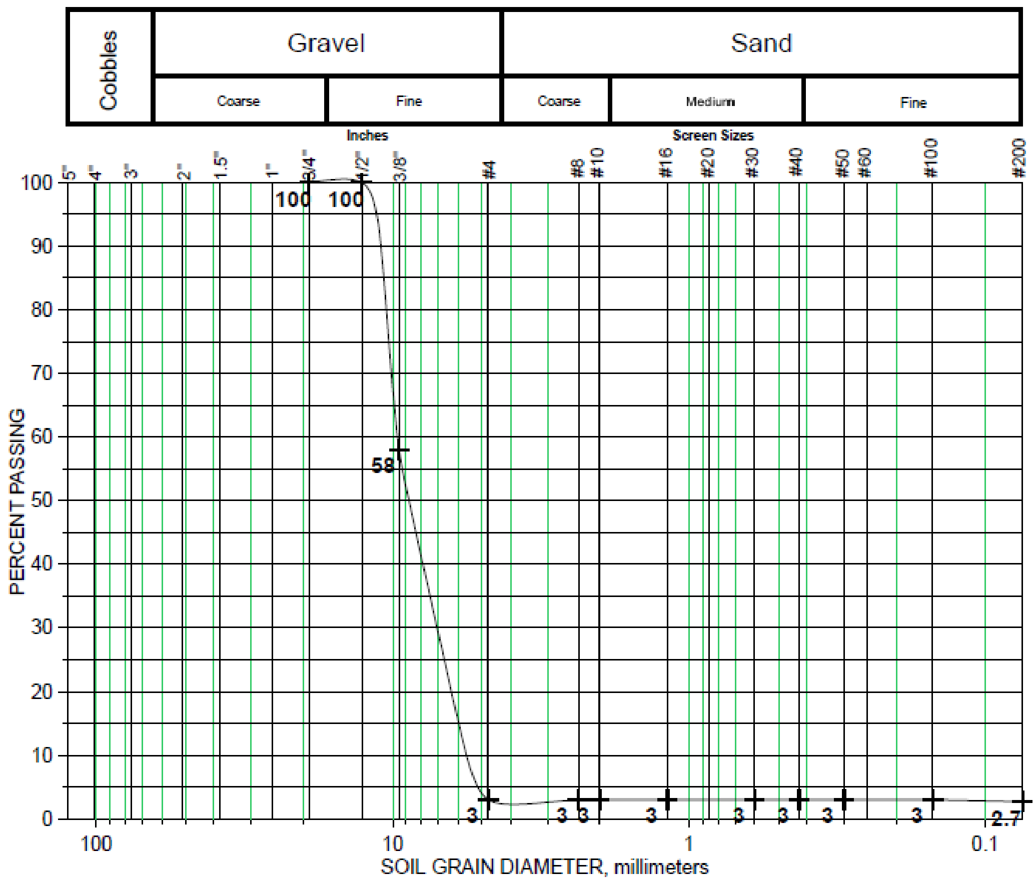

Sieve Analysis Laboratory Report
3/4-inch Base

Sample Source:	Idaho Rock and Sand
Sample Location:	3/4-inch Base Stockpile
Sample Description:	Silty Gravel with Sand (GM)
Sampled By:	M. Tangarife
Date Sampled:	10/5/2020
Date Received:	10/19/2020

Sieve Size	Metric	Percent Passing
1"	12.5 mm	100
3/4"	9.5 mm	100
1/2"	12.5 mm	94
3/8"	9.5 mm	88
No. 4	4.75 mm	65
No. 8	2.36 mm	51
No. 10	2.00 mm	49
No. 16	1.18 mm	43
No. 30	0.6 mm	39
No. 40	0.425 mm	38
No. 50	0.3 mm	37
No. 100	0.15 mm	35
No. 200	0.075 mm	34.3

GRADATION ANALYSIS
ASTM C136

Sample Location: 3/4-inch Base - Idaho Rock and Sand
Sample Classification: Silty Gravel with Sand (GM)
Date Sampled: 10/5/2020
Date Tested: 10/19/2020

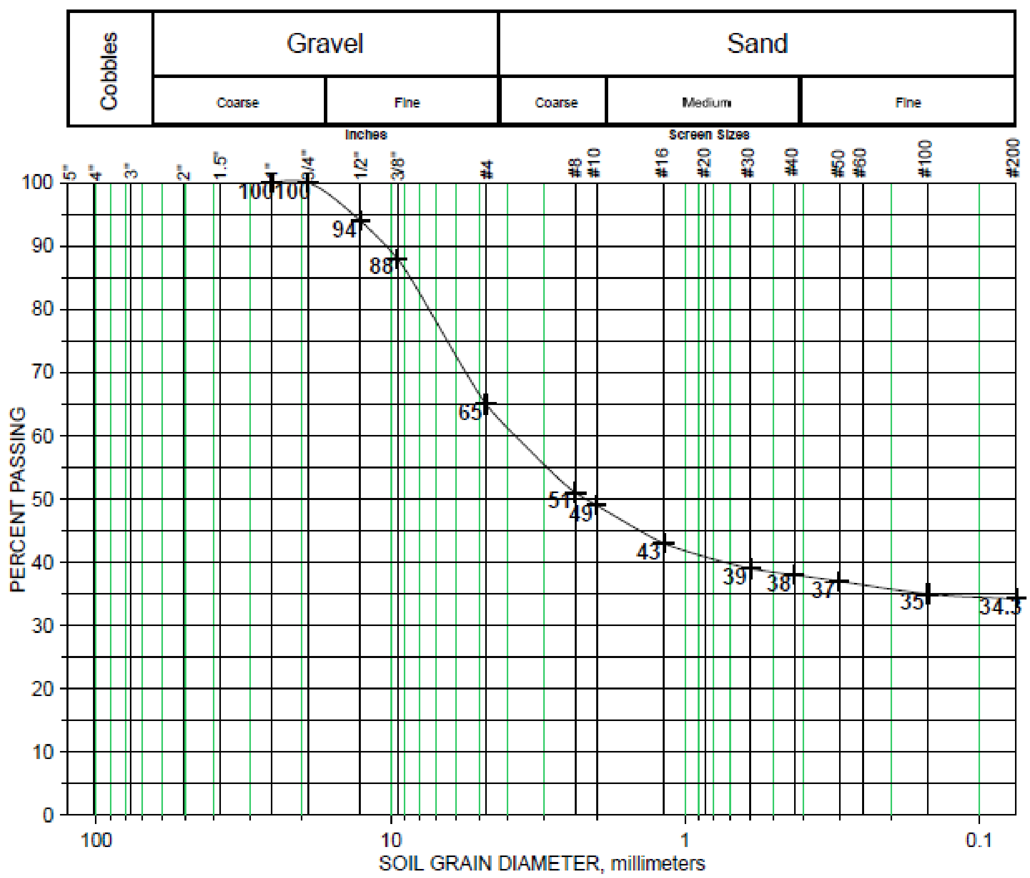

Appendix F – In-Situ Test Results

F1 – Density Determinations

Moist Density Determination Medium Sand (West) - CIP Model

Sample Source:	Pocatello Ready Mix
Sample Location:	Medium Sand Stockpile
Sample Description:	Well graded sand with silt (SW-SM)
Sampled By:	M. Tangarife
Date Backfilled:	9/29/2020

		Mass of Soil	
Bucket Number	Tare Weight (lb)	Bucket + Moist Soil (lb)	Moist Soil (lb)
5	2.4	57.8	55.4
6	2.2	57.3	55.1
4	2.2	61.5	59.3
2	1.5	55.1	53.6
5	2.4	55.3	52.9
4	2.2	61.1	58.9
2	1.5	53.0	51.5
5	2.4	56.2	53.8
6	2.2	57.8	55.6
2	1.5	58.6	57.1
4	2.2	57.8	55.6
2	1.5	50.2	48.7
6	2.2	64.6	62.4
4	2.2	56.7	54.5
1	2.0	58.0	56.0
2	1.5	56.9	55.4
5	2.4	57.1	54.7
6	2.2	61.3	59.1
1	2.0	57.1	55.1
5	2.4	57.8	55.4
1	2.0	54.5	52.5
5	2.4	56.0	53.6
6	2.2	60.0	57.8
4	2.2	59.7	57.5
2	1.5	57.8	56.3
1	2.0	64.2	62.2
5	2.4	63.9	61.5
6	2.2	65.0	62.8
5	2.4	59.3	56.9
4	2.2	59.5	57.3
1	2.0	63.3	61.3
4	2.2	61.3	59.1
6	2.2	47.2	45.0
1	2.0	15.0	-13.0
		Total	1840.9

Volume					
Height (in)	**Avg Height (in)**	**Width Short Leg (in)**	**Width Long Leg (in)**	**Depth (in)**	**Volume (ft^3)**
13.750 13.813 12.875	13.479	59.320	83.250	30.625	17.03

Wet Unit Weigth, pcf = **108.1**

Moist Density Determination Medium Sand (East) - CIP Model

Sample Source:	Pocatello Ready Mix
Sample Location:	Medium Sand Stockpile
Sample Description:	Well graded sand with silt (SW-SM)
Sampled By:	M. Tangarife
Date Backfilled:	9/29/2020

		Mass of Soil	
Bucket Number	Tare Weight (lb)	Bucket + Moist Soil (lb)	Moist Soil (lb)
1	2.0	47.6	45.6
2	1.5	47.2	45.7
4	2.2	52.2	50.0
5	2.4	56.9	54.5
6	2.2	56.7	54.5
7	1.8	53.6	51.8
9	1.8	60.4	58.6
10	2.4	64.4	62.0
4	2.2	54.7	52.5
5	2.4	61.7	59.3
2	1.5	55.6	54.1
6	2.2	59.1	56.9
4	2.2	57.8	55.6
2	1.5	57.1	55.6
1	2.0	59.3	57.3
5	2.4	59.1	56.7
6	2.2	64.8	62.6
4	2.2	58.0	55.8
2	1.5	57.3	55.8
6	2.2	63.7	61.5
5	2.4	61.9	59.5
4	2.2	63.1	60.9
2	1.5	60.6	59.1
6	2.2	59.3	57.1
2	1.5	63.5	62.0
4	2.2	57.5	55.3
5	2.4	62.8	60.4
6	2.2	66.8	64.6
4	2.2	59.7	57.5
5	2.4	61.3	58.9
2	1.5	52.2	50.7
6	2.2	60.4	58.2
4	2.2	60.6	58.4
1	2.0	63.1	61.1
5	2.4	56.7	54.3
4	2.2	30.0	-27.8
		Total	1956.6

Height (in)	Avg Height (in)	Volume Width Short Leg (in)	Width Long Leg (in)	Depth (in)	Volume (ft^3)
12.125 13.500 13.750	13.125	59.320	83.250	31.688	17.16

Wet Unit Weigth, pcf = **114.0**

Moist Density Determination Pea Gravel - CIP Model

Sample Source:	Pocatello Ready Mix
Sample Location:	Pea Gravel Stockpile
Sample Description:	Poorly Graded Gravel (GP)
Sampled By:	M. Tangarife
Date Backfilled:	9/29/2020

Bucket Number	Tare Weight (lb)	Mass of Soil Bucket + Moist Soil (lb)	Moist Soil (lb)
9	1.8	42.7	40.9
10	2.4	47.4	45.0
7	1.8	52.2	50.4
4	2.2	47.2	45.0
1	2.0	50.8	48.8
2	1.5	49.6	48.1
6	2.2	51.9	49.7
4	2.2	51.5	49.3
2	1.5	48.7	47.2
9	1.8	51.0	49.2
7	1.8	45.2	43.4
1	2.0	42.6	40.6
		Total	557.6

Height (in)	Width (in)	Volume Depth (in)	Volume (ft^3)
11.750	26.700	31.000	5.63

Wet Unit Weigth, pcf = **99.1**

Moist Density Determination Medium Sand (East) - Hollow-Core Model

Sample Source:	Pocatello Ready Mix
Sample Location:	Medium Sand Stockpile
Sample Description:	Well graded sand with silt (SW-SM)
Sampled By:	M. Tangarife
Date Backfilled:	9/29/2020

		Mass of Soil	
Bucket Number	**Tare Weight (lb)**	**Bucket + Moist Soil (lb)**	**Moist Soil (lb)**
1	2.4	54.9	52.5
2	2.0	55.1	53.1
4	1.5	50.0	48.5
5	2.4	52.0	49.6
6	2.2	52.9	50.7
7	2.4	56.7	54.3
8	1.8	53.4	51.6
9	2.4	52.7	50.3
4	1.5	57.5	56.0
5	2.4	57.5	55.1
2	2.0	52.5	50.5
6	2.2	54.2	52.0
4	1.5	53.6	52.1
2	2.0	51.4	49.4
1	2.4	56.2	53.8
5	2.4	52.0	49.6
6	2.2	56.9	54.7
4	1.5	56.4	54.9
2	2.0	52.5	50.5
6	2.2	56.9	54.7
5	2.4	58.9	56.5
4	1.5	58.9	57.4
2	2.0	59.1	57.1
6	2.2	52.2	50.0
2	2.0	57.3	55.3
4	1.5	53.1	51.6
5	2.4	41.0	38.6
6	2.2	38.6	36.4
4	1.5	41.0	39.5
5	2.4	42.8	40.4
2	2.0	38.1	36.1
6	2.2	39.7	37.5
4	1.5	47.2	45.7
1	2.4	55.1	52.7
5	2.4	47.6	45.2
4	1.5	48.3	46.8
2	2.0	44.3	42.3
6	2.2	30.2	28.0
4	1.5	34.2	32.7
1	2.4	37.9	35.5
5	2.4	50.5	48.1
4	1.5	41.0	39.5
		Total	2016.8

			Volume		
Height (in)	**Avg Height (in)**	**Width Short Leg (in)**	**Width Long Leg (in)**	**Depth (in)**	**Volume (ft^3)**
13.750 14.000 14.500	14.083	59.220	83.875	30.750	17.93

Wet Unit Weigth, pcf = **112.5**

Moist Density Determination Medium Sand (West) - Hollow-Core Model

Sample Source:	Pocatello Ready Mix
Sample Location:	Medium Sand Stockpile
Sample Description:	Well graded sand with silt (SW-SM)
Sampled By:	M. Tangarife
Date Backfilled:	11/2/2020

		Mass of Soil	
Bucket Number	Tare Weight (lb)	Bucket + Moist Soil (lb)	Moist Soil (lb)
3	2.2	52.2	50.0
4	1.5	55.6	54.1
5	2.4	59.5	57.1
6	2.2	52.9	50.7
2	2.0	64.4	62.4
1	2.4	58.0	55.6
5	2.4	56.4	54.0
2	2.0	48.7	46.7
3	2.2	52.9	50.7
6	2.2	56.0	53.8
3	2.2	55.6	53.4
4	1.5	55.1	53.6
5	2.4	46.5	44.1
6	2.2	51.4	49.2
5	2.4	49.2	46.8
1	2.4	52.9	50.5
2	2.0	53.4	51.4
4	1.5	51.1	49.6
3	2.2	54.5	52.3
5	2.4	51.6	49.2
6	2.2	54.0	51.8
4	1.5	53.1	51.6
6	2.2	49.6	47.4
5	2.4	51.1	48.7
2	2.0	50.7	48.7
4	1.5	52.5	51.0
6	2.2	56.0	53.8
3	2.2	54.2	52.0
5	2.4	55.8	53.4
6	2.2	56.0	53.8
3	2.2	58.9	56.7
4	1.5	50.5	49.0
3	2.2	52.2	50.0
4	1.5	51.1	49.6
6	2.2	56.0	53.8
3	2.2	52.9	50.7
5	2.4	59.9	57.5
6	2.2	54.1	51.9
3	2.2	52.9	50.7
4	1.5	53.8	52.3
3	2.2	53.8	51.6
6	2.2	48.9	46.7
2	2.0	46.7	44.7
		Total	2212.6

			Volume		
Height (in)	Avg Height (in)	Width Short Leg (in)	Width Long Leg (in)	Depth (in)	Volume (ft^3)
15.000 16.875 16.750	16.208	57.600	82.875	31.313	20.63

Wet Unit Weigth, pcf = **107.3**

Moist Density Determination Pea Gravel - Hollow-Core Model

Sample Source:	Idaho Rock and Sand
Sample Location:	3/4-inch Base Stockpile
Sample Description:	Silty Gravel with Sand (GM)
Sampled By:	M. Tangarife
Date Backfilled:	11/2/2020

		Mass of Soil	
Bucket Number	**Tare Weight (lb)**	**Bucket + Moist Soil (lb)**	**Moist Soil (lb)**
1	1.8	71.2	69.4
2	2.0	62.2	60.2
3	1.5	67.7	66.2
4	1.8	64.8	63.0
5	1.8	72.6	70.8
6	2.0	74.1	72.1
1	1.8	69.3	67.5
2	2.0	52.0	50.0
3	1.5	64.0	62.5
4	1.8	63.5	61.7
5	1.8	32.0	30.2
6	2.0	53.5	51.5
		Total	725.1

		Volume	
Height (in)	**Width (in)**	**Depth (in)**	**Volume (ft^3)**
12.000	25.500	31.000	5.49

Wet Unit Weigth, pcf = **132.1**

F2 – Sand Cone Tests

Sand Cone Test - Medium Sand CIP Model

Sample Source:	Pocatello Ready Mix
Sample Location:	Medium Sand Stockpile
Sample Description:	Well graded sand with silt (SW-SM)
Sampled By:	M. Tangarife
Date Tested:	10/12/2020

DENSITY					
Test Number	1 (east)	2 (west)	3	4	5
Weight of Sand Cone Before (lb)	13.375	13.580			
Weight of Sand Cone After (lb)	8.220	7.780			
Weight of Sand in Cone and Hole (lb)	5.155	5.800			
Weight of Sand in Cone (lb)	3.124	3.124			
Weight of Sand in Hole (lb)	2.031	2.676			
Unit Weight of Sand (pcf)	79.0	79.0			
Volume of Hole (ft^3)	0.026	0.034			
Weight of Bag and Wet Soil from Hole (lb)	2.945	3.813			
Weight of Bag (lb)	0.055	0.055			
Weight of Wet Soil (lb)	2.890	3.758			
Weight of Wet Soil and Tare (g)	504.8	536.9			
Weight of Dry Soil and Tare (g)	500.9	532.2			
Weight of Tare (g)	404.5	405.1			
Weight of Water (g)	3.9	4.7			
Weight of Dry Soil (g)	96.4	127.1			
Moisture Content (%)	4.0	3.70			
Wet Density (pcf)	112.4	110.9			
Dry Density (pcf)	108.1	107.0			

Sand Cone Test - Coarse Sand CIP Model

Sample Source:	Pocatello Ready Mix
Sample Location:	Coarse Sand Stockpile
Sample Description:	Silty Sand (SM)
Sampled By:	M. Tangarife
Date Tested:	10/8/2020

DENSITY					
Test Number	1	2	3	4	5
Weight of Sand Cone Before (lb)	14.110				
Weight of Sand Cone After (lb)	9.420				
Weight of Sand in Cone and Hole (lb)	4.690				
Weight of Sand in Cone (lb)	3.124				
Weight of Sand in Hole (lb)	1.566				
Unit Weight of Sand (pcf)	79.0				
Volume of Hole (ft^3)	0.020				
Weight of Bag and Wet Soil from Hole (lb)	1.909				
Weight of Bag (lb)	0.055				
Weight of Wet Soil (lb)	2.160				
Weight of Wet Soil and Tare (g)	517.5				
Weight of Dry Soil and Tare (g)	512.0				
Weight of Tare (g)	405.2				
Weight of Water (g)	5.5				
Weight of Dry Soil (g)	106.8				
Moisture Content (%)	5.1				
Wet Density (pcf)	109.0				
Dry Density (pcf)	104.8				

Appendix G – Equipment Calibrations

G1 – Break Machine

Form: 188 Rev 7, 9 Jan 15

ACCREDITED CALIBRATION 2521.01

3998 Commerce Circle
Idaho Falls, ID 83401
Ph: (208) 523-5557

Certificate of Calibration

Qal-Tek

Innovating Solutions for Those Building a Better and More Secure World

Calibrated On Site At:
Customer: Strata Engineering, Inc Pocatello
Att.: Mike Hitchcock (Lab and RSO)
Address: 2055 Garrett Way, Suite 1
City: Pocatello State: ID Zip: 83201
Phone: 208-237-3400

Serial Number: **94114(ID#4007)** Mfg: Cal Teck Inc. Model: CT-400K-AT 7000 Ref. #: W30339-142031

Calibration/Ver. Date: 17-Jan-2020

Compression

Calibration/Ver. Due Date: 17-Jan-2021

Basic Information

Load Range Full Scale (range 1)	400000
Mach. Ind. Resolution (range 1)	10
Load Range Full Sacle (range 2)	40000
Mach. Ind. Resolution (range 2)	10
Mach. Units	lbf
Ambient Temperature	75

Range 1 As Found

Mach. Ind. Reading	Proof Load Run 1	Proof Load Run 2	Error Run 1 (lbf)	Error Run 1 (%)	Error Run 2 (lbf)	Error Run 2 (%)	Repeatability Error (%)	Pass/Fail	Uncertainty %FS
40000	39870	39930	-130	0.326	-70	0.175	0.151	Pass	0.12
80000	80030	79870	30	-0.037	-130	0.163	-0.2	Pass	0.12
160000	159240	159710	-760	0.477	-290	0.182	0.295	Pass	0.12
280000	278150	278620	-1850	0.665	-1380	0.495	0.17	Pass	0.12
400000	396840	397170	-3160	0.796	-2830	0.713	0.083	Pass	0.12
Machine zero	-25	-25						Pass	0
Max Error						0.796	0.295		

Range 2 As Found

Mach. Ind. Reading	Proof Load Run 1	Proof Load Run 2	Error Run 1 (lbf)	Error Run 1 (%)	Error Run 2 (lbf)	Error Run 2 (%)	Repeatability Error (%)	Pass/Fail	Uncertainty %FS
4000	4010	4010	10	-0.249	10	-0.249	0	Pass	0.014
8000	8030	8010	30	-0.374	10	-0.125	-0.249	Pass	0.014
16000	16040	16020	40	-0.249	20	-0.125	-0.124	Pass	0.014
28000	27980	27930	-20	0.0709	-70	0.251	-0.18	Pass	0.014
40000	39930	39870	-70	0.175	-130	0.326	-0.151	Pass	0.014
Machine zero	45	25						Pass	0
Max Error						0.374	0.249		

Range 1 As Left

Mach. Ind. Reading	Proof Load Run 1	Proof Load Run 2	Error Run 1 (lbf)	Error Run 1 (%)	Error Run 2 (lbf)	Error Run 2 (%)	Repeatability Error (%)	Pass/Fail	Uncertainty %FS
40000	39820	39930	-180	0.452	-70	0.175	0.277	Pass	0.12
80000	80030	79870	30	-0.037	-130	0.163	-0.2	Pass	0.12
160000	159240	159710	-760	0.477	-290	0.182	0.295	Pass	0.12
280000	278150	278620	-1850	0.665	-1380	0.495	0.17	Pass	0.12
400000	396840	397170	-3160	0.796	-2830	0.713	0.083	Pass	0.12
Machine zero	-25	-25						Pass	0
Max Error						0.796	0.295		

Range 2 As Left

Mach. Ind. Reading	Proof Load Run 1	Proof Load Run 2	Error Run 1 (lbf)	Error Run 1 (%)	Error Run 2 (lbf)	Error Run 2 (%)	Repeatability Error (%)	Pass/Fail	Uncertainty %FS
4000	4010	4010	10	-0.249	10	-0.249	0	Pass	0.014
8000	8030	8010	30	-0.374	10	-0.125	-0.249	Pass	0.014
16000	16040	16020	40	-0.249	20	-0.125	-0.124	Pass	0.014
28000	27980	27930	-20	0.0709	-70	0.251	-0.18	Pass	0.014
40000	39930	39870	-70	0.175	-130	0.326	-0.151	Pass	0.014
Machine zero	45	25						Pass	0
Max Error						0.374	0.249		

Platen Flatness Verification

	Lower Platen Compliance	Upper Platen Compliance
Gap Less than or Equal to 0.001 (in)	Acceptable	NEEDS TO BE RESURFACED

Tolerance <= 0.001" over 6" unless limited by platen size.

Machined and rechecked 4/2020

17-Jan-2020 Page 1 of 2 SN 94114(ID#4007)

G2 – Sieve Analysis Equipment

Worksheet 2

Mechanical Sieve Shaker Efficiency Check

Check Procedure: ITD-D-5 Check Frequency: 12 months

Date Checked: 5-8-2020	Shaker Manufacturer: Gilson
Model No. : PS-3	Identification No. : 4041
Standard Balance Number: 4865	Mass of Total Sample: 4000.1

Sieve ID	Sieve Size	~~Sieve Ident. No.~~ Mass Retain.	~~Mass retained by mechanical sieving~~ Mass Retain.	~~Hand Sieving Mass Passing~~ Mass Retain.	~~Hand Sieving % Passing~~ 9-10 .1' change	Acceptable (Y/N)[1]
4703	1"	571.2	571.1	571.0	0.01	yes
4204	3/8"	358.2	357.9	357.7	0.08	yes
	~~No. 8~~ Time	9 min.	10 min.	11 min.		

Note 1: No more than 0.5%, by mass, of the total sample shall pass any one sieve after one minute of continuous hand sieving.

Minimum mechanical shaking time required 9 minutes	
Shaker was cleaned: ☑	Shaker was lubricated: ☑

Remarks:	
Checked By: Codey Spencer	Signature: Codey Spencer
WAQTC NO. 23558	
PREVIOUS CHECK DATE:	RE- CHECK DUE DATE: 5-8-2021

Worksheet 2

Mechanical Sieve Shaker Efficiency Check

Check Procedure: ITD-D-5 Check Frequency: 12 months

Date Checked: 5/11/2020	Shaker Manufacturer: Gilson
Model No. : SS-12R	Identification No. : 4271
Standard Balance Number: 4865	Mass of Total Sample: 2000.5

Sieve ID#

Sieve Size	~~Sieve Ident. No.~~ MASS Retain.	~~Mass retained by mechanical sieving~~ Mass Retain.	~~Hand Sieving Mass Passing~~ Mass Retain.	~~Hand Sieving % Passing~~ 8-9 min .1' change	Acceptable (Y/N)[1]
~~1st~~ Time	7 min	8 min	9 min		
3/8"	148.9	150.2	150.6	0.3	Yes
No. 8	429.7	426.1	424.6	0.4	yes

Note 1: No more than 0.5%, by mass, of the total sample shall pass any one sieve after one minute of continuous hand sieving.

Minimum mechanical shaking time required 8 minutes	
Shaker was cleaned: ☑	Shaker was lubricated: ☑

Remarks:	
Checked By: David S. Myers	Signature: David S. Myers
WAQTC NO. 23284	
PREVIOUS CHECK DATE:	RE- CHECK DUE DATE: 5/11/2021

Worksheet 5

Sieve Measurements

Check Procedure ITD D11

Identification Number:	Check Date:	Nominal sieve opening,
4703	2/11/2020	w =1" in. (25.0 mm)

Opening #	Opening Size X Vertical	Opening #	Opening Size Y Horizontal
1	24.89	1	25.10
2	24.92	2	24.92
3	25.12	3	24.93
4	24.87	4	24.90
5	24.89	5	24.91
6	25.02	6	24.89
7	24.89	7	25.04
8	25.01	8	25.01
9	25.00	9	24.98
10	24.95	10	25.01
11	25.04	11	24.98
12	24.98	12	25.02
13	24.99	13	24.87
14	25.03	14	25.01
15	24.89	15	25.10
Average X	24.97	Average Y	24.98

a = General Condition of Sieve Frame (Section 6.3 and Table 2)	Met ☒ Not Met ☐
Max. Individual sieve Opening, b = 26.38 mm (table 1, column 6),	Met ☒ Not Met ☐
Maximum allowable tolerance of average openings, c = 24.24 to 25.76 mm (Table 1,column 1 + or - column 4)	Met ☒ Not Met ☐

From Table 1 in AASHTO M 2 (ASTM E11):

Verify general condition of sieve frame a; maximum opening size does not exceed b; and the average of the sieve openings meets the requirements of c.

Sieve Disposition: ☒ Acceptable ☐ Unacceptable	
Remarks:	
Checked By: Codey Spencer	Signature: Codey Spencer
WAQTC NO. 23558	
PREVIOUS CHECK DATE: 2/2019	RE-CHECK DUE DATE: 2/11/2021

Worksheet 5

Sieve Measurements

Check Procedure ITD D11

Identification Number:	Check Date:	Nominal sieve opening, w =3/4 in. (19.0 mm)
4202	2-12-20	14x14

Opening #	Opening Size X Vertical	Opening #	Opening Size Y Horizontal
1	18.84	1	18.88
2	18.98	2	19.14
3	18.91	3	18.86
4	19.01	4	19.01
5	18.83	5	18.94
6	19.14	6	19.00
7	18.98	7	18.81
8	18.89	8	19.21
9	18.85	9	18.77
10	19.35	10	19.04
11	18.83	11	18.93
12	18.98	12	19.05
13	18.95	13	18.83
14	19.07	14	19.14
15	18.91	15	18.92
Average X	18.97	Average Y	18.97

a = General Condition of Sieve Frame (Section 6.3 and Table 2)	Met ☒ Not Met ☐
Max. Individual sieve Opening, b = 20.13 mm (table 1, column 6),	Met ☒ Not Met ☐
Maximum allowable tolerance of average openings, c = 18.25 to 19.75 mm (Table 1,column 1 + or - column 4)	Met ☒ Not Met ☐

From Table 1 in AASHTO M 92 (ASTM E11):

Verify general condition of sieve frame a; maximum opening size does not exceed b; and the average of the sieve openings meets the requirements of c.

Sieve Disposition: ☒ Acceptable ☐ Unacceptable	
Remarks:	
Checked By: Kevin Koompin	Signature:
WAQTC NO. 22634	
PREVIOUS CHECK DATE: 2-2019	RE-CHECK DUE DATE: 2-12-2024

Worksheet 5

Sieve Measurements

Check Procedure ITD D11

Identification Number:	Check Date:	Nominal sieve opening, w =1/2 in. (12.5 mm)
4264	2/11/2020	

Opening #	Opening Size X Vertical	Opening #	Opening Size Y Horizontal
1	12.42	1	12.32
2	12.37	2	12.34
3	12.46	3	12.36
4	12.30	4	12.34
5	12.32	5	12.38
6	12.39	6	12.34
7	12.44	7	12.38
8	12.40	8	12.39
9	12.30	9	12.35
10	12.36	10	12.37
11	12.37	11	12.30
12	12.33	12	12.30
13	12.39	13	12.33
14	12.39	14	12.31
15	12.38	15	12.35
Average X	12.37	Average Y	12.34

a = General Condition of Sieve Frame (Section 6.3 and Table 2)	Met ☒ Not Met ☐
Max. Individual sieve Opening, b = 13.33 mm (table 1, column 6),	Met ☒ Not Met ☐
Maximum allowable tolerance of average openings, c = 12.12 to 12.89 mm (Table 1,column 1 + or - column 4)	Met ☒ Not Met ☐

From Table 1 in AASHTO M 92 (ASTM E11):

Verify general condition of sieve frame a; maximum opening size does not exceed b; and the average of the sieve openings meets the requirements of c.

Sieve Disposition: ☒ Acceptable ☐ Unacceptable	
Remarks:	
Checked By: Cody Spencer	Signature: Cody Spencer
WAQTC NO. 23558	
PREVIOUS CHECK DATE: 4/10/19	RE-CHECK DUE DATE: 2/11/2021

Worksheet 5

Sieve Measurements

Check Procedure ITD D11

Identification Number: 4204	Check Date: 2/11/2020	Nominal sieve opening, w =3/8 in. (9.5 mm)

Opening #	Opening Size X Vertical	Opening #	Opening Size Y Horizontal
1	9.37	1	9.34
2	9.39	2	9.32
3	9.41	3	9.32
4	9.34	4	9.42
5	9.37	5	9.47
6	9.40	6	9.32
7	9.36	7	9.44
8	9.40	8	9.40
9	9.40	9	9.42
10	9.37	10	9.38
11	9.40	11	9.50
12	9.39	12	9.42
13	9.37	13	9.50
14	9.34	14	9.49
15	9.39	15	9.51
Average X	9.38	Average Y	9.42

a = General Condition of Sieve Frame (Section 6.3 and Table 2)	Met ☒ Not Met ☐
Max. Individual sieve Opening, b = 10.18 mm (table 1, column 6),	Met ☒ Not Met ☐
Maximum allowable tolerance of average openings, c 9.21 to 9.80 mm (Table 1,column 1 + or - column 4)	Met ☒ Not Met ☐

From Table 1 in AASHTO M 92 (ASTM E11):

Verify general condition of sieve frame a; maximum opening size does not exceed b; and the average of the sieve openings meets the requirements of c.

Sieve Disposition: ☒ Acceptable	☐ Unacceptable
Remarks:	
Checked By: Codey Spencer	Signature: Codey Spencer
WAQTC NO. 23558	
PREVIOUS CHECK DATE: 2/2019	RE-CHECK DUE DATE: 2/11/2021

Worksheet 5

Sieve Measurements

Check Procedure ITD D11

Identification Number: 4205	Check Date: 2/11/2020	Nominal sieve opening, w =#4 (4.75 mm)

Opening #	Opening Size X Vertical	Opening #	Opening Size Y Horizontal
1	4.73	1	4,70
2	4.76	2	4.75
3	4.74	3	4.71
4	4.68	4	4.72
5	4.75	5	4.73
6	4.71	6	4.74
7	4.74	7	4.76
8	4.73	8	4.71
9	4.70	9	4.75
10	4.71	10	4.76
11	4.74	11	4.68
12	4.73	12	4.73
13	4.69	13	4.74
14	4.75	14	4.75
15	4.71	15	4.71
Average X	4.72	Average Y	4.73

a = General Condition of Sieve Frame (Section 6.3 and Table 2)	Met ☒ Not Met ☐
Max. Individual sieve Opening, b = 5.16 mm (table 1, column 6),	Met ☒ Not Met ☐
Maximum allowable tolerance of average openings, c = 4.60 to 4.90 mm (Table 1,column 1 + or - column 4)	Met ☒ Not Met ☐

From Table 1 in AASHTO M 92 (ASTM E11):

Verify general condition of sieve frame a; maximum opening size does not exceed b; and the average of the sieve openings meets the requirements of c.

Sieve Disposition: ☒ Acceptable ☐ Unacceptable	
Remarks:	
Checked By: Codey Spencer WAQTC NO. 23558	Signature: Codey Spencer
PREVIOUS CHECK DATE: 2/2019	RE-CHECK DUE DATE: 2/11/2021

Worksheet 4

Wire Cloth Sieves Check Procedure

Check Procedure: ITD-D-11

Check Frequency: 12 months

Identification No.: 4729	Date: 1/31/2020
Manufacturer: Forney	Sieve size: #8 12" Round

General condition of sieve frame:	[X] Acceptable [ ] Unacceptable
General condition of sieve cloth, Annex A1.1.1 Observation of deviations, such as weaving defects, creases, wrinkles	[X] Acceptable [ ] Unacceptable
Sieve opening appearance, Annex A1.1.2 Observation of oversized openings must be less than Column 6 (Table 1, Column 1 + Column 5)	[X] Acceptable [ ] Unacceptable

Remarks:	
Checked By: Kevin Koompin	Signature: Kevin Koompin
WAQTC NO. 22634	
PREVIOUS CHECK DATE: 2-2019	RE-CHECK DUE DATE: 1/31/2021

Worksheet 4

Wire Cloth Sieves Check Procedure

Check Procedure: ITD-D-11

Check Frequency: 12 months

Identification No.: 4694	Date: 1/31/2020
Manufacturer: Dual	Sieve size: #10 12" Rounds

General condition of sieve frame:	☒ Acceptable ☐ Unacceptable
General condition of sieve cloth, Annex A1.1.1 Observation of deviations, such as weaving defects, creases, wrinkles	☒ Acceptable ☐ Unacceptable
Sieve opening appearance, Annex A1.1.2 Observation of oversized openings must be less than Column 6 (Table 1, Column 1 + Column 5)	☒ Acceptable ☐ Unacceptable

Remarks:	
Checked By: Kevin Koompin	Signature:
WAQTC NO. 22634	
PREVIOUS CHECK DATE: 2-2019	RE-CHECK DUE DATE: 1/31/2021

Worksheet 4

Wire Cloth Sieves Check Procedure

Check Procedure: ITD-D-11

Check Frequency: 12 months

Identification No.: 4184	Date: 1/31/2020
Manufacturer: Dual	Sieve size: #16 12" Round

General condition of sieve frame:	☒ Acceptable ☐ Unacceptable
General condition of sieve cloth, Annex A1.1.1 Observation of deviations, such as weaving defects, creases, wrinkles	☒ Acceptable ☐ Unacceptable
Sieve opening appearance, Annex A1.1.2 Observation of oversized openings must be less than Column 6 (Table 1, Column 1 + Column 5)	☒ Acceptable ☐ Unacceptable

Remarks:	
Checked By: Kevin Koompin WAQTC NO. 22634	Signature:
PREVIOUS CHECK DATE: 2-2019	RE-CHECK DUE DATE: 1/31/2021

Worksheet 4

Wire Cloth Sieves Check Procedure

Check Procedure: ITD-D-11 Check Frequency: 12 months

Identification No.: 4693	Date: 1/31/2020
Manufacturer: Dual	Sieve size: #30 12" Round #30

General condition of sieve frame:	☑ Acceptable ☐ Unacceptable
General condition of sieve cloth, Annex A1.1.1 Observation of deviations, such as weaving defects, creases, wrinkles	☒ Acceptable ☐ Unacceptable
Sieve opening appearance, Annex A1.1.2 Observation of oversized openings must be less than Column 6 (Table 1, Column 1 + Column 5)	☒ Acceptable ☐ Unacceptable

Remarks:	
Checked By: Kevin Koompin	Signature: [signature]
WAQTC NO. 22634	
PREVIOUS CHECK DATE: 2-2019	RE-CHECK DUE DATE: 1/31/2021

Worksheet 4

Wire Cloth Sieves Check Procedure

Check Procedure: ITD-D-11

Check Frequency: 12 months

Identification No.: 4278	Date: 1/31/2020
Manufacturer: Dual	Sieve size: #40 12" Round

General condition of sieve frame:	☒ Acceptable ☐ Unacceptable
General condition of sieve cloth, Annex A1.1.1 Observation of deviations, such as weaving defects, creases, wrinkles	☒ Acceptable ☐ Unacceptable
Sieve opening appearance, Annex A1.1.2 Observation of oversized openings must be less than Column 6 (Table 1, Column 1 + Column 5)	☒ Acceptable ☐ Unacceptable

Remarks:	
Checked By: Kevin Koompin	Signature: Kevin Koompin
WAQTC NO. 22634	
PREVIOUS CHECK DATE: ~~2/219~~ 2/2019	RE-CHECK DUE DATE: 1/31/2021

Worksheet 4

Wire Cloth Sieves Check Procedure

Check Procedure: ITD-D-11 Check Frequency: 12 months

Identification No.: 4751	Date: 1/31/20
Manufacturer: Dual	Sieve size: #50 12" Round

General condition of sieve frame:	[X] Acceptable [ ] Unacceptable
General condition of sieve cloth, Annex A1.1.1 Observation of deviations, such as weaving defects, creases, wrinkles	[X] Acceptable [ ] Unacceptable
Sieve opening appearance, Annex A1.1.2 Observation of oversized openings must be less than Column 6 (Table 1, Column 1 + Column 5)	[X] Acceptable [ ] Unacceptable

Remarks:	
Checked By: Kevin Koompin	Signature:
WAQTC NO. 22634	
PREVIOUS CHECK DATE: 2-2019	RE-CHECK DUE DATE: 1/31/~~2001~~ 2021

Worksheet 4

Wire Cloth Sieves Check Procedure

Check Procedure: ITD-D-11 Check Frequency: 12 months

Identification No.: 4726	Date: 1/31/2020
Manufacturer: Dual	Sieve size: #100 12" Rounds

General condition of sieve frame:	☒ Acceptable ☐ Unacceptable
General condition of sieve cloth, Annex A1.1.1 Observation of deviations, such as weaving defects, creases, wrinkles	☒ Acceptable ☐ Unacceptable
Sieve opening appearance, Annex A1.1.2 Observation of oversized openings must be less than Column 6 (Table 1, Column 1 + Column 5)	☒ Acceptable ☐ Unacceptable

Remarks:	
Checked By: Kevin Koompin	Signature:
WAQTC NO. 22634	
PREVIOUS CHECK DATE: 2-2019	RE-CHECK DUE DATE: 1/31/2021

Worksheet 4

Wire Cloth Sieves Check Procedure

Check Procedure: ITD-D-11 Check Frequency: 12 months

Identification No.: 4819	Date: 1/31/2020
Manufacturer: Dual	Sieve size: #200 12" Round

General condition of sieve frame:	☒ Acceptable ☐ Unacceptable
General condition of sieve cloth, Annex A1.1.1 Observation of deviations, such as weaving defects, creases, wrinkles	☒ Acceptable ☐ Unacceptable
Sieve opening appearance, Annex A1.1.2 Observation of oversized openings must be less than Column 6 (Table 1, Column 1 + Column 5)	☒ Acceptable ☐ Unacceptable

Remarks:	
Checked By: Kevin Koompin	Signature: Kevin Koompin
WAQTC NO. 22634	
PREVIOUS CHECK DATE: 2-2019	RE-CHECK DUE DATE: 1/31/2021

G3 – Proctor Compaction Equipment

Worksheet 16

4" Moisture Density (Proctor) Mold Standardization Record

Standardization Procedure: ITD-D42 | Standardization Frequency: 12 months

Identification Number: 4830	Date Standardized: 2/5/2020
Manufacturer:	
Calibration Standard: Caliper No: 4890 Scale: 4992 Thermometer: 10588	**New Mold Tolerances:** Inside Diameter 101.19 to 102.01 Height 116.27 to 116.53 **Used Mold Tolerances:** Inside Diameter 100.99 to 102.21 Height 116.27 to 116.53

DIMENSIONAL DATA: ☑ As Found

	Inside Diameter - Top, in.	Inside Diameter - Bottom, in.	Inside Height - in.
Measurement #1	101.56	101.28	116.34
	(90°)	(90°)	(180°)
Measurement #2	101.32	101.34	116.22
AVERAGE	D_t= 101.44	D_b= ~~101.34~~ 101.31	H= 116.28

New Mold : ☐	Used Mold: ☑	
Mold Average Inside Diameter within tolerance :	☑ Yes	☐ No
Mold Average Inside Height within tolerance :	☑ Yes	☐ No
Calculated Volume of Mold: $V = \frac{B-C}{A}$	V= Volume of Mold, ft^3 75.9° A= Density of Water: 997.20 B= Mass of Water, Glass, and Mold: 5605.3 C= Mass of Glass and Mold: 4668.2	Volume of Mold: 0.0332
Disposition of Mold:	☑ Acceptable	☐ Not Acceptable

Remarks:	
Standardized By: J. Kofoed	Signature: [signature]
WAQTC NO. 23477	
PREVIOUS STANDARDIZATION DATE: 2/2019	RE-STANDARDIZATION DUE DATE: 2/2021

1/17

Worksheet 17

5.5 lb Manual Rammer Check Record

Check Procedure : ITD-D40

Check Frequency: 12 months

Identification Number: 4893	Date Checked: 3/12/2020	
Manufacturer:	Rammer: 5.5 Nominal Weight: yes Nominal Drop: yes	
Calibration Standards:	Caliper Number: 004890	Balance Number: 4992

DIMENSIONAL DATA: ☒ As Found ☐ As Adjusted

	Measurement #1	Measurement#2		ASTM REQUIREMENTS
Rammer Circular Face Diameter: mm	50.68	50.67		50.55 to 51.05 mm
Rammer Weight: grams	2490.8	2490.8		2486 to 2504 g
Rammer Height of Drop: mm	305	305		303 to 307 mm

Guide sleeve holes: min dia, 9.5 mm:				
TOP	#1 9.82	#2 9.78	#3 9.76	#4 9.79
BOTTOM	#1 9.84	#2 9.78	#3 9.60	#4 10.17
Guide sleeve holes: distance from end of sleeve: 18 to 20 mm				
TOP	#1 19.67	#2 19.15	#3 19.26	#4 19.55
BOTTOM	#1 19.52	#2 18.08	#3 18.15	#4 18.43

Disposition of Rammer: ☒ Acceptable ☐ Not Acceptable

Remarks:	
Checked By: Kevin Koompin	Signature: Kevin Koompin
WAQTC NO. 22634	
PREVIOUS CHECKED DATE: 2-2019	RE-CHECKED DUE DATE: 3/12/2021

1/17

Appendix H – Correlation Charts

H1 – Representative Values of Relative Density

Table 4-3 Representative Values of Relative Density

Descriptive Condition	Relative Density, %	Typical Range of Unit Weight and Density		
		pcf	kN/m^3	Mg/m^3
Loose	<35	<90	<14	<1.4
Medium dense	35–65	90–110	14–17	1.4–1.7
Dense	65–85	110–130	17–20	1.7–2.0
Very dense	>85	>130	>20	>2.0

H2 – Modulus of Elasticity and Poisson's Ratio Values

Table 14-1 Range of Values: Modulus of Elasticity and Poisson's Ratio

Soil Type	Modulus of Elasticity, E (ksf)	Modulus of Elasticity, E (kN/m²)
Sand, loose	200–500	9,000–25,000
Sand, dense	1,000–1,700	45,000–80,000
Sand, silty	150–450	7,000–21,000
Sand and gravel, loose	1,000–3,000	45,000–145,000
Sand and gravel, dense	2,000–4,000	90,000–180,000
Silt	50–400	2,400–20,000
Loess	300–1,100	15,000–50,000
Clay, soft	10–100	500–5,000
Clay, medium	100–200	4,000–10,000
Clay, firm	150–400	7,000–20,000
Clay, sandy	550–850	25,000–40,000

Soil Type	Poisson's Ratio, ν
Sand, loose	0.10–0.30
Sand, dense	0.30–0.40
Silt	0.30–0.40
Loess	0.20–0.40
Clay, saturated	0.40–0.50
Clay, partially saturated	0.30–0.40
Clay, with sand and silt	0.20–0.40

Note: Values for Poisson's ratio lie within a narrow range and for analytical studies are usually estimated. The modulus of elasticity varies widely, being affected by stress history, water content, density, and grain–size distributions; with a given soil, values will vary according to the applied load range.

Appendix I – Experimental Test Results

I1 – Test No. 1 CIP Model

Test No. 1 - Pea Gravel CIP Model

TIMESTAMP	Load	Actuator	TCY2 (Corrected)	TCY1 (Corrected)	TCY3 (Corrected)	LS1
TS	lbs	in	in	in	in	in
53:27.8	141.5554	-0.0258379	-0.000003502	-0.00000757	-0.00009336	-0.003443778
54:16.8	249.4006	-0.03812313	-0.000124306	-0.00001127	-0.00021152	-0.003608376
54:57.8	369.7825	-0.05633259	-0.000306159	-0.00004321	-0.00041993	-0.00362885
57:49.8	557.7181	-0.0755558	-0.000538372	-0.003030837	-1.19E-07	-0.003030837
04:58.6	700.0614	-0.1112213	-0.000644758	-0.00064921	-0.00066911	-0.006111681
06:20.6	832.6656	-0.1303988	-0.000782818	-0.00077242	-0.00067914	-0.005530804
10/5/2020 11:07	927.3735	-0.1505594	-0.001026452	-0.00096333	-0.00077048	-0.004972309
10:18.2	1079.57	-0.1702948	-0.001326501	-0.00120670	-0.00098717	-0.008813322
11:49.6	1164.846	-0.1746426	-0.001447141	-0.00132328	-0.00113636	-0.008709222
12:41.4	1392.834	-0.2038727	-0.001794890	-0.00156242	-0.00146242	-0.008800149
13:48.4	1558.308	-0.2222204	-0.002188794	-0.00191927	-0.00180596	-0.009473503
14:55.2	1742.932	-0.2404184	-0.002499633	-0.00215221	-0.00209694	-0.0103634
16:21.6	1839.18	-0.2602339	-0.002786852	-0.00233084	-0.00240569	-0.01115119
10/5/2020 11:17	2075.886	-0.2786598	-0.003092103	-0.00254422	-0.00263833	-0.0127399
19:12.6	2179.706	-0.2953091	-0.003413908	-0.00282759	-0.00297417	-0.01366124
20:55.2	2350.513	-0.3148661	-0.003770791	-0.00310975	-0.00334151	-0.01486996
21:49.2	2551.018	-0.3319101	-0.004070662	-0.00332212	-0.00360619	-0.01631045
24:11.2	2606.676	-0.34305	-0.004242636	-0.00331354	-0.00407010	-0.01734486
26:50.8	2630.479	-0.3892164	-0.004231817	-0.003336306	-0.005209074	-0.01820156
27:53.6	2789.15	-0.4054632	-0.004539586	-0.003369208	-0.005599874	-0.01868033
30:01.6	2913.927	-0.4246645	-0.004957131	-0.00358152	-0.006286824	-0.01920396
31:37.6	3075.925	-0.4454088	-0.005319617	-0.003778871	-0.006852034	-0.02024916
34:38.4	3311.829	-0.4754591	-0.005847431	-0.004115339	-0.007382484	-0.02246973
35:44.4	3480.192	-0.499651	-0.006145752	-0.004420813	-0.007691884	-0.02396026
38:19.8	3660.472	-0.5264635	-0.006448544	-0.02566418	0.000158787	-0.02566418
38:38.2	3672.782	-0.5405951	-0.006662659	-0.004819985	-0.008455694	-0.02707994
39:39.2	3818.953	-0.5529127	-0.006806738	-0.02779961	0.000147581	-0.02779961
45:00.8	3931.221	-0.6165171	-0.007329739	-0.005288243	-0.009336744	-0.03153041
10/5/2020 11:47	4191.262	-0.6243439	-0.007636524	-0.03212494	0.000107884	-0.03212494
49:26.2	4219.01	-0.6826696	-0.007905982	-0.00567013	-0.010060164	-0.03514022
50:57.8	4259.198	-0.7178659	-0.00809852	-0.005839824	-0.010275634	-0.03684354

Test No. 1 - Pea Gravel CIP Model

TIMESTAMP	LS2	TSX	TNX	TEZ	TWZ	WIX	EIX
TS	in	in	in	in	in	in	in
53:27.8	-1.07E-06	-0.000115037	9.66E-06	1.78E-05	-6.68E-06	-2.09E-05	3.46E-06
54:16.8	-2.68E-07	-0.000153542	1.70E-05	1.35E-05	-5.25E-06	3.93E-06	-4.65E-06
54:57.8	6.74E-06	-4.60E-05	3.70E-06	1.61E-05	1.31E-06	-9.54E-07	2.03E-06
57:49.8	-4.92E-06	-1.19E-07	-4.89E-06	2.26E-06	-1.34E-05	-1.22E-05	5.36E-06
04:58.6	-5.94E-05	8.11E-06	-1.07E-05	1.19E-06	1.79E-06	-0.01950634	-1.25E-05
06:20.6	-6.92E-05	1.79E-06	4.53E-06	2.15E-06	3.46E-06	-0.0194664	1.19E-07
10/5/2020 11:07	-5.77E-05	5.48E-06	-1.30E-05	-7.87E-06	5.96E-06	-0.01947451	-9.66E-06
10:18.2	-6.49E-05	4.74E-05	1.31E-05	-2.50E-06	-2.86E-06	0.2602279	4.17E-06
11:49.6	-7.51E-05	1.07E-06	-1.79E-06	3.93E-06	-5.84E-06	0.2602348	8.34E-06
12:41.4	-6.58E-05	-3.19E-05	1.08E-05	-3.58E-07	1.66E-05	0.260213	9.32E-05
13:48.4	-7.02E-05	-6.70E-05	5.72E-06	-2.26E-06	-1.51E-05	0.2602206	0.000185847
14:55.2	-0.000204593	-3.09E-05	1.23E-05	1.67E-06	-4.41E-06	0.2602303	0.000257134
16:21.6	-0.000549197	2.48E-05	-2.16E-05	3.22E-06	2.98E-06	0.260231	0.000281096
10/5/2020 11:17	-0.001257747	5.11E-05	-2.59E-05	-1.38E-05	-2.62E-06	0.2602755	0.000331163
19:12.6	-0.001430452	5.69E-05	6.91E-06	1.07E-06	1.55E-06	0.2604003	0.00041461
20:55.2	-0.001954883	7.19E-05	-1.43E-06	-1.29E-05	-8.70E-06	0.2605329	0.000453353
21:49.2	-0.002695441	7.64E-05	9.54E-06	-5.13E-06	7.39E-06	0.2606102	0.000516057
24:11.2	-0.003379673	8.49E-05	-5.60E-06	1.31E-06	8.46E-06	0.2620283	0.000592351
26:50.8	-0.003522038	6.54E-05	-3.22E-06	2.86E-06	9.42E-06	0.2644919	0.002558947
27:53.6	-0.003525048	2.54E-05	7.39E-06	5.72E-06	9.18E-06	0.2644845	0.002624273
30:01.6	-0.00351879	0.000109315	-7.51E-06	-6.20E-06	-4.29E-06	0.2645483	0.002732396
31:37.6	-0.003642291	0.000142574	1.96E-05	-5.96E-06	1.01E-05	0.2647332	0.002839208
34:38.4	-0.004654408	0.000144482	-2.26E-06	1.54E-05	-6.56E-06	0.2649696	0.003008723
35:44.4	-0.005512089	0.00016427	-8.58E-06	-7.15E-06	-9.54E-06	0.2651249	0.003022909
38:19.8	-0.00647226	0.000158787	-1.59E-05	-1.35E-05	-1.17E-05	0.265314	0.003834248
38:38.2	-0.007105708	0.000142336	-3.05E-05	-1.19E-07	-1.31E-06	0.2654077	0.003813863
39:39.2	-0.007522732	0.000147581	5.60E-06	1.17E-05	-4.65E-06	0.2655014	0.003825784
45:00.8	-0.009425581	0.00013423	7.75E-06	2.40E-05	-5.01E-06	0.2658032	0.003842235
10/5/2020 11:47	-0.009435594	0.000107884	-5.84E-06	-1.43E-06	-5.36E-06	0.2659454	0.003831506
49:26.2	-0.01091617	0.000115275	-1.08E-05	-1.61E-05	2.26E-06	0.2661248	0.003827929
50:57.8	-0.01178247	0.000123382	-8.34E-06	-1.51E-05	-5.96E-06	0.2662468	0.003851771

Test No. 1 - Pea Gravel CIP Model

TIMESTAMP	WOX	EOX	SOZ	NOZ	TBSY	TBNY	BEAM
TS	in	in	in	in	in	in	in
53:27.8	-1.55E-06	-7.81E-06	7.30E-06	7.72E-06	3.22E-06	1.04E-05	-1.89E-05
54:16.8	2.59E-05	8.64E-06	2.55E-06	5.69E-06	-7.36E-06	-4.59E-06	-0.000236273
54:57.8	3.70E-06	3.52E-06	-3.67E-06	-1.19E-07	-5.93E-06	-7.45E-06	-0.000279039
57:49.8	-1.50E-05	-8.58E-06	3.11E-06	5.81E-06	-1.04E-05	1.58E-06	-0.000487
04:58.6	6.32E-06	-1.43E-06	-1.39E-05	-1.22E-05	-2.80E-06	-1.07E-05	-0.000802428
06:20.6	-2.01E-05	-1.36E-05	4.26E-06	-1.03E-05	-3.52E-06	4.71E-06	-0.002069384
10/5/2020 11:07	4.77E-07	3.52E-06	4.77E-07	-8.14E-06	-4.44E-06	5.60E-06	-0.001160681
10:18.2	-3.44E-05	4.17E-07	6.32E-06	-6.14E-06	-1.07E-06	-9.54E-07	-0.000772834
11:49.6	-1.05E-05	-5.72E-06	-3.55E-06	-1.24E-05	-1.98E-05	9.45E-06	-0.001922607
12:41.4	1.68E-05	5.01E-06	-3.80E-06	-7.87E-06	1.55E-06	6.79E-06	-0.001036108
13:48.4	6.14E-06	-1.19E-07	-1.31E-05	-1.85E-06	-1.50E-05	3.25E-06	-0.002938479
14:55.2	-6.26E-06	4.71E-06	6.02E-06	-1.33E-05	2.32E-06	7.45E-07	-0.003178656
16:21.6	-9.48E-06	6.62E-06	-1.67E-05	-1.17E-05	-2.15E-06	1.55E-06	-0.003485829
10/5/2020 11:17	1.92E-05	6.20E-06	-5.62E-06	-5.48E-06	-2.56E-06	1.34E-06	-0.004973859
19:12.6	-1.25E-06	3.70E-06	-0.000272572	1.70E-06	1.34E-06	1.08E-05	-0.004654765
20:55.2	-1.45E-05	-1.07E-06	-0.000290275	-1.71E-05	-1.16E-05	7.30E-06	-0.004886329
21:49.2	-2.46E-05	-2.92E-06	-0.000272587	-6.65E-06	1.43E-05	1.48E-05	-0.006775856
24:11.2	3.56E-05	2.15E-05	-0.000520587	-6.20E-06	-3.55E-06	-1.70E-06	-0.006954044
26:50.8	-0.00454253	0.002079546	-0.003077492	0.000306934	0.001081944	3.46E-06	-0.006786555
27:53.6	-0.004670203	0.002070963	-0.003073752	0.000314027	0.001078933	-1.20E-05	-0.006478727
30:01.6	-0.004871964	0.002078593	-0.003394336	0.000342935	0.001087934	3.73E-06	-0.006936014
31:37.6	-0.005176365	0.002152205	-0.003523052	0.000507861	0.001103491	-1.52E-06	-0.006628782
34:38.4	-0.005133033	0.002172589	-0.003669307	0.000521004	0.001129538	3.58E-07	-0.007945538
35:44.4	-0.005143881	0.002212822	-0.003785312	0.000686616	0.001124173	-6.44E-06	-0.008838713
38:19.8	-0.005158067	0.002252758	-0.003985077	0.000747442	0.001198351	-0.000135124	-0.009688169
38:38.2	-0.005252361	0.002248704	-0.004027829	0.000792265	0.001185924	-0.000142634	-0.01030403
39:39.2	-0.005371332	0.002253652	-0.004023895	0.000810117	0.00118345	-0.000133872	-0.01040208
45:00.8	-0.005533993	0.002341151	-0.004327342	0.000959724	0.001589596	-0.000293762	-0.01058346
10/5/2020 11:47	-0.00554657	0.002316654	-0.004323527	0.000958741	0.00158149	-0.0003272	-0.01018977
49:26.2	-0.005636215	0.002336621	-0.004548162	0.001012117	0.00177896	-0.000411093	-0.01117176
50:57.8	-0.005725801	0.002341509	-0.004574418	0.001056403	0.001844525	-0.000417233	-0.01192042

I2 – Test No. 2 CIP Model

Test No. 2 - 3/4-inch Base CIP Model

TIMESTAMP	RECORD	Load	Actuator Corrected	TCY2	TCY1	TCY3	LS1
TS	RN	lbs	in	in	in	in	in
26:28.4	153857	680.9325	-0.02490997	-1.03E-05	-0.000266433	1.97E-06	7.36E-06
27:07.6	154053	876.2721	-0.03899479	-0.000252068	-0.00039798	-8.72E-06	7.30E-06
31:52.6	155478	1165.721	-0.06012249	-0.000766903	-0.000768364	-0.000528306	-0.00034982
33:18.6	155908	1332.059	-0.07789135	-0.001194268	-0.001077771	-0.000909045	-0.001299173
37:09.2	157061	1506.584	-0.0936985	-0.00156346	-0.001349509	-0.001252249	-0.001829833
42:56.6	158798	1788.724	-0.1135912	-0.002012327	-0.001743197	-0.001803711	-0.0026097
45:56.6	159698	2184.763	-0.1476841	-0.002637744	-0.002330244	-0.002420813	-0.004763663
49:55.2	160891	2323.32	-0.166707	-0.002999663	-0.002642989	-0.002763048	-0.006039351
52:30.6	161668	2428.271	-0.1874914	-0.003292263	-0.002919436	-0.003034785	-0.007238925
55:05.4	162442	2807.06	-0.2236357	-0.004020423	-0.003504753	-0.003715813	-0.009857535
56:24.6	162838	3027.597	-0.2422123	-0.004184827	-0.00366658	-0.003886506	-0.0111669
59:10.4	163667	3161.672	-0.2579708	-0.004542992	-0.003919959	-0.004194856	-0.01207274
02:20.4	164617	3255.763	-0.2829046	-0.004784971	-0.004100502	-0.004427776	-0.01340196
10/6/2020 11:06	165755	3675.705	-0.3087673	-0.005609646	-0.004685402	-0.005201772	-0.0159207
08:21.2	166421	3973.196	-0.3359919	-0.006006598	-0.005034506	-0.005602896	-0.01766881
10:40.4	167117	4139.938	-0.3733921	-0.0064082	-0.005401254	-0.006018713	-0.01970145
10/6/2020 11:17	169055	4366.267	-0.4169397	-0.00683865	-0.005720735	-0.006466985	-0.02219114
18:28.2	169456	4466.944	-0.4530611	-0.007211626	-0.006083786	-0.006812021	-0.02442589
10/6/2020 11:21	170300	4593.72	-0.4901695	-0.007533535	-0.00634551	-0.007136881	-0.02630889
22:29.4	170662	4709.535	-0.5232935	-0.007805616	-0.006591976	-0.007375151	-0.02798021
23:43.8	171034	4858.424	-0.5551929	-0.008026481	-0.006781399	-0.007581666	-0.02913088
10/6/2020 11:25	171470	4906.222	-0.5983772	-0.008320019	-0.006968677	-0.007890493	-0.03097627
10/6/2020 11:26	171995	4936.486	-0.640893	-0.008565769	-0.007165909	-0.008131936	-0.03270105
28:22.2	172426	5105.884	-0.6703854	-0.008751854	-0.007328749	-0.008279786	-0.03341067
30:59.4	173212	5064.466	-0.7083921	-0.008991763	-0.007497132	-0.008441851	-0.03461099
32:26.8	173649	5191.196	-0.7470474	-0.009207293	-0.007712662	-0.008659154	-0.03623646
34:13.6	174183	5284.018	-0.7777233	-0.009332687	-0.007849872	-0.008731693	-0.03679705
35:19.4	174512	5335.7	-0.8155079	-0.009394363	-0.007967114	-0.008839875	-0.03789437
36:46.8	174949	5407.466	-0.8559418	-0.009600937	-0.008125067	-0.008976862	-0.03905275
10/6/2020 11:38	175345	5402.977	-0.8975868	-0.009811714	-0.008255422	-0.009223014	-0.04010656
39:26.4	175747	5456.274	-0.9310131	-0.009863943	-0.008303046	-0.009242281	-0.04066402
40:14.8	175989	5503.185	-0.9738789	-0.01004119	-0.008484483	-0.009390742	-0.04183573

Test No. 2 - 3/4-inch Base CIP Model

TIMESTAMP	LS2	TSX	TNX	TEZ	TWZ	WIX	EIX
TS	in	in	in	in	in	in	in
26:28.4	-6.79E-06	1.55E-05	2.17E-05	7.63E-06	1.17E-05	2.50E-05	2.49E-05
27:07.6	-9.33E-06	-5.36E-06	3.22E-06	-5.60E-06	-4.77E-06	1.14E-05	1.26E-05
31:52.6	-0.000131339	3.83E-05	-1.31E-06	-1.03E-05	-2.86E-06	-8.11E-06	7.87E-06
33:18.6	-0.000798494	2.00E-05	1.19E-06	-7.15E-06	2.50E-06	6.56E-06	4.77E-06
37:09.2	-0.001130939	5.70E-05	8.23E-06	4.17E-06	7.75E-06	0.001089454	8.82E-06
42:56.6	-0.001571119	6.59E-05	3.70E-06	5.72E-06	8.94E-06	0.001060843	2.17E-05
45:56.6	-0.003035188	8.92E-05	2.38E-06	-2.62E-06	-2.26E-06	0.001050711	0.000195265
49:55.2	-0.003824055	0.000103116	5.96E-06	1.51E-05	9.66E-06	0.001076221	0.000297308
52:30.6	-0.004592001	7.30E-05	-1.19E-05	2.38E-07	-2.50E-06	0.03905559	0.000377417
55:05.4	-0.00615564	8.57E-05	-2.15E-06	5.60E-06	2.86E-06	0.03907824	0.000547051
56:24.6	-0.006983578	9.72E-05	6.79E-06	-2.98E-06	2.03E-05	0.03908026	0.000586987
59:10.4	-0.007542014	8.93E-05	3.58E-06	0	-1.01E-05	0.03907585	0.000651717
02:20.4	-0.008626372	0.000120759	3.81E-06	1.43E-06	1.24E-05	0.03916585	0.000714779
10/6/2020 11:06	-0.009952277	0.000119567	-2.26E-06	1.05E-05	5.48E-06	0.03945291	0.000869632
08:21.2	-0.01100057	0.000155211	1.55E-06	8.82E-06	8.23E-06	0.03964365	0.000951052
10:40.4	-0.01234296	0.00014472	-8.23E-06	1.23E-05	1.20E-05	0.03981435	0.001037836
10/6/2020 11:17	-0.01378495	0.000172138	-4.89E-06	-2.62E-06	2.50E-06	0.2095034	0.001091719
18:28.2	-0.01515684	0.000163078	5.96E-07	1.23E-05	1.42E-05	0.2096341	0.001201034
10/6/2020 11:21	-0.01635486	0.000148773	-1.07E-05	1.19E-07	3.93E-06	0.2097561	0.001267195
22:29.4	-0.01739898	0.000139594	2.26E-06	1.85E-05	1.17E-05	0.2098446	0.001320958
23:43.8	-0.01816046	0.000120759	-1.45E-05	-1.79E-06	-2.03E-06	0.2099147	0.001310706
10/6/2020 11:25	-0.01929298	0.000137925	9.54E-06	4.89E-06	8.34E-06	0.2100303	0.001406431
10/6/2020 11:26	-0.02027965	0.00013864	-7.87E-06	-6.08E-06	-6.32E-06	0.2101707	0.001460075
28:22.2	-0.02073768	0.000124812	-4.17E-06	-1.87E-05	-7.27E-06	0.2102348	0.001460552
30:59.4	-0.02156758	0.000169754	6.44E-06	3.58E-07	-7.15E-07	0.210323	0.001527667
32:26.8	-0.0224961	0.000169873	1.00E-05	1.31E-05	1.14E-05	0.2103994	0.001609445
34:13.6	-0.02296555	0.000172496	-2.38E-06	7.39E-06	9.54E-07	0.2104264	0.001611352
35:19.4	-0.02364388	0.000168443	9.30E-06	9.54E-07	1.99E-05	0.2105069	0.001626968
36:46.8	-0.02436823	0.000180721	4.77E-06	-7.03E-06	-7.39E-06	0.2105526	0.001670837
10/6/2020 11:38	-0.02511027	0.000198245	9.89E-06	-9.06E-06	5.48E-06	0.2106447	0.001714945
39:26.4	-0.02555996	0.000208736	1.55E-06	-2.22E-05	7.51E-06	0.2106615	0.001764536
40:14.8	-0.02609953	0.000188351	1.67E-06	1.60E-05	-7.51E-06	0.4886388	0.001814008

Test No. 2 - 3/4-inch Base CIP Model

TIMESTAMP	WOX	EOX	SOZ	NOZ	TBSY	TBNY	BEAM
TS	in	in	in	in	in	in	in
26:28.4	-2.18E-05	2.03E-06	1.61E-05	4.92E-06	-5.07E-06	9.51E-06	-0.002121061
27:07.6	-2.43E-05	-5.42E-06	1.41E-05	-3.31E-06	-8.70E-06	4.53E-06	-0.002148449
31:52.6	-4.63E-05	1.76E-05	5.90E-06	-1.49E-06	1.40E-06	1.28E-05	-0.002677202
33:18.6	-1.82E-05	8.40E-06	1.89E-06	5.30E-06	8.31E-06	1.38E-05	-0.003445655
37:09.2	-8.45E-05	1.90E-05	-2.71E-06	-8.17E-06	-4.44E-06	2.29E-06	-0.004172057
42:56.6	-8.18E-05	1.16E-05	5.66E-07	3.49E-06	2.11E-05	4.08E-06	-0.004472315
45:56.6	-0.000159085	4.17E-06	9.09E-07	1.25E-05	4.07E-05	3.81E-06	-0.005357623
49:55.2	-0.000356197	7.63E-06	-1.60E-05	1.40E-05	3.99E-06	1.22E-05	-0.005881578
52:30.6	-0.000374854	4.65E-06	5.08E-06	2.71E-06	2.01E-05	2.21E-06	-0.006195396
55:05.4	-0.000762463	6.74E-06	-6.26E-07	5.28E-06	1.28E-05	1.16E-06	-0.00712052
56:24.6	-0.000809193	-4.05E-06	-4.63E-05	4.86E-06	-1.49E-07	1.19E-06	-0.007714659
59:10.4	-0.000876784	4.35E-06	-0.000111327	9.95E-06	1.79E-06	-7.15E-06	-0.007288247
02:20.4	-0.000941753	1.20E-05	-0.000207081	1.24E-05	-9.03E-06	1.34E-06	-0.007410765
10/6/2020 11:06	-0.001223385	1.19E-05	-0.000396386	4.05E-06	1.30E-05	2.26E-06	-0.00835982
08:21.2	-0.001356423	1.75E-05	-0.000432119	1.52E-05	-3.61E-06	-2.06E-06	-0.008484691
10:40.4	-0.001364112	2.46E-05	-0.000491247	2.31E-05	7.99E-06	-6.35E-06	-0.01018724
10/6/2020 11:17	-0.001437366	5.01E-06	-0.000668496	1.64E-05	2.78E-05	-1.49E-06	-0.01037657
18:28.2	-0.00156045	2.09E-06	-0.000772521	4.65E-06	2.60E-05	5.81E-06	-0.0106183
10/6/2020 11:21	-0.001541495	1.55E-06	-0.000885397	6.74E-06	0.000102311	-5.19E-06	-0.01187116
22:29.4	-0.001609266	1.01E-05	-0.000985444	2.08E-05	6.70E-05	9.60E-06	-0.01197371
23:43.8	-0.001736462	5.36E-07	-0.001003534	1.18E-05	8.04E-05	2.44E-06	-0.01280689
10/6/2020 11:25	-0.001761973	1.07E-05	-0.001064718	6.23E-06	0.000116974	5.96E-08	-0.01258051
10/6/2020 11:26	-0.001765966	1.47E-05	-0.001171187	4.05E-06	0.000104696	1.01E-05	-0.01367092
28:22.2	-0.001830697	1.20E-05	-0.001213953	2.04E-05	0.000128001	9.12E-06	-0.01385224
30:59.4	-0.001844943	2.06E-05	-0.001256511	1.76E-05	0.000176638	5.07E-07	-0.01366651
32:26.8	-0.001859009	1.26E-05	-0.001351655	1.68E-05	0.000206888	-1.25E-06	-0.01462957
34:13.6	-0.001937628	2.14E-05	-0.001568601	1.87E-05	0.000249326	7.15E-07	-0.01454595
35:19.4	-0.0019207	7.69E-06	-0.001547277	1.48E-05	0.000276595	-7.00E-06	-0.01518044
36:46.8	-0.002040327	9.12E-06	-0.001525447	1.80E-05	0.000344783	-4.44E-06	-0.01541862
10/6/2020 11:38	-0.002090454	2.19E-05	-0.001546487	1.16E-05	0.000393868	-1.54E-05	-0.01533377
39:26.4	-0.002010524	1.69E-05	-0.001570731	2.05E-05	0.00045532	-2.71E-06	-0.01563489
40:14.8	-0.002088249	6.56E-07	-0.001562208	1.25E-05	0.000475615	-7.06E-06	-0.0162783

I3 – Test No. 3 CIP Model

Test No. 3 - Concrete Trapezoid with Backfill CIP Model

TIMESTAMP	RECORD	Load	Actuator	TCY2	TCY1	TCY3	LS1
TS	RN	lbs	in	in	in	in	in
		Smp	Smp	Smp	Smp	Smp	Smp
10/9/2020 12:34	205879	1278.91	0.03419018	-0.000115335	-0.000852406	-1.18E-05	-8.67E-06
35:37.4	206156	3058.134	0.04769039	-0.002484895	-0.003009379	-0.002142504	0.000455856
42:55.6	208347	6022.808	0.07858086	-0.007246114	-0.007159531	-0.006986275	0.001737565
45:52.8	209233	7459.23	0.1027079	-0.01042498	-0.009775817	-0.01022489	0.003021091
47:21.4	209676	8958.522	0.1211376	-0.01367862	-0.01241708	-0.01368994	0.004088879
49:04.8	210193	10262.81	0.1406898	-0.01656014	-0.01482219	-0.01675677	0.005368114
50:44.6	210692	11642.52	0.1575766	-0.01964063	-0.01732558	-0.02001669	0.006254852
52:24.4	211191	12283.87	0.1757765	-0.02187441	-0.01908642	-0.02235842	0.007259071
54:36.6	211852	13087.63	0.1934328	-0.02326741	-0.02009887	-0.02403203	0.00812161
56:57.4	212556	14077.34	0.211874	-0.0256215	-0.02209759	-0.02674611	0.008579165
01:09.8	213818	17091.53	0.2469759	-0.03145502	-0.02655125	-0.03315371	0.009530067
03:58.4	214661	18276.27	0.2638483	-0.03430168	-0.02871376	-0.03645925	0.01041606
06:48.2	215510	18643.17	0.2855091	-0.03634129	-0.03009725	-0.03867833	0.01125202
08:14.4	215941	19259.28	0.2955904	-0.0373117	-0.03087217	-0.03969347	0.0112572

Test No. 3 - Concrete Trapezoid with Backfill CIP Model

TIMESTAMP	LS2	TSX	TNX	TEZ	TWZ	WIX	EIX
TS	in	in	in	in	in	in	in
	Smp	Smp	Smp	Smp	Smp	Smp	Smp
10/9/2020 12:34	-1.25E-05	5.72E-06	3.22E-06	7.27E-06	-7.39E-06	9.00E-06	1.91E-06
35:37.4	-4.49E-05	-1.14E-05	-3.58E-06	4.41E-06	-2.62E-06	0.000343561	0.000335574
42:55.6	-2.39E-05	5.46E-05	1.29E-05	-1.32E-05	-6.44E-06	0.002792537	0.001475692
45:52.8	0.00014925	2.52E-05	1.55E-06	1.08E-05	-4.89E-06	0.003984153	0.002329946
47:21.4	0.00065124	1.31E-05	3.58E-07	4.89E-06	8.34E-07	0.00530225	0.003346682
49:04.8	0.00129956	2.62E-06	2.86E-06	2.17E-05	2.26E-06	0.006406367	0.004200101
50:44.6	0.001664042	-2.15E-06	1.47E-05	0	8.94E-06	0.216681	0.005168796
52:24.4	0.002230078	1.31E-05	2.15E-06	3.10E-06	-7.27E-06	0.2174306	0.005819678
54:36.6	0.002697855	7.10E-05	2.50E-06	5.25E-06	-4.77E-06	0.218079	0.006311059
56:57.4	0.002802402	6.53E-05	1.91E-06	-1.79E-06	1.39E-05	0.2191021	0.007178187
01:09.8	0.003410816	-7.15E-06	1.37E-05	1.01E-05	1.67E-06	0.444663	0.009210944
03:58.4	0.003912687	-2.66E-05	1.60E-05	-2.38E-06	2.38E-07	0.4457005	0.01024747
06:48.2	0.004688621	-2.80E-05	1.42E-05	7.51E-06	-1.07E-06	0.4464949	0.01090288
08:14.4	0.004690647	-1.35E-05	1.79E-05	1.47E-05	-7.15E-07	0.4469876	0.01134813

Test No. 3 - Concrete Trapezoid with Backfill CIP Model

TIMESTAMP	WOX	EOX	SOZ	NOZ	TBSY	TBNY	BEAM
TS	in	in	in	in	in	in	in
	Smp	Smp	Smp	Smp	Smp	Smp	Smp
10/9/2020 12:34	3.46E-06	-4.05E-06	1.11E-05	-8.67E-06	-7.21E-06	1.07E-05	-0.001158297
35:37.4	2.82E-05	-8.11E-06	1.17E-05	5.01E-06	-5.39E-06	1.47E-05	-0.004969507
42:55.6	4.89E-05	-1.85E-06	-0.000222445	-7.27E-06	0.00026989	3.58E-05	-0.01503983
45:52.8	-2.55E-05	4.17E-07	-0.000627711	-0.000478804	0.000597298	0.000240088	-0.02783555
47:21.4	-0.00052917	7.03E-06	-0.000984132	-0.000745833	0.000785112	0.000511855	-0.03480875
49:04.8	-0.001273692	6.62E-06	-0.001202032	-0.001233041	0.001187354	0.000781894	-0.04503942
50:44.6	-0.001695156	-6.20E-06	-0.00147365	-0.001273364	0.001212329	0.000800222	-0.0542261
52:24.4	-0.002128422	1.04E-05	-0.001707107	-0.001411378	0.001262933	0.000988066	-0.06622532
54:36.6	-0.002386987	3.46E-06	-0.001842096	-0.001706272	0.001499593	0.001119554	-0.07961458
56:57.4	-0.002501309	1.15E-05	-0.002238989	-0.001732349	0.001498222	0.001134396	-0.09237027
01:09.8	-0.003516138	1.53E-05	-0.00312233	-0.001959562	0.001724541	0.001144052	-0.1114397
03:58.4	-0.004081488	0.000663221	-0.003360748	-0.002625465	0.002062947	0.001145869	-0.1220233
06:48.2	-0.004490137	0.001264632	-0.0038919	-0.002874643	0.002137452	0.001143217	-0.1391709
08:14.4	-0.004490793	0.001297832	-0.004173577	-0.002877712	0.002150416	0.001150757	-0.1469035

I4 – Test No. 4 CIP Model

Test No. 4 - Concrete Trapezoid Without Backfill CIP Model

TIMESTAMP	RECORD	Load	Actuator	TCY2 Corrected	TCY1 Corrected	TCY3 Corrected	LS1
TS	RN	lbs	in	in	in	in	in
14:09.4	240119	216.1506	0.01010799	-0.00000294	8.52346E-06	-0.000005427	2.22E-05
14:45.6	240300	2627.783	0.02997494	-0.00458027	-0.003660113	-0.003949424	0.000385761
16:50.2	240923	5421.788	0.04741096	-0.01008219	-0.008383065	-0.009341970	0.000490844
18:36.6	241455	8182.803	0.06493187	-0.01572801	-0.01304096	-0.014808510	0.000205874
21:35.6	242350	10851.02	0.08440781	-0.02194817	-0.01830667	-0.021078550	-0.001180232
29:04.4	244594	15536.4	0.1197128	-0.03399913	-0.02700216	-0.033163150	-0.005271018
33:34.2	245943	17727.61	0.1389627	-0.04282263	-0.034266325	-0.042935030	-0.009637415
38:17.6	247360	17622.7	0.1445045	-0.04790411	-0.038251045	-0.048922610	-0.01190227
40:34.4	248044	19469.79	0.1746101	-0.07038340	-0.055736245	-0.074745450	-0.009988368
43:56.8	249056	20412.7	0.1912231	-0.08260824	-0.065515285	-0.088996020	-0.009987772

Test No. 4 - Concrete Trapezoid Without Backfill CIP Model

TIMESTAMP	LS2	TSX	TNX	TEZ	TWZ	WIX	EIX
TS	in	in	in	in	in	in	in
14:09.4	-4.11E-06	8.34E-06	-3.34E-06	1.37E-05	7.15E-06	-2.98E-07	-1.41E-05
14:45.6	1.07E-05	-9.18E-06	9.18E-06	4.95E-05	7.39E-06	0.000511885	0.000229895
16:50.2	1.41E-05	2.15E-06	-1.62E-05	5.20E-05	-1.20E-05	0.002573788	0.002074778
18:36.6	0.000789583	2.83E-05	1.62E-05	5.20E-05	1.44E-05	0.004679263	0.003800273
21:35.6	0.003372848	0.000107884	8.46E-06	3.11E-05	8.34E-07	0.007267654	0.005818903
29:04.4	0.01147878	0.000691652	6.68E-06	0.000351906	-3.34E-06	0.05006725	0.01102537
33:34.2	0.01705885	0.000935555	2.15E-06	-3.59E-05	8.34E-07	0.05684423	0.02156597
38:17.6	0.02017629	0.000947952	-6.79E-06	-0.000106573	-1.19E-06	0.05772054	0.02984512
40:34.4	0.01732779	0.001430511	-1.81E-05	-0.002508163	-3.93E-06	0.09167963	0.03618699
43:56.8	0.01723504	0.001452565	-8.34E-06	-0.002449751	3.58E-07	0.1127105	0.03690594

Test No. 4 - Concrete Trapezoid Without Backfill CIP Model

TIMESTAMP	WOX	EOX	SOZ	NOZ	TBSY	TBNY	BEAM
TS	in	in	in	in	in	in	in
14:09.4	3.61E-06	-2.24E-06	-7.77E-06	-2.75E-06	1.46E-06	4.82E-06	-0.001265675
14:45.6	-1.06E-06	-8.13E-07	1.36E-07	-2.75E-06	1.46E-06	-7.62E-06	-0.00631386
16:50.2	6.97E-06	1.91E-06	3.63E-06	2.43E-06	4.31E-06	-1.95E-05	-0.01127243
18:36.6	-9.21E-07	1.52E-06	3.51E-06	-3.26E-06	3.80E-06	-3.22E-05	-0.01764107
21:35.6	6.20E-06	-6.12E-06	5.84E-06	1.53E-06	-3.59E-06	-2.90E-05	-0.02418587
29:04.4	1.36E-05	-3.01E-06	1.37E-07	-3.78E-06	-1.91E-06	-6.14E-05	-0.03931633
33:34.2	2.20E-05	4.37E-06	2.99E-06	-9.48E-06	-2.42E-06	-6.99E-05	-0.0445762
38:17.6	4.39E-05	-5.60E-06	2.60E-06	3.99E-06	-3.51E-07	-7.20E-05	-0.04617101
40:34.4	4.00E-05	1.19E-05	1.36E-07	3.61E-07	-1.91E-06	-7.29E-05	-0.04949507
43:56.8	4.09E-05	7.09E-06	5.84E-06	3.34E-06	-9.18E-08	-8.03E-05	-0.05230314

I5 – Test No. 5 CIP Model

Test No. 5 - Concrete Trapezoid Without Backfill to Failure CIP Model

TIMESTAMP	RECORD	Load	Actuator	TCY2	LS1	LS2
TS	RN	lbs	in	in	in	in
09:20.4	256674	-50.78882	0.01078796	-2.01E-06	-8.34E-06	2.32E-06
10:47.2	257108	711.0209	0.01764965	-0.001007684	1.06E-05	1.21E-05
12:12.4	257534	3293.489	0.03726864	-0.006585285	1.08E-05	1.45E-05
14:06.8	258106	5828.799	0.05359077	-0.01225951	-2.67E-05	0.000425994
17:29.4	259119	11092.71	0.08970928	-0.0243149	-0.000831485	0.00112766
19:15.2	259648	13922.21	0.1087446	-0.03097111	-0.002519369	0.003380656
22:32.8	260636	16633.67	0.1272526	-0.03821509	-0.003973603	0.004669249
24:30.2	261223	18090.75	0.1457357	-0.04966624	-0.008146584	0.007492483
26:10.8	261726	21044.02	0.163003	-0.05536754	-0.007926345	0.007657528
27:30.8	262126	21856.59	0.1820583	-0.07082094	-0.008691192	0.008797169
29:46.2	262803	22992.91	0.2035341	-0.08586301	-0.008678496	0.008100867
31:10.4	263224	26288.2	0.2497015	-0.1142378	-0.009234846	0.007846832
32:44.2	263693	27091.33	0.256587	-0.1176969	-0.009245753	0.007872343
34:18.2	264163	28145.75	0.2763348	-0.1318187	-0.009753883	0.008217335
36:16.8	264756	29630.46	0.3171606	-0.1661446	-0.01660126	0.01644737
36:36.2	264853	18177.12	0.3336573	-0.2536882	-0.01818854	0.01840043

I6 – Test No. 1 Hollow-Core Model

Test No. 1 - 3/4-inch Base Hollow-Core Model

TIMESTAMP	RECORD	Load	Actuator	TCY2	TCY1	TCY3	LS2
TS	RN	lbs	in	in	in	in	in
11/4/2020 12:52	306756	48.28003	0.000487328	1.01E-06	1.61E-05	-9.30E-06	-2.91E-06
53:27.4	307193	814.9254	0.05589199	-0.000798762	-1.54E-05	-0.00037992	2.14E-06
54:13.6	307424	1099.433	0.09352875	-0.001269639	-0.000365138	-0.00072217	3.56E-06
11/4/2020 12:55	307671	1240.386	0.1272459	-0.001480997	-0.000534654	-0.000807822	1.75E-06
57:05.6	308284	1334.018	0.1499138	-0.001615047	-0.000746965	-0.000825405	3.56E-06
58:36.4	308738	1448.842	0.2013922	-0.001838982	-0.000923753	-0.001008511	-1.62E-06
01:16.2	309537	1546.27	0.2662048	-0.002030671	-0.001185656	-0.001130044	8.10E-06
02:02.8	309770	1678.361	0.3008919	-0.002206028	-0.001380563	-0.001277149	-1.23E-06
04:37.2	310542	1805.302	0.3846378	-0.002584517	-0.001800537	-0.001573145	-3.30E-06
05:52.2	310917	1959.895	0.4761648	-0.002868831	-0.002144814	-0.001787424	-1.93E-07
11/4/2020 13:08	311746	2066.665	0.5491934	-0.003181458	-0.002498507	-0.002001643	-3.17E-06

Test No. 1 - 3/4-inch Base Hollow-Core Model

TIMESTAMP	TSX	TNX	TEZ	TWZ	WIX	EIX	WOX
TS	in	in	in	in	in	in	in
11/4/2020 12:52	0.005581379	-2.13E-05	7.93E-06	-2.15E-05	1.72E-05	1.00E-05	5.91E-05
53:27.4	0.01047564	9.54E-06	-3.93E-06	1.55E-06	-1.23E-05	-8.34E-07	-2.84E-05
54:13.6	0.01850164	-3.52E-06	1.43E-05	1.07E-06	1.18E-05	1.28E-05	2.49E-05
11/4/2020 12:55	0.02222419	-5.42E-06	-1.03E-05	6.20E-06	-1.23E-05	1.37E-05	-7.75E-06
57:05.6	0.01467764	2.68E-06	-3.22E-06	1.54E-05	-1.19E-07	4.09E-05	1.34E-05
58:36.4	0.007333398	1.10E-05	1.36E-05	-1.49E-05	1.18E-05	0.000107169	-1.55E-05
01:16.2	0.03598356	-1.85E-06	1.45E-05	6.91E-06	4.17E-06	-0.1117623	4.17E-06
02:02.8	0.0368135	1.85E-06	1.49E-06	2.50E-06	1.17E-05	-0.1117522	7.39E-06
04:37.2	0.03736031	-6.02E-06	6.02E-06	4.41E-06	1.37E-05	-0.1117517	2.28E-05
05:52.2	0.03732467	-1.31E-05	6.20E-06	-1.47E-05	0.000136018	-0.111742	8.65E-05
11/4/2020 13:08	0.03731048	1.31E-05	-7.45E-06	3.10E-06	0.000270486	-0.1117442	4.97E-05

Test No. 1 - 3/4-inch Base Hollow-Core Model

TIMESTAMP	EOX	SOZ	NOZ	TBSY	TBNY	BEAM
TS	in	in	in	in	in	in
11/4/2020 12:52	3.22E-06	-7.09E-06	7.20E-06	-1.83E-05	1.22E-05	0.000223488
53:27.4	-9.60E-06	2.09E-05	8.79E-07	4.92E-05	-2.92E-06	-0.001360387
54:13.6	2.68E-06	-4.54E-05	9.16E-06	-1.76E-05	-8.46E-06	-0.002725571
11/4/2020 12:55	5.78E-06	-5.14E-05	1.56E-07	-5.37E-05	-8.76E-06	-0.003400713
57:05.6	-3.46E-06	-0.000198185	-1.82E-06	6.38E-06	3.81E-06	-0.00333643
58:36.4	8.82E-06	-0.000444472	8.63E-06	-1.40E-05	-3.22E-06	-0.00353387
01:16.2	-2.03E-05	-0.000419021	-4.52E-06	8.40E-06	-1.07E-06	-0.003535151
02:02.8	-4.05E-06	-0.000447989	-1.51E-06	-4.53E-05	-8.82E-06	-0.003258079
04:37.2	-4.23E-06	-0.000661969	-2.97E-06	-2.49E-05	-5.54E-06	-0.003447056
05:52.2	-3.10E-06	-0.000638306	-2.35E-06	-7.15E-07	-2.32E-05	-0.00423938
11/4/2020 13:08	9.18E-06	-0.000879943	5.14E-06	-1.14E-05	-7.03E-06	-0.004525065

I7 – Test No. 2a Hollow-Core Model

Test No. 2a - Trapezoid with Backfill Hollow-Core Model

TIMESTAMP	RECORD	Load	Actuator	TCY2	TCY1	TCY3	LS2
TS	RN	lbs	in	in	in	in	in
31:34.8	335111	-4.089111	9.54E-07	-7.33E-06	9.89E-06	-3.58E-07	-4.64E-06
33:12.2	335598	1553.057	0.01642895	-0.002241373	-0.001868367	-0.001598895	4.81E-06
11/5/2020 10:36	336482	4143.442	0.03674221	-0.008633733	-0.008461118	-0.006162345	-5.55E-06
38:12.4	337099	6530.947	0.05541229	-0.01578075	-0.01647937	-0.01111799	-2.40E-07

Test No. 2a - Trapezoid with Backfill Hollow-Core Model

TIMESTAMP	TSX	TNX	TEZ	TWZ	WIX	EIX	WOX
TS	in	in	in	in	in	in	in
31:34.8	1.92E-05	3.58E-07	-1.40E-05	-1.79E-06	-7.99E-06	-2.03E-06	-4.05E-06
33:12.2	-0.000213981	1.14E-05	-1.35E-05	1.07E-05	-2.91E-05	5.25E-06	-1.47E-05
11/5/2020 10:36	0.00034368	5.25E-06	1.65E-05	-1.19E-05	0.001449406	0.000842691	1.23E-05
38:12.4	0.000275731	1.28E-05	-7.03E-06	6.44E-06	0.00333792	0.002015233	-0.000405669

Test No. 2a - Trapezoid with Backfill Hollow-Core Model

TIMESTAMP	EOX	SOZ	NOZ	TBSY	TBNY	BEAM
TS	in	in	in	in	in	in
31:34.8	1.47E-05	-4.29E-06	1.01E-05	-4.28E-05	1.88E-05	-1.20E-05
33:12.2	4.05E-06	-5.72E-06	-8.73E-06	1.97E-06	1.03E-05	-0.003542244
11/5/2020 10:36	-7.87E-06	3.78E-05	-8.05E-07	2.16E-05	2.32E-06	-0.009269655
38:12.4	-2.48E-05	-1.70E-05	-6.32E-06	0.000560045	2.24E-05	-0.01541451

I8 – Test No. 2b Hollow-Core Model

Test No. 2b - Trapezoid with Backfill Hollow-Core Model

TIMESTAMP	RECORD	Load	Actuator	TCY2	TCY1	TCY3	LS2
TS	RN	lbs	in	in	in	in	in
46:39.2	339633	-14.59448	0.02664089	7.47E-05	4.16E-05	5.60E-05	3.72E-07
47:00.8	339741	5907.345	0.08481312	-0.01294219	-0.01318574	-0.009070873	-4.29E-06
11/5/2020 10:49	340437	7823.081	0.1033363	-0.02095252	-0.02214134	-0.01422524	4.00E-06
50:51.8	340896	9061.949	0.1199989	-0.03036505	-0.03447568	-0.01992667	-5.59E-06
54:24.6	341960	10033.05	0.140214	-0.04396927	-0.05304325	-0.02821577	5.42E-06
11/5/2020 10:55	342342	11151.89	0.1556635	-0.05310553	-0.06578469	-0.03364229	2.83E-06
58:26.4	343169	12072.2	0.1767101	-0.06733918	-0.08602309	-0.04226464	1.67E-06
00:13.2	343703	12837.29	0.1922617	-0.07867014	-0.1023797	-0.04874182	1.54E-06
11/5/2020 11:01	344227	13509.98	0.2116613	-0.09357858	-0.1241031	-0.05693603	4.65E-06
11/5/2020 11:04	344857	14275.65	0.2300348	-0.1085297	-0.1463096	-0.06517869	-1.57E-06
11/5/2020 11:06	345617	14559.5	0.2406607	-0.116473	-0.1577824	-0.06938714	4.52E-06
09:52.2	346598	13706.06	0.2589636	-0.1382646	-0.1899171	-0.08110058	7.60E-07

Test No. 2b - Trapezoid with Backfill Hollow-Core Model

TIMESTAMP	TSX	TNX	TEZ	TWZ	WIX	EIX (Corrected)
TS	in	in	in	in	in	in
46:39.2	0.000221729	6.79E-06	1.25E-06	5.13E-06	-4.59E-06	0.000015974
47:00.8	-3.85E-05	1.69E-05	-4.17E-06	1.67E-05	0.002453923	0.001481414
11/5/2020 10:49	-3.40E-05	-3.34E-06	8.23E-06	-1.39E-05	0.004653156	0.002818227
50:51.8	-6.04E-05	3.04E-06	1.70E-05	1.69E-05	0.00685221	0.004172921
54:24.6	-0.0121299	0.000113487	-2.15E-06	5.48E-06	0.009890318	0.005112645
11/5/2020 10:55	0.004315972	0.00024277	1.62E-05	4.89E-06	0.01224643	0.006418225
58:26.4	0.008626819	0.000382006	5.48E-06	1.08E-05	0.01569247	0.008387205
00:13.2	0.008760214	0.000456154	2.29E-05	-5.25E-06	0.0182392	0.009797695
11/5/2020 11:01	0.008802295	0.000553608	8.76E-06	2.25E-05	0.02128661	0.011427285
11/5/2020 11:04	0.008705497	0.000652432	1.19E-06	1.91E-06	0.02488089	0.013198975
11/5/2020 11:06	0.003048897	0.000722408	-7.33E-06	3.93E-06	0.02666897	0.014354345
09:52.2	0.00350821	0.000807405	-2.92E-06	-0.001059294	0.02701229	0.014057515

Test No. 2b - Trapezoid with Backfill Hollow-Core Model

TIMESTAMP	WOX	EOX	SOZ	NOZ	TBSY	TBNY	BEAM
TS	in	in	in	in	in	in	in
46:39.2	-1.73E-05	5.84E-06	-2.26E-06	4.75E-06	1.90E-05	9.60E-06	0.000223309
47:00.8	-3.96E-05	-1.55E-05	-1.30E-05	-2.98E-07	2.44E-05	7.63E-06	-0.01314706
11/5/2020 10:49	-0.001204014	-3.71E-05	-1.85E-05	2.07E-06	0.000728488	7.21E-06	-0.01869476
50:51.8	-0.003402352	-4.97E-05	-0.00071758	3.31E-06	0.001491129	2.01E-05	-0.02299252
54:24.6	-0.005865812	-3.39E-05	-0.000888109	-1.39E-06	0.002132118	0.000157118	-0.02643469
11/5/2020 10:55	-0.007834196	-1.35E-05	-0.001047492	2.28E-06	0.002436519	0.000172794	-0.02896848
58:26.4	-0.009555697	-5.13E-05	-0.00176388	8.94E-07	0.002903223	0.00017643	-0.03169817
00:13.2	-0.01074159	-3.93E-05	-0.002225518	-1.12E-05	0.003122687	0.000156641	-0.03384319
11/5/2020 11:01	-0.01204133	-5.16E-05	-0.002852261	-1.71E-05	0.003228426	0.000166774	-0.03586751
11/5/2020 11:04	-0.01330447	-7.02E-05	-0.003715575	7.60E-07	0.003274977	0.000187874	-0.0371716
11/5/2020 11:06	-0.01383805	-5.69E-05	-0.004437864	-8.34E-07	0.003454804	0.000328541	-0.03824392
09:52.2	-0.01437736	-5.13E-05	-0.005215406	-1.04E-05	0.004066765	0.000308991	-0.03691679

I9 – Test No. 3 Hollow-Core Model

Test No. 3 - Trapezoid Without Backfill to Failure Hollow-Core Model						
TIMESTAMP	RECORD	Load	Actuator	TCY2	LS1	LS2
TS	RN	lbs	in	in	in	in
21:22.8	357609	8.937988	0.0733137	8.24E-05	2.89E-05	-5.08E-06
11/9/2020 15:22	358085	1940.909	0.0929718	-0.008519	3.63E-05	-3.14E-06
23:35.8	358274	3528.274	0.1137915	-0.019039	2.38E-05	3.60E-07
24:49.2	358641	3612.311	0.1207037	-0.02573	2.04E-05	-2.89E-08
26:18.2	359086	3205.451	0.145319	-0.053147	-1.82E-06	2.69E-06
28:29.2	359741	3326.699	0.1728783	-0.08063	-1.82E-06	2.04E-06
11/9/2020 15:29	359955	3636.753	0.2116508	-0.118973	-7.87E-06	1.14E-06
30:36.8	360379	3928.3	0.2466068	-0.15298	-7.86781E-06	-2.36057E-06
44144.64775	361021	3717.17	0.2886562	-0.197277	-7.86781E-06	-4.95098E-06
36:51.8	362254	3730.681	0.3314314	-0.237375	-7.67E-05	1.14E-06
37:29.2	362441	4251.761	0.3695965	-0.270227	-8.71E-05	-6.12E-06
38:12.4	362657	4671.391	0.4031086	-0.300294	-9.20E-05	-1.97E-06
44144.65214	362919	4613.595	0.4445181	-0.343003	-8.88705E-05	-3.00798E-06
44144.65353	363522	5157.496	0.4940567	-0.390612	0.0004659	-2.74842E-06
11/9/2020 15:41	363765	5531.385	0.5384798	-0.437038	0.000656575	-7.28E-06
44:39.6	364593	5663.027	0.5985651	-0.496376	0.004170716	-5.04E-05
47:37.2	365481	5249.955	0.6358328	-0.5367	0.005755931	-0.001830066
48:51.4	365852	4370.819	0.7172203	-0.621678	0.007250071	-0.00388967
50:26.6	366328	5354.8	0.7983742	-0.697398	0.008354038	-0.00467947

Appendix J – FEM Simulations

J1 – 2D Analysis Simulation CIP Model

FINITE ELEMENT ANALYSIS WITH ANSYS
CAST-IN-PLACE CULVERT 2D ANALISYS

Step-by-Step model:

1. Create a directory for the ANSYS files; for example, call it "ANSYS Model"
2. Start ANSYS
   a. Change directory: From Utility Menu (top menu) select *File*, *Change Directory*…
   b. Set Jobname to "CIP Culvert Analysis": From Utility Menu select, *File*, *Change Jobname*…
3. From ANSYS Main Menu (located on the left side of the screen), select *Preferences* …
   a. Select *Structural* → Click on *OK*
4. From ANSYS *Main Menu*, select *Preprocessor*
   a. *Element Type* → *Add/Edit/Delete*… →
      i. *Add*… → *Solid* → *Quad 4 Node 182* (also known as *Plane 182)* → for *Element T*
      1 → *OK* →
      ii. *Options*… → For *Element Behavior K3*, select *Plane Stress*, and no other changes ar
      necessary → *OK*
      iii. *Close* → Close *Element Type* submenu of the *Main Menu*
   b. *Material Properties* →
      i. *Material Models*… → *Structural* → *Linear* → *Elastic* → *Isotropic* → Enter value for EX: 5.35e6 → Enter value for PRXY: 0.2 → *OK*

Note: The concrete will have a modulus of elasticity of 5.35 x10^6 psi and Poisson's ratio of 0.2.

      ii. *Material* → *New Model* → Enter a 2 for material ID
      iii. *Material Models*… → *Structural* → *Linear* → *Elastic* → *Isotropic* → Enter value for EX: 5200 → Enter value for PRXY: 0.3 → *OK*

Note: The backfill soil (sand) will have a modulus of elasticity of 4,514 psi and Poisson's ratio of 0.3.

      iv. *Material* → *New Model* → Enter a 3 for material ID
      v. *Material Models*… → *Structural* → *Linear* → *Elastic* → *Isotropic* → Enter value for EX: 2080 → Enter value for PRXY: 0.35 → *OK*

Note: The top 12 inches of backfill soil (gravel) will have a modulus of elasticity of 11,600 psi and Poisson's ratio of 0.3.

      vi. *Material* → *New Model* → Enter a 4 for material ID
      vii. *Material Models*… → *Structural* → *Linear* → *Elastic* → *Isotropic* → Enter value for EX: 29e6 → Enter value for PRXY: 0.3 → *OK*

Note: The steel plate will have a modulus of elasticity of 4.514 x10^3 psi and Poisson's ratio of 0.3.

      i. From the *Material* pull-down menu of the "*Define Material Model Behavior*" window, select *Exit*.
   c. *Modeling* → *Create*
      i. *Keypoints* → *In Active CS*
      Included the following nodes:

Node	X-Coordinate	Y-Coordinate	Z-Coordinate
1	33.0904	0.0000	0.0000
2	51.7154	0.0000	0.0000
3	51.7154	11.2154	0.0000
4	63.7154	32.0000	0.0000
5	84.5000	44.0000	0.0000
6	108.5000	44.0000	0.0000
7	129.2846	32.0000	0.0000
8	141.2846	11.2154	0.0000

9	141.2846	0.0000	0.0000
10	159.9096	0.0000	0.0000
11	159.9096	14.2154	0.0000
12	146.4808	14.2154	0.0000
13	133.6769	36.3923	0.0000
14	110.1077	50.0000	0.0000
15	82.8923	50.0000	0.0000
16	59.3231	36.3923	0.0000
17	46.5192	14.2154	0.0000
18	33.0904	14.2154	0.0000
19	0.0000	0.0000	0.0000
20	193.0000	0.0000	0.0000
21	193.0000	50.0000	0.0000
22	193.0000	62.0000	0.0000
23	0.0000	62.0000	0.0000
24	0.0000	50.0000	0.0000
25	91.5000	62.0000	0.0000
26	91.5000	63.0000	0.0000
27	101.5000	62.0000	0.0000
28	101.5000	63.0000	0.0000

ii. *Areas* → *Arbitrary* → *Through KPs* →
Select nodes 1 through 18 presented above in increasing order to create the culvert area.
iii. *Areas* → *Arbitrary* → *Through KPs* →
Select nodes 19, 1,18,17,16,15 and 14 presented above to create a soil area left of the culvert which represents the sand backfill soil mass.
iv. *Areas* → *Arbitrary* → *Through KPs* →
Select nodes 10, 20, 21, 14,13,12,11 and 10 presented above to create a soil area right of the culvert which represents the sand backfill soil mass.
v. *Areas* → *Arbitrary* → *Through KPs* →
Select nodes 24,15,14,21,22 and 23 presented above to create a soil area on top of the culvert which represents the gravel backfill soil mass.
vi. *Areas* → *Arbitrary* → *Through KPs* →
Select nodes 25 through 28 presented above to create the steel plate area to be located on top of the 12 inches of gravel.
vii. Close *Arbitrary* and *Create* submenus of the *Main Menu*

d. *Modeling* → *Operate* → *Booleans* →
   i. *Glue* → *Areas* → With the vertical arrow pick all areas (soil masses, culvert and steel plate) → *Apply*
   ii. Close the *Glue* and *Operate* submenus of the *Main Menu*
e. *Meshing* →
   i. *Size Controls* → *Manual Size* → *Areas – Picked Areas* → With the vertical arrow pick the soil masses and culvert areas → *Apply* → For the *SIZE* include a 1 → *OK*
   ii. *Size Controls* → *Manual Size* → *Areas – Picked Areas* → With the vertical arrow pick the steel plate area → *Apply* → For the *SIZE* include a 0.2 → *OK*
   iii. Close the *Size Controls* submenu of the *Main Menu*.
   iv. *Mesh Attributes* → *Picked Areas* → with the vertical arrow pick the concrete culvert → *OK* → make sure that MAT=1 and TYPE 1 = Plane 182 → *OK*

v. *Mesh Attributes* → *Picked Areas* → with the vertical arrow pick the sand soil masses (left and right of the culvert) → *OK* → enter MAT=2 and Type 1 = Plane 182 and leave everything else unchanged → *OK*

vi. *Mesh Attributes* → *Picked Areas* → with the vertical arrow pick the gravel soil mass (top) → *OK* → enter MAT=3 and Type 1 = Plane 182 and leave everything else unchanged → *OK*

vii. *Mesh Attributes* → *Picked Areas* → with the vertical arrow pick the steel plate area → *OK* → enter MAT=4 and Type 1 = Plane 182 and leave everything else unchanged → *OK*

viii. Close the *Mesh Attributes* submenu.

f. *Meshing* → *Mesh* → *Areas* → *Free* → With the vertical arrow, pick all areas to be meshed → *OK*.

At this point, all elements will be meshed, in somewhat of a random pattern.

g. Close the *Mesh* submenu of the *Main Menu*.

h. *Loads* → *Define Loads* → *Apply* → *Structural* → *Displacements* → *On Lines* → With the vertical arrow, select the bottom edge of the model → *OK* → In the "*Apply U, ROT on Lines*" window, select (highlight) *ALL DOF* (i.e., all degrees of freedoms to be zero) → *Apply*

i. With the vertical arrow, select the right and left edges of the soil masses → *OK* → In the "*Apply U, ROT on Lines*" window, select (highlight) *UX* (i.e., roller) → *OK*

j. Close *Displacement* and *Apply* submenus.

k. *Loads* → *Define Loads* → *Apply* → *Structural* → *Pressure* → *On Lines* → with the vertical arrow select the top line of steel plate → *OK* → For *VALUE Load PRESS value*, type in 1,820 → *OK*

Note: Here a pressure of 1,820 lb/in acting down in the y-direction will be applied on the top of the steel plate.

l. Close the *Pressure* and *Apply* submenus. Close the *Preprocessor* menu.

5. From ANSYS Main Menu select *Solution*
   a. *Solve* → *Current LS* → *OK* → close the "Note" window → close "STATUS Command" window
   b. Close the *Solution* window
6. Save the active drawing window.
   a. From Utility Menu, select PlotCtrls → Symbols → click on All Applied BCs → In front of *Surface Load Symbols*, select *Pressure* → In front of *Show pres and convect as*, select *Arrows* (this will show the show the pressure as arrows).
7. From Utility Menu, select *Select* → *Entities* →
   a. From the first pull-down menu select *Elements* → from the second pull-down menu select *By Attributes* → click on *Material num* → enter 1 in the box → *Apply* → *Invert*
   b. From the first pull-down menu now select *Nodes* → from the second pull-down menu select *Attached to* → click on *Elements* → *OK*

Note: This will allow ANSYS to analyze the stresses in the soil masses and the concrete culvert but neglect those in the steel plate.

   c. Close the Select Entities window

8. See and/or save results:
   a. From the *Main Menu*, select *General Postproc*
      i. *Plot Results* → *Contour Plot – Element Solution…* → For the item to be contoured, select *Stress* → Then select *Stress, Y-Component of Stress.*
      ii. *Plot Results* → *Contour Plot – Nodal Solution…* → For the item to be contoured, select *Stress* → Then select *Stress, Y-Component of Stress.*
      iii. *List Results* → *Nodal Solution* → *Stress* → *Y-Component of Stress* → *OK*.
9. To exit ANSYS:
   a. From *ANSYS Utility Menu*, select *File* → *Exit …* → Click on *Save Geom+Loads* → *OK*

J2 – 3D Analysis Simulation CIP Model

FINITE ELEMENT ANALYSIS WITH ANSYS
CAST-IN-PLACE 3D CULVERT ANALSYS

Step-by-Step model:

1. Create a directory for the ANSYS files; for example, call it "ANSYS 3D Model"
2. Start ANSYS
   a. Change directory: From Utility Menu (top menu) select *File, Change Directory…*
   b. Set Jobname to "CIP Culvert Analysis 3D": From Utility Menu select, *File, Change Jobname*..
3. From ANSYS Main Menu (located on the left side of the screen), select *Preferences* …
   a. Select *Structural* → Click on *OK*
4. From ANSYS *Main Menu*, select *Preprocessor*
   a. *Element Type* →*Add/Edit/Delete*…→
      i. *Add*…→ *Solid* → *Brick 8 Node 185* → for *Element Type 1* → *OK* →
      ii. *Close* → Close *Element Type* submenu of the *Main Menu*
   b. *Material Properties* →
      i. *Material Models*…→ *Structural* → *Linear* → *Elastic* → *Isotropic* → Enter value for EX: 3.83e6 → Enter value for PRXY: 0.2 → *OK*.

Note: The concrete will have a modulus of elasticity of 3.83 x10^6 psi and Poisson's ratio of 0.2.

      ii. *Material* →*New Model* →Enter a 2 for material ID
      iii. *Material Models*…→ *Structural* → *Linear* → *Elastic* → *Isotropic* → Enter value for EX: 4514→ Enter value for PRXY: 0.3 → *OK*.

Note: The backfill soil (sand) will have a modulus of elasticity of 4,514 psi and Poisson's ratio of 0.3.

      i. *Material* →*New Model* →Enter a 3 for material ID
      ii. *Material Models*…→ *Structural* → *Linear* → *Elastic* → *Isotropic* → Enter value for EX: 11600→ Enter value for PRXY: 0.3 → *OK*.

Note: The backfill soil (gravel) will have a modulus of elasticity of 11,600 psi and Poisson's ratio of 0.3.

      iii. *Material* →*New Model* →Enter a 4 for material ID
      iv. *Material Models*…→ *Structural* → *Linear* → *Elastic* → *Isotropic* → Enter value for EX: 29e6 → Enter value for PRXY: 0.3 → *OK*.

Note: The steel plate will have a modulus of elasticity of 29 x10^6 psi and Poisson's ratio of 0.3.

      v. From the *Material* pull-down menu of the "*Define Material Model Behavior*" window, select *Exit*.
   c. *Modeling* → *Create*
      i. *Keypoints* →*In Active CS*
      Included the following nodes:

Node	X-Coordinate	Y-Coordinate	Z-Coordinate
1	33.0904	0.0000	0.0000
2	51.7154	0.0000	0.0000
3	51.7154	11.2154	0.0000
4	63.7154	32.0000	0.0000
5	84.5000	44.0000	0.0000
6	108.5000	44.0000	0.0000
7	129.2846	32.0000	0.0000
8	141.2846	11.2154	0.0000
9	141.2846	0.0000	0.0000
10	159.9096	0.0000	0.0000
11	159.9096	14.2154	0.0000
12	146.4808	14.2154	0.0000

13	133.6769	36.3923	0.0000
14	110.1077	50.0000	0.0000
15	82.8923	50.0000	0.0000
16	59.3231	36.3923	0.0000
17	46.5192	14.2154	0.0000
18	33.0904	14.2154	0.0000
19	0.0000	0.0000	0.0000
20	193.0000	0.0000	0.0000
21	193.0000	50.0000	0.0000
22	193.0000	62.0000	0.0000
23	0.0000	62.0000	0.0000
24	0.0000	50.0000	0.0000
25	77.8923	62.0000	0.0000
26	77.8923	63.0000	0.0000
27	87.8923	62.0000	0.0000
28	87.8923	63.0000	0.0000

i. *Areas* → *Arbitrary* → *Through KPs* →
   Select nodes 1 through 18 presented above in increasing order to create the culvert area.
ii. *Areas* → *Arbitrary* → *Through KPs*→
   Select nodes 19, 1,18,17,16,15 and 14 presented above to create a soil area left of the culvert which represents the sand backfill soil mass.
iii. *Areas* → *Arbitrary* → *Through KPs*→
   Select nodes 10, 20, 21, 14,13,12,11 and 10 presented above to create a soil area right of the culvert which represents the sand backfill soil mass.
iv. *Areas* → *Arbitrary* → *Through KPs*→
   Select nodes 24,15,14,21,22 and 23 presented above to create a soil area on top of the culvert which represents the gravel backfill soil mass.
v. *Areas* → *Arbitrary* → *Through KPs*→
   Select nodes 25 through 28 presented above to create the steel plate area to be located on top of the 12 inches of gravel.
vi. Close *Arbitrary* and *Create* submenus of the *Main Menu*

d. *Modeling* → *Operate* → *Extrude* → *Areas* → *By XYZ Offset* → Select the soil and culvert areas → *Apply* → Type 0 for DX and DY, and a -15 for the DZ offset of extrusion. Leave RX, RY and RZ scales without any values.

Note: This will create volumes having a depth of 15 inches for the soil and culvert.

a. *Modeling* → *Operate* → *Extrude* → *Areas* → *By XYZ Offset* → Select the steel plate area → *Apply* → Type 0 for DX and DY, and a -2.5 for the DZ offset of extrusion. Leave RX, RY and RZ scales without any values.

Note: This will create a volume having a depth of 2.5 inches for the steel plate.

i. *Modeling* → *Operate* → *Booleans* → *Glue* → *Volumes* → With the vertical arrow pick the soil, culvert and plate volumes → *Apply*
ii. Close the *Glue* and *Operate* submenus of the *Main Menu*

b. *Meshing* →
iii. *Size Controls* → *Manual Size* → *Areas – Picked Areas* → Select all areas that represent the soil and the culvert → *Apply* → *SIZE* → type in 2 → *OK*
iv. *Size Controls* → *Manual Size* → *Areas – Picked Areas* → Select all faces of the steel plate except the bottom one → *Apply* → *SIZE* → type in 1 → *OK*
v. *Size Controls* → *Manual Size* → *Areas – Picked Areas* → Select the bottom face of the steel plate → *Apply* → *SIZE* → type in 0.5 → *OK*

vi. Close the *Size Controls* submenu of the *Main Menu.*
vii. *Mesh Attributes* → *Picked Volumes* → with the vertical arrow pick the concrete culvert → *OK* → make sure that MAT=1 and TYPE 1 = Solid 185 is selected → *OK*
viii. *Mesh Attributes* → *Picked Volumes* → with the vertical arrow pick the sand soil volumes → *OK* → make sure that MAT=2 and TYPE 1 = Solid 185 is selected → *OK*
ix. *Mesh Attributes* → *Picked Volumes* → with the vertical arrow pick the gravel soil volume → *OK* → make sure that MAT=3 and TYPE 1 = Solid 185 is selected → *OK*
x. *Mesh Attributes* → *Picked Volumes* → with the vertical arrow pick the steel plate → *OK* → make sure that MAT=4 and TYPE 1 = Solid 185 is selected → *OK*
xi. Close the *Mesh Attributes* submenu.

c. *Meshing* → *Mesh* → *Volumes* → *Free* → With the vertical arrow pick the volumes to be meshed → *OK.*

Note: At this point, the five volumes will be meshed, in somewhat of a random pattern. In addition, ANSYS might show some warnings and suggestions related to element shapes and possible ways to obtain more accurate results using alternative element types. Close said warnings signs.

d. Close the *Mesh* submenu of the *Main Menu.*
e. *Loads* → *Define Loads* → *Apply* → *Structural* → *Displacements* → *On Lines* → With the vertical arrow select the front and back face lines of the soil and culvert edges and the front lines of the plate edges → *OK* → In the "*Apply U, ROT on Lines*" window, select (highlight) UZ (i.e., Z coordinate to be zero) → *Apply*
f. *Loads* → *Define Loads* → *Apply* → *Structural* → *Displacements* → *On Lines* → With the vertical arrow select the right and left face lines of the soil edges → *OK* → In the "*Apply U, ROT on Lines*" window, select (highlight) UX (i.e., X coordinate to be zero) → *Apply*
g. *Loads* → *Define Loads* → *Apply* → *Structural* → *Displacements* → *On Lines* → With the vertical arrow select the bottom edge lines → *OK* → In the "*Apply U, ROT on Lines*" window, select (highlight) All DOF (i.e., X, Y and Z coordinates to be zero) → *Apply*
h. *Loads* → *Define Loads* → *Apply* → *Structural* → *Pressure* → *On Areas* → with the vertical arrow select the top face of the steel plate → *OK* → For *VALUE Load PRESS value*, type in 364 → *OK*

Note: Here a pressure of 364 lb/in^2 acting down in the y-direction will be applied on the top of the steel plate.

i. Close the *Pressure* and *Apply* submenus. Close the *Preprocessor* menu.

5. From ANSYS Main Menu select *Solution*
   a. *Solve* → *Current LS* → *OK* → close the "Note" window → close "STATUS Command" window
   b. Close the *Solution* window
6. Save the active drawing window.
   a. From Utility Menu, select PlotCtrls → Symbols → click on All Applied BCs → In front of *Surface Load Symbols*, select *Pressure* → In front of *Show pres and convect as*, select *Arrows* (this will show the show the pressure as arrows).
7. From Utility Menu, select *Select* → *Entities* →
   a. From the first pull-down menu select *Elements* → from the second pull-down menu select *By Attributes* → click on *Material num* → enter 4 in the box → *Apply* → *Invert*
   b. From the first pull-down menu now select *Nodes* → from the second pull-down menu select *Attached to* → click on *Elements* → *OK*

Note: This will allow ANSYS to analyze the stresses in the soil mass and the concrete culvert but neglect those in the steel plate.

c. Close the Select Entities window

8. See and/or save results:
   a. From the *Main Menu*, select *General Postproc*
      i. *Plot Results* → *Contour Plot – Element Solution…* → For the item to be contoured, select *Stress* → Then select *Stress, Y-Component of Stress.*
      ii. *Plot Results* → *Contour Plot – Nodal Solution…* → For the item to be contoured, select *Stress* → Then select *Stress, Y-Component of Stress.*

iii. *List Results* → *Nodal Solution* → *Stress* → *Y-Component of Stress* → *OK.*

9. To exit ANSYS:
   a. From *ANSYS Utility Menu*, select *File* → *Exit ...* → Click on *Save Geom+Loads* → *OK*

J3 – CIP Model ANSYS Nodal Solutions

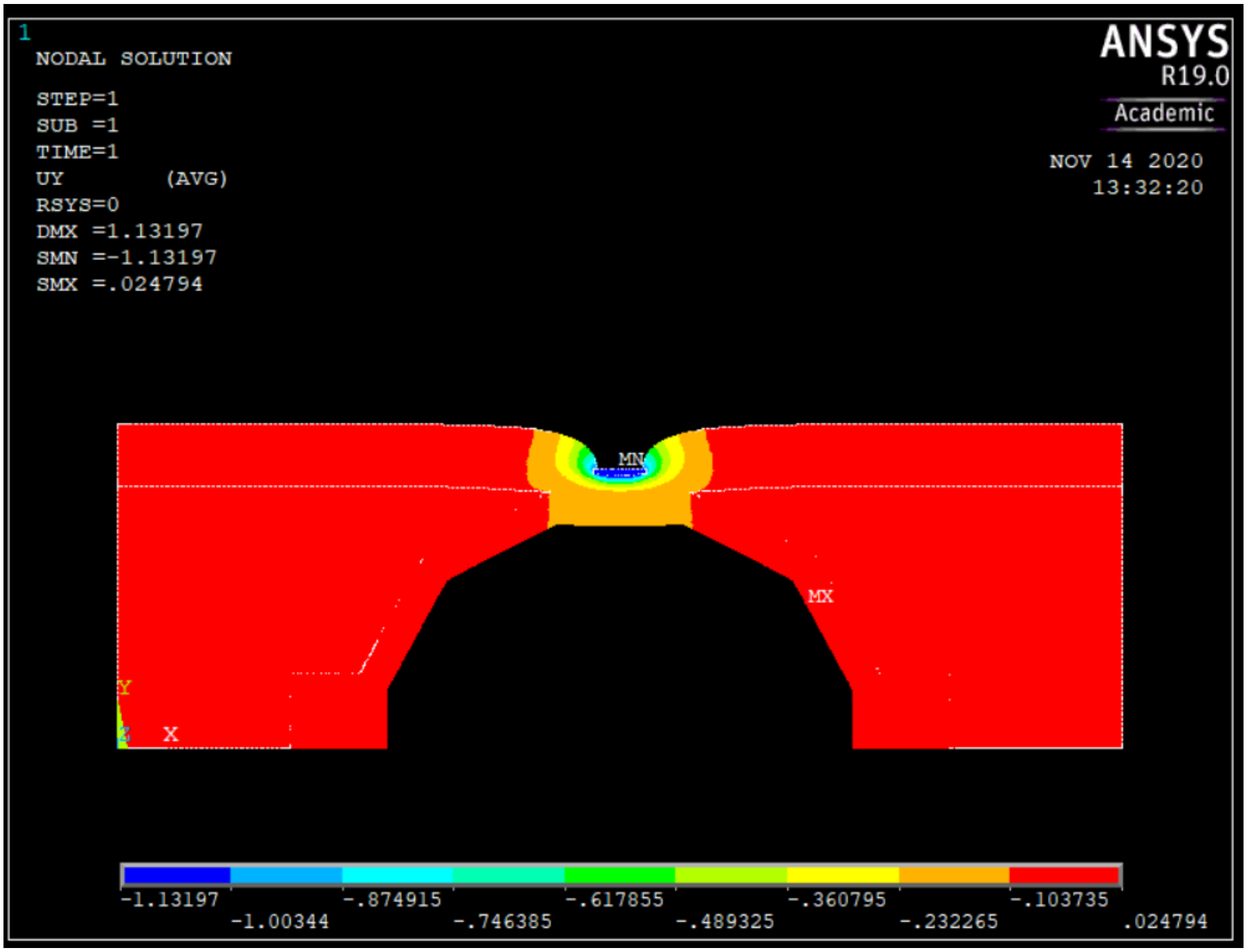

Figure 119 - 2D Nodal Y-Displacements Initial Predictions Test No. 1 CIP Model

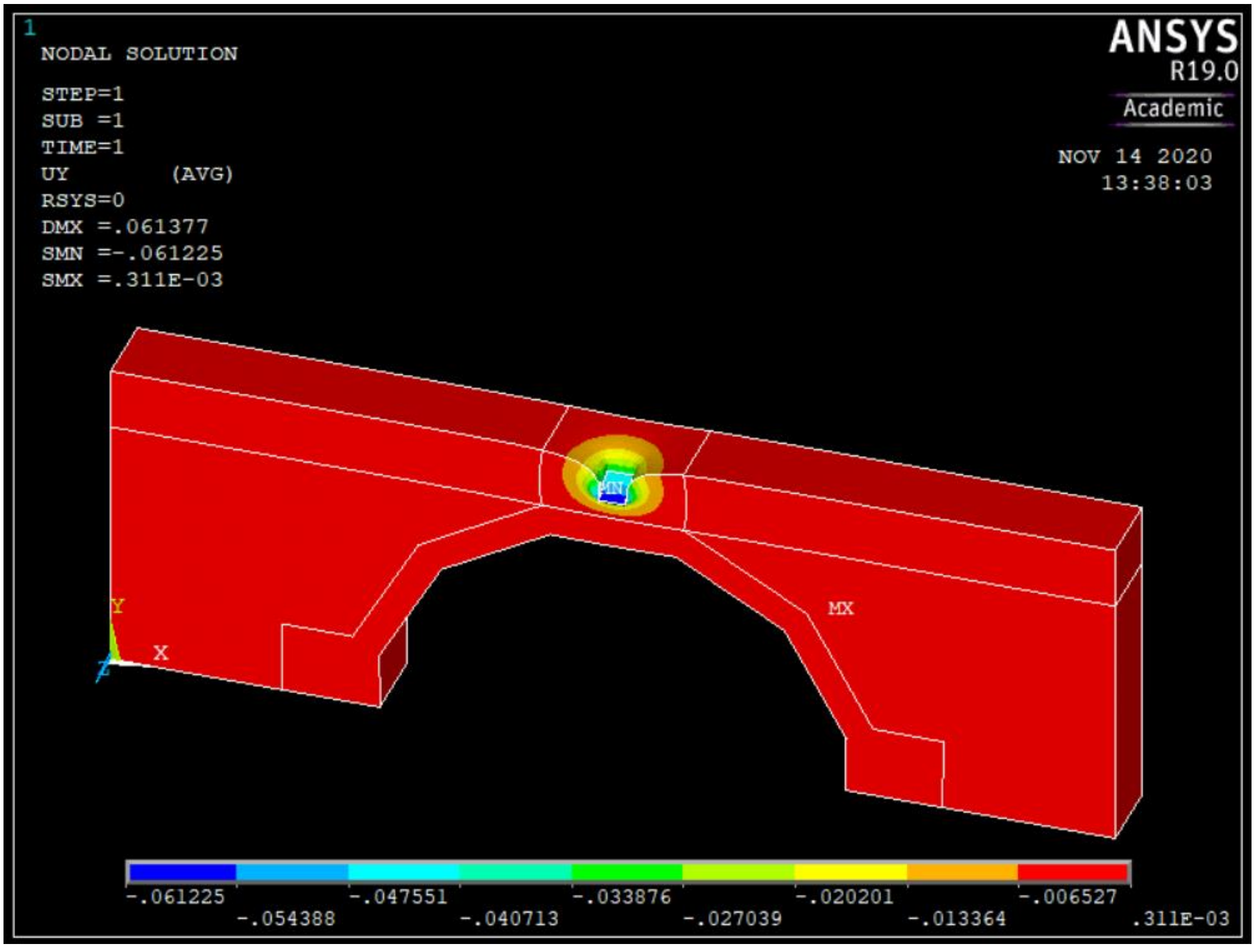

Figure 120 - 3D Nodal Y-Displacements Initial Predictions Test No. 1 CIP Model

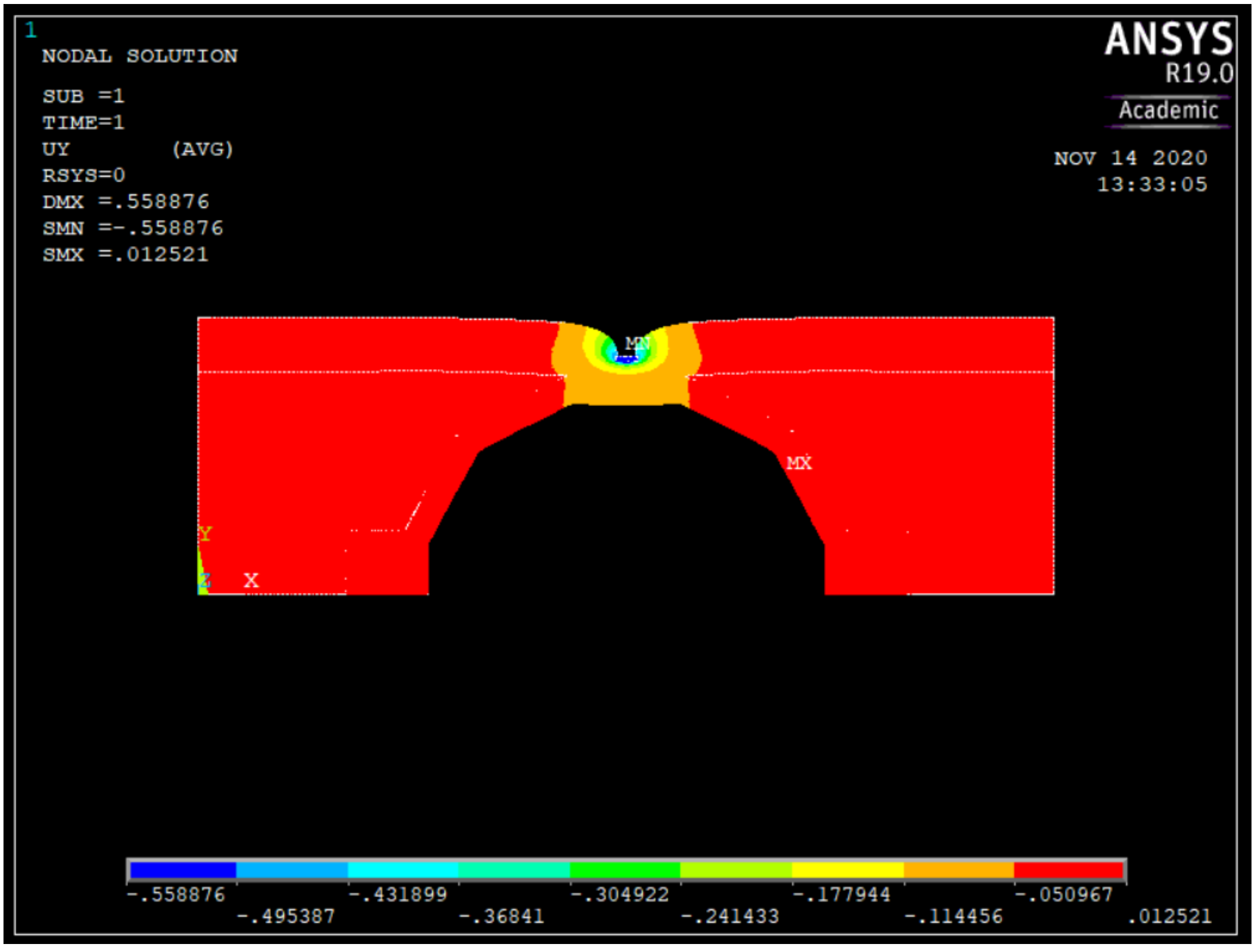

Figure 121 - 2D Nodal Y-Displacements Initial Predictions Test No. 2 CIP Model

Figure 122 - 3D Nodal Y-Displacements Initial Predictions Test No. 2 CIP Model

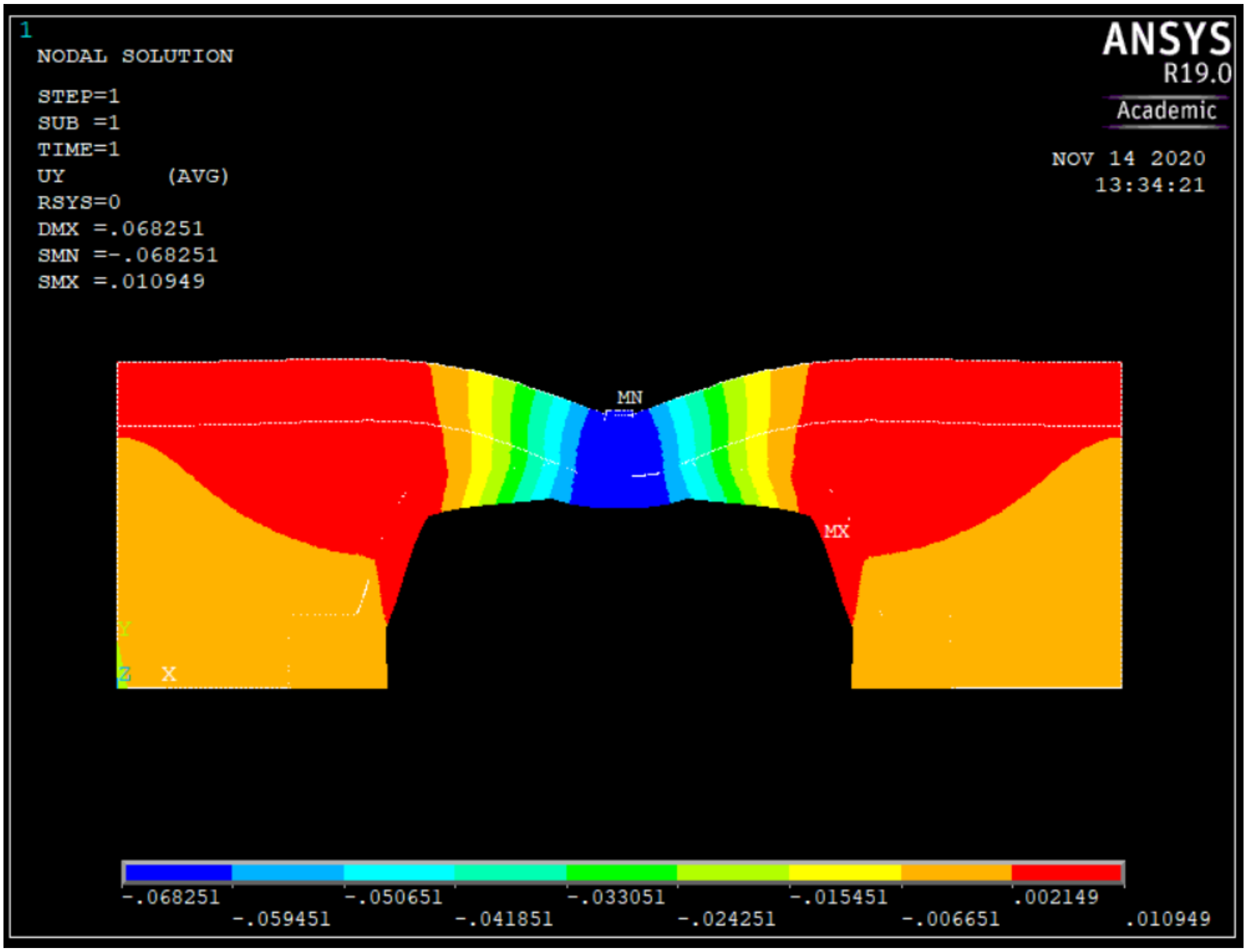

Figure 123 - 2D Nodal Y-Displacements Initial Predictions Test No. 3 CIP Model

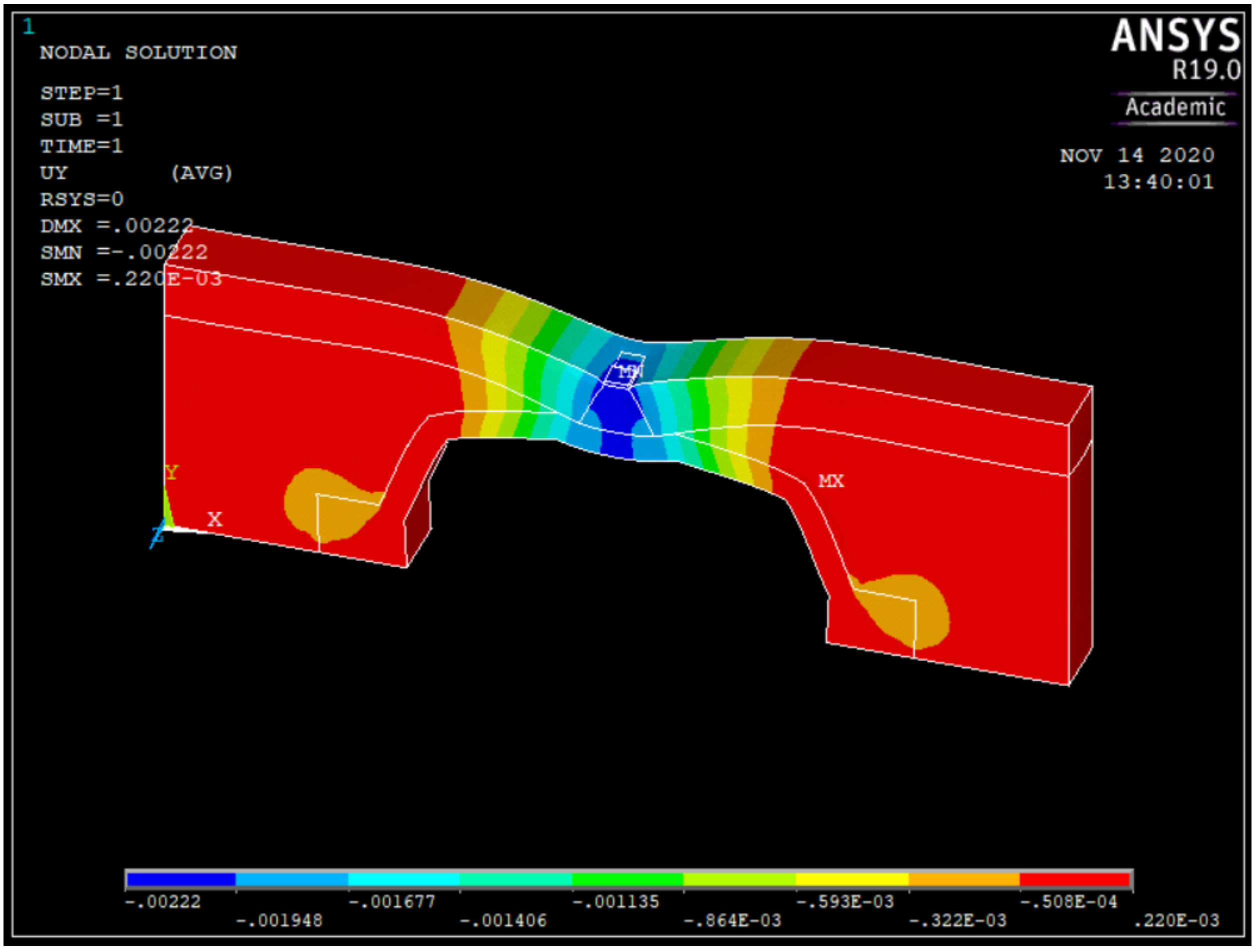

Figure 124 - 3D Nodal Y-Displacements Initial Predictions Test No. 3 CIP Model

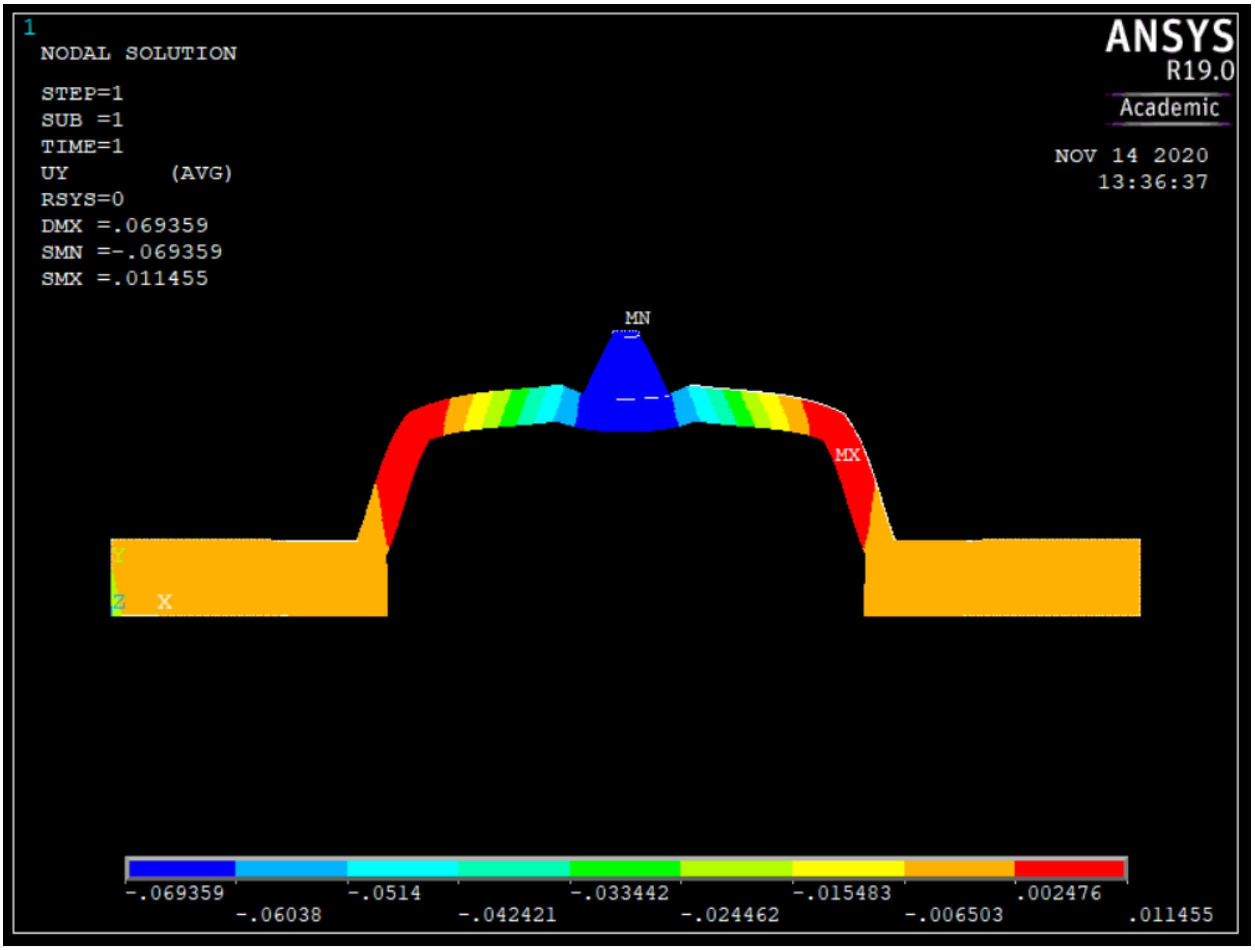

Figure 125 - 2D Nodal Y-Displacements Initial Predictions Test No. 4 CIP Model

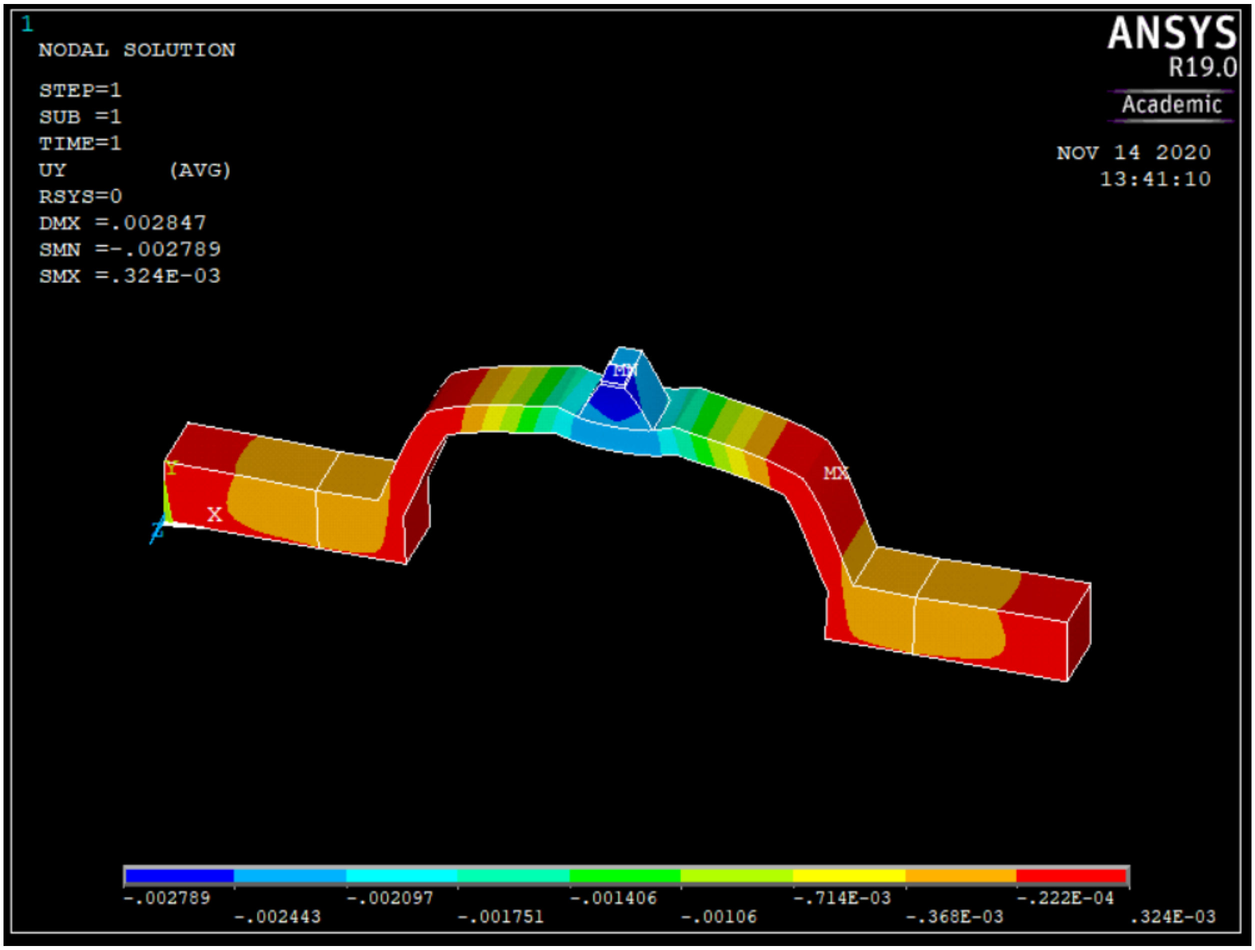

Figure 126 - 3D Nodal Y-Displacements Initial Predictions Test No. 4 CIP Model

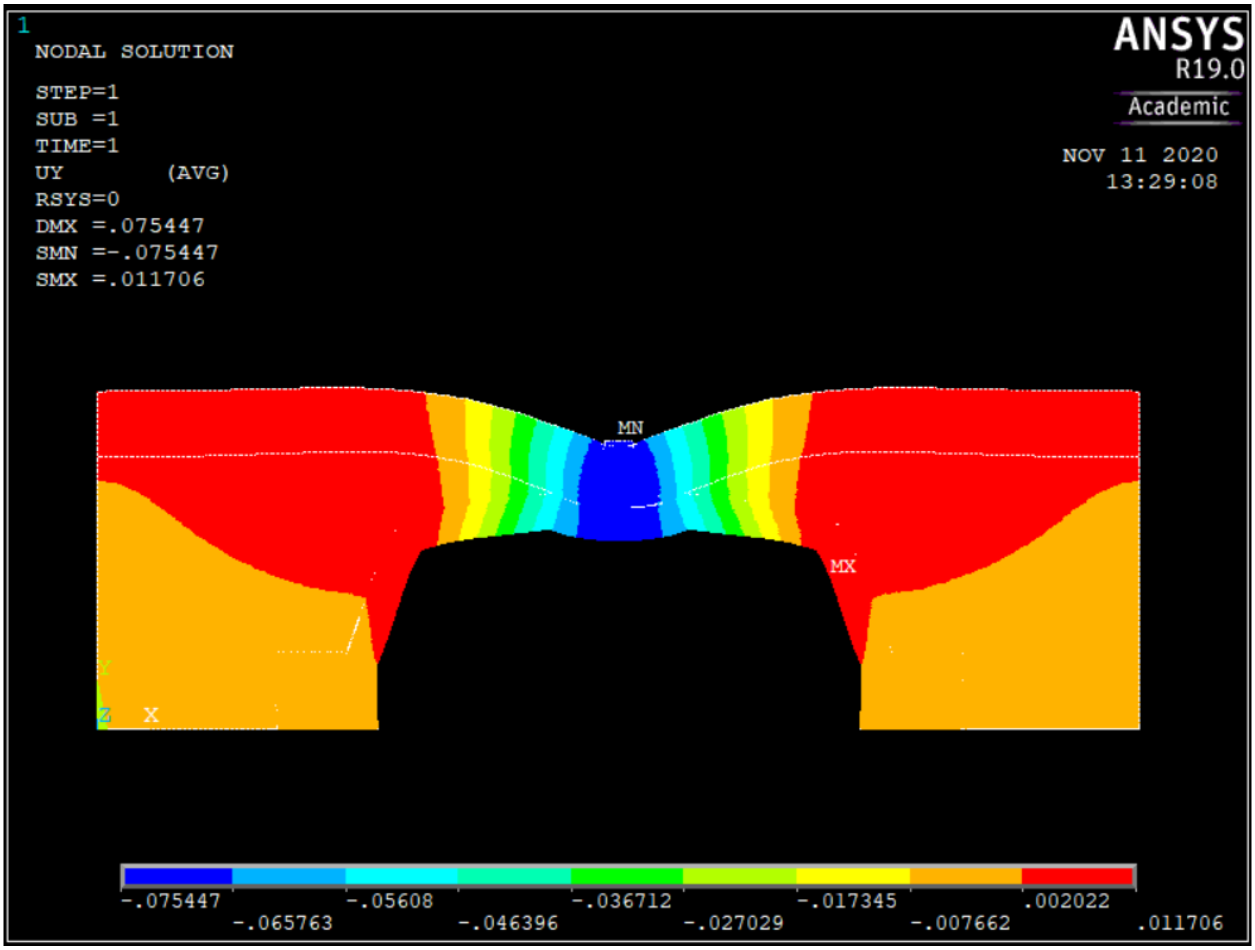

Figure 127 - 2D Nodal Y-Displacements Rerun No. 1 - Test No. 3 CIP Model

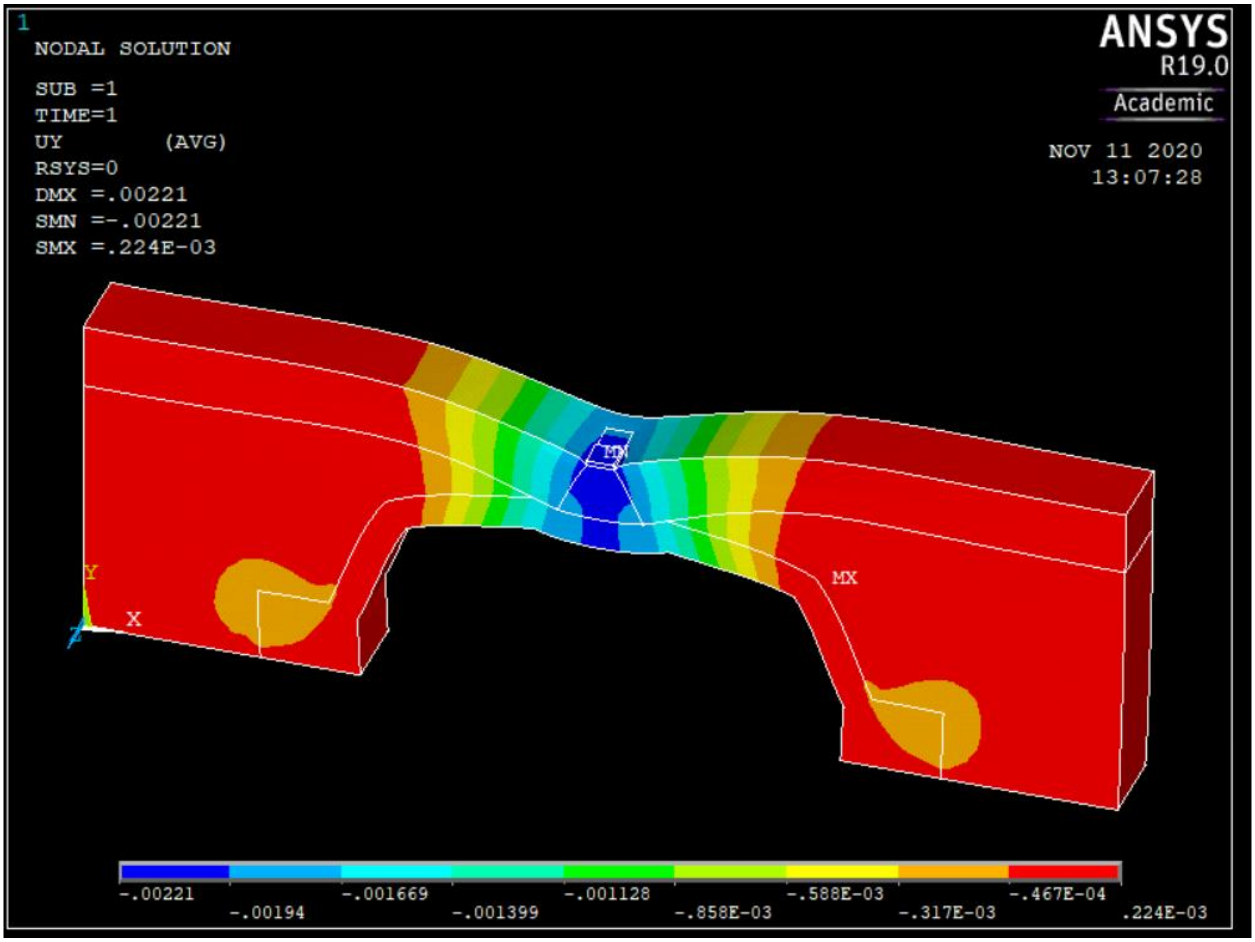

Figure 128 - 3D Nodal Y-Displacements Rerun No. 1 - Test No. 3 CIP Model

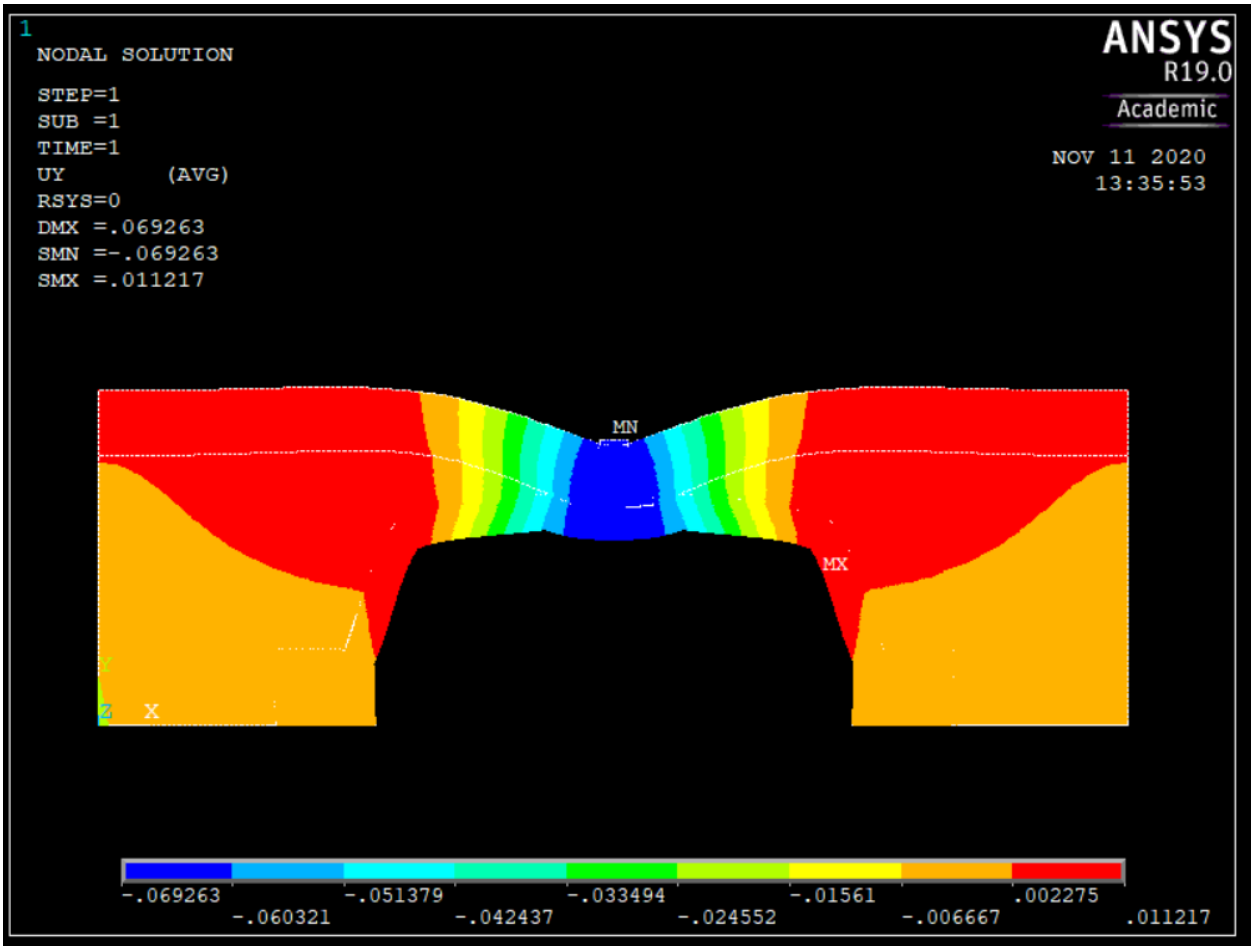

Figure 129 - 2D Nodal Y-Displacements Rerun No. 2 - Test No. 3 CIP Model

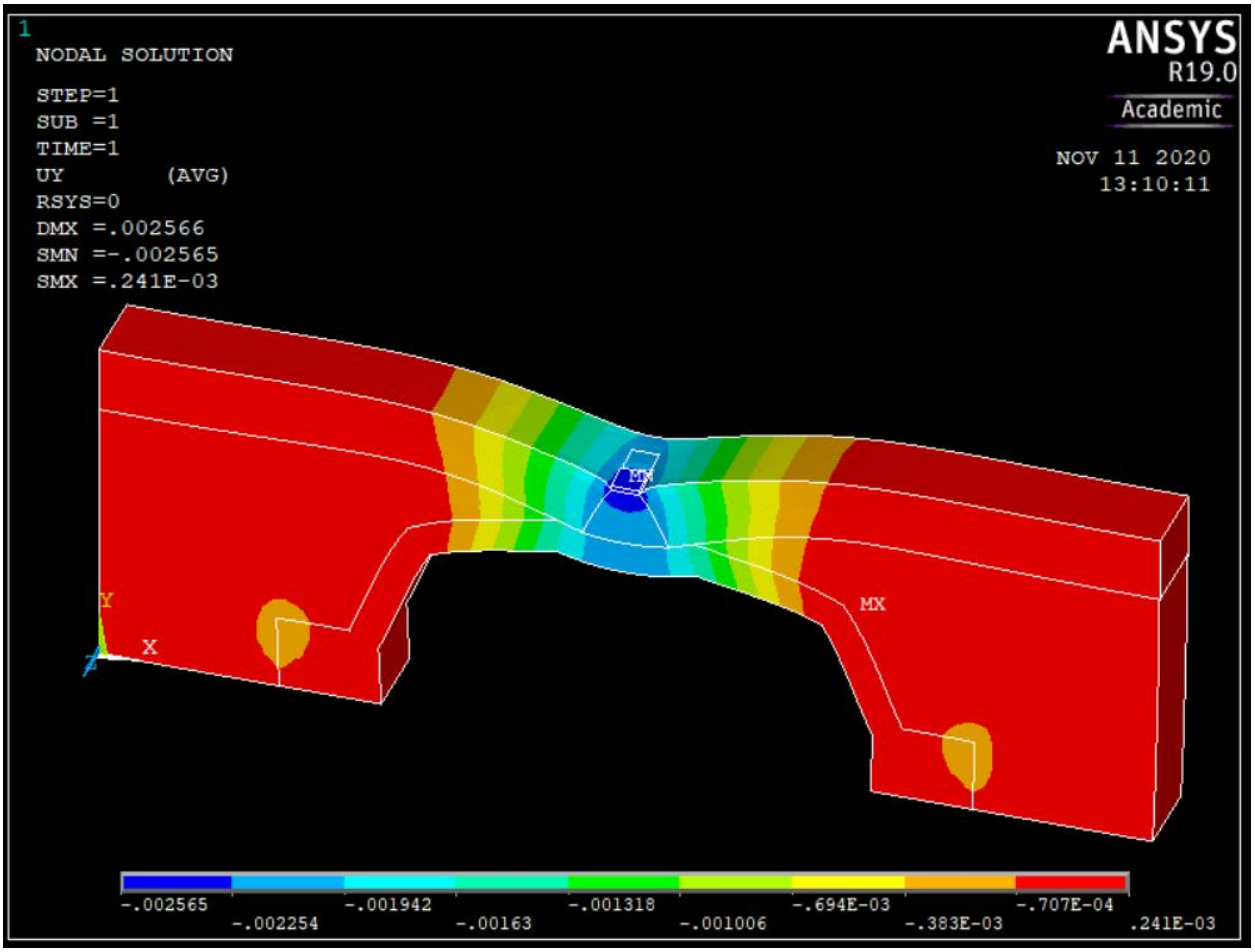

Figure 130 - 3D Nodal Y-Displacements Rerun No. 2 - Test No. 3 CIP Model

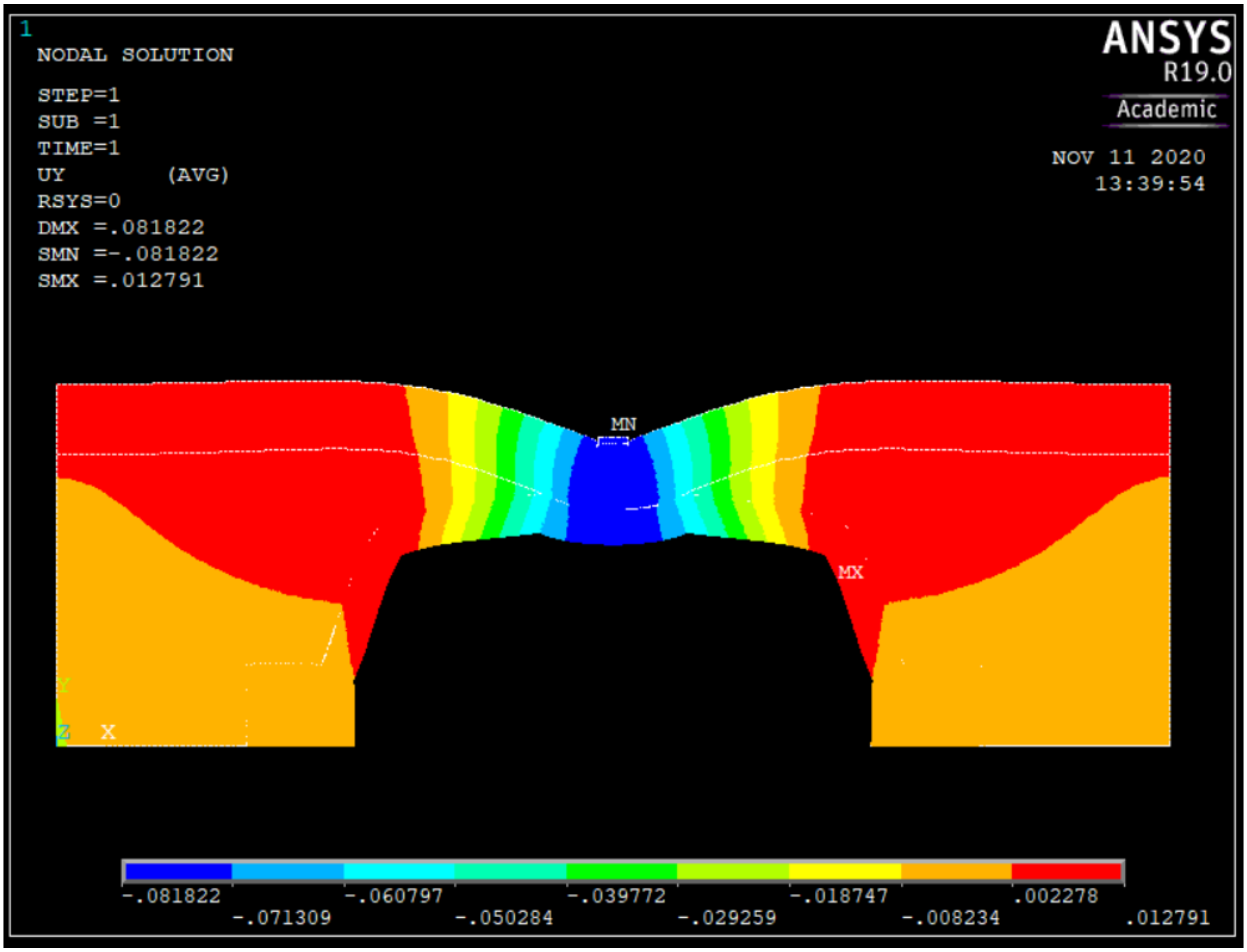

Figure 131 - 2D Nodal Y-Displacements Rerun No. 3 - Test No. 3 CIP Model

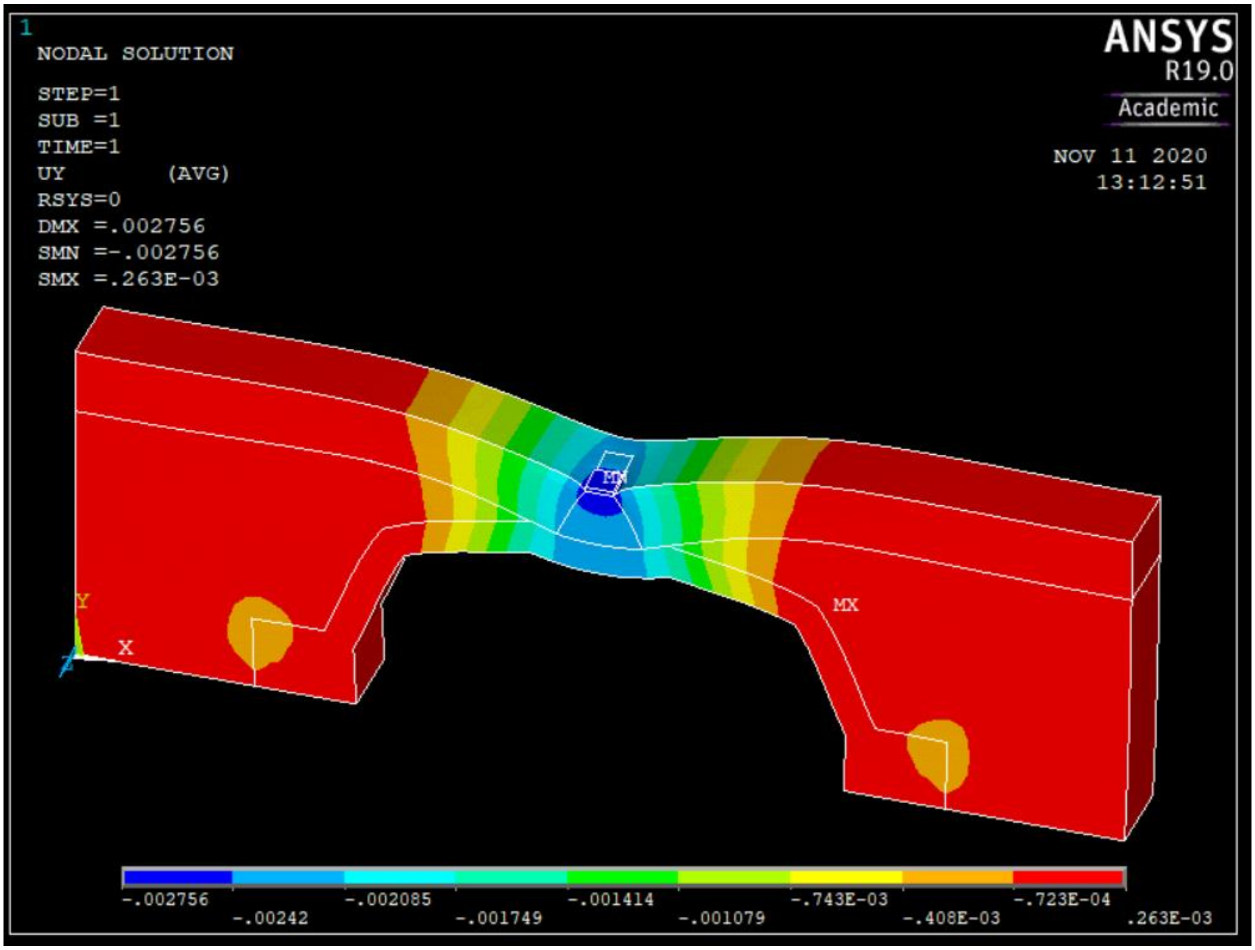

Figure 132 - 3D Nodal Y-Displacements Rerun No. 3 - Test No. 3 CIP Model

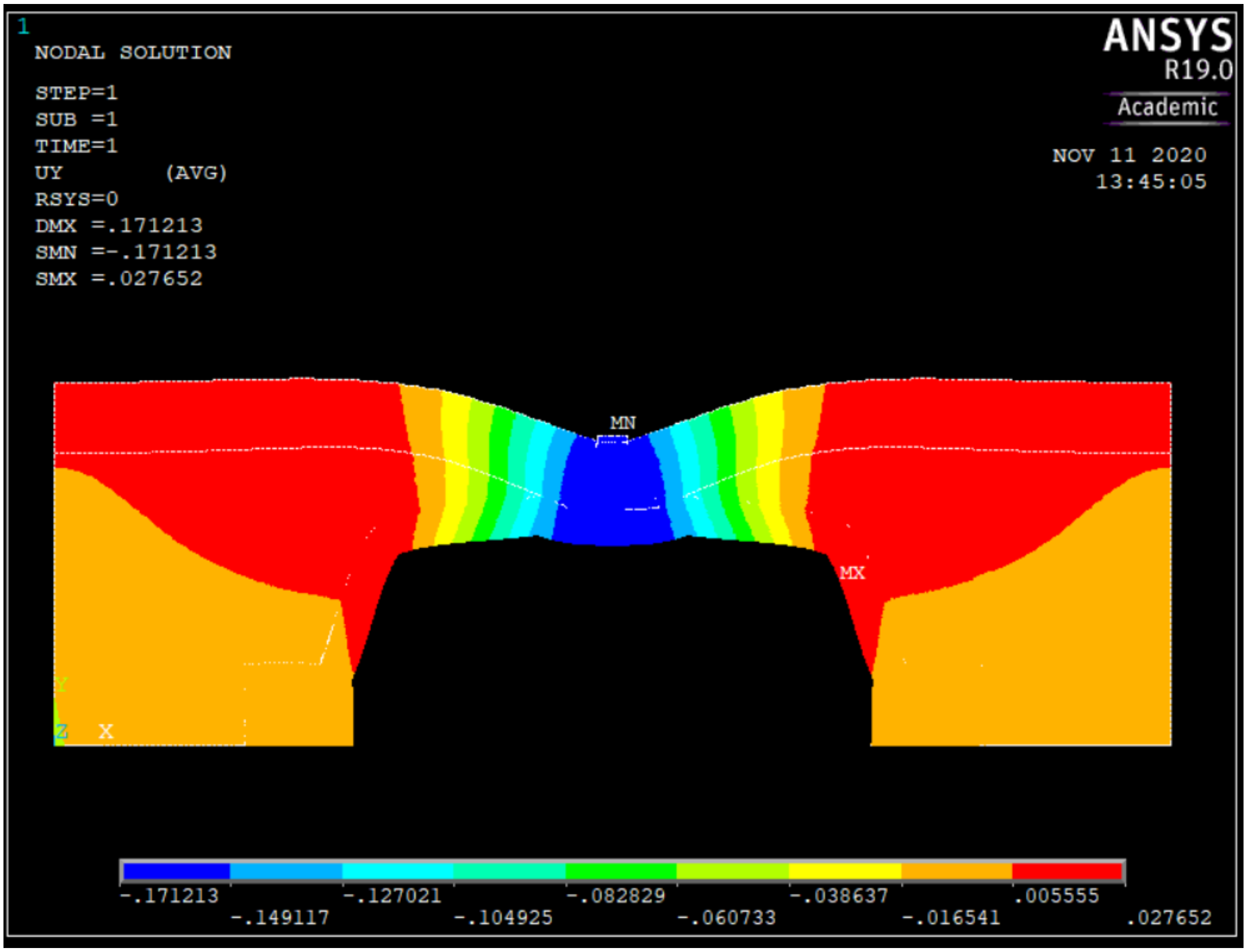

Figure 133 - 2D Nodal Y-Displacements Rerun No. 4 - Test No. 3 CIP Model

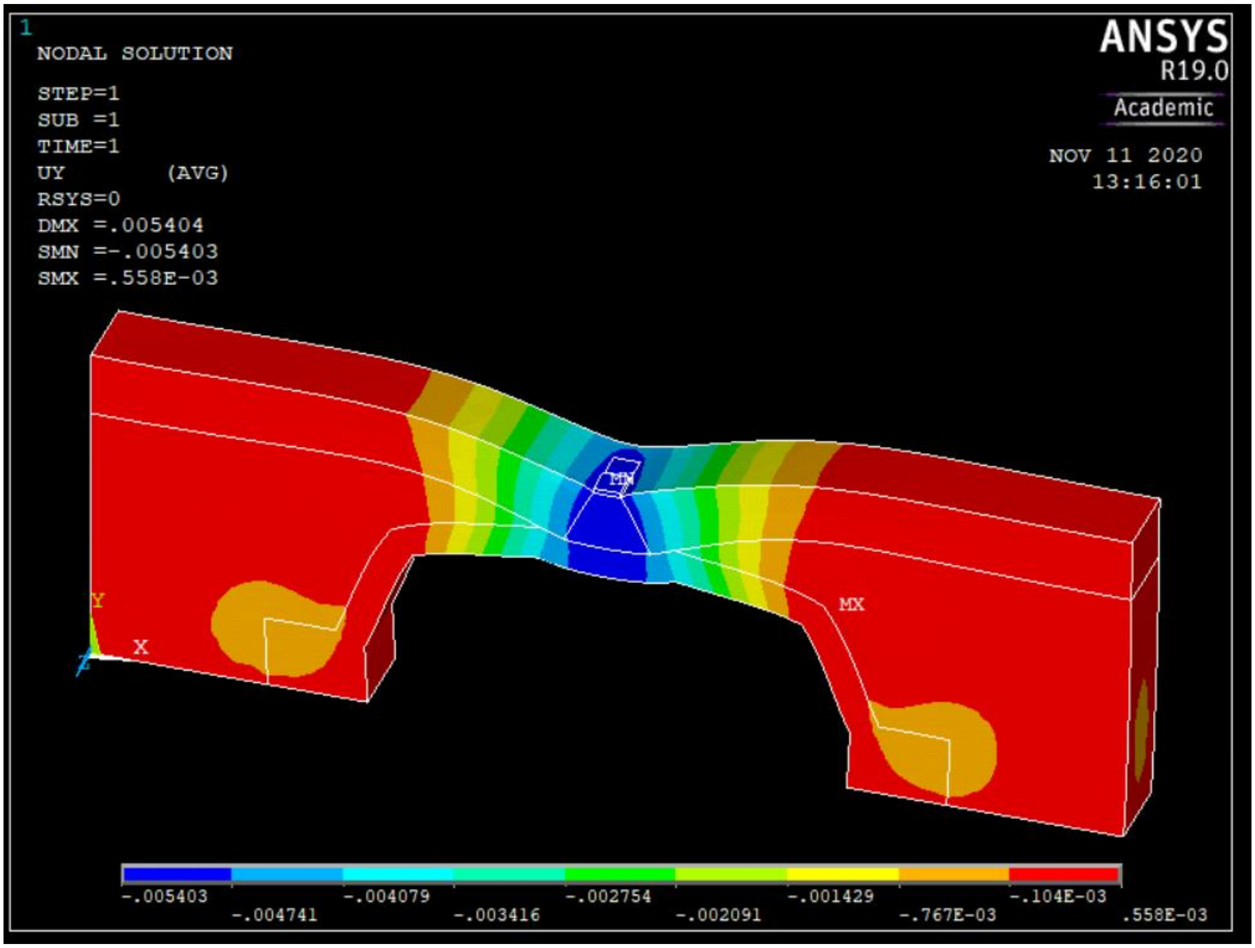

Figure 134 - 3D Nodal Y-Displacements Rerun No. 4 - Test No. 3 CIP Model

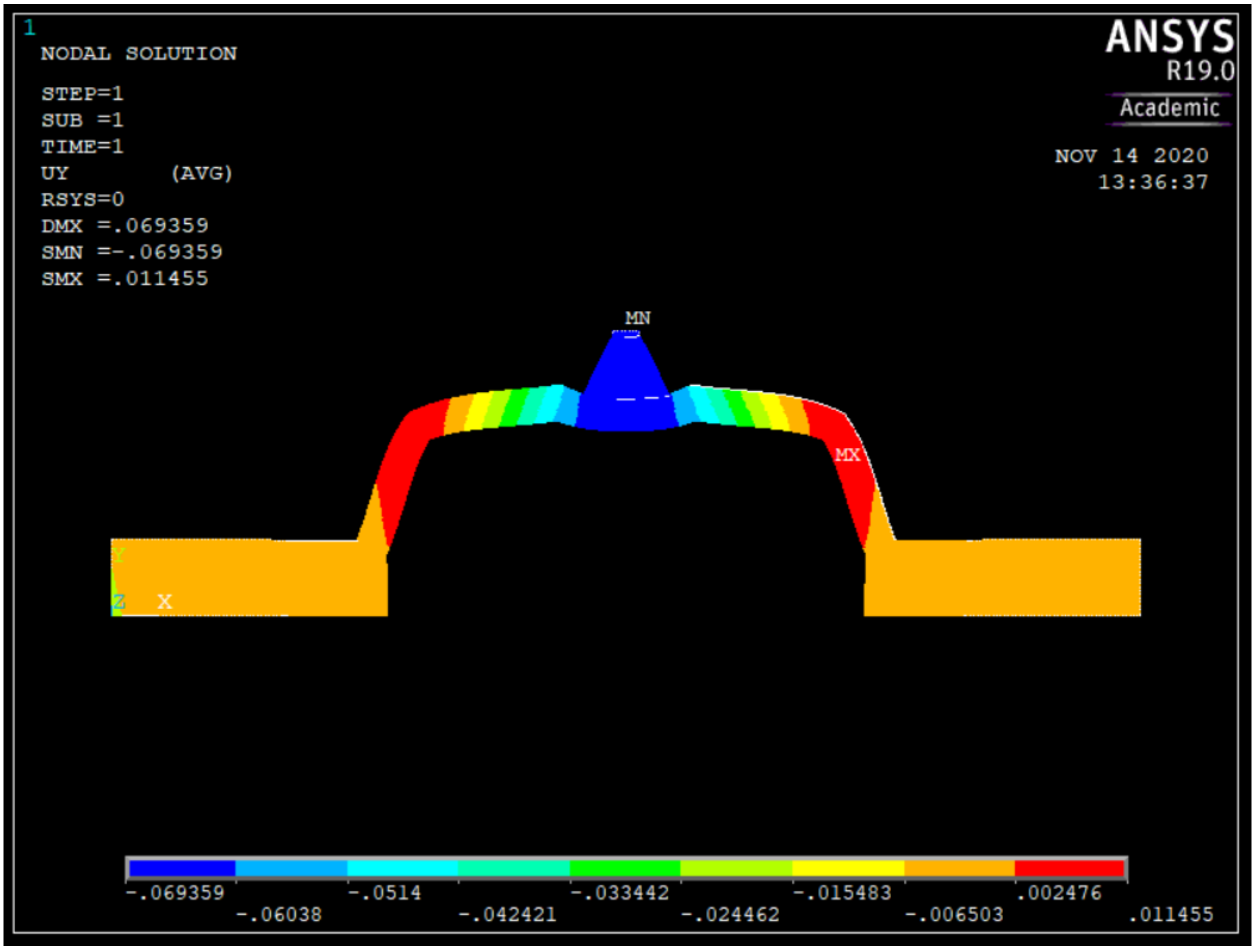

Figure 135 - 2D Nodal Y-Displacements Rerun No. 1 - Test No. 4 CIP Model

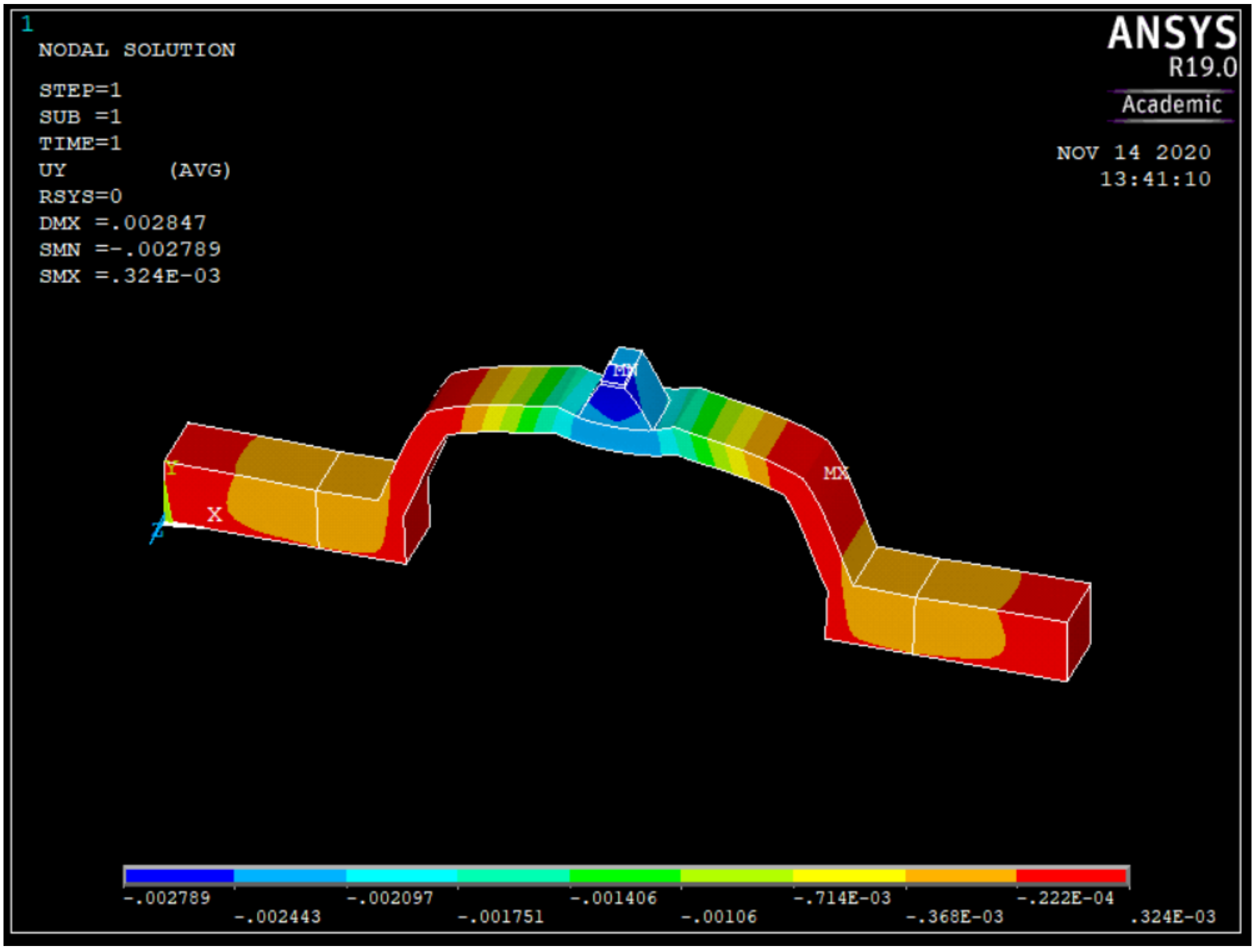

Figure 136 - 3D Nodal Y-Displacements Rerun No. 1 - Test No. 4 CIP Model

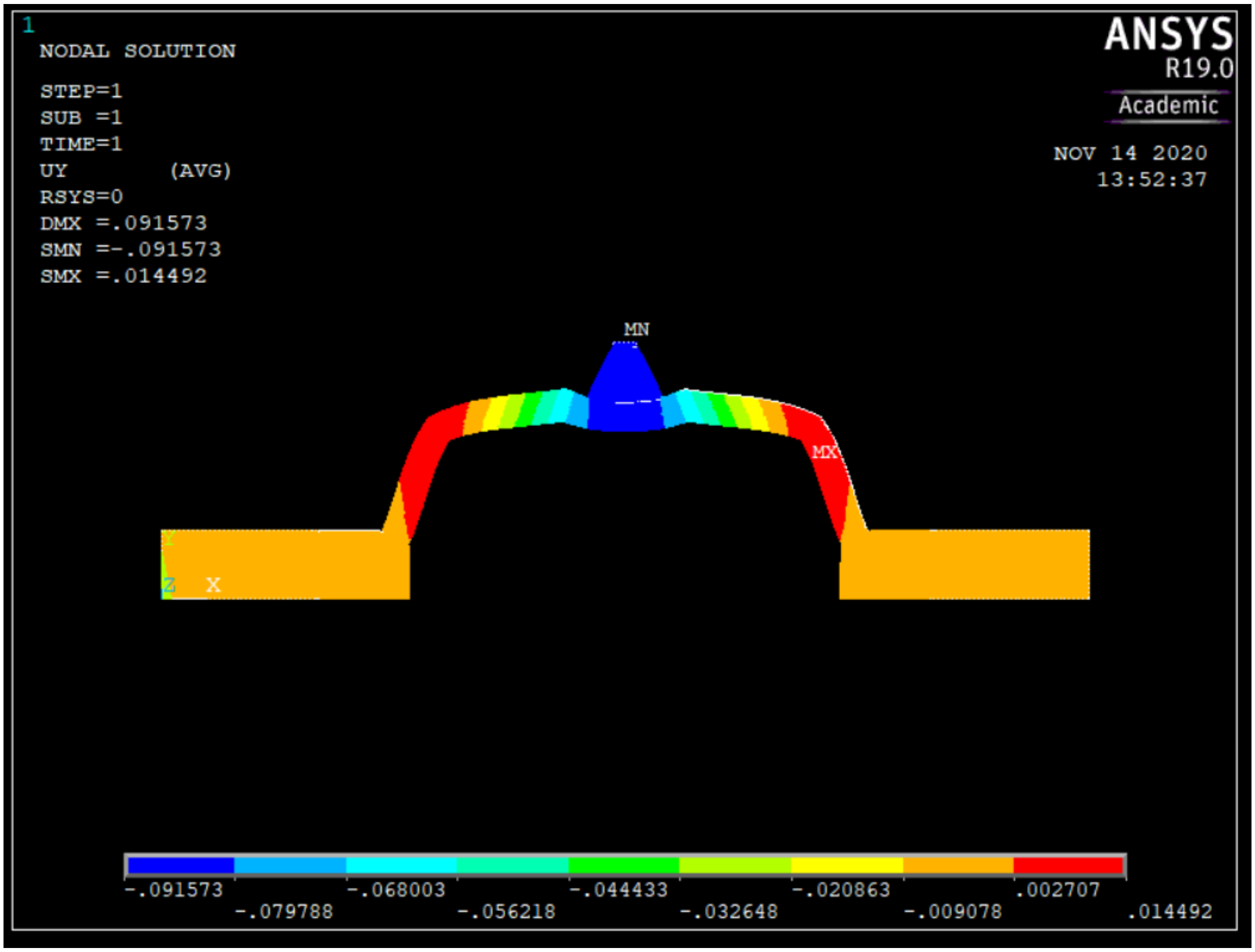

Figure 137 - 2D Nodal Y-Displacements Rerun No. 2 - Test No. 4 CIP Model

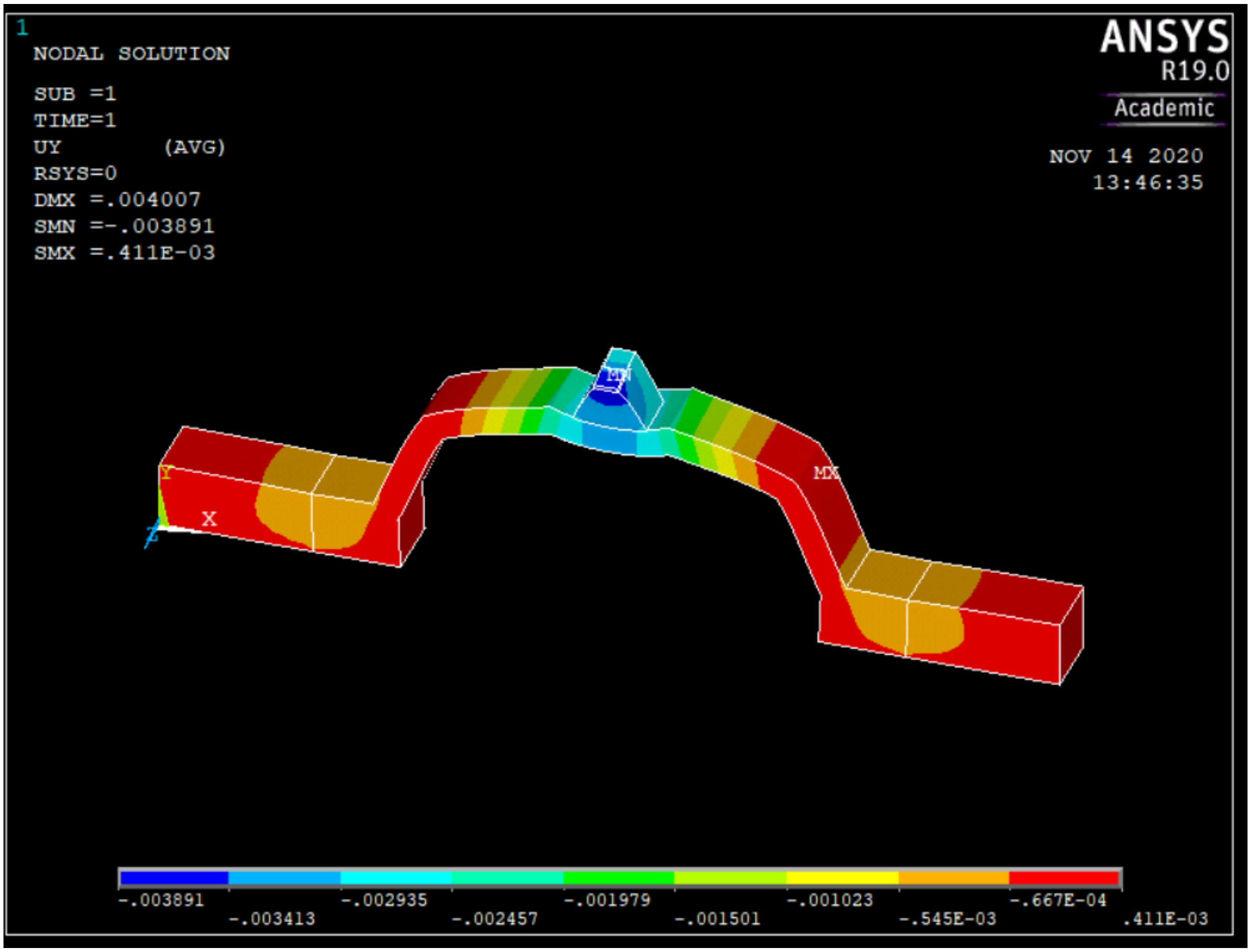

Figure 138 - 3D Nodal Y-Displacements Rerun No. 2 - Test No. 4 CIP Model

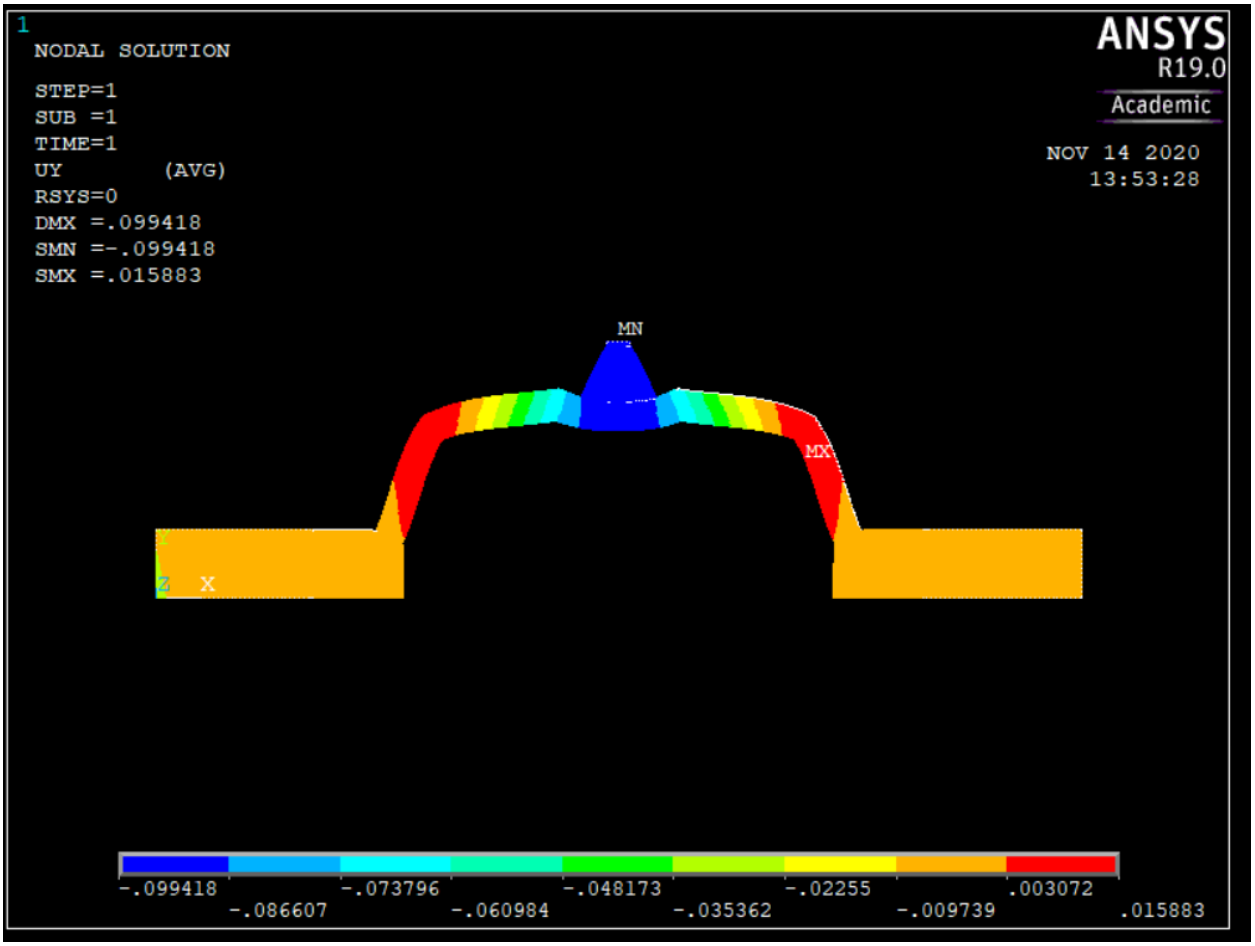

Figure 139 - 2D Nodal Y-Displacements Rerun No. 3 - Test No. 4 CIP Model

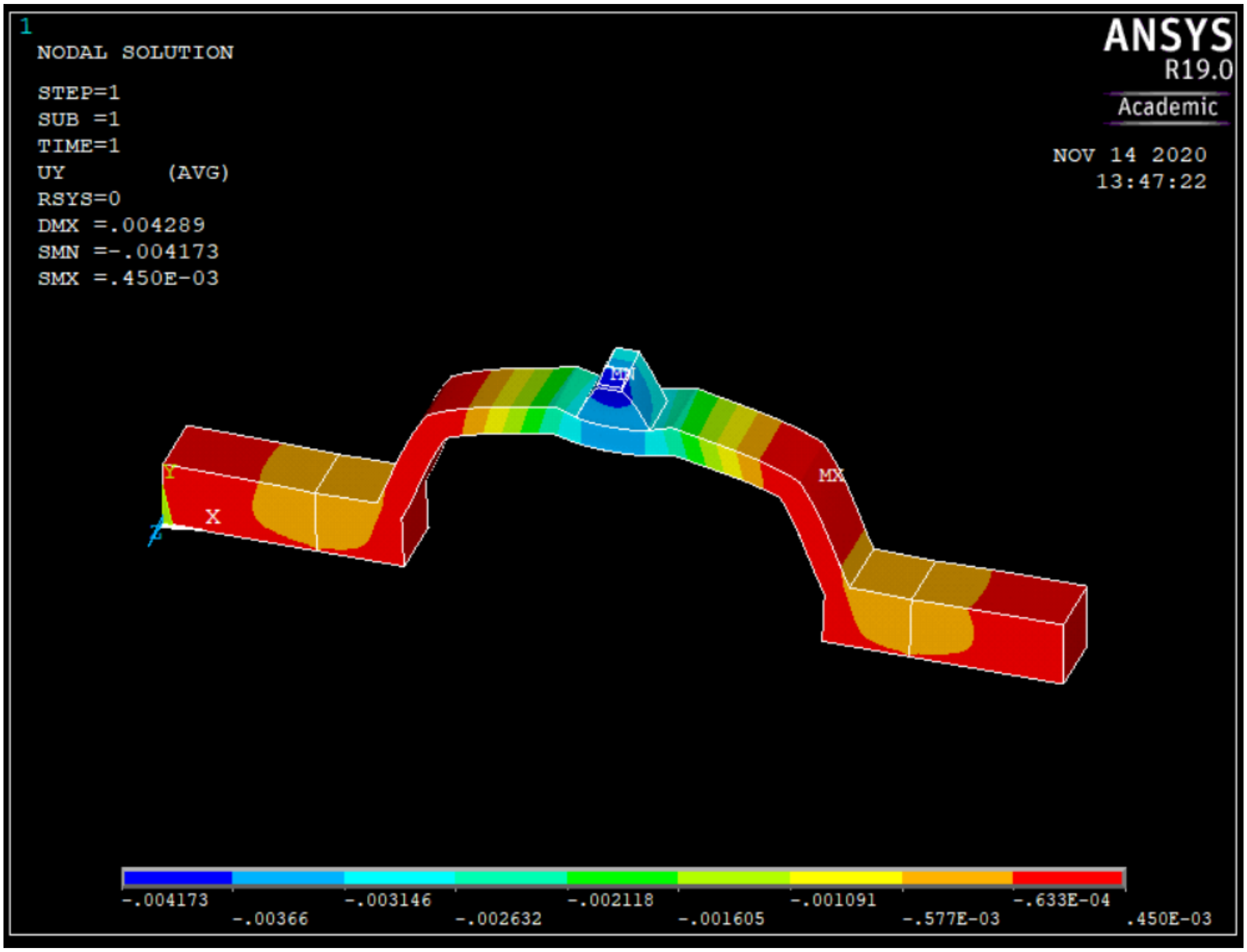

Figure 140 - 3D Nodal Y-Displacements Rerun No. 1 - Test No. 3 CIP Model

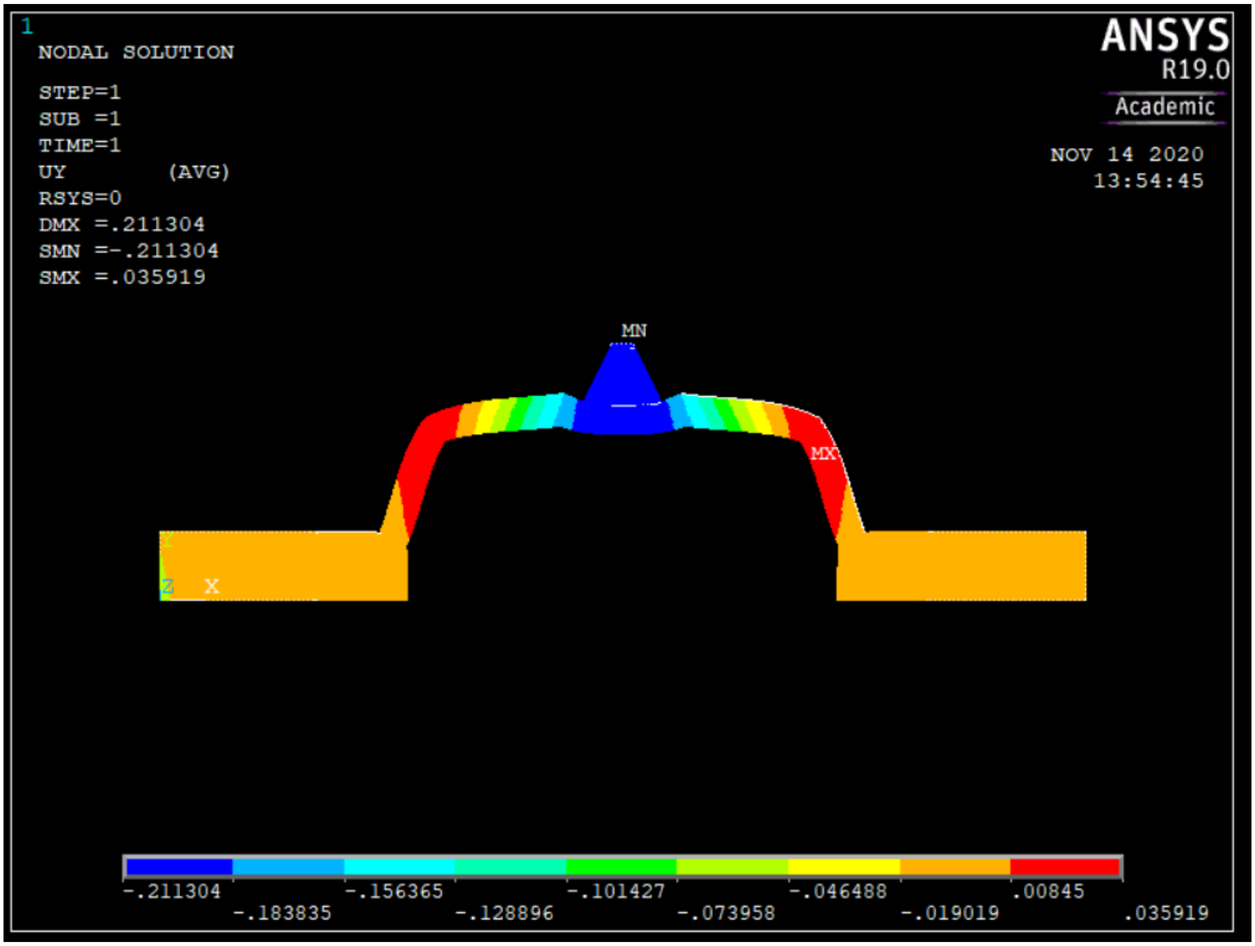

Figure 141 - 2D Nodal Y-Displacements Rerun No. 4 - Test No. 4 CIP Model

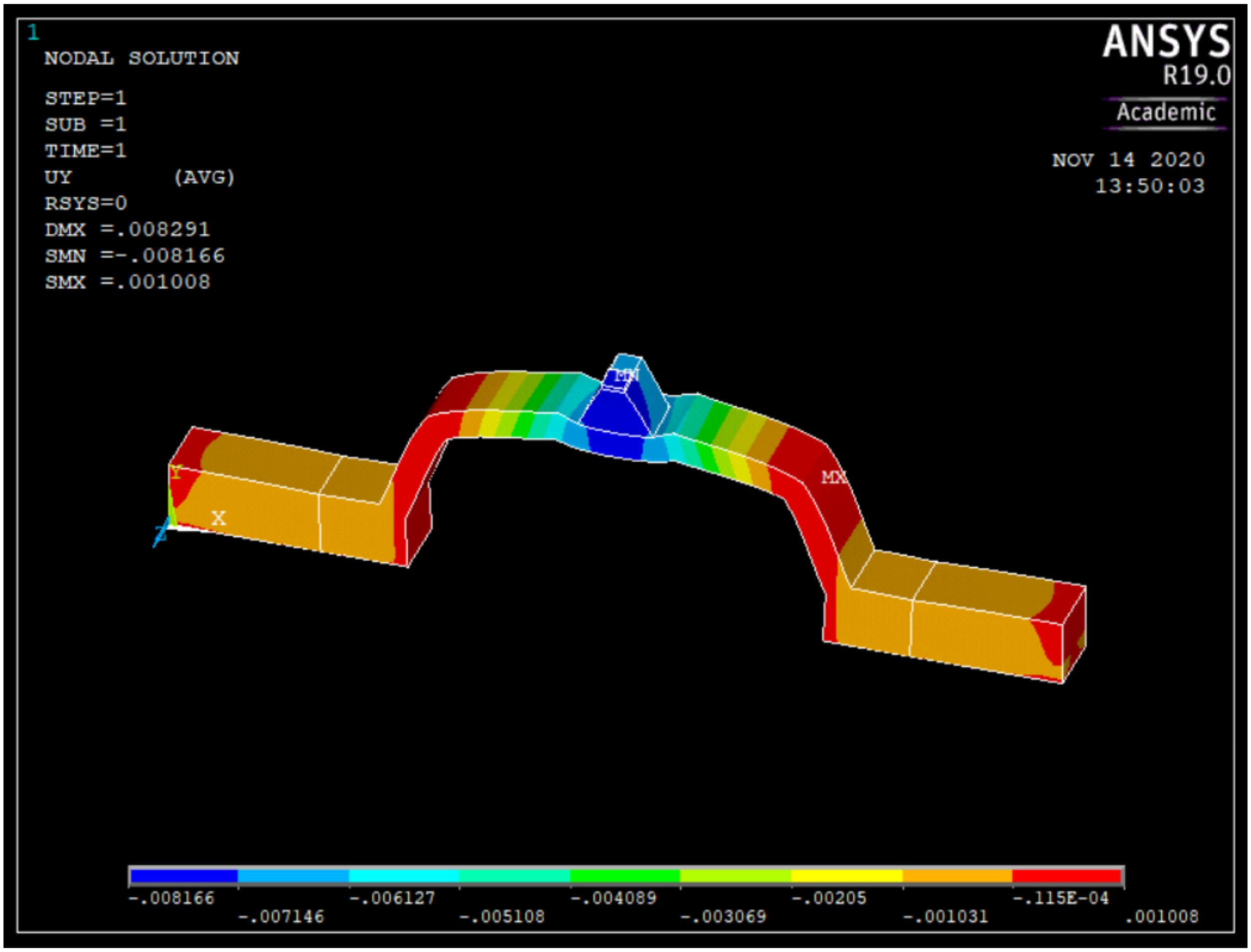

Figure 142 - 3D Nodal Y-Displacements Rerun No. 5 - Test No. 4 CIP Model

J4 - 2D Analysis Simulation Hollow-Core Model

FINITE ELEMENT ANALYSIS WITH ANSYS
HOLLOW CORE 2D CULVERT ANALSYS

Step-by-Step model:

1. Create a directory for the ANSYS files; for example, call it "ANSYS Model"
2. Start ANSYS
   a. Change directory: From Utility Menu (top menu) select *File*, *Change Directory*…
   b. Set Jobname to "CIP Culvert Analysis": From Utility Menu select, *File*, *Change Jobname*…
3. From ANSYS Main Menu (located on the left side of the screen), select *Preferences* …
   a. Select *Structural* → Click on *OK*
4. From ANSYS *Main Menu*, select *Preprocessor*
   a. *Element Type* →*Add/Edit/Delete*…→
      i. *Add*…→ *Solid* → *Quad 4 Node 182* (also known as *Plane 182*) → for *Element Type 1* → *OK* →
      ii. *Options*… → For *Element Behavior K3*, select *Plane Stress*, and no other changes are necessary → *OK*
      iii. *Close* → Close *Element Type* submenu of the *Main Menu*
   b. *Material Properties* →
      i. *Material Models*…→ *Structural* → *Linear* → *Elastic* → *Isotropic* → Enter value for EX: 3.83e6 → Enter value for PRXY: 0.2 → *OK*.

Note: The concrete will have a modulus of elasticity of 3.83 x10^6 psi and Poisson's ratio of 0.2.

      ii. *Material* →*New Model* →Enter a 2 for material ID
      iii. *Material Models*…→ *Structural* → *Linear* → *Elastic* → *Isotropic* → Enter value for EX: 4,514 → Enter value for PRXY: 0.3 → *OK*.

Note: The backfill soil (sand) will have a modulus of elasticity of 4,514psi and Poisson's ratio of 0.3.

      iv. *Material* →*New Model* →Enter a 3 for material ID
      v. *Material Models*…→ *Structural* → *Linear* → *Elastic* → *Isotropic* → Enter value for EX: 11,600 → Enter value for PRXY: 0.3 → *OK*.

Note: The top 12 inches of backfill soil (gravel) will have a modulus of elasticity of 11,600psi and Poisson's ratio of 0.3.

      vi. *Material* →*New Model* →Enter a 4 for material ID
      vii. *Material Models*…→ *Structural* → *Linear* → *Elastic* → *Isotropic* → Enter value for EX: 29e6 → Enter value for PRXY: 0.3 → *OK*.

Note: The steel plate will have a modulus of elasticity of 29 x10^6 psi and Poisson's ratio of 0.3.

      i. *Material* →*New Model* →Enter a 5 for material ID
      ii. *Material Models*…→ *Structural* → *Linear* → *Elastic* → *Isotropic* → Enter value for EX: 3e6 → Enter value for PRXY: 0.25 → *OK*.

Note: The grout will have a modulus of elasticity of 3 x 10^6 psi and Poisson's ratio of 0.25.

      i. From the *Material* pull-down menu of the "*Define Material Model Behavior*" window, select *Exit*.

   c. *Modeling* → *Create*
      i. *Keypoints* →*In Active CS*
         Included the following nodes:

Key Point No.	X-Coordinate	Y-Coordinate	Z-Coordinate
1	33.09	0.00	0.00
2	51.72	0.00	0.00
3	51.72	14.22	0.00

4	63.72	35.00	0.00
5	84.50	47.00	0.00
6	108.50	47.00	0.00
7	129.28	35.00	0.00
8	141.28	14.22	0.00
9	141.28	0.00	0.00
10	159.91	0.00	0.00
11	159.91	14.22	0.00
12	148.21	14.22	0.00
13	146.48	17.22	0.00
14	134.48	38.00	0.00
15	133.68	39.39	0.00
16	132.28	40.20	0.00
17	111.50	52.20	0.00
18	110.11	53.00	0.00
19	108.50	53.00	0.00
20	84.50	53.00	0.00
21	82.89	53.00	0.00
22	81.50	52.20	0.00
23	60.72	40.20	0.00
24	59.32	39.39	0.00
25	58.52	38.00	0.00
26	46.52	17.22	0.00
27	44.79	14.22	0.00
28	33.09	14.22	0.00
29	0.00	0.00	0.00
30	193.00	0.00	0.00
31	193.00	53.00	0.00
32	193.00	65.00	0.00
33	0.00	65.00	0.00
34	0.00	53.00	0.00
35	91.50	65.00	0.00
36	101.50	65.00	0.00
37	101.50	66.00	0.00
38	91.50	66.00	0.00
39	50.78	18.60	0.00
40	53.67	23.60	0.00
41	56.56	28.61	0.00
42	59.45	33.62	0.00
43	65.10	39.26	0.00
44	70.10	42.15	0.00
45	75.11	45.04	0.00
46	80.12	47.93	0.00
47	87.83	50.00	0.00
48	93.61	50.00	0.00
49	99.39	50.00	0.00
50	105.17	50.00	0.00
51	112.88	47.93	0.00

52	117.89	45.04	0.00
53	122.90	42.15	0.00
54	127.90	39.26	0.00
55	133.55	33.62	0.00
56	136.44	28.61	0.00
57	139.33	23.60	0.00
58	142.22	18.60	0.00

ii. *Areas* → *Arbitrary* → *Through KPs* →
Select the nodes for the footing, grout and hollow-core members separately.

iii. *Areas* → *Arbitrary* → *Through KPs* →
Select nodes 21 to 29 and 34 presented above to create a soil area left of the culvert which represents the sand backfill soil mass.

iv. *Areas* → *Arbitrary* → *Through KPs* →
Select nodes 10 to 18, 30 and 31 presented above to create a soil area right of the culvert which represents the sand backfill soil mass.

v. *Areas* → *Arbitrary* → *Through KPs* →
Select nodes 31 to 34, 18 to 21, 35 and 36 presented above to create a soil area on top of the culvert which represents the gravel backfill soil mass.

vi. *Areas* → *Arbitrary* → *Through KPs* →
Select nodes 35 through 38 presented above to create the steel plate area to be located on top of the 12 inches of gravel.

vii. *Areas* → *Circle* → *Solid Circle* →
Enter the coordinates from Key Points 39 to 58 for each circle.
Enter a value of 1.58 for the radius of each circle
Note: X- and Y-coordinates represent the center of the circles

viii. Close *Arbitrary* and *Create* submenus of the *Main Menu*

d. *Modeling* → *Operate* → *Booleans* →

i. *Subtract* → *Areas* → With the vertical arrow pick the lower left hollow core rectangle member → *OK* → Now pick the four circles of that member → *OK* → holes should appear within the member.

ii. Repeat Step 4.d.i. for all hollow-core members.

iii. *Glue* → *Areas* → With the vertical arrow pick all areas (soil masses, culvert, grout and steel plate) → *Apply*

iv. Close the *Glue* and *Operate* submenus of the *Main Menu*

e. *Meshing* →

i. *Size Controls* → *Manual Size* → *Areas – Picked Areas* → With the vertical arrow pick the soil masses → *Apply* → For the *SIZE* include a 2 → *OK*

ii. *Size Controls* → *Manual Size* → *Areas – Picked Areas* → With the vertical arrow pick the footings, hollow core slabs, grout and steel plate area → *Apply* → For the *SIZE* include a 0.5 → *OK*

iii. Close the *Size Controls* submenu of the *Main Menu*.

iv. *Mesh Attributes* → *Picked Areas* → with the vertical arrow pick the hollow core slabs → *OK* → make sure that MAT=1 and TYPE 1 = Plane 182 → *OK*

v. *Mesh Attributes* → *Picked Areas* → with the vertical arrow pick the sand soil masses (left and right of the culvert) → *OK* → enter MAT=2 and Type 1 = Plane 182 and leave everything else unchanged → *OK*

vi. *Mesh Attributes* → *Picked Areas* → with the vertical arrow pick the gravel soil mass (top) → *OK* → enter MAT=3 and Type 1 = Plane 182 and leave everything else unchanged → *OK*

vii. *Mesh Attributes* → *Picked Areas* → with the vertical arrow pick the steel plate area → *OK* → enter MAT=4 and Type 1 = Plane 182 and leave everything else unchanged → *OK*
viii. *Mesh Attributes* → *Picked Areas* → with the vertical arrow pick the grout segments → *OK* → make sure that MAT=5 and TYPE 1 = Plane 182 → *OK*
ix. Close the *Mesh Attributes* submenu.

f. *Meshing* → *Mesh* → *Areas* → *Free* → With the vertical arrow, pick all areas to be meshed → *OK*.

At this point, all elements will be meshed, in somewhat of a random pattern.

g. Close the *Mesh* submenu of the *Main Menu*.
h. *Loads* → *Define Loads* → *Apply* → *Structural* → *Displacements* → *On Lines* → With the vertical arrow, select the bottom edge of the model → *OK* → In the "*Apply U, ROT on Lines*" window, select (highlight) *ALL DOF* (i.e., all degrees of freedoms to be zero) → *Apply*
i. With the vertical arrow, select the right and left edges of the soil masses → *OK* → In the "*Apply U, ROT on Lines*" window, select (highlight) *UX* (i.e., roller) → *OK*
j. Close *Displacement* and *Apply* submenus.
k. *Loads* → *Define Loads* → *Apply* → *Structural* → *Pressure* → *On Lines* → with the vertical arrow select the top line of steel plate → *OK* → For *VALUE Load PRESS value*, type in 1,820 → *OK*

Note: Here a pressure of 1,820 lb/in acting down in the y-direction will be applied on the top of the steel plate.

l. Close the *Pressure* and *Apply* submenus. Close the *Preprocessor* menu.

5. From ANSYS Main Menu select *Solution*
   a. *Solve* → *Current LS* → *OK* → close the "Note" window → close "STATUS Command" window
   b. Close the *Solution* window
6. Save the active drawing window.
   a. From Utility Menu, select PlotCtrls → Symbols → click on All Applied BCs → In front of *Surface Load Symbols*, select *Pressure* → In front of *Show pres and convect as*, select *Arrows* (this will show the show the pressure as arrows).
7. From Utility Menu, select *Select* → *Entities* →
   a. From the first pull-down menu select *Elements* → from the second pull-down menu select *By Attributes* → click on *Material num* → enter 4 in the box → *Apply* → *Invert*
   b. From the first pull-down menu now select *Nodes* → from the second pull-down menu select *Attached to* → click on *Elements* → *OK*

Note: This will allow ANSYS to analyze the stresses in the soil masses and the concrete culvert but neglect those in the steel plate.

   c. Close the Select Entities window

8. See and/or save results:
   a. From the *Main Menu*, select *General Postproc*
      i. *Plot Results* → *Contour Plot – Element Solution…* → For the item to be contoured, select *Stress* → Then select *Stress, Y-Component of Stress.*
      ii. *Plot Results* → *Contour Plot – Nodal Solution…* → For the item to be contoured, select *Stress* → Then select *Stress, Y-Component of Stress.*
      iii. *List Results* → *Nodal Solution* → *Stress* → *Y-Component of Stress* → *OK.*
9. To exit ANSYS:
   a. From *ANSYS Utility Menu*, select *File* → *Exit …* → Click on *Save Geom+Loads* → *OK*

J5 – 3D Analysis Simulation Hollow-Core Model

FINITE ELEMENT ANALYSIS WITH ANSYS
HOLLOW CORE CULVERT 3D ANALSYS

Step-by-Step model:

1. Create a directory for the ANSYS files; for example, call it "ANSYS 3D Model"
2. Start ANSYS
   a. Change directory: From Utility Menu (top menu) select *File, Change Directory…*
   b. Set Jobname to "CIP Culvert Analysis 3D": From Utility Menu select, *File, Change Jobname…*
3. From ANSYS Main Menu (located on the left side of the screen), select *Preferences …*
   a. Select *Structural* → Click on *OK*
4. From ANSYS *Main Menu*, select *Preprocessor*
   a. *Element Type* →*Add/Edit/Delete…* →
      i. *Add…* → *Solid* → *Brick 8 Node 185* → for *Element Type 1* → *OK* →
      ii. *Close* → Close *Element Type* submenu of the *Main Menu*
   b. *Material Properties* →
      i. *Material Models…* → *Structural* → *Linear* → *Elastic* → *Isotropic* → Enter value for EX: 3.83e6 → Enter value for PRXY: 0.2 → *OK*.

Note: The concrete will have a modulus of elasticity of 3.83 x10^6 psi and Poisson's ratio of 0.2.

      ii. *Material* → *New Model* → Enter a 2 for material ID
      iii. *Material Models…* → *Structural* → *Linear* → *Elastic* → *Isotropic* → Enter value for EX: 4,514→ Enter value for PRXY: 0.3 → *OK*.

Note: The backfill soil (sand) will have a modulus of elasticity of 4,514psi and Poisson's ratio of 0.3.

      i. *Material* → *New Model* → Enter a 3 for material ID
      ii. *Material Models…* → *Structural* → *Linear* → *Elastic* → *Isotropic* → Enter value for EX: 11,600→ Enter value for PRXY: 0.3 → *OK*.

Note: The backfill soil (gravel) will have a modulus of elasticity of 11,600psi and Poisson's ratio of 0.3.

      iii. *Material* → *New Model* → Enter a 4 for material ID
      iv. *Material Models…* → *Structural* → *Linear* → *Elastic* → *Isotropic* → Enter value for EX: 29e6 → Enter value for PRXY: 0.3 → *OK*.

Note: The steel plate will have a modulus of elasticity of 29 x10^6 psi and Poisson's ratio of 0.3.

      v. From the *Material* pull-down menu of the "*Define Material Model Behavior*" window, select *Exit*.
   c. *Modeling* → *Create*
      i. *Keypoints* → *In Active CS*
      Included the following nodes:

Key Point No.	X-Coordinate	Y-Coordinate	Z-Coordinate
1	33.09	0.00	0.00
2	51.72	0.00	0.00
3	51.72	14.22	0.00
4	63.72	35.00	0.00
5	84.50	47.00	0.00
6	108.50	47.00	0.00
7	129.28	35.00	0.00
8	141.28	14.22	0.00
9	141.28	0.00	0.00
10	159.91	0.00	0.00
11	159.91	14.22	0.00
12	148.21	14.22	0.00

13	146.48	17.22	0.00
14	134.48	38.00	0.00
15	133.68	39.39	0.00
16	132.28	40.20	0.00
17	111.50	52.20	0.00
18	110.11	53.00	0.00
19	108.50	53.00	0.00
20	84.50	53.00	0.00
21	82.89	53.00	0.00
22	81.50	52.20	0.00
23	60.72	40.20	0.00
24	59.32	39.39	0.00
25	58.52	38.00	0.00
26	46.52	17.22	0.00
27	44.79	14.22	0.00
28	33.09	14.22	0.00
29	0.00	0.00	0.00
30	193.00	0.00	0.00
31	193.00	53.00	0.00
32	193.00	65.00	0.00
33	0.00	65.00	0.00
34	0.00	53.00	0.00
35	91.50	65.00	0.00
36	101.50	65.00	0.00
37	101.50	66.00	0.00
38	91.50	66.00	0.00
39	50.78	18.60	0.00
40	53.67	23.60	0.00
41	56.56	28.61	0.00
42	59.45	33.62	0.00
43	65.10	39.26	0.00
44	70.10	42.15	0.00
45	75.11	45.04	0.00
46	80.12	47.93	0.00
47	87.83	50.00	0.00
48	93.61	50.00	0.00
49	99.39	50.00	0.00
50	105.17	50.00	0.00
51	112.88	47.93	0.00
52	117.89	45.04	0.00
53	122.90	42.15	0.00
54	127.90	39.26	0.00
55	133.55	33.62	0.00
56	136.44	28.61	0.00
57	139.33	23.60	0.00
58	142.22	18.60	0.00

i. *Areas* → *Arbitrary* → *Through KPs* →
Select the nodes for the footing, grout and hollow-core members separately.

ii. *Areas* → *Arbitrary* → *Through KPs* →
Select nodes 21 to 29 and 34 presented above to create a soil area left of the culvert which represents the sand backfill soil mass.

iii. *Areas* → *Arbitrary* → *Through KPs* →
Select nodes 10 to 18, 30 and 31 presented above to create a soil area right of the culvert which represents the sand backfill soil mass.

iv. *Areas* → *Arbitrary* → *Through KPs* →
Select nodes 31 to 34, 18 to 21, 35 and 36 presented above to create a soil area on top of the culvert which represents the gravel backfill soil mass.

v. *Areas* → *Arbitrary* → *Through KPs* →
Select nodes 35 through 38 presented above to create the steel plate area to be located on top of the 12 inches of gravel.

vi. *Areas* → *Circle* → *Solid Circle* →
Enter the coordinates from Key Points 39 to 58 for each circle.
Enter a value of 1.58 for the radius of each circle

Note: X- and Y-coordinates represent the center of the circles

vii. Close *Arbitrary* and *Create* submenus of the *Main Menu*

d. *Modeling* → *Operate* → *Booleans* →

i. *Subtract* → *Areas* → With the vertical arrow pick the lower left hollow core rectangle member → *OK* → Now pick the four circles of that member → *OK* → holes should appear within the member.

ii. Repeat Step 4.d.i. for all hollow-core members.

e. *Modeling* → *Operate* → *Extrude* →

i. *Areas* → *By XYZ Offset* → Select the soil and culvert areas (including the grouted connections) → *Apply* → Type 0 for DX and DY, and a -15 for the DZ offset of extrusion. Leave RX, RY and RZ scales without any values.

Note: This will create volumes having a depth of 15 inches for the soil and culvert.

ii. *Areas* → *By XYZ Offset* → Select the steel plate area → *Apply* → Type 0 for DX and DY, and a -2.5 for the DZ offset of extrusion. Leave RX, RY and RZ scales without any values.

Note: This will create a volume having a depth of 2.5 inches for the steel plate.

f. *Modeling* → *Operate* → *Booleans* →

i. *Glue* → *Volumes* → With the vertical arrow pick the soil, culvert and plate volumes → *Apply*

i. Close the *Glue* and *Operate* submenus of the *Main Menu*

g. *Meshing* →

i. *Size Controls* → *Manual Size* → *Areas – Picked Areas* → Select all areas that represent the soil and the culvert → *Apply* → *SIZE* → type in 2 → *OK*

ii. *Size Controls* → *Manual Size* → *Areas – Picked Areas* → Select all faces of the steel plate except the bottom one → *Apply* → *SIZE* → type in 1 → *OK*

iii. *Size Controls* → *Manual Size* → *Areas – Picked Areas* → Select the bottom face of the steel plate → *Apply* → *SIZE* → type in 0.5 → *OK*

iv. Close the *Size Controls* submenu of the *Main Menu*.

v. *Mesh Attributes* → *Picked Volumes* → with the vertical arrow pick the concrete culvert → *OK* → make sure that MAT=1 and TYPE 1 = Solid 185 is selected → *OK*

vi. *Mesh Attributes* → *Picked Volumes* → with the vertical arrow pick the sand soil volumes → *OK* → make sure that MAT=2 and TYPE 1 = Solid 185 is selected → *OK*

vii. *Mesh Attributes* → *Picked Volumes* → with the vertical arrow pick the gravel soil volume → *OK* → make sure that MAT=3 and TYPE 1 = Solid 185 is selected → *OK*

viii. *Mesh Attributes* → *Picked Volumes* → with the vertical arrow pick the steel plate → *OK* → make sure that MAT=4 and TYPE 1 = Solid 185 is selected → *OK*

ix. Close the *Mesh Attributes* submenu.

x. *Mesh* → *Volumes* → *Free* → With the vertical arrow pick the volumes to be meshed → *OK*.

Note: At this point, the five volumes will be meshed, in somewhat of a random pattern. In addition, ANSYS might show some warnings and suggestions related to element shapes and possible ways to obtain more accurate results using alternative element types. Close said warnings signs.

xi. Close the *Mesh* submenu of the *Main Menu*.

5. *Loads* → *Define Loads* → *Apply* → *Structural* →
   i. *Displacements* → *On Lines* → With the vertical arrow select the front and back face lines of the soil and culvert edges and the front lines of the plate edges → *OK* → In the "*Apply U, ROT on Lines*" window, select (highlight) UZ (i.e., Z coordinate to be zero) → *Apply*
   ii. *Displacements* → *On Lines* → With the vertical arrow select the right and left face lines of the soil edges → *OK* → In the "*Apply U, ROT on Lines*" window, select (highlight) UX (i.e., X coordinate to be zero) → *Apply*
   iii. *Displacements* → *On Lines* → With the vertical arrow select the bottom edge lines → *OK* → In the "*Apply U, ROT on Lines*" window, select (highlight) All DOF (i.e., X, Y and Z coordinates to be zero) → *Apply*
   iv. *Pressure* → *On Areas* → with the vertical arrow select the top face of the steel plate → *OK* → For *VALUE Load PRESS value*, type in 364 → *OK*

Note: Here a pressure of 364 lb/in^2 acting down in the y-direction will be applied on the top of the steel plate.

   v. Close the *Pressure* and *Apply* submenus. Close the *Preprocessor* menu.

6. From ANSYS Main Menu select *Solution*
   a. *Solve* → *Current LS* → *OK* → close the "Note" window → close "STATUS Command" window
   b. Close the *Solution* window
7. Save the active drawing window.
   a. From Utility Menu, select PlotCtrls → Symbols → click on All Applied BCs → In front of *Surface Load Symbols*, select *Pressure* → In front of *Show pres and convect as*, select *Arrows* (this will show the show the pressure as arrows).
8. From Utility Menu, select *Select* → *Entities* →
   a. From the first pull-down menu select *Elements* → from the second pull-down menu select *By Attributes* → click on *Material num* → enter 4 in the box → *Apply* → *Invert*
   b. From the first pull-down menu now select *Nodes* → from the second pull-down menu select *Attached to* → click on *Elements* → *OK*

Note: This will allow ANSYS to analyze the stresses in the soil mass and the concrete culvert but neglect those in the steel plate.

   c. Close the Select Entities window
9. See and/or save results:
   a. From the *Main Menu*, select *General Postproc*
      i. *Plot Results* → *Contour Plot – Element Solution…* → For the item to be contoured, select *Stress* → Then select *Stress, Y-Component of Stress*.
      ii. *Plot Results* → *Contour Plot – Nodal Solution…* → For the item to be contoured, select *Stress* → Then select *Stress, Y-Component of Stress*.
      iii. *List Results* → *Nodal Solution* → *Stress* → *Y-Component of Stress* → *OK*.
10. To exit ANSYS:
   a. From *ANSYS Utility Menu*, select *File* → *Exit …* → Click on *Save Geom+Loads* → *OK*

J6 – Hollow-Core Model ANSYS Nodal Solutions

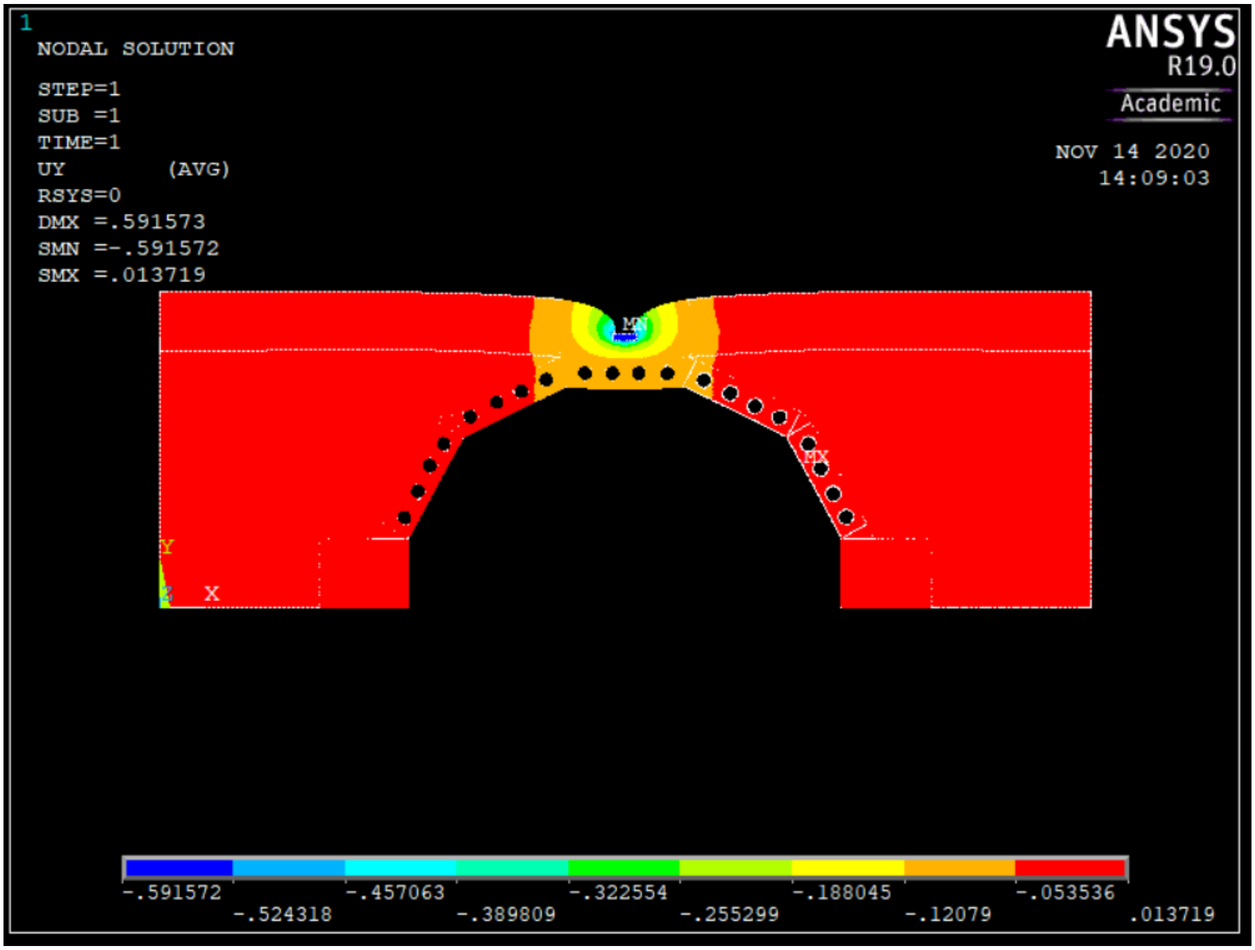

Figure 143 - 2D Nodal Y-Displacements Initial Predictions Test No. 1 Hollow-Core Model

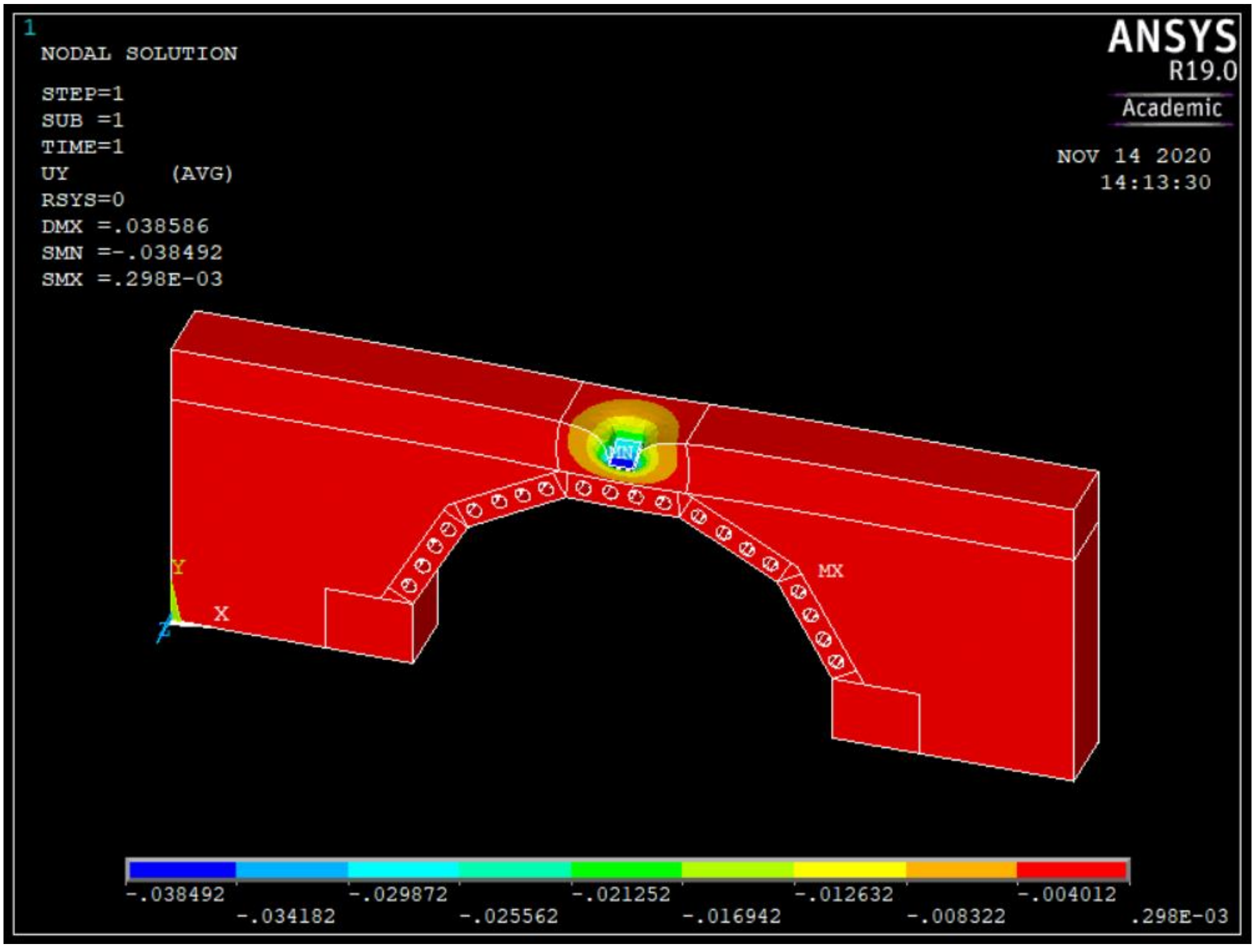

Figure 144 - 3D Nodal Y-Displacements Initial Predictions Test No. 1 Hollow-Core Model

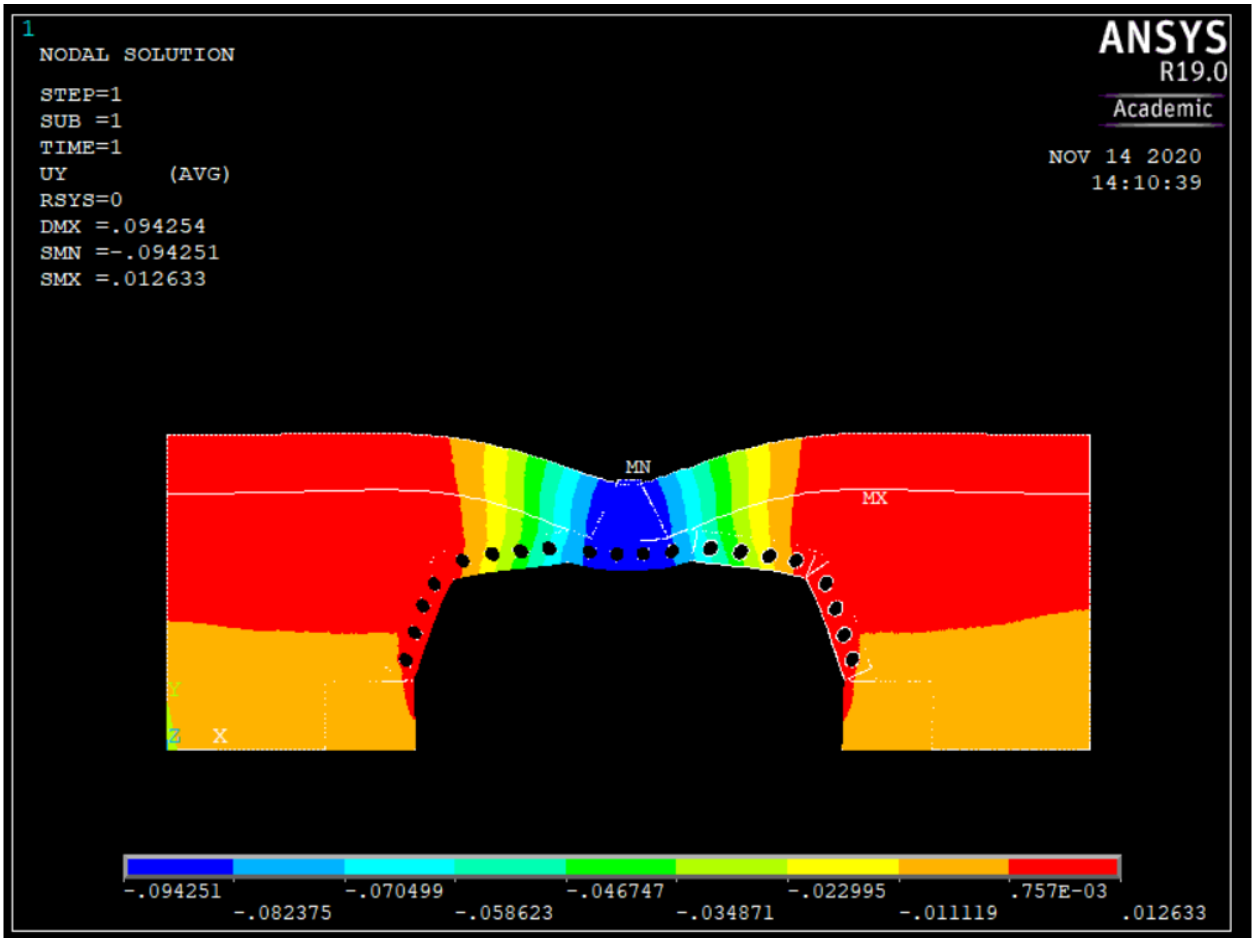

Figure 145 - 2D Nodal Y-Displacements Initial Predictions Test No. 2 Hollow-Core Model

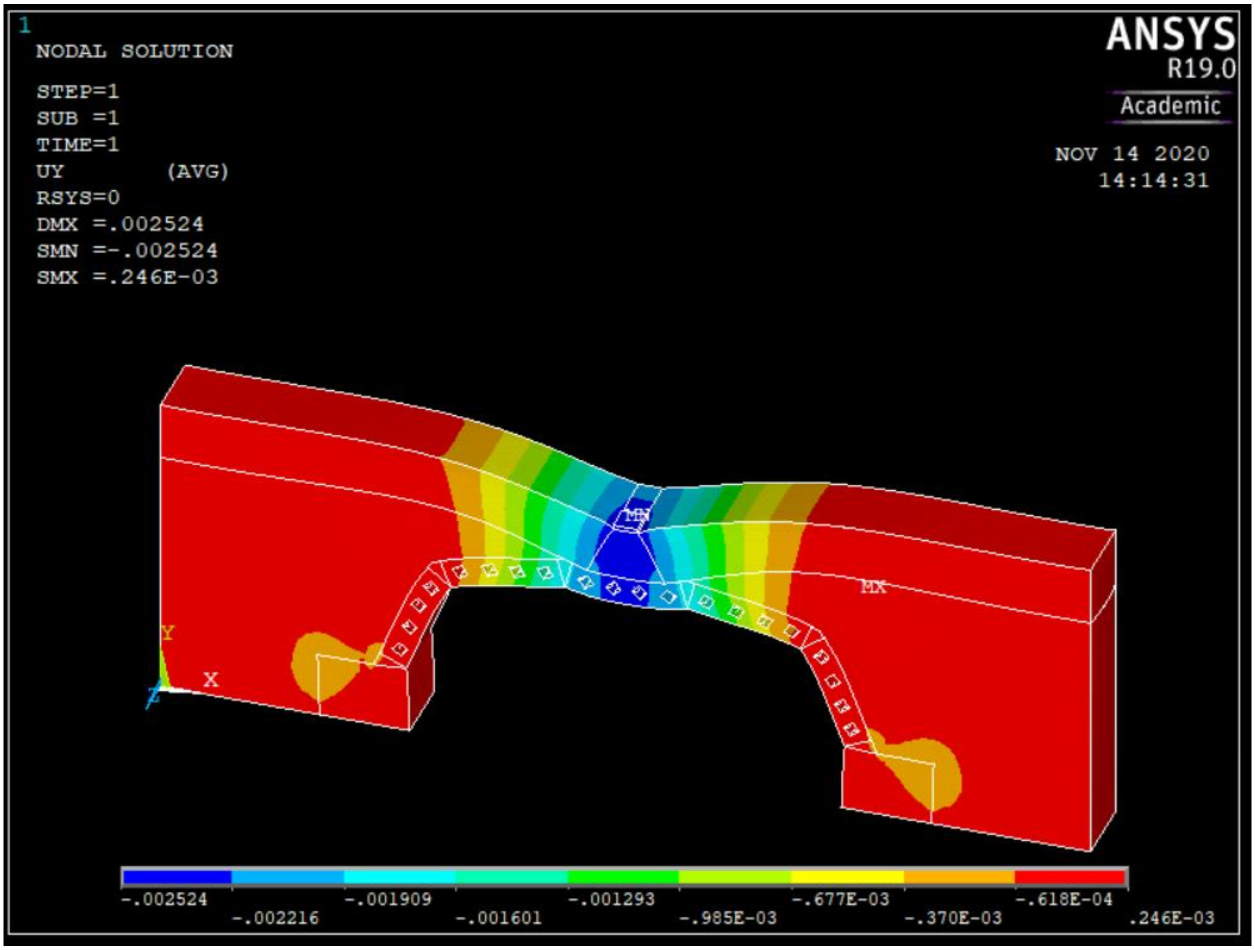

Figure 146 - 3D Nodal Y-Displacements Initial Predictions Test No. 2 Hollow-Core Model

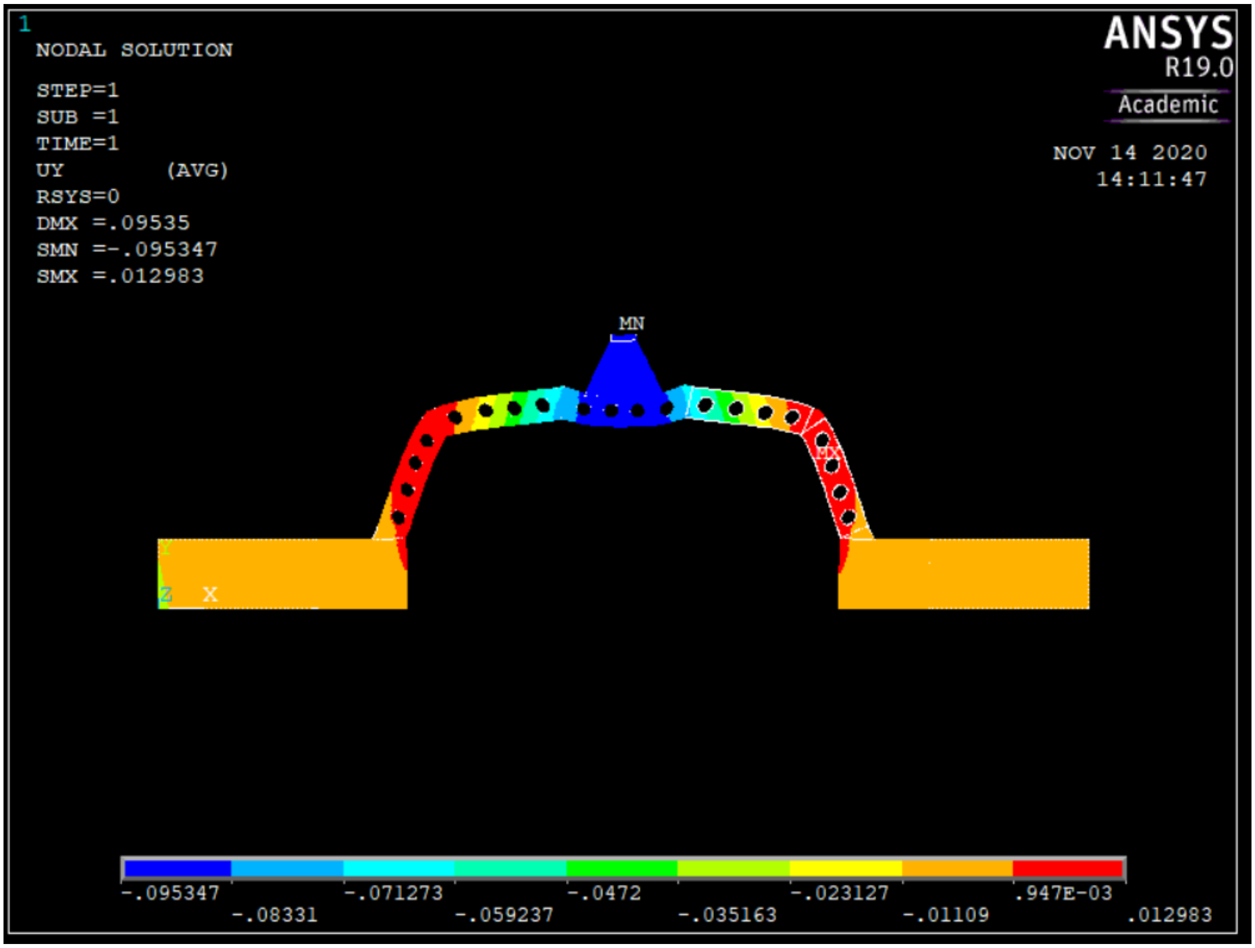

Figure 147 - 2D Nodal Y-Displacements Initial Predictions Test No. 3 Hollow-Core Model

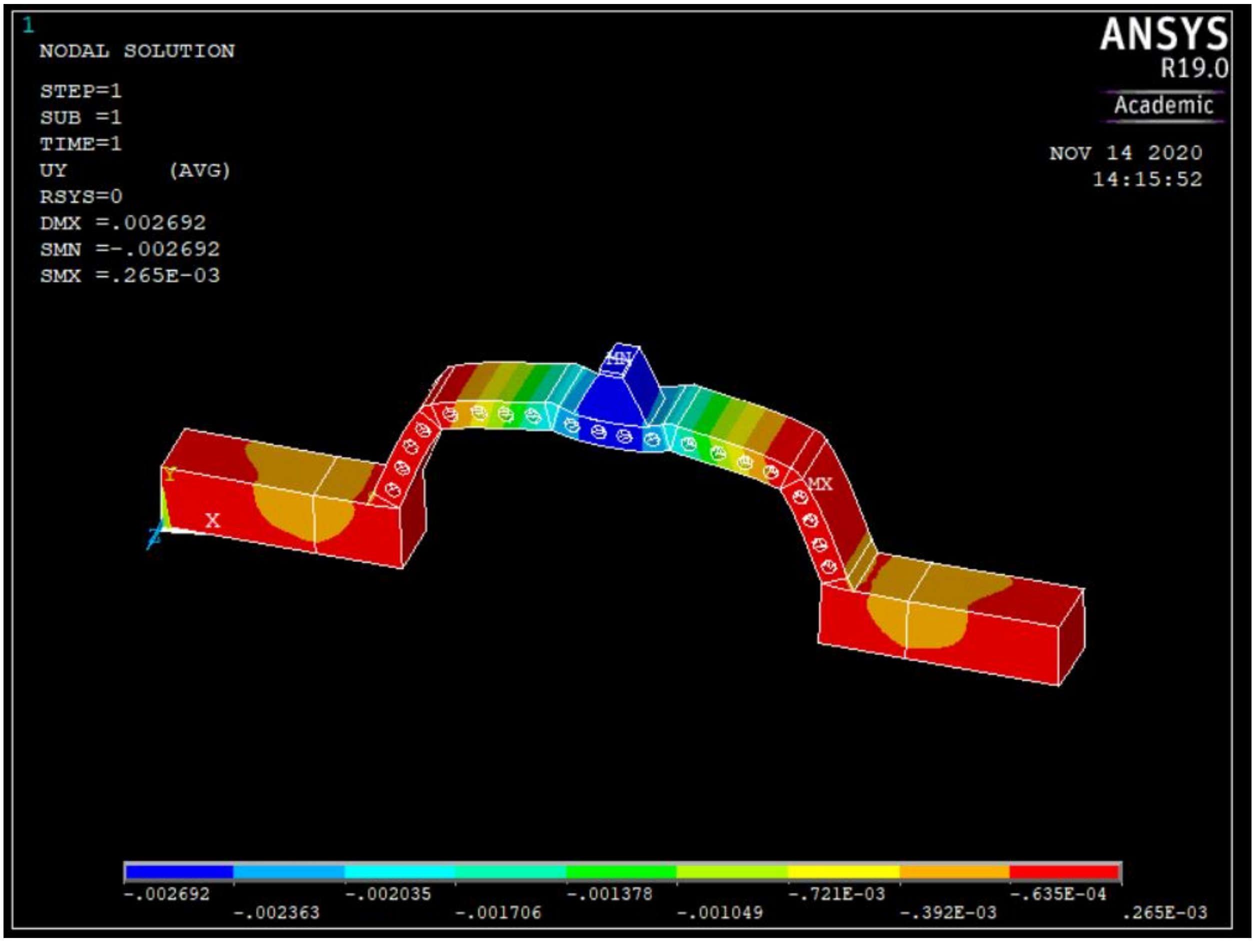

Figure 148 - 3D Nodal Y-Displacements Initial Predictions Test No. 3 Hollow-Core Model

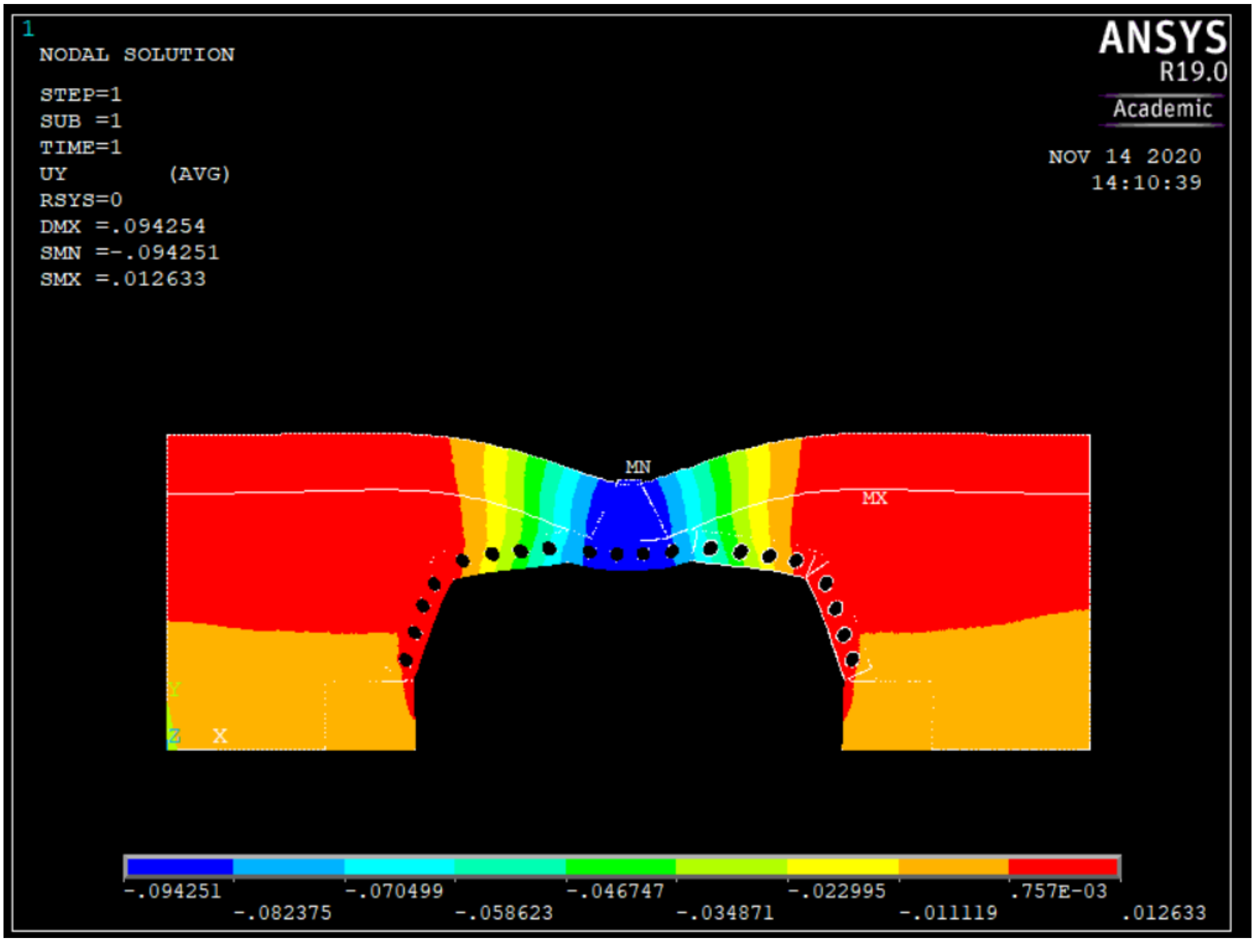

Figure 149 - 2D Nodal Y-Displacements Rerun No. 1 - Test No. 2 Hollow-Core Model

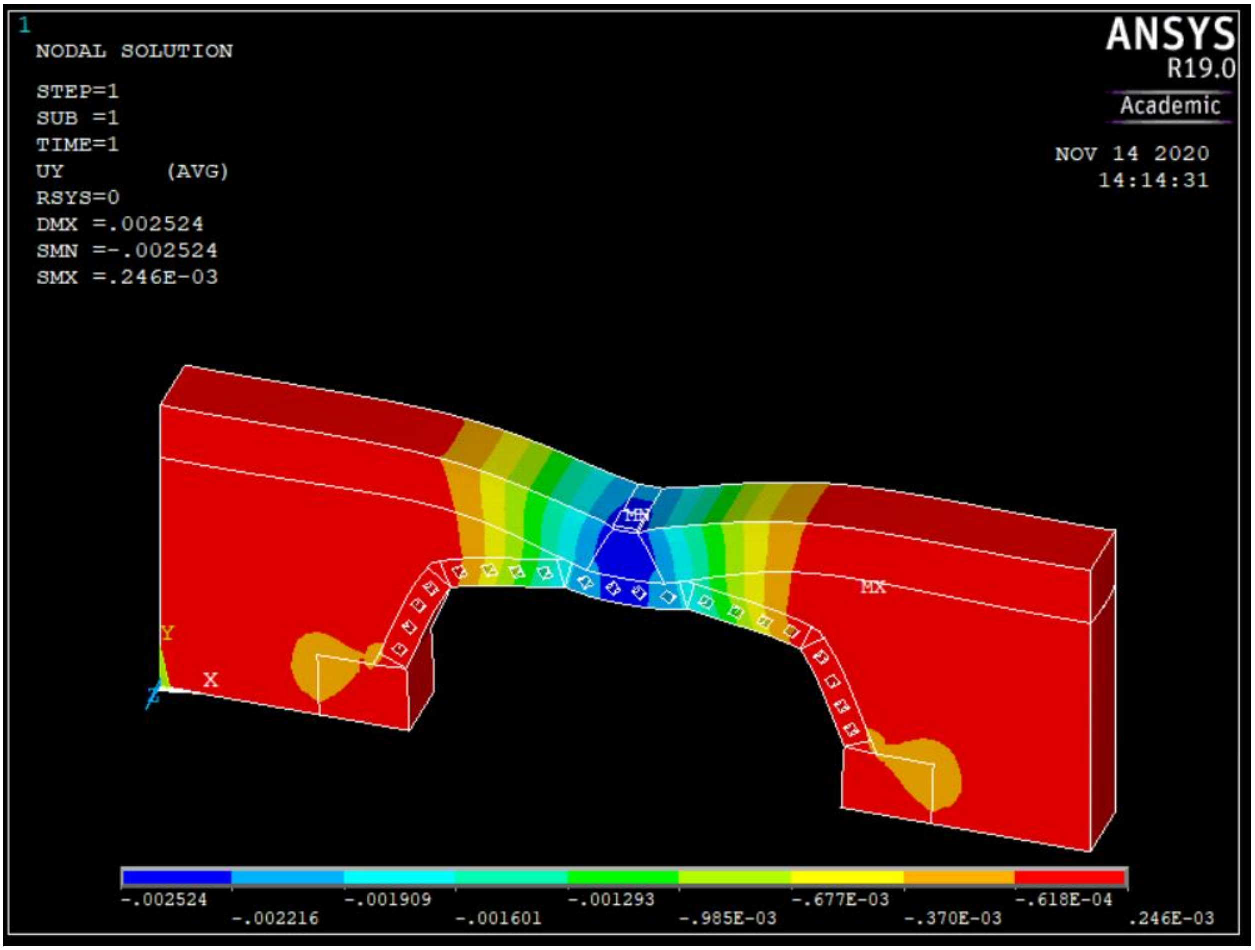

Figure 150 - 3D Nodal Y-Displacements Rerun No. 1 - Test No. 2 Hollow-Core Model

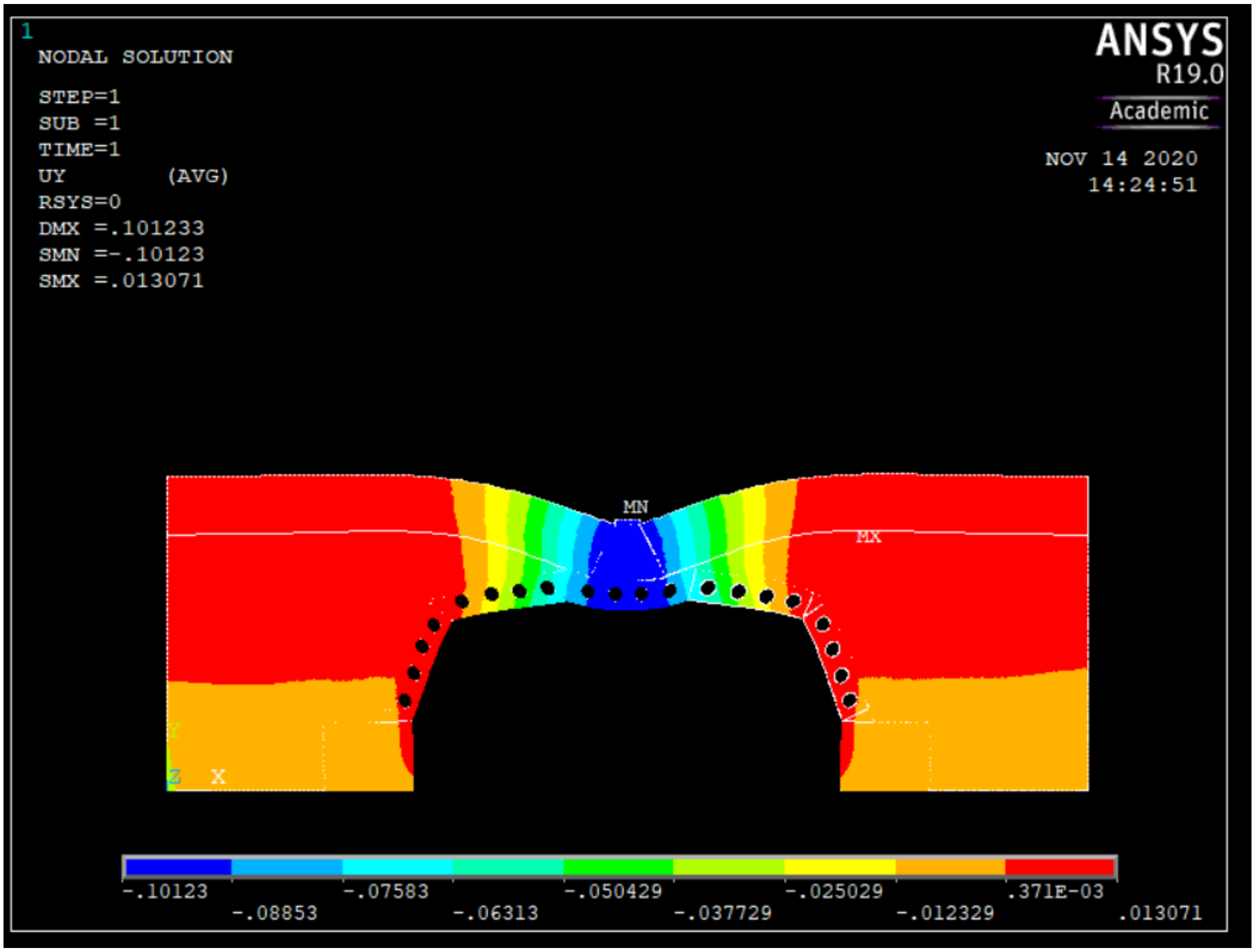

Figure 151 - 2D Nodal Y-Displacements Rerun No. 2 - Test No. 2 Hollow-Core Model

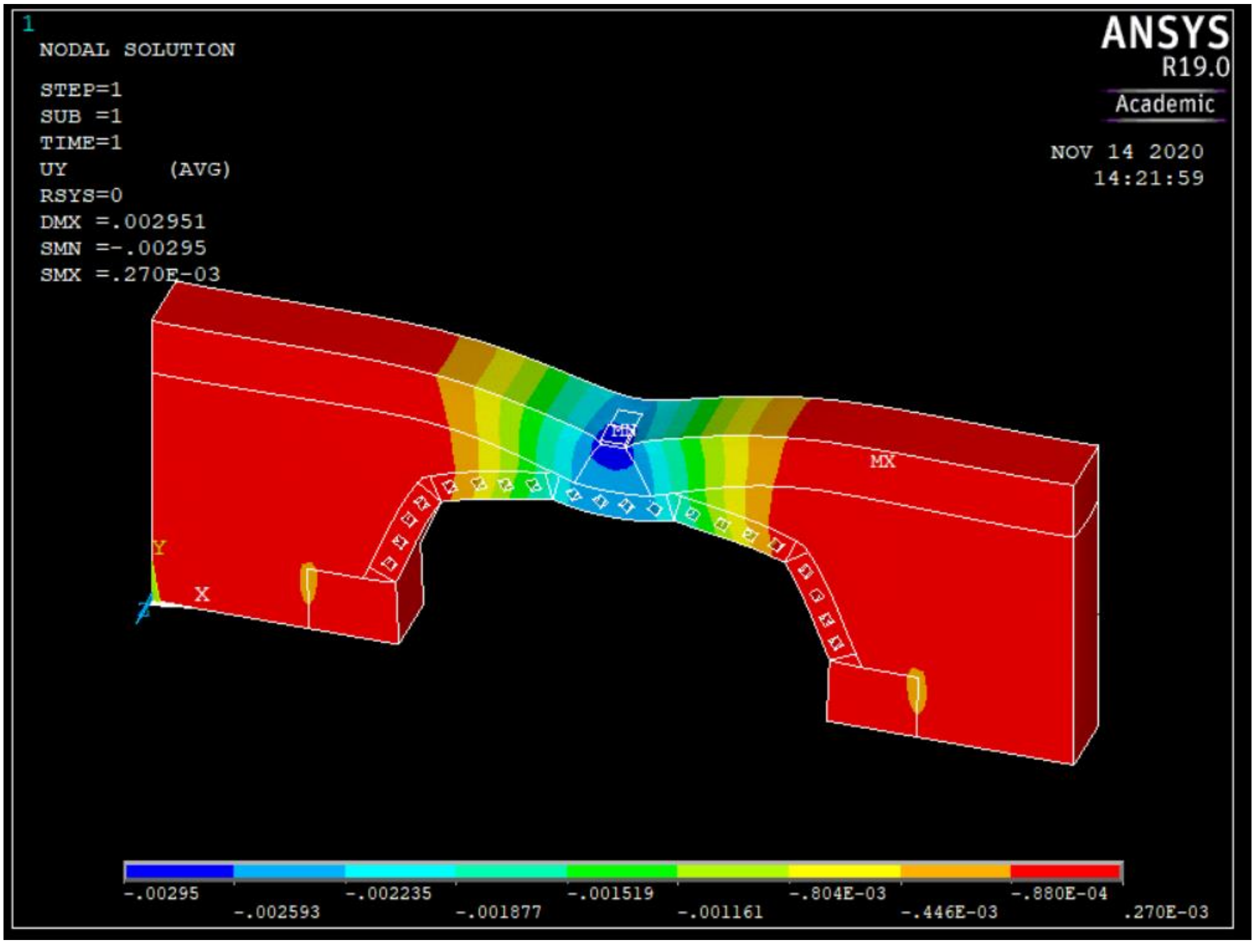

Figure 152 - 3D Nodal Y-Displacements Rerun No. 2 - Test No. 2 Hollow-Core Model

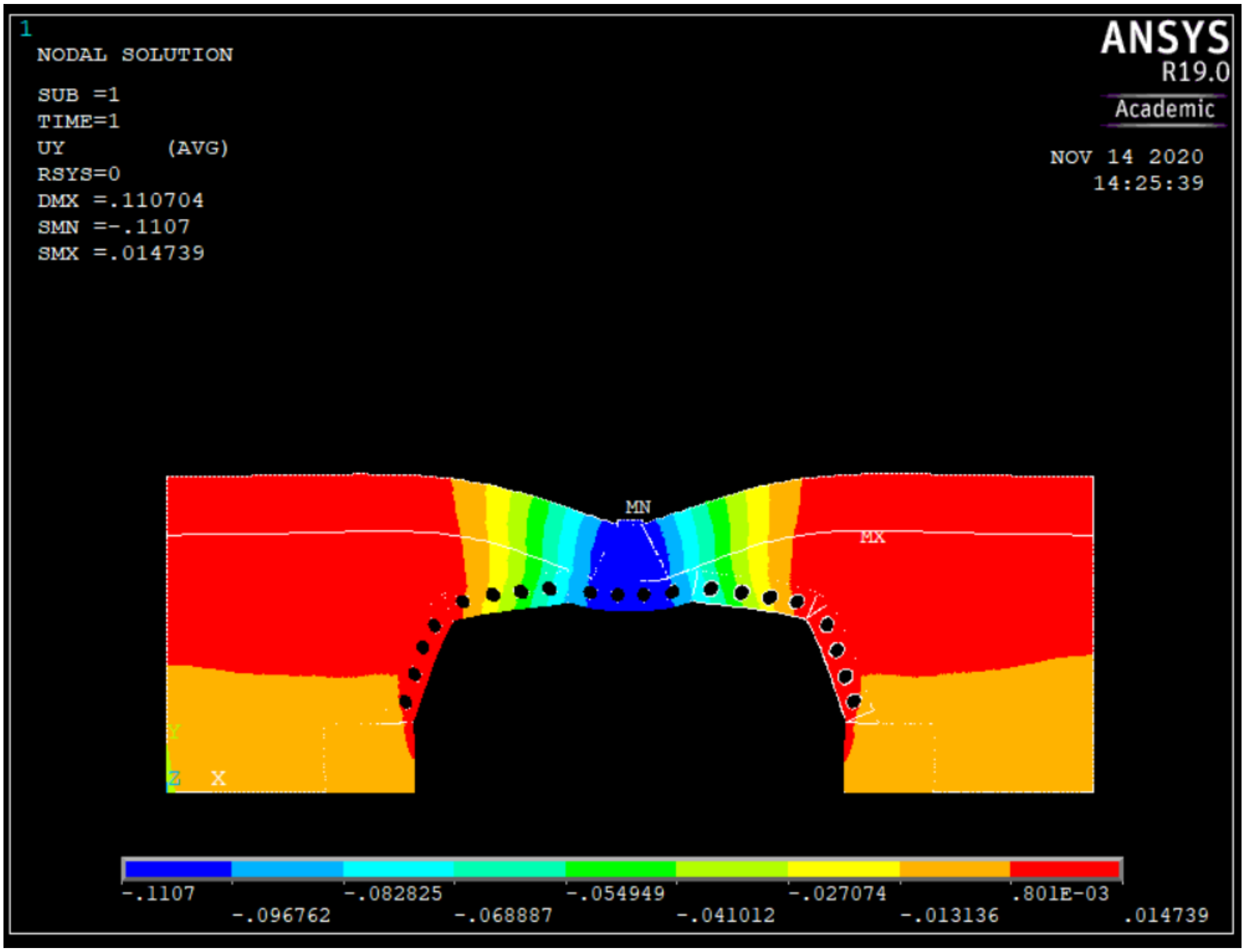

Figure 153 - 2D Nodal Y-Displacements Rerun No. 3 - Test No. 2 Hollow-Core Model

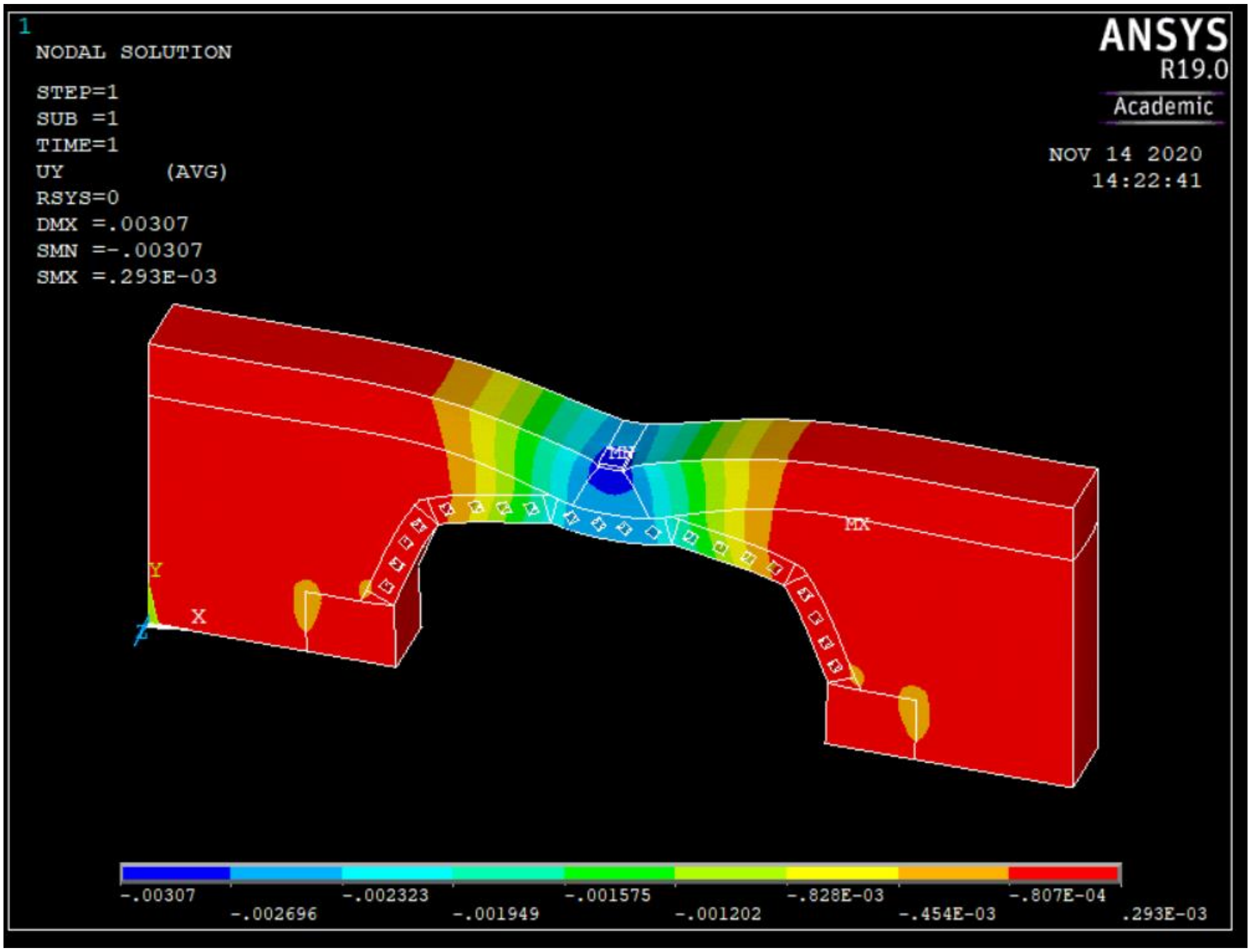

Figure 154 - 3D Nodal Y-Displacements Rerun No. 3 - Test No. 2 Hollow-Core Model

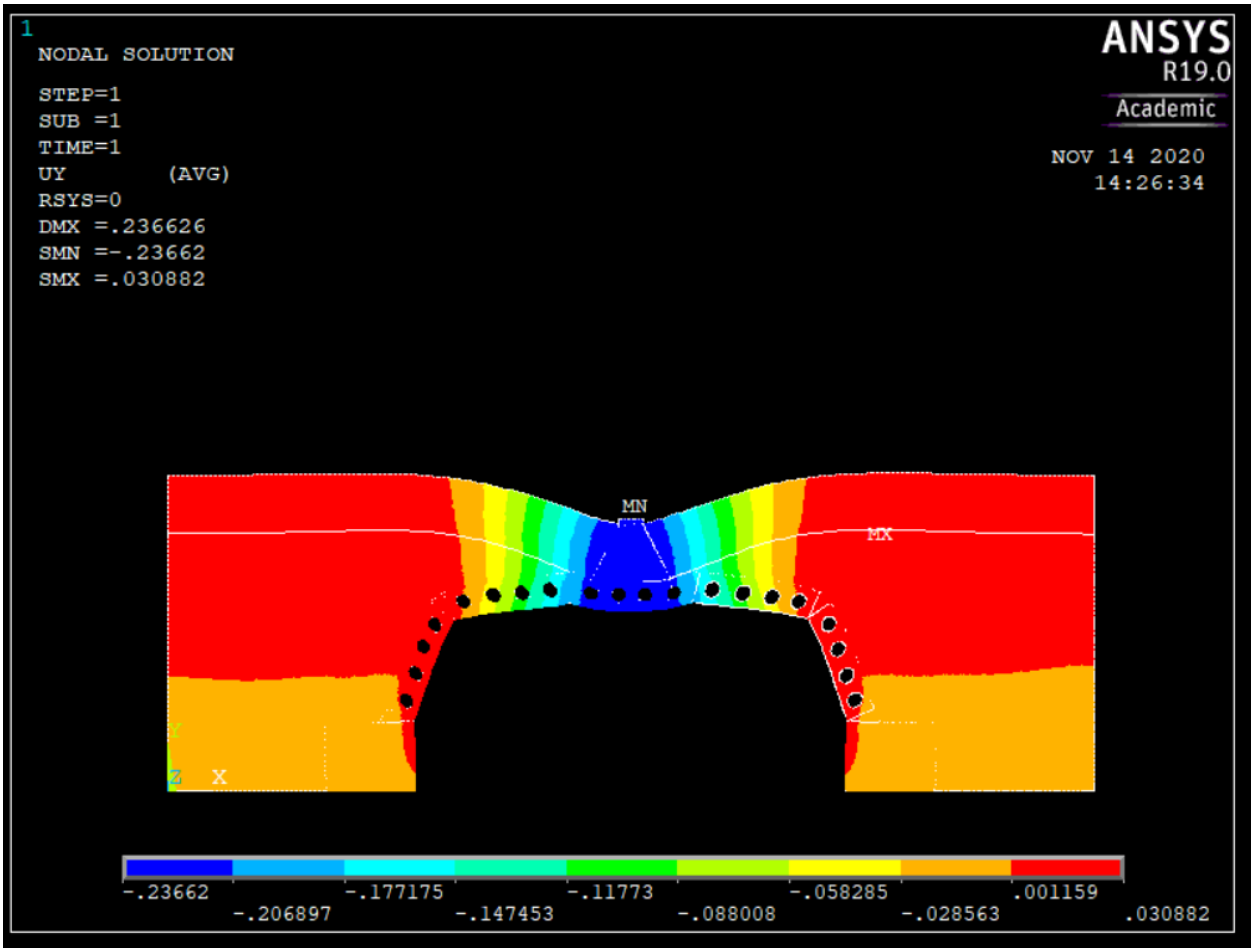

Figure 155 - 2D Nodal Y-Displacements Rerun No. 4 - Test No. 2 Hollow-Core Model

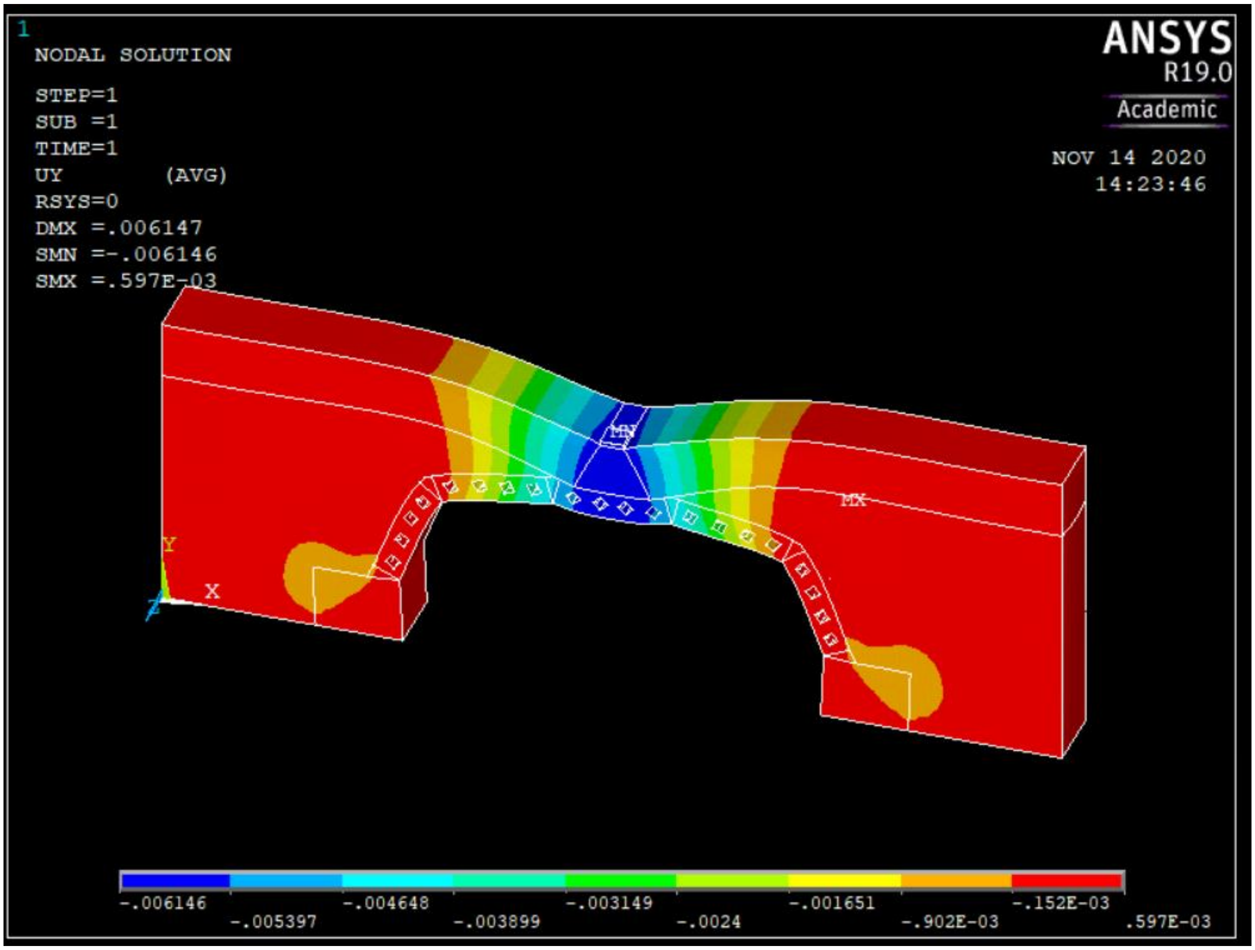

Figure 156 - 3D Nodal Y-Displacements Rerun No. 4 - Test No. 2 Hollow-Core Model

Appendix K – STAAD Analyses

K1 – Test No. 4 CIP Model Fixed Supports (27-inch Beam)

Job Information

	Engineer	Checked	Approved
Name:	Maria Tangarife	Dr. James Mahar	
Date:	11/9/2020		

Project ID	
Project Name	

Structure Type	SPACE FRAME

Number of Nodes	2	Highest Node	2
Number of Elements	1	Highest Beam	1

Number of Basic Load Cases	2
Number of Combination Load Cases	0

Included in this printout are data for:

All	The Whole Structure

Included in this printout are results for load cases:

Type	L/C	Name
Primary	1	DEAD LOAD
Primary	2	LIVE LOAD

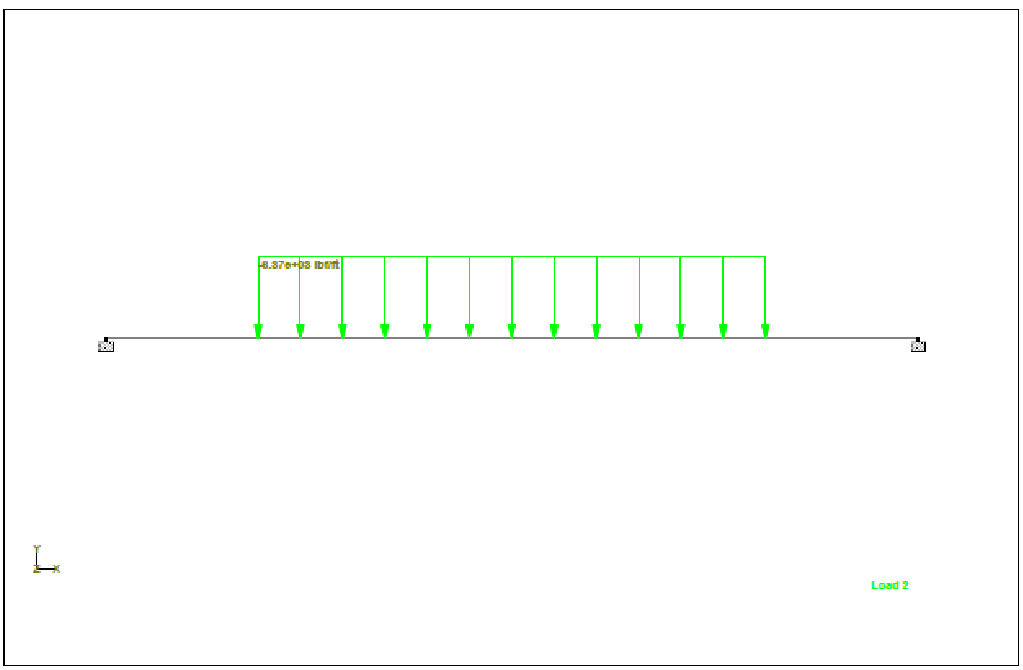

Loading Diagram

Reactions

Node	L/C	Horizontal FX (kip)	Vertical FY (kip)	Horizontal FZ (kip)	Moment MX (kip`in)	Moment MY (kip`in)	Moment MZ (kip`in)
1	1:DEAD LOAD	0	0.341	0	-0	0	1.905
	2:LIVE LOAD	0	4.511	0	-0	0	26.704
2	1:DEAD LOAD	0	0.341	0	0	0	-1.906
	2:LIVE LOAD	0	4.516	0	0	0	-26.720

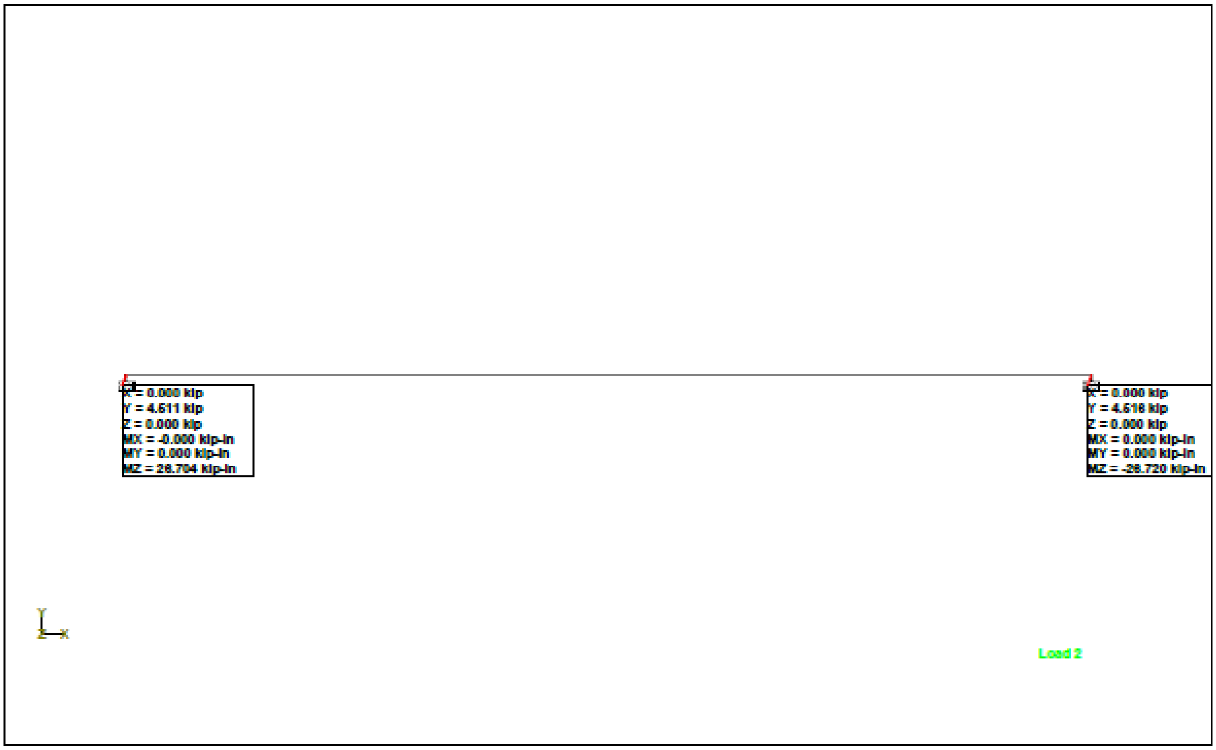

Reactions

Beam End Forces

Sign convention is as the action of the joint on the beam.

Beam	Node	L/C	Axial Fx (kip)	Shear Fy (kip)	Shear Fz (kip)	Torsion Mx (kip`in)	Bending My (kip`in)	Bending Mz (kip`in)
1	1	1:DEAD LOAD	0	0.341	0	0	0	1.905
		2:LIVE LOAD	0	4.511	0	0	0	26.704
	2	1:DEAD LOAD	0	0.341	0	0	0	-1.906
		2:LIVE LOAD	0	4.516	0	0	0	-26.720

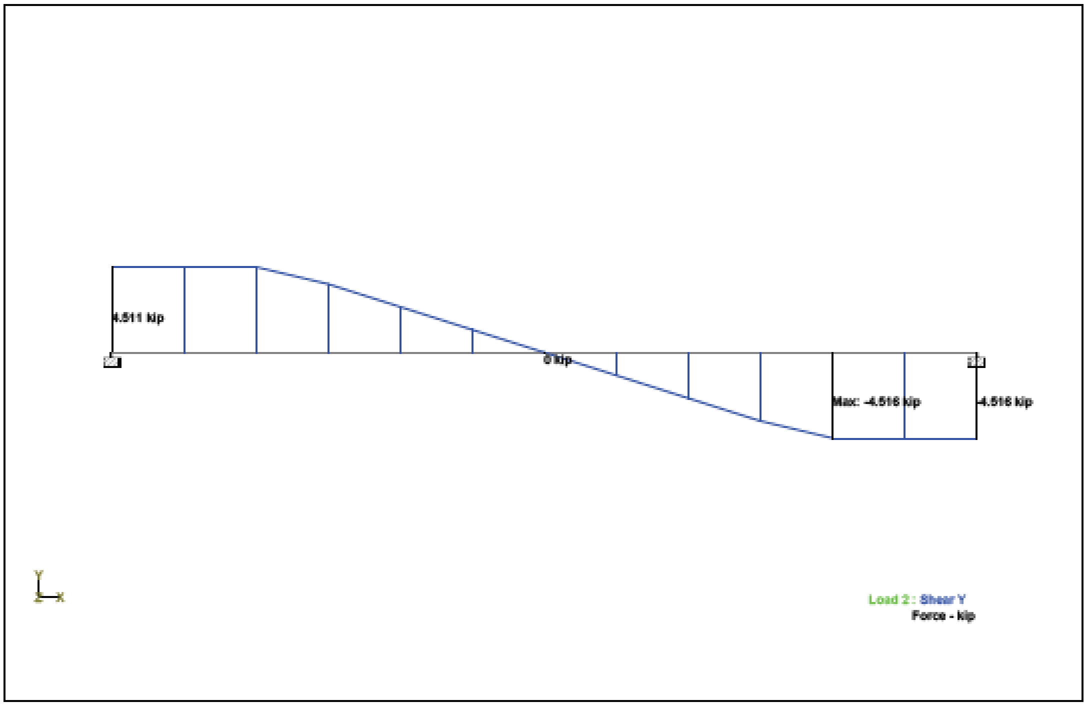

Shear

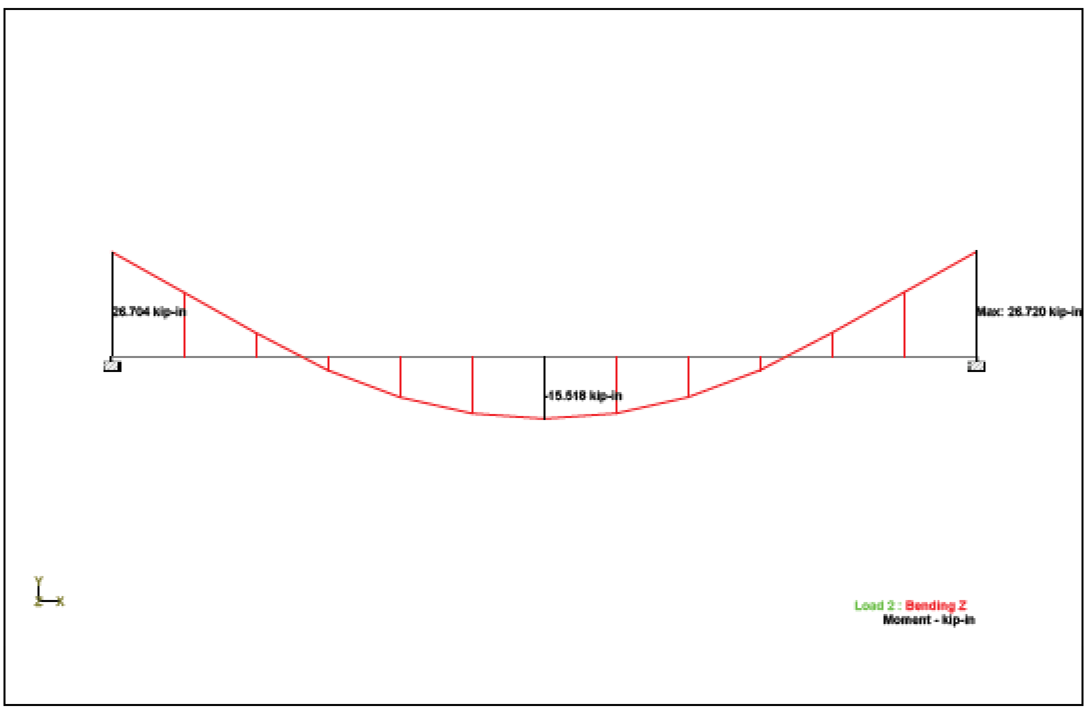

Moment

Beam Displacement Detail

Displacements shown in italic indicate the presence of an offset

Beam	L/C	d (ft)	X (in)	Y (in)	Z (in)	Resultant (in)
1	1:DEAD LOAD	0	0	0	0	0
		0.227	0.000	-0.000	0	0.000
		0.454	0.000	-0.000	0	0.000
		0.680	0.000	-0.000	0	0.000
		0.907	0.000	-0.000	0	0.000
		1.134	-0.000	-0.000	0	0.000
		1.361	0.000	-0.000	0	0.000
		1.588	-0.000	-0.000	0	0.000
		1.814	-0.000	-0.000	0	0.000
		2.041	-0.000	-0.000	0	0.000
		2.268	0	0	0	0
	2:LIVE LOAD	0	0	0	0	0
		0.227	0.000	-0.000	0	0.000
		0.454	0.000	-0.000	0	0.000
		0.680	0.000	-0.000	0	0.000
		0.907	0.000	-0.001	0	0.001
		1.134	-0.000	-0.001	0	0.001
		1.361	0.000	-0.001	0	0.001
		1.588	-0.000	-0.000	0	0.000
		1.814	-0.000	-0.000	0	0.000
		2.041	-0.000	-0.000	0	0.000
		2.268	0	0	0	0

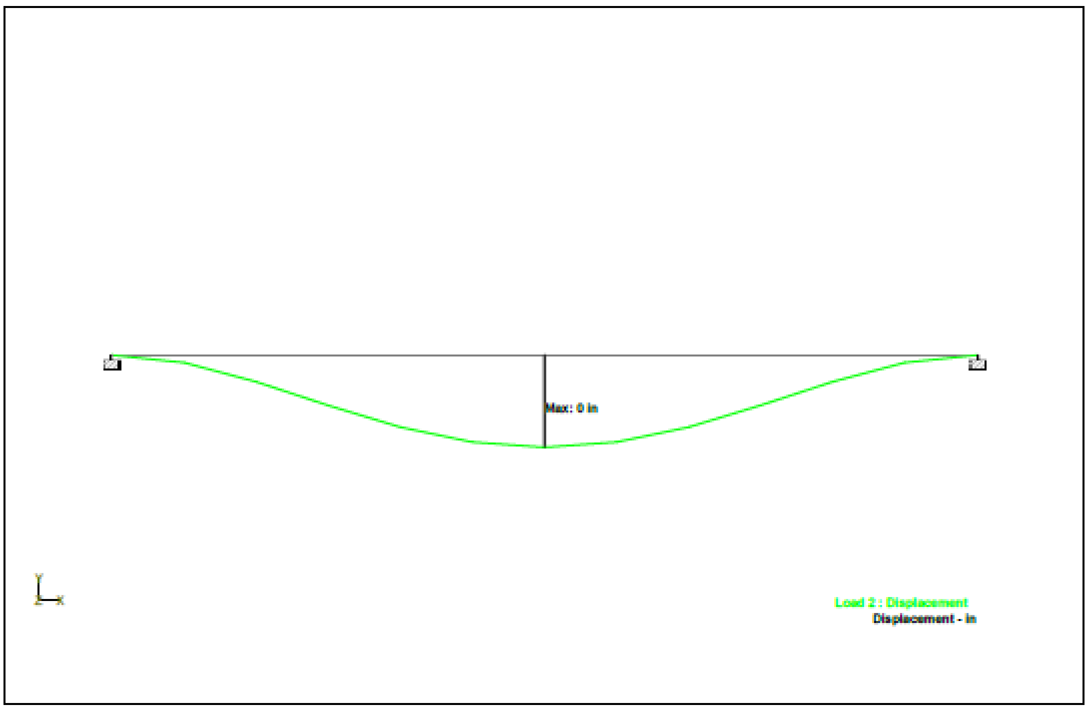

Displacement

K2 – Test No. 4 CIP Model Pinned Supports (27-inch Beam)

Job Information

	Engineer	Checked	Approved
Name:	Maria Tangarife	Dr. James Mahar	
Date:	11/9/2020		

Project ID	
Project Name	

Structure Type	SPACE FRAME

Number of Nodes	2	Highest Node	2
Number of Elements	1	Highest Beam	1

Number of Basic Load Cases	2
Number of Combination Load Cases	0

Included in this printout are data for:

All	The Whole Structure

Included in this printout are results for load cases:

Type	L/C	Name
Primary	1	DEAD LOAD
Primary	2	LIVE LOAD

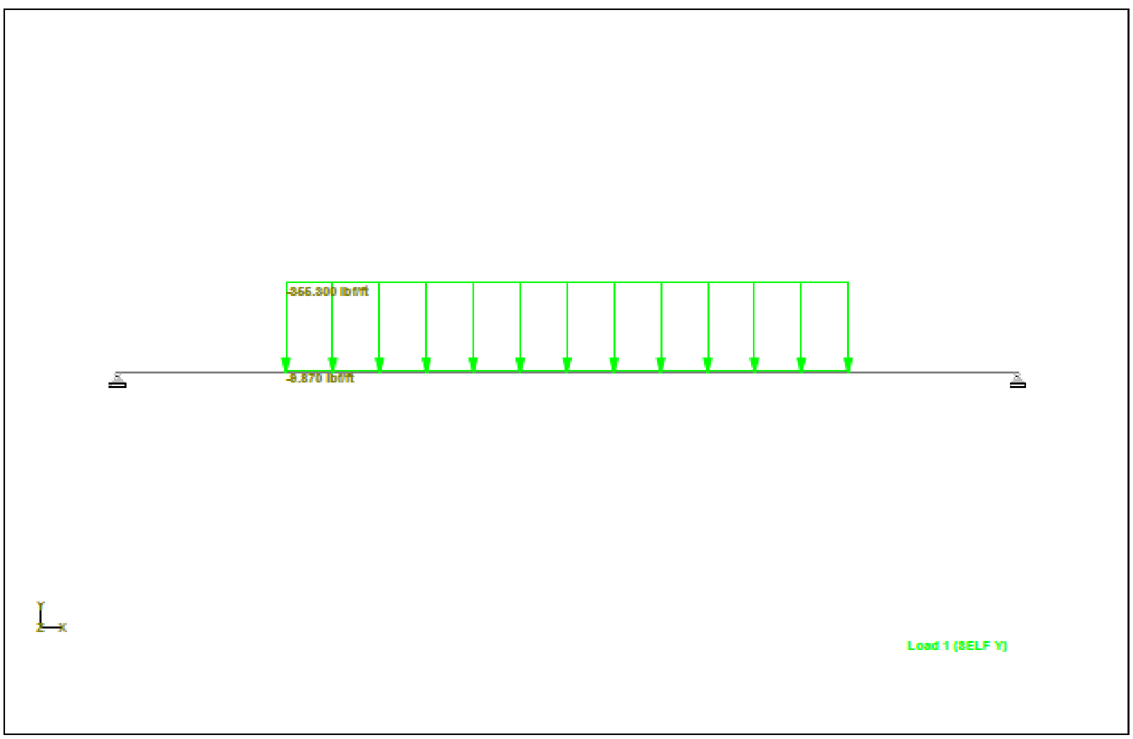

Loading Diagram

Reactions

		Horizontal	Vertical	Horizontal	Moment		
Node	L/C	FX (kip)	FY (kip)	FZ (kip)	MX (kip`in)	MY (kip`in)	MZ (kip`in)
1	1:DEAD LOAD	0	0.341	0	0	0	0
	2:LIVE LOAD	0	4.511	0	0	0	0
2	1:DEAD LOAD	0	0.341	0	0	0	0
	2:LIVE LOAD	0	4.515	0	0	0	0

Beam End Forces

Sign convention is as the action of the joint on the beam.

			Axial	Shear		Torsion	Bending	
Beam	Node	L/C	Fx (kip)	Fy (kip)	Fz (kip)	Mx (kip`in)	My (kip`in)	Mz (kip`in)
1	1	1:DEAD LOAD	0	0.341	0	0	0	0.000
		2:LIVE LOAD	0	4.511	0	0	0	0.000
	2	1:DEAD LOAD	0	0.341	0	0	0	0.000
		2:LIVE LOAD	0	4.515	0	0	0	0.000

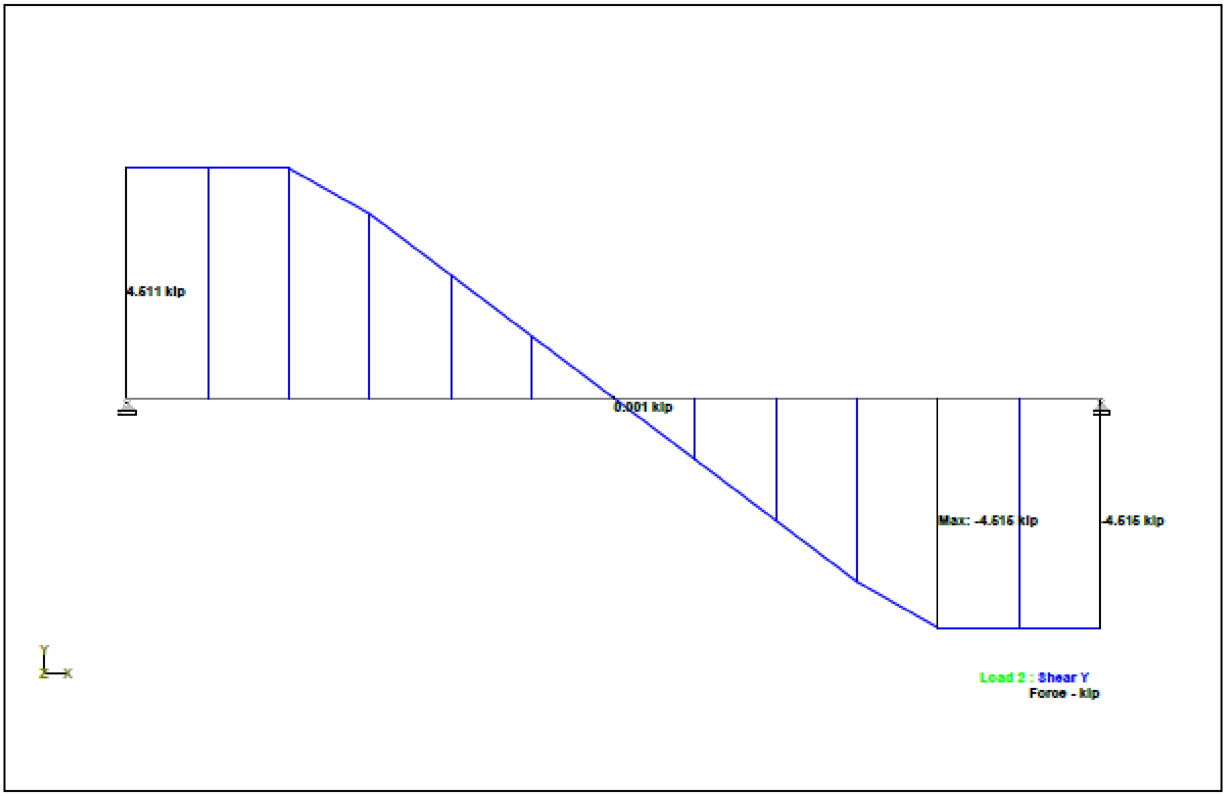

Shear Diagram

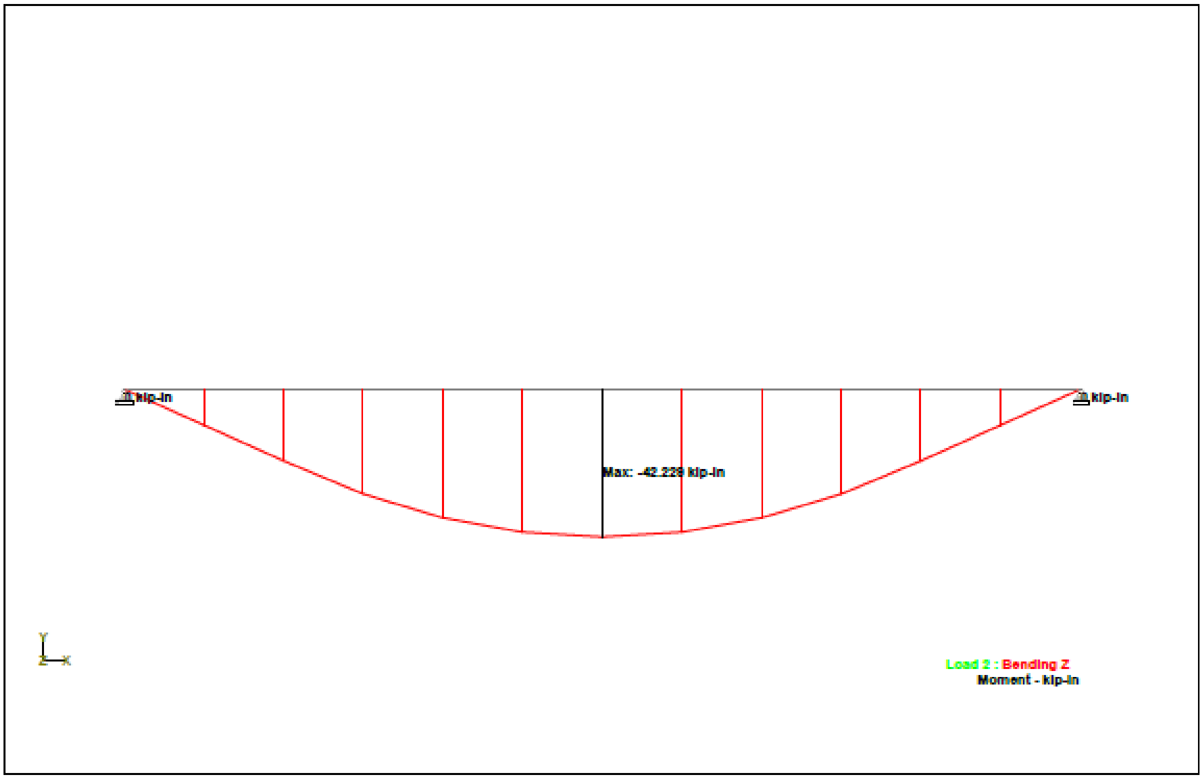

Moment Diagram

Beam Displacement Detail

Displacements shown in italic indicate the presence of an offset

Beam	L/C	d (ft)	X (in)	Y (in)	Z (in)	Resultant (in)
1	1:DEAD LOAD	0	0	0	0	0
		0.227	0.000	-0.000	0	0.000
		0.454	0.000	-0.000	0	0.000
		0.680	0.000	-0.000	0	0.000
		0.907	0.000	-0.000	0	0.000
		1.134	-0.000	-0.000	0	0.000
		1.361	0.000	-0.000	0	0.000
		1.588	-0.000	-0.000	0	0.000
		1.814	-0.000	-0.000	0	0.000
		2.041	-0.000	-0.000	0	0.000
		2.268	0	0	0	0
	2:LIVE LOAD	0	0	0	0	0
		0.227	0.000	-0.001	0	0.001
		0.454	0.000	-0.002	0	0.002
		0.680	0.000	-0.002	0	0.002
		0.907	0.000	-0.003	0	0.003
		1.134	-0.000	-0.003	0	0.003
		1.361	0.000	-0.003	0	0.003
		1.588	-0.000	-0.002	0	0.002
		1.814	-0.000	-0.002	0	0.002
		2.041	-0.000	-0.001	0	0.001
		2.268	0	0	0	0

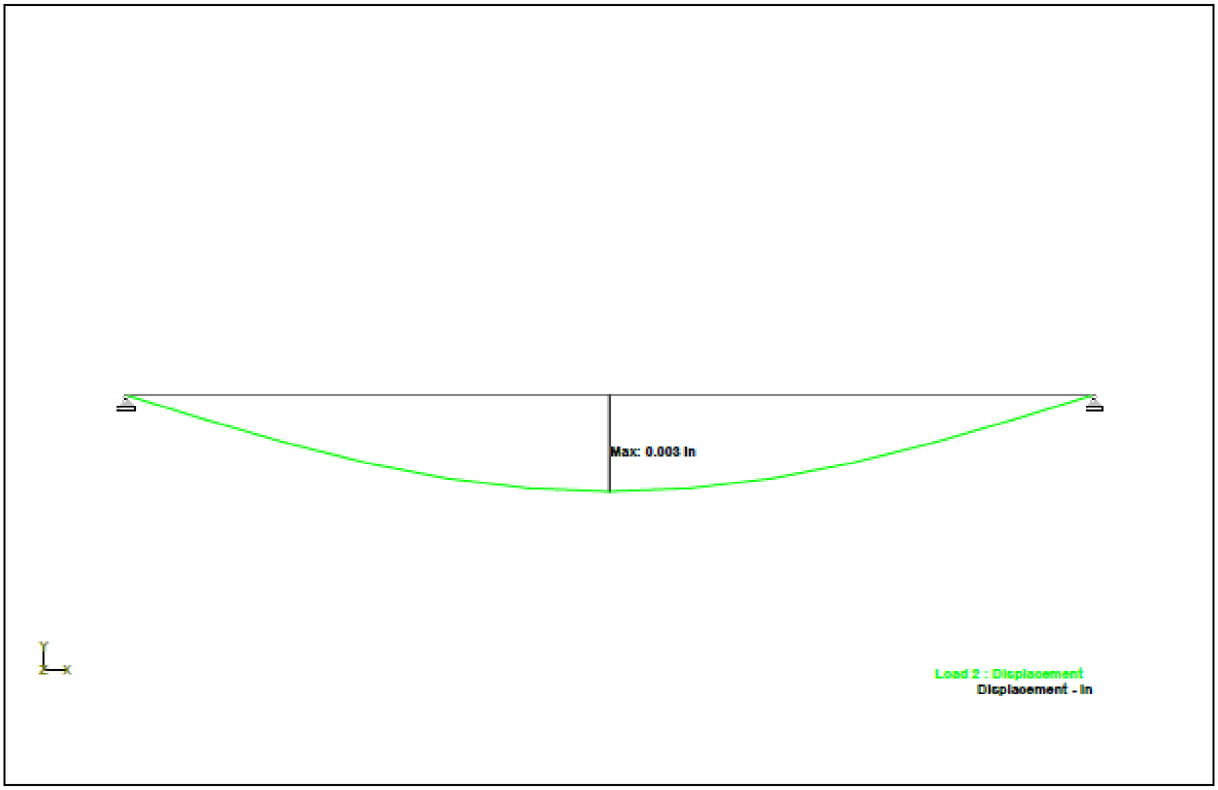

Displacement

K3 – Test No. 4 CIP Model Fixed Supports (Three 27-inch Segments)

Job Information

	Engineer	Checked	Approved
Name:	Maria Tangarife	Dr. James Mahar	
Date:	11/9/2020		

Project ID	
Project Name	

Structure Type	SPACE FRAME

Number of Nodes	4	Highest Node	4
Number of Elements	3	Highest Beam	3

Number of Basic Load Cases	2
Number of Combination Load Cases	0

Included in this printout are data for:

All	The Whole Structure

Included in this printout are results for load cases:

Type	L/C	Name
Primary	1	DEAD LOAD
Primary	2	LIVE LOAD

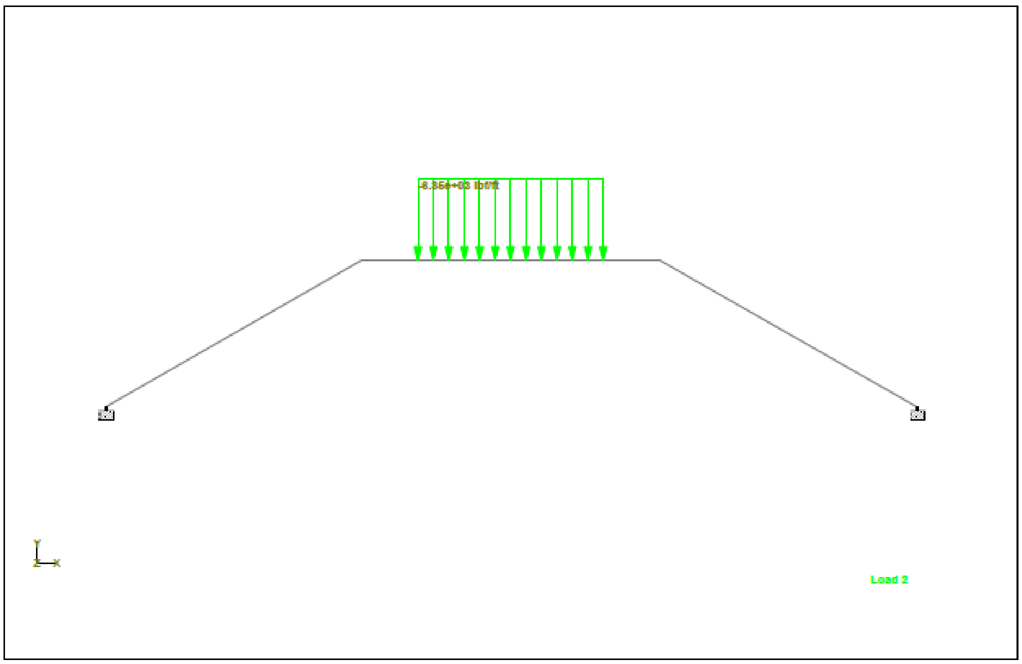

Loading Diagram

Reactions

		Horizontal	Vertical	Horizontal	Moment		
Node	L/C	FX (kip)	FY (kip)	FZ (kip)	MX (kip`in)	MY (kip`in)	MZ (kip`in)
1	1:DEAD LOAD	0.256	0.247	0	0	0	0.617
	2:LIVE LOAD	8.485	4.506	0	0	0	2.883
4	1:DEAD LOAD	-0.256	0.248	0	0	0	-0.626
	2:LIVE LOAD	-8.485	4.492	0	0	0	-2.938

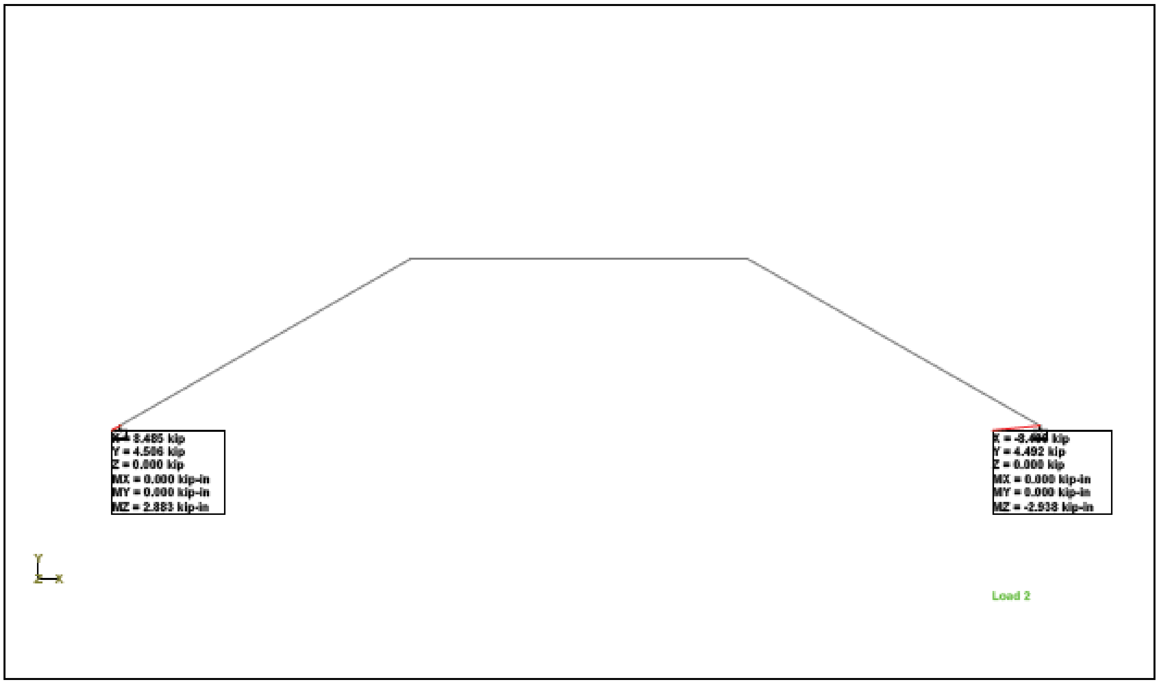

Reactions

Beam End Forces

Sign convention is as the action of the joint on the beam.

			Axial	Shear		Torsion	Bending	
Beam	Node	L/C	Fx (kip)	Fy (kip)	Fz (kip)	Mx (kip`in)	My (kip`in)	Mz (kip`in)
1	1	1:DEAD LOAD	0.345	0.087	0	0	0	0.617
		2:LIVE LOAD	9.602	-0.334	0	0	0	2.883
	2	1:DEAD LOAD	-0.263	0.056	0	0	0	-0.204
		2:LIVE LOAD	-9.602	0.334	0	0	0	-11.956
2	2	1:DEAD LOAD	0.256	0.082814	0	0	0	0.204
		2:LIVE LOAD	8.485	4.506	0	0	0	11.956
	3	1:DEAD LOAD	-0.256	0.082	0	0	0	-0.197
		2:LIVE LOAD	-8.485	4.492	0	0	0	-11.813
3	3	1:DEAD LOAD	0.263	0.056	0	0	0	0.197
		2:LIVE LOAD	9.595	0.326	0	0	0	11.813
	4	1:DEAD LOAD	-0.345	0.087	0	0	0	-0.626
		2:LIVE LOAD	-9.595	-0.326	0	0	0	-2.938

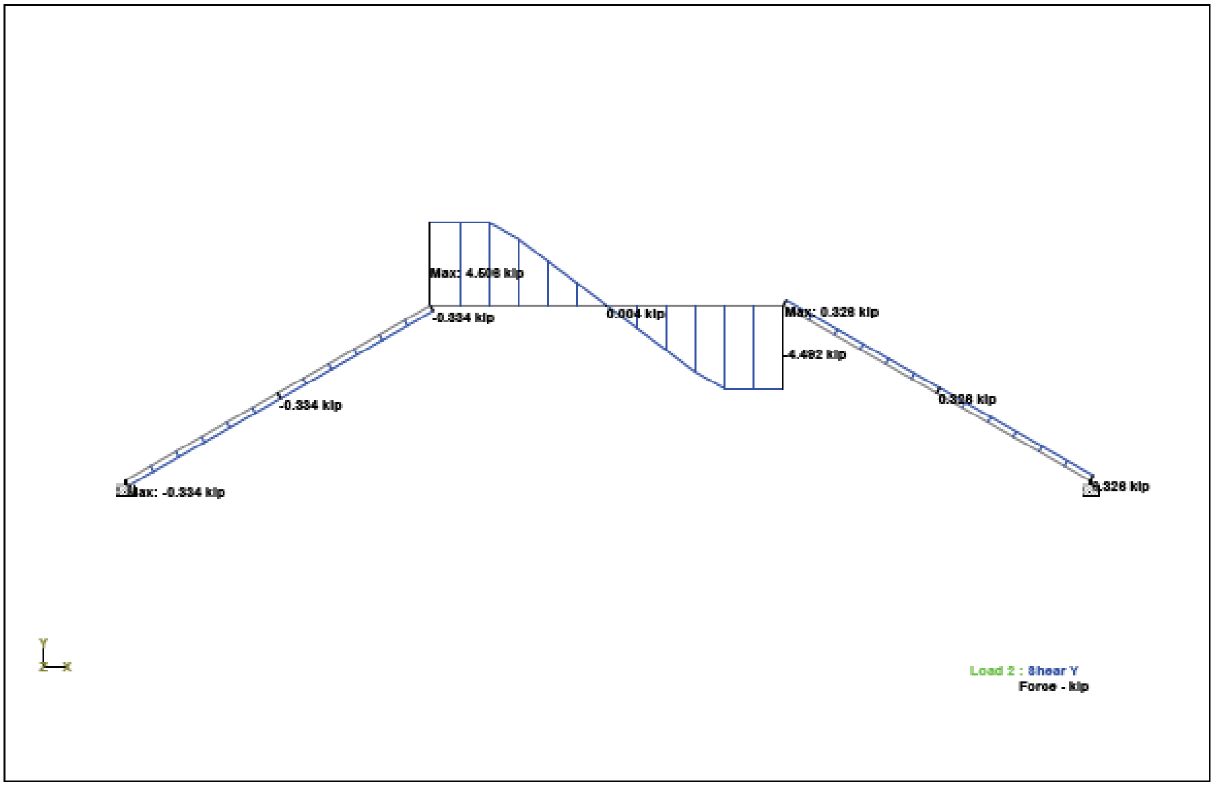

Shear Diagram

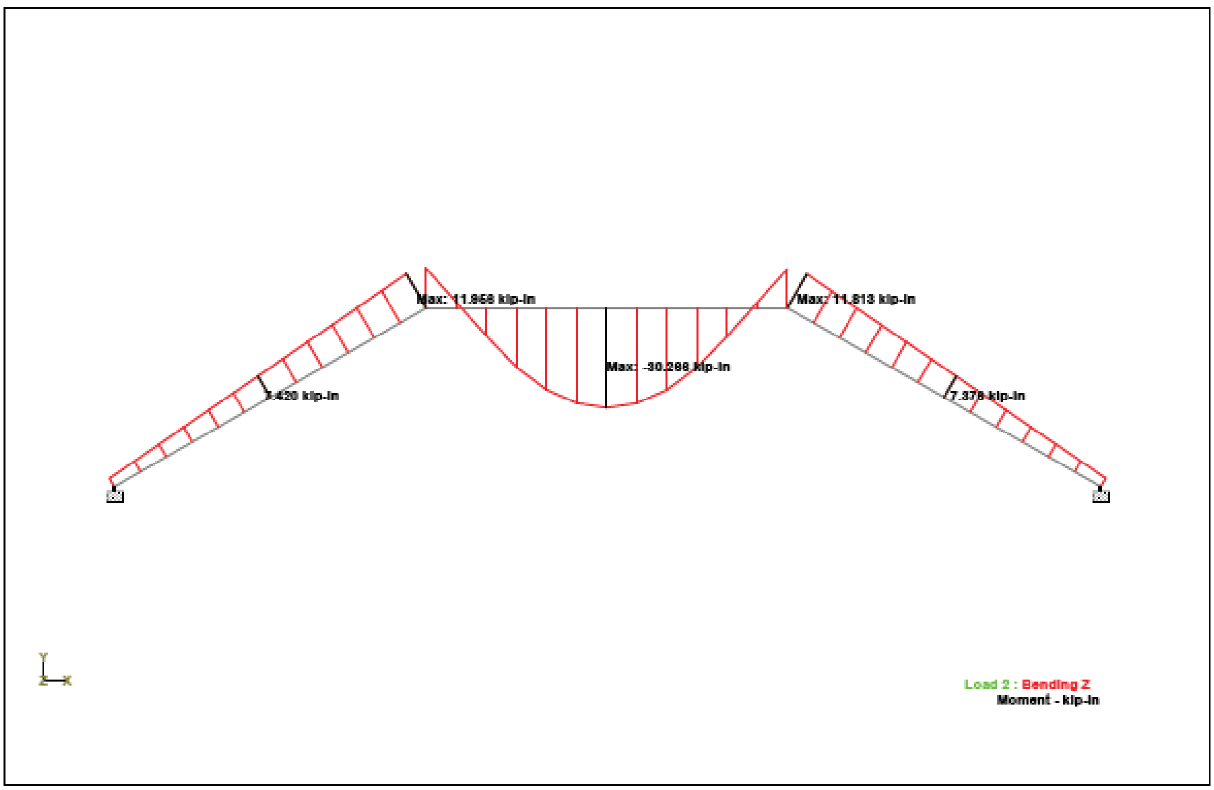

Moment Diagram

Beam Displacement Detail

Displacements shown in italic indicate the presence of an offset

Beam	L/C	d (ft)	X (in)	Y (in)	Z (in)	Resultant (in)
1	1:DEAD LOAD	0	0	0	0	0
		0.226	-0.000	-0.000	0	0.000
		0.452	-0.000	-0.000	0	0.000
		0.679	0.000	-0.000	0	0.000
		0.905	0.000	-0.000	0	0.000
		1.131	0.000	-0.000	0	0.000
		1.357	0.000	-0.000	0	0.000
		1.584	0.000	-0.000	0	0.000
		1.810	0.000	-0.000	0	0.000
		2.036	0.000	-0.000	0	0.000
		2.262	0.000	-0.000	0	0.000
	2:LIVE LOAD	0	0	0	0	0
		0.226	-0.000	-0.000	0	0.000
		0.452	-0.000	-0.000	0	0.000
		0.679	-0.000	-0.000	0	0.000
		0.905	-0.000	-0.000	0	0.000
		1.131	-0.000	-0.000	0	0.000
		1.357	-0.000	-0.001	0	0.001
		1.584	-0.000	-0.001	0	0.001
		1.810	0.000	-0.001	0	0.001
		2.036	0.000	-0.001	0	0.001
		2.262	0.000	-0.002	0	0.002
2	1:DEAD LOAD	0	0.000	-0.000	0	0.000
		0.227	0.000	-0.000	0	0.000
		0.454	0.000	-0.000	0	0.000
		0.681	0.000	-0.000	0	0.000
		0.908	0.000	-0.000	0	0.000
		1.135	-0.000	-0.000	0	0.000
		1.362	-0.000	-0.000	0	0.000
		1.589	-0.000	-0.000	0	0.000
		1.816	-0.000	-0.000	0	0.000
		2.043	-0.000	-0.000	0	0.000
		2.270	-0.000	-0.000	0	0.000
	2:LIVE LOAD	0	0.000	-0.002	0	0.002
		0.227	0.000	-0.002	0	0.002
		0.454	0.000	-0.003	0	0.003
		0.681	0.000	-0.003	0	0.003
		0.908	0.000	-0.004	0	0.004
		1.135	-0.000	-0.004	0	0.004
		1.362	-0.000	-0.004	0	0.004
		1.589	-0.000	-0.003	0	0.003
		1.816	-0.000	-0.003	0	0.003
		2.043	-0.000	-0.002	0	0.002
		2.270	-0.000	-0.002	0	0.002
3	1:DEAD LOAD	0	-0.000	-0.000	0	0.000
		0.227	-0.000	-0.000	0	0.000
		0.454	-0.000	-0.000	0	0.000
		0.681	-0.000	-0.000	0	0.000
		0.908	-0.000	-0.000	0	0.000
		1.136	-0.000	-0.000	0	0.000
		1.363	0.000	-0.000	0	0.000
		1.590	-0.000	-0.000	0	0.000
		1.817	0.000	-0.000	0	0.000

Beam Displacement Detail Cont...

Beam	L/C	d (ft)	X (in)	Y (in)	Z (in)	Resultant (in)
		2.044	-0.000	-0.000	0	0.000
		2.271	0	0	0	0
	2:LIVE LOAD	0	-0.000	-0.002	0	0.002
		0.227	-0.000	-0.001	0	0.001
		0.454	-0.000	-0.001	0	0.001
		0.681	0.000	-0.001	0	0.001
		0.908	0.000	-0.001	0	0.001
		1.136	0.000	-0.000	0	0.000
		1.363	0.000	-0.000	0	0.000
		1.590	0.000	-0.000	0	0.000
		1.817	0.000	-0.000	0	0.000
		2.044	0.000	-0.000	0	0.000
		2.271	0	0	0	0

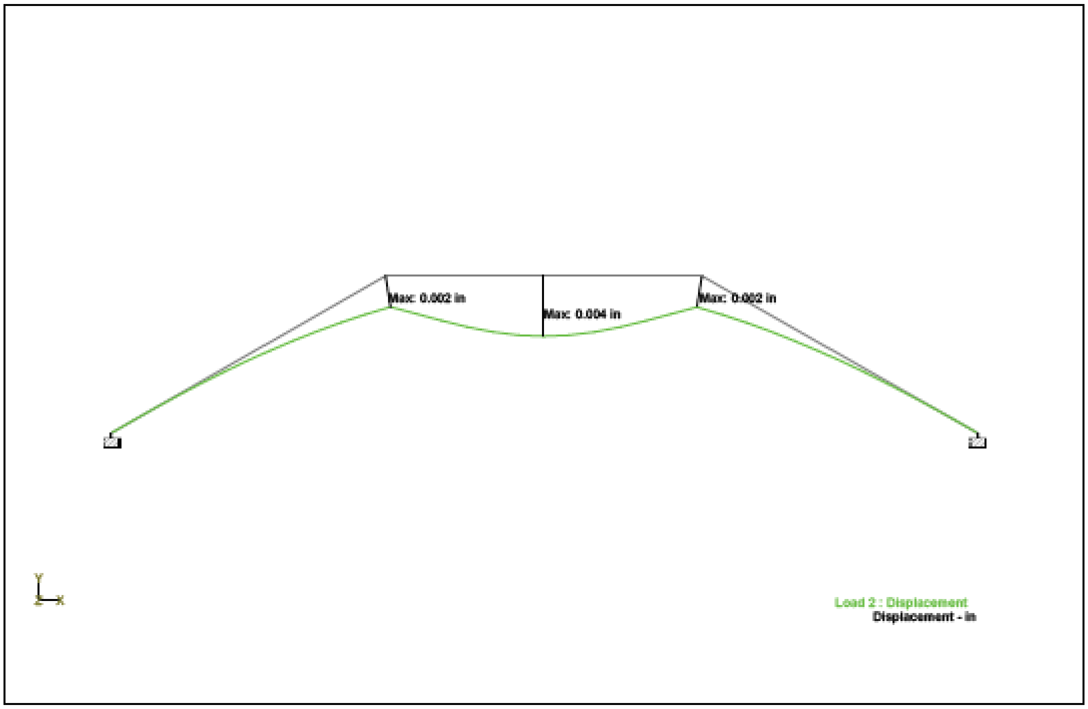

Displacements

K4 – Test No. 4 CIP Model Fixed Supports (81-inch Beam)

Job Information

	Engineer	Checked	Approved
Name:	Maria Tangarife	Dr. James Mahar	
Date:	11/9/2020		

Project ID	
Project Name	

Structure Type	SPACE FRAME

Number of Nodes	2	Highest Node	2
Number of Elements	1	Highest Beam	1

Number of Basic Load Cases	2
Number of Combination Load Cases	0

Included in this printout are data for:

All	The Whole Structure

Included in this printout are results for load cases:

Type	L/C	Name
Primary	1	DEAD LOAD
Primary	2	LIVE LOAD

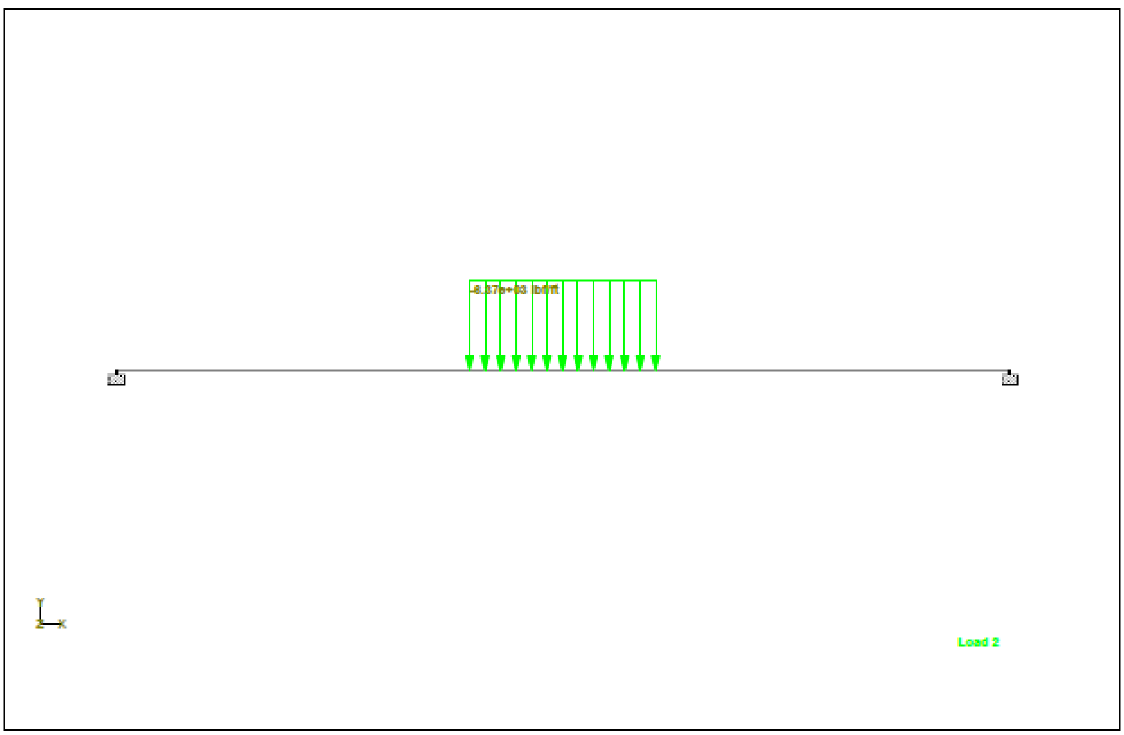

Loading Diagram

Reactions

		Horizontal	Vertical	Horizontal	Moment		
Node	L/C	FX (kip)	FY (kip)	FZ (kip)	MX (kip`in)	MY (kip`in)	MZ (kip`in)
1	1:DEAD LOAD	0	0.506	0	-0	0	8.571
	2:LIVE LOAD	0	4.511	0	-0	0	90.758
2	1:DEAD LOAD	0	0.506	0	0	0	-8.572
	2:LIVE LOAD	0	4.513	0	0	0	-90.786

Reactions

Beam End Forces

Sign convention is as the action of the joint on the beam.

			Axial	Shear		Torsion	Bending	
Beam	Node	L/C	Fx (kip)	Fy (kip)	Fz (kip)	Mx (kip`in)	My (kip`in)	Mz (kip`in)
1	1	1:DEAD LOAD	0	0.506	0	0	0	8.571
		2:LIVE LOAD	0	4.511	0	0	0	90.758
	2	1:DEAD LOAD	0	0.506	0	0	0	-8.572
		2:LIVE LOAD	0	4.513	0	0	0	-90.786

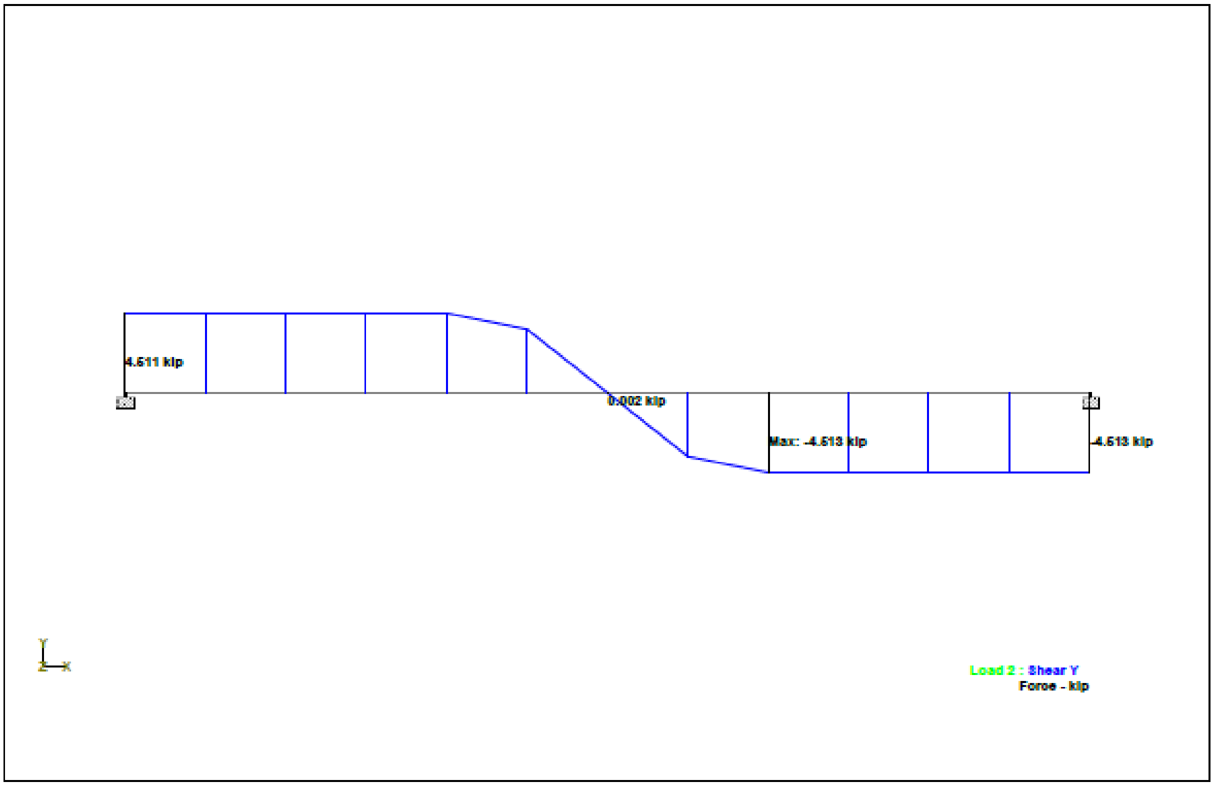

Shear Diagram

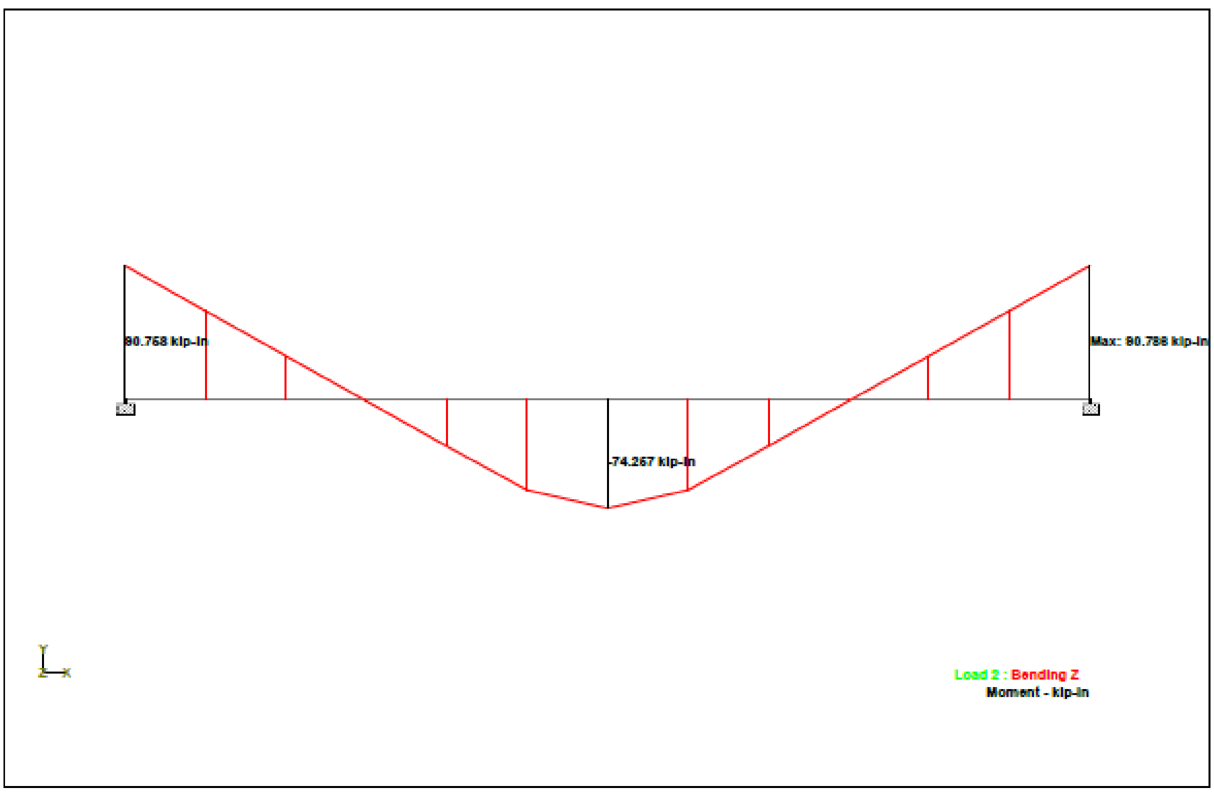

Moment Diagram

Beam Displacement Detail

Displacements shown in italic indicate the presence of an offset

Beam	L/C	d (ft)	X (in)	Y (in)	Z (in)	Resultant (in)
1	1:DEAD LOAD	0	0	0	0	0
		0.680	-0.000	-0.000	0	0.000
		1.361	-0.000	-0.001	0	0.001
		2.041	-0.000	-0.001	0	0.001
		2.722	0.000	-0.002	0	0.002
		3.402	-0.000	-0.002	0	0.002
		4.082	0.000	-0.002	0	0.002
		4.763	-0.000	-0.001	0	0.001
		5.443	0.000	-0.001	0	0.001
		6.124	-0.000	-0.000	0	0.000
		6.804	0	0	0	0
	2:LIVE LOAD	0	0	0	0	0
		0.680	-0.000	-0.002	0	0.002
		1.361	-0.000	-0.007	0	0.007
		2.041	-0.000	-0.014	0	0.014
		2.722	0.000	-0.019	0	0.019
		3.402	-0.000	-0.021	0	0.021
		4.082	0.000	-0.019	0	0.019
		4.763	-0.000	-0.014	0	0.013575
		5.443	0.000	-0.007	0	0.007
		6.124	-0.000	-0.002	0	0.002
		6.804	0	0	0	0

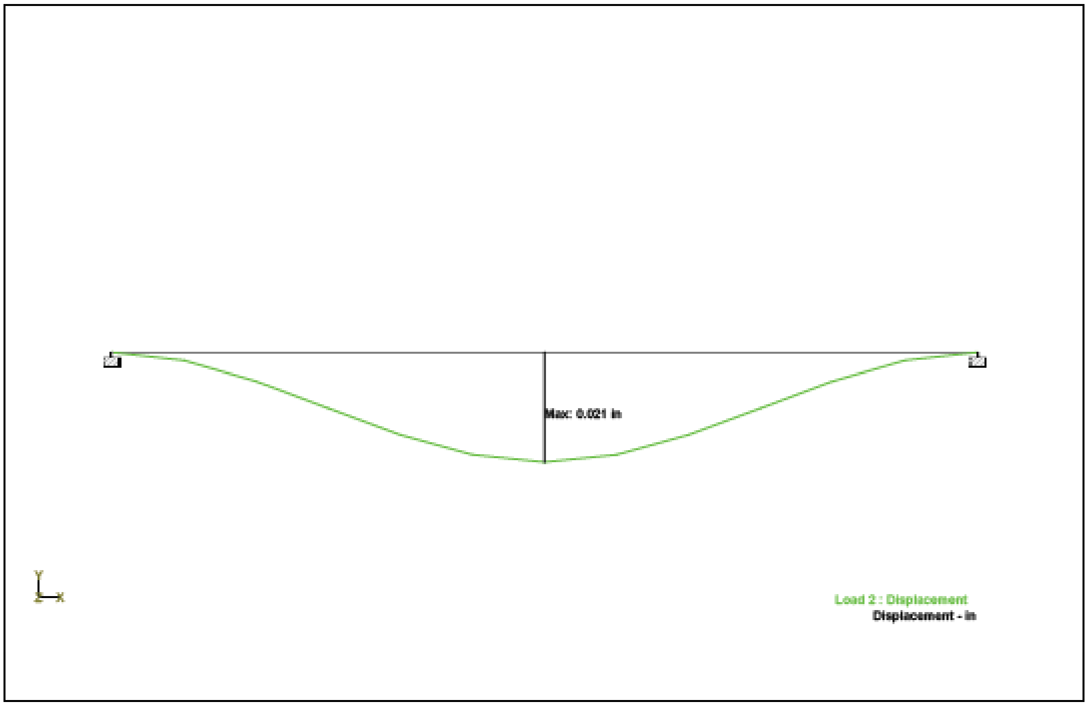

Displacement